Gebhard Mathis
Editor

Chest Sonography

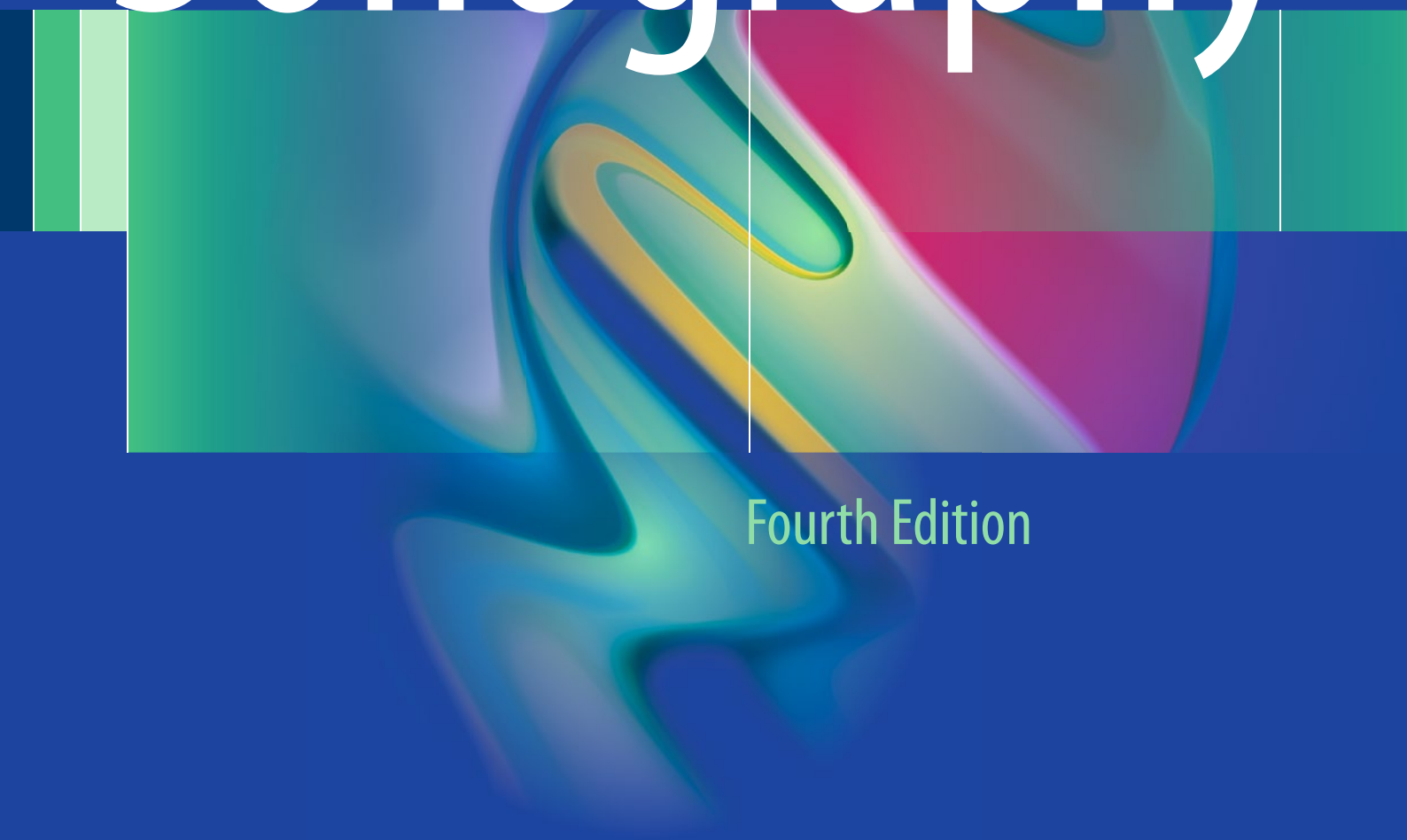

Fourth Edition

Springer

Chest Sonography

Gebhard Mathis
Editor

Chest Sonography

Fourth Edition

Springer

Editor
Gebhard Mathis
Rankweil
Austria

ISBN 978-3-319-44071-2 ISBN 978-3-319-44072-9 (eBook)
DOI 10.1007/978-3-319-44072-9

Library of Congress Control Number: 2017940481

Printed on acid-free paper

This Springer imprint is published by Springer Nature
The registered company is Springer International Publishing AG
The registered company address is: Gewerbestrasse 11, 6330 Cham, Switzerland

Preface

The scope of ultrasonography of the lung has been substantially extended over the last few years. Portable ultrasound systems are being used to an increasing extent in the preclinical setting, at accident sites, in the ambulance, or in the rescue helicopter. A paradigm shift is under way. With the ultrasound stethoscope, we are immediately at the patient's side during a clinical investigation. Patients no longer need to be transported to an ultrasound laboratory. This has proven successful in emergency medicine, in emergency departments, at the intensive care unit, as well as in the preclinical setting and the doctor's office. In daily clinical practice, chest ultrasound is a strategic instrument to determine further steps: What type of immediate treatment should one use? Where should the patient be transferred?

In the differential diagnosis of dyspnea and in non-cardiac chest pain, a pneumothorax can be proven accurately or ruled out with certainty. In patients with an interstitial syndrome, the investigator is able to visualize a pulmonary edema and also follow up the treatment process semiquantitatively. The fact that inflammatory, neoplastic, and embolism-related peripheral lung consolidations have a typical appearance on ultrasonography has been known for a long time. Recent studies and meta-analyses have confirmed previous data on the subject. An international consensus conference initiated by Winfocus has produced certain recommendations in this regard. Ultrasound of the lung has been incorporated into a number of guidelines, such as those for the evaluation of a lung carcinoma invading the chest wall.

However, the method calls for very thorough knowledge of the subject and a meticulous investigation technique. The analysis of numerous studies has shown that superficial applications – in terms of method – produce poor results. This is true of the diagnostic investigation of pulmonary embolism, among other conditions.

For the abovementioned reasons, we present a current update on the subject, which incorporates a large body of recent publications and is accompanied by a number of new illustrations and photographs. My most heartfelt thanks to the team of authors for their renewed creative teamwork and timely submissions. My thanks to Springer-Verlag for their positive cooperation and meticulous production of the book.

I hope this illustrated atlas will help many colleagues and serve many patients by enabling clinicians to establish diagnoses accurately, efficiently, and economically at the patient's bedside and initiate the appropriate therapeutic measures promptly.

Gebhard Mathis
Rankweil, Austria
October 2016

Contents

Indications, Technical Equipment and Investigation Procedure

Sonja Beckh

G. Mathis (ed.), *Chest Sonography*, DOI 10.1007/978-3-319-44072-9_1

1

1.1 Indications

Ultrasonography of the lung has now become an established imaging procedure for chest diseases. The diagnostic value of this procedure has been described and proven in several comprehensive scientific investigations and studies (Beckh et al. 2002; Beaulieu and Marik 2005; Mathis et al. 2005; Niemann et al. 2009; Reuß 2010; Reissig et al 2012; Volpicelli et al. 2012; von Bartheld et al. 2013; Squizzato et al. 2013).

The acceptance of the method is reflected in a number of well-known international guidelines (AWMF 2010; Goeckenjan et al. 2010, 2011; Havelock et al. 2010; Hooper et al. 2010; Piscaglia et al. 2012; Bamber et al. 2013; Cosgrove et al. 2013; Detterbeck et al. 2013). Furthermore, ultrasound investigation of the lung has been established as a fundamental diagnostic procedure in emergency situations and intensive medicine (Diacon et al. 2005; Soldati et al. 2006; Arbelot et al. 2008; Copetti and Cattarossi 2008; Copetti et al. 2008; Noble et al. 2009; Moore and Copel 2011; Blank and Heinzmann 2012; Volpicelli et al. 2012; Böer et al. 2014)

The ultrasound image does not provide a complete overview of the chest. However, it does show a certain portion of the chest and thus provides diagnostic information about a variety of problems (Fig. 1.1).

About 99 % of the ultrasonic wave is reflected by the healthy lung. Intrapulmonary processes can be registered by ultrasound only when they extend to the visceral pleura or can be visualized through a sound-conducting medium such as fluid or consolidated lung tissue (Fig. 1.2).

Acoustic shadowing occurs due to nearly complete absorption of the ultrasonic wave on bone, especially behind the sternum, the scapula, and the spine. Impairment due to the rib shadow can be balanced, at least in part, by appropriate breathing techniques.

The immediate retrosternal and posterior portions of the mediastinum cannot be viewed from the percutaneous aspect. Transesophageal and transbronchial ultrasound may

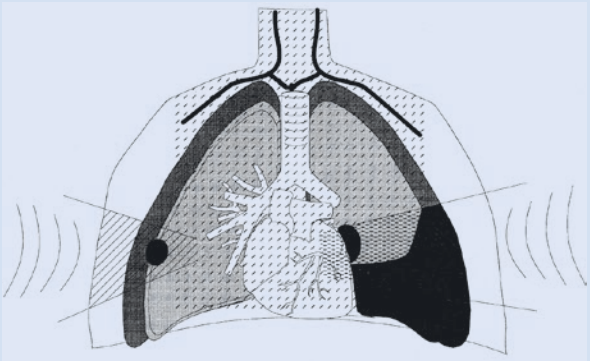

Fig. 1.2 Entities and pathological changes that can be accessed by ultrasound

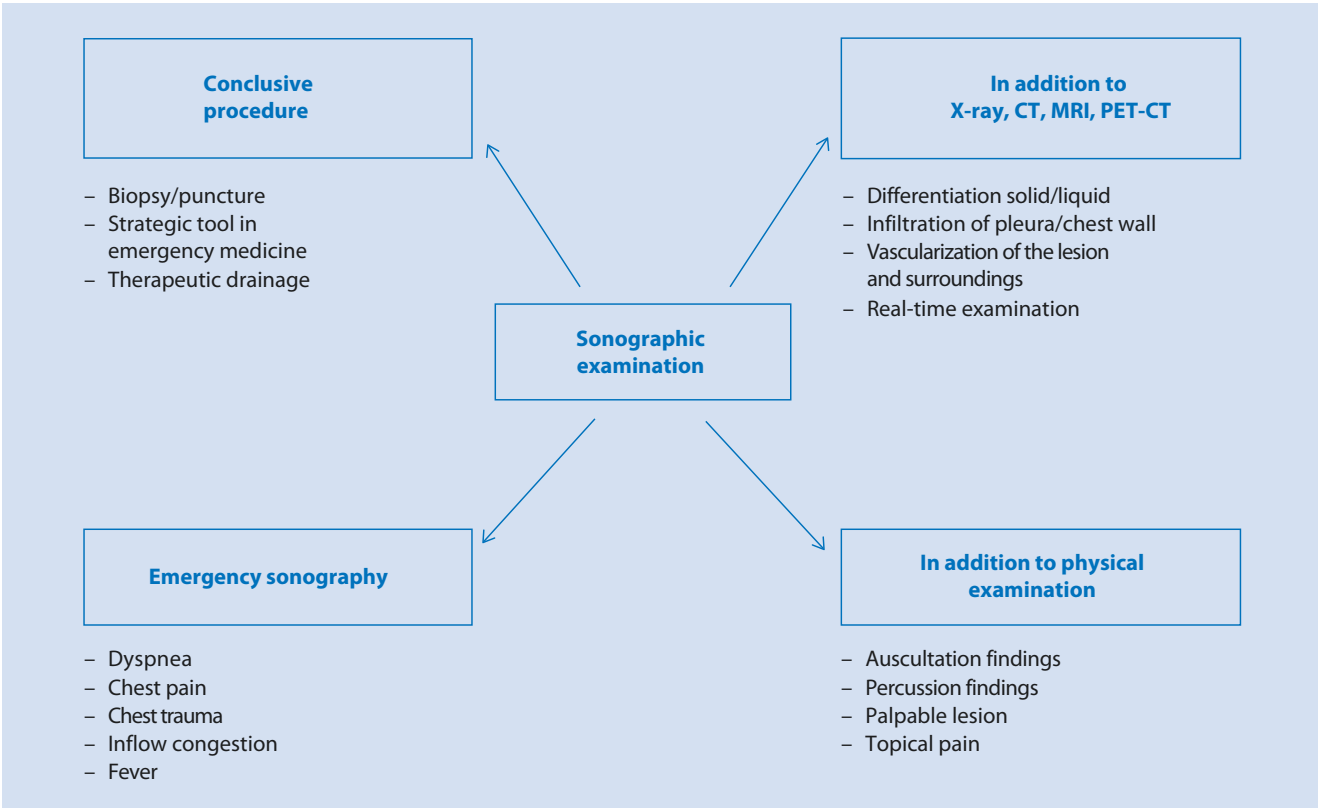

Fig. 1.1 Spectrum of applications of ultrasonography for pleural and pulmonary diseases

be used additionally, but it should be noted that these examination procedures are invasive in terms of effort and handling (Lam and Becker 1996; Aabakken et al. 1999; Herth et al. 2004; Annema et al. 2010; Haas et al. 2010; Walker et al. 2012; Silvestri et al. 2013; ▶ Sect. 6.2, ▶ Chap. 7).

Ultrasonography provides diagnostic information during the investigation of individual entities in the chest (Overview).

Diagnostic information during the investigation of individual entities in the chest

- Chest wall
  - Benign lesions:
    - Benign neoplasms (such as lipoma)
    - Hematoma
    - Abscess
    - Reactivated lymph nodes
    - Perichondritis, Tietze syndrome
    - Rib fracture
  - Malignant lesions:
    - Lymph node metastases (primary diagnosis and the course of disease under treatment)
    - Growing invasive carcinomas
    - Osteolyses
- Pleura
  - Solid structures:
    - Thickening of the pleura, callosity, calcification, asbestos-induced plaques
  - Space-occupying lesion:
    - *Benign*: fibrous tumor, lipoma
    - *Malignant*: clearly identifiable metastases, diffuse carcinosis, pleural mesothelioma
  - Fluid:
    - Effusion, hemothorax, pyothorax, chylothorax
  - Dynamic investigation:
    - Pneumothorax
    - Differentiating between an effusion and a callosity
    - Adherence of a space-occupying lesion
    - Invasion by a space-occupying lesion
    - Mobility of the diaphragm
- Lung
  - Interstitial syndrome
  - *Benign peripheral lesions*:
    - Inflammation, abscess, embolism, atelectasis
  - *Malignant peripheral lesions*:
    - Peripheral metastasis, peripheral carcinoma, tumor/atelectasis
  - Mediastinum, percutaneous:
    - Space-occupying lesions in the upper anterior mediastinum
    - Lymph nodes in the aortopulmonary window
    - Suspected thrombosis in the vena cava and its afferent vessels
    - Visualization of collateral circulation
    - Pericardial effusion

Additional pathologies of the heart that can be visualized by ultrasonography will not be addressed in this book; for further information the reader may consult appropriate echocardiography textbooks.

1.2 Required Technical Equipment

Devices used for ultrasound investigation of the abdomen and the thyroid may also be used for investigation of the chest. A high-resolution linear transducer of 5–10 MHz is suitable for imaging the **chest wall** and the **parietal pleura** (Mathis 2004). Additionally, the recently introduced probes of 7.5–18 MHz are very useful for evaluating **lymph nodes** (Prosch et al. 2014), the **pleura,** and the **surface of the lung.**

A convex or sector probe of 3–4 MHz ensures sufficient depth of penetration for investigation of the **lung** (Mathis 2004).

Vector, sector or narrow convex probes are recommended for the **mediastinum**. The smaller the footprint, the better the probe can be placed on the jugulum or the supraclavicular fossa. The frequency range should be 3.5–5 Mhz. It should be noted that the device settings commonly used for examining the heart are not suitable for the rest of the mediastinum. Contrast, image rates and the grayscale balance must be aligned to the visualization of mediastinal structures.

A special probe with an appropriate connecting channel to the ultrasound device is needed to perform a transesophageal ultrasound investigation.

Endobronchial ultrasonography is performed with special thin high-frequency probes (12–20 MHz) which are introduced through the working channel of the flexible bronchoscope.

1.3 Investigation Procedure

1.3.1 Chest Wall, Pleura, Diaphragm, Lung

The investigation should be performed, as far as possible, with the patient seated, during inspiration and expiration, and if necessary in combination with respiratory maneuvers such as coughing or "sniffing". Raising the arms and crossing them behind the head expands the intercostal spaces and facilitates the access. The transducer is moved from ventral to dorsal along the longitudinal lines in the chest (◘ Fig. 1.3):

- the parasternal line,
- the middle and lateral clavicular line,
- the anterior, middle and posterior axillary line,
- the lateral and medial scapular line, and
- the paravertebral line.

The respective anatomic location of the findings should be mentioned in the report.

Subsequent transverse transducer movement parallel to the ribs in the intercostal spaces (◘ Fig. 1.4) provides the additional information needed for accurate localization of the respective finding.

The investigation of lesions behind the scapula should be performed under maximum adduction of the arm with encirclement of the contralateral shoulder (◘ Fig. 1.5).

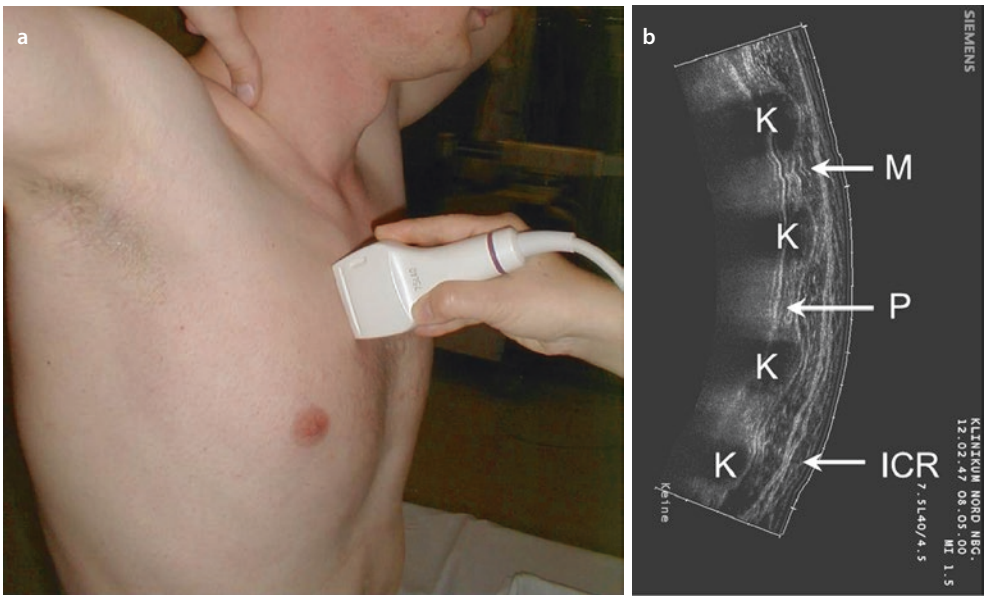

Fig. 1.3 Investigation of the seated patient. **a** Linear probe placed longitudinally on the right parasternal line. **b** Corresponding longitudinal panoramic ultrasound image (SieScape). *K* cartilaginous insertion of a rib, *ICR* intercostal space, *M* muscle, *P* pleural line

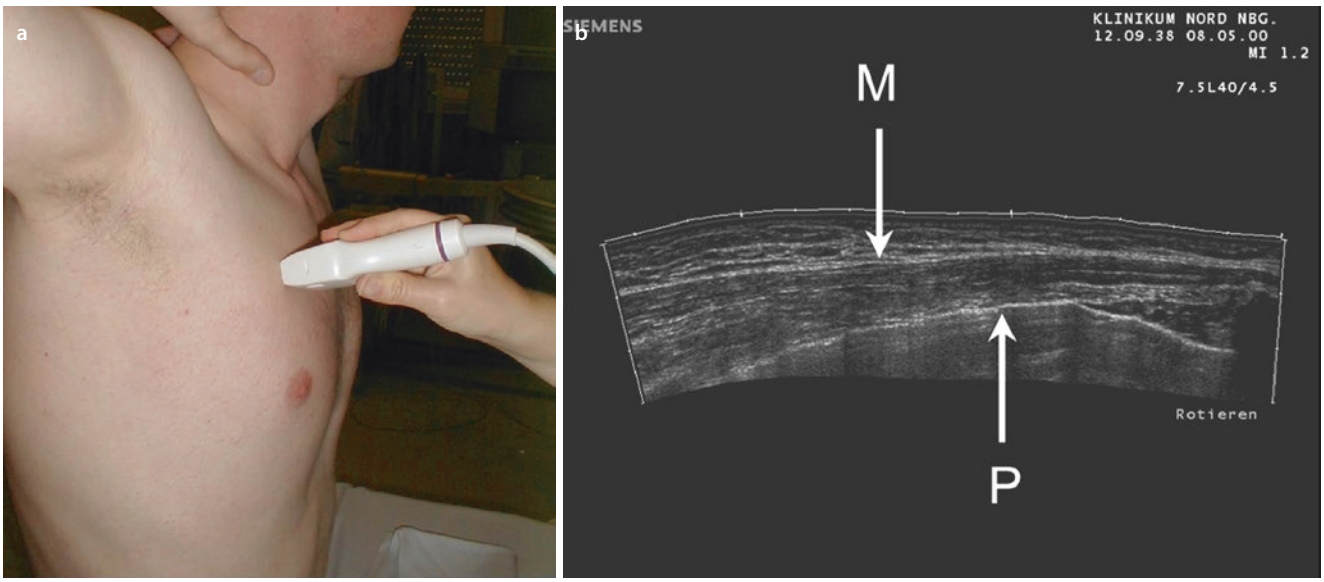

Fig. 1.4 Investigation of the seated patient. **a** Linear probe placed parallel to the ribs in the third intercostal space. **b** Corresponding transverse panoramic ultrasound image (SieScape). *M* muscle, *P* pleural line

The supraclavicular access enables the investigator to view the apex of the lung (Sect. 1.3.2).

From the suprasternal aspect one is able to inspect the upper anterior mediastinum (Sect. 5.1). From the abdominal aspect one can investigate the diaphragm from the subcostal approach through the transhepatic route on the right side (Fig. 1.6), and to a limited extent from the trans-splenic route on the left side.

Additionally, the longitudinal acoustic plane from the flank shows both costodiaphragmatic recesses (Fig. 1.7).

The supine patient is examined in the same manner. The abdominal access is better in this setting, but the intercostal view might be more difficult because the mobility of the pectoral girdle is limited.

1.3.2 Investigation of the Upper Thoracic Aperture

Special approaches are needed to investigate the upper thoracic aperture. The patient is required to lie flat for the investigation of cervical and supraclavicular lymph nodes, ideally with a hyperextended cervical spine (Prosch et al. 2014). The axillary region is investigated with the patient's arm in elevated position. High-resolution transducers of 5–18 MHz are used to view the structure of lymph nodes and the brachial plexus, including its branches. The thoracic aperture and the supraclavicular region should be investigated by ultrasound in cases of the following questions:

- Invasion of a Pancoast tumor
- Lymph node staging
- Trauma (parturition, accident)
- Puncture of the upper thoracic aperture
- Brachial plexus block (anesthesia)

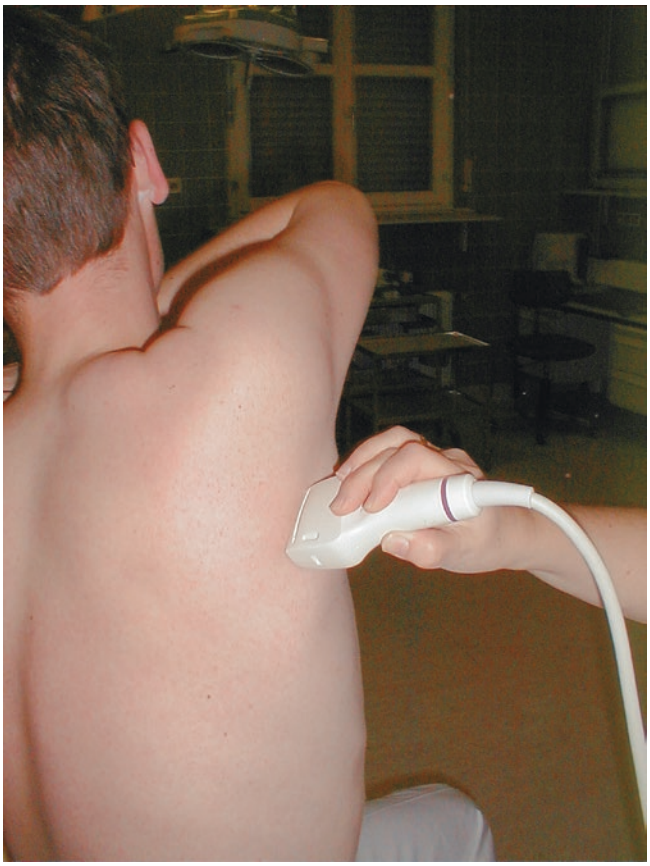

Fig. 1.5 Position of the patient for investigating retroscapular entities

The investigation is started at the base of the lateral cervical region (Fig. 1.8a, b).

The nerve branches pass through the gap between the anterior and middle scalene muscle, in lateral and downward direction. The branches reach the axilla by passing between the first rib and the clavicle. The course of the nerve branches along the axillary artery is registered by the infraclavicular approach (Fig. 1.9a–d).

The investigation is concluded by using the transaxillary approach (Fig. 1.10a–c).

With regard to transesophageal and transbronchial ultrasonography, please refer to the corresponding chapters.

1.4 Conclusion

Thanks to excellent resolution and the possibility of dynamic investigation, ultrasonography provides crucial information in patients with chest disease. Entities of the chest wall and changes in pleura can be visualized directly with ultrasound; pulmonary processes can be registered by ultrasound when they extend to the visceral pleura or when the ultrasonic wave is able to pass through a sound-conducting medium. The anterior portions of the mediastinum can be viewed percutaneously by the use of special sonic windows. To investigate the chest, one should use a combination of a linear transducer (5–7.5 MHz) for the near field and a convex or sector probe (3.5–5 MHz) for the deeper regions. High-resolution transducers of 5–18 MHz are needed to investigate the upper thoracic aperture and the supraclavicular region, in order to visualize the nerve branches of the brachial plexus and the structure of lymph nodes.

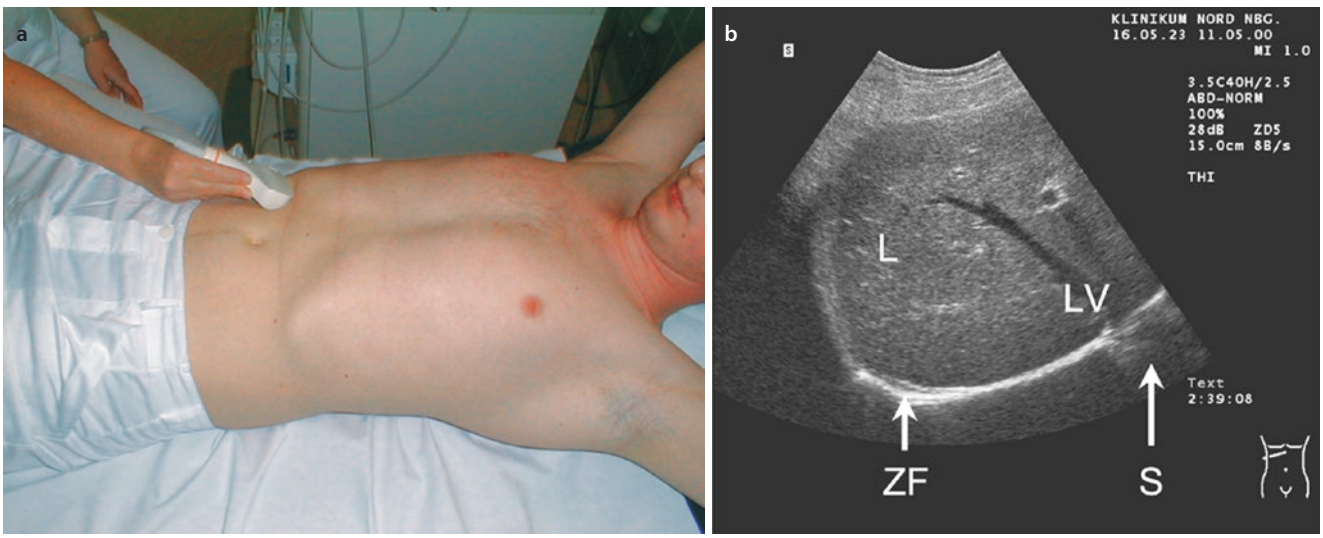

Fig. 1.6 Transhepatic investigation. **a** Convex probe placed subcostally from the right side, tilted slightly in cranial direction. **b** Corresponding ultrasound image. *L* liver, *LV* hepatic vein, *S* reflection of the liver above the diaphragm, *ZF* diaphragm

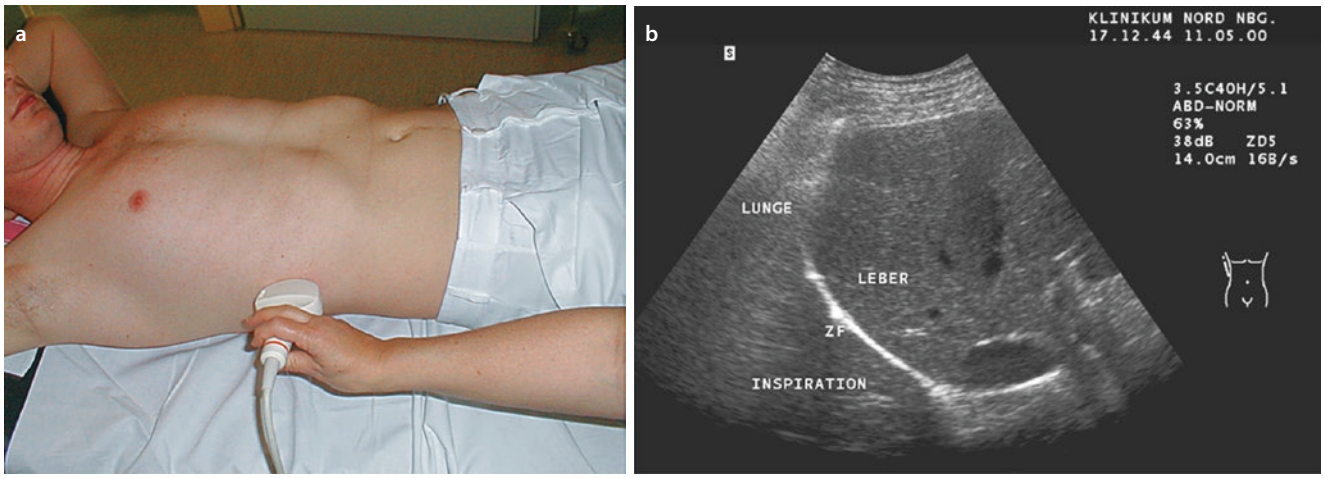

Fig. 1.7 Investigation from the lateral aspect. **a** Convex probe placed longitudinally in the mid-axillary line on the right side. **b** Corresponding ultrasound image (*ZF* diaphragm). A lung with normal mobility is shifted during inspiration into the costodiaphragmatic recess and obscures the upper margin of the liver

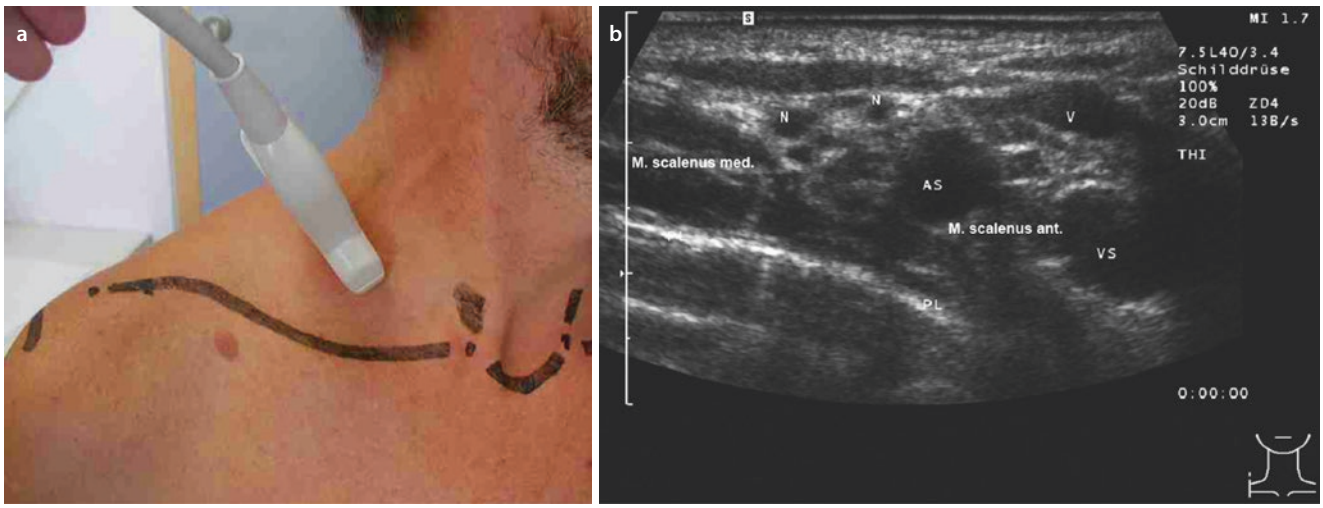

Fig. 1.8 Investigation of the upper thoracic aperture. **a** Semisagittal longitudinal section at the base of the lateral cervical region. **b** Corresponding ultrasound image. *AS* subclavian artery, *VS* subclavian vein, *PL* pleura, *N* branches of the brachial plexus, *V* innominate vein

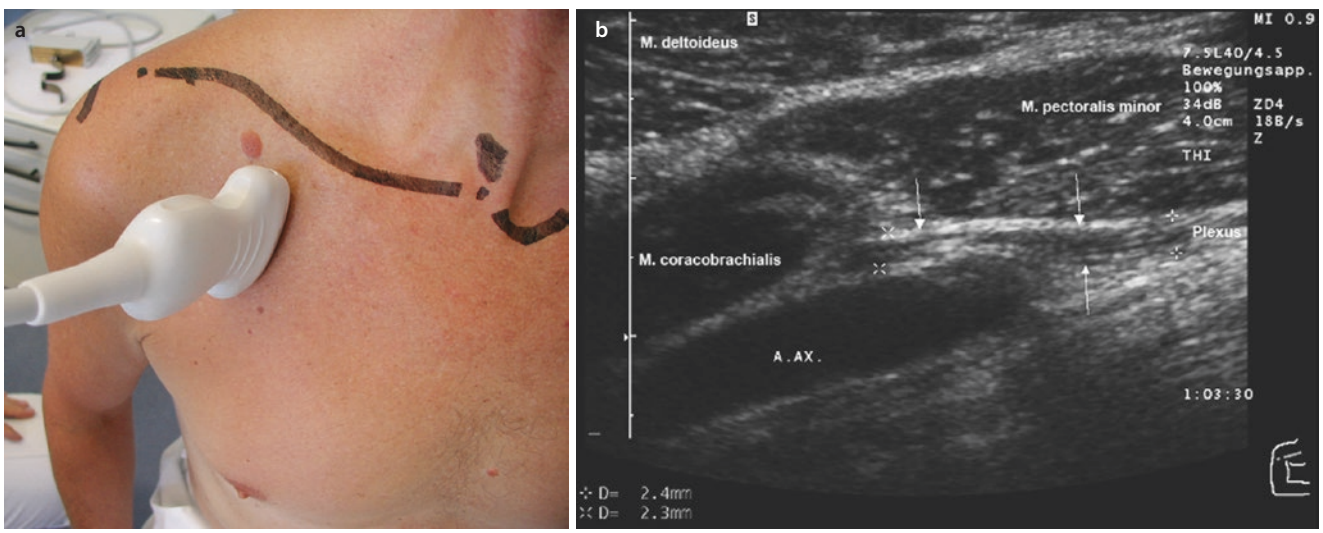

Fig. 1.9 **a** Oblique infraclavicular longitudinal section in the medioclavicular line. **b** Corresponding ultrasound image (*A.Ax* axillary artery). *Arrows* and *crosses mark* the course of the plexus nerve. **c** Infraclavicular cross-section parallel to the clavicle in the mid-clavicular line. **d** Corresponding ultrasound image. *Arrow* on the pleural line

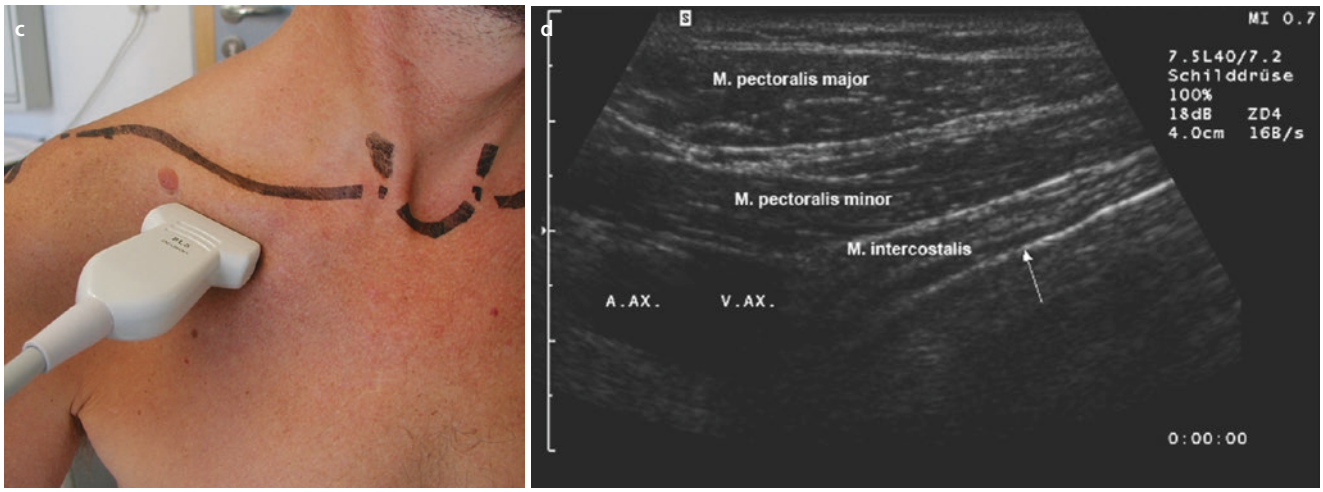

Fig. 1.9 (continued)

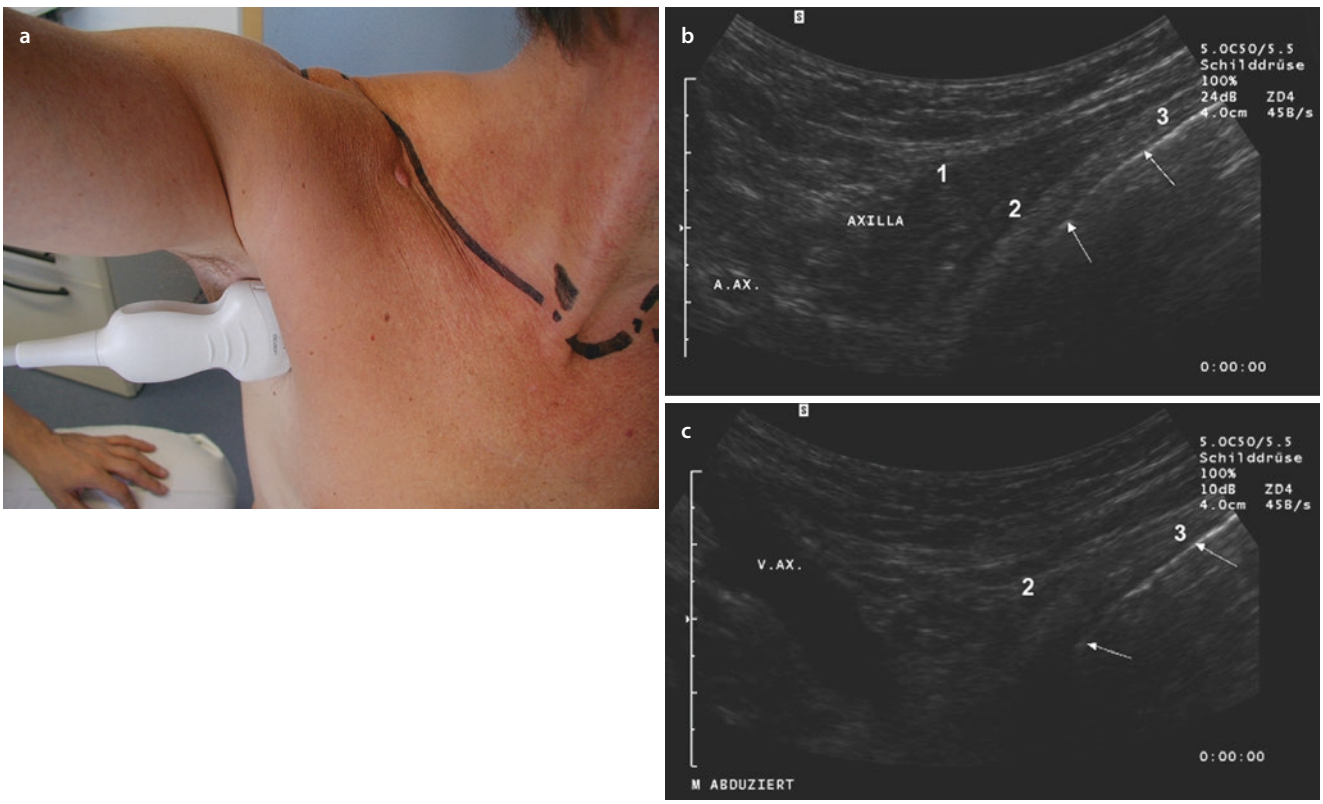

Fig. 1.10 **a** Transaxillary longitudinal section in the mid-axillary line. **b** Corresponding ultrasound image – dorsally tilted view. *1* anterior serratus muscle, *2* Intercostal muscle, *3* pleural line (*arrows*). **c** Corresponding ultrasound image – ventrally tilted view

1

References

Aabakken L, Silvestri GA, Hawes R et al (1999) Cost-efficacy of endoscopic ultrasonography with fine-needle aspiration vs. mediastinotomy in patients with lung cancer and suspected mediastinal adenopathy. Endoscopy 31:707–711

Annema JT, van Meerbeck JP, Rintoul RC et al (2010) Mediastinoscopy versus endosonography for mediastinal nodal staging of lung cancer: a randomized trial. JAMA 304:2245–2252

Arbelot C, Ferrari F, Bouhemad B, Rouby JJ (2008) Lung ultrasound in acute respiratory distress syndrome and acute lung injury. Curr Opin Crit Care 14:70–74

Bamber J, Cosgrove D, Dietrich CF (2013) EFSUMB guidelines and recommendations on the clinical use of ultrasound elastography. Part 1: basic principles and technology. Ultraschall Med 34:169–184

Beaulieu Y, Marik PE (2005) Bedside ultrasonography in the ICU. Part 1, Part 2. Chest 128:881–895, 1766–1781

Beckh S, Bölcskei PL, Lessnau KD (2002) Real-time chest ultrasonography: A comprehensive review for the pulmonologist. Chest 122:1759–1773

Blank W, Heinzmann A (2012) Thoraxsonographie im Notfall. Klinikarzt 41:28–32

Böer J, Braun B, Heinzmann A (2014) Notfallsonographie an Thorax und Abdomen. In: Ultraschalldiagnostik- Lehrbuch und Atlas. EcomedMEDIZIN Heidelberg 65.ErgLfg, Kap. III–5, 1–8

Copetti R, Cattarossi L (2008) Ultrasound diagnosis of pneumonia in children. Radiol Med 113:190–198

Copetti R, Soldati G, Copetti P (2008) Chest sonography: a useful tool to differentiate acute cardiogenic pulmonary edema from acute respiratory distress syndrome. Cardiovasc Ultrasound 6:16

Cosgrove D, Piscaglia F, Bamber J et al (2013) EFSUMB guidelines and recommendations on the clinical use of ultrasound elastography. Part 2: clinical applications. Ultraschall Med 34:238–253

Detterbeck FC, Zelman Lewis S, Diekemper R et al (2013) Executive Summary. Diagnosis and management of lung cancer, 3rd ed: American College of Chest Physicians evidence-based clinical practice guidelines. Chest 143:7S–37S

Diacon AH, Theron J, Bolliger CT (2005) Transthoracic ultrasound for the pulmonologist. Curr Opin Pulm Med 11:307–312

Goeckenjan G, Sitter H, Thomas M et al (2010) Prävention, Diagnostik, Therapie und Nachsorge des Lungenkarzinoms. Interdisziplinäre S3- Leitlinie der Deutschen Gesellschaft für Pneumologie und Beatmungsmedizin und der Deutschen Krebsgesellschaft. Pneumologie 64(S2):S23–S155

Goeckenjan G, Sitter H, Thomas M et al (2011) Prevention, diagnosis, therapy and follow-up of lung cancer: interdisciplinary guideline of the German Respiratory Society and the German Cancer Society. Pneumologie 65:39–59

Haas AR, Vachani A, Sterman DH (2010) Advanvces in diagnostic bronchoscopy. Am J Respir Crit Care Med 182:589–597

Havelock T, Teoh R, Laws D et al (2010) Pleural procedures and thoracic ultrasound: British Thoracic Society Pleural Disease Guideline 2010. Thorax 65:ii61–ii76

Herth FJ, Becker HD, Eberhardt R (2004) Endobronchialer Ultraschall beim Bronchialkarzinom. Radiologe 44:457–464

Hooper C, Gary Lee YC, Maskell N (2010) Investigation of a unilateral pleural effusion in adults: British Thoracic Society Pleural Disease Guideline 2010. Thorax 65:ii 4–ii 17

Lam S, Becker HD (1996) Future diagnostic procedures. Chest Surg Clin N Am 6:363–380

AWMF Leitlinie (2010) Diagnostik und Therapie der Venenthrombose und der Lungenembolie. S2-Leitlinie der Deutschen Gesellschaft für Angiologie. www.awmf.org/leitlinien

Mathis G (2004) Thoraxsonography – part I: chest wall and pleura. Praxis 93:615–621

Mathis G, Blank W, Reißig A et al (2005) Thoracic ultrasound for diagnosing pulmonary embolism. A prospective multicenter study of 352 patients. Chest 128:1531–1538

Moore CL, Copel JA (2011) Point-of-care ultrasonography. N Engl J Med 364:749–757

Niemann T, Egelhof T, Bongratz G (2009) Transthoracic sonography for the detection of pulmonary embolism – a meta- analysis. Ultraschall Med 30:150–156

Noble VE, Lamhaut L, Capp R et al (2009) Evaluation of a thoracic ultrasound training module for the detection of pneumothorax and pulmonary edema in the prehospital physician care providers. BMC Med Educ 9:3

Piscaglia F, NolsØe C, Dietrich CF et al (2012) The EFSUMB Guidelines and Recommendations on the Clinical Practice of Contrast Enhanced Ultrasound (CEUS): update 2011 on non-hepatic applications. Ultraschall Med 32:33–59

Prosch H, Meng S, Bernathova M (2014) Supradiaphragmale Lymphknoten. In: Ultraschalldiagnostik – Lehrbuch und Atlas. EcomedMEDIZIN Heidelberg 63.Erg.Lfg. Kap III–1.6.2, 1–36

Reissig A, Copetti R, Mathis G et al (2012) Lung ultrasound in the diagnosis and follow-up of community- acquired pneumonia: a prospective multicenter diagnostic accuracy study. Chest 142:965–972

Reuß J (2010) Sonografie der Pleura. Ultraschall Med 31:8–25

Silvestri GA, Gonzalez AV, Jantz MA et al (2013) Methods for staging non-small cell lung cancer. Diagnosis and management of lung cancer, 3rd ed: American College of Chest Physicians evidence-based clinical practice guidelines. Chest 143:e211S–e250S

Soldati G, Testa A, Silva F et al (2006) Chest ultrasonography in lung contusion. Chest 130:533–538

Squizzato A, Rancan E, Dentali F et al (2013) Diagnostic accuracy of lung ultrasound for pulmonary embolism: a systematic review and meta-analysis. J Thromb Haemost 11:1269–1278

Volpicelli G, Elbarbary M, Blaivas M et al (2012) International evidence-based recommendations for point-of-care lung ultrasound. Intensive Care Med 38:577–591

von Bartheld MB, Dekkers OM, Szlubowski A et al (2013) Endosonography vs conventional bronchoscopy for the diagnosis of sarcoidosis: the GRANULOMA randomized clinical trial. JAMA 309:2457–2464

Walker CM, Chung JH, Abbott GF (2012) Mediastinal lymph node staging: from noninvasive to surgical. AJR 199:W54–W64

Ultrasonography of the Chest Wall

Helmut Prosch

G. Mathis (ed.), *Chest Sonography*, DOI 10.1007/978-3-319-44072-9_2

2.1 Introduction

Due to its rather superficial location, the chest wall is almost ideally suited for ultrasound investigation. The primary indications for performing an ultrasonography of the chest wall include the clarification of swelling or suspicious findings in the chest wall on palpation, and targeted investigation of painful sites in the chest wall (Summary). Furthermore, ultrasonography of the chest wall plays an important role in performing biopsies and planning surgery for tumors of the chest wall or space-occupying lesions of the lung invading the chest wall . Last but not least, ultrasound plays an important role in the investigation of lymph nodes.

Indications for an Ultrasound Investigation of the Chest Wall

Swelling of the chest wall
Pain
Ambiguous findings on palpation
Ambiguous findings on X-rays
Chest trauma
Tumor staging
Intervention
Follow-up, monitoring progress

2.2 Accumulation of Fluid

2.2.1 Hematomas

Depending on their red blood cell content and degree of organization, hematomas may cause a variety of echo patterns. Usually they are anechoic or hypoechoic (Fig. 2.1). Occasionally one finds subtle veil-like internal echoes. Intermediate forms may be seen in rare cases, which include more dense echoes in the internal spaces. Organized hematomas may be very inhomogeneous in terms of their echo pattern.

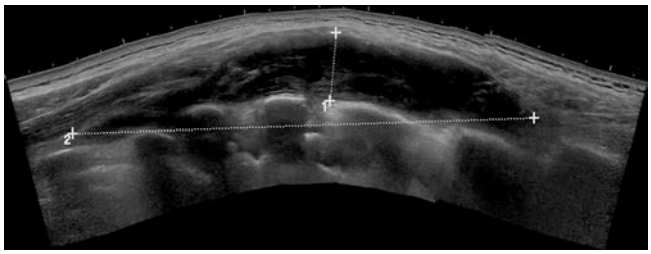

Fig. 2.1 Hematoma. Extensive hematoma of the dorsal portion of the chest wall after a fracture of the scapula and a serial rib fracture. Ultrasound investigation reveals an anechoic septated hematoma measuring 15 cm in length

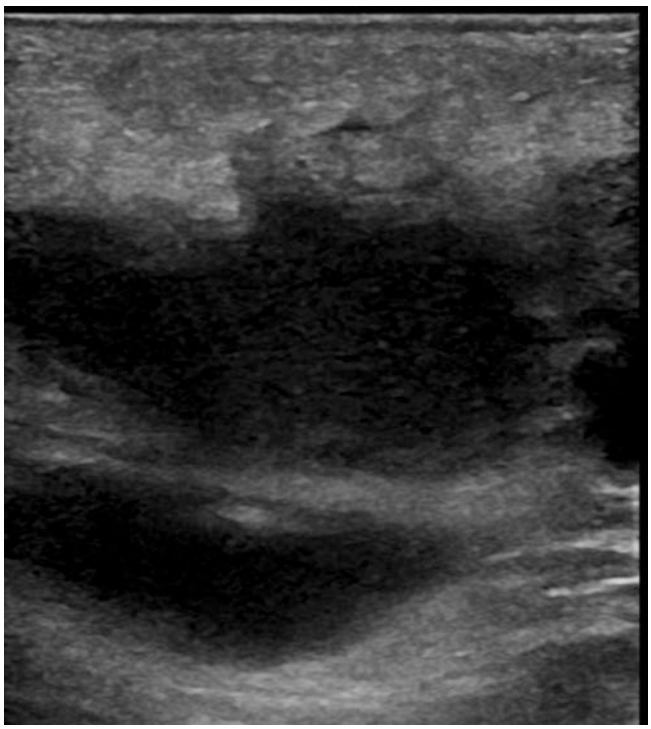

Fig. 2.2 A painful swelling in the right armpit raises suspicion of a sweat gland abscess. Ultrasonography reveals a largely anechoic space-occupying lesion measuring 3 × 1.5 cm in size. The moderately echogenic margin is indicative of an incipient capsule. The ultrasound-guided puncture reveals pus

2.2.2 Abscesses of the Chest Wall

Depending on their cell and protein content, a variety of internal structures may be found in an abscess cavity. Thus, the content of abscesses may be similar to that of hematomas. Quite often they cannot be delineated by ultrasound investigation alone, especially because there may be many intermediate stages such as infected hematomas. A major difference between abscesses and sterile hematomas is that abscesses tend to be accompanied by a capsule of differing shape, with floating internal structures (Fig. 2.2). In the majority of cases, clinical features such as reddening of the overlying skin clearly indicate the presence of an abscess.

2.2.3 Postoperative Seromas

Postoperative seromas are frequently observed after a muscle-sparing lateral thoracotomy. Postoperative seromas are largely anechoic, round or bizarre in shape, and do not have a capsule. Lymphatic cysts have a similar structure and are mainly round or -oval. Occasionally the occluded lymphatic vessel can be visualized.

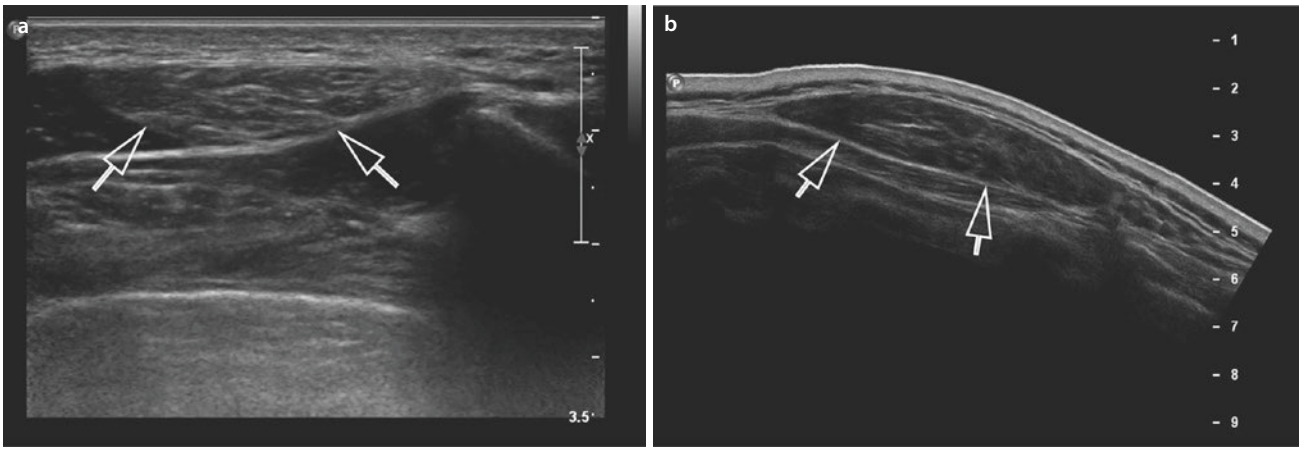

Fig. 2.3 Lipomas of the chest wall. **a** Lipoma with a hyperechoic texture, **b** Lipoma with a hypoechoic texture

2.3 Space-Occupying Lesions of the Chest Wall

Tumors of the chest wall are rather rare and usually benign. In most cases, the clinical symptoms alone permit conclusions about the benign or malignant nature of the lesion. Benign tumors are usually asymptomatic, grow slowly, and retain their tissue margins. In some tumors such as lipomas or fibromas, the combination of clinical symptoms and ultrasound features are so typical that a biopsy is not required. In contrast, malignant tumors grow rather rapidly, invasively, and are painful.

2.3.1 Lipoma and Fibroma

Lipomas are the most common tumors of the chest wall and are usually diagnosed by clinical investigation. The echogenicity of lipomas and fibromas depends on their cellular fat content, the quantity of connective tissue, and interstitial impedance differences. The texture may range from hypoechoic to relatively echodense (Fig. 2.3). Their demarcation from the environs may be blurred, and a capsule may develop.

2.3.2 Neurogenic Tumors

Neurogenic tumors such as schwannomas or neuromas are seen on ultrasound as oval hypoechoic lesions with sharp demarcations, and therefore do not differ significantly from space-occupying lesions of a different etiology. Evidence of the corresponding nerve is a diagnostic sign of a neurogenic tumor (Fig. 2.4).

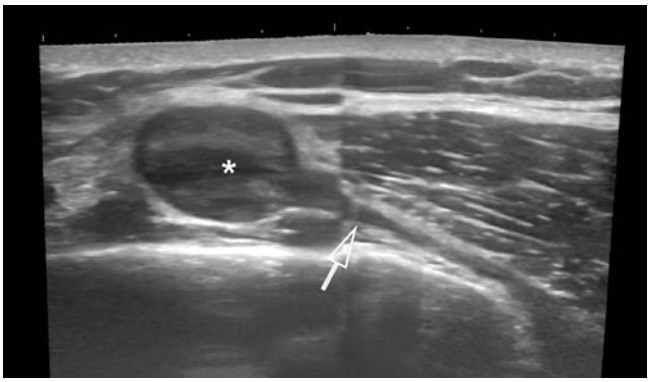

Fig. 2.4 Neurofibroma of the chest wall (*) in a patient with known neurofibromatosis. Evidence of the corresponding nerve is a diagnostic sign of a neurogenic tumor (*arrow*) (Courtesy of Gerd Brodner, Medical University of Vienna)

2.3.3 Sarcoma and Soft Tissue Metastases

A major criterion of a malignant space-occupying lesion is the presence of invasive growth (Fig. 2.5). In terms of echotexture it is frequently hypoechoic, with inhomogeneous hyperechoic portions. The use of color-Doppler ultrasonography may be helpful in assessing hypoechoic structures suspected of being malignant. The suspicion of a malignant lesion may be confirmed by the type of vascularization and the course of vessels.

Knowledge of the pattern of vascularization is also very helpful in performing ultrasound-guided punctures. In this convenient location, which is usually very close to the transducer, an ultrasound-guided puncture is very useful because it provides material for histological investigation and subsequent confirmation of the diagnosis.

The treatment of choice for a sarcoma is usually radical surgery. The resection margins and microscopic nodules can be determined better by performing a preoperative ultrasound investigation than by CT or MRT (Briccoli et al. 2007). However, a preoperative CT and MRI are necessary to determine the intraosseous spread of the tumors, their depth, and exclude pulmonary metastases.

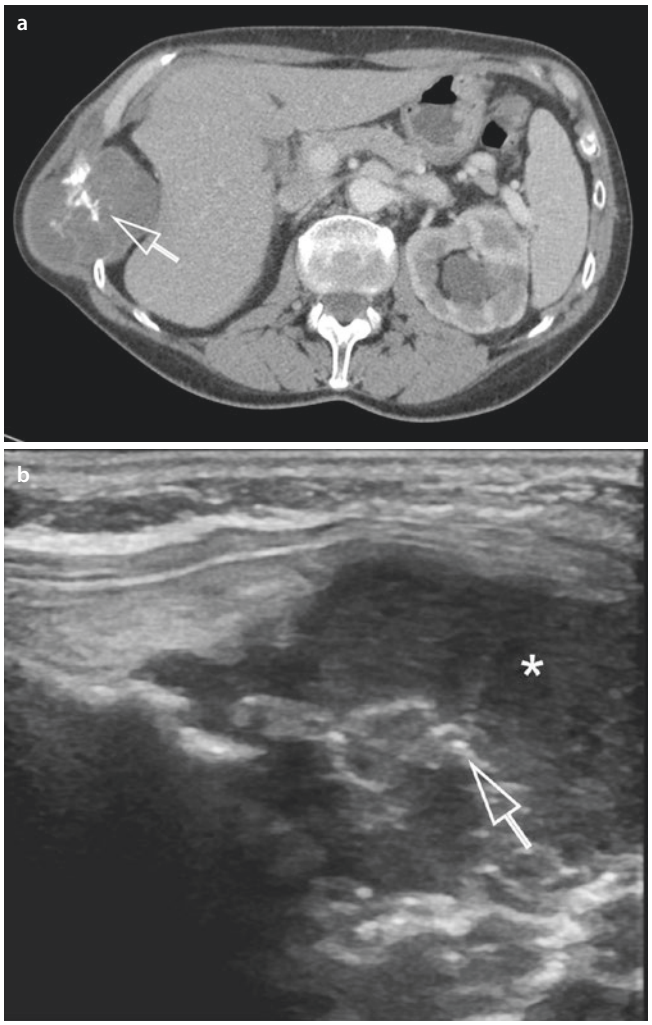

Fig. 2.5 Chondrosarcoma of the chest wall. **a** CT reveals an extensive space-occupying lesion with dense soft tissue and chondroid calcifications (*arrow*). **b** Ultrasonography shows an inhomogeneous hypoechoic space-occupying lesion (*) with coarse cloddy calcifications (*arrow*). An ultrasound-guided biopsy was able to confirm the suspected chondrosarcoma

2.4 Lymph Nodes

Subcutaneous palpable swellings are usually caused by enlarged lymph nodes. The ultrasound morphology of lymph nodes is indicative of their etiology and permits a tentative assessment of the malignant or benign nature of the lesions in accordance with the patient's clinical condition (Table 2.1). High-frequency probes provide a highly differentiated B-mode image. The pattern of vascularization on color Doppler provide information about the type of lymph nodes. The possibility of assessing the malignant or benign nature of a lesion has certainly been improved by the better resolution of the B-mode image as well as the use of various Doppler procedures for the assessment of vascularization patterns (Ying et al. 2004).

However, the benign or malignant nature of a lesion can only be established tentatively by its ultrasound morphology. Confirmation of the diagnosis requires a histological investigation of tissue obtained by performing a puncture. Alternatively, the course of the disease will confirm the diagnosis. In clinical practice, changes in ultrasound morphology are especially significant. Thus, ultrasound follow-up investigations are useful to confirm the diagnosis of inflammatory disease and document the success of treatment in cases of malignant lymph nodes.

2.4.1 Inflammatory Lymph Nodes

Inflammatory lymph nodes are rarely larger than 20 mm in size. They usually have smooth margins, are oval, triangular, or longitudinal (Fig. 2.6). A typical feature of lymphadenitis is the presence of lymph nodes arranged like a pearl necklace along lymph node stations. In accordance with the anatomical structure, one frequently finds a more or less echogenic internal zone which is referred to as the hilar fat sign and corresponds to the fatty and connective tissue in the center of the lymph nodes. This sign is especially seen in healing inflammatory processes. The zone, with sharp edges as opposed to the surroundings, is

Table 2.1 Ultrasound morphology of lymph nodes

	Inflammatory	Malignant lymphoma	Lymph node metastasis
Shape	Oval, longitudinal	Round, oval	Round
Edge	Smooth	Smooth	Irregular
Demarcation	Sharp	Sharp	Blurred
Growth	Pearl-necklace-like	Expansive, displacing	Invasive
Movability	Good	Good to moderate	Poor
Echogenicity	Hypoechoic margin, "hilar fat sign"	Hypoechoic, pseudocystic	Inhomogeneous, hypoechoic
Vascularization	Regular, central	Irregular	Corkscrew-like

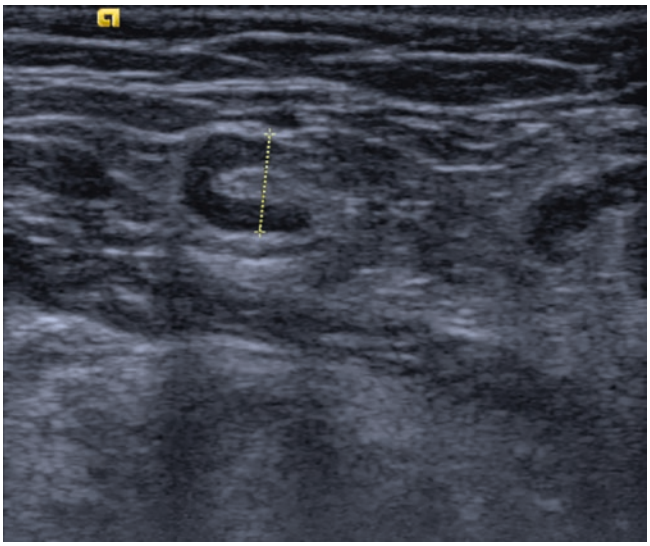

Fig. 2.6 Ultrasound image of a normal lymph node with a bean-shaped appearance, a hyperechoic hilum, and a hypoechoic cortex

hypoechoic. One commonly finds regular courses of vessels in this region on Doppler ultrasound. The lymph node hilum with the afferent and efferent vessels are also seen.

2.4.2 Tuberculosis

After the lung, lymph nodes are the second most common site of manifestation of tuberculosis (TB). Lymph node tuberculosis occurs in about 90 % of patients without accompanying pulmonary tuberculosis.

On the B-mode ultrasonography image, TB lymph nodes are seen in various forms. Some patients have rather sharply demarcated and sequentially arranged lymph nodes, whereas others have lymph nodes spreading into the environs diffusely or centrally fused hypoechoic lymph nodes with blurred margins, similar to metastases of solid tumors (Figs. 2.7 and 2.8). The pattern of vascularization of tuberculotic lymph nodes cannot be distinguished from that of lymph node metastases.

2.4.3 Malignant Lymphoma

On the B-mode ultrasound image, lymph nodes in the presence of lymphoma are usually round, hypoechoic, with sharp margins, without a hilum, and thus cannot be distinguished from lymph node metastases of solid tumors (Fig. 2.9). Markedly poor echogenicity of the lymph node could be interpreted as sign of lymphoma. On older ultrasound devices the lymph nodes look almost like cysts. On modern ultrasound devices, high-resolution transducers usually show a micronodular reticular internal echo (Fig. 2.10) (Ahuja et al. 2001). Lymph nodes arranged bilaterally around a vessel ("sandwich-like") may be interpreted as a sign of a

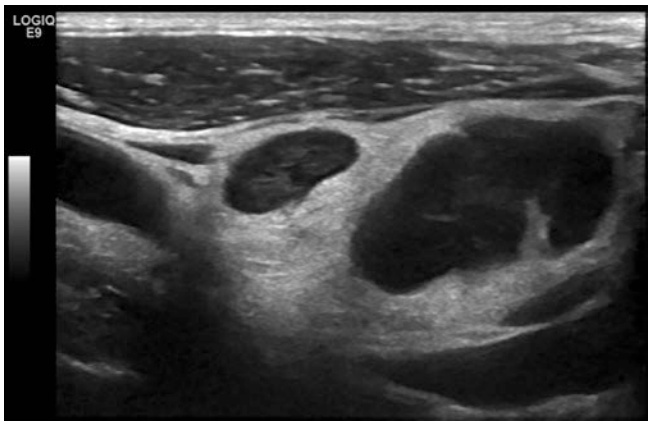

Fig. 2.7 Bean-shaped hypoechoic lymph nodes with sharp margins and a significant surrounding soft tissue edema

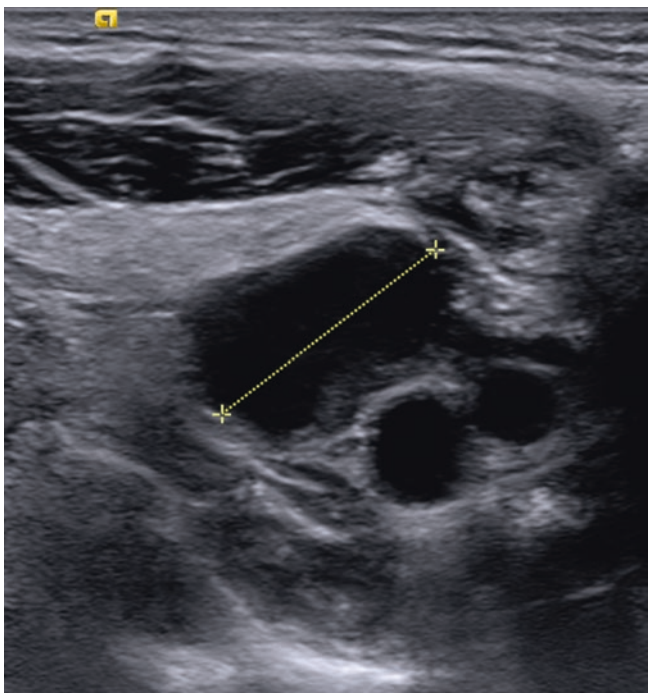

Fig. 2.8 Pseudocystic necrosis of a lymph node in the presence of lymph node tuberculosis

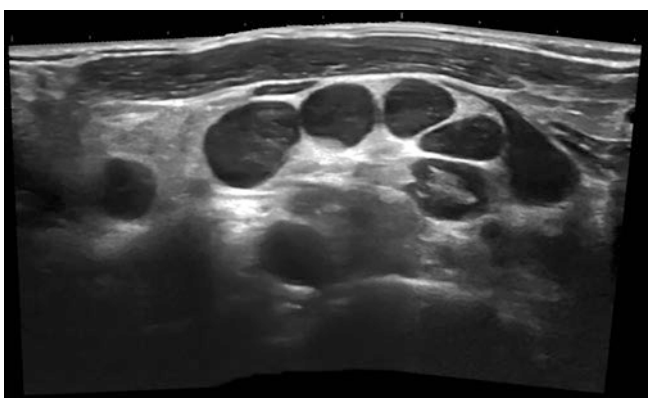

Fig. 2.9 Lymph nodes arranged sequentially in a cobblestone-like pattern, in a patient with a small-cell lymphocytic lymphoma. The lymph nodes are round, with sharp margins, hypoechoic, and without a hilum

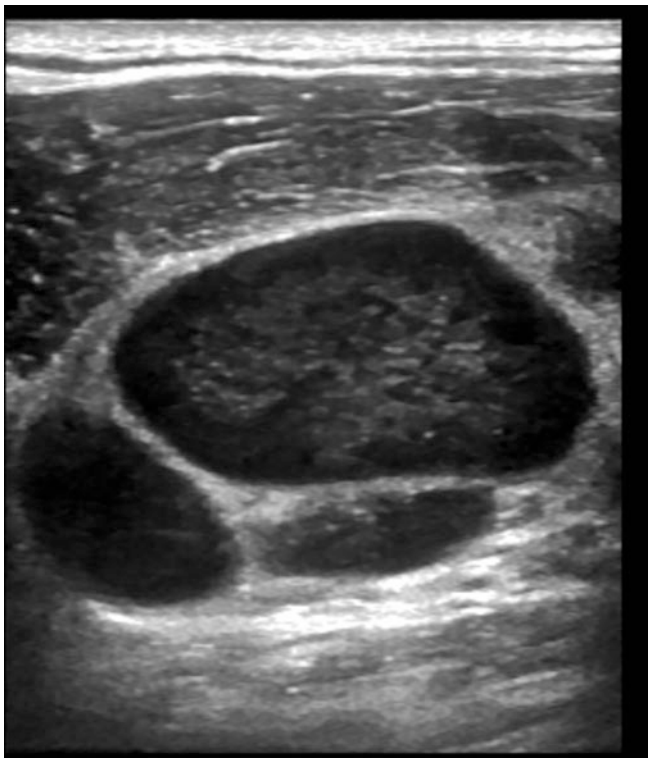

Fig. 2.10 Micronodular pattern of a lymph node in a patient with a small-cell lymphocytic lymphoma

malignant lymphoma. The vascularization of malignant lymphomas may be regularly enhanced or even irregular at the edges.

2.4.4 Lymph Node Metastases

On the B-mode ultrasonography image, round lymph nodes and the loss of the hyperechoic hilum are signs of lymph node metastases (Fig. 2.11). The demarcation is frequently blurred. Aggressive growth in terms of the invasion of muscles and vessels may be observed. Lymph node metastases are usually irregularly hypoechoic. Lymph node metastases of papillary thyroid carcinomas may be hyperechoic due to thyroglobulin deposits (Esen 2006). Size is an unreliable criterion of malignancy. In supraclavicular lymph nodes, a transverse diameter of 5 mm or more is considered pathological. Occasionally one also finds reactive lymph nodes in the vicinity of metastatic lymph nodes. The pattern of vascularization of lymph node metastases is very characteristic: vessels tend to be located at the edges, are distributed unevenly, follow a chaotic route, flow in various directions, and show changes in color (Tschammler et al. 2002).

Non-palpable lymph node metastases can be seen on ultrasound. Therefore, in the presence of breast cancer an ultrasound investigation of the axilla is recommended in preoperative staging and when monitoring the progress of disease (Ciatto et al. 2007; Krishnamurthy et al. 2002; Johnson et al. 2011).

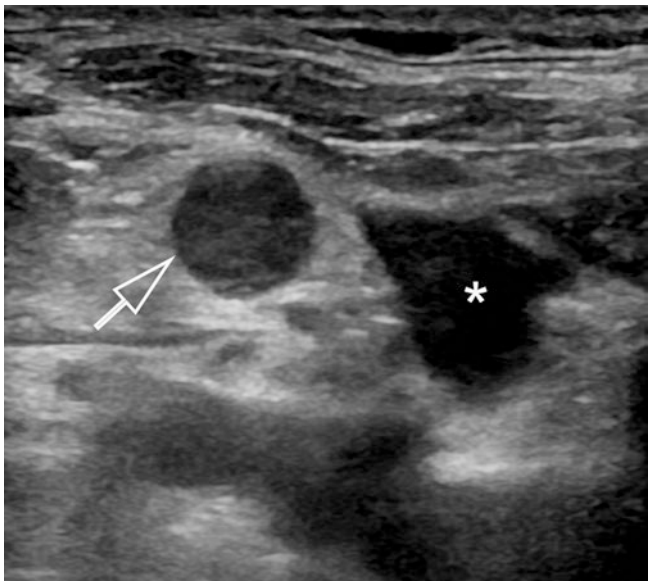

Fig. 2.11 Lymph node metastasis of a supraclavicular lymph node (*arrow*) immediately adjacent to the jugular vein (*). On ultrasound the lymph node has rounded contours and no fatty hilum

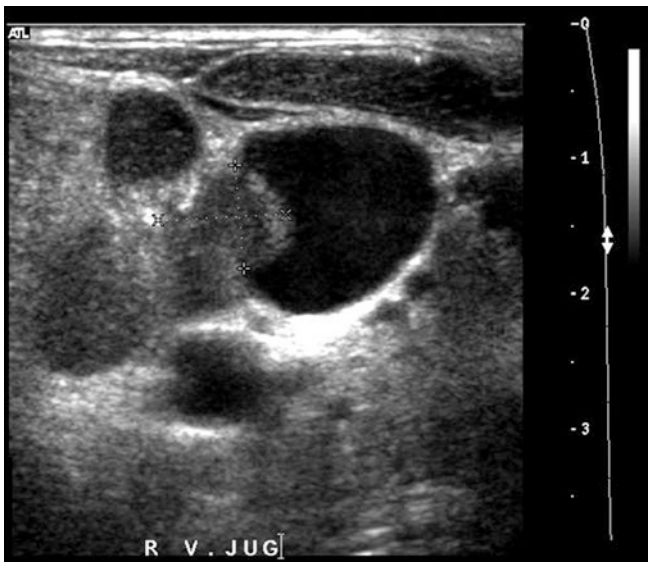

Fig. 2.12 Supraclavicular lymph node metastasis of a squamous cell carcinoma of the lung with disruption of the capsule and invasion into the adjacent jugular vein

An ultrasound investigation of the supraclavicular region is especially important in staging bronchial carcinoma because enlarged and usually non-palpable supraclavicular lymph nodes are found in as many as 51 % of patients with mediastinal N3 lymph nodes (Prosch et al. 2007; van Overhagen et al. 2004). An inoperable tumor stage (III B) can be demonstrated with minimal risk, at a low cost, by performing an ultrasound-guided biopsy of the lymph nodes (Figs. 2.12, 2.13, and 2.14).

The change in the size of lymph node metastases is a useful parameter of its progress. Despite the fact that the patient responds to chemotherapy or radiotherapy, reactive lymph nodes may persist.

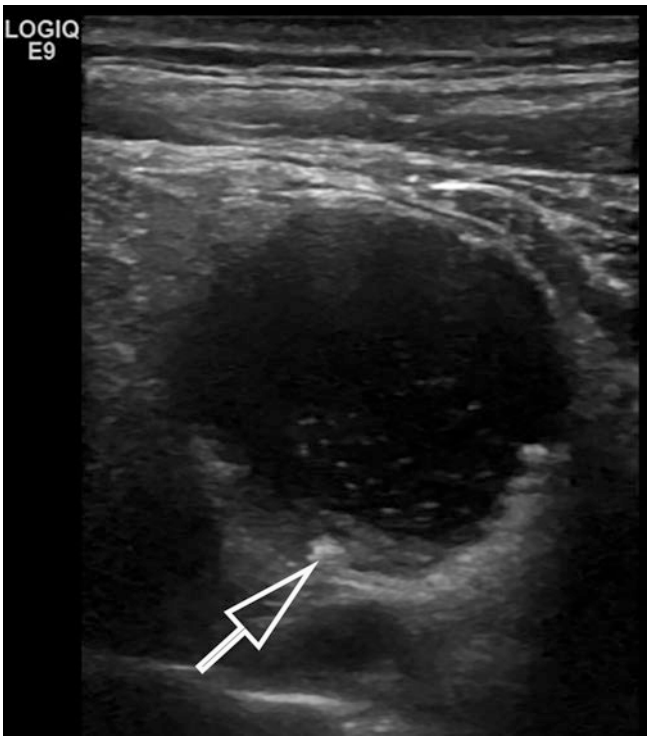

Fig. 2.13 Supraclavicular lymph node metastasis of an ovarian carcinoma. The lymph node is seen on ultrasound as a nearly anechoic (cystic) rounded lesion with sharp margins and calcified edges (*arrow*)

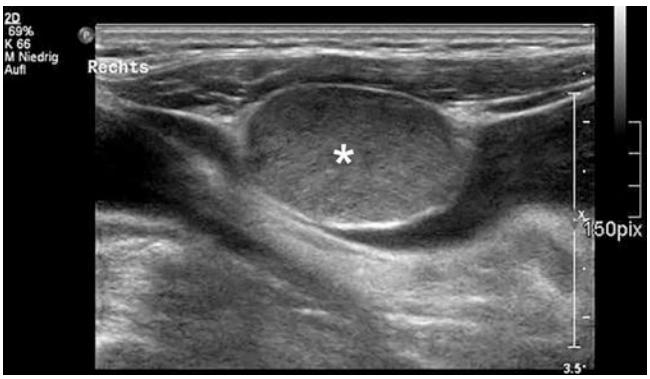

Fig. 2.14 Supraclavicular lymph node metastasis of an adenocarcinoma of the lung. On high-resolution ultrasound it is seen as a largely homogenous hyperechoic oval lymph node with sharp margins and without a hyperechoic hilum (*)

2.5 Bony Thorax

2.5.1 Fractures of the Ribs and the Sternum

Non-displaced rib fractures may be difficult to diagnose in clinical routine because rib fractures frequently escape detection even on targeted X-rays of the ribs. However, timely detection of a rib fracture is important for early initiation of appropriate pain treatment on the one hand, and for differential diagnosis on the other. A number of studies performed in the last few decades have shown that rib fractures

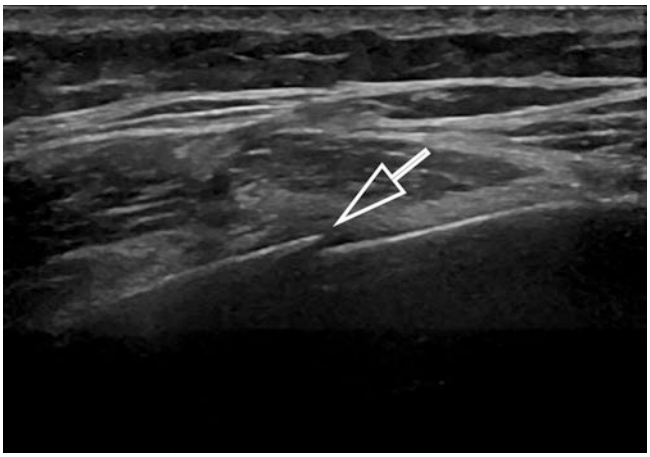

Fig. 2.15 Rib fracture with a cortical step (*arrow*) directly at the site of pain

are demonstrated with much greater sensitivity by a targeted ultrasound investigation than by an X-ray of the ribs (Bitschnau et al. 1997; Griffith et al. 1999; Turk et al. 2010). In 19 of 20 patients with no rib fractures on conventional X-rays, Turk et al. found rib fractures in the ultrasound investigation (Turk et al. 2010).

By performing a targeted investigation at the site of pain, a rib fracture can be detected quite rapidly even by an inexperienced investigator. In contrast, the diagnostic reliability of ultrasonography in demonstrating fractures of the sternum is poor.

Criteria of a fracture on ultrasound investigation include direct evidence of a fracture gap or a cortical step (Fig. 2.15). In cases of a very narrow fracture gap (more narrow than the lateral resolution capacity of ultrasound), the fracture may be demonstrated indirectly by the evidence of reverberation echoes or the so-called "chimney phenomenon". These reverberation artefacts arise at the boundaries of fracture fragments and extend vertically into the deeper aspect. In non-displaced fractures, the chimney phenomenon can be triggered by gentle pressure on the point of pain. Some patients have a circumscribed hematoma , which is an indirect sign of a fracture.

Demonstration or exclusion of concomitant injuries like a pneumothorax, a hemothorax , a lung contusion, or injuries to the organs of the upper abdomen are clinically more important than the detection of rib fractures. In clinically stable patients, the rib fracture itself *and* the concomitant injuries can be clarified by performing an ultrasound investigation (Wüstner et al. 2005).

The narrow gap between the osseous cartilaginous portion of the rib and the primary bony rib, a regular phenomenon in elderly patients, may lead to the false-positive diagnosis of a rib fracture (Fig. 2.16).

Anatomical conditions and normal variants should be considered when assessing the sternum as well, in order to rule out the risk of false-positive diagnoses. The normal discrete cortical interruption in the synchondrosis between the corpus and the manubrium should not be mistaken for a

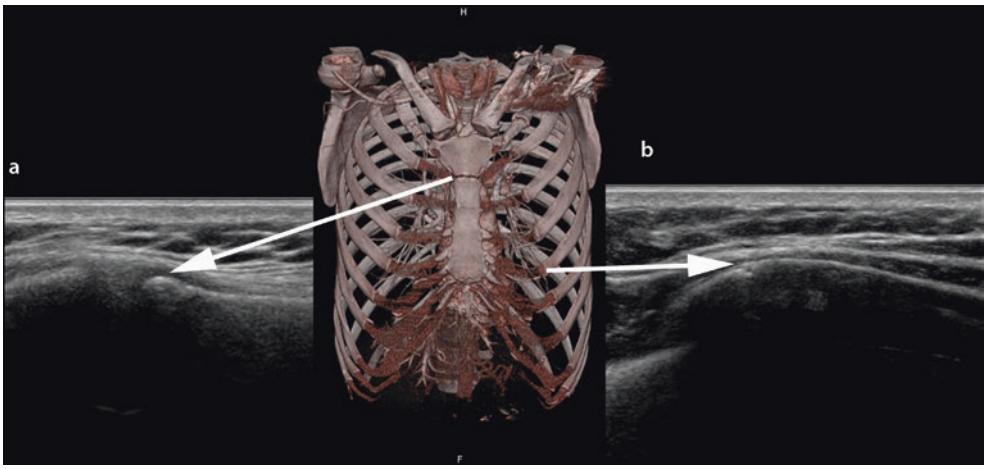

Fig. 2.16 Potential reasons for a false-positive diagnosis of a rib fracture on ultrasound investigation. **a** Cortical interruption in the region of the synchondrosis between the corpus and the manubrium. **b** Gap between the osseous cartilaginous portion of the rib and the primary osseous rib

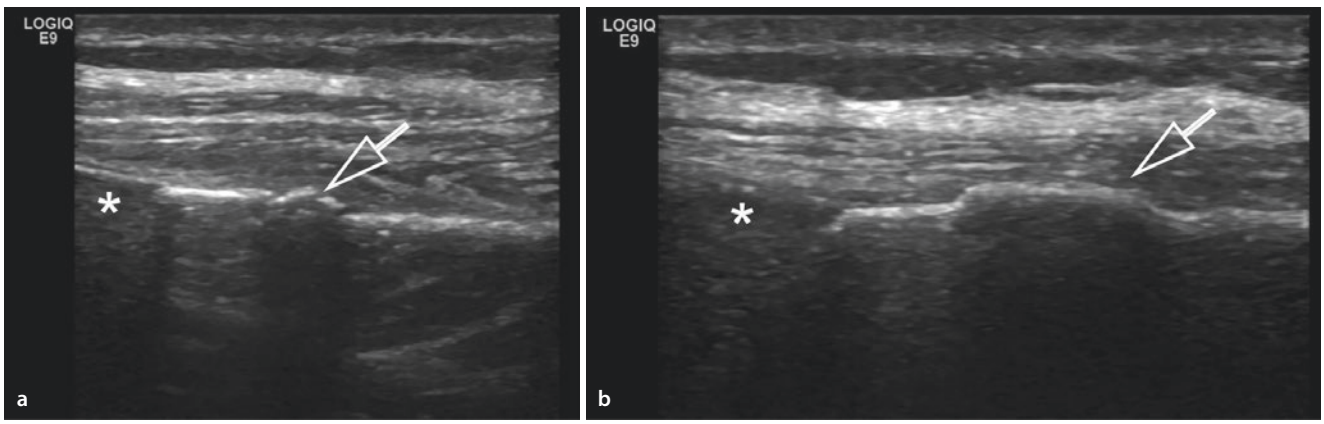

Fig. 2.17 Fracture. **a** A recent fracture (*arrow*) of a rib in the ventral portion of the costal arch, close to the cartilaginous part (*). **b** Complete healing and a minimal hump: a residual finding after 3 months (*arrow*)

fracture. Various forms of missing fusion or bone appositions that may occur in rare cases should also be taken into account (Chan 2009; Hyacinthe et al. 2012).

In clinical monitoring one first finds a local hematoma as a hypoechoic/anechoic edge in the region of the fracture gap. The subsequent formation of callus is marked by incipient organization and consolidation. The beginning calcification causes fine acoustic shadows or even complete ossification. Once this has been concluded, all that remains is a forward hump of the continuous and strong cortical reflex (Fig. 2.17). Disrupted healing can be easily established by the absence of continuous ossification. Consolidation starts from the third to fourth week after an injury; in normal cases complete restitution is achieved after a few months (Friedrich and Volkenstein 1994).

2.5.2 Osteolytic Metastases

An osteolysis is usually a tumor metastasis. A notable aspect of an osteolysis is an interrupted and destroyed cortical reflex with pathological echo transmission. Osteolytic metastases are usually well demarcated, round or oval space-occupying lesions, partly hypoechoic, and of gross echostructure. Color-coded duplex ultrasonography demonstrates corkscrew-like newly formed vessels. In tumor staging, ultrasound is a reliable procedure to differentiate rib fractures from bone metastases (Paik et al. 2005). In cases of doubt, an ultrasound-guided biopsy can be used at minimal risk for histological investigation and confirmation.

During ongoing treatment, osteolysis in the bony portion of the chest serves as a progress parameter in the presence of multiple myeloma, small-cell bronchial carcinoma, prostate or breast carcinoma. An increase or decrease in size on the one hand, and a change in internal structures in terms of ultrasound morphology on the other, can be compared and documented. Recalcification under treatment is seen earlier on ultrasonography than on X-rays.

Cave

The staging of bone metastases cannot be performed by ultrasonography. Ultrasound, however, is meaningful to examine the sites of positive scintigraphy findings, palpable swellings, and painful sites.

2.5.3 Invasion of the Chest Wall By Bronchial Carcinoma

Percutaneous ultrasonography is especially informative for the assessment of an invasion of the chest wall by a lung carcinoma. According to the TNM staging system, an invasion of the chest wall is defined as a T3 tumor and is found in 6 % of patients at the time of diagnosis (Mountain 1997; Facciolo et al. 2001). Invasion of the chest wall as such is no exclusion criterion for curative resection of the tumor, but is of crucial importance for the surgical procedure because parts of the chest wall also must be resected in these cases (Fig. 2.18).

Owing to its high spatial resolution, ultrasonography is markedly superior to CT for evaluating an invasion of the chest wall (sensitivity 89–100 % versus 42–68 %) (Bandi et al. 2007; Suzuki et al. 1993). Reliable signs of invasion include direct evidence of tumor spread into the chest wall or rib destruction (cf. Overview, Fig. 2.19) (Bandi et al. 2007). Widening of the pleura and/or limited respiratory motion of the tumor are interpreted as indirect signs because an inflammatory reaction of tissue surrounding a tumor may also cause both of these changes.

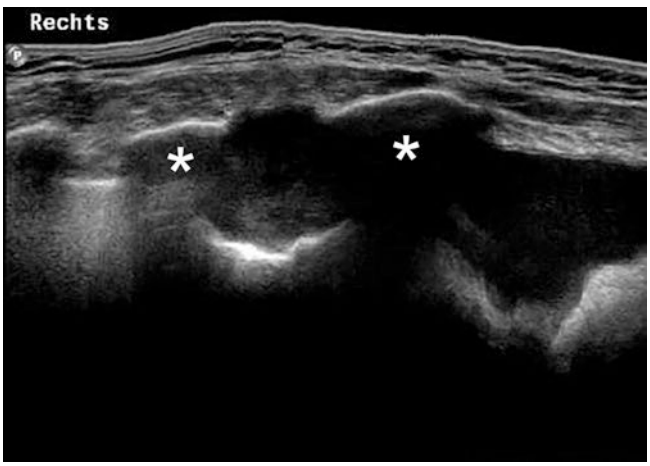

Fig. 2.18 Panoramic view of a lung carcinoma invading the chest wall (*arrow*) between two ribs (*)

Signs of Invasion of the Chest Wall

Reliable Signs
- Extra-organ invasion
- Rib destruction

Additional Signs
- Pleural thickening
- Limited respiratory motion

Preoperative clarification of an invasion of the chest wall is especially significant in tumors that invade the chest wall at the apex of the lung; these are referred to as Pancoast tumors. According to the TNM staging system, Pancoast tumors are T3 tumors as long as they do not invade the mediastinum, a vertebral body, the subclavian artery or vein, the C8 nerve root or higher (Detterbeck et al. 2013). The imaging procedure of choice for the investigation of a Pancoast tumor is an MRI scan. In patients who cannot be investigated by MRI due to contraindications, invasion of the nerve roots or the plexus can be determined by a targeted ultrasound investigation (Fig. 2.20).

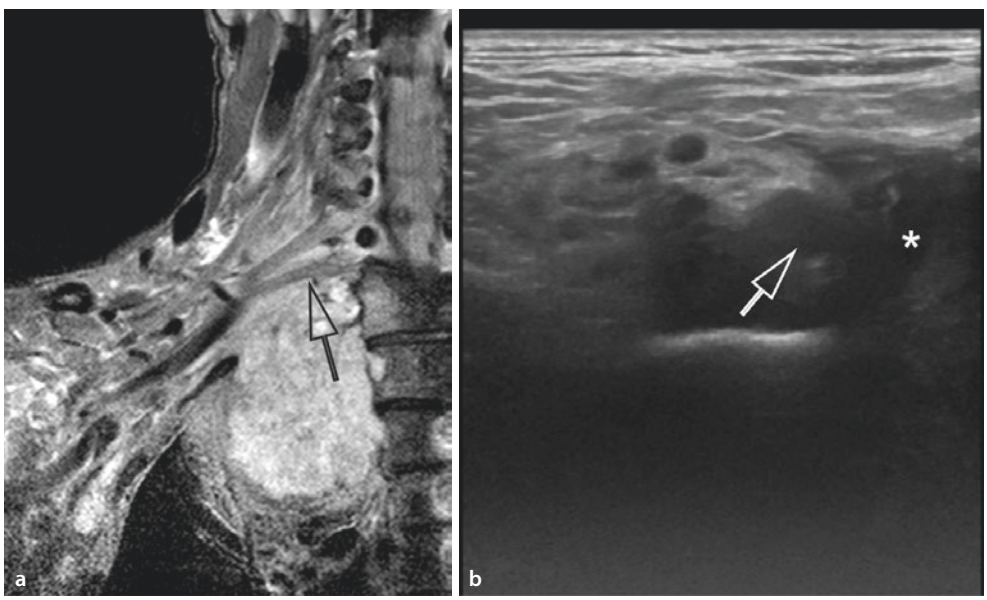

Fig. 2.19 Pancoast tumor on the right side. **a** MRI (coronal T2 STIR) shows an extensive tumor growing around the C8 nerve root and touching the C7 root. **b** High-resolution ultrasound. The C8 nerve root (*arrow*) in the efferent portion is entirely ensheathed by the tumor (*) and swollen

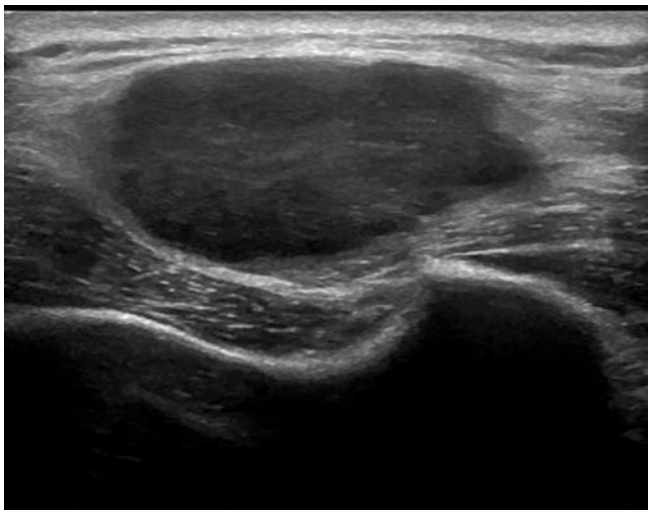

Fig. 2.20 Soft tissue metastasis of a squamous cell carcinoma. On ultrasound the metastasis is seen as a hypoechoic space-occupying lesion with partly sharp and partly blurred margins

2.6 Conclusion

Fractures of the ribs as well as the sternum are seen well on ultrasound. Fracture diagnosis based on ultrasound is not only much more sensitive than conventional X-rays, but also provides reliable and rapid views of soft tissue lesions, hematomas and pleural effusions.

The visualization of lymph nodes and a tentative assessment of the malignant or benign nature of a lesion are important indications to perform an ultrasound investigation of the chest wall. In case a puncture needs to be performed for the purpose of treatment, all ambiguous lesions of the chest wall can be easily accessed for an ultrasound-guided puncture and subsequent histological confirmation of the diagnosis. The risk associated with puncture are very low because of the convenient location of the lesions. When the malignant nature of a chest wall lesion has been proven, its progress under treatment can be monitored by ultrasonography.

References

Ahuja AT, Ying M, Yuen HY, Metreweli C (2001) "Pseudocystic" appearance of non-Hodgkin's lymphomatous nodes: an infrequent finding with high-resolution transducers. Clin Radiol 56(2):111–115. doi:10.1053/crad.2000.0642

Bandi V, Lunn W, Ernst A, Eberhardt R, Hoffmann H, Herth FJ (2008) Ultrasound vs. computed tomography in detecting chest wall invasion by tumor: a prospective study. Chest 133(4):881–886. doi: chest.07-1656 [pii] 10.1378/chest.07-1656

Bitschnau R, Gehmacher O, Kopf A, Scheier A, Mathis G (1997) Ultraschalldiagnostik von Rippen- und Sternumfrakturen. Ultraschall Med 18(4):158–161

Briccoli A, Galletti S, Salone M, Morganti A, Pelotti P, Rocca M (2007) Ultrasonography is superior to computed tomography and magnetic resonance imaging in determining superficial resection margins of malignant chest wall tumors. JUM J Ultrasound Med 26(2):157–162

Chan SS (2009) Emergency bedside ultrasound for the diagnosis of rib fractures. Am J Emerg Med 27(5):617–620. doi:10.1016/j.ajem.2008.04.013

Ciatto S, Brancato B, Risso G, Ambrogetti D, Bulgaresi P, Maddau C, Turco P, Houssami N (2007) Accuracy of fine needle aspiration cytology (FNAC) of axillary lymph nodes as a triage test in breast cancer staging. Breast Cancer Res Treat 103(1):85–91. doi:10.1007/s10549-006-9355-0

Detterbeck FC, Postmus PE, Tanoue LT (2013) The stage classification of lung cancer: diagnosis and management of lung cancer, 3. Aufl. American college of chest physicians evidence-based clinical practice guidelines. Chest J 143(5. Suppl):e191S–e210S. doi:10.1378/chest.12-2354

Esen G (2006) Ultrasound of superficial lymph nodes. Eur J Radiol 58(3):345–359. doi:10.1016/j.ejrad.2005.12.039

Facciolo F, Cardillo G, Lopergolo M, Pallone G, Sera F, Martelli M (2001) Chest wall invasion in non-small cell lung carcinoma: a rationale for en bloc resection. J Thorac Cardiovasc Surg 121(4):649–656. doi: S0022-5223(01)72517-2 [pii] 10.1067/mtc.2001.112826

Friedrich RE, Volkenstein RJ (1994) Diagnose und Repositionskontrolle von Jochbogenfrakturen. Ultraschall Med 15(4):213–216. doi:10.1055/s-2007-1003967

Griffith JF, Rainer TH, Ching ASC, Law KC, Cocks RA, Metreweli C (1999) Sonography compared with radiography in revealing acute rib fracture. AJR Am J Roentgenol 173(6):1603–1609

Hyacinthe AC, Broux C, Francony G, Genty C, Bouzat P, Jacquot C, Albaladejo P, Ferretti GR, Bosson JL, Payen JF (2012) Diagnostic accuracy of ultrasonography in the acute assessment of common thoracic lesions after trauma. Chest 141(5):1177–1183. doi:10.1378/chest.11-0208

Johnson S, Brown S, Porter G, Steel J, Paisley K, Watkins R, Holgate C (2011) Staging primary breast cancer. Are there tumour pathological features that correlate with a false-negative axillary ultrasound? Clin Radiol 66(6):497–499. doi:10.1016/j.crad.2010.11.015

Krishnamurthy S, Sneige N, Bedi DG, Edieken BS, Fornage BD, Kuerer HM, Singletary SE, Hunt KK (2002) Role of ultrasound-guided fine-needle aspiration of indeterminate and suspicious axillary lymph nodes in the initial staging of breast carcinoma. Cancer 95(5):982–988. doi:10.1002/cncr.10786

Mountain CF (1997) Revisions in the international system for staging lung cancer. Chest 111(6):1710–1717

Paik SH, Chung MJ, Park JS, Goo JM, Im JG (2005) High-resolution sonography of the rib: can fracture and metastasis be differentiated? AJR Am J Roentgenol 184(3):969–974. doi:10.2214/ajr.184.3.01840969

Prosch H, Strasser G, Sonka S, Oschatz E, Mashaal S, Mohn-Staudner A, Mostbeck GH (2007) Cervical ultrasound (US) and US-guided lymph node biopsy as a routine procedure for a staging of lung cancer. Ultraschall Med 28(6):598–603. doi:10.1055/s-2007-963215

Suzuki N, Saitoh T, Kitamura S (1993) Tumor invasion of the chest wall in lung cancer: diagnosis with US. Radiology 187(1):39–42

Tschammler A, Beer M, Hahn D (2002) Differential diagnosis of lymphadenopathy: power Doppler vs color Doppler sonography. Eur Radiol 12(7):1794–1799

Turk F, Kurt AB, Saglam S (2010) Evaluation by ultrasound of traumatic rib fractures missed by radiography. Emerg Radiol 17(6):473–477. doi:10.1007/s10140-010-0892-9

van Overhagen H, Brakel K, Heijenbrok MW, van Kasteren JH, van de Moosdijk CN, Roldaan AC, van Gils AP, Hansen BE (2004) Metastases in supraclavicular lymph nodes in lung cancer: assessment with palpation, US, and CT. Radiology 232(1):75–80

Wüstner A, Gehmacher O, Hammerle S, Schenkenbach C, Hafele H, Mathis G (2005) Ultraschalldiagnostik bei stumpfen Thoraxtrauma. Ultraschall Med 26(4):285–290. doi:10.1055/s-2005-858524

Ying M, Ahuja A, Brook F (2004) Accuracy of sonographic vascular features in differentiating different causes of cervical lymphadenopathy. Ultrasound Med Biol 30(4):441–447. doi:10.1016/j.ultrasmedbio.2003.12.009

Pleura

Joachim Reuß

G. Mathis (ed.), *Chest Sonography*, DOI 10.1007/978-3-319-44072-9_3

In the normal thorax the transthoracic sonographic view reaches to the pleura at the most. The healthy air containing lung is not depictable due to the total sound reflection at its surface. In the early years of ultrasound up to the nineteen eighties the presentation of pleural effusions was considered the only reasonable application for chest sonography apart from echokardiography.

The bony chest cage impedes the presentation of the pleura because of the shadows behind the ribs and the sternum. An appropriate examination technique allows an insight to the pleura through the intercostal spaces, when angulating the transducer also to the parietal pleura behind the ribs. By respiratory maneuvers the lungs move up and down. The visceral pleura slides through the intercostal field of view and thereby becomes sonographically visible. The diaphragmatic pleura is seen best in deep inspiration through the abdomen using liver and spleen as an acoustic window. The pleura of the apex of the lung is directly detectable through the supraclavicular fossa. The scapula as an osseous obstacle can be shifted or rotated by arm movements in medial or lateral direction. The mediastinal pleura and its continuation along the spine is largely invisible by transthoracic examination (▶ see Chap. 1).

3.1 Technical Visualization of the Pleura

The pleural surface of the lung can be approximately estimated by means of CT sectional images. Supposing the invisibility of the mediastinal pleura about 70 % of the pleural surface can be visualized by a transthoracical approach (Reuß 2010). Fortunately most of the pathologic changes of the pleura are in this region. Pathologic changes exclusively located at the mediastinal pleura are rare.

The normal pleura is approximately 0.2 mm thick. This is within the range of the axial resolution of 0.2 mm of a 10 MHz-transducer. Nevertheless the visualization of the pleura also succeeds with a transducer with lower frequency due to the differences in the impedance between the pleura and the neighbouring layers of fat and fluid (Fig. 3.1). The visceral pleura covers the aerated lung. At this interface arises a total reflection of the ultrasound, visible on the screen as a very bright line including the visceral pleura (Reuß 2010). Actually the visceral pleura is not really visible when the healthy lung is filled with air. In case of an usually hypoechogenic subpleural consolidation of the lung the visceral pleura is demarcated with the same echogenicity and thickness as the parietal pleura (Fig. 3.2).

3.2 Indications for Pleural Sonography

The clinical questions that indicate an ultrasound examination of the pleura are manifold (Reuß 2010) (Table 3.1). However wide overlap with indications for ultrasound of the chest wall, lung, diaphragm and abdomen is present. Only the symptom dyspnea may be triggered by sonographically

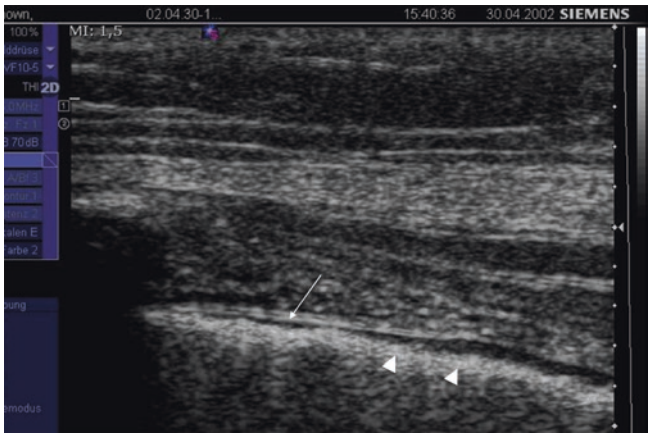

Fig. 3.1 Clearly identifiable double contour in the region of the parietal pleura (*arrow*) corresponding to the actual parietal pleura and the endothoracic fascia. Disproportionately thick visceral pleura (*arrow heads*), due to an artifact

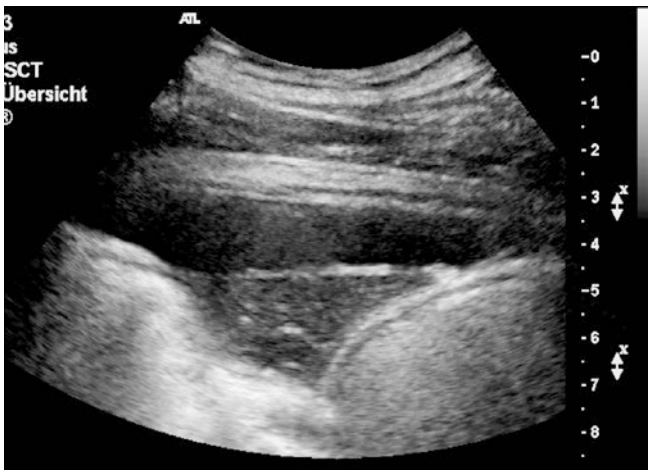

Fig. 3.2 Subpleural consolidation in a patient with lung embolism and pleural effusion. Thus the pleura is delineated separately from the total reflection at the air in the lung. Visceral and parietal pleura are displayed equally thick and equally echogenic

visible changes such as pleural effusion, pleurisy, pleural tumor, pleural fibrosis or pneumothorax, but also by interstitial syndrom in cardiac failure, ARDS, pneumonia, lung atelectasis due to a central lung tumor and lung embolism, a diaphragmatic paresis or diaphragmatic eventration due to ascites. The broad use of thoracic ultrasound is worthwile (Mathis 1997).

3.3 Normal Pleura

In transthoracic intercostal examinations the intercostal space is smoothly limited by the very thin, moderately echogenic parietal pleura. Provided good examination conditions there is occasionally a double line visible representing the parietal pleura and the endothoracic fascia (Reuß et al. 2002) (Fig. 3.1). Between parietal pleura and intercostal muscles

Table 3.1 Symptoms and situations indicating ultrasound of the pleura

Dyspnea +/– attenuation of percussion sounds	Pleural effusion	Size/volume Suspected cause Parapneumonic Heart failure Malignant Concomitant effusion in Pancreatitis Polyserositis Liver cirrhosis Renal failure Septicemia
Dyspnea + pain	Pneumothorax Pleurisy	
Respiratory dependant chest pain	Pleurisy	Concomitant pleurisy in Pneumonia Lung embolism Chest wall processes Rib fracture Abscess Metastasis Hematoma/seroma
Before intended thoracocentesis	Verification of effusion Free floating/loculated effusion	Diaphragmatic eventration Solid lesion/tumor Diagnostic/therapeutic thoracocentesis possible?
	Cathether pleurodesis Before after	Pleural space empty? Pleurodesis successful?
Radiologically proven pleural based lung consolidation	Solid/liquid Pleural mass	Mass starting from Chest wall Lung Diaphragm
Known underlying disease	Tumor Diagnosis/staging	Effusion Pleural metastasis
	Pneumonia	Parapneumonic effusion Size/volume Septated? Echogenic = > empyema?
	Cardiac failure	Decompensated with effusion?
	Renal failure/liver cirrhosis	Concomitant effusion
	Lupus erythematodes/other systemic diseases	Polyserositis
Trauma	Pleural effusion Hematothorax Pneumothorax	
Artificial ventilation	Conventionally-radiologically occult pneumothorax Conventionally-radiologically occult effusion	Sulcus anterior syndrome

is an individually very different hypoechoic layer, the extrapleural fat layer. The visceral pleura is separated from the parietal layer by the thin anechoic pleural space. Inwards the pleural space follows the normally hyperechogenic line of the visceral pleura sliding up and down with respiration. Pleural sliding is diagnostically important to prove normal conditions. Missing pleural sliding may have different causes (Table 3.2).

Normally both pleural sheets are completely smooth. Occasionally comet-tail-artifacts with a ring-down-effect are originating from the visceral pleura, mostly in elder persons due to small scars in the pleura or subpleural lung. Particularly

Table 3.2 Missing pleural sliding, differential diagnosis

Pneumothorax	Pleural space not visible Missing lung puls No B-lines Occasionally "lung point" (see below)
Emphysema	Minimal or missing pleural sliding, minimal respiratory excursions
Pleural fibrosis	Hypoechoic or mostly hyperechoic pleural thickening
Apex of lung	Also normally minimal sliding

common are comet-tail-artifacts starting from the diaphragmatic pleura, depicted in a transhepatic or translienal view. Similar artifacts also originating from the visceral pleura must be differentiated. These artifacts are laser-like traversing to the bottom of the screen without ring-down-effect and move breath dependent with the visceral pleura. These artifacts are called B-lines and represent interstitial subpleural changes in the lung, mostly in cardic lung edema, less often in lung fibrosis or in the border area of focal malignant or benign subpleural lung lesions (▶ see Chap. 4). Hence B-lines are not of real pleural origin.

3.4 Pleural Effusion

In erect position free floating effusion is located in the lowest parts of the costo-diaphragmatic pleural recessus. The effusion is surrounded by the chest wall, the diaphragm and the inferior parts of the lung (Figs. 3.3 and 3.4). most pleural effusions are echofree, especially in cardiac failure, severe hypalbuminemia, overhydration in renal insufficiency and in decompensated liver cirrhosis. Even in small effusions an airfree sonolucent cuspidate compression atelectasis waving breath-dependently is visible (▶ see Sect. 5.4). In the sitting position also minute effusions of 20 ml are detectable (Gryminski et al. 1976; Kocijancic et al. 2004) (Fig. 3.5). In conventional X-ray of the chest the minimal detectable volume is about 100 ml (Collins et al. 1972).

Color Doppler demonstrates the breath-dependent and pulse-dependent internal movement in the effusion and differentiates effusions from hypoechoic or anechoic solid lesions (Fig. 3.6). From the author's point of view this respiratory dependent color signal is not very reliable to distinguish echopoor thickenings of the pleura from minute strip like effusions. However, a color signal is triggered also by the lung movement.

Large pleural effusions can fill the whole hemithorax forming a serothorax. Then the lung is completely collapsed and can only be seen as a small airfree lobed structure in the hilus, possibly a residual bronchoaerogram of the large bronchi in the hilus. In a serothorax after pneumonectomy the collapsed lung is lacking.

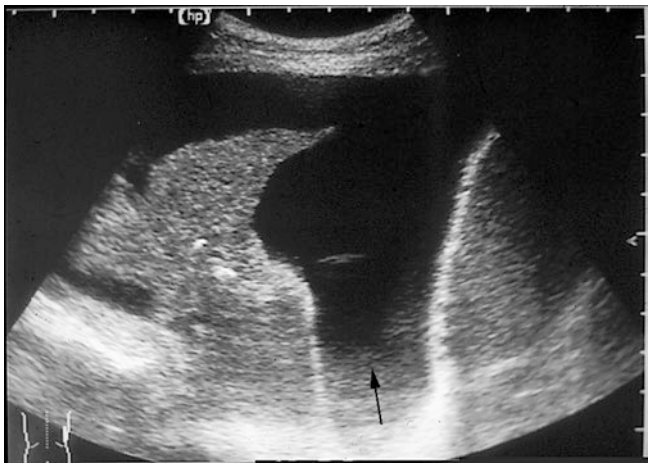

Fig. 3.3 Large nearly echofree pleural effusion. The echoes in the deep parts of the effusion are artifacts (*arrow*). Lung compressed with minimal residual air in central bronchi

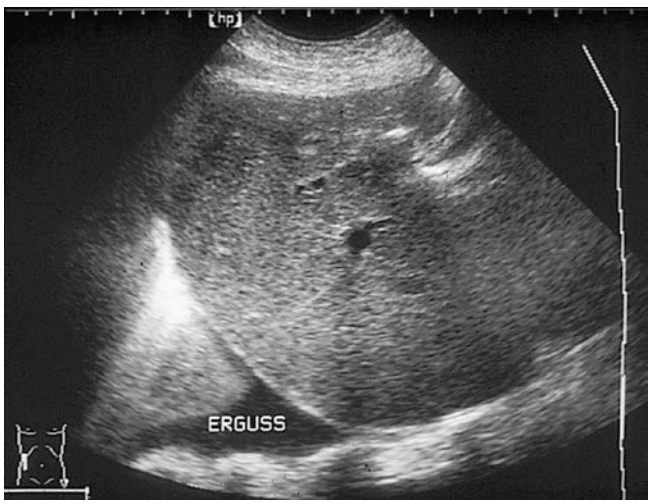

Fig. 3.4 Small posterior pleural effusion between spine and diaphragm in a transhepatic examination

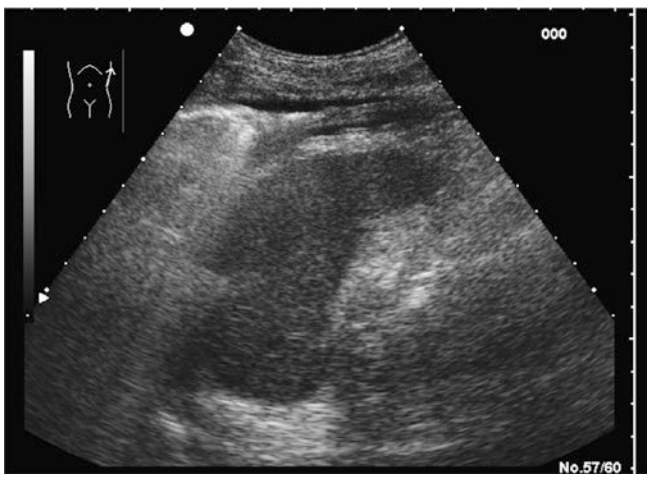

Fig. 3.5 Very small strip-like postoperative pleural effusion in the angle between ribs and diaphragm. The deformation during respiration in the dynamic examination excludes a circumscribed pleural thickening

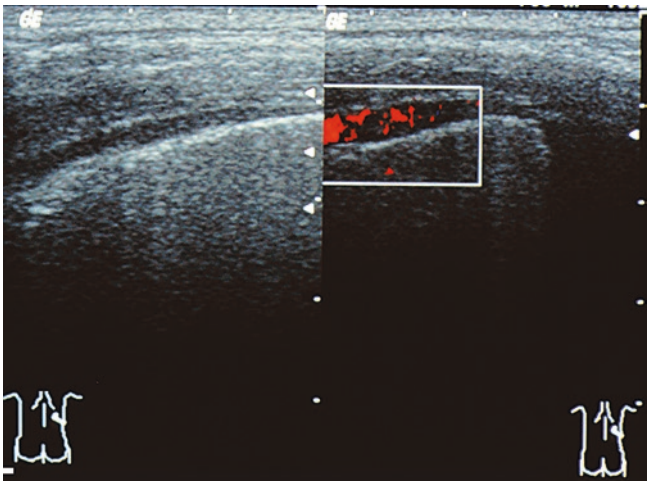

Fig. 3.6 Small pleural effusion. The flow signals in the effusion are produced by the pulse and breath synchronous inner shift and characterize the anechoic region as fluid

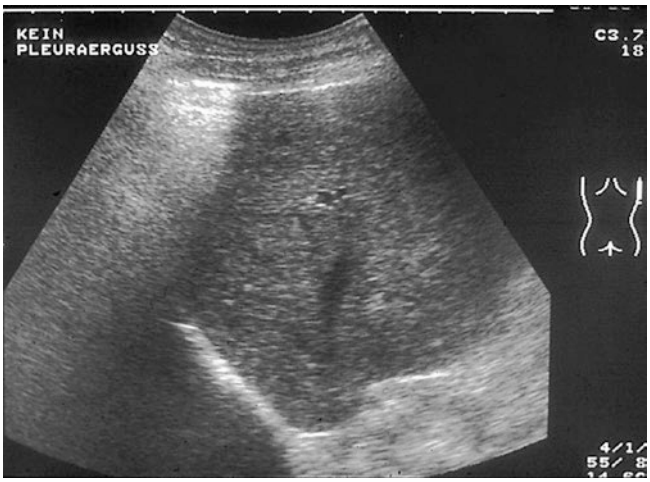

Fig. 3.7 No presentation of fluid between lung and liver, thus ruling out free floating pleural effusion. To rule out a captured effusion, the whole pleura must be examined

In the supine patient the pleural effusion is extending along the lateral chest wall. In a conventional chest-X-ray such an effusion is noticed only as a slight uniform unilateral opacification. Owing to a missing difference in lung transparency bilateral effusions are not detectable even under study conditions. The ultrasound examination of the supine patient must be performed from the posterior axillary line possibly after slight rotation of the patient.

In the erect patient a free floating effusion can be ruled out by examining the whole inferior pleura. Only aerated lung with its typical reflection is visible. For this purpose a supine patient has to be rotated completely on the left or right side (Fig. 3.7).

Volume assessment

Measuring of the volume of a pleural effusion by means of ultrasound is not possible. Several proposals have been made to estimate the volume reaching correlation coefficients up to 0.75. The difference to the actual volume may be substantially. But for clinical purposes the estimation is mostly sufficient. Volume estimation may be important in the follow up of effusions under conservative treatment or to forecast a positive effect of a thoracocentesis in dyspnoeic patients. Thoracocentesis of an effusion volume less than 500 ml is successful only in exceptional cases concerning the respiratory function. For less experienced examinators it may be helpful to estimate the volume by a formula. In the erect patient suffering from cardiac failure the success of a diuretic therapy may be well documented by measuring the perpendicular extension of the subpulmonary. The main part of the effusion volume is situated subpulmonary whereas the part of the effusion ascending along the chest wall contributes less to the total volume (Fig. 3.8). The estimation of the effusion volume in supine patients is more difficult and less exact (Table 3.3).

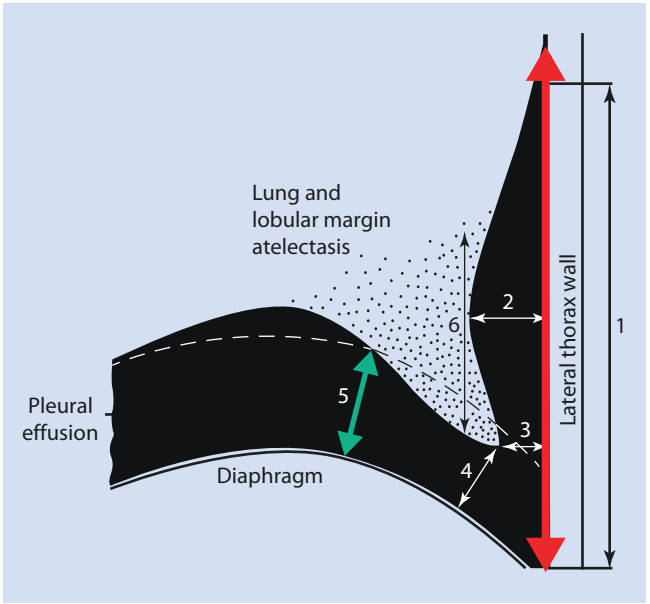

Fig. 3.8 Schematic presentation of volume estimation of pleural effusions. Valuable parameters are maximal extension of the effusion (*1*), inferior distance between lung and diaphragm (*4*), and the subpulmonary extension of the effusion (*5*). The thickness of the layer between lung and chest wall (*2*), the distance beween an inferior atelectasis and the chest wall (*3*) and the extension of the atelectasis (*6*) are not suitable for the volume estimation (According to Goecke and Schwerk 1990)

Etiology of pleural effusion

Depending on the etiology of the effusion, the content may present differently. Transudates in cardiac failure, hypoproteinemia or liver cirrhosis are usually echofree. Due to considerable differences in the impedances in the effusion and in the aerated lung or the chest wall arise scatter artifacts in the effusion. These artifacts shift typically with the transducer movements (Fig. 3.3).

Table 3.3 Estimation of the effusion volume in supine patients

Author	Result	Comment
Roch et al. 2005	PLDbasal >5 cm corresponding >500 ml effusion volume PLDbasal = distance between basal lung and posterior chest wall end expiratorically	Sens. 83 %, spec. 90 % Low interobserver variance
Balik et al. 2006	V(ml) = 20 × Sep(mm) V = effusion volume Sep = separation distance between basal lung and chestwall in posterior axillary line	Correlation coefficient $r = 0.72$
Eibenberger et al. 1994	Effusion thickness dorsobasal 20 mm corresponding 380 ± 130 ml 40 mm corresponding 1000 ± 330 ml Measurement expiratorically	Correlation coefficient $r = 0.80$
Vignon et al. 2005	Effusion thickness dorsobasal >45 mm right/> 50 mm left corresponding >800 ml effusion volume	Sens. 94 % right, 100 % left Spec. 76 % right, 67 % left

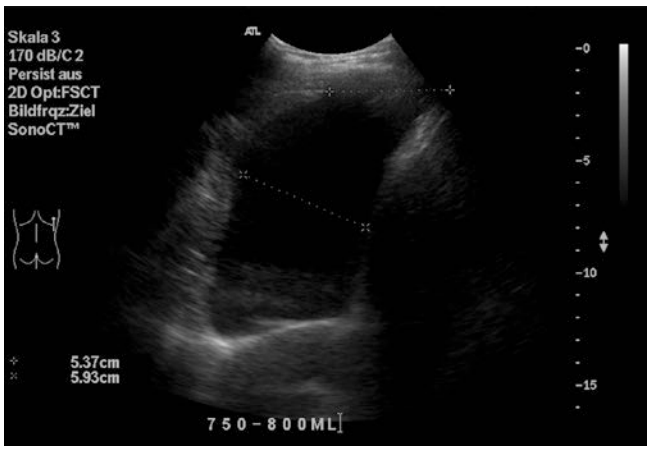

Fig. 3.9 Exclusively subpulmonary pleural effusion in severe right heart failure, latero-posterior longitudinal section. The infrapulmonary and lateral diameters of the effusion add up to an estimated volume 720 ml, according to the formula of Goecke and Schwerk. In exclusively subpulmonary effusions this formula underestimates the actual volume. Actually aspirated volume 850 ml

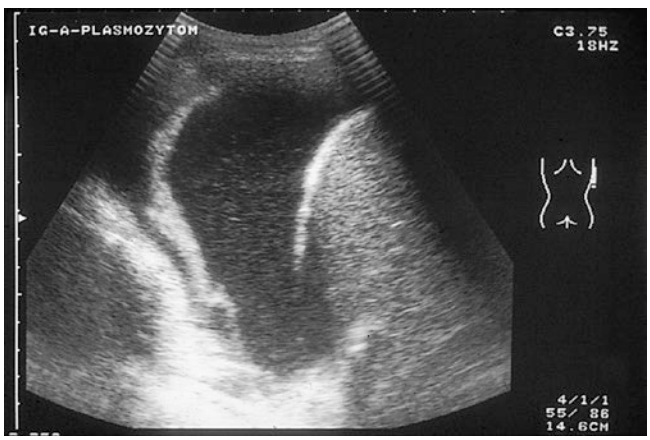

Fig. 3.10 Echogenic protein containing pleural effusion in a patient suffering from a IgA-myeloma. In contrast to artificial echoes these echoes move swinging or rotating synchronous with breath or pulse. Inflammatory, hemorrhagic or chylous effusions present in a similar manner. Transudates are usually echofree

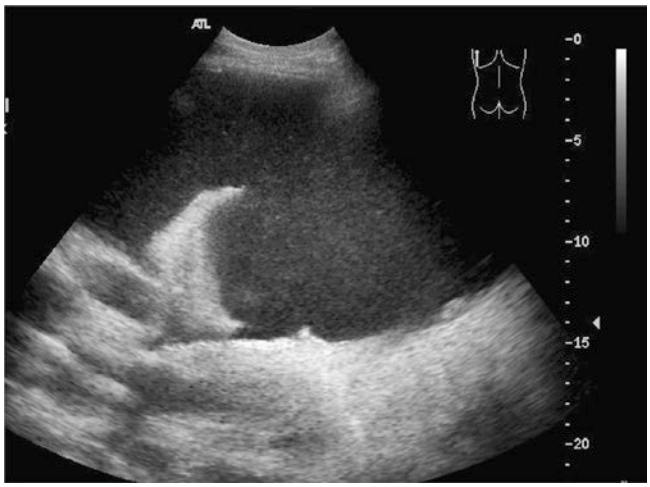

Fig. 3.11 Homogenous echogenic pleural effusion with atelectasis of the lower lobe of the lung. Lack of fever or clinical signs of inflammation and no trauma in the history is unlikely for an empyema or hematothorax. Aspiration reveals a chylous effusion due to metastases of a lung carcinoma in the mediastinum with destruction of the thoracic duct

Blood, pus or chylus reflect the ultrasound differently, therefore these effusions are echogenic (Figs. 3.9 and 3.10). The internal echoes shift breath and pulse dependant in the effusion, sometimes nearly circular. Protein agglomerates in inflammatory and malignant effusions also cause an echogenic appearance of the effusion (Chian et al. 2004). A reliable distinction between transudates and exudates by ultrasound is impossible. Also one third of exudates appear echofree. Modern ultrasound devices are highly sensitive and show occasionally internal echoes also in transudates (Fig. 3.11). If diagnostically necessary a thoracocentesis is required. The indication should be provided generously (Hooper 2010). With the patient's consent this is possible immediately after sonographically establishing a puncture site. The aspirate is then further analyzed in the laboratory depending on the specific issue (Table 3.4).

Table 3.4 Analysis of aspirate from pleural effusions

Macroscopy	Appearance	Clear, turbid, purulent, bloody
	Consistency	Runny, viscous, ropy, frothy
Leucozytes	Transudate <1000/µl Exudate >1000/µl	
Hemoglobin	Hematocrit	Almost equal to blood = > hematothorax
Clinical chemistry	pH	<7.2 = > parapneumonic, empyema
	Total protein	Limit transudate/exudate 3 g/dl
	Glucose	<60 mg/dl or quotient effusion/serum < 0.5 = > parapneumonic, rheumatic, tbc
	LDH	Quotient effusion/serum > 0.6 = > parapneumonic
Bacteriology	Culture aerobic and anaerobic and	Gram staining
In case of clinical suspicion	Tbc-PCR and –culture, cytology, virology, tumor-marker, cholesterol, triglycerides, chylomicrones, lipase	

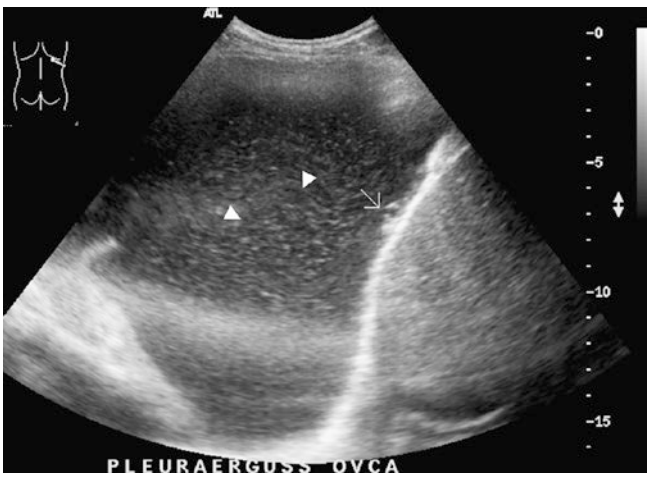

Fig. 3.12 Malignant pleural effusion in metastasized ovarian carcinoma. Even on the stationary image one suspects the dynamic circular movement of the echoes in the effusion (*arrowheads*). Deep in the effusion strip-like artifacts. Small pleural metastasis on the diaphragm (*arrow*)

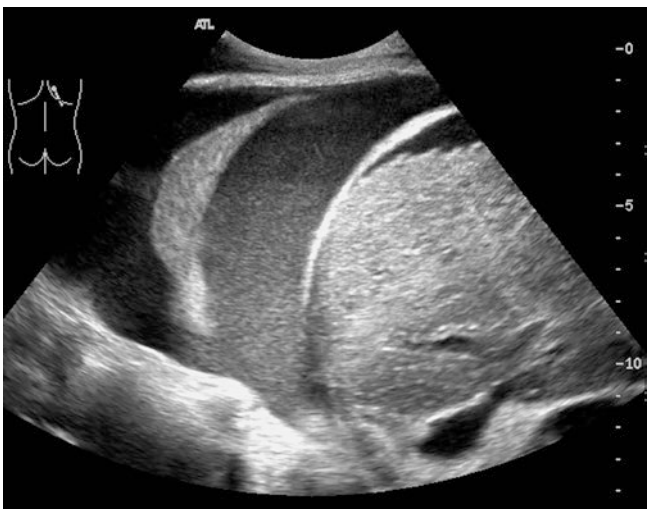

Fig. 3.13 Partly clear echogenic effusion, the subphrenic ascites and the humpy cirrhotic liver clearly depictable. The aspirate of the effusion clear, with a protein content of 29 g/l formally a transudate

3.4.1 Complicated Parapneumonic Effusion

Infected, septated and captured pleural effusions are referred to as complicated (Light 2006). Rounded margins due to the adhesion of the pleural layers are characteristic for captured pleural effusions, a finding similar to that in CT and MRI. Captured and loculated effusions show less deformation as free floating effusions when holding the transducer fixed to the chest wall. Compared to CT and MRI ultrasound is the best method to detect septations. Septations often develop spontaneously in a parapneumonic effusion or in an empyema (Figs. 3.12 and 3.13). Inadaquately treated parapneumonic effusions have a high risk of prolonged hospitalization, prolonged systemic toxicity, increased mortality after late or inadequate tube drainage, a residual decline of respiratory function, a local spreading of the inflammation and an increased mortality (Light 2006). The prognostic risk of parapneumonic effusions is rising correlated to an increasing volume. Captured or septated effusions and a thickened pleura are typical signs of an increased risk. Ultrasound is best suitable to detect effusion volume, loculation and pleural thickening. A negative bacterial culture or Gram staining and a pH > 7.20 in the aspirate mark a low risk. Aspirates with positive culture or Gram staining, purulent aspirates or a pH < 7.20 are typical for an empyema (Colice et al. 2000; Heffner 2010) (Table 3.5).

Hemorrhagic as well as malignant effusion can also appear septated or loculated. Also as a result of multiple thoracocenteses fibrinous strings and bands appear. Fibrinous strands, pleural thickenings and accompanying consolidations of the lung are nearly always indicating an exudate, except the typical compression atelectasis of the lower lobe of the lung.

Table 3.5 Parapneumonic pleural effusion and empyema

	Uncomplicated PPE	Complicated PPE	Empyema
Pleural morphology	Thin	Fibrinous exudates, septations	Thickened, granulation tissue, septae and loculations
Pleural aspirate	Clear	Turbid	Purulent
pH[a]	>7.30	7.1–7.2 (7.3)	<7.1
Lactatdehydrogenase[a]	<500 U/l	>1000 U/l	>1000U/l
Glucose[a]	>60 mg/dl	<40 mg/dl	<40 mg/dl
Cytology	PMN +	PMN ++	PMN +++
Microbiology	Sterile aspirate	Occasionally positive (microscopically and in culture)	Often positive (microscopically and in culture)

According to Tasci 2005
PMN polymorphonuclear cells, *PPE* parapneumonic effusion
[a]Examination of pleural fluid

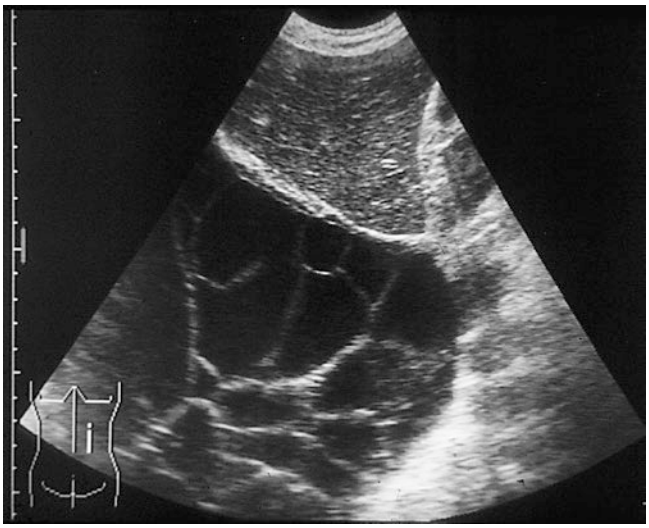

Fig. 3.14 Honeycomb-like loculated post-inflammatory pleural effusion. Ultrasound avoids frustraneous puncture attempts with a possible risk of injury

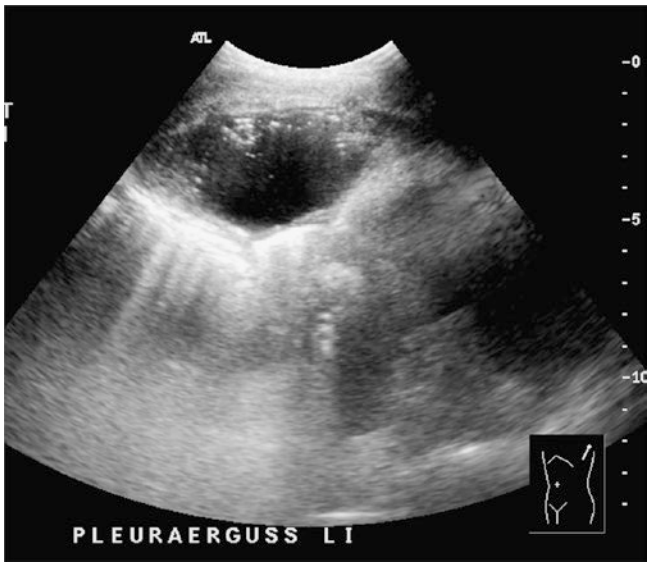

Fig. 3.15 Captured effusion after pancreatitis. Radiologically the effusion the formation impresses as a pleural based tumor. A reliable differentiation of a unilocular empyema is impossible, therefore a diagnostic puncture is needed

To exclude septations prior to each diagnostic pleurocentesis and especially prior to a therapeutic thoracocentesis an ultrasound scan should be done. Punctering of single chambers, if necessary, may be carried out under ultrasound guidance. Different echogenic content of chambers may indicate a partial empyema or hemorrhage.

3.4.2 Pleural Empyema

Pleural empyemas usually present as capsulated, low to moderately echogenic and relatively homogenic effusions. Owing to the adhesions they are not free floating when changing the patients position. Usually the pleura is thickened. With the panoramic function of modern ultrasound scanners also large empyemas can be mapped in their whole extension.

In CT empyemas appear with moderately and uniformly thickend pleura with relatively smooth margins to the cavity (Light 2006). The separation of the pleural sheets, known as "split pleura sign", may also be depicted by ultrasound. Usually the inflammatory infiltration into the surrounding lung is limited. Passive atelectases close to the empyema may occur. Complex septations and passive atelectases support with a sensitivity of only 40 % the diagnosis of an empyema. A pleural puncture is needed to confirm the diagnosis.

A careful and differentiated transthoracic ultrasound examination can already clarify the therapeutic pathway with establishing the diagnosis (Figs. 3.14 and 3.15). Loculated empyema are not suitable for percutaneous tube drainage. Such

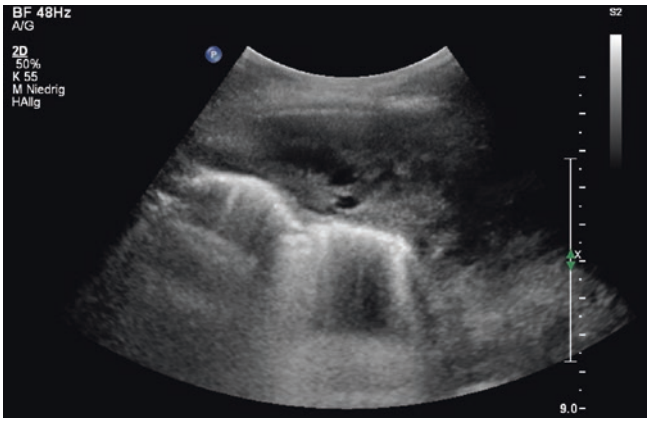

Fig. 3.16 Thirty year old patient suffering from pneumonia, only few residual air in the lung parenchyma. Around the consolidated lung a septated effusion with irregular thickened and not well demarcated pleural sheets (*arrows*). Sonographically the image of a complicated effusion. The aspirate showed 8.500/µl leucocytes and pH 7.05 according to an empyema. Drainage by video-assisted thoracoscopy

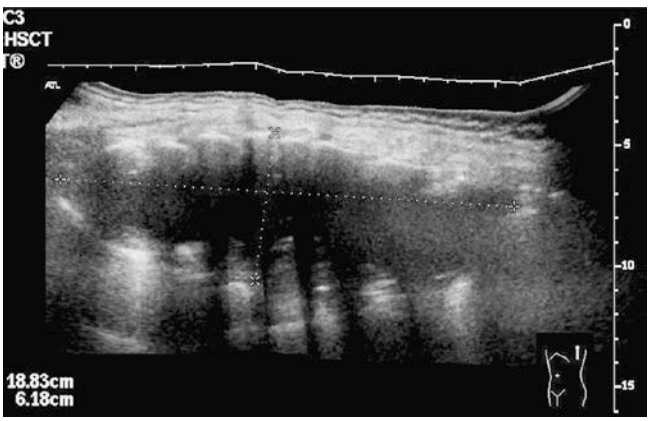

Fig. 3.17 Pleural empyema spreading over multiple intercostal spaces. The ribs with their shadows clearly visible. Volumetry and overall view is possible with the panoramic function

empyema need a surgically or video assisted thoracoscopically guided drainage with destruction of the septae (Fig. 3.16). Unilocular empyema nowadays are drained transthoracically with tubes of 10–30 Char. under ultrasound guidance. Highly viscous contents of an empyema need a greater diameter of the tube (Figs. 3.17, 3.18, and 3.19) (▶ see Chap. 10).

A lung abscess may be difficult to differentiate from a pleural empyema. Lung abscesses often have an extended inflammatory infiltration and atelectatic parts of the surrounding lung, mimicking a very thick wall. Repositioning the patient air containing lung abscesses present with a change of the air-fluid level. Air content is a reliable sign for a connection of a lung abscess to a bronchus. After multiple previous punctures also pleural empyema may contain a few air. Gas-forming bacteria are rare in pleural empyema. The prove of vessels in the pericavitary consolidation occurs more frequently around an abscess and is not typical for an empyema. But using CEUS vessels may be found also around an empyema.

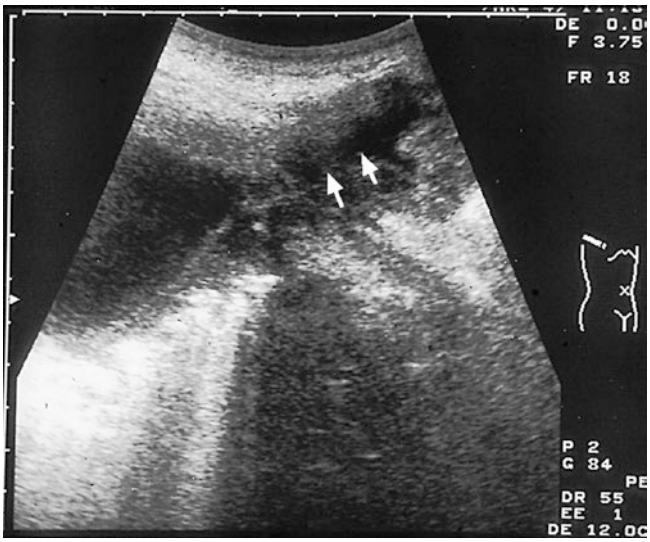

Fig. 3.18 Pleural empyema with thickened wall with relatively smooth margins and clearly visible split pleura. Partial evacuation of the empyema via a fistula through the chest wall, surrounded by inflammatory infiltrations (*arrows*)

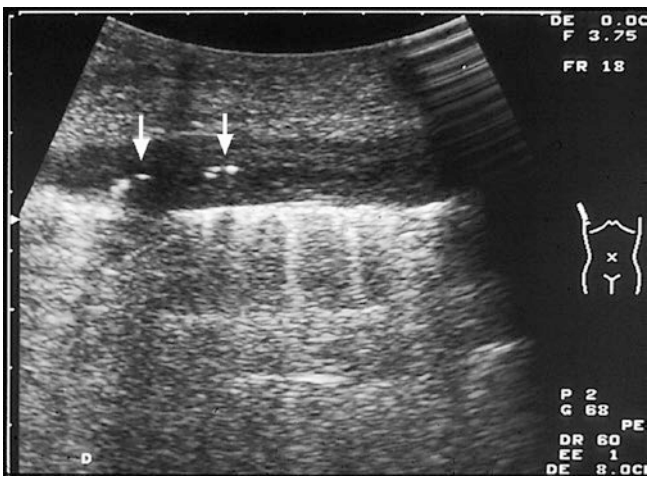

Fig. 3.19 Clearly visible thickening of the pleural sheets in an already drained empyema. Small air bubbles in the otherwise empty cavity

For the transthoracic therapy of a lung abscess it is crucial not to drain through aerated lung. The drainage should strictly be performed in an area where the pleural sheets are glued together, otherwise there is a high risk for the development of an additional pleural empyema.

3.4.3 Hematothorax, Chylothorax

A hematothorax develops posttraumatic, occasionally after interventions, e.g. after faulty puncture with injury of the lung or a vessel in the chest wall. A hematothorax induced by a disease-related or anticoagulant-related coagulopathy is rare. Not so rare is a hematothorax or hemorrhagic effusion in primary or secondary tumor diseases of the pleura, especially pleural mesothelioma.

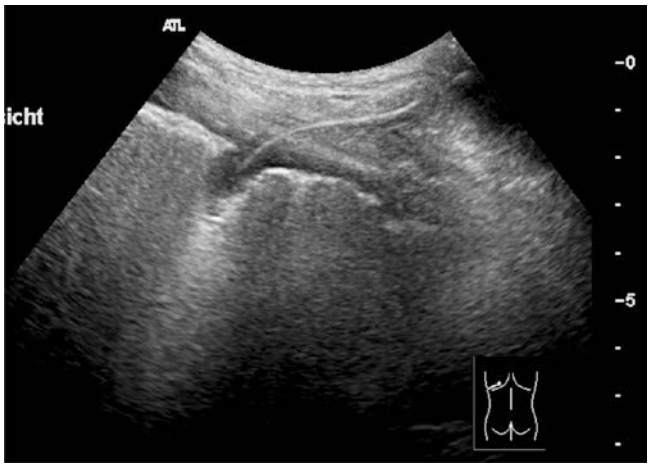

Fig. 3.20 After successful pleurodesis. The drainage tube used for application of the talc suspension still in situ. The surrounding pleura hypoechoic and thickened. In the dynamic examination no gliding sign

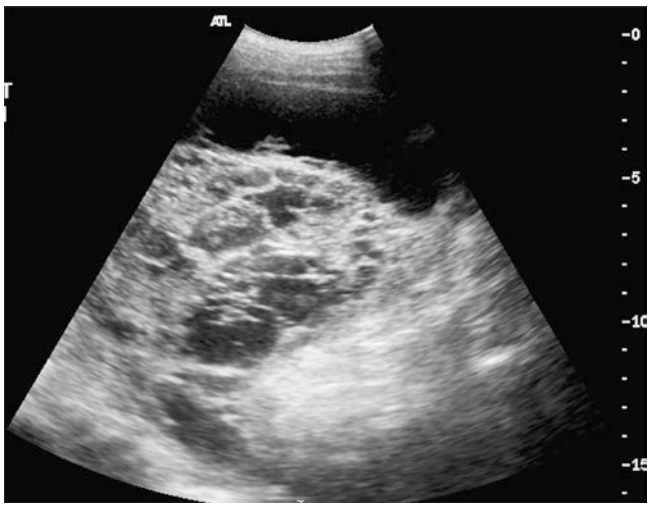

Fig. 3.21 Extended fibrinous clot after attempted pleurodesis. Inferior lung fixed to the diaphragm but not to the chest wall. Beneath the clot a significant effusion, included in the clot also liquid parts

Blood in the pleural cavity may present very differently. Fresh blood is mostly echofree similar to the flowing blood in the vessels. Newly coagulated blood may be considerably echogenic, clots are usually moderately echogenic and may appear like solid tissue, frequently with cystic inclusions. After secondary liquefaction of the clots the pleural content is again echofree. Frequently septae develop in hematothoraces. Septae are obstacles for a sufficient drainage, therefore hematothoraces should be drained very early, e.g. immediately after admission to a hospital in the emergency room. Thick drainage tubes should be preferred. Determining the puncture site by ultrasound reduces the risk of secondary intervention related injuries of diaphragm, liver or spleen, especially in case of an unknown elevation of the diaphragm. Without a sufficient drainage of

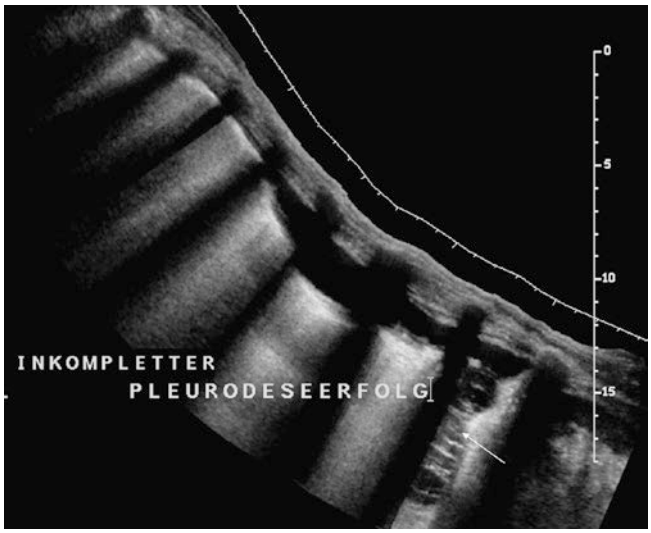

Fig. 3.22 Incomplete pleurodesis. In the left part of the image the visceral pleura fits tight to the parietal pleura, there no gliding sign. In the right part of the image the pleural sheets apart with effusion in between. The inferior lung fixed with multiple fibrinous strings (*arrow*). Panoramic view with eight ribs in cross section and their shadows

a hematothorax frequently develops a pleural peel with restriction of ventilation.

Injuries or tumor related destructions of the thoracic duct lead to a chylothorax. The effusion mostly appears moderately echogenic, sometimes highly echogenic. The aspirate looks milky, with a high concentration of triglycerides and chylomicrons. The cause for the leakage may be very small tumors or metastases e.g. due to breast cancer or lung cancer. These small tumors may be very difficult to localize.

3.4.4 Pleurodesis

In malignant pleural diseases with recurrent large effusions and consecutive dyspnea, mainly due to pleural carcinosis, pleurodesis is a beneficent palliative therapy. Spraying talc solution thoracoscopically over the pleura achieves the best results. But this procedure cannot be performed in every patient and everywhere. For catheter pleurodesis the pleura is emptied via an ultrasound guided drainage tube. Through this tube the talc solution is instillated into the pleural cavity. In successful pleurodesis pleural gliding is no more visible by ultrasound (Figs. 3.20, 3.21, 3.22, and 3.23). In inadequate pleurodesis ultrasound differentiates much better between residual effusion, septation, lung consolidation or partial lung atelectasis than conventional chest-X-ray does. This success can be secured by ultrasound after thoracoscopical pleurodesis too. For clarification of this problem a computed tomography is nearly never necessary. Ultrasound nowadays has the advantage to be available nearly everywhere in hospitals and private practice.

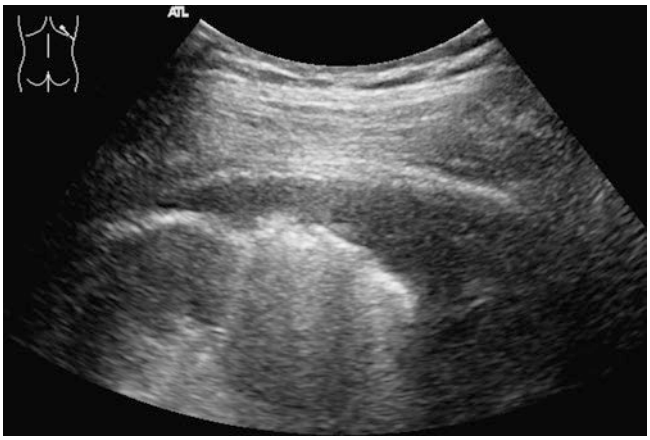

Fig. 3.23 Successful pleurodesis with formation of a broad hypoechoic pleural peel. Owing to the scarred distortions the lung surface irregular

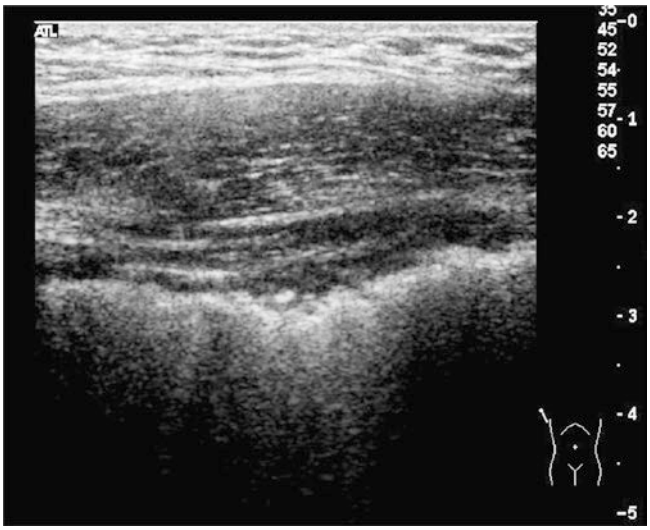

Fig. 3.24 Acute pleuritic with moderately thickened pleura, the line of the parietal pleura irregular edged. Examination in the painful area of the chest

3.5 Solid Pleural Changes

Pleural thickenings may occur diffuse, circumscribed, ribbon-shaped, nodular, regular, irregular, hypoechoic or complex structured. The changes may be limited to a single pleural sheet or affect both sheets. In an effusion or in case of a preserved gliding sign the thickening can be clearly assigned to the parietal or visceral pleura, depending on the movement with the lung. In case of interconnected pleural sheets the original pleural cavity can only be guessed by an echogenic partly interrupted line. Pleural thickenings can be observed in inflammatory diseases as well as in primary or secondary tumorous diseases. From the sonographic shape or structure of a pleural thickening cannot be deduced the etiology even though hypoechoic nodules are typical for metastases.

3.5.1 Pleuritis

Breath dependant chest pain and pleural rales are typical for pleuritis. To confirm the diagnosis multiple diseases like cardiac chest pain and myocardial infarction have to be ruled out. Conventional chest X-ray may present an opacification corresponding to a small effusion, but is often completely inconspicuous and therefore does not rule in nor rule out pleuritis. In most of these patients abnormalities of the pleura can be detected by ultrasound (overview).

Sonographical findings in pleuritis (acc. to Gehmacher et al. 1997)

- rough appearance and interruption of the normally smooth pleura (89.4 %)
- small subpleural consolidations with a diameter between 0.2 and 2.0 cm (63.8 %)
- localized parietal or basal pleural effusions (63.8 %)
- CEUS: early marked contrast enhancement of the pleura

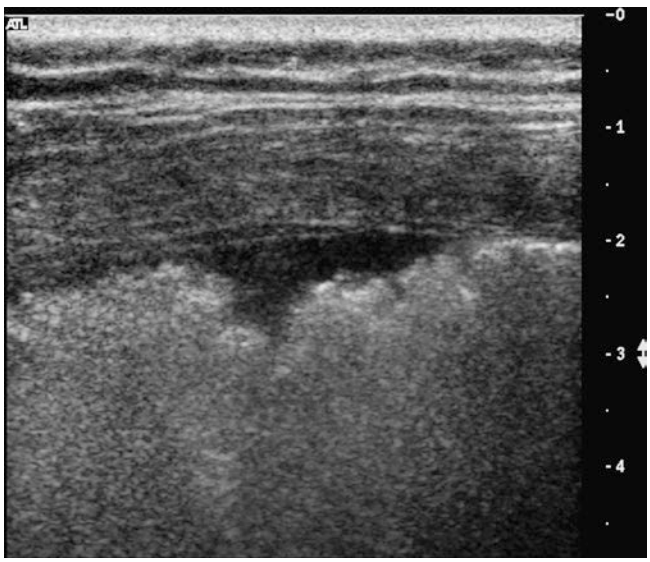

Fig. 3.25 Thirty Five year old female patient in the 24 week of gestation with localized breath dependent pain. Small subpleural consolidation in pleuritis. This small consolidation could also be assigned to a lung embolism, but there was no other evidence for that

In most cases the parietal pleura is hypoechoic to moderately echogenic thickened. The lung gliding is restricted due to the pain (Fig. 3.24) (Gehmacher 1997; Volpicelli et al. 2012). Small wedge-shaped echopoor subpleural consolidations occur as a sign of inflammatory co-reaction of the lung (Fig. 3.25). This is interpreted as a focal interstitial syndrome, especially when B-lines appear at the edges (▶ see Chap. 4; Lichtenstein et al. 1997). More extended hypoechoic consolidations suggest the suspicion of subpleural infiltrations in a viral pneumonia. Typical consolidations of a bacterial pneumonia can be accompanied by a pleuritis (Fig. 3.26,

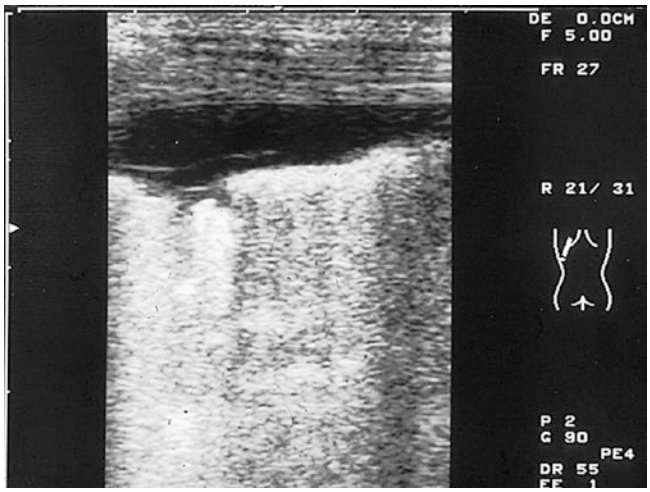

Fig. 3.26 Tuberculous pleuritis without thickening of the parietal pleura, irregular visceral pleura and tiny nodular subpleural consolidations. Thin fibrinous strands in the effusion. Diagnosis confirmed by detection of mycobacterium tuberculosis in the aspirate

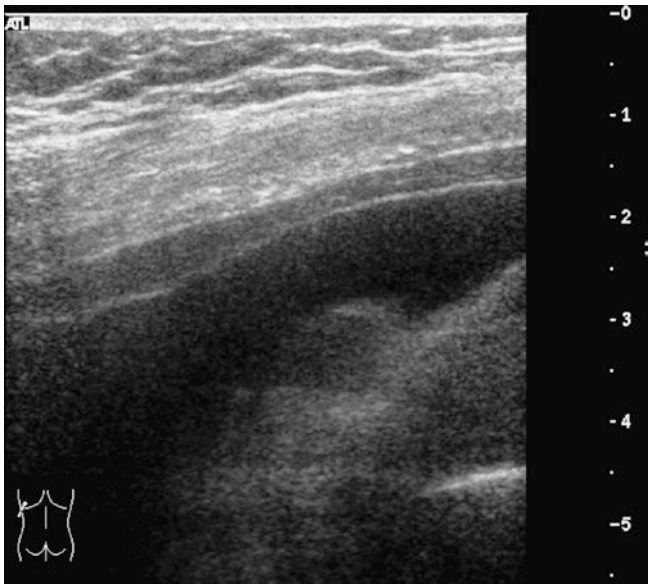

Fig. 3.27 Unusual pleural peel. The parietal pleura is thickened up to 6 mm, but smooth demarcated. The visceral pleura is not involved. Large pleural effusion due to cardiac failure

▶ see Sect. 5.1). Apart from the real pleural thickening ribbon-shaped moderately echogenic fibrinous deposits are detectable continuing as strings and bands through the accompanying effusion. In the late phase they are responsible for the loculation (Fig. 3.14).

Perfusion in the thickened pleura is only detectable by color Doppler in 23.4 % of patients (Gehmacher et al. 1997). In contrast enhanced ultrasound (CEUS) the hyperemia is visible. The inflammatory thickened pleura and particularly the accompanying pneumonic consolidations display after application of contrast medium (e.g. Sonovue®) a very short time to enhancement in contrary to peels, tumors or the muscles in the chest wall (Görg et al. 2005). Though contrast enhancing agents are rarely necessary to confirm the diagnosis.

3.5.2 Pleural Peels

A pleural peel is a fibrosis of the pleura and develops as a result of different diseases like pleuritis or empyema, but also postoperatively. Initially the pleural sheets glue together. The subsequent fibrosis spreads from one sheet to the other and produces a thickening of the pleura of sometimes several centimeters. Lung gliding is no more possible. Calcified peels are easily detectable by X-ray. Non-calcified peels manifest radiologically as parietal opacification at the chest wall or in the angle between chest wall and diaphragm. Sonographically peels are moderately echogenic, in the individual case sometimes nearly echofree, mimicking a small shell-like effusion. The missing of lung gliding and deformation during breathing rules an effusion out. The demarcation of the fibrosis against the chest wall or the lung may be smooth, but often bizarre irregular (Fig. 3.27). In the latter case the differentiation from an infiltration by a pleural carcinosis or mesothelioma is difficult (Fig. 3.28). Hyperechoic calcifications with shadows are typical for old fibroses. Residual air in adjacent lung consolidations must be excluded. Extended shell-like calcifications prevent any deeper sonographical insight into the chest. Cyst-like inclusions in peels as probable residuals of former effusions are not so rare. Atypical vessels can be ruled out by color Doppler (Tables 3.6 and 3.7).

3.5.3 Pleural Tumors

Primary benign and malignant pleural tumors are rare in contrast to metastases. Sometimes pleural tumors are accidentally discovered during a chest ultrasound. In most cases parietal tumors are previously detected by other imaging procedures like conventional chest-X-ray, computed tomography or magnetic resonance imaging. For further clarification a "point-of-care"- ultrasound examination is performed.

Benign Pleural Tumors

Benign tumors like lipomas, neurinomas, chondromas, fibromas or benign mesotheliomas account for less than 5 % of all pleural tumors. In chest-X-ray they are noticed as pleural based opacifications with smooth margins. Frequently they give rise to extended diagnostic examinations to rule out a pleural metastasis or a peripheral lung cancer. Sonographically most of the benign pleural tumors are moderately echogenic and clearly demarcated by a thin capsule. Depending on the size they displace neighboring structures, but are not growing invasively (Fig. 3.29). However, displacement and invasion are not always clearly to distinguish. Transpleural growth with missing lung gliding is compatible with malignant infiltration. Small accompanying pleural effusion can also occur with benign pleural tumors. A distinction of the different benign pleural tumors by means of ultrasound is

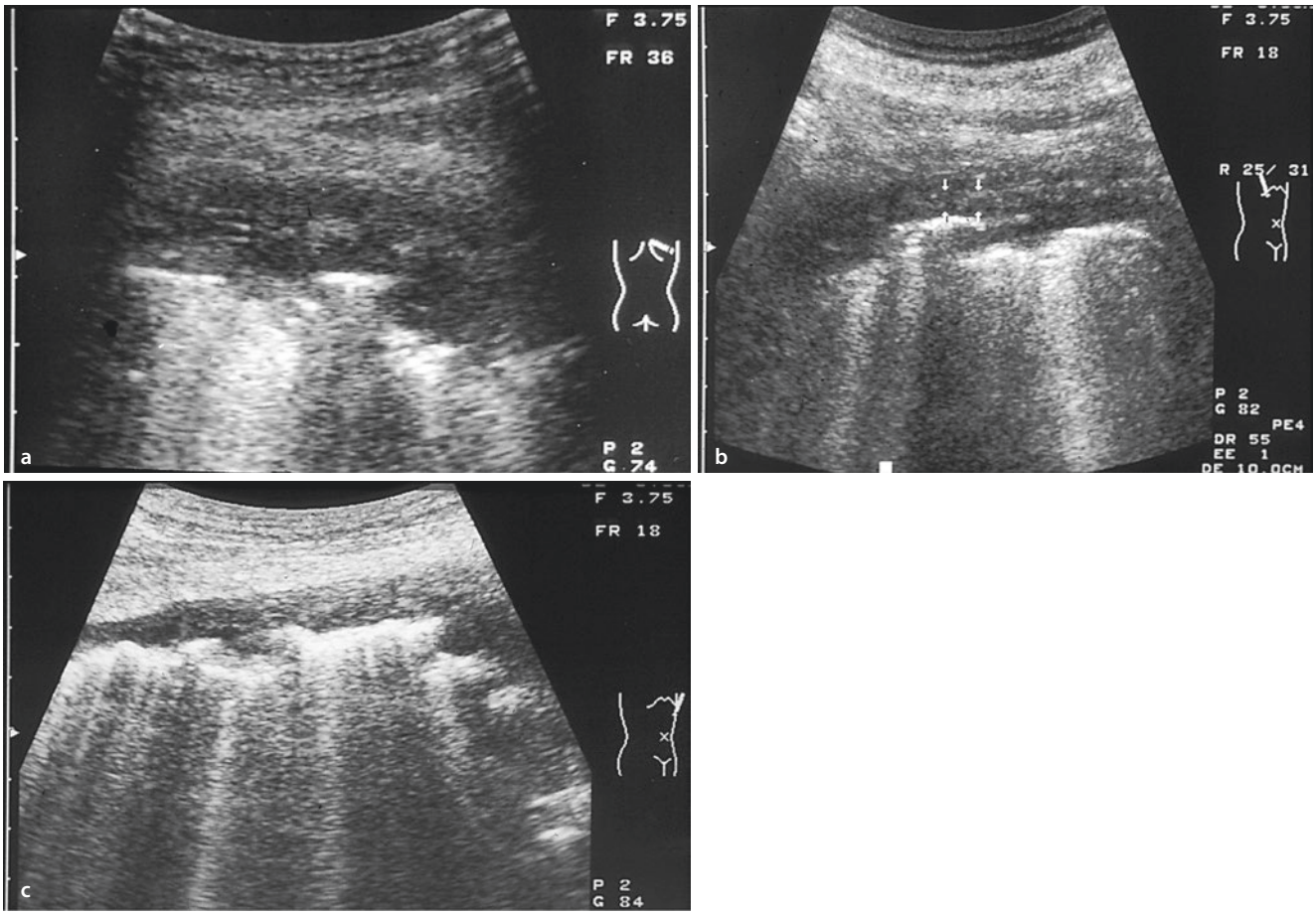

Fig. 3.28 Extended moderately echogenic masses with irregular demarcation in the pleural area are ambiguous without otherwise reliable clinical data and therefore need to be proven histologically. A differentiation between fibrosis, pleural carcinosis and pleural mesotheliom solely by ultrasound is difficult or impossible. **a** Extended pleural fibrosis in a young woman after several operations in the chest. The cause for the first operation was a already existing peel of unknown origin suspected to be a tumor. **b** Slowly growing radiologically detectable non-calcified "pleural peel". Because of the clinical suspicion of a occult carcinoma repeated transthoracic biopsies which revealed at last the "peel" as pleural carcinosis in CUP-syndrome. Between the *arrows* one believes to recognize the former pleural cavity. **c** Nearly identical ultrasound image as in **a, b**, but histologically a pleural mesothelioma in a former asbestos worker

Table 3.6 Causes of pleural fibrosis

Spontaneously arising inflammatory diseases	Pleuritis Pleural empyema
Induced inflammation	Pleurodesis
Trauma	Chest wall trauma with pleural injury Hematothorax Recurrent pneumothorax Postoperatively, especially after pleurectomy

Table 3.7 Differential diagnosis of pleural fibrosis

Pleural effusion
Acute fibrinous pleuritis
Pleural carcinosis
Pleural mesothelioma
After pleurodesis
Extended pleural plaques after asbestos exposition
Subpleural consolidations, e.g. Lung contusion Lymphomatous infiltrations
Subpleural lipomatosis

impossible. The classification of the benign tumors by small needle biopsy specimens or only by cytology is often very difficult or impossible for the pathologist. Calcifications are more common in benign tumors. Density measurements as in CT, e.g. in lipomas, are not available in ultrasound.

Solitary fibrous tumors of the pleura, formerly known as hemangiopericytoma, are often asymptomatic and are discovered by chance in an advanced stage. Two thirds of all cases are originating from the visceral pleura. Occasionally this can be depicted by CEUS. However, the often existing peduncle comes up during the operation. The tumor shows beside well perfused areas also necroses and cystic parts. Most

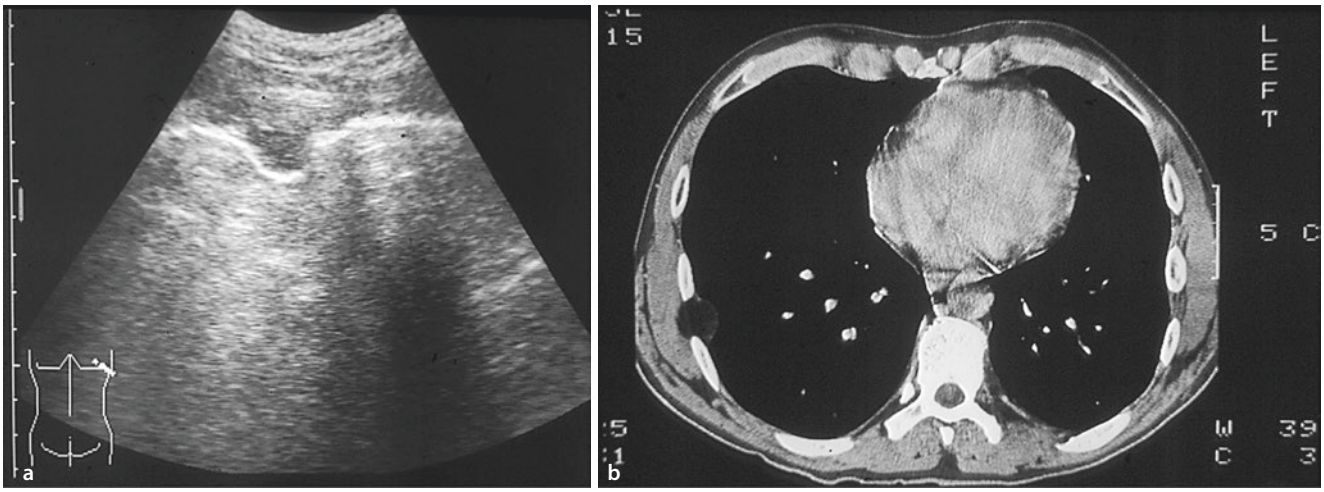

Fig. 3.29 **a** Small round clearly demarcated tumor of the parietal pleura. The lung is gliding breath-dependently unimpeded over the tumor. The tumor is isoechogenic compared to the chest wall muscles. In chest-X-ray a small pleural based lesion was noticed. **b** Also in computed tomography a well demarcated tumor with fat density corresponding to a lipoma. No histological confirmation, but stable over many years in follow-up

of these tumors turn out as benign, also histologically, but may metastasize after decades. Even after malignant transformation the tumors have a good prognosis, also after operation of recurrent masses. The secretion of insulin-like- growth-factor in large tumors can cause recurrent and difficult to treat hypoglycemias (Abu Arab 2012; Cardillo et al. 2012; Travis 2010).

Pleural Metastasis

Pleural metastases are frequently occurring in advanced breast and lung cancers, but in many other tumors as well. The development of pleural metastases is often combined with pleural effusions. This acoustic window facilitates the displaying of the metastases. If suspicious lesions are already located by other imaging procedures, also the rare metastases without effusion are easily to depict by ultrasound. Ultrasound is in these cases usually used for the assignment of the lesion either to the lung, pleura or chest wall, to distinguish whether they are solid or liquid and to guide the transthoracic biopsy.

In a newly discovered pleural effusion of unknown origin the pleura should be scanned for suspicious metastatic lesions. A regular search for a pleural effusion in oncologic patients can reveal the occurrence of pleural metastases the first time. But since ultrasound is only a conditionally appropriate procedure for intrapulmonary metastases, an additional CT is mandatory.

Most of the metastases are located on the pleura along the chest wall, the diaphragm and in the pleural recessus, that is in regions well accessible for ultrasound (Figs. 3.30, 3.31, 3.32, and 3.33). Pleural metastases are mainly hypoechoic to moderately echogenic. In rare cases they seem to be echofree, mimicking liquid formations. Metastases are nodular, round, hemispherical or broad-based polyp-like protruding into the effusion. Metastases are, of course, of varying size and are detectable from a size of 1–2 mm. Large metastases can invade deeply the underlying lung or chest

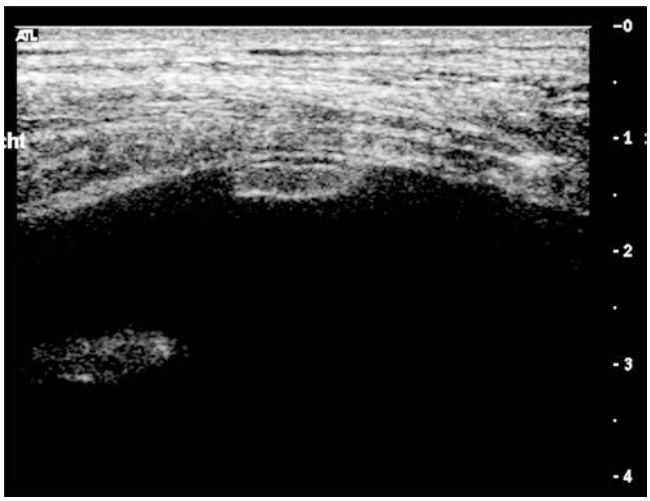

Fig. 3.30 Metastasis located on an otherwise normal parietal pleura. Metastasized breast carcinoma. Large pleural effusion

wall. An interrupted or missing demarcation of the vicinity or pseudopodia-like branches indicate malignancy. Due to the lower echogenicity they are distinguishable from the chest wall or the diaphragm. Single, well demarcated metastases cannot be differentiated from benign pleural tumors by means of ultrasound alone. Multiple occurrence of identical possibly different sized formations is nearly proving metastases especially in a known underlying malignant disease. Therefore a biopsy is not required in every case. In first detected and suspected, but not proved primary tumor an ultrasound guided needle biopsy may clarify the tumor diagnosis. Single metastases located in the visceral pleura may occur like a peripheral lung cancer. Both lesions can spread to the other pleural sheet in the same way leading to an adhesion of the pleural sheets.

Fibrinous clots adjacent to the pleura after trauma or interventions may appear like metastases. In the real time examination

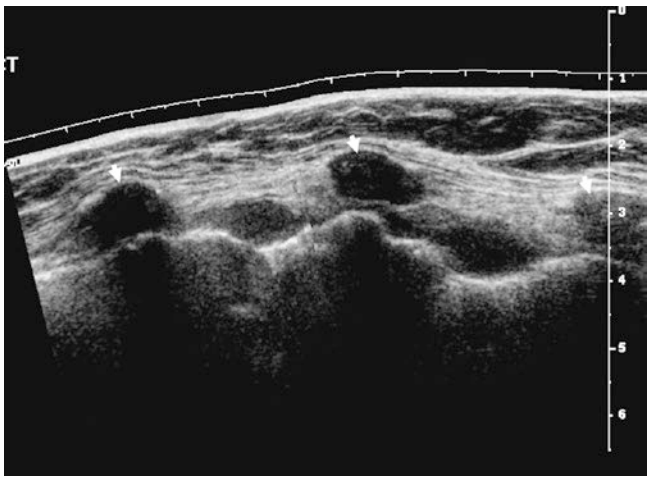

Fig. 3.31 Pleural metastases in a patient with breast carcinoma and ovarian carcinoma in her history. The origin of the metastasis can only be proven by biopsy and histology. The parietal metastases are invading the chest wall and the visceral pleura, discernable by the rough lung surface and the missing gliding sign. Parasternal longitudinal section on the right side in the region of the cartilaginous ribs

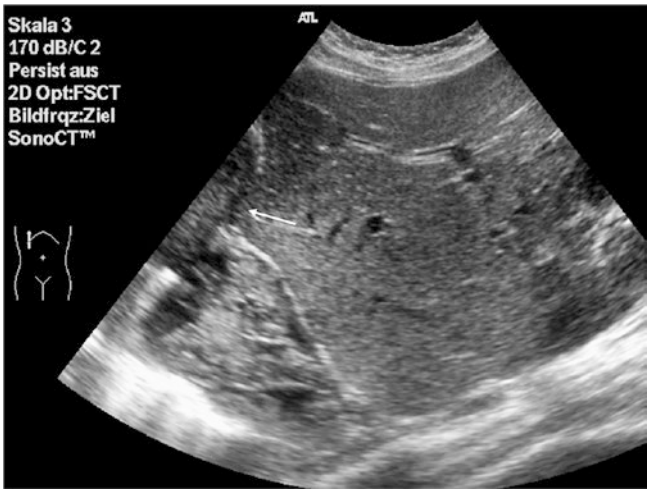

Fig. 3.33 Extended pleural carcinosis due to an endometrial cancer, known since 2 years. The diaphragm walled in, deformed and partially destructed by the carcinosis (*arrow*),furthermore invasion of the liver

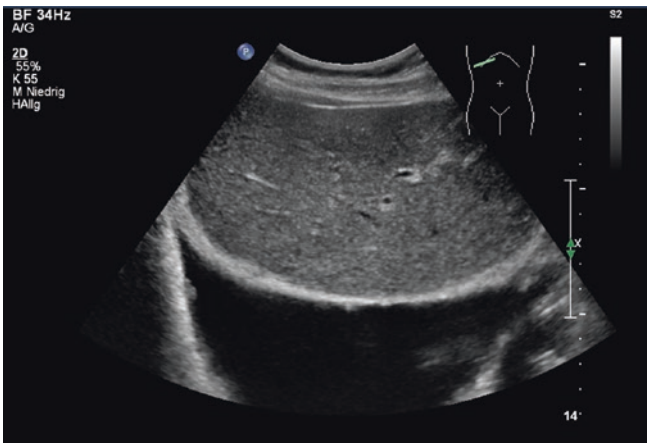

Fig. 3.32 Patient with breast carcinoma supposed to have a singular liver metastasis. Sonographically a pleural effusion with small metastasis in the pleural recesses

metastases are rigid whereas fibrin clots slosh forth and back. In CEUS fibrin clot do not enhance contrast medium.

An expanded plate-like carcinosis of the pleura with or without effusion is rare. The sonomorphological distinction from peels or a mesothelioma is difficult. Even the needle biopsy may fail, when malignant, inflammatory-reactive and fibrinous areas and small blood clots are close together.

In CEUS most metastases enhance only moderately, dependent also from the grade of vascularization of the primary tumor. In the early arterial phase the supply through parietal pleural vessels or peripheral bronchial vessels may be observed. Visceral pleural metastases are not supplied by pulmonary arterial vessels, therefore the beginning of the early arterial phase in the metastases is markedly later (>10 s) than in a surrounding atelectasis or pneumonia (3–10 s). (See Table 3.8).

Table 3.8 Differential diagnosis of pleural metastasis

Single benign pleural tumor
Fibrinous clot after trauma or intervention
Chest wall tumor
Subpleural lung tumor/metastasis Peripheral lung cancer Subpleural metastasis Lung embolism Granuloma/rheumatic nodule Atelectasis/obstructive atelectasis Lung contusion
Capsuled pleural effusion
Localized pleural empyema
Irregular shaped and demarcated pleural peel
Uni- or oligolocalized pleural mesothelioma
Pancoast tumor with chest wall infiltration

Malignant Pleural Mesothelioma

The malignant pleural mesothelioma with an incidence of about 20/1 Mio inhabitants is one of the less frequent tumors in Germany. Most affected patients had contact to asbestos in their history (Neumann 2013). Asbestos as well known trigger of this disease is banned in the whole European Union since 2005. In western Germany sprayed asbestos is prohibited already since 1979, a general prohibition followed in 1993 (Switzerland and Austria 1990, Great Britain 1999, no general asbestos ban up to now in the United States of America). Today a delay between exposition and disease outbreak up to 50 years is accepted, explaining the still rising incidence. In Germany a plateau is expected for the year 2030 (Lehnert 2009).

Asbestos plaques in the pleura characterize people with previous exposure to asbestos. These patients bear a risk to develop a mesothelioma. Asbestos plaques occur as calcified or non calcified pleural thickenings typically in the posterior-inferior parts of the parietal pleura. Their appearance in chest-X-ray and computed tomography is well known. Members of risk groups are surveyed radiologically. Plaques are not only shaped like a table mountain, but also flat tapering plaques are common. Preferably with high resolution transducers the moderately echogenic plaques with their smooth boundaries are detected in the parietal pleura with breath dependent gliding of the lung. The internal structure of the plaques is according to previous observations homogenous. About 10 % of the plaques calcify and then present high echogenic and with shadows. Tiny effusions may occur.

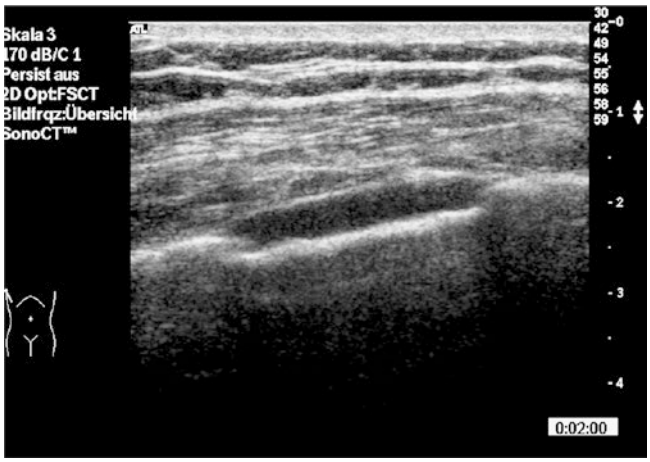

Fig. 3.34 Hypoechoic asbestos plaque with typical table-mountain-like appearance in the posterior-inferior pleura on the right side

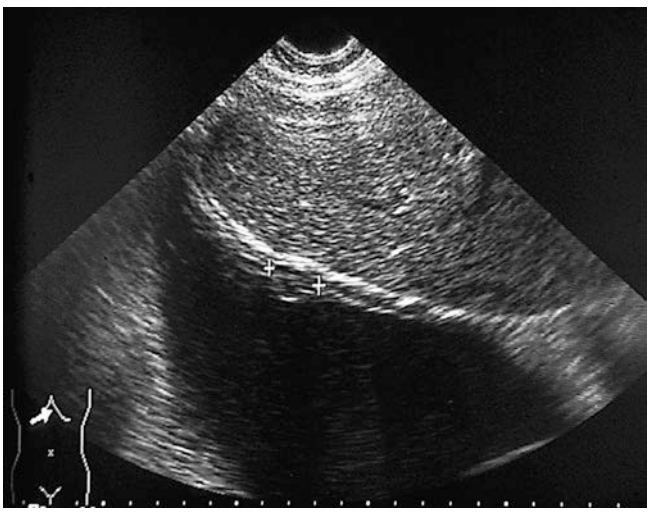

Fig. 3.35 Newly diagnosed mesothelioma spreading tapestry-like nearly over the whole pleura of the right hemithorax, single nodules (between the *markers*). The patient was admitted to the hospital because of dyspnea within 2 days. In the chest-X-ray a "white hemithorax". Decade-long asbestos exposition

Compared to the plaques mesotheliomas have an irregular edged and often unclear boundary. Beside tumorous mesotheliomas exist also tapestry-like spreaded mesotheliomas with embedded nodules in the pleura (Figs. 3.34 and 3.35).

The infiltration of the chest wall and the diaphragm is best depicted with high frequency transducers as hypoechoic streaky branches (Figs. 3.36 and 3.37). The tumor spreads early to the other pleural sheet. In an ultrasound study in 28 % of the patients both sheets of the pleura were affected at first diagnosis (Geiger et al. 2003). Accompanying pleural effusions may be echogenic due to hemorrhage.

Making the diagnosis by cytology of the effusion or blind pleural biopsy (Abrams needle) is only in about 30 % of patients successful. Thoracoscopically gathered biopsies achieve a positive diagnosis in over 90 %. Percutaneous imaging guided biopsies have a comparable good success rate.

After biopsies by operation or thoracoscopy about 40 % of patients develop metastases in the biopsy channel in the

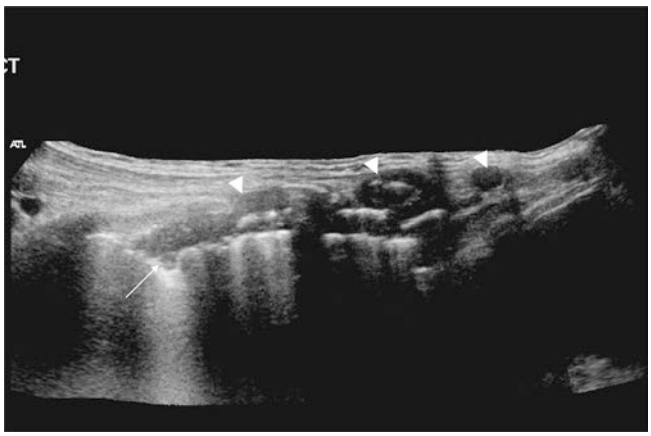

Fig. 3.36 Pleural mesothelioma. Already extended chest wall infiltration with inclusion of the ribs (*arrow heads*), and lung infiltration (*arrow*)

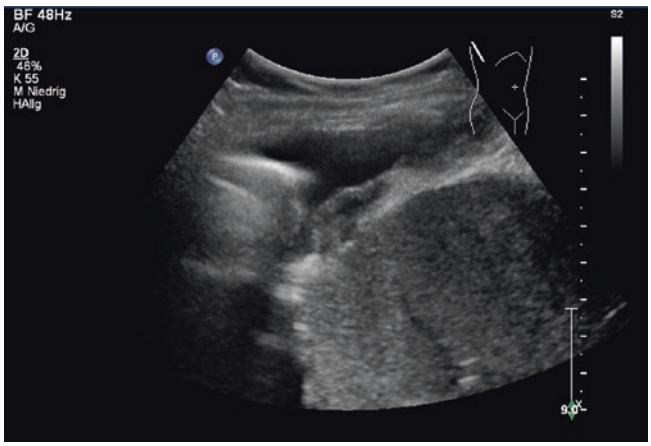

Fig. 3.37 Former asbestos worke with pleural mesothelioma. In the pleural recesses markedly thickened hypoechoic inhomogeneous pleura corresponding to the tumor (*closed arrows*). Deep infiltration into diaphragm and chest wall. The diaphragm at the dome destroyed (*open arrow*). Small tumor dependent effusion

chest wall, but also 0–15 % of patients after percutaneous biopsies, especially along the channels of the drainage tubes (Geiger et al. 2003). Therefore a short time radiation of the concerned area of the chest wall is recommended e.g. with 3 × 7 Gy. Curative operations in pleural mesothelioma are possible only in few patients.

Computed tomography is the standard procedure for the lymph node situation in mesotheliomas. For lack of detailed ultrasonographic studies the magnetic resonance imaging is the goldstandard for treatment planning concerning infiltration of chest wall and diaphragm. In an older study ultrasonography was also very sensitive in detecting this infiltration. The presentation of the pericardial invasion by ultrasound is highly specific (Layer et al. 1999). Data from large studies are lacking.

3.6 Pneumothorax

A pneumothorax can occur spontaneously, but also after trauma. Symptoms may be mild dyspnea to severe rapidly increasing shortness of breath in tension pneumothorax. A spontaneous pneumothorax represents often predominantly with chest pain.

The air penetrated into the pleural cavity nearly totally reflects the ultrasound in a similar manor as air in the alveoli (Fig. 3.38). At first glance there seems to be no difference in the sonographic image between air containing lung and air in the pleural cavity. Four signs of positive or negative demonstration of the visceral pleura and thus the lung are the basis of the ultrasound diagnosis of pneumothorax. The **gliding sign**, the synchronous up and down of the lung along the chest wall with breathing, is only visible when the lung is directly attached to the chest wall (Lichtenstein and Menu 1995). **B-lines** arise in the subpleural interstitium and can only be demonstrated, when the lung is adjacent to the chest wall. Air between the pleural sheets prevents the depiction of the lung surface. The **lung pulse**, a pulsation of the lung synchronous with the heart frequency, can normally be demonstrated during real time examination. But the lung excursions are very low. It is much better visible using color- or power-Doppler (Fig. 3.39). For this the close attachment of the lung to the chest wall is also a prerequisite. If the lung is only partially attached to the lateral the chest wall the lung gliding is visible in this area whereas in the ventral parts the lung gliding is missing. The transition zone is called the **lung point**. The demonstration of a lung point proves a partial pneumothorax (Lichtenstein et al. 2000). Lung gliding, B-lines, lung pulse and lung point definitely rule in or rule out a pneumothorax (Volpicelli 2011; Volpicelli et al. 2012). Diagnosing n.u. pneumothorax by ultrasound is superior to conventional Chest-X-ray in numerous studies concerning sensitivity with nearly identical specificity and nearly equal to computed tomography (Abu Arab 2012; Herth et al. 2003; Soldati et al. 2008; Wilkerson and Stone 2010). It is a great advantage, that ultrasound can be used everywhere, also outside the hospital in the emergency situation and gives a reliable result as basis for a therapeutical decision, the tube drainage (Fig. 3.40). This is not only advantageous in trauma but also after interventions with complications. Hereby the emerging pneumothorax can be observed in real time. But many pneumothoraces develop later within 4 h, a follow up is therefore recommended (Garofalo et al. 2006; Reißig and Kroegel 2005; Sartori et al. 2007). In patients under mechanical ventilation on the intensive care unit a pneumothorax occurs in 4–15 % as complication

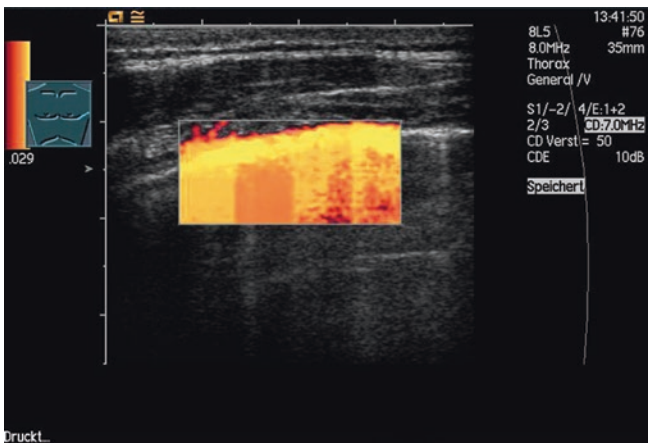

Fig. 3.39 Color sign to rule out a pneumothorax. The color signal can represent either the lung gliding or the lung pulse

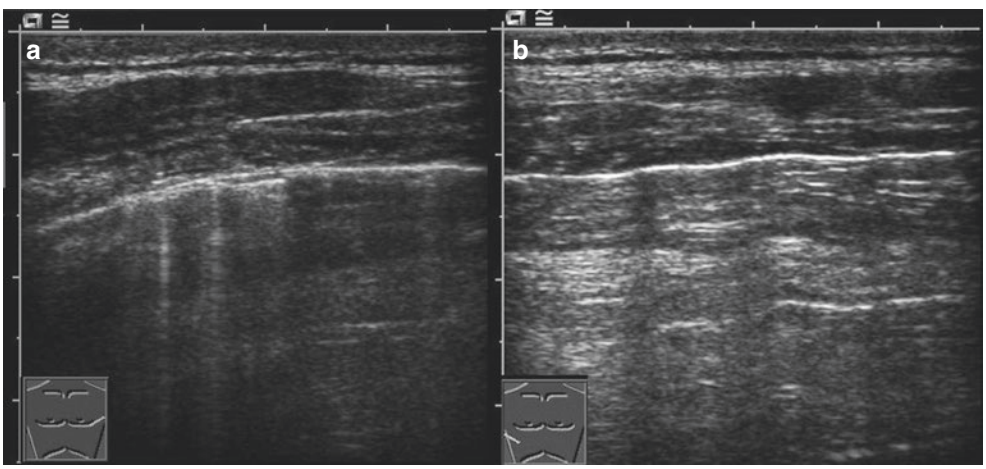

Fig. 3.38 Pneumothorax. **a** Ventilated side with pleural reflex and few B-lines. The ventilated lung is gliding synchronous with breathing. **b** Inforced pleural reflex at the entering of the air-filled pleural cavity with multiple horizontal reverberation artifacts

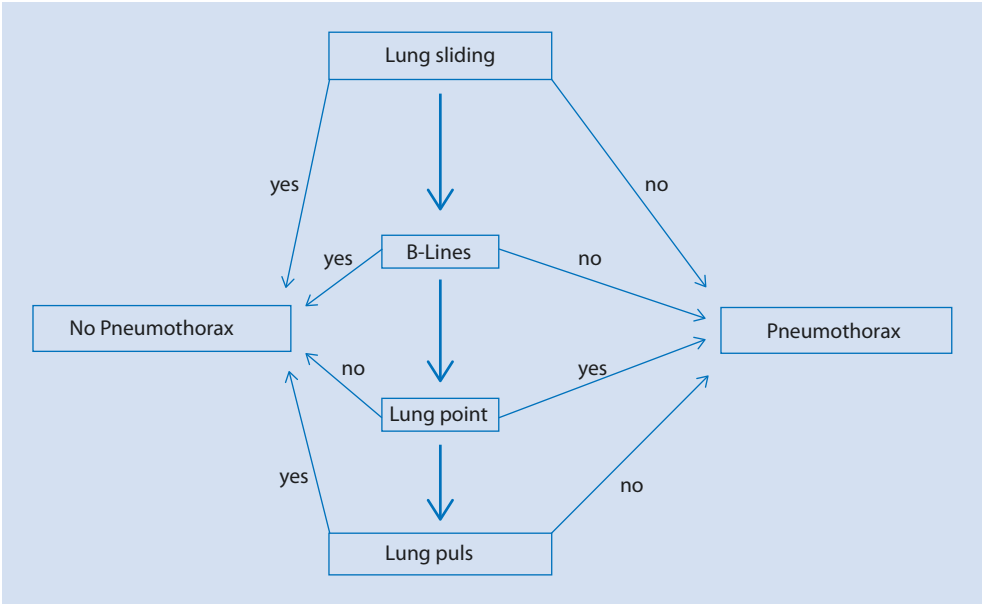

Fig. 3.40 Algorithm in suspected pneumothorax (acc. to Volpicelli 2012)

Table 3.9 Diagnostic signs to detect or exclude a pneumothorax

Pneumothorax	No	Gliding sign	Yes	No pneumothorax
	No	B-lines	Yes	
	No	Lung puls	Yes	
	Yes	Lung point	No	

(Gardelli et al. 2012; Yarmus and FellerKopman 2012). A sulcus- anterior-syndrome, a partial pneumothorax in the anterior-inferior parts of the pleura remains often undiagnosed in the chest-X-ray in supine position, but is detectable by ultrasound (Hsu and Sun 2014). See also Table 3.9.

In patients with emphysema the extend of lung gliding is reduced and may be difficult to detect. B-lines in a healthy lung are often completely lacking.

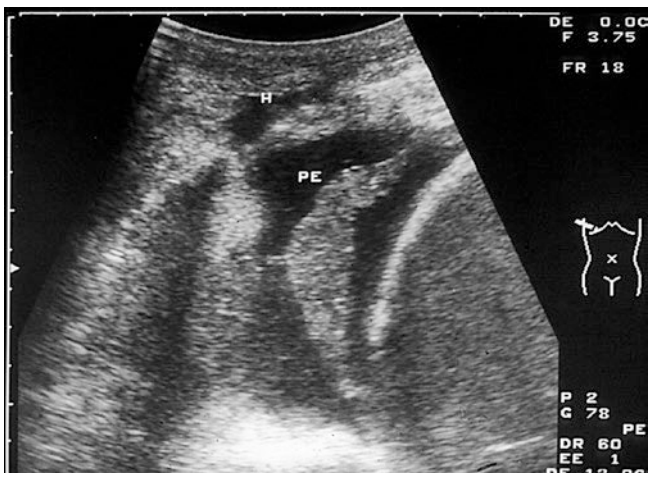

Fig. 3.41 Emergency examination in the surgical emergency room in a roofer, fallen from the roof. Dyspnea and severe chest pain on the right side. Echofree but still bloody effusion with lung atelectasis and partial rupture of the chest wall. Fluid mass included in the chest wall at the same location as a visible hematoma at the skin

3.7 Traumatic Changes in the Pleural Cavity

Small pleural effusions without compromising respiratory effects are common after mild to moderate chest trauma. E-fast (extended focused abdominal sonography in trauma) detects these usually non-hemorrhagic effusions. Merely then sonographic follow up is needed.

The result of a primary or secondary bleeding into an effusion is a hemorrhagic effusion. Depending on the content of blood the effusion appears more or less echogenic. The internal echoes are moving breath dependent, often circular. The hemoglobin concentration is usually significantly lower than in a venous blood sample.

A hemothorax contains pure blood in the pleura, the hemoglobin concentrations in a punctured and venous sample are almost equal. A hemothorax results usually due to a trauma, occasionally spontaneously in patients with not well adjusted anticoagulation. Liquid blood is often completely anechoic (Fig. 3.41). Coagulation develops different grades of echogenicity. Then the echogenic pleural content is deformable, e.g. by respiration, but is obviously not liquid. Later the hemorrhage gets organized and fibrosis develops. To prevent this process a hemothorax should be drained early with large-caliber tubes. Patients with a severe chest

trauma should be examined soon by ultrasound already in the emergency room, if possible earlier at the scene or in the ambulance. If fluid is detected in the pleura and a bloody effusion is confirmed by aspiration, immediately a tube drainage is administered after previous sonographical localization of a suitable puncture site. The following computed tomography then shows possible further injuries, especially at the spine and the big vessels.

As a result of stab injuries, rib fractures with pike-like broken ribs penetrating into the lung or due to an explosion trauma with lung rupture a pneumothorax can occur. Patients with a tension pneumothorax develop rapidly increasing dyspnea and a shock. By ultrasound the diagnosis of a pneumothorax is established within a few seconds (Table 3.6) and the mandatory chest tube immediately can be administered. Supine chest-X-ray displays in only 50 % a traumatic pneumothorax. Many emergency physicians nowadays know about the high potentials of ultrasound to prove a pleural effusion or a pneumothorax with high sensitivity and specifitity.

A chest wall emphysema may prohibit the sonographical examination of the pleura (see chapter). A posttraumatic chest wall emphysema is often combined with a pneumothorax.

3.8 Diaphragm

The diaphragm is routinely displayed by ultrasound during a transabdominal examination of spleen and liver, but attracts little attention. Many studies in the last few years dealt with the diaphragm.

3.8.1 Normal Diaphragm

The muscular part of the diaphragm inserts in the region of the lower aperture of the thorax at the ribs, the sternum and the spine. The diaphragmatic muscle presents in the ultrasound image as a narrow three-layered structure, the real muscle in the middle hypoechoic. During respiration, especially during forced respiration, the thickening in the contraction is visible (Fig. 3.42). In particular in patients suffering from chronic obstructive lung disease the contraction-dependent thickening can be well recognized. The dome of the diaphragm consists of only a thin aponeurosis, sonographically often not to separate from the line of total reflection at the bottom of the lung. The diaphragmatic crura can be discovered on both sides of the upper abdominal aorta cranial of the origin of the celiac axis. In posterior longitudinal sections through liver or spleen the diaphragmatic crura can be found as strictly muscular organ along the spine. Normally the trigonum sternocostalis on both sides cannot be seen as well as the posterior hiatus pleuroperitonealis Bochdalek on both sides.

Normally the diaphragm bulges like a dome into the lower thorax. The flattening of the diaphragm in obstructive lung diseases can be detected in the individual case by ultrasound, not only radiologically. In severe emphysema the diaphragm may be bulged inversely.

In obese or COLD- patients often exist furrows of the diaphragm, impressing consecutively the liver. The diaphragmatic duplication is well detectable in the furrow at the liver surface. An "unsuccessful" flat transverse section through such a furrow can fake a focal liver lesion. Furrows at the spleen are usually only detectable in splenomegaly.

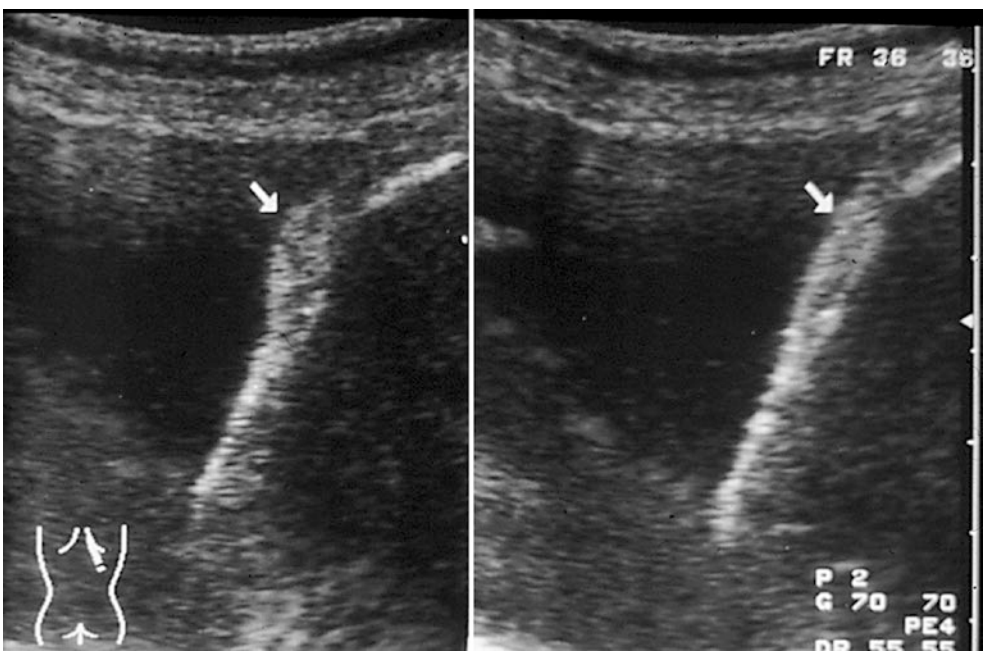

Fig. 3.42 Diaphragm with pleural effusion, the transition of the thicker muscular part into the aponeurosis in the dome is well to differentiate. In inspiration the muscle shortens and becomes thicker **a**, *arrow*) and slackens during expiration **b**, *arrow*)

3.8.2 Visualization

Because of the pleural recesses and the normal air-filled lung the diaphragm is only depictable through the abdomen, through the liver on the right side and through the spleen on the left side. A pleural effusion enables to demonstrate the complete diaphragm through the pleural cavity. Then the aponeurosis in the dome is also clearly to visualize. Under real time conditions the diaphragmatic motion can be observed and, if necessary, recorded in a short video clip.

3.8.3 Diaphragmatic Hernia

Congenital hernias are only exceptionally discovered in the adult. The most important findings are abdominal organs, located in the thorax, e.g. mostly gut, less common liver, spleen or kidneys. In newborns with severe respiratory insufficiency a congenital diaphragmatic hernia has to be considered. According to a S1-guideline (Guideline of the German Society for Pediatric Surgery 2010) the standard diagnostic procedure is a chest-X-ray. But gut in the chest can also be proven by means of ultrasound. Skilled ultrasound specialists are able to find a diaphragmatic hernia also in fetuses beyond the 18 week of gestation (Fig. 3.43).

The esophagogastric transition zone can be nearly regularly demonstrated as round multilayered formation. Axial sliding hernias are occasionally visible by ultrasound, but its evidence is of limited value. In reflux complaints endoscopy is mandatory to find a possible Barrett's esophagus.

3.8.4 Diaphragmatic Rupture

Ruptures of the diaphragm after severe abdominal or chest traumas occur in 1–3 %. Only in one quarter of the patients these ruptures are detected preoperatively (Rubikas 2001; Ozpolat 2009). The displacement of abdominal organs into the chest is the main sonographical symptom. The patients often have a hemorrhagic effusion. This ultrasound window improves the visualization of the diaphragm.

The margins of the rupture and the gap in the diaphragm are only depictable in individual cases (Fig. 3.44). A seeming gap in the diaphragm caused by an edge shadow artifact should not be misleading. The changing localization of the gap with changing the position of the transducer excludes an actual gap. These severe ill patients need a computed tomography to visualize preoperatively additional findings in the chest, abdomen, retroperitoneum and skeleton which are not demonstrable by ultrasound. In many of these cases the sonographic proof of liquid in the abdomen by FAST leads to an emergency operation. Then intraoperatively the diaphragmatic rupture turns out (Hansen and Muhl 1997).

Occasionally diaphragmatic ruptures are diagnosed years after the trauma, e.g. due to small rupture without severe symptoms. With time, the traumatic hernia canal widens and larger parts of the abdominal organs are displaced into the chest and cause respiratory insufficiency or perfusion disturbances at the herniated organs.

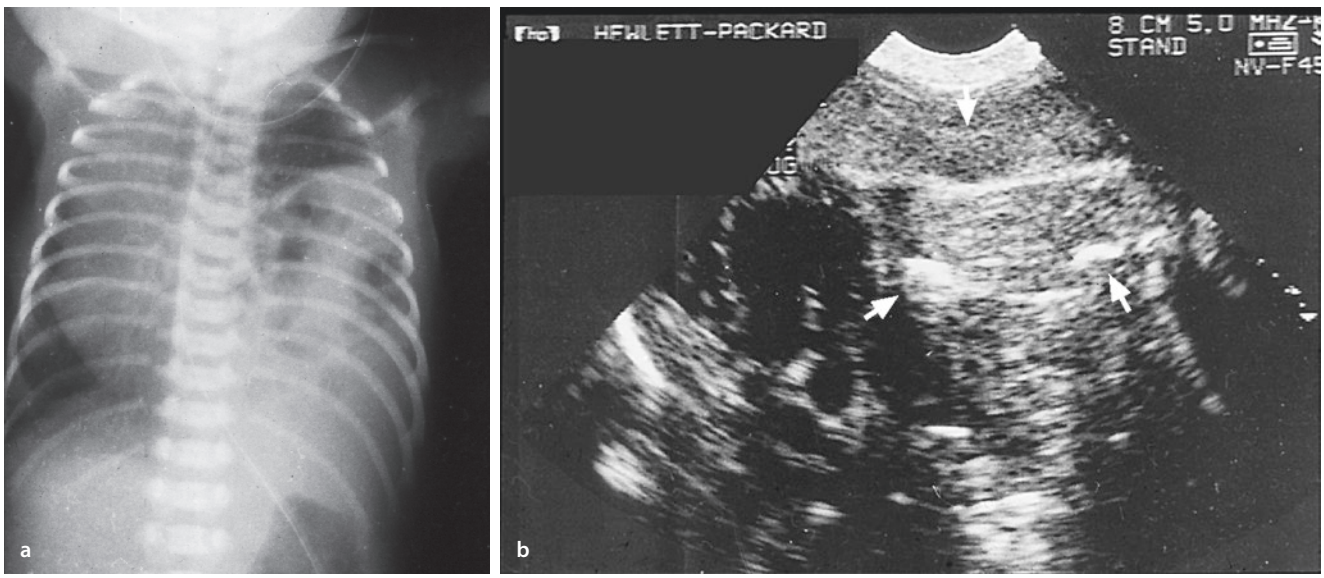

Fig. 3.43 **a** Chest-X-ray of an infant with gas-containing intestinal organs in the left hemithorax indicating a large congenital diaphragmatic hernia. **b** Typical ultrasound image of a congenital diaphragmatic left-sided hernia with the stomach beneath the clearly identifiable heart. Subxiphoidal cross section (Courtesy Prof. Manfred Teufel, Children's hospital, Klinikverbund Südwest, Bunsenstr.120, D 71032 Böblingen)

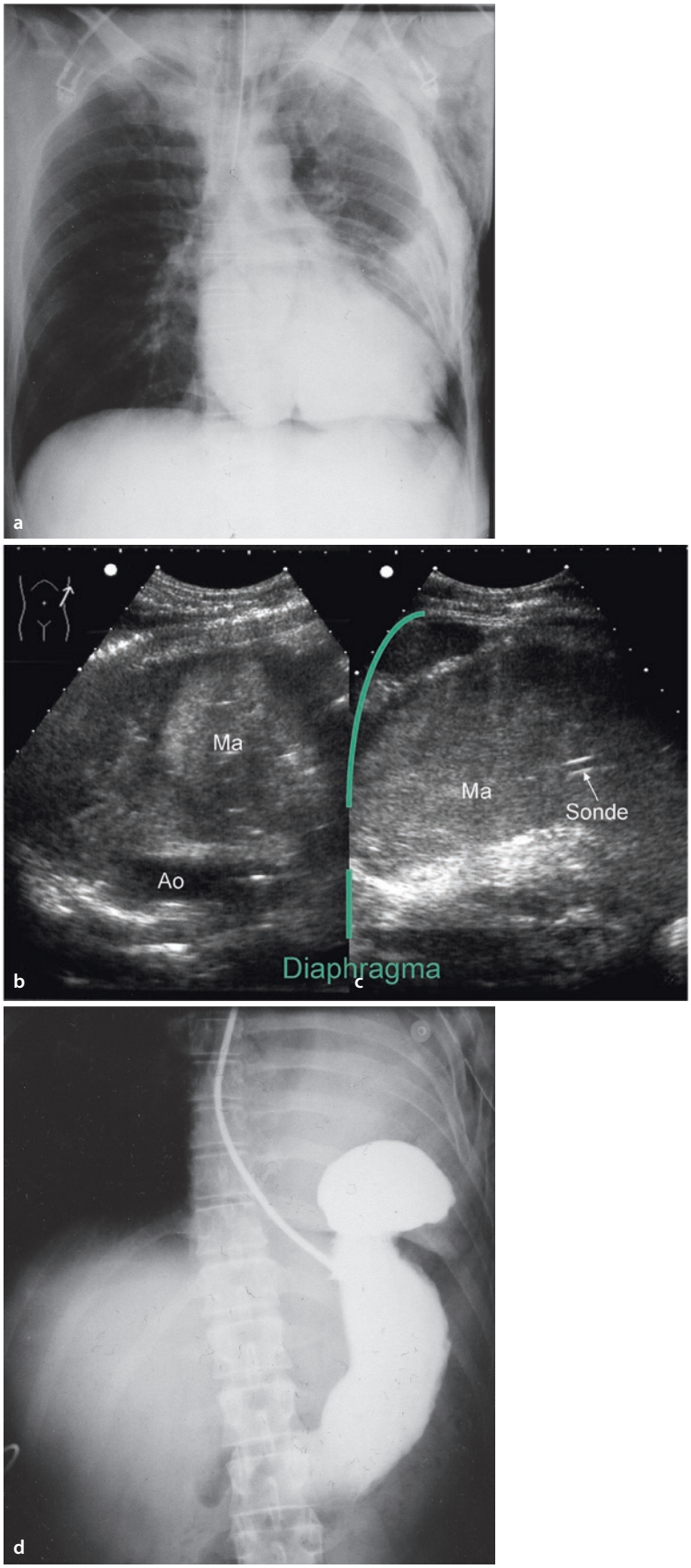

Fig. 3.44 Male patient after fall from a balcony in the fourth floor. Despite tube drainage due to hematothorax worsening oxygen saturation in mechanical ventilation. **a** In the chest-X-ray opacification infero-lateral on the left, therefore immediate ultrasound examination because of suspected not drained part of the hematothorax. **b** Sonographically in the chest a round inderterminable structure filled with echogenic fluid. **c** Below the diaphragm parts of the stomach with tube. In the dynamic examination the stomach can be tracked through the diaphragm into the chest (composite image) **d** confirmation of the diagnosis by filling the stomach with contrast via the tube. In CT the diaphragmatic rupture shown but misinterpreted

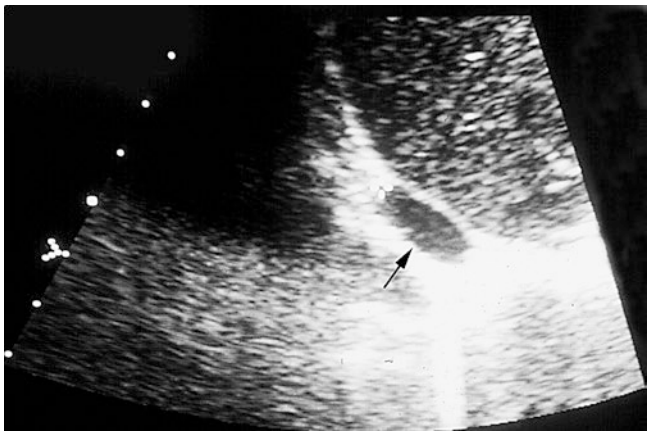

Fig. 3.45 Rare finding of a lipoma in the diaphragm. Smoothly demarcated tumor (*arrow*) presenting in similar fashion in CT showing fat density

3.8.5 Diaphragmatic Tumors

Primary tumors of the diaphragm are rare and the diagnosis is usually not made in early stages, at most as an incidental finding (Belaabidia et al. 2006) (Figs. 3.45 and 3.46). Also metastases in the diaphragm are rare, but may cause pain by infiltrating adjacent nerve plexuses (Figs. 3.47 and 3.48). Diaphragmatic metastases are typically enclosed in the diaphragm in contrary to pleural or – less common – peritoneal metastases placed on the diaphragm. Large pleural metastases may infiltrate into or break through the diaphragm (Figs. 3.47, 3.48, and 3.49). Pleural mesotheliomas may present an infiltration of the diaphragm as well as into the liver or spleen. By ultrasound not only the tumor infiltration is visible but also the tumor related fixation and paresis of the diaphragm.

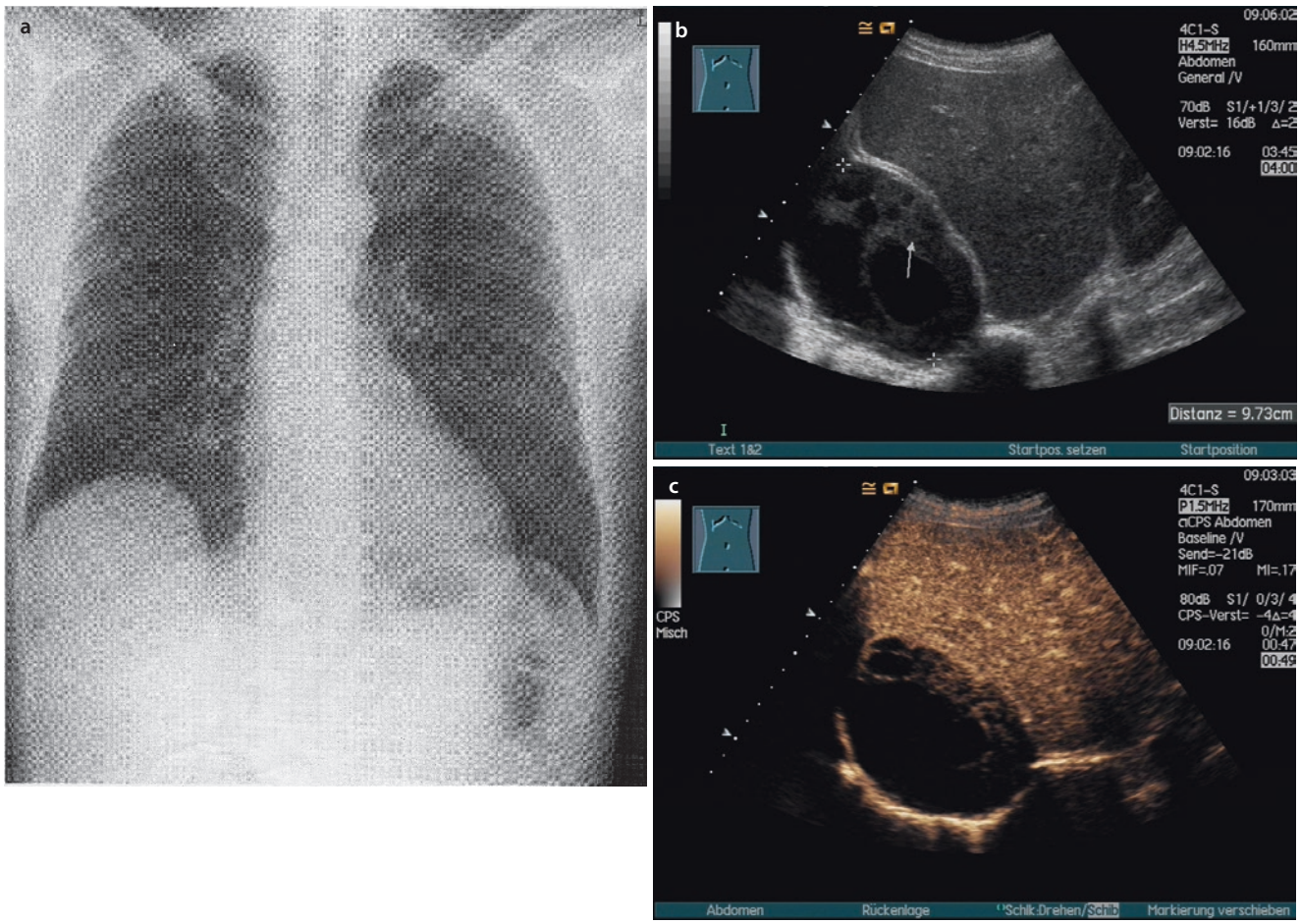

Fig. 3.46 **a** Smoothly demarcated opacification at the diaphragm in chest-X-ray, incidental finding. In retrospect this lesion was already guessed on a previous chest-X-ray 7 years earlier. **b** By ultrasound a cyst-like lesion with solid parts and septae seeming to originate from the diaphragmatic pleura. No calcifications, with color-Doppler no vessels detectable. **c** By CEUS in the bronchial-arterial phase the solid parts and the septae contrast enhancing, the vessels originating from the diaphragm. Thus a hydatid disease ruled out, the echinococcus titer negative. The tumor was removed by operation, histologically a solitary fibrous tumor of the diaphragm with low malignant tendency (Prof. Katenkamp, Jena, Germany), formerly known as hemangiopericytoma

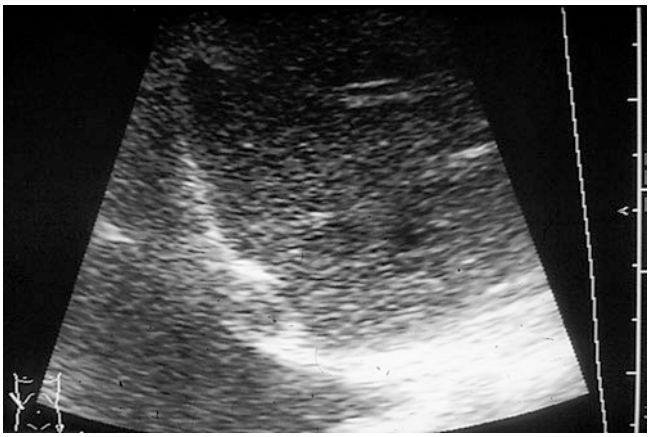

Fig. 3.47 In ultrasound a similar finding like in Fig. 3.40 in a patient with known lung cancer, so far no metastases. The lesion was found during a routine follow up examination. Computed tomography could not comprehend the lesion. By ultrasound guided puncture a metastasis of the known lung cancer confirmed

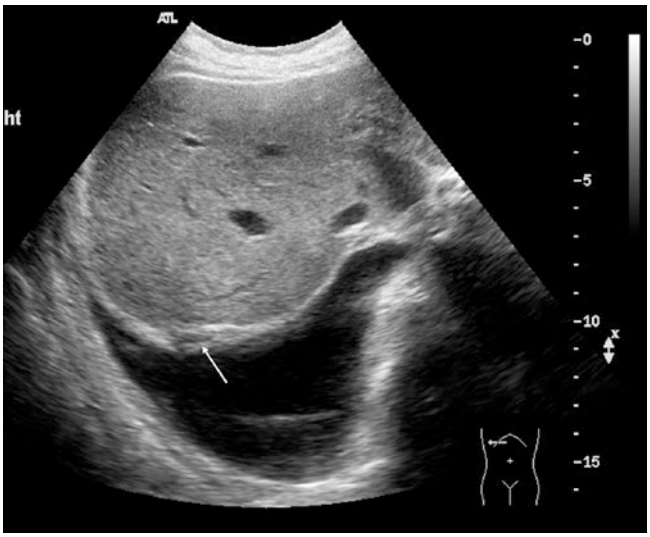

Fig. 3.48 Metastasis of a breast cancer in the diaphragm. Artificial echoes in a large pleural effusion

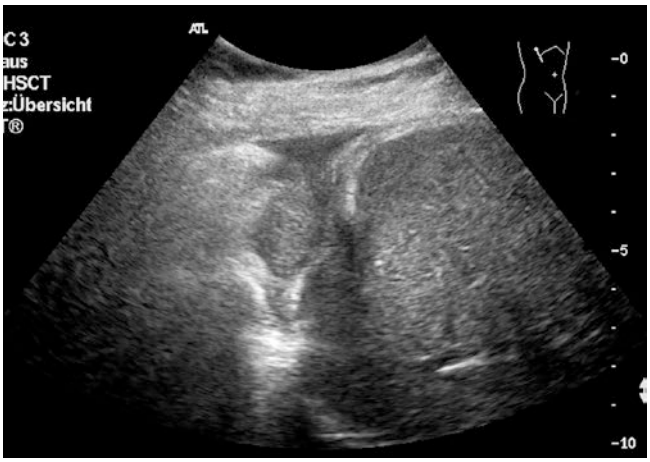

Fig. 3.49 Pleural metastasis with deep infiltration, deformation and destruction of the diaphragm. Pleural carcinosis with effusion. 19 years ago diagnosis of a breast cancer, 2 years ago diagnosis of a ovarian cancer

Table 3.10 Sonographically discernable causes of a diaphragmatic eventration

Unilateral	Abdominal cause	Large liver or spleen Large liver tumors Subphrenical capsulated liquid formations (seroma, bilioma, abscess) Unilateral paresis of the diaphragm
	Cause in the chest = seemingly eventration	Atypical inferior lung consolidation (pneumonia, atelectasis) Subpulmonary effusion, capsulated or loculated Inferior pulmonary, pleural or diaphragmatic tumor, possibly in combination with lung atelectasis
Bilateral	Abdominal cause	Abdominal obesity Ascites
	Cause in the chest = seemingly eventration	Bilateral subpulmonary effusion Bilateral inferior atelectasis

3.8.6 Diaphragmatic Eventration

Behind the radiological description of a diaphragmatic eventration different situations may be hidden. The diaphragm can in fact be dislocated due to paresis or due to displacement by giant organs or liquid collections. Unusual inferior lung consolidations or tumors or a subpulmonary effusion can pretend a diaphragmatic eventration. By ultrasound the situation can soon be clarified (Table 3.10).

3.8.7 Functional Examination

The real time ultrasound examination offers the best conditions for the functional examination of the diaphragm. A normal bilateral up-and-down-movement of the diaphragm with respiration, identical on both sides, is clearly visible. Pleural peels close to the chest wall cause a immobility of the parietal part of the diaphragm. A residual motion can be detected, ruling out a complete phrenical paresis. Old pleural lesions may be very discrete in the image, so that the dynamic examination with demonstration of the "sticking" is important. Short video clips are optimal for the documentation of the diaphragmatic motion. Using the time-motion-mode not only the movement of the diaphragm can be detained, but also the extent of the motion can approximately be measured. For this measurement the transducer, preferably a phased-array-transducer, is positioned on the abdomen in the medioclavicular or anterior axillary line, directed to the posterior part of the diaphragm, thus ensuring that the diaphragm in the B-mode is well detectable and during

Table 3.11 Benchmarks for diaphragmatic motion measured by ultrasound (according to Matamis 2013)

		Normal values	
		m	f
Motion (cm)	Normal breathing	1.8	1.6
	Forced breathing	7.0	5.7
	Sniffing	2.9	2.6
	Mechanical ventilation	1.8	
Contraction velocity (cm/s)	Slope	1.3	

respiration is moving towards the transducer. From the time-motion-curve different parameters can be picked out. The most frequently used parameter is the shift of the diaphragm in centimeter during normal and forced breathing. Other values are the contraction velocity of the diaphragm as well as the inspiration and breath cyclus time (Lloyd et al. 2006; Matamis 2013; Soilemezi et al. 2013). See Table 3.11.

A phrenical paresis is immediately noticed by missing or paradoxical diaphragmatic movement (Lloyd et al. 2006). Tumors at the neck or in the mediastinum causing the paresis are detectable by ultrasound. Diaphragmatic pareses acquired during birth can be recorded sonographically by the pediatrician (Urvoas et al. 1994). Normal chest_X-rays do not allow a reliable conclusion concerning the diaphragmatic function, but ultrasound (Epelman et al. 2005). Patients after stroke and residual dysphagia show a markedly reduced diaphragmatic motility, in normal breathing as well as under forced breathing and when coughing. The reduced motility correlates with lung function. In studies these date are already included in the rehabilitation planning (Jung 2014; Park 2014). A sonographical assessment after long-term mechanical ventilation in adults provides information about the function and the respiratory mechanical function can be estimated – sufficient experience and expertise provided (Dorffner et al. 1998). Measuring of the thickness of the diaphragmatic muscle yields also good results to estimate the diaphragmatic function after long term mechanical ventilation (Francis et al 2016, Noda et al 2016). This protects the patients against premature extubation and serves as basis for an additional forced training in the weaning phase.

References

Abu Arab W (2012) Solitary fibrous tumours of the pleura. Eur J Cardiothorac Surg 41:587–597

Balik M, Plasil P, Waldauf P et al (2006) Ultrasound estimation of volume of pleural fluid in mechanically ventilated patients. Intensive Care Med 32:318–321

Belaabidia B, Sellami S, Benelkhayat R et al (2006) Le léiomyosarcome diaphragmatique : revue de la littérature, à propos d'une observation. Cancer Radiother 10:137–141

Cardillo G, Lococo F, Carleo F, Martelli M (2012) Solitary fibrous tumors of the pleura. Curr Opin Pulm Med 18:339–346

Chian CF, Su WL, Soh LH et al (2004) Echogenic swirling pattern as a predictor of malignant pleural effusions in patients with malignancies. Chest 126:129–134

Colice GL, Cutis A, Deslauriers J et al (2000) Medical and surgical treatment of parapneumonic effusions, an evidencebased guideline. Chest 18:1158–1171

Collins JD, Burwell D, Furmanski S et al (1972) Minimal detectable pleural effusions. Radiology 105:51–53

Dorffner R, Eibenberger K, Youssefzadeh S et al (1998) The value of sonography in the intensive care unit for the diagnosis of diaphragmatic paralysis. RöFo 169:274–277

Eibenberger KL, Dock WI, Ammann ME et al (1994) Quantification of pleural effusion: sonography versus radiography. Radiology 191:681–684

Epelman M, Navarro OM, Daneman A, Miller SF (2005) Mmode sonography of diaphragmatic motion: description of technique and experience in 278 pediatric patients. Pediatr Radiol 35:661–667

Francis CA, Hoffer JA, Reynolds S (2016) Ultrasonographic evaluation of diaphragm thickness during mechanical ventilation in intensive care patients, Am J Crit Care 25:e1–8. doi: 10.4037/ajcc2016563

Gardelli G, Feletti F, Nanni A, Mughetti M, Piraccini A, Zompatori M (2012) Chest ultrasonography in the ICU. Respir Care 57:773–781

Garofalo G, Busso M, Perotto F, De Pascale A, Fava C (2006) Ultrasound diagnosis of pneumothorax. Radiol Med 111:516–525

Gehmacher O, Kopf A, Scheier M et al (1997) Ist eine Pleuritis sonographisch darstellbar? Ultraschall Med 18:214–219

Geiger D, Düll T, von Pawel J et al (2003) Thoraxwandinfiltration und Stichkanalinvasion beim malignen Pleuramesotheliom. Ultraschall Med 24:34, abstract

Goecke W, Schwerk WB (1990) Die RealTimeSonographie in der Diagnostik von Pleuraergüssen. In: Gebhardt J, Hackelöer BJ, Klinggräff GV, Seitz K (eds) Ultraschalldiagnostik, vol 89. Springer, Berlin

Görg C, Bert T, Görg K (2005) Contrastenhanced sonography for differential diagnosis of pleurisy and focal pleural lesions of unknown cause. Chest 128:3894–3899

Gryminski J, Krakówka P, Lypacewicz G (1976) The diagnosis of pleural effusion by ultrasonic and radiologic techniques. Chest 70:33–37

Hansen M, Muhl E (1997) Blunt thoracic trauma – therapeutic relevance of results of roentgen image, ultrasound and computerized tomography. Langenbecks Arch Chir Suppl Kongressbd 114:458–460

Heffner JE (2010) Management of the patient with a malignant pleural effusion. Semin Respir Crit Care Med 31:723–733

Herth F, Schmitteckert H, Schulz M, Becker H (2003) Diagnostik des Pneumothorax mittels transthorakalem Ultraschall – eine prospektive Untersuchung. Ultraschall Med 24(Suppl 1):30, abstract

Hooper C, Lee YCG, Maskell N et al. (2010) Investigation of a unilateral pleural effusion in adults: British Thoracic Society disease guidelines 2010, Thorax;65(Suppl 2):ii4eii17. doi: 10.1136/thx.2010.136978

Hsu CW, Sun SF (2014) Latrogenic pneumothorax related to mechanical ventilation. World J Crit Care Med 3:8–14

Jung KJ, JY Park, DW Hwang et al. (2014) Ultrasonographic Diaphragmatic Motion Analysis and Its Correlation With Pulmonary Function in Hemiplegic Stroke Patients, Ann Rehabil Med 38(1):29–37

Layer G, Schmitteckert H, Steudel A et al (1999) MRT, CT und Sonographie in der präoperativen Beurteilung der Primärtumorausdehnung beim malignen Pleuramesotheliom. Fortschr Roentgenstr 170:365–370

Lehnert M, Taeger D, Wiethege Tet al., Update zur Epidemiologie des Pleuramesothelioms in Deutschland, IPA – Institut für Prävention und Arbeitsmedizin der Deutschen Gesetzlichen Unfallversicherung,

Institut der Ruhr-Universität Bochum, Deutsche Gesetzliche Unfallversicherung, 2009
Lichtenstein DA, Menu Y (1995) A bedside ultrasound sign ruling out pneumothorax in the critically ill: lung sliding. Chest 108:345–348
Lichtenstein DA, Mezière GA (2008) Relevance of lung ultrasound in the diagnosis of acute respiratory failure. The BLUEprotocol. Chest 134:117–125
Lichtenstein DA, Mezière GA, Bidermann P (1997) The comet tail artifact: an ultrasound sign of alveolarinterstitial syndrome. Am J Respir Crit Care Med 156:1640–1646
Lichtenstein DA, Mezière GA, Bidermann P, Gepner A (2000) The »lung point«: an ultrasound sign specific to pneumothorax. Intensive Care Med 26:1434–1440
Light RW (2006) Parapneumonic effusions and empyema. Proc Am Thorac Soc 3:75–80
Lloyd T, Tang YM, Benson MD, King S (2006) Diaphragmatic paralysis: the use of Mmode ultrasound for diagnosis in adults. Spinal Cord 44:505–508
Loddenkemper R (1994) Pleuraerkrankungen. In: Ferlinz R (Hrsg) Pneumologie in Praxis und Klinik. Thieme, Stuttgart, S 712–717
Loff S, Zwerchfellhernie, Zwerchfelldefekt (Congenital Diaphragmatic Hernia [CDH]), S1-Leitlinie der Deutschen Gesellschaft für Kinderchirurgie, AWMF-Register Nr. 006/087, 2016
Matamis D, Soilemezi E, Tsagourias M et al. (2013) Sonographic evaluation of the diaphragm in critically ill patients. Technique and clinical applications, Intensive Care Med 39:801–810. doi: 10.1007/s00134-013-2823-1
Mathis G (1997) Thoraxsonogrphy – Part I: Chest wall and pleura. Ultrasound Med Biol 23:1131–1139
Neumann V, Löseke S, Nowak D et al. (2013) Malignes Pleuramesotheliom. Inzidenz, Ätiologie, Diagnostik, Therapie und Arbeitsmedizin, Deutsches Ärzteblatt 110: 319–326
Noda Y, Sekiguchi K, Kohara N et al. (2016) Sonographic diaphragm thickness correlates with compound muscle action potentialamplitude and forced vital capacity, MuscleNerve 53:522–527. Doi: 10.1002/mus.24902
Ozpolat B1, Kaya O, Yazkan R, Osmanoğlu G (2009) Diaphragmatic injuries: a surgical challenge. Report of forty-one cases,Thorac Cardiovasc Surg 57(6):358–62. doi: 10.1055/s-0029-1185579
Park GY, Kim SR, Kim YW et al. (2014) Decreased diaphragm excursion in stroke patients with dysphagia as assessed by M- mode sonography, Arch Phys Med Rehabil. pii: S0003-9993(14)01033-8. doi: 10.1016/j.apmr.2014.08.019.
Reißig A, Kroegel C (2005) Accuracy of transthoracic sonography in excluding postinterventional pneumothorax and hydropneumothorax. Comparison to chest radiography. Eur J Radiol 53:463–470
Reuß J (2010) Sonography of the pleura. Sonography of the pleura. Ultraschall Med 31:8–22
Reuß J, Blank W, Drews U et al (2002) Sonographischanatomischer Vergleich des Aufbaus der inneren Thoraxwand zwischen Interkostalmuskulatur und Pleuraspalt. Ultraschall Med 23(Suppl 1):70, abstract
Roch A, Bojan M, Michelet P et al (2005) Usefulness of ultrasonography in predicting pleural effusions >500 ml in patients receiving mechanical ventilation. Chest 127:224–232
Rubikas R (2001) Diaphragmatic injuries. Eur J Cardiothorac Surg 20:53–57
Sartori S, Tombesi P, Trevisani L, Nielsen I, Tassinari D, Abbasciano V (2007) Accuracy of transthoracic sonography in detection of pneumothorax after sonographically guided lung biopsy: prospective comparison with chest radiography. AJR Am J Roentgenol 188:37–41
Soilemezi E, Tsagourias M, Talias MA, Soteriades ES, Makrakis V, Zakynthinos E, Matamis D (2013) Sonographic assessment of changes in diaphragmatic kinetics induced by inspiratory resistive loading. Respirology 18:468–473
Soldati G, Testa A, Sher S, Pignataro G, La Sala M, Silveri NG (2008) Occult traumatic pneumothorax – diagnostic accuracy of lung ultrasonography in the emergency department. Chest 133:204–211
Tacsi S, Burghard A, Schäfer H, Rabe C, Ewig S, Lüderitzt B (2005) Longterm outcome of intrapleural fibrinolytic therapy via smallbore catheter drainage in the management of complicated parapneumonic effusion and a empyemaa case series. Med Klin (Munich) 100:181–185
Travis WD (2010) Sarcomatoid neoplasms of the lung and pleura, Arch Pathol Lab Med 134(11):1645–1658. doi: 10.1043/2010-0086-RAR.1
Urvoas E, Pariente D, Fausser C et al (1994) Diaphragmatic paralysis in children: diagnosis by TMmode ultrasound. Pediatr Radiol 24:564–568
Vignon P, Chastagner C, Berkane V et al (2005) Quantitative assessment of pleural effusion in critically ill patients by means of ultrasonography. Crit Care Med 33:1757–1763
Volpicelli G (2011) Sonographic diagnosis of pneumothorax, Intensive Care Med 37(2):224–232. doi: 10.1007/s00134-010-2079-y
Volpicelli G et al (2012) International evidencebased recommendations for pointofcare lung ultrasound. Intensive Care Med 38:577–591
Wilkerson RG, Stone MB (2010) Sensitivity of bedside ultrasound and supine anteroposterior chest radiographs for the identification of pneumothorax after blunt trauma. Acad Emerg Med 17:11–17
Yarmus L, FellerKopman D (2012) Pneumothorax in the critically ill patient. Chest 141:1098–1105

Interstitial Syndrome

Giovanni Volpicelli and Luna Gargani

G. Mathis (ed.), *Chest Sonography*, DOI 10.1007/978-3-319-44072-9_4

4

4.1 General Considerations

It is standard textbook knowledge that «because ultrasound energy is rapidly dissipated by air, ultrasound imaging is not useful for the evaluation of the pulmonary parenchyma» (Manaker and Weinberger 2008). The concept that ultrasound cannot be employed for evaluating the lung is linked to the presence of air, which determines a very high acoustic mismatch with the surrounding tissues, causing a complete reflection of the ultrasound beam, which prevents the creation of real imaging of the pulmonary parenchyma. In a normally aerated lung, the only detectable structure is the pleura, visualized as a hyperechoic horizontal line. Even this image is an artefact due to a reverberation phenomenon at the interface between alveolar air and the soft tissues of the thoracic wall. Below the pleural line, the artefact image of the lung moves synchronously with respiration against the chest wall. In addition, some hyperechoic, horizontal lines arising at regular intervals from the pleural line can be seen: the A-lines (Fig. 4.1). However, even if the corresponding lung area is imaged only as artifacts at ultrasound, these give many important clinical information (Volpicelli 2013).

When combined with a respiratory movement, the reverberation artefacts represent a sign of normal or excessive content of air in the alveolar spaces. When the air content decreases and lung density increases due to the presence in the lung of exudate, transudate, collagen, blood, hyper cellularity, the acoustic mismatch between the lung and the surrounding tissues is lowered, and the ultrasound beam will be partly reflected at deeper zones and repeatedly. This phenomenon creates on the screen some vertical reverberation hyperechic artefacts, known as B-lines, formed by multiple short horizontal lines that are repeated in a vertical tight sequence (Fig. 4.2). B-lines belong to the family of the comet-tail artefacts, very well known in abdominal ultrasound (Ziskin et al. 1982). In some studies, published before an experts agreement on nomenclature that was obtained in the recent consensus conference on lung ultrasound (LUS), B-lines have also been addressed as comet-tail artifacts or ultrasound lung comets (Volpicelli et al. 2012). B-lines are defined as discrete laser-like vertical hyperechoic reverberation artifacts that arise from the pleural line, extend to the bottom of the screen without fading, and move synchronously with lung sliding. Multiple B-lines are considered the sonographic sign of lung interstitial syndrome, and their number increases along with decreasing air content and increase in lung density (Volpicelli et al. 2012).

Therefore, although air limits the reconstruction of a real image of the normal lung, the alteration in the balance between air and fluids of the diseased lung significantly modifies the normal ultrasound pattern. This can happen both in case of deflation of the lung with maintenance of a constant weight, but also when the weight of the lung rises for the increase in fluids, cells, connective tissue or blood content. In other words, whether the cause is a simple deflation or an increase in fluids and cellularity of the lung parenchyma, ultrasound is highly sensible to variations of the organ density as deduced by studies on phantoms, animal models and humans (Volpicelli 2013).

Thus, the acoustic limitations of ultrasound in the assessment of an air-rich organ such as the lung can paradoxically become a diagnostic advantage. The artifacts created by the mismatch between air and tissues in the lung are easy to detect and correspond to their quantitative balance.

However, the diagnostic approach based on LUS can vary according to different settings and clinical situations, following the main principle of what is today known as "point-of-care ultrasound" (Moore and Copel 2011). On occasion, the best efficacy of the method is obtained by a clinically driven,

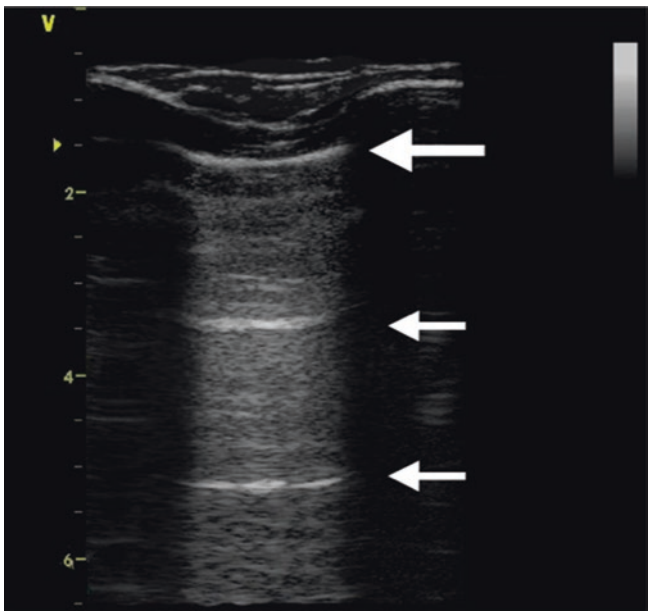

Fig. 4.1 The white arrows indicate the linear echoic images corresponding to the pleural line (*large arrow*) and the A-lines (*small arrows*)

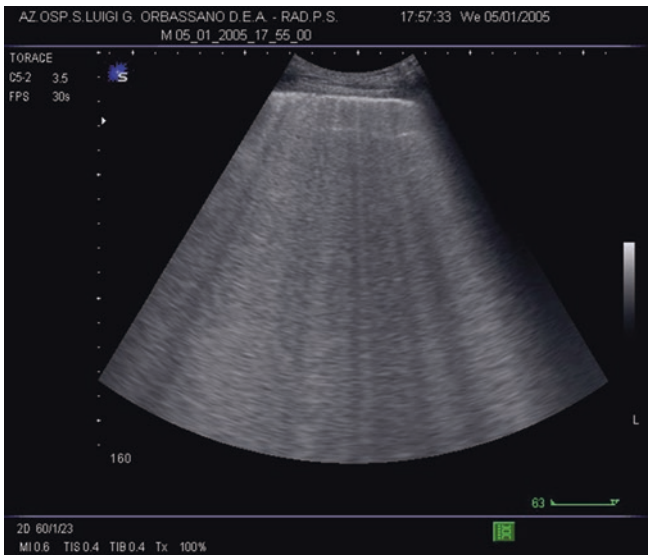

Fig. 4.2 An ultrasound lung scan showing multiple B-lines, in a case of acute pulmonary edema

focused assessment. If properly driven and correctly interpreted, even signs that have low significance in the general population become highly accurate for diagnosing specific pulmonary conditions (Gargani and Volpicelli 2014). The correlation with the specific setting and patient's symptoms of presentation, the clinical history, but also the evolution of the clinical situation and the corresponding change in the ultrasound pattern during the time course of our observation and treatment, may be crucial for a correct interpretation.

4.2 Interstitial Syndrome

The interstitial syndrome is a condition where alveolar air is impaired due to increase of fluids in the interstitium, but some lung aeration is still preserved as opposed to a condition of complete consolidation of the lung. The potential of LUS for the diagnosis of the interstitial syndrome has been mainly shown in studies on critically ill patients and in patients attending the emergency department (Lichtenstein and Meziere 2008; Pivetta et al. 2015). Also, some other studies showed the usefulness in chronic fibrosis and in chronic renal failure patients submitted to dyalisis (Mallamaci et al. 2010; Reissig and Kroegel 2003).

The main principle of the ultrasound diagnosis of interstitial syndrome is based on the recognition of B-lines, a rough and very basic count in the single scan and the count and distribution of positive scans. At least three B-lines visualized in a longitudinal, view define a positive scan. The bilateral distribution of multiple positive scans in at least two different chest areas per side, generally define the condition of diffuse interstitial syndrome. Isolated positive scans, or more than one but not bilateral, are diagnostic of a focal interstitial syndrome (Volpicelli et al. 2012).

Even if detection of the B-line pattern cannot differentiate between cardiogenic edema, ARDS and pulmonary fibrosis, this simple bedside technique has immediate effect in the real-time diagnostic process of the critically ill and dyspneic patients. The use of a simplified LUS protocol was more accurate than the conventional tools in the first 2 h initial diagnoses in acute respiratory failure, showing a better immediate effect and yielding correct prompt diagnoses in 90.5% of patients (Lichtenstein and Meziere 2008).

In the evaluation of patients with acute respiratory failure, the B-line pattern allows for a differentiation between a cardiogenic and a respiratory origin of the disorder, because exacerbation of COPD, pulmonary embolism, pneumonia, pneumothorax yield a non-interstitial ultrasound pattern (Gargani et al. 2008; Zanobetti et al. 2011). In selected patients with acute decompensated heart failure or end stage renal failure, B-lines represent a sign of extravascular lung water, which allows monitoring of pulmonary congestion by simply observing its clearance at repeated LUS examinations (Volpicelli et al. 2008). In ARDS patients submitted to invasive ventilation with positive pressure, sonographic evaluation for B-lines allows monitoring of re-aeration and can be used to guide therapeutic maneuvers (Bouhemad et al. 2011).

4.3 Technique

In a patient with acute dyspnea, if cardiogenic pulmonary edema is in the differential diagnosis, LUS will be used to examine the anterior and lateral chest to detect the diffuse signs of interstitial and alveolar edema, which usually respect three highly specific features: they are correlated with the severity of the respiratory failure, follow a regular and symmetric spatial distribution, and usually progress from the lateral inferior (dependent zones) to the anterior upper chest areas. The scanning technique that should be employed in the emergency setting is the eight-zone examination, consisting of scanning four chest areas per side: areas 1 and 2 denote the upper anterior and lower anterior chest, while areas 3 and 4 denote the upper lateral and basal lateral chest, respectively (Fig. 4.3) (Volpicelli et al. 2006). In the critically ill patient with acute respiratory failure, a more rapid anterior two-region scan may be even sufficient to rule out the interstitial syndrome due to cardiogenic acute pulmonary edema (Lichtenstein and Meziere 2008). However, this focused anterior scanning, while still highly accurate in acute situations in the critically ill, may not be sufficient in patients who are not so severely dyspnoic, since presence of B-lines on the anterior chest usually denotes a more severe degree of pulmonary congestion in case of heart failure. This interpretation is an example of adaptation of the LUS technique and signs to the specific setting and clinical condition.

In the setting of chronic patients, with less time pressure and more borderline cases, the scanning technique should always be more comprehensive. It can include the anterior,

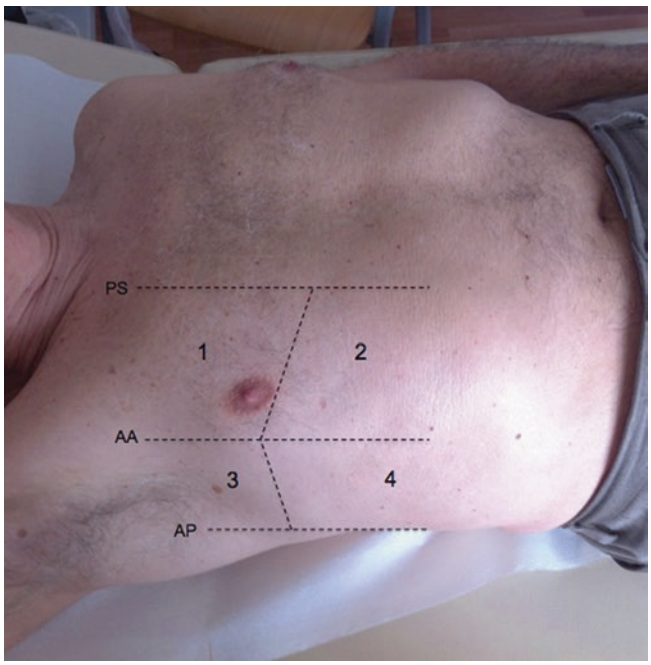

Fig. 4.3 The eight zones examination consisting of scanning four chest areas per side: the upper *(1)* and lower *(2)* anterior, the upper *(3)* and basal *(4)* lateral. *PS* parasternal line, *AA* anterior axillary line, *AP* posterior axillary line

lateral, but also the dorsal chest. Different approaches have been proposed: a detailed scanning scheme has been used in many studies on patients with heart failure, on dialysis, and with pulmonary fibrosis, focused on the assessment of the consistency and distribution of B-lines. This comprehensive approach is particularly useful for quantifying the extent of the LUS abnormalities, and for assessing intra-patient variations after therapeutic interventions, including dialysis. Ultrasound scanning of the anterior and lateral chest is obtained on the right and left hemithorax, from the second to the fourth (on the right side to the fifth) intercostal spaces, and from the parasternal line to the axillary line. The posterior chest is scanned along the paravertebral line, scapularis line and posterior axillary line. The sum of the B-lines found on each scanning site yields a score denoting the extent of the pulmonary interstitial syndrome (see below for the techniques of quantifications).

In the case of limited time, even in a chronic setting the examination can be more focused and should be clinically driven. In patients with heart failure, it is important to scan also the dependent zones, i.e., lung posterior basis if we are evaluating an out-patient, or along the posterior and mid-axillary lines if we are scanning an in-patient who has been lying down for many hours. In patients with interstitial lung disease such as pulmonary fibrosis, it is mandatory to scan the posterior chest, because the disease generally starts in this region of the lung (Gargani and Volpicelli 2014).

The patient can be scanned in any decubitus, since lung abnormality distribution does not change so rapidly that significant information would be missed (apart from pleural effusion) just by changing the patient's position. Moreover, in the case of pulmonary congestion, even if the position of B-lines changes, the overall distribution tends to remain the same, without clinically relevant differences. The supine position is ideal for scanning the anterior chest, whereas the lateral chest may be examined in the semi-supine position (on the left decubitus to scan the right axillary lines, and on the right decubitus to scan the left axillary lines). The optimum position for scanning the posterior chest is with the patient sitting on the bed, his/her back turned to the operator. Indeed, it is possible also to scan patients while they are standing, sitting or lying flat, without significant differences in results. The only real limitation is when LUS needs to be extended to the dorsal chest of a patient lying down who is intubated in the intensive care unit, or a patient who is unconscious and cannot be moved. In these situations, using small probes that may be better placed between the bed and the patient may allow the best result (Fig. 4.4).

Although the number of B-lines may be slightly different when using different probes in a specific chest site, the overall clinical picture does not change by changing the transducer. The possibility of easily assessing B-lines with any kind of transducer is one of the advantages of this technique, so no one should give up on scanning a patient just because the "ideal" probe is not available. Portable machines and pocket-sized devices have also been proposed for assessing B-lines. There is no need for a second harmonic or Doppler imaging mode, so even very old ultrasound machines can be employed. Normally the focus should be positioned at the pleural line level.

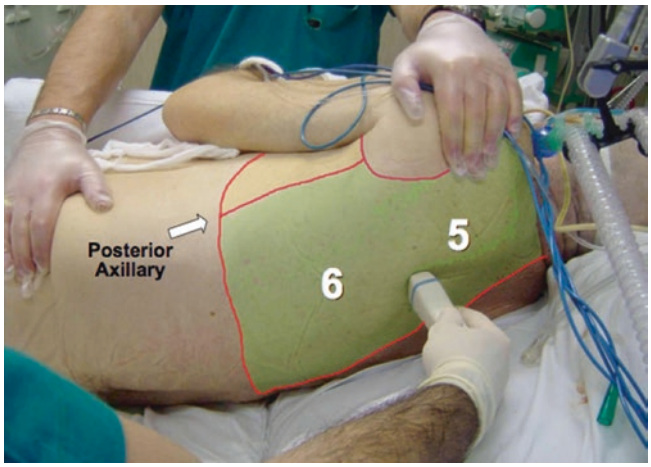

Fig. 4.4 The use of small probes may be helpful in examining the dorsal scans in bedridden patients

4.4 Interpretation of the Sonographic Interstitial Syndrome

Interpretation of LUS images is usually not very challenging. We must keep in mind that LUS is more affected by lack of specificity than lack of sensitivity. A LUS pattern showing multiple B-lines may be not enough to establish a specific diagnosis, since it can be linked to different pathologic conditions. Indeed, this limitation in specificity is a common feature of several diagnostic tools that we routinely interpret in daily clinical practice, from physical examination to EKG, from chest X-ray to more sophisticated instrumental findings. The power of these tools resides in the interpretation of signs when combined with each other at bedside, together with a consideration of the overall clinical picture. When all patient characteristics are taken into account, including history, symptoms, physical examination, setting, comorbidities, medications, etc., specificity can increase significantly. For example, in a patient with systemic sclerosis and without any known left heart conditions, presence of multiple B-lines is more probably related to pulmonary fibrosis than to extravascular lung water. On the other hand, presence of multiple diffuse bilateral B-lines in a patient with reduced cardiac function is more likely to be related to extravascular lung water than to fibrosis.

Distribution of B-lines and pleural line characteristics are also crucial to increasing the specificity of LUS. B-lines due to cardiogenic pulmonary edema are usually bilateral, start appearing in the dependent zones and usually diffusing or recovering symmetrically. B-lines due to pulmonary fibrosis generally start at the posterior lung basis, and are often associated with irregularity of the pleural line and subpleural small consolidations. In contrast to pulmonary edema due to congestion or overhydration, acute lung injury/ARDS shows

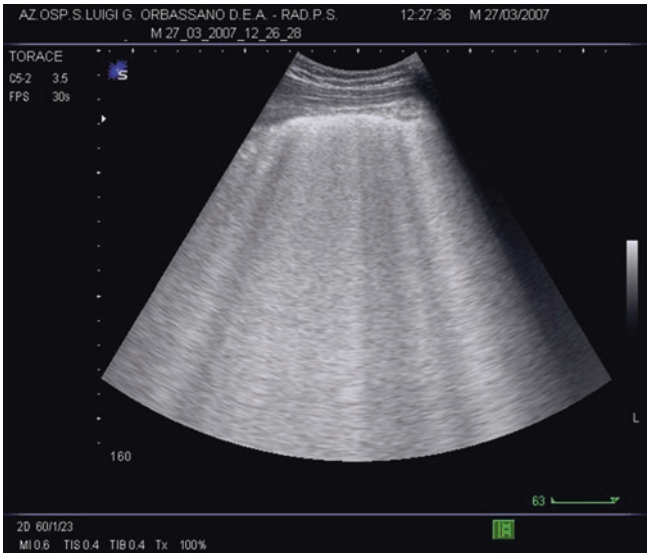

Fig. 4.5 This lung scan shows highly fragmented pleural line and intense hyperlucent multiple B-lines alternating with spared areas. This pattern is typical of ARDS

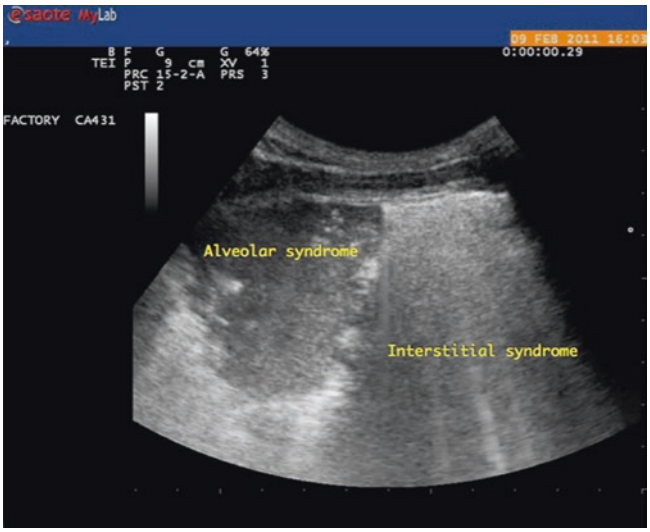

Fig. 4.6 This lung scan shows a focal *interstitial syndrome* around the pulmonary consolidation (*alveolar syndrome*), in a case of pneumonia

a inhomogeneous and irregular pattern, featuring many subpleural consolidations, highly fragmented pleural line and intense hyperlucent multiple B-lines alternating with spared areas (Fig. 4.5). This irregular distribution of B-lines contrasts with that observed in cardiogenic pulmonary edema, where B-lines are usually detected in more homogenous distribution, which is gravity-related, while it is quite rare when visualizing subpleural consolidations.

Dynamic response to therapy can also be useful for increasing the accuracy of LUS. In the case of multiple bilateral B-lines that are dissolved in days during ordinary treatment, or even in a few hours by an acute diuretic load, the cardiogenic or volume overload origin of B-lines is strongly suggested (Volpicelli et al. 2008). Similarly, in end-stage renal disease patients, B-lines decreasing or even disappearing after either a hemodialysis or peritoneal dialysis session, indicate pulmonary congestion due to overload (Mallamaci et al. 2010).

Additional information deriving from a bedside focused ultrasound evaluation of other organs may also be helpful. This approach has been recently described in patients with undifferentiated hypotension, where the integrated point-of-care multiorgan ultrasonography of the heart, inferior vena cava, lungs and abdomen significantly agreed with a final clinical diagnosis obtained by retrospective chart review (Volpicelli et al. 2013).

A controversial issue is quantification of B-lines. In critically ill patients the assessment can be qualitative, since the ultrasound finding of acute conditions is usually well defined and clear. For instance, in a critically ill patient with acute respiratory failure, if the underlying condition is cardiogenic pulmonary edema, the sonographic appearance of the lungs will be striking, with multiple diffuse bilateral B-lines to convey a picture of "white sonographic lung". In these patients, B-lines can also be found in the least dependent zones, i.e. the anterior chest. On the contrary, finding a limited number of B-lines (even if bilateral) in a very symptomatic respiratory failure patient should lead to excluding the diagnosis of a cardiogenic origin of the actual condition.

In non-critical patients, a more careful assessment and quantification of B-lines may be useful, especially for the follow-up of a chronic condition. A semi-quantification of B-lines has been proposed and subsequently used in many papers from different research groups. This quantification is made possible by counting all B-lines in a specific scanning site. Zero is defined as a complete absence of B-lines in the investigated area, whereas when using a cardiac probe the full white screen in a single scanning site is considered as corresponding to ten B-lines (Gargani and Volpicelli 2014). However, B-lines cannot always be easily enumerated, especially if they are many, since they often tend to be confluent. A helpful rule is to consider the percentage of the scanning site occupied by B-lines (i.e. the percentage of white screen compared to black screen below the pleural line) and then divide it by ten. For clinical purposes, the final number of B-lines can then be categorized ranging from mild to severe degrees, similar to what is done for most echocardiographic parameters (Gargani and Volpicelli 2014). This counting approach can be imprecise when considering single scanning sites, but nevertheless provides a reliable overall LUS picture, allowing more accurate monitoring of patients, both in acute conditions – i.e., rapid changes after diuretic therapy or dialysis but also in stable outpatients. Moreover, this approach has shown good intraobserver and interobserver variability, around 4–5 % in many studies and never superior to 7 %.

A focal interstitial syndrome can sometimes be the "peripheral alarm" of a more medial pathological condition, for example in the case of peri-lesional interstitial edema, due to either inflammation or impaired lymphatic drainage (Fig. 4.6).

4.5 Limitations

It must be emphasized that LUS does not rule out pulmonary abnormalities that do not reach the pleura. The pulmonary interstitial syndrome from some specific etiologies sometimes may save the subpleural space, which will prevent its visualization by sonography. However, these are only rare conditions particularly in emergency situations. Indeed, most of the lung conditions observed in the critically ill and emergency situations are characterized by lesions that reach the lung surface. The analysis of the lung anatomy may help to understand the reason. The secondary pulmonary lobule is the fundamental unit of the lung structure. In different pulmonary regions the lobule is variably surrounded by the interlobular septa, which are connective structures that envelope the lung like a network and contain pulmonary veins and lymphatics. Secondary pulmonary lobules in the periphery are relatively large and are marginated by interlobular septa that are thicker than in other parts of the lung. Thus, the periphery of the lung is highly representative of systemic diseases and conditions, and alterations of the most peripheral septa can be studied by LUS (Volpicelli 2013).

Conditions that alter the regular interaction between the emitting surface of the probe and the chest wall, may limit the ultrasound evaluation of the interstitial syndrome. Very obese patients are occasionally difficult to be studied. Combination with other pulmonary conditions, like pneumothorax or large pleural effusion, may make difficult or impossible the evaluation of the interstitial syndrome. Bandages, wounds and other hindrances may sometimes prevent the ultrasound study.

References

Bouhemad B, Brisson H, Le-Guen M, Arbelot C, Lu Q, Rouby JJ (2011) Bedside ultrasound assessment of positive end-expiratory pressure-induced lung recruitment. Am J Respir Crit Care Med 183(3):341–347

Gargani L, Volpicelli G (2014) How I do it: lung ultrasound. Cardiovasc Ultrasound 12:25

Gargani L, Frassi F, Soldati G, Tesorio P, Gheorghiade M, Picano E (2008) Ultrasound lung comets for the differential diagnosis of acute cardiogenic dyspnoea: a comparison with natriuretic peptides. Eur J Heart Fail 10(1):70–77

Lichtenstein DA, Meziere GA (2008) Relevance of lung ultrasound in the diagnosis of acute respiratory failure: the BLUE protocol. Chest 134(1):117–125

Mallamaci F, Benedetto FA, Tripepi R, Rastelli S, Castellino P, Tripepi G, Picano E, Zoccali C (2010) Detection of pulmonary congestion by chest ultrasound in dialysis patients. JACC Cardiovasc Imaging 3(6):586–594

Manaker S, Weinberger S (2008) Diagnostic procedures in respiratory diseases. In: Fauci AS, Kasper DL, Braunwald E, Hauser SL, Longo DL, Jameson JL, Loscalzo J (eds) Harrison's principles of internal medicine. McGraw-Hill Medical, New York

Moore CL, Copel JA (2011) Point-of-care ultrasonography. N Engl J Med 364(8):749–757

Pivetta E, Goffi A, Lupia E, Tizzani M, Porrino G, Ferreri E, Volpicelli G, Balzaretti P, Banderali A, Iacobucci A, Locatelli S, Casoli G, Stone MB, Maule MM, Baldi I, Merletti F, Cibinel G (2015) Lung ultrasound-implemented diagnosis of acute decompensated heart failure in the Emergency Department – A SIMEU multicenter study. Chest 148(1):202–210. doi:10.1378/chest.14-2608

Reissig A, Kroegel C (2003) Transthoracic sonography of diffuse parenchymal lung disease: the role of comet tail artifacts. J Ultrasound Med 22(2):173–180

Volpicelli G (2013) Lung sonography. J Ultrasound Med 32(1):165–171

Volpicelli G, Mussa A, Garofalo G, Cardinale L, Casoli G, Perotto F, Fava C, Frascisco M (2006) Bedside lung ultrasound in the assessment of alveolar-interstitial syndrome. Am J Emerg Med 24(6):689–696

Volpicelli G, Caramello V, Cardinale L, Mussa A, Bar F, Frascisco MF (2008) Bedside ultrasound of the lung for the monitoring of acute decompensated heart failure. Am J Emerg Med 26(5):585–591

Volpicelli G, Elbarbary M, Blaivas M, Lichtenstein DA, Mathis G, Kirkpatrick AW, Melniker L, Gargani L, Noble VE, Via G, Dean A, Tsung JW, Soldati G, Copetti R, Bouhemad B, Reissig A, Agricola E, Rouby JJ, Arbelot C, Liteplo A, Sargsyan A, Silva F, Hoppmann R, Breitkreutz R, Seibel A, Neri L, Storti E, Petrovic T, International Liaison Committee on Lung Ultrasound for International Consensus Conference on Lung Ultrasound (2012) International evidence-based recommendations for point-of-care lung ultrasound. Intensive Care Med 38(4):577–591

Volpicelli G, Lamorte A, Tullio M, Cardinale L, Giraudo M, Stefanone V, Boero E, Nazerian P, Pozzi R, Frascisco MF (2013) Point-of-care multiorgan ultrasonography for the evaluation of undifferentiated hypotension in the emergency department. Intensive Care Med 39(7):1290–1298

Zanobetti M, Poggioni C, Pini R (2011) Can chest ultrasonography replace standard chest radiography for evaluation of acute dyspnea in the ED? Chest 139(5):1140–1147

Ziskin MC, Thickman DI, Goldenberg NJ, Lapayowker MS, Becker JM (1982) The comet tail artifact. J Ultrasound Med 1(1):1–7

Lung Consolidation

Gebhard Mathis, Sonja Beckh, and Christian Görg

G. Mathis (ed.), *Chest Sonography*, DOI 10.1007/978-3-319-44072-9_5

5.1 Inflammatory Consolidations in the Lung

Gebhard Mathis

Summary

Pneumonic lung infiltrations are characterized by typical changes in terms of sonomorphology (bronchoaerograms, colliquations, parapneumonic effusions). Pneumonias may be first discovered at the bedside. The extent of infiltration may be underestimated owing to artifacts on sonography. Reventilation is well correlated with clinical progression.

The value of chest sonography in pneumonia lies in the assessment of accompanying pleural fluid, timely detection of abscess formation, sonography-guided collection of pathogens, and controls particularly in pregnant women and children.

In cases of tuberculosis and diseases of the frame of the lung, sonography is the optimum method to visualize small pleural effusions and subpleural consolidations; therefore, it is indispensable to control the progress of the disease.

5.1.1 Pneumonia

Pathophysiological Prerequisites

In cases of lobular and segmental pneumonia, large amounts of air are displaced from the lung as a result of extensive fibrinous exudation. Affected lobes or segments are depleted of air and sink in water. The phase of engorgement offers good conditions for pathological echo transmission. In this phase, pneumonia is imaged well on the sonogram. In the phase of lysis, the inflamed portion of the lung is ventilated to an increasing extent.

Focal pneumonias and interstitial pneumonias barely extend up to the pleura and are therefore poorly accessible to sonographic imaging. However, bronchial pneumonias are often accompanied by involvement of the pleura and are therefore partly visualized by sonography.

Sonomorphology of Pneumonia

A number of sonomorphological criteria are characteristic for pneumonic infiltrations. They are of varying intensity in the course of disease.

Sonomorphology of pneumonia:

- Liver or tissue like in the early stage
- Lentil-shaped air trappings
- Bronchoaerogram
- Fluid bronchogram (poststenotic)
- Blurred or serrated margins
- Reverberation echoes at the margin
- Hypoechoic to anechoic in the presence of abscess

Phase of Engorgement

In the initial phase of disease, i.e., in the phase of engorgement, the pneumonic lesion is hypoechoic, relatively homogeneous, and hepatoid in form. Its configuration is bizarre. It is rarely explicitly segmental like the pulmonary infarction or rounded like carcinomas and metastases. Its margins are irregular, serrated, and somewhat blurred (Figs. 5.1 and 5.2).

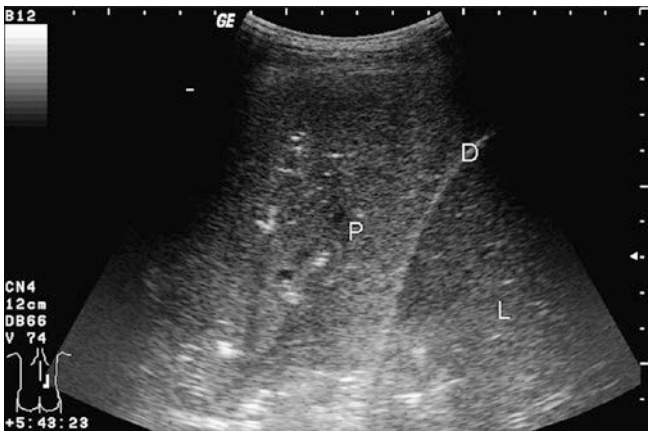

Fig. 5.1 Oblique section of lobar pneumonia in the right lower lobe. The pneumonic infiltrate (*P*) is similar to the liver in terms of echotexture (*L*). *D* diaphragm

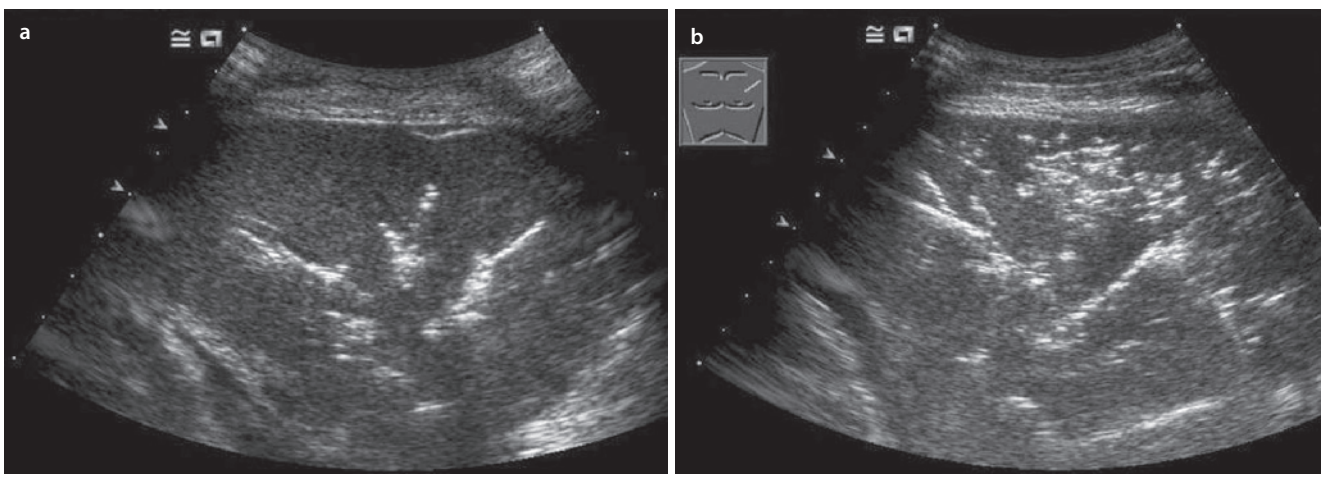

Fig. 5.2 A 68-year-old severely ill man with clinical signs of acute pneumonia. **a** In the upper lobe of the lung on the left side, there is a liver-like consolidation with a bronchoaerogram. **b** A subpleural fluid alveologram

Air Bronchogram

A marked bronchogram (bronchopneumogram, air bronchogram) with treelike ramifications is seen in up to 90 % of cases. The intensive reflexes of the bronchial tree run between consolidated portions of the parenchyma. In all stages of the disease the bronchoaerogram is more pronounced than in cases of pulmonary embolism. Quite often one finds a small number of, and in most cases numerous, lenticular internal echoes just a few millimeters in size (Fig. 5.1b). These echoes indicate the presence of air in the small bronchi. In other words, this is a partial image of a bronchoaerogram. These internal echoes can be partly explained by congested secretion of highly diverse impedance (Weinberg et al. 1986; Mathis et al. 1992; Gehmacher et al. 1995; Reissig and Kroegel 2007; Reissig et al. 2012 Figs. 5.2 and 5.3). The air bronchogram moves dynamically in a breath-dependent manner. This is an important difference between an air bronchogram and obstructive atelectasis: the latter is accompanied by a less prominent air bronchogram and is static (Lichtenstein et al. 2009).

The bronchogram visualized by sonography cannot be equated with that seen on a radiograph. Viral pneumonias are often less ventilated and/or reveal less pronounced bronchoaerograms. These are smaller and more compact than bacterial pneumonia and may resemble large pulmonary infarctions. In contrast to pulmonary infarctions, they are strongly perfused with blood (Fig. 5.4).

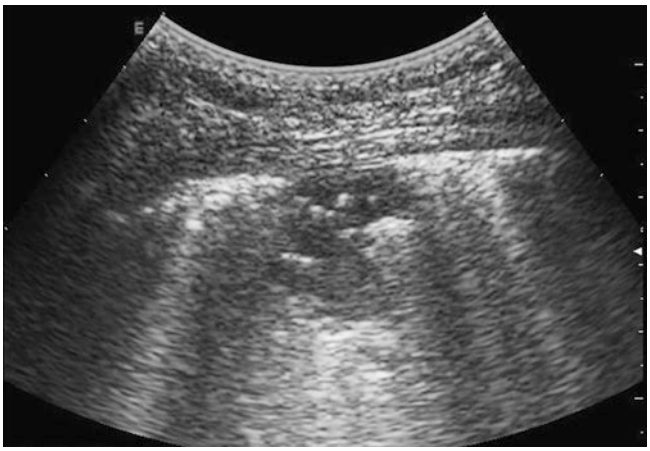

Fig. 5.3 Pneumonia after H1N1-Influenza

Fluid Bronchogram

The fluid bronchogram is marked by anechoic tubular structures along the bronchial tree. The bronchial wall is echogenic and the fluid in the segmental bronchi is hypoechoic. The reflexes around the bronchi are wider than those along vessel walls. Given good resolution, the bronchial walls are ribbed and the vessel walls are smooth; therefore, tubular

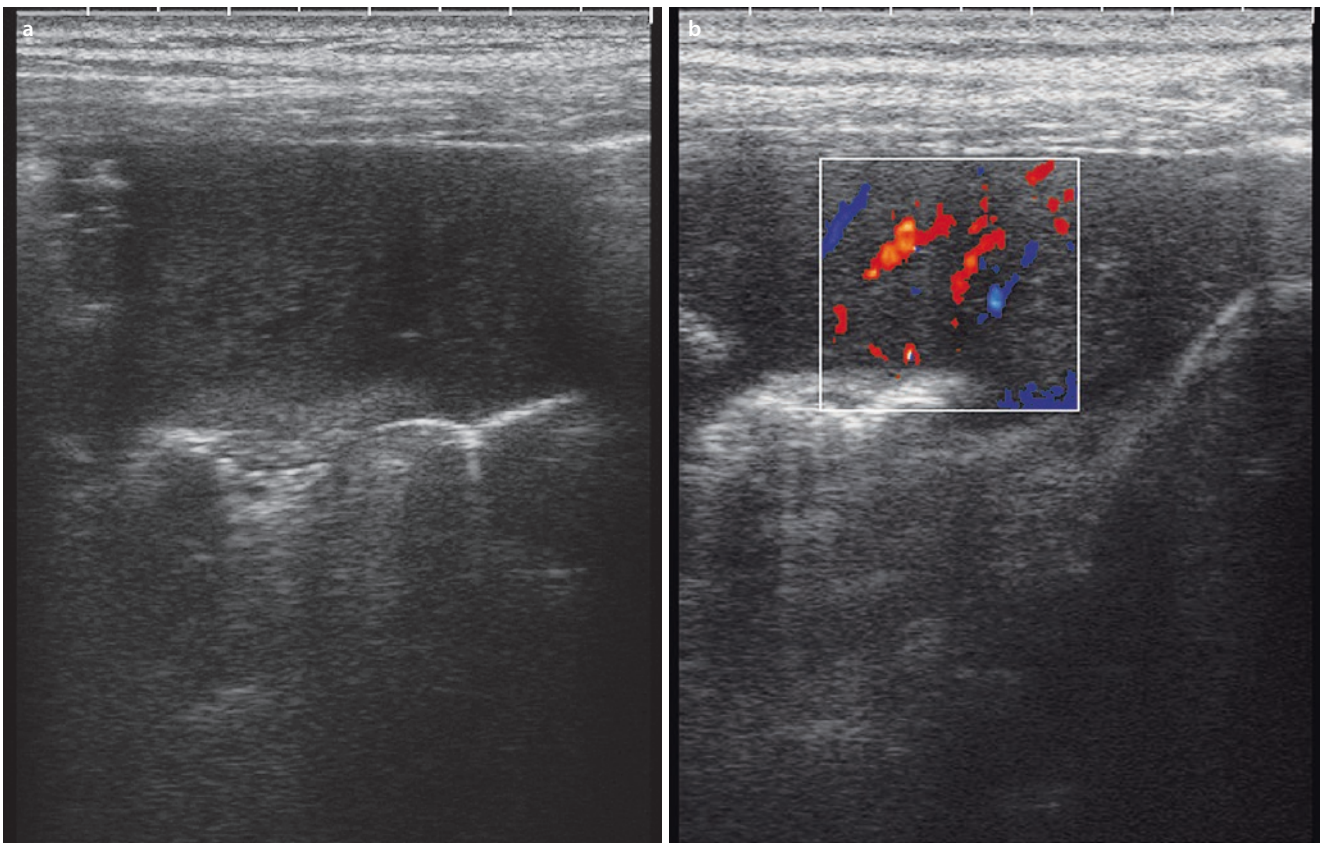

Fig. 5.4 A 52-year-old woman with pain on inspiration, fever, and hemoptysis. **a** Sonography reveals a consolidation measuring 5 × 3.5 cm in size, with a small bronchoaerogram. **b** Color-Doppler shows regular perfusion – viral pneumonia

structures can be easily classified on B-mode image. In the case of doubt, color-coded duplex sonography helps to distinguish between vessels and bronchi. The fluid bronchogram is seen in approximately 8 % of patients with pneumonia and develops in the early phase of the disease as a result of bronchial secretion or owing to bronchial obstruction. A persistent fluid bronchogram always raises suspicion of poststenotic pneumonia and is an indication for bronchoscopic investigation (◘ Fig. 5.5). A tumor may be found or ruled out; the obstructive secretory embolus is aspirated and material obtained for bacteriological investigation (Mathis 1997; Reissig et al. 2012).

Poststenotic Pneumonia

Poststenotic pneumonias that develop in the periphery or the margin of carcinomas are better delineated from the tumor by means of sonography than by X-ray investigation. Poststenotic pneumonia is typically characterized by a fluid bronchogram (◘ Fig. 5.5d). Monitoring the effectiveness of therapy is important in this setting – is the pneumonia subsiding or is the tumor increasing in size?

Circulation

On color-coded duplex sonography pneumonia has a typical appearance: Circulation is uniformly increased, ramified, and the vessels run a normal course. In fact, circulation is increased in the entire infiltrate up to beneath the pleura (◘ Fig. 5.6). This is interesting when pneumonia needs to be differentiated from pulmonary infarctions that have poor or no blood flow, or even from tumors with an irregular circulation pattern. Carcinomas are strongly vascularized in their margins. Owing to neovascularization, vessels in the margins of carcinomas are characterized by a typical corkscrew pattern (Gehmacher et al. 1995; Mathis 1997).

On contrast-enhanced sonography pneumonias are rapidly enriched with contrast medium and achieve intensive saturation after just 8–10 s (Goerg 2007; Bertolini et al. 2008; ◘ Fig. 5.7; ▶ Chap. 9).

Parapneumonic Effusion

Parapneumonic fluid accumulations can be imaged better on ultrasound than on conventional X-rays (55 % versus 25 %). These must be discovered and their course monitored in order to initiate invasive therapy in terms of puncture or video-assisted thoracoscopy on a timely basis (Reissig et al. 2012, ◘ Fig. 5.8).

Abscess Formation

Bacterial pneumonias tend to develop colliquations and form abscesses. This is the case in approximately 6 % of patients with lobar pneumonia (this figure refers to radiographic investigations). Sonography more commonly reveals *microabscess* (Yang et al. 1991, 1992; Mathis 1997).

The *sonomorphology of pulmonary abscess* is highly characteristic: round or oval and largely anechoic lesions. Depending on whether a capsule is formed, the margin is smooth, echodense, and white (◘ Fig. 5.9). Blurred internal echoes are indicative of high cell content or viscous pus rich in protein. In cases of abscesses due to gas-forming pathogens, highly echogenic small air trappings move actively within the fluid in concordance with the respiratory rhythm. Microabscesses cannot be easily distinguished from vessels on color-Doppler imaging.

Considering the scarce quantity of material for bacteriological investigation obtained from the sputum or from bronchial lavage, it is useful to taken *a specimen for the detection of pathogens* by means of sonography-guided aspiration. When the

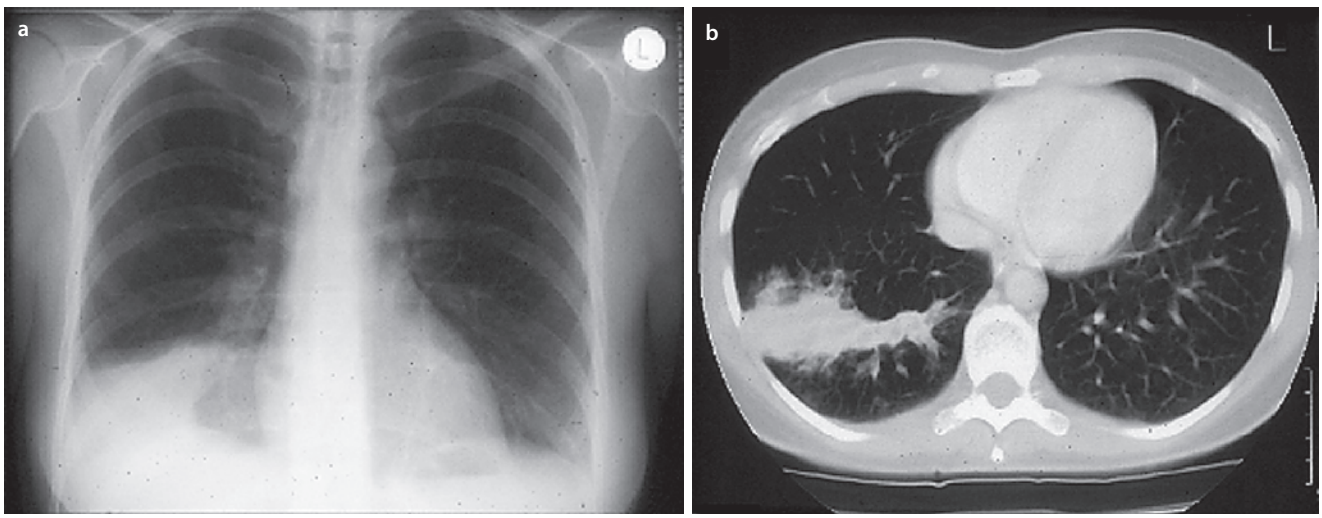

◘ **Fig. 5.5** A 32-year-old woman who had experienced segmental pneumonia for the third time in 1 year. **a** Sharply demarcated segmental shadow on the X-ray. **b** Largely homogeneous consolidation on computed tomography. **c** The morphology of the lesion on sonography is very similar to that on computed tomography. The echotexture contains significantly few air trappings. In the center, there is a small anechoic fluid area. **d** On the longitudinal section one finds tubular structures; parallel to the vessel a typical fluid bronchogram. **e** The adenocarcinoma is verified on bronchoscopy; on surgery, it is staged T1 N0

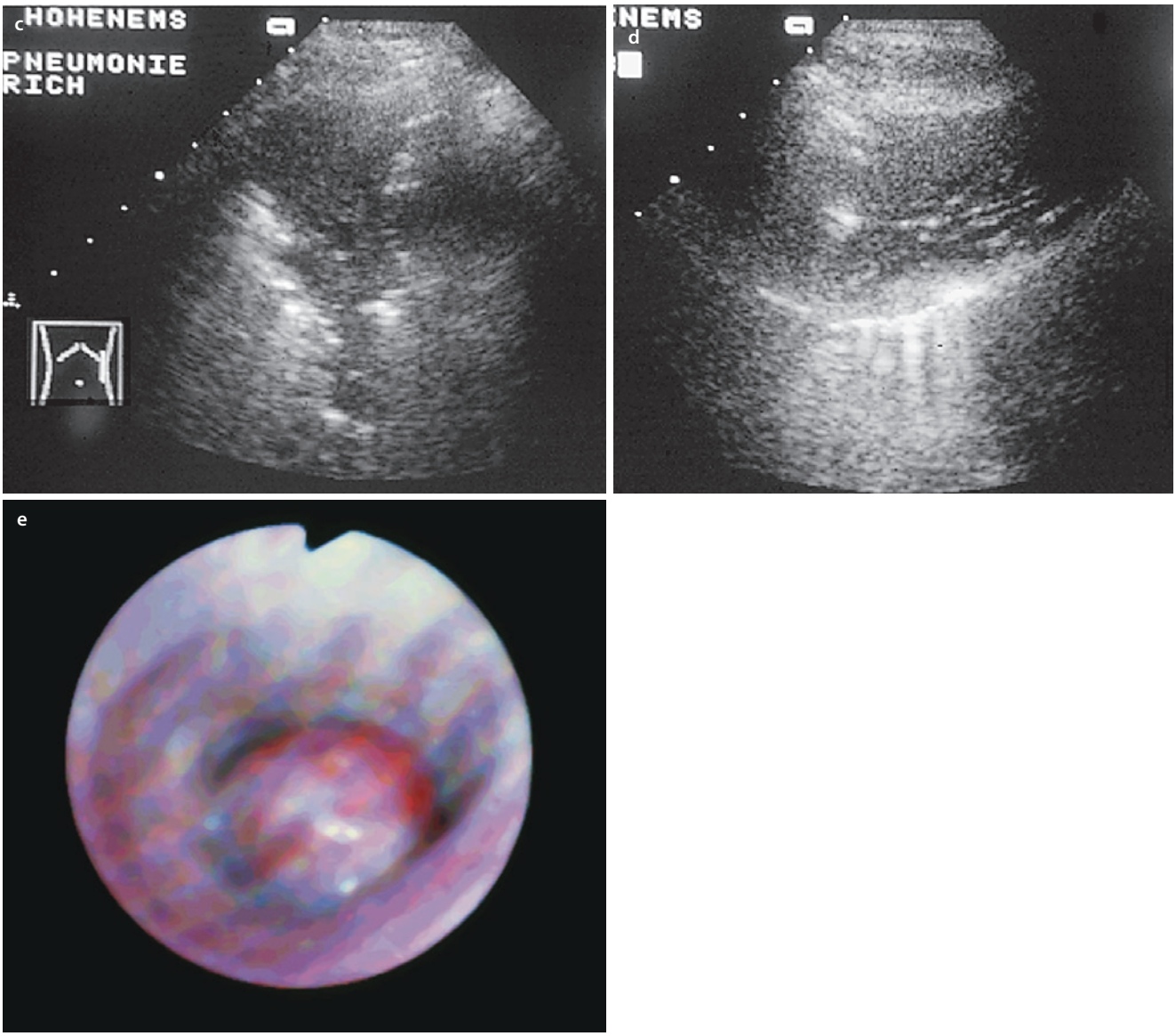

Fig. 5.5 (continued)

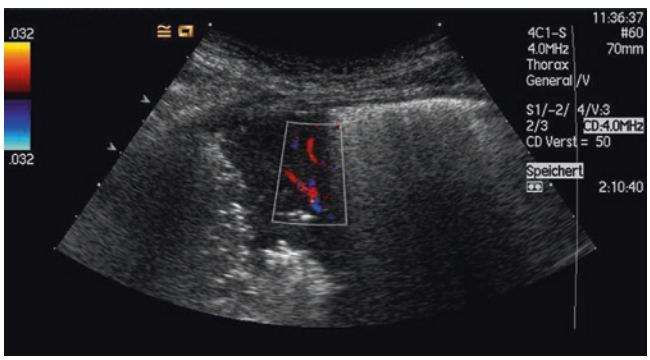

Fig. 5.6 On color-coded duplex sonography pneumonia is seen as an accentuated, regular pattern of circulation

puncture is performed with an ordinary injection needle, a thorough sonographic preinvestigation should be performed, if necessary under sonographic visual guidance, to ensure that air-filled lungs and vessels are avoided. The cause of pulmonary infections can be determined by this method in 80% of cases (Yang et al. 1992; Chen et al. 1993; Liaw et al. 1994; Mathis 1997).

Lung abscess drainage may be performed under sonographic or computed tomography visual monitoring. The risk of a pneumothorax is minimized when one passes through the chest wall obliquely, in a regular fashion, and enters the lung at the site where the abscess is closest to the pleura. The risk of a dreaded bronchopleural fistula is minimized when the correct approach is used, i.e., when one only traverses the homogeneous infiltrate and avoids ventilated areas (Yang et al. 1991; van Sonnenberg et al. 1991; Talayanagi et al. 2010).

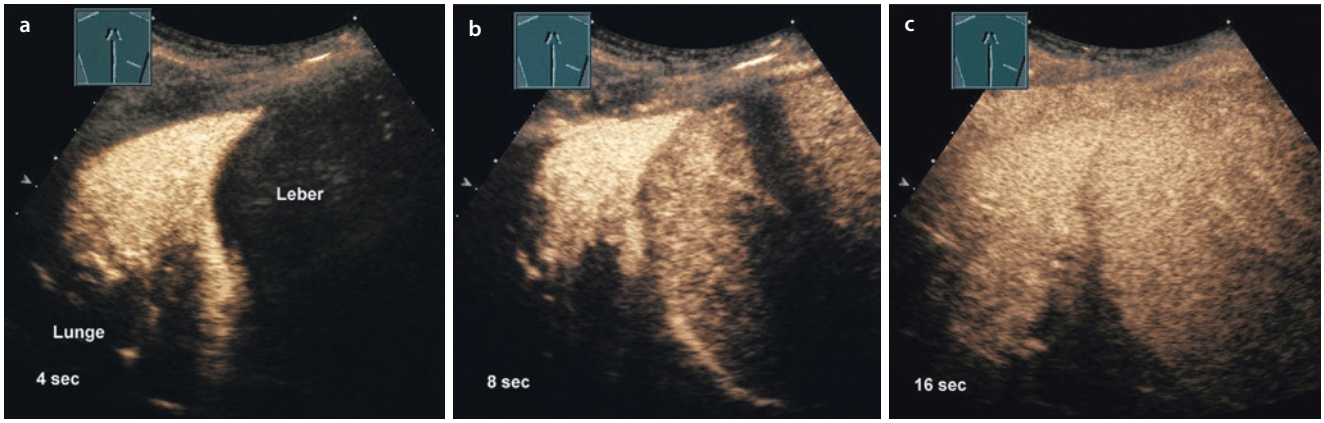

Fig. 5.7 Signal-enhanced sonography in pneumonia. The saturation starts very early and achieves its maximum after 5–10 s

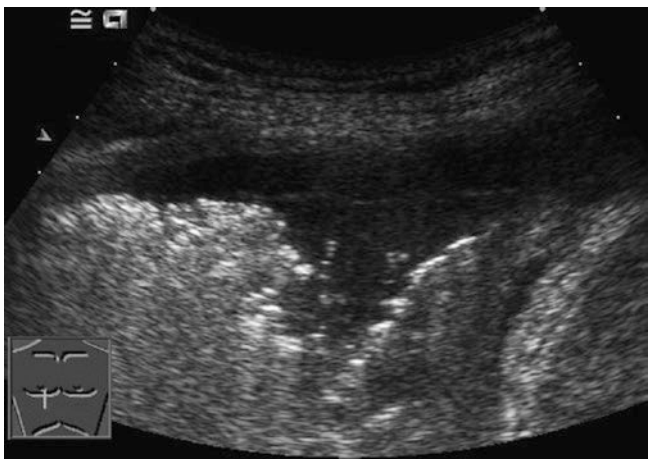

Fig. 5.8 Parapneumonic effusion. Remission observed by ultrasound

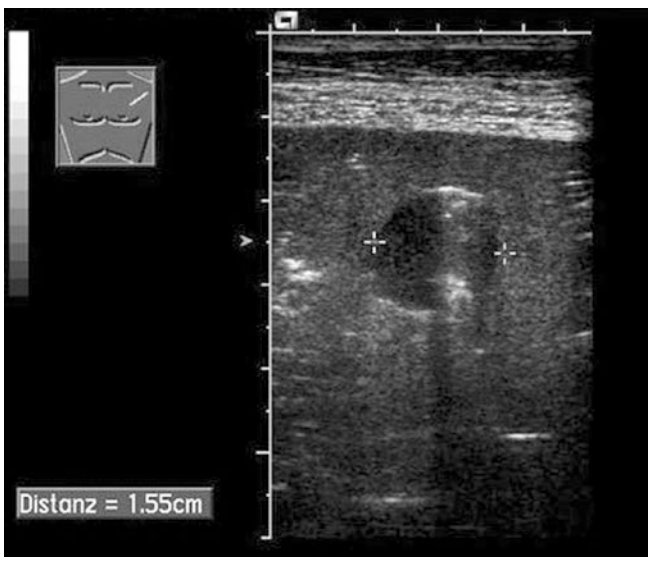

Fig. 5.9 Colliquated abscesses with persistent fever. Sonography-guided aspiration showed a surprisingly large number of tubercle bacilli

Healing Phase

When pneumonia is in the phase of healing, the infiltrated lung tissue is ventilated to an increasing extent. Such air gives rise to reflection and reverberation artifacts. The pneumonia recedes on the sonography image and usually appears smaller than on the chest radiograph. The resolution of these lesions on ultrasound correlates well with the patient's clinical progress (Fig. 5.10).

Diagnostic Value

Primary diagnosis of pneumonia is usually performed on the basis of clinical signs and chest X-rays. The extent of infiltration may be underestimated on ultrasound. Central pneumonias are not seen on sonography.

Can ultrasonography of the lung replace conventional X-rays as a diagnostic imaging procedure? The authors of older studies have compared ultrasound with chest X-rays and achieved favorable results (89 % sensitivity) (Mathis et al. 1992; Gehmacher et al. 1995). With CT as the reference method, ultrasound was able to show 12–25 % more pneumonias than the chest X-ray (Copetti and Cattarossi 2008). A large multicenter study comprising 362 patients confirmed ultrasound morphology criteria on the one hand, and yielded a sensitivity of 93,4 % and a specificity of 97,7 % on the other. In combination with auscultation the accuracy was even higher (Reissig et al. 2012). In multimorbid patients admitted to an acute geriatric ward, lung ultrasound was more accurate than chest x-ray for the diagnosis of pneumonia (90 % vs 67 %), particularly in those with frailty (Tiniesi 2016).

Bedside chest ultrasound is a reliable tool for the diagnosis of pneumonia in the emergency dempartement, probably being superior to Chest x-ray in this setting (sensitivity 98% vs 67%). It is likely that its wider use will allow a faster diagnosis, conducive to a more appropriate and timely therapy (Cortellaro 2012).

Two metanaylyses of nine and 12 studies comprising 1080 and 1353 patients, respectively, yielded a pooled sensitivity of 95–97 % and a specificity of 94–96 %. Pneumonia cannot be ruled out with absolute certainty by ultrasound (Hu et al. 2014; Chavez et al. 2014). In cases of clinical suspicion of pneumonia, further radiological investigations will be

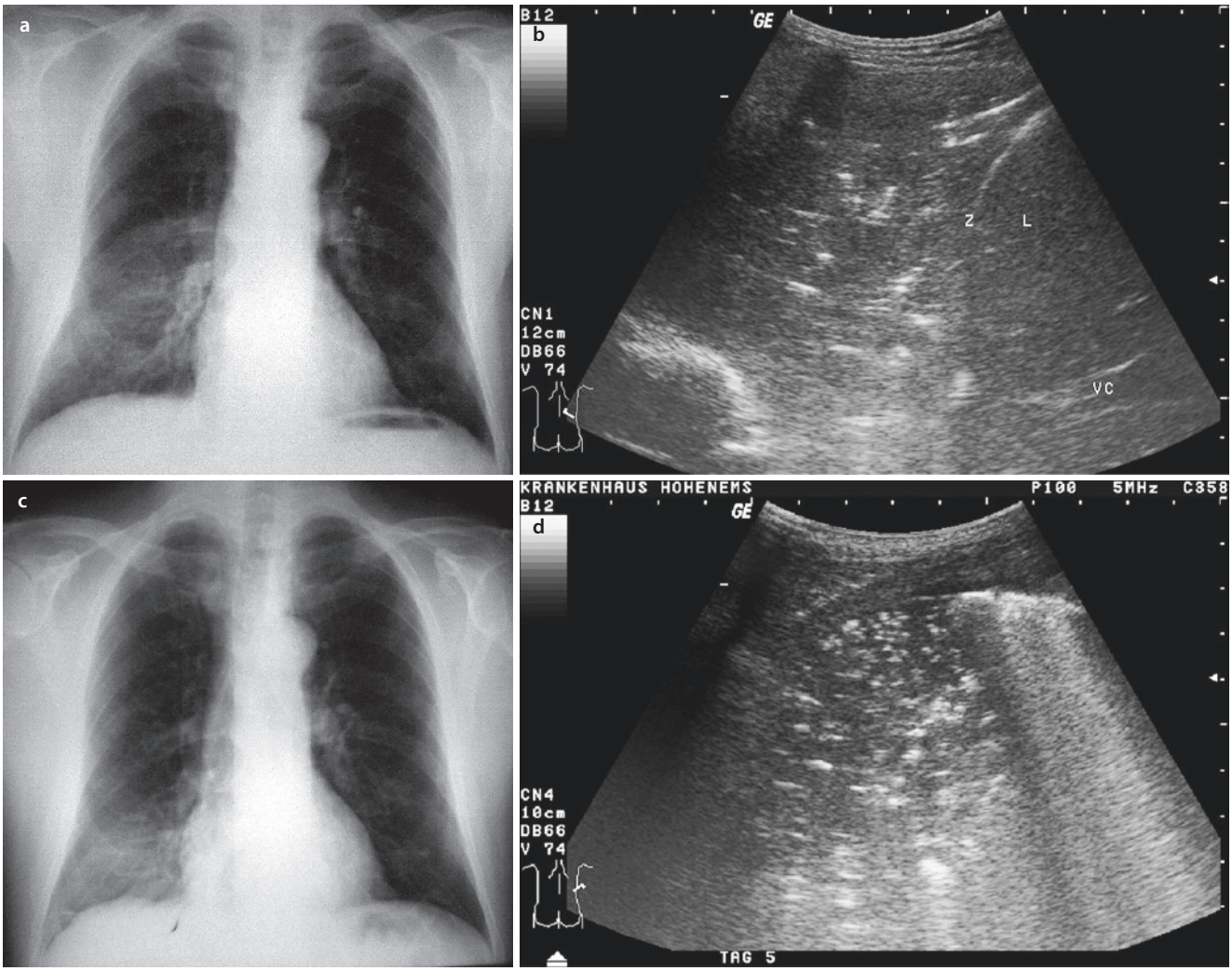

Fig. 5.10 A 72-year-old man with clinically severe pneumonia. **a** Typical appearance on X-ray. **b** On sonography the echotexture is similar to that of the liver, with a pronounced bronchoaerogram. *Z* diaphragm, *L* liver, *VC* vena cava. After 1 week of antibiotic therapy the patient is afebrile and has recovered to the extent that he can be discharged. **c** On the X-ray there still is a marked residual infiltrate. **d** Sonography only shows a receding infiltration

necessary. However, after the clinical investigation and after obtaining the required laboratory data concerning inflammatory parameters, immediate antibiotic treatment can be initiated almost everywhere: at the medical office, the emergency department, the intensive care unit, and in stroke patients among others (Busti et al. 2014; Chavez et al. 2015).

5.1.2 Tuberculosis

In pulmonary tuberculosis, ultrasonography is helpful in detecting pleural effusions, subpleural consolidations and pneumonic infiltrates. Ultrasound-guided diagnostic punctures are meaningful in this setting. Chest X-rays and computed tomography are indispensable to obtain an overview of the condition (Yuan et al. 1993; Kopf et al. 1994; Mathis 1997; Figs. 5.11, 5.12, and 5.13).

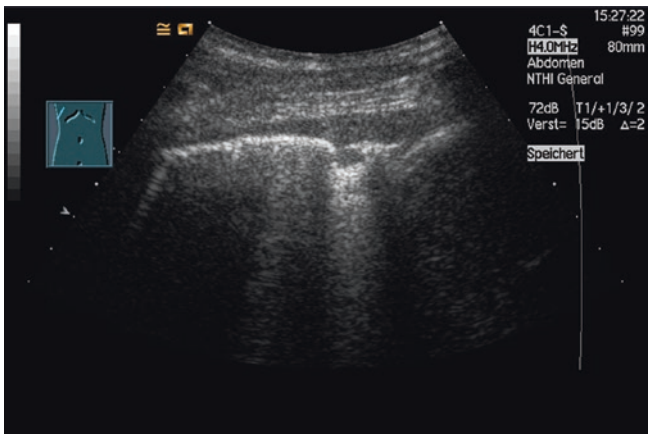

Fig. 5.11 Small lymphocytic pleural effusion. US-guided biopsy of the nodule showed tuberculosis

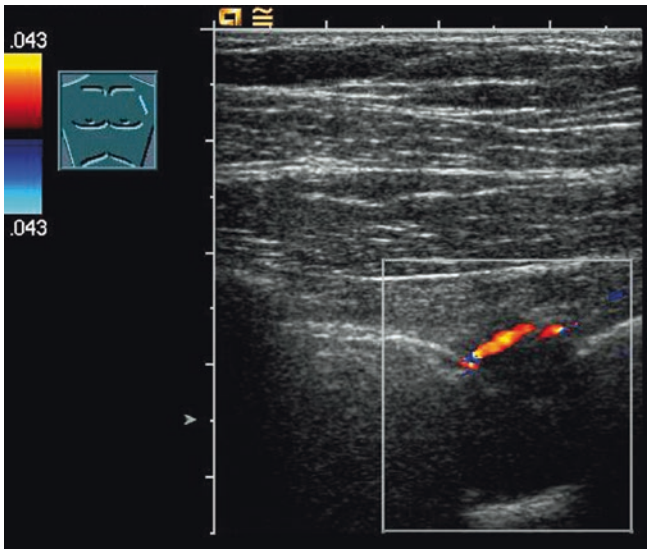

Fig. 5.12 Peripheral lung lesion on a routine X-ray of a young woman. On sonography one finds a hypoechoic, poorly vascularized lesion. Biopsy indicated tuberculosis

Tuberculotic lung lesions may be seen on sonography as rounded or irregular structures of relatively homogeneous texture. Depending on the size of the lesion, these infiltrates may also be accompanied by air trappings as in pneumonia. Nodular dissemination, as in miliary tuberculosis, is visualized as multiple subpleural nodes measuring a few millimeters in size (Fig. 5.13).

Colliquations can be imaged well, but air in cavities might be a disturbing factor and might limit visualization. Even very small quantities of the specific pleural effusion are seen. Pleural thickening may also be revealed. A patient's response to tuberculostatic therapy can be monitored well with sonography, especially in cases of pleural and subpleural tuberculosis lesions.

In cases of rarer infectious lung consolidations such as aspergillosis or echinococcus, typical lesions can be visualized and significant additional information (in addition to the information available from radiographs) obtained (Fig. 5.14).

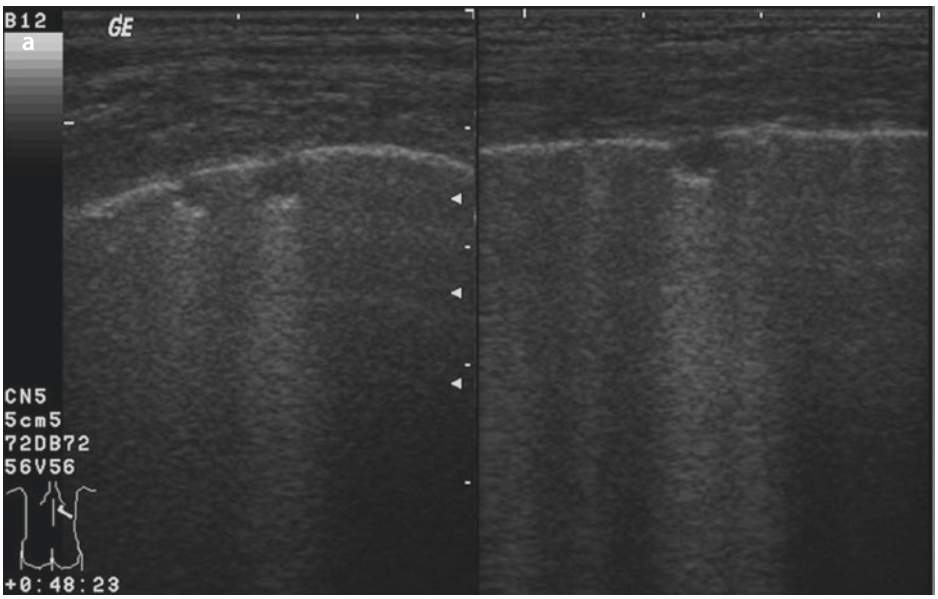

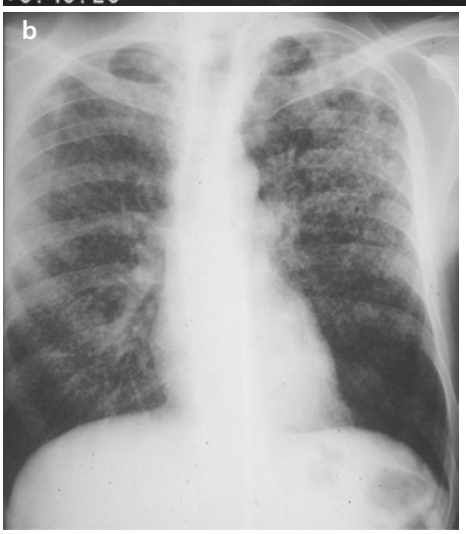

Fig. 5.13 Miliary tuberculosis. **a** Fragmented pleura (*arrowheads*) with numerous subpleural nodes measuring 2–3 mm in size. **b** Chest X-ray showing miliary tuberculosis

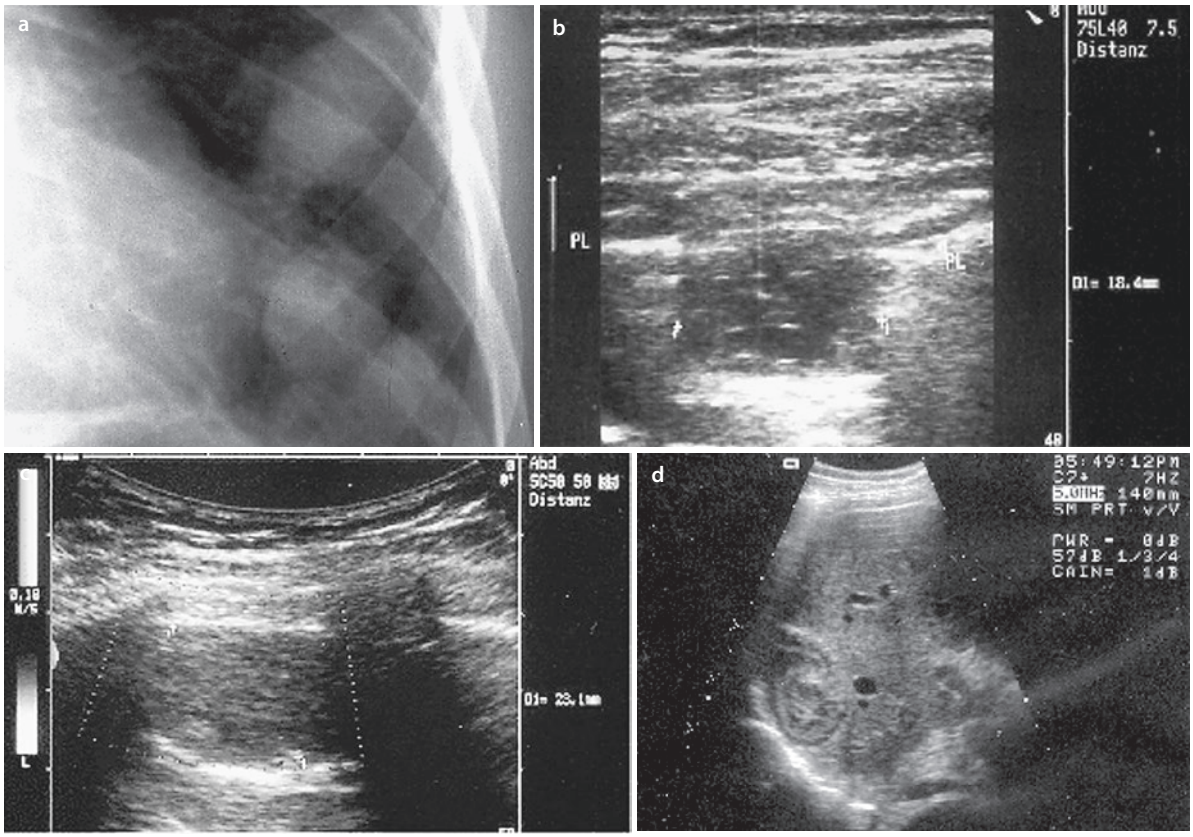

Fig. 5.14 Echinococcus cysticus. A 28-year-old man with pulmonary echinococcosis in his medical history. The patient was admitted to the hospital because of fever, cough, and marked dyspnea. **a**, **b** The X-ray shows multiple round lesions in the lung and pneumonic infiltrates. **c** Sonography revealed the round lesions extending to the surface of the lung. Thick-walled cysts (*crosses*) with internal secondary cysts showing no vascularization on color-Doppler sonography. Additionally one finds several areas indicative of pneumonia. **d** An echinococcal lesion is present in the liver as well. Further diagnostic procedures confirmed bilateral pneumonia in terms of superinfection and preexisting pulmonary echinococcosis. The patient subsequently developed severe pulmonary hypertension despite antibiotic therapy plus albendazole

5.1.3 Interstitial Lung Disease

Technically sonography is entirely unsuitable to diagnose diseases of the lung framework. However, it was shown that such diseases are frequently accompanied by *involvement of the pleura* and the latter is significantly better visualized by sonography than by other imaging procedures:

- Minimal pleural effusions
- Fragmented pleura with several comet-tail artifacts (B-lines)
- Subpleural consolidations (Figs. 5.15, 5.16, 5.17, and 5.18)

The value of the method lies in the detection of a grave condition and in steering the diagnostician's attention towards a specific target.

Therapy controls are highly efficient in cases of minimal pleural effusions and subpleural infiltrations; no method is superior to sonography in this regard (Wohlgenannt et al. 2001; Reissig and Kroegel 2003).

5.2 Neoplastic Consolidations in the Lung: Primary Lung Tumors and Metastases

Sonja Beckh

Summary

Sonography does not permit the investigator to make a distinction between metastases and peripheral carcinoma. The interpretation must take the patient's medical history and survey radiographs into account. In terms of differential diagnosis, the formation of lesions in the parietal pleura must be excluded by dynamic investigation. Even benign pulmonary lesions, e.g., hamartoma or hemangiofibroma, might extend to the periphery of the lung as hypoechoic formations. Cyst walls may be of varying thickness. They usually have an anechoic content. Occasionally they contain fluid with internal echoes. In order to differentiate between a cyst and a pulmonary abscess or an encapsulated empyema, the diagnostic procedure must take clinical parameters and computed tomography investigations into account. In the final

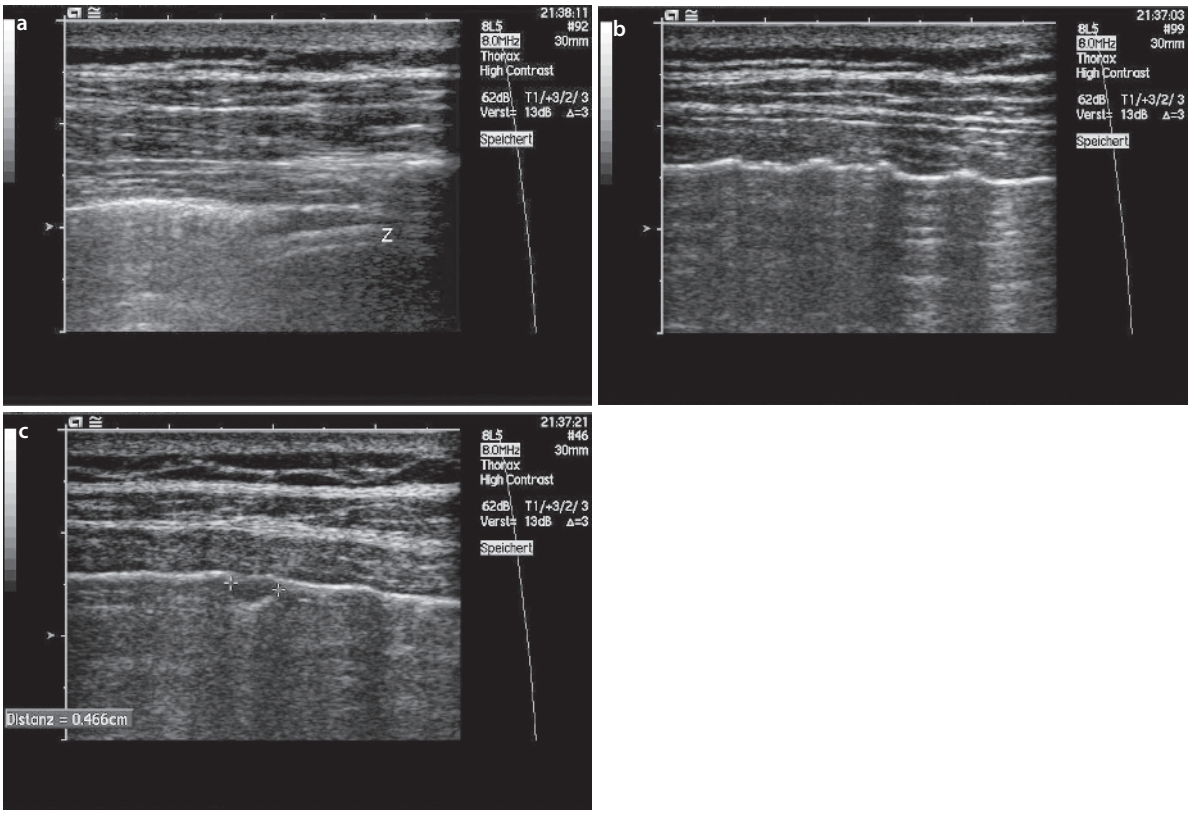

Fig. 5.15 Sarcoidosis. **a** Minimal basal pleural effusion. *Z* diaphragm. **b** Uneven, fragmented visceral pleura with several reverberation echoes (comet-tail artifacts). **c** Subpleural nodes measuring about 5 mm in size

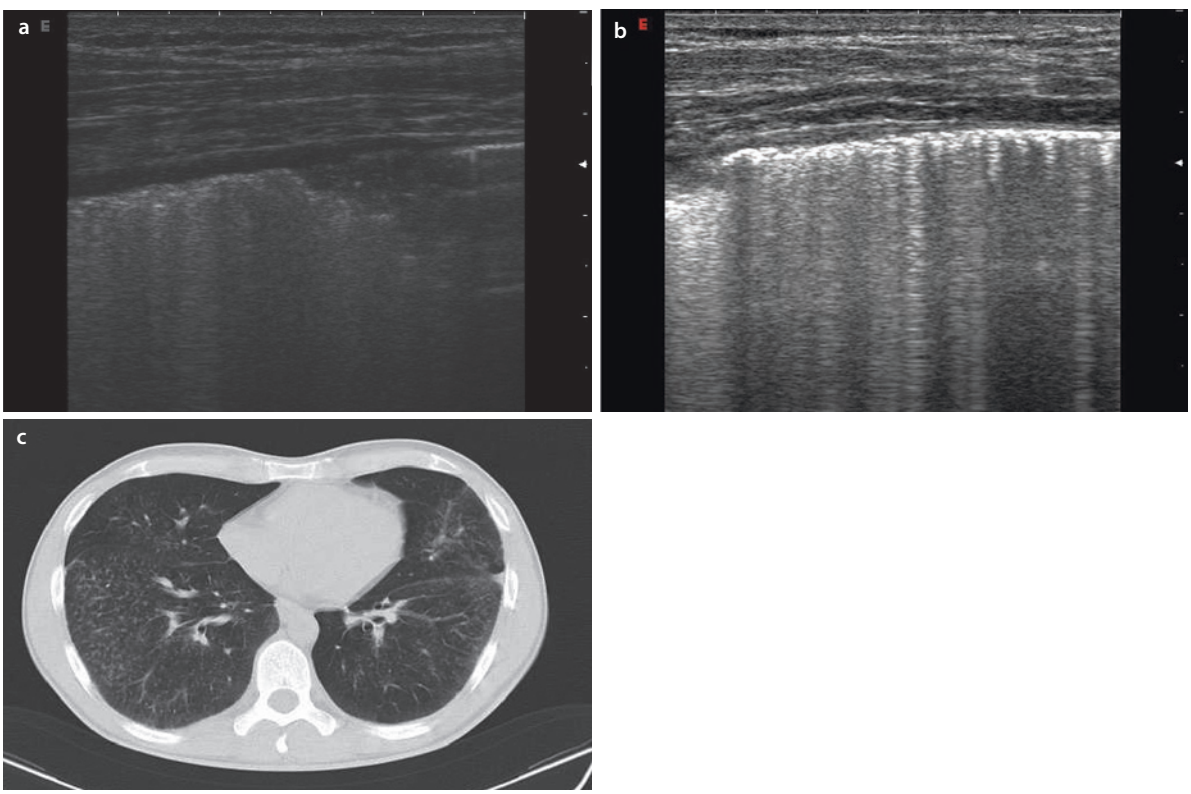

Fig. 5.16 Sarcoidosis. A 26-year-old man with creepy appearance of dyspnea and plueritic pain. **a** Left sided subpleural consolidations with narrow pleural effusion. **b** Diffuse interstitial syndrome in a nonhomogeneous distribution. **c** Corresponding CT

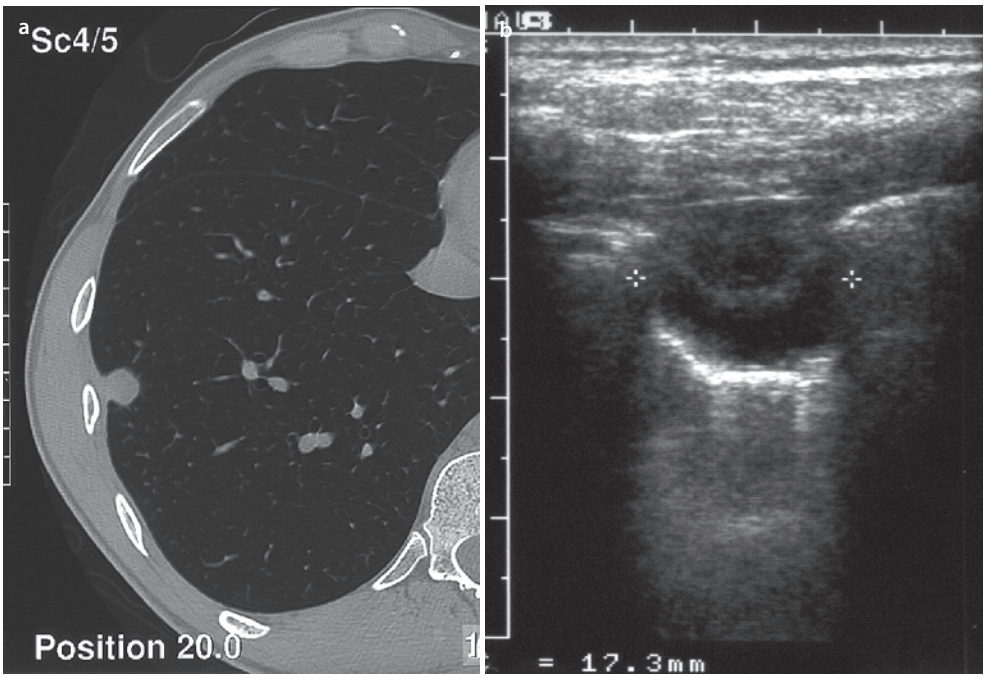

Fig. 5.17 **a** The patient was referred for identification of the primary lesion in the presence of a "metastatic lung". **b** Sonopgraphy-guided biopsy of the subpleural lesion indicated a rheumatic nodule

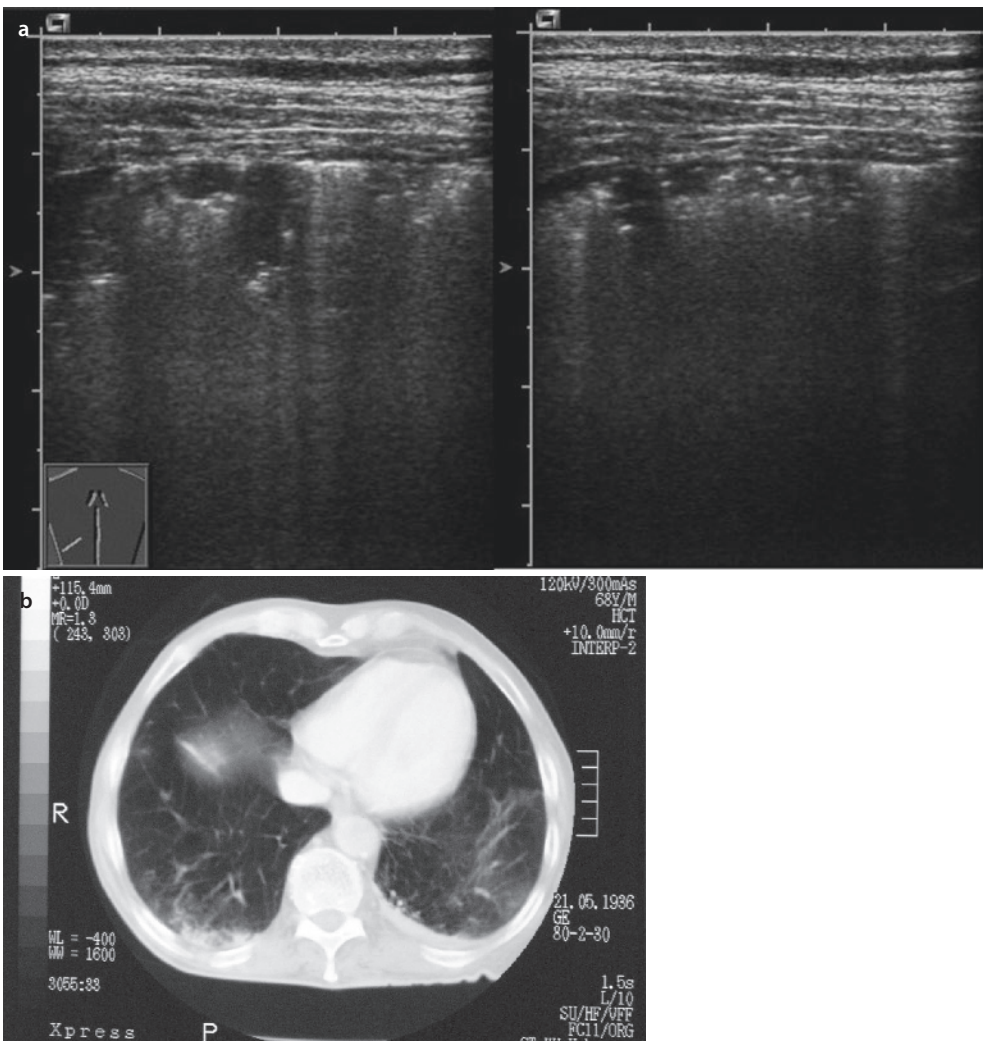

Fig. 5.18 Chronic organizing pneumonia. **a** Extensive subpleural infiltrations, indicated with US-guided biopsy. **b** Corresponding CT

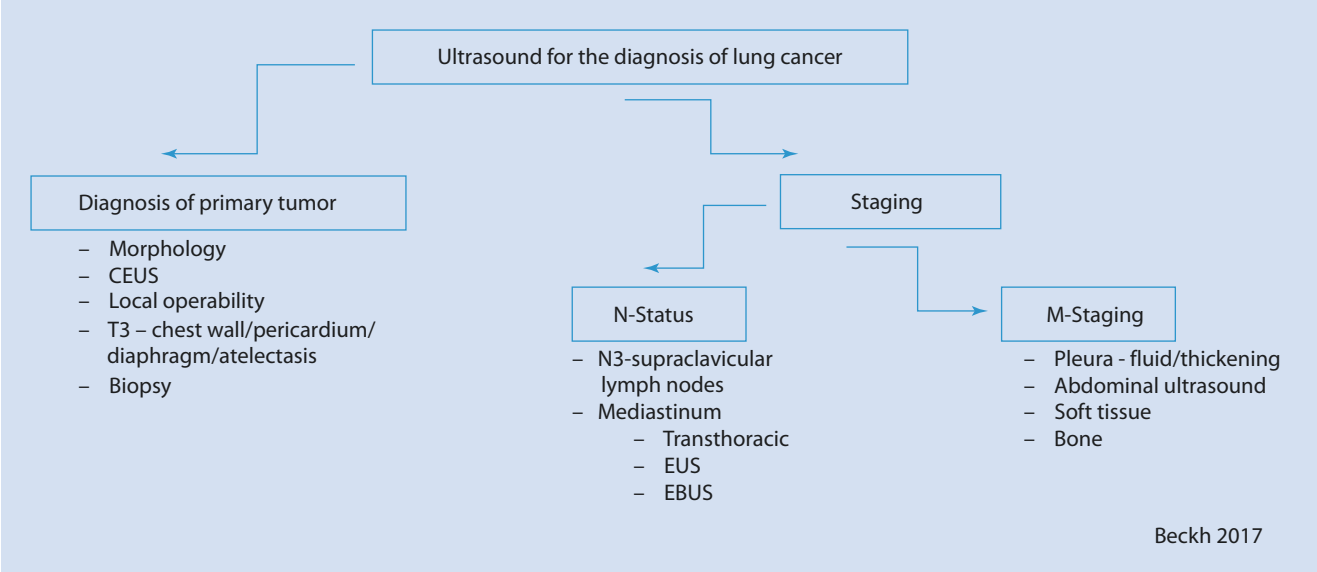

Fig. 5.19 Role of lung ultrasound in diagnosis and staging of lung cancer

Table 5.1 Sonomorphology of lung carcinomas

Morphology	Echotexture	Vessels	Complex structures
Sharp margins	Inhomogeneous	Displacement of vessels	Residual ventilated areas
Rounded	Hypoechoic	Destruction of vessels	Accompanying pneumonia at the margin
Polypoid	Rarely echogenic	Interruption of vessels	Solid space-occupying lesion/pneumonia
Ramifications	Rarely anechoic	Neovascularization	Bacterial/fungal colonization
Serrated margin	Necrotic areas	–	Bizarre pattern in large necroses

analysis, bacteriological, cytological, and histological investigations are of decisive importance.

Thanks to ongoing scientific work, the recent international guidelines and recommendations have incorporated ultrasound as a part of the diagnostic procedure for the investigation of lung carcinoma (Pan et al. 1993; Suzuki et al. 1993; Yuan et al. 1994; Yang 1996; Hsu et al. 1996, 1998; Mathis 1997, 1999; Beckh et al. 2002; Detterbeck et al. 2003; Goerg and Bert 2004; Bandi et al. 2008; Hoosein et al. 2011; Volpicelli et al. 2012). Due to its excellent resolution, ultrasound has proved equivalent to nuclear resonance tomography in the investigation of the chest wall affected by tumor invasion (Goeckenjan et al. 2011). Percutaneous diagnostic and therapeutic ultrasound-guided puncture is recommended, and has been accepted as a reliable procedure (Goeckenjan et al. 2011; Detterbeck et al. 2013a, b; Rivera et al. 2013). Endobronchial and endoesophageal ultrasound is the state of the art for staging mediastinal disease (Goeckenjan et al. 2011; Detterbeck et al. 2013a, b; Silvestri et al. 2013). The visualization of vessels with color-Doppler or ultrasound contrast medium provides valuable additional information for the differential diagnosis of space-occupying lesions (Piscaglia et al. 2012, ▶ Chap. 8).

Lung consolidations are seen on sonography only when no aerated tissue hinders the echo transmission. For staging of the disease and planning treatment in cases of malignant lung disease, procedures that provide sectional images such as computed tomography or magnetic resonance tomography are absolutely essential in order to obtain an overview of the entire chest (van Kaick and Bahner 1998; Knopp et al. 1998; Schoenberg 2003). As a rule, the sonographic investigation is performed when the findings of various radiographic procedures are known. Given specific symptoms, however, a targeted symptom-oriented investigation is also meaningful (▶ Chap. 11) (Fig. 5.19).

Pulmonary malignancies may have a highly variable *echotexture*. They are usually hypoechoic, moderately echodense, or very inhomogeneously structured; more rarely they are nearly anechoic (Mathis 1997; Mathis et al. 1999; Table 5.1). However, the echotexture alone does not allow the investigator to draw conclusions about the malignant or benign nature of the disease (Figs. 5.20 and 5.21).

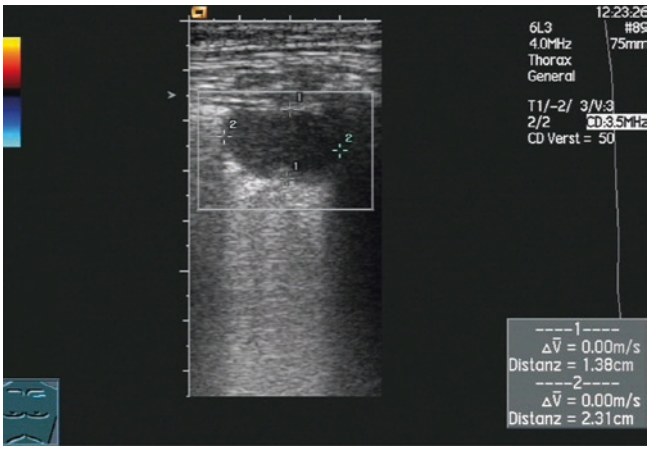

Fig. 5.20 A small hypoechoic lesion in a 78-year-old man: an incidental finding in the upper lobe of the left lung, in infraclavicular location. Sonography-guided biopsy indicated squamous cell carcinoma

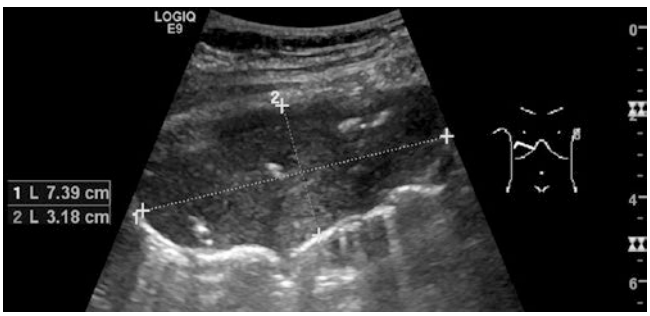

Fig. 5.21 A 40-year-old man with recurrent eosinophilic pleural effusion. X-rays showed a peripheral lesion in the upper lobe of the left lung. On sonography in the anterior axillary line in the second intercostal region, there is a hypoechoic peripheral pulmonary lesion with central vessels and rather sharp margins. Removal of the lesion by thoracoscopy led to the diagnosis of hyalinosis and callus. The source of the pleural effusions is still not clear

In contrast to acute inflammatory infiltrations, the sonomorphology of malignant lesions does not change during a short course of disease. Chronic carnifying pneumonia and peripheral callused cicatricial lesions are problematic in terms of differential diagnosis; it may be difficult to differentiate these entities from malignant disease (Mathis 1997).

Decisive criteria to grade the malignant or benign nature of a pulmonary lesion are the following:

- *Contours* of the lung surface
- *Margins* to ventilated lung tissue
- *Invasion* of adjacent structures (chest wall, diaphragm, pericardium)
- *Destruction* of normal tissue architecture
- *Displacement* of regular vessels
- *Neovascularization*
- *Differentiation between a central space-occupying lesion and a poststenotic invasion/atelectasis*

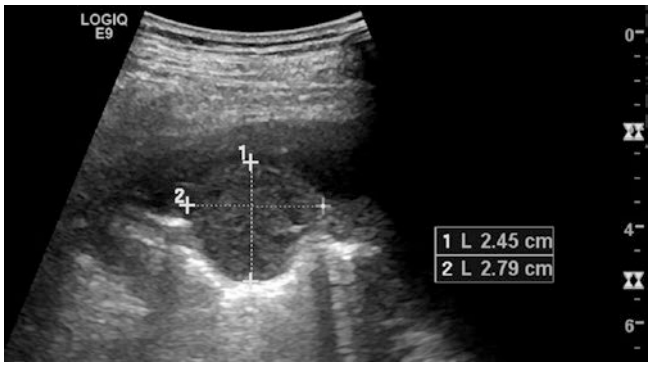

Fig. 5.22 Small-cell lung carcinoma invading the lower lobe of the left lung (diagnosed by bronchoscopic biopsy), irregular lung surface, narrow pleural effusion

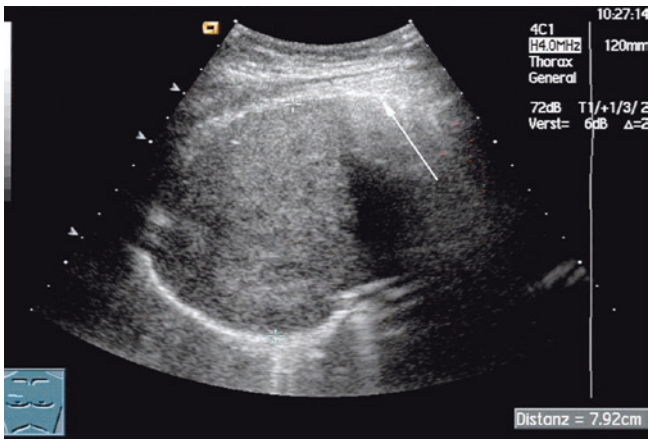

Fig. 5.23 Large hypoechoic space-occupying lesion in the upper lobe of the right lung, sharply demarcated from ventilated lung tissue. In medial location (*arrow*) one finds an unremarkable echogenic pleural line. Sonography-guided biopsy indicated poorly differentiated neuroendocrine carcinoma G4

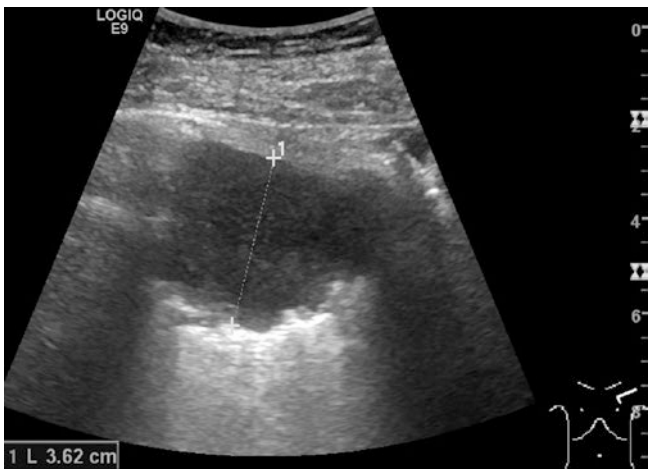

Fig. 5.24 Hypoechoic space-occupying lesion in the upper lobe of the right lung with fringed branches into the ventilated lung tissue (*arrows*). Histological investigation of the resected upper lobe yielded a mixed-cell lung carcinoma (squamous cell or large-cell carcinoma)

5.2.1 Contours of the Lung Surface

The *contours* of the lung surface are very well delineated from the surrounding pleural fluid. Figure 5.22 shows the convex swelling surface of the lung by a lung carcinoma. A benign inflammatory infiltration would never lead to such irregular deformation of the lung surface.

5.2.2 Delineation of Margins from Ventilated Lung Tissue

Malignant lesions are often very *sharply demarcated* from lung tissue (Fig. 5.23). Occasionally, however, one finds *fringed or finger-shaped ramifications* into the normally ventilated parenchyma – a sign of invasive growth (Fig. 5.24).

In contrast to inflammatory lesions, such solid malignant formations in marginal zones are not ventilated and therefore are more sharply demarcated from the surrounding tissue.

5.2.3 Invasion of Adjacent Structures: Chest Wall, Diaphragm, and Pericardium

Practically at first glance, a malignancy *invading* adjacent structures is indicative of the aggressive nature of the tumor (Suzuki et al. 1993; Bandi et al. 2008). In the case of a Pancoast's tumor, a space-occupying lesion penetrating the dome of the pleura is clearly visualized (Fig. 5.25).

Malignant invasion of the chest wall frequently causes local pain. Targeted investigation of the region with the transducer will help to diagnose the condition early (Fig. 5.26).

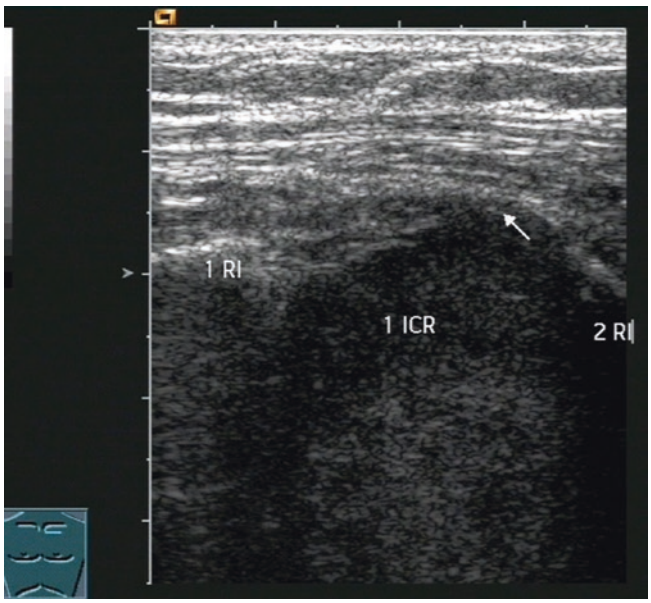

Fig. 5.26 This woman slipped on a staircase 6 months ago and has been experiencing renewed pain in the left chest for 4 weeks. Computed tomography shows a suspected hematoma. On sonography there is a space-occupying lesion invading the muscles of the chest wall and causing obvious destruction of the third and fourth rib laterally. Sonography-guided biopsy indicated poorly differentiated adenocarcinoma

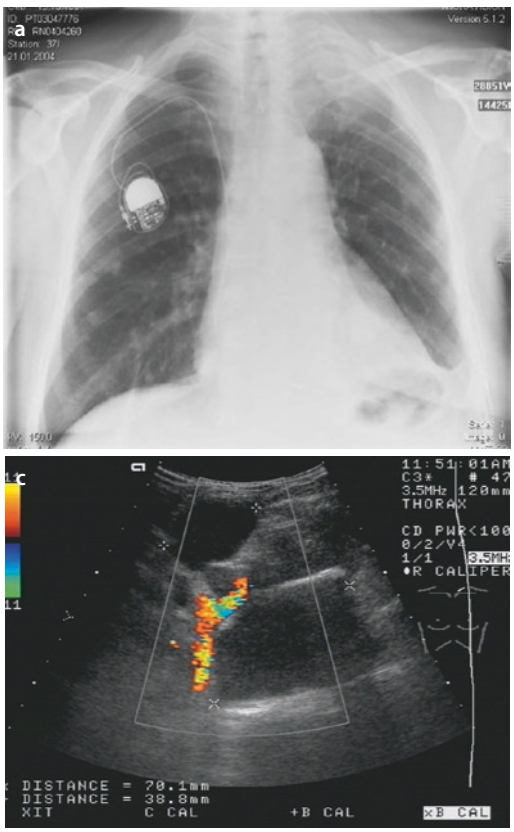

Fig. 5.25 **a** A 72-year-old man with pain in the left chest for several months; initially interpreted as angina pectoris. On the overview X-ray a shadow was noted on the left side in apical location. **b** On the coronary computed tomography section there was a space-occupying lesion on the left side in apical location, surrounding the first rib and penetrating the soft tissue. **c** Corresponding sonographic image: large hypoechoic tumor formation penetrating the dome of the pleura and invading the supraclavicular soft tissue. The subclavian artery is slightly compressed and displaced medially by the tumor. Sonography-guided biopsy indicated moderately differentiated adenocarcinoma developing within scar and connective tissue

Invasion into adjacent structures of the chest wall is a very reliable sign of malignant growth. Therefore, the current S-3 guidelines demand a sonography for staging in lung cancer (Goeckenjan et al. 2011). In terms of differential diagnosis only one disease is likely to be present here, namely, actinomycosis or nocardiosis (Corrin 1999).

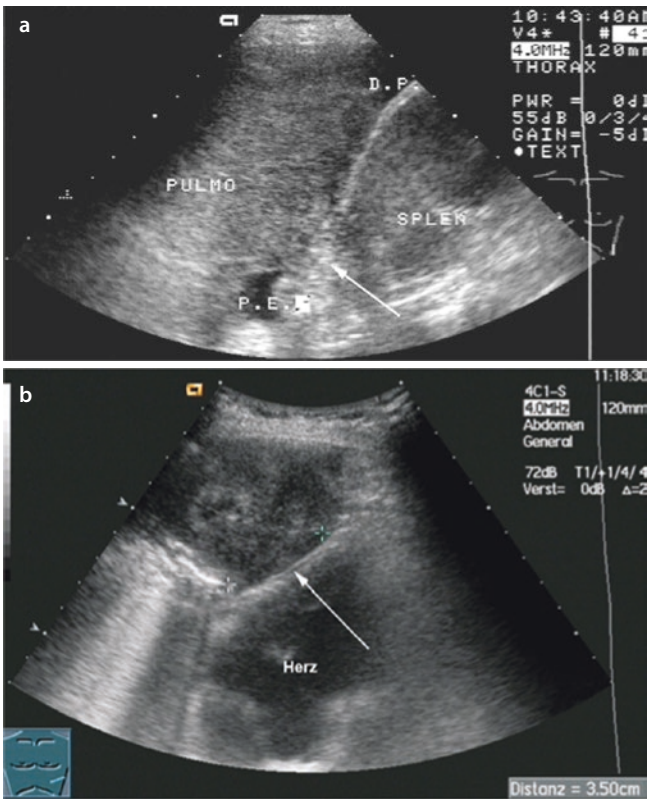

Fig. 5.27 **a** Large tumor below the left lower lobe, inserting into the diaphragm (*arrow*). Histology of the sonographic biopsy and the operation specimen indicated benign fibrous tumor of the pleura. **b** Tumor in the lingula, invading about 3.5 cm of the parietal pericardium (*arrow*). Sonographic biopsy indicated poorly differentiated adenocarcinoma

The diaphragm on the right side of the chest is usually fully visible, with the liver serving as the sonic window. On the left side, tumors lying medial to the spleen are only seen if there is an effusion or when the tumor itself serves as the sonic window. In the latter case the insertion at the diaphragm may be seen as in Fig. 5.27a.

For staging of the disease and planning therapy, among other factors the relation between the tumor and the pericardium is important. Owing to the excellent resolution and the possibility of dynamic investigation, tumor invasion of the parietal pericardium can be clearly visualized (Fig. 5.27b).

5.2.4 Destruction of the Normal Tissue Architecture and Displacement of Regular Vessels

Malignant invasion *destroys* the normal texture of tissue. Bronchial branches may be displaced or fully destroyed (Fig. 5.28).

The original normal vessels are either displaced (Figs. 5.25 and 5.28) or disappear altogether.

In some cases, vessels of the tumor itself are found particularly in the margin (Fig. 5.29b). Such vessels are convoluted and marked by changes in diameter (Yuan et al. 1994; Mathis 1997; Hsu et al. 1996, 1998).

5.2.5 Additional Investigations to Assess the Possibility of Resection

For further planning of treatment in terms of *whether the entity can be operated on and resected*, a detailed dynamic investigation has to be performed (Beckh and Boelcskei 2003). In order to decide between video-assisted thoracoscopy (VATS) and thoracotomy, it is important to know whether the pathological entity is widely fixed to the parietal pleura or is freely movable in conjunction with the lung (Landreneau et al. 1998). However, adherence alone does

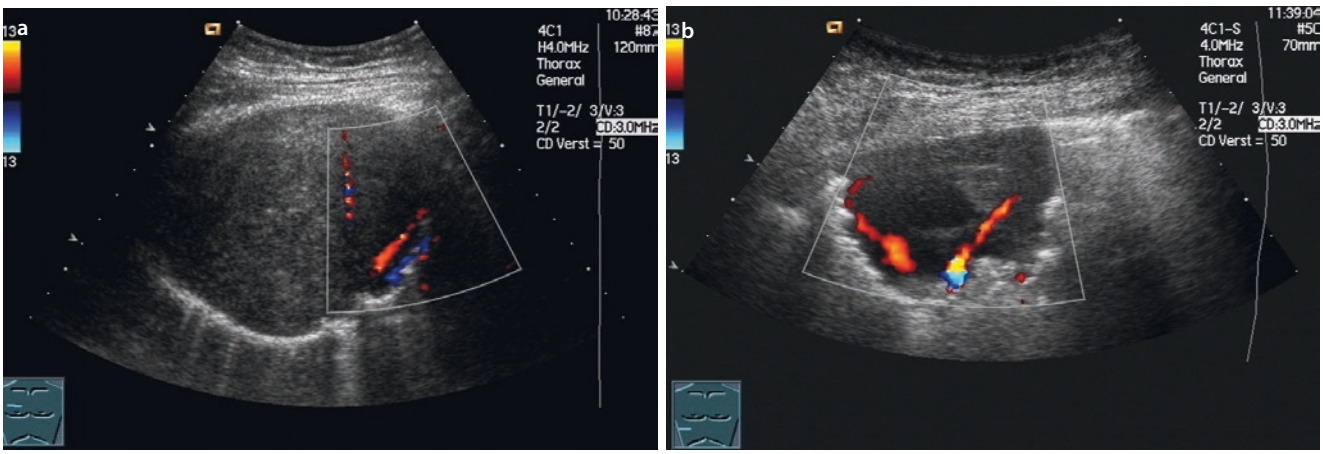

Fig. 5.28 **a** Large tumor in the upper lobe of the right lung, displacing the artery and vein of the upper lobe in medial direction. Sonographic biopsy indicated poorly differentiated neuroendocrine carcinoma. **b** Tumor in the lateral middle lobe with central necrosis; in the marginal areas there are strong, convoluted vessels of changing diameter

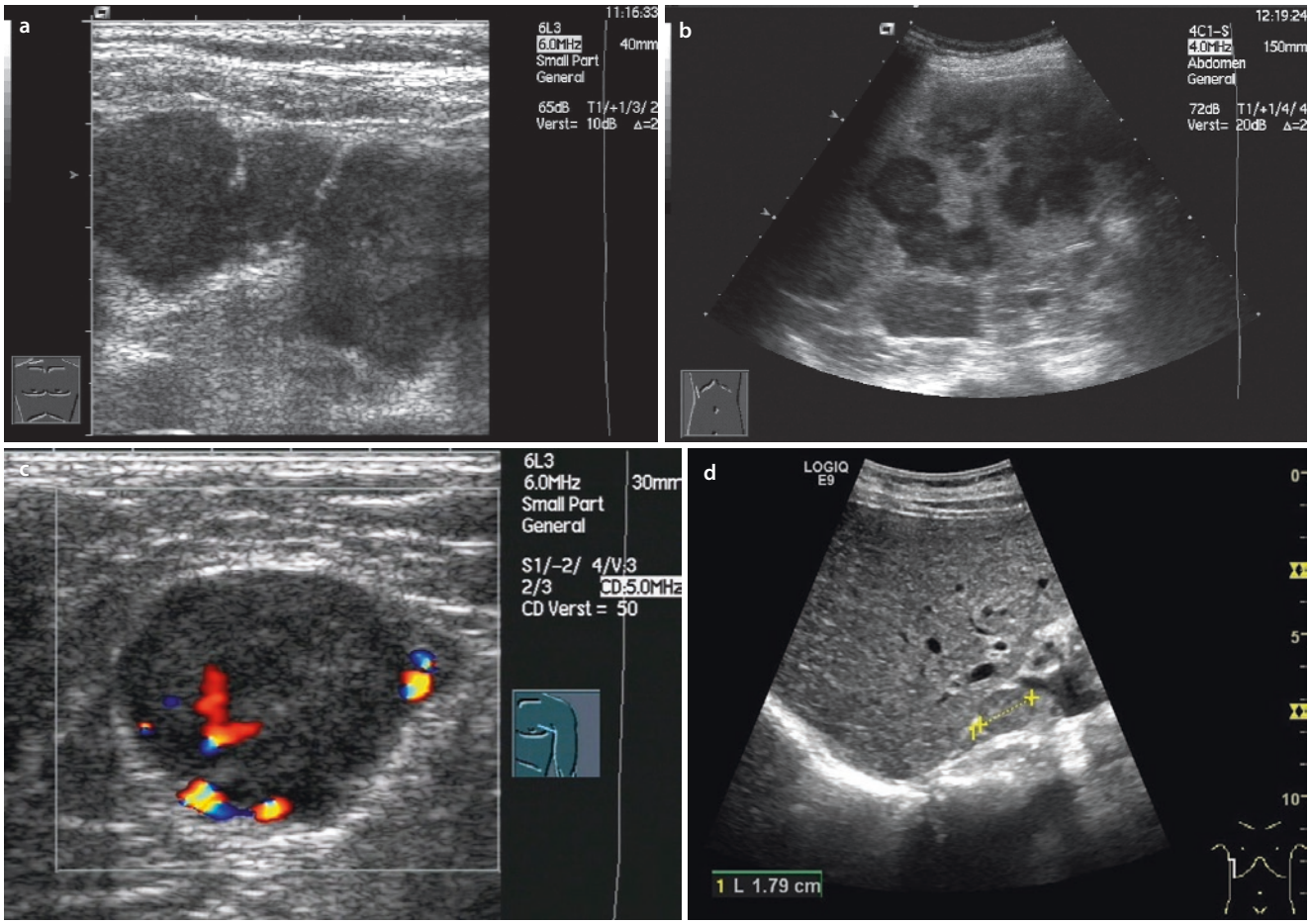

Fig. 5.29 **a** Supraclavicular lymph node metastases in a woman with a bronchial adenocarcinoma. **b** Diffuse metastatic invasion of the entire right lobe of the liver in a man with a non-small-cell lung carcinoma. **c** Axillary lymph node metastasis in lung cancer, round and echopoor, irregular vascularization central and at the margin. **d** Adrenal metastasis in lung cancer

not permit the investigator to decide whether the lesion is malignant or benign.

In the course of tumor staging, sonography is more suitable than computed tomography to demonstrate metastases in supraclavicular lymph node regions (Fultz et al. 2002; Prosch et al. 2007; Hoosein et al. 2011; Rettenbacher 2014; Fig. 5.29a).

The basic diagnostic procedures must include sonography of the abdomen in order to identify metastases (Fig. 5.29b, d).

Tumor-Related Complications in Mediastinal Vessels

In case of mediastinal tumor spread, the vena cava and its supplying vessels must be examined in order to identify compression syndromes or thrombosis (Ko et al. 1994).

Differentiation of a Central Space-Occupying Lesion from an Atelectasis

Atelectatic lung tissue is a suitable sonic window to the tumor that occludes the branch of the bronchus. Quite often sonography (Fig. 5.30a) allows better differentiation of the tumor from nonventilated lung tissue than computed tomography (Fig. 5.30b).

In some cases, vessels of the tumor itself are found particularly in the margin (Fig. 5.29b). Such vessels are convoluted and marked by changes in diameter (Yuan et al. 1994; Mathis 1997; Hsu et al. 1996, 1998).

5.2.6 Heterogeneous Structural Pattern

The assessment of malignant lesions might be rendered difficult by their highly *heterogeneous structural pattern* (Pan et al. 1993).

Tumor consolidations may still contain residually ventilated bronchial branches (Fig. 5.27) or *colliquations* and/or *necrotic zones* (Figs. 5.28b and 5.31).

Lung tissue adjacent to a tumor might be affected by inflammation (Fig. 5.32) or contain calcifications.

In a diseased portion of the lung, solid portions of the tumor might exist along with complex inflammatory infiltrations (Fig. 5.31).

Sonographic assessment of an adenocarcinoma lepidic pattern (earlier bronchoalveolar carcinoma) is highly problematic. On the one hand, multiple peripheral consolidations with variable air content might mimic multifocal pneumonia (Goerg et al. 2002; Fig. 5.32). On the other hand, one may only find an uncharacteristic uneven lung surface.

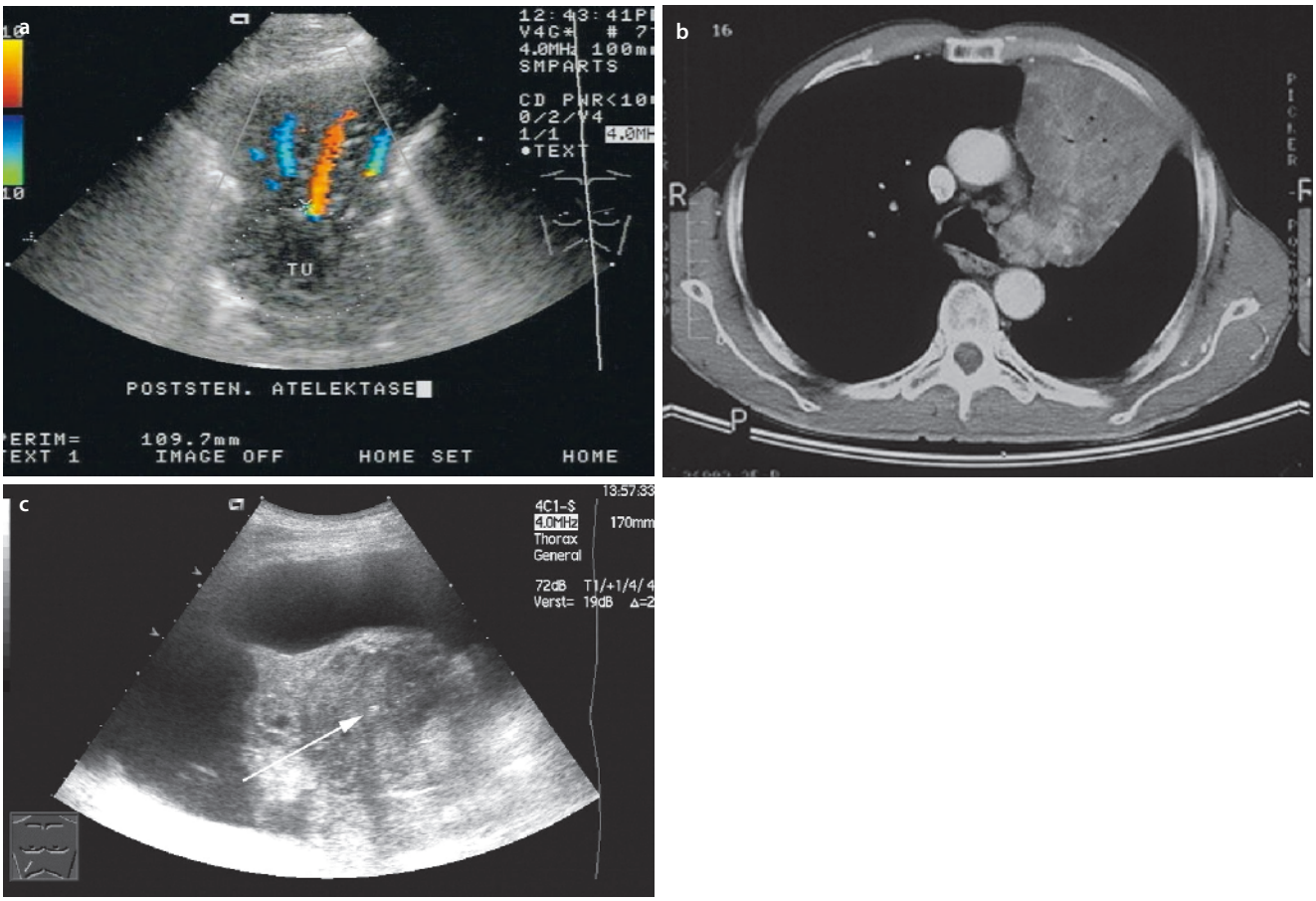

Fig. 5.30 **a** Central tumor in the left upper lobe (*broken line*); behind it there is atelectatic lung tissue with a regular vascular architecture. **b** Computed tomography image of the tumor and the atelectasis in the upper lobe. **c** Large tumor (*arrow*) in the right lower lobe; in the marginal area there is atelectatic lung tissue surrounded by a pleural effusion. Sonographic biopsy of the tumor indicated small-cell carcinoma

In all cases of ambiguous pulmonary lesions, sonography may serve as an important aid in decision-making. It helps the investigator to decide about the subsequent diagnostic procedure – either immediately in terms of a sonography-assisted biopsy (Mathis et al. 1999; Beckh et al. 2002; Gompelmann et al. 2012), or as a complementary imaging method to select the appropriate surgical procedure.

Pulmonary Metastases

Pulmonary metastases are documented on sonography when they reach the margin of the lung. Owing to poor visibility in this region, sonography is not a suitable screening method. Metastases have no small air trappings and are usually homogeneously hypoechoic; occasionally, they have branches extending into tissue (Mathis et al. 1999). Pathological vessels are predominantly found at the margin (Figs. 5.33 and 5.34; Table 5.2).

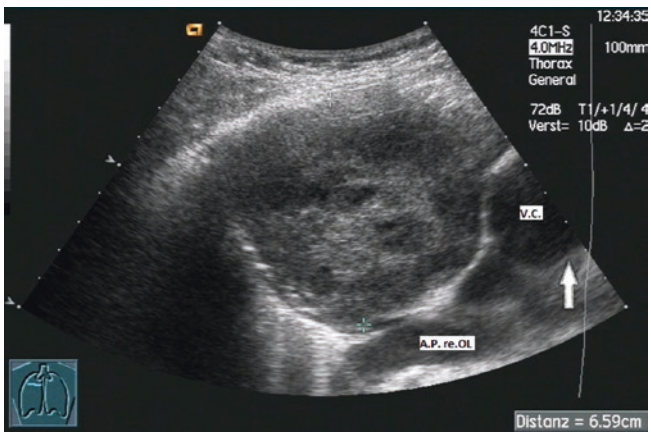

Fig. 5.31 Space-occupying lesion in the upper and middle lobe with several necrotic zones (*arrowheads*). Initially there were marked signs of inflammation on clinical examination. Under antibiotic therapy the invasive pneumonic portion resolved (*arrow*). Sonographic biopsy from solid portions of the space-occupying lesion indicated squamous cell carcinoma

Summary

Sonography does not permit the investigator to make a distinction between metastases and peripheral carcinoma. The interpretation must take the patient's medical history and survey radiographs into account. In terms of differential diagnosis, the formation of lesions in the parietal pleura must be excluded by dynamic investigation. Even benign pulmonary lesions,

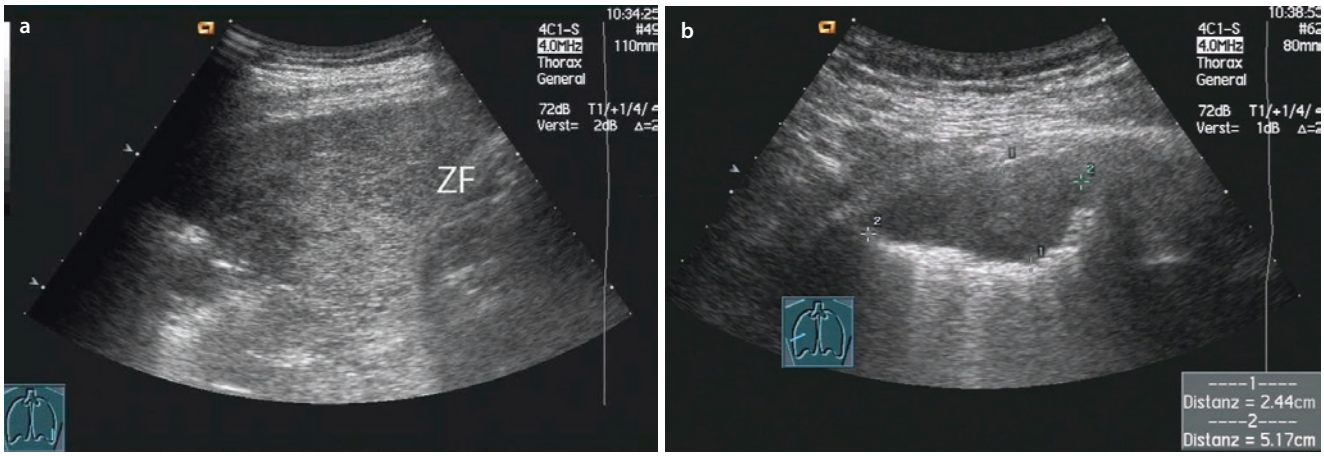

Fig. 5.32 Space-occupying lesion in the upper and middle lobe with several necrotic zones (*arrowheads*). Initially there were marked signs of inflammation on clinical examination. Under antibiotic therapy the invasive pneumonic portion resolved (*arrow*). Sonographic biopsy from solid portions of the space-occupying lesion indicated squamous cell carcinoma

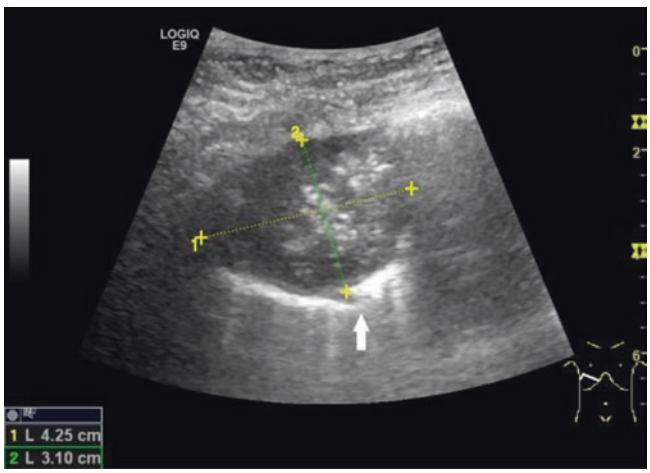

Fig. 5.33 This 77-year-old man complained of pain in the right chest. Sonography revealed a large tumor formation extending from the lung to the chest wall and leading to osteolytic destruction of a rib (*arrow*). Sonography-guided biopsy indicated metastasis of a urothelial carcinoma operated on 2 years ago

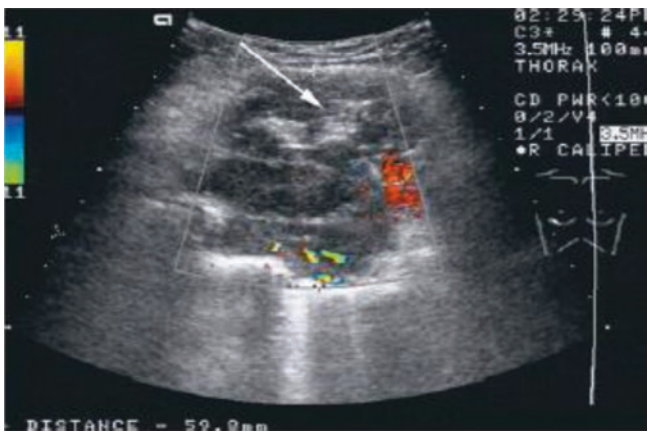

Fig. 5.34 In the right lower lobe a metastasis from breast cancer infiltrating in lung tissue (*arrow*)

Table 5.2 Sonomorphology of pulmonary metastases

Morphology	Echotexture	Vessels
Round	Hypoechoic	Bizarre new vessel formation at the margin
Oval	No ventilated portions	–
Serrated	Necrosis possible	–
Sharp margins	–	–

e.g., hamartoma or hemangiofibroma, might extend to the periphery of the lung as hypoechoic formations. Cyst walls may be of varying thickness. They usually have an anechoic content. Occasionally they contain fluid with internal echoes. In order to differentiate between a cyst and a pulmonary abscess or an encapsulated empyema, the diagnostic procedure must take clinical parameters and computed tomography investigations into account. In the final analysis, bacteriological, cytological, and histological investigations are of decisive importance.

5.3 Vascular Lung Consolidations: Pulmonary Embolism and Pulmonary Infarction

Gebhard Mathis

Pulmonary embolism is the most frequent clinically nondiagnosed cause of death. Autopsy studies have demonstrated a frequency of 10–15 %. In cases of chronic heart failure the rate is as high as 30 %. Again, pulmonary embolism is the cause of death in 40 % of these. Ten percent of deaths in clinics are due to pulmonary embolism. In a further 10 %, pulmonary embolism is involved in a causal way.

Clinical symptoms are rare and tend to be quite harmless and unspecific. The chest X-ray is not very sensitive. Even in times of MSCT, one must assume that 40 % of fatal pulmonary embolisms remain undiagnosed (Reissig et al. 2010). The crucial diagnostic step still is to consider the investigation procedure in the first place. The clinician is called upon to use any method that improves the diagnosis of pulmonary embolism and reduces mortality – which still is as high as 15 % (Goldhaber et al. 1999; Janata et al. 2002; Burge et al. 2008; Newman and Schriger 2011).

5.3.1 Pathophysiological Prerequisites for Sonographic Imaging of Pulmonary Embolism

A few minutes after a secondary pulmonary artery has been occluded, the surfactant collapses. Interstitial fluid and erythrocytes flow into the alveolar space. A hemorrhagic congestion offers the most ideal conditions for sonographic imaging. These consolidations are oriented towards the pleura. Practically along with their base they are open at the periphery, which creates good conditions for transthoracic sonography (Fig. 5.35).

The pulmonary embolism is a dynamic process. Small hemorrhages are rapidly absorbed by local fibrinolysis, as the intimal layer of pulmonary arteries has a substantial fibrinolytic capacity. The rather frequent condition of a recent reperfusable transient hemorrhage (early infarction) as well as the rare condition of a genuine pulmonary infarction with tissue necrosis (late infarction) can be visualized on ultrasound. Small premonitory embolisms (signal embolisms) may occur before a massive or fulminant pulmonary embolism and lead to the initiation of appropriate therapeutic measures (Mathis and Dirschmid 1993).

5.3.2 Sonomorphology of Pulmonary Embolism

Form and Echotexture

Peripheral pulmonary embolisms are hypoechoic and largely homogenous on ultrasound. Older and larger infarctions may be grainy in terms of structure. Embolism-related lung consolidations are largely triangular, with a pleural base, and may protrude slightly. The lesions may be rounded towards the hilum or polygonal in shape. The margin may be initially somewhat blurred, but is usually sharp. A pseudo acoustic enhancement may be seen behind it (Fig. 5.36; Mathis and Dirschmid 1993; Reissig and Kroegel 2003; Mathis et al. 2005)

Distinction between an early infarction that can be reperfused and a late infarction with tissue necrosis is rarely achieved; it is achieved only in larger lesions beyond a size of 2–3 cm. Nevertheless, these criteria are important to differentiate these from inflammatory infiltrates, which are usually larger.

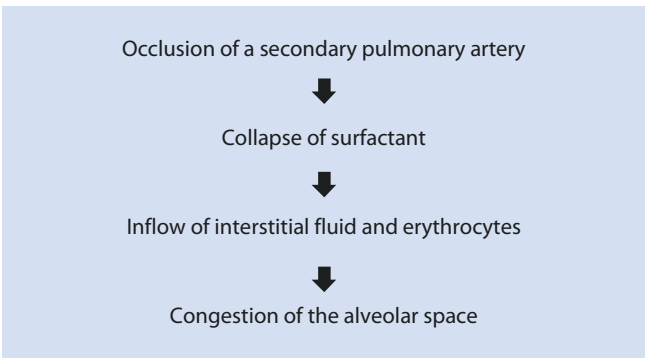

Fig. 5.35 Pathophysiological prerequisites for sonographic imaging in cases of pulmonary embolism. Peripheral engorgement of the alveolar lumen is a good prerequisite for pathological echo transmission

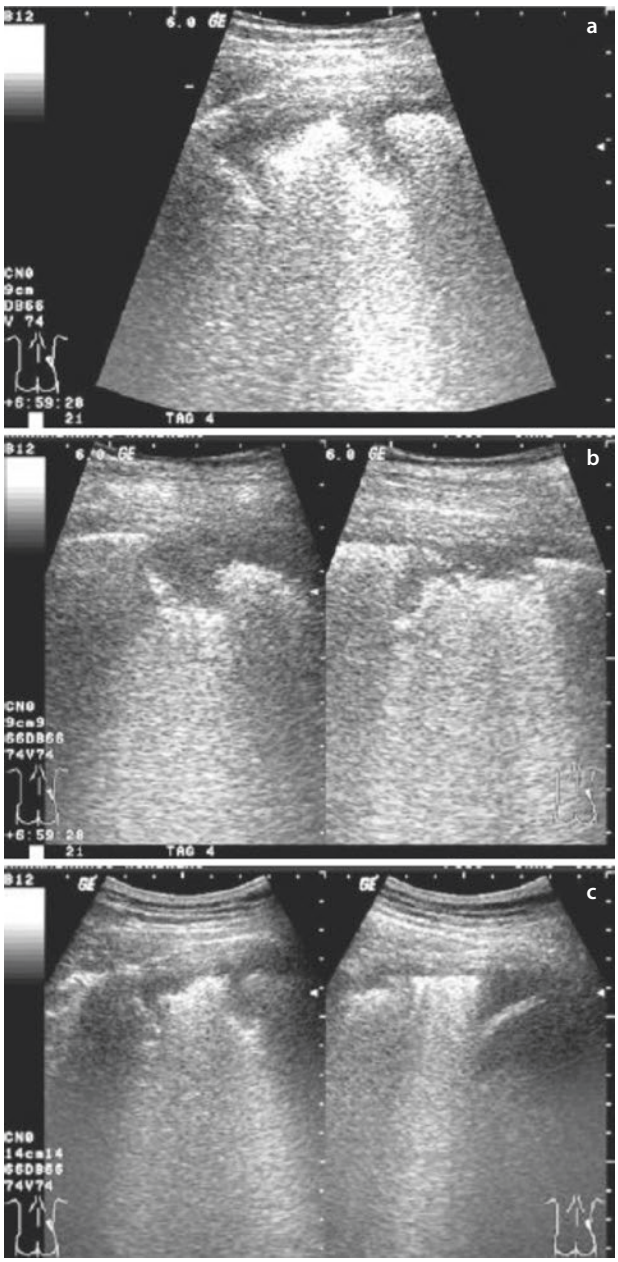

Fig. 5.36 **a** Two adjacent pulmonary infarctions in the same region of terminal flow in the presence of an obstructed pulmonary secondary artery.**b** Two further infarctions in the same woman. **c** Accompanying pleuraö effusion

Studies published in the last few years have provided a much more precise description of the sonomorphology of hemorrhage and infarctions in the presence of pulmonary embolism (Mathis and Dirschmid 1993; Reissig and Kroegel 2003; Mathis et al. 2005).

Localization

Two-thirds of lung infarctions are located dorsally in the lower lobes of the lung, more often on the right side than on the left side. This is because of anatomical factors and because of hemodynamics: basal pulmonary arteries tend to run straight, while arteries of the upper lobe tend to branch off at a steeper angle. The dorsobasal region is particularly accessible to transcutaneous sonography (Figs. 5.44, 5.45 and 5.46).

Number

The improved resolution available today allows the investigator to detect more lesions than he/she could several years ago. In cases of pulmonary embolism, on average 2.4 infarctions are seen on sonography. Given two or more lesions and the clinical likelihood of pulmonary embolism, the specificity of sonography is 99 %. In slim patients it would be advisable to investigate the pleural reflex with a high-frequency transducer as well (Fig. 5.38).

Size

The mean size of pulmonary infarctions is 12 mm × 16 mm (range 5–70 mm). Lesions less than 5 mm in size should not be taken into account because they might be merely scars. If at all, their progress should be monitored. Pleuritis may be marked by a similar appearance. However, pleuritis will be found at the site of pain and is usually characterized by extensive fragmentation of the pleural reflex (Figs. 5.36, 5.37, 5.38, 5.39, 5.40, 5.41, 5.42, and 5.43).

Morphology

Pulmonary infarctions are usually triangular in shape and have their base at the pleura. The pleural base may be slightly protruded. Quite often the lesions are rounded towards the hilum; occasionally they are also polygonal in shape (Reissig et al. 2001; Mathis et al. 2005; Fig. 5.45).

Vascular Signs

In some cases one finds an anechoic *band of vessels* on the B-mode image. The band of vessels is oriented from the tip of the lesion towards the hilum. It corresponds to the branch of the pulmonary artery congested by thromboembolism, as evidenced in computed tomography investigations as well (so-called vessel sign or vascular sign) (Figs. 5.44 and 5.47).

Pleural Effusion

In approximately half of cases the investigator finds small pleural effusions either focally above the lesion or in the pleural sinuses. The effusion is largely anechoic and smaller than an infarction, which is an important criterion to distinguish this entity from compression atelectasis. The pleural effusion may also lead to apparent echo enhancement in the pulmonary infarction. Internal echoes in the effusion and fibrin strands are indicative of infarction pneumonia (Mathis et al. 1993; Fig. 5.45).

Signal Embolism

A massive pulmonary embolism is frequently accompanied by smaller embolic events, which then appear as *signal embolisms*. They are visualized as individual triangular or rounded small lesions. Several such small defects lying adjacent to each other create the image of a lacerated margin between the nonventilated portion of the lung lying close to the pleura and the normally ventilated portion of the lung. Such small lesions may be a precursor of an imminent pulmonary embolism or may even be present in conjunction with a massive central pulmonary embolism and thus confirm the diagnosis without the central embolus itself being demonstrated on chest sonography; it escapes detection because of air in the intervening space (Fig. 5.46).

Color-Coded Duplex Sonography in Pulmonary Embolism

In very few cases is the investigator able to visualize, on color-coded duplex sonography, a circulation stop caused by embolism (Fig. 5.47). This limitation has several reasons:

- Patients with dyspnea cannot hold their breath long enough, which causes several artifacts on color-coded duplex sonography.
- It is difficult to locate the supplying vessel at the right level.
- When reperfusion occurs rapidly, the lesion is revascularized early. However, such perfusion is markedly less than that in pneumonic infiltrates.

Nevertheless, color-Doppler sonography is an important tool to differentiate subpleural pulmonary lesions (Yuan et al. 1993; Gehmacher and Mathis 1994).

Contrast-Assisted Sonography

Pulmonary infarctions and hemorrhage due to embolism are marked by the absence of circulation and the absence of contrast on contrast-assisted sonography as well as color-Doppler sonography. At the margin of the lesion there may be delayed or poor contrast enhancement because this area is supplied by a bronchial artery. Pleuritis and pneumonia, on the other hand, are contrasted early and strongly by a pulmonal artery supply. In case of doubt pleural consolidations can be distinguished from embolic ones by the use of signal-enhanced ultrasound (Goerg 2007; Bertolini et al. 2008; Fig. 5.48 ▶ Chap. 8).

Phase of Healing: Infarction Pneumonia

Several weeks after a pulmonary embolism, the sonomorphology of the pulmonary infarction is no longer characteristic. As reventilation progresses, the sonographic image resembles that of pneumonia (Fig. 5.41). Infarction pneumonias may develop in the region of infarction or even in the vicinity of the infarction and between multiple infarctions. Coughing up sequestrated infarctions creates infarction cavities, which may become subject to secondary infection

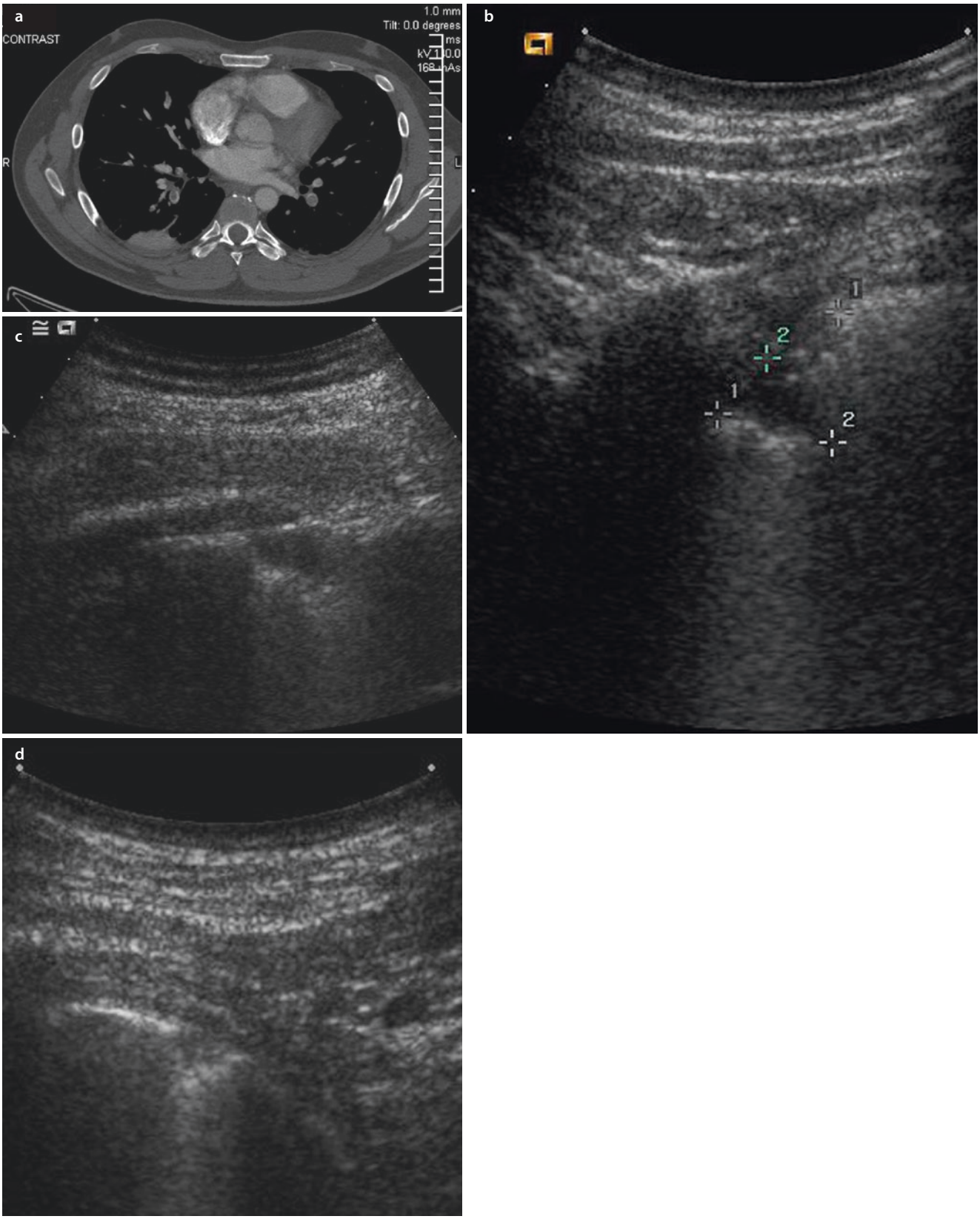

Fig. 5.37 A 42 year-old male patient 2 weeks after dyspnea following appendectomy. **a** MSCT cemonstrates the pulmonary embolism in central and peripheral location. **b** The pulmonary embolism measuring 2 cm on ultrasound corresponds to the peripheral consolidation on MSCT. **c**, **d** Two pulmonary infarctions measuring 1 cm in size were not seen on the 32-slice CT

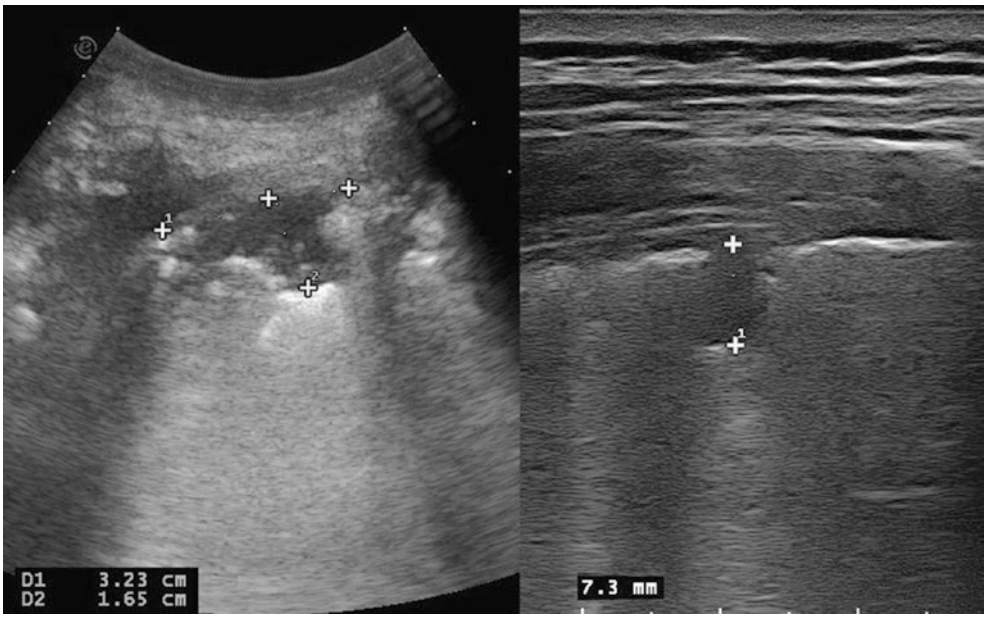

Fig. 5.38 A 42-year-old male patient 2 weeks after dyspnea following appendectomy. **a** MSCT demonstrates the pulmonary embolism in central peripheral location. **b** The pulmonary embolism measuring 2 cm on ultrasound corresponds to the peripheral consolidation on MSCT. **c**, **d** Two pulmonary infarctions measuring 1 cm in size were not seen on the 32-slice CT

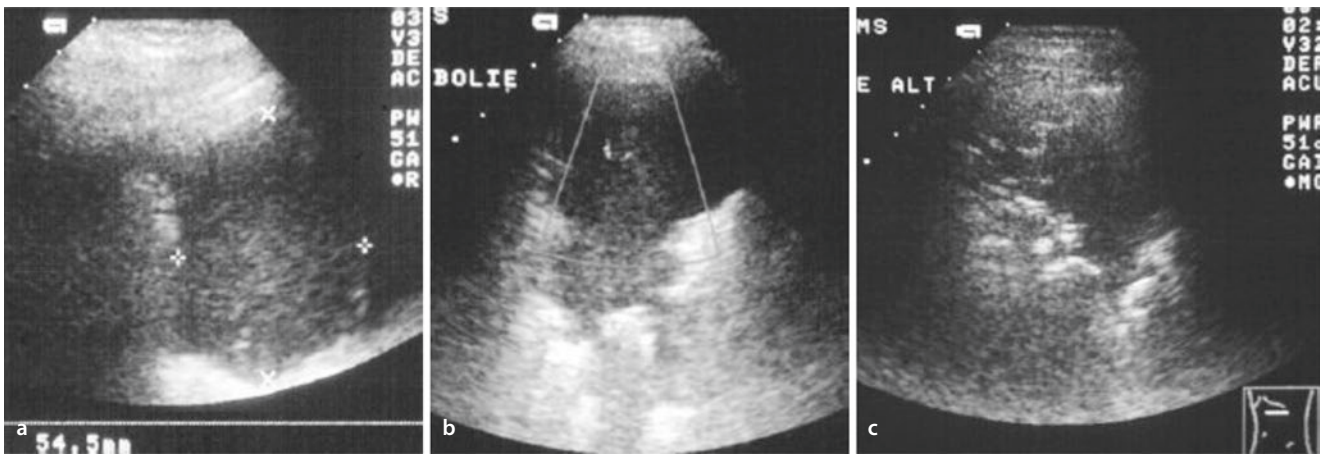

Fig. 5.39 **a** Five hours after the embolic event there is a rounded, homogeneous early infarction. **b** After 5 days the lesion is triangular in shape. **c** After 12 days the lesion has developed into a classic pulmonary infarction that is somewhat smaller than the original lesion, triangular in shape and marked by serrated margins

and lead to a pulmonary abscess. Therefore, the processes of repair in late infarctions create diverse conditions for sonographic imaging. A sonomorphological distinction between this entity and other peripheral lung consolidations now becomes difficult. In patients who arrive for sonographic investigation in the stage of infarction pneumonia, 1 or 2 weeks after the event the lesion can be imaged by sonography but the sonomorphology offers very few criteria for differential diagnosis.

Tips on the Procedure

Many patients with a pulmonary embolism report pleuritic chest pain. Others report discomfort in a specific region. The clinician first looks at the region of pain and is able to establish the cause very rapidly. When the patient does not mention a specific location, the clinician starts the investigation in the dorsobasal aspect, where the large majority of pulmonary embolisms can be seen. In cases of continued clinical suspicion the clinician should perform an echo investigation of the entire lung, which may take several minutes. The dorsobasal region must be examined in all cases.

5.3.3 Sonomorphological Differential Diagnosis

Various criteria permit sonomorphological differential diagnosis between pneumonia and peripheral pulmonary lesions of other origin. *Pneumonias* are characterized by blurred margins on the sonogram, are inhomogenously structured, have numerous lenticular internal echoes, bronchoaerograms, and in cases of poststenotic pneumonias even fluid bronchograms. In the early stage pneumonia may be similar to the liver (Sect. 5.1).

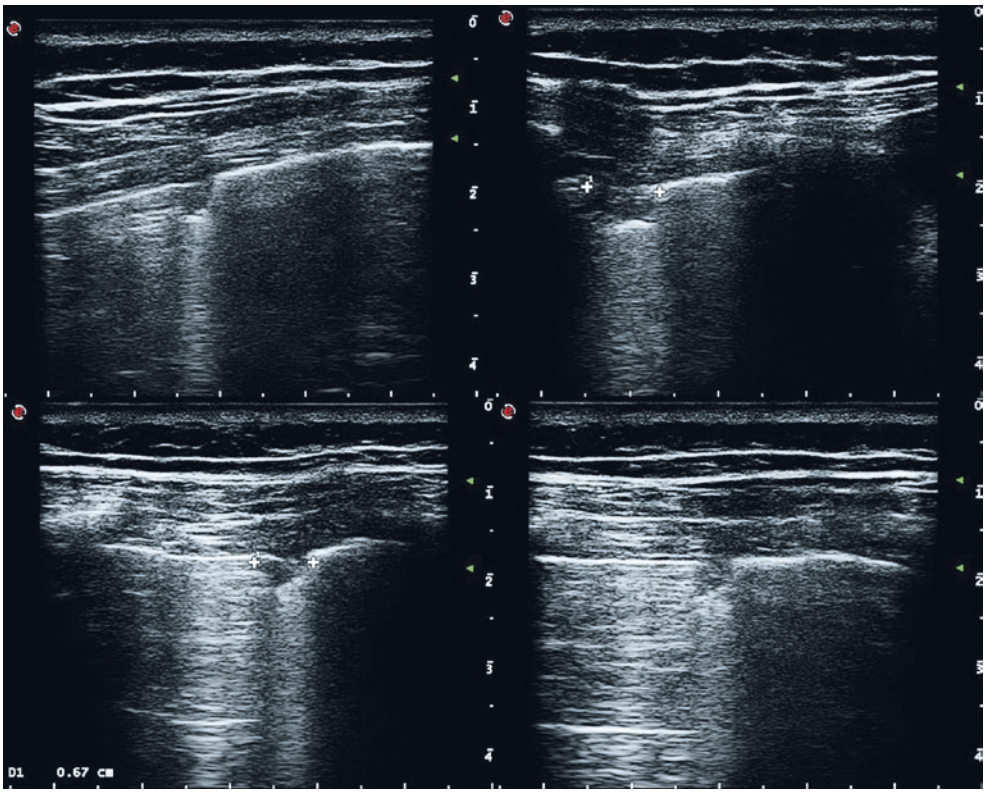

Fig. 5.40 24-year-old woman in pregnancy, deep vein and pelvis thrombosis, slight dyspnea. Several near 1 cm small pulmonary embolisatzions

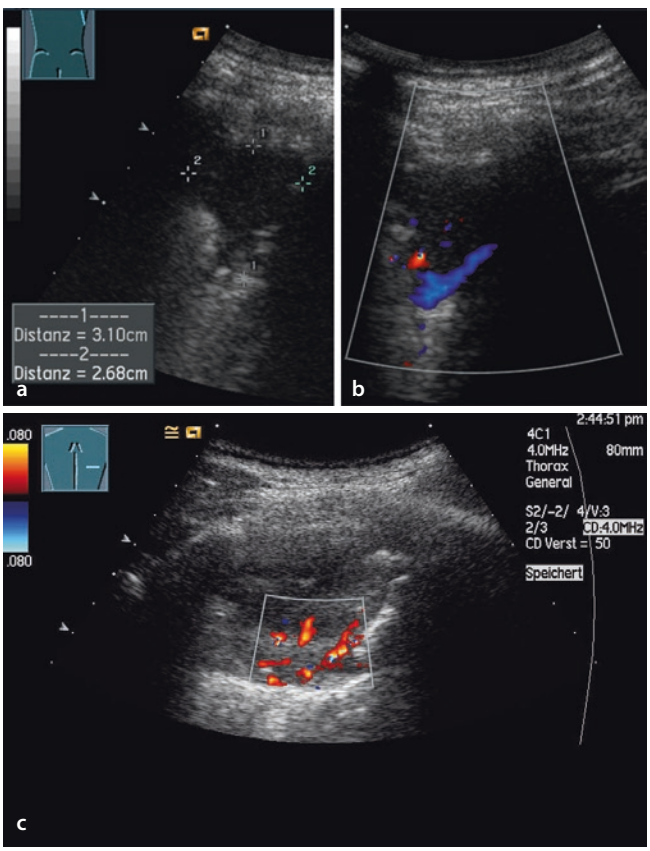

Fig. 5.41 **a** Early triangular pulmonary infarction. The D-dimer test was still negative at this time. **b** The infarction is vascularized only at the margin and not in the center. **c** Four days later the patient had an infarction pneumonia that was seen clinically as well. This is larger than the original lesion, partly ventilated, and revascularized

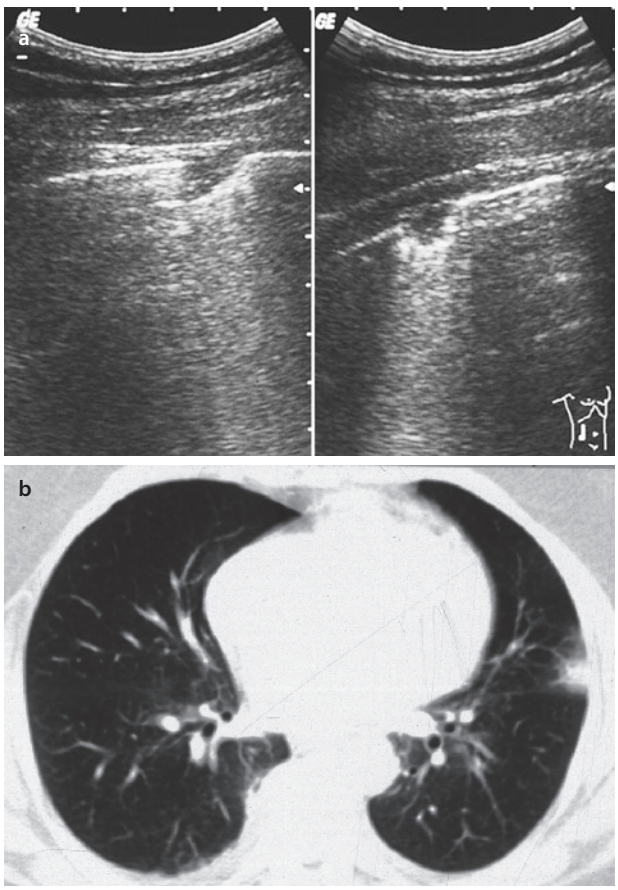

Fig. 5.42 A 25-year-old woman with sudden dyspnea and mild respiratory chest pain. **a** Sonography revealed two small pulmonary infarctions. **b** On spiral computed tomography the central pulmonary embolism was confirmed and only one lesion was seen in the periphery

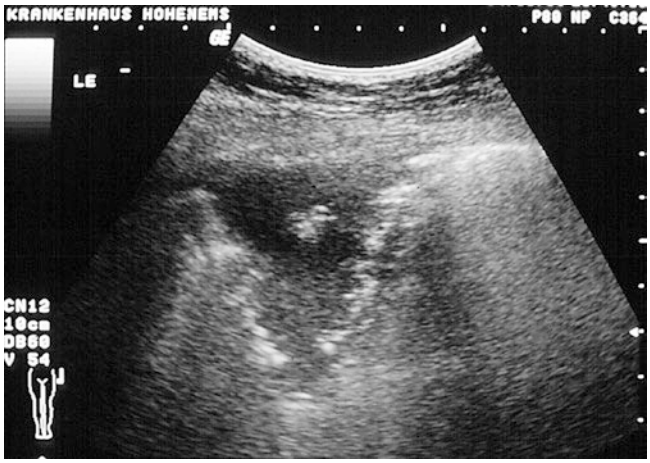

Fig. 5.43 Large, classic pulmonary infarction with highly serrated margins and a central bronchial reflex

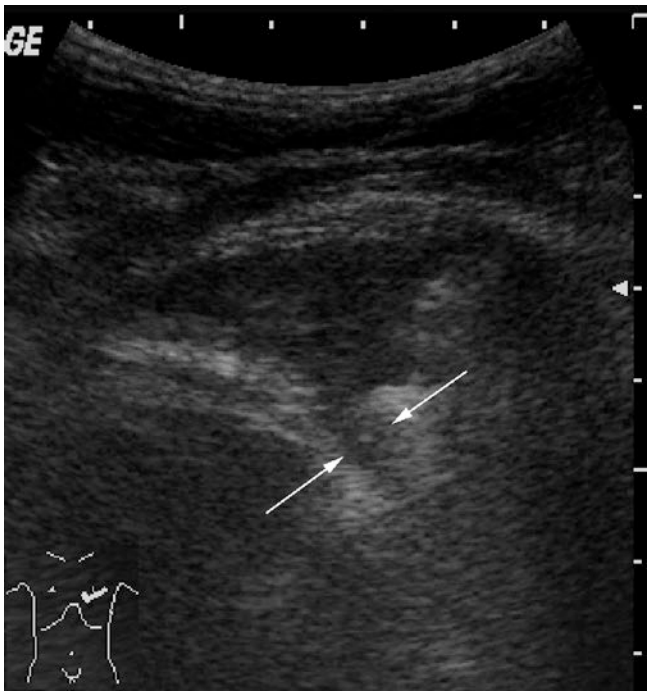

Fig. 5.44 Most pulmonary infarctions are found in dorsobasal location owing to anatomical and hemodynamic factors

Carcinomas and metastases tend to be rounded or polycyclic, grow in an invasive fashion, have crow's feet, tumor cones and, occasionally, central necrotic zones.

Compression atelectases are narrow, shaped like a pointed cap, concave at least on one side, and float in the effusion, which is much larger than the atelectasis (Mathis et al. 1993; Mathis 2014).

Color-coded duplex sonography is also suitable to differentiate between pneumonic and neoplastic lesions: Pneumonias have a marked, regular central pattern of circulation, while carcinomas and metastases are nourished by atypical corkscrew-shaped vessels at their margins. Contrast-assisted sonography allows the investigator to distinguish between pulmonary infarctions and inflammatory infiltrates.

5.3.4 Accuracy of Chest Sonography in the Diagnosis of Pulmonary Embolism

A large multicenter study comprising 352 patients in the ordinary clinical setting round the clock, which included less experienced investigators, showed that three-fourths of patients with pulmonary embolism have typical peripheral lesions on sonography. A surprisingly high specificity of 95% was achieved in this study (Mathis et al. 2005). These figures concur with those reported for the demonstration of peripheral pulmonary embolisms in pathological studies. The results are worse, if the dorsal region is not examined (Nazerian et al. 2014).

Two recent meta-analyses of five resp 10 studies on 652/887 patients, the pooled sensitivity and specificity was 80–87% and 82–93%. The authors conclude that, in view of the increasing numbers of CT investigations and the increasing collective radiation dose for specific clinical situations, such also emergency, pregnancy, renal failure, and contrast allergy chest ultrasound serves as a diagnostic alternative to CT (Niemann et al. 2009; Squizzato et al. 2013). This is recommended it actual Consensus and guidelines (Volpicelli et al. 2012; AWMF 2016).

Caution: A normal chest sonogram does not exclude the presence of pulmonary embolism, as is true for a negative computed tomography or a negative D-dimer test as well.

5.3.5 Triple-Organ-Ultrasound in Thromboemplism

In several anatomical locations, sonography has become the method of choice to diagnose thromboembolism. In a single investigation step the experienced investigator is able to inspect several actual clinically or potentially involved regions of the body using a single imaging procedure. He/she is able to study the *source*, *pathway*, and *target* of the embolic event.

Duplex Sonography of Leg Veins

Much more than half of pulmonary embolisms originate from leg veins. Compression sonography is a safe procedure to confirm that an embolism is originating from a deep vein thrombosis. In cases of suspected leg vein thrombosis the median sensitivity is 95% and the median specificity is 97%. Even in cases of the relatively frequent isolated lower leg thrombosis the median sensitivity is 89% and the median specificity is 92% (Jaeger et al. 1993). Patients who have anticoagulation withheld following a negative or inconclusive whole-leg compression ultrasound for suspected deep vein thrombosis have a low rate of adverse events (Horner et al. 2014).

Visualization of the thrombus and the absence of flow are direct signs of leg vein thrombosis (Fig. 5.49). Detection of the thrombus in the B-mode is indirectly improved by the application of color-Doppler sonography. The thrombosed vein is not compressible or is only partially compressible, which is indicative of an occluding coagulation. However,

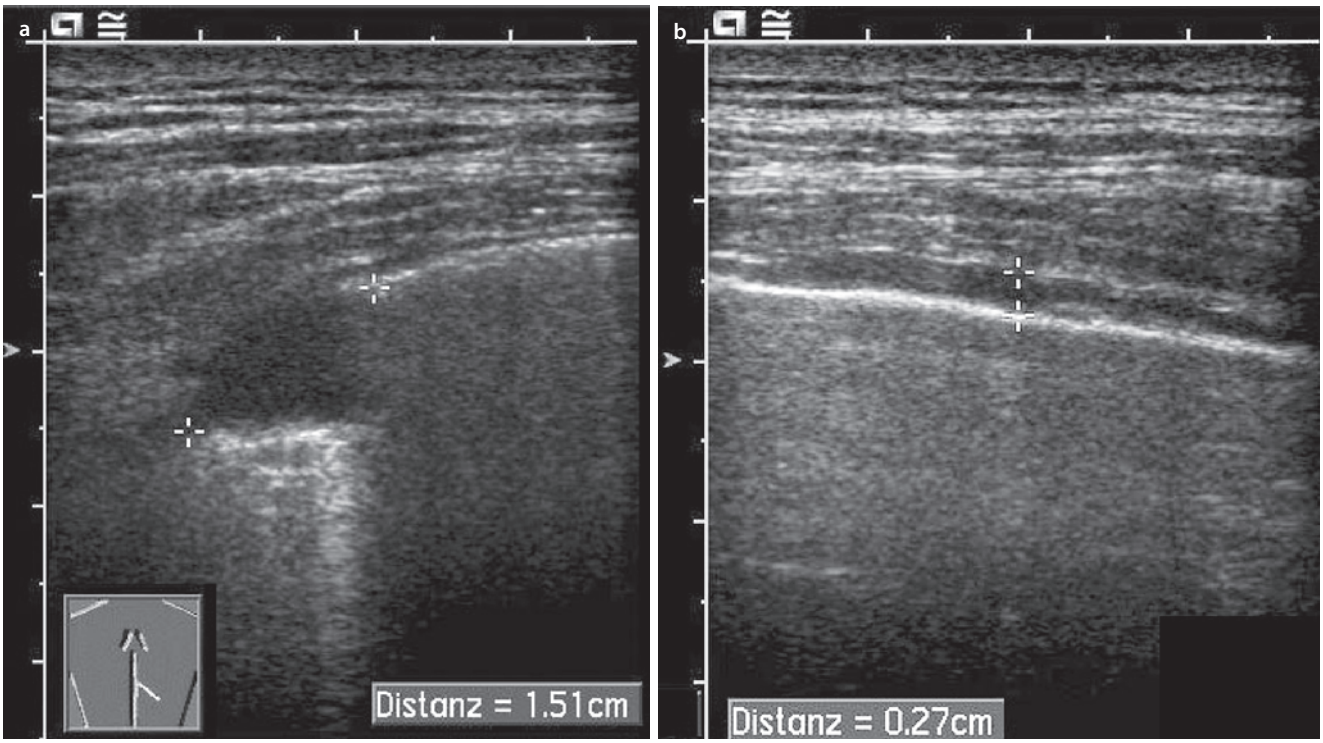

Fig. 5.45 **a** Triangular lung infarction of typical form and size with pleural protrusion. **b** Small loculated pleural effusion

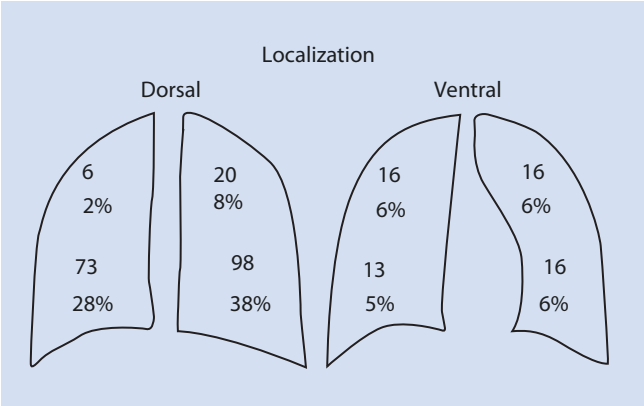

Fig. 5.46 Most pulmonary infarctions are found in the dorsobasal location owing to anatomical and hemodynamic factors

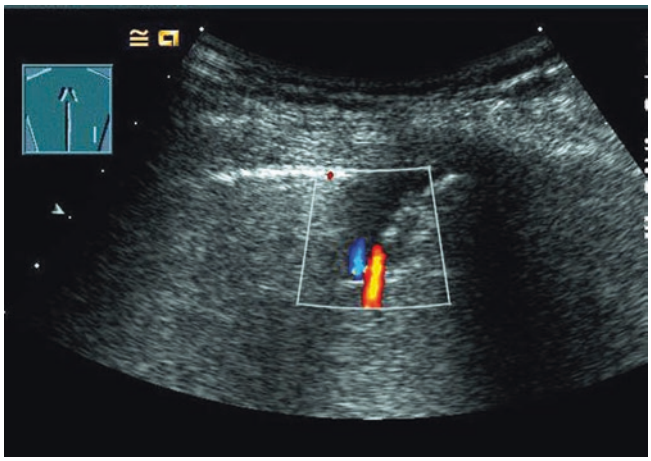

Fig. 5.47 Circulatory stop at the tip of the wedge-shaped pulmonary infarction

signs of compressibility are only reliable when they are found in the inguinal or popliteal region. The vena cava and pelvic veins are not sufficiently compressible. In cases of calf thrombosis the compression is painful on palpation. The respiratory phase of venous flow is lost at a location distal to any hindrance of flow. In cases of acute thrombosis the vein is markedly dilated and valvular movements are absent.

Echocardiography

About 40% of patients with acute pulmonary embolism have a right heart load. This specifically includes patients at hemodynamic risk who have to undergo lysis or embolectomy as a life-saving measure. The first hours after the onset of symptoms are of decisive importance for the prognosis of hemodynamically relevant pulmonary embolism. On echocardiography one can obtain a rapid overview of the degree of risk for the patient, establish the intensity of monitoring, and devise a treatment plan.

The following parameters are used to assess acute right heart load (Wacker et al. 2003; McConell et al. 1996; Jackson et al. 2000; Miniati et al. 2001; Konstantinides et al. 2014):

- Size of the right ventricle (Fig. 5.50)
- Contraction of the free right-ventricular wall
- Movement of the interventricular septum
- Size of the right atrium
- Are embolisms seen in the right heart?
- Exclusion of atrial myxoma

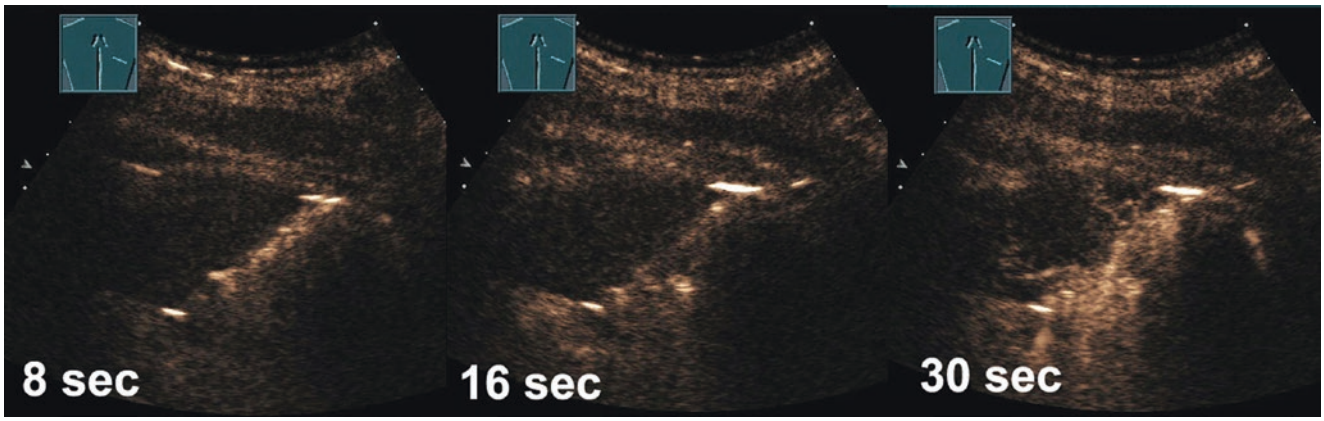

Fig. 5.48 In contrast enhanced ultrasound pulmonary embolism shows a very late and less intensive enhancement – very well for differentiation of inflammatory consolidations

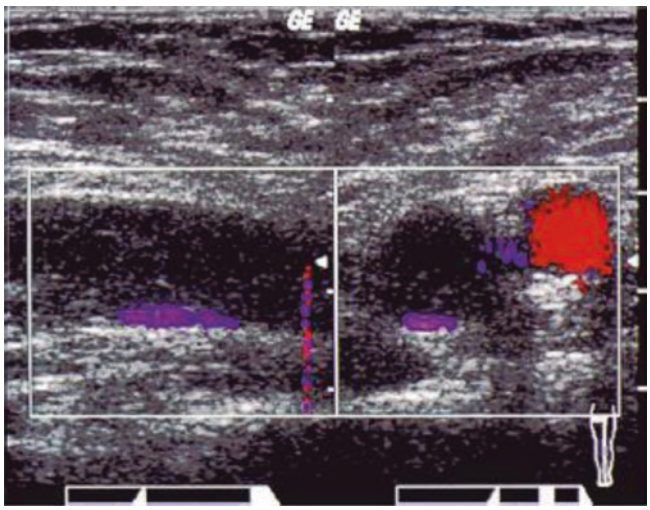

Fig. 5.49 Searching for the source of embolism: leg vein thrombosis in the femoral vein. The vein is larger than the artery, congested with echogenic material, and cannot be compressed. A small amount of flow is seen at the margin

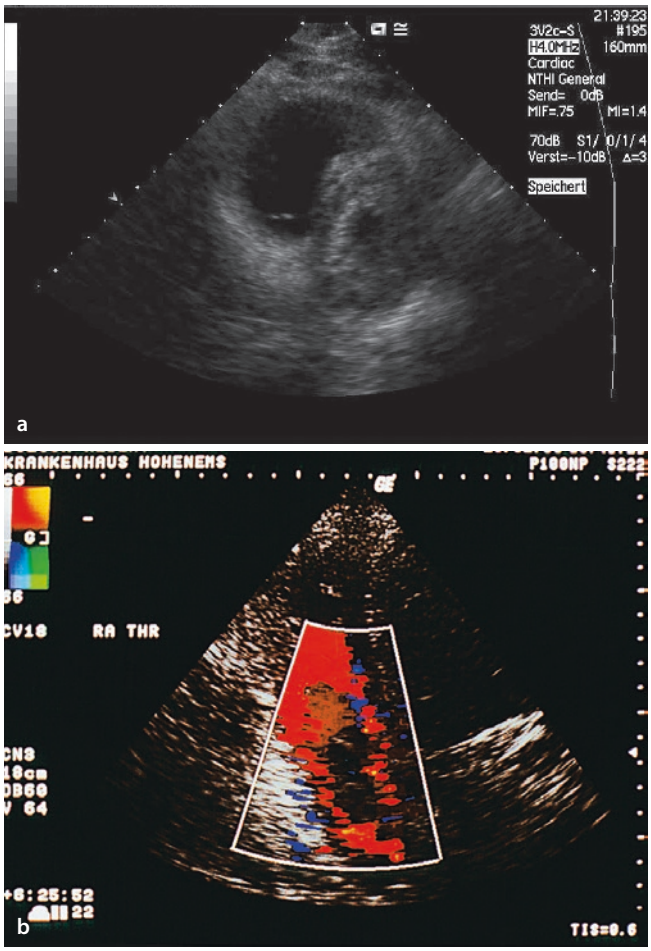

Fig. 5.50 **a** Acute load of the right side of the heart with massive dilatation of the right ventricle. **b** At the level of the valve there is a floating thrombus in the right side of the heart

These parameters are frequently assessed, determined individually, but not conclusively. This "over-view" focussed echocardiogram provides important subjective impressions, a few measured data, and occasionally an inadequate range of differential diagnoses concerning the various causes of right heart load.

Right-ventricular dysfunction typically occurs in basal location and is more pronounced medially in cases of acute right heart failure while the kinetics of the apex of the heart is relatively intact (McConell et al. 1996). In cases of chronic right heart load the right ventricle is uniformly adynamic and dilated. Measurement of the tricuspid annulus plane systolic excursion (TAPSE) may also be useful.

Echocardiographic examination is not recommended as part of the diagnostic work-up in haemodynamically stable, normotensive patients with suspected (not high-risk) pulmonary embolsim. This is in contrast to suspected high-risk PE, in which the absence of echocardiographic signs of RV overload or dysfunction practically excludes PE as the cause of haemodynamic instability. In the latter case, echocardiography may be of further help in the differential diagnosis of the cause of shock, by detecting pericardial tamponade, acute valvular dysfunction, severe global or regional LV dysfunction, aortic dissection, or hypovolaemia (Konstantinides et al. 2014).

Since the introduction of transesophageal echocardiography, the source of embolism is increasingly looked for in the heart as well. Transthoracic echocardiography may disclose sessile and floating thrombi in the right atrium. In transesophageal location, one may also find riding thrombi in the central main trunks of the pulmonary arteries.

A major advantage of sonographic investigation of embolism is its manifold applicability and its availability at the bedside, whether in the emergency department or in the intensive care unit. Echocardiography and leg vein compression sonography yield a sensitivity of more than 90 % for pulmonary embolism (Mathis et al. 2006; Nazerian et.al. 2014).

5.4 Mechanical Lung Consolidations: Atelectasis

Christian Görg

5.4.1 Definition

Atelectasis is defined as the absence of ventilation in portions of the lung or the entire lung. Such lack of ventilation may be permanent or transient, complete or partial (dysatelectasis), congenital or acquired (Fig. 5.51).

5.4.2 Pathomorphology

Depending on the origin, a distinction is made between compression atelectasis and resorption atelectasis (obstructive atelectasis). Compression atelectasis may be anticipated when an accumulation of fluid causes intrapleural pressure to increase to a level higher than that of external air. This may be expected when the effusion is more than 2 l (Grundmann 1986).

Resorption atelectasis occurs when a bronchus is displaced in terms of its region of vascular supply, as a result of external compression or endobronchial obliteration.

In cases of resorption or obstructive atelectasis, a distinction is made between the central and the peripheral forms. Central obstruction is usually caused by endobronchial processes (e.g., bronchial carcinoma or foreign body) or extrabronchial alterations (e.g., enlarged lymph nodes), whereas peripheral bronchial obstructions are marked by inflammatory mucus plugs and displacement of small bronchial branches. Displacement of the lumen of the middle lobe by mucus or pus, scarred kinking of the bronchus, external lymph node compression or tumor leads to the middle lobe syndrome.

Atelectasis impairs circulation in parenchyma, causing undersaturation of arteries owing to reduced gas exchange in perfused but not ventilated atelectatic lung parenchyma.

In terms of pathological anatomy, the early phase of obstructive atelectasis is marked by high-protein fluid in intraalveolar spaces. The next stage is characterized by the migration of macrophages and lymphocytic infiltration. In cases of compression or even obstructive atelectasis of longer duration, the parenchyma shrinks and fibrous induration of lung tissue occurs.

Additional attendant phenomena or complications in cases of bronchial obstruction include retention of secretion; bronchiectasis is seen in approximately 40 % of cases (Burke and Fraser 1988; Yang et al. 1990; Liaw et al. 1994). In rare cases the patient develops bacterial superinfection and microscopic or gross abscesses; necrotic or hemorrhagic lesions in atelectatic tissue may also be found.

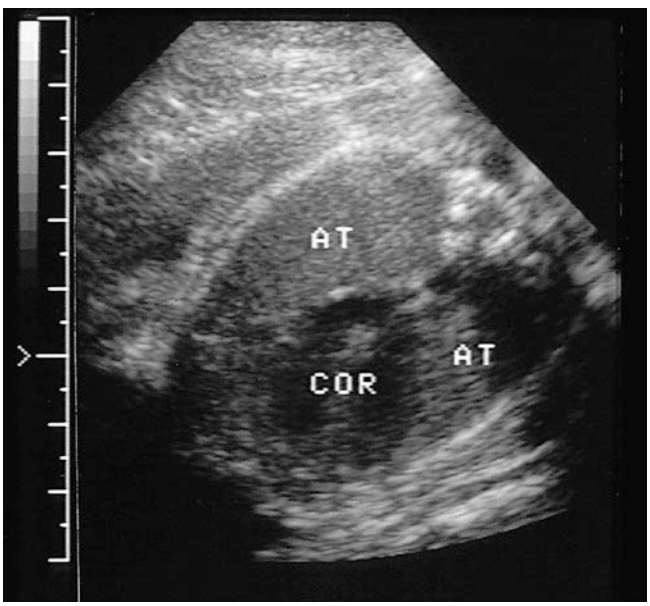

Fig. 5.51 Echo through the chest of a fetus in the 32nd gestational week. Both lungs are homogeneously hypoechoic, as in complete atelectasis (*AT*)

5.4.3 Sonomorphology

Lung atelectases are characterized by partial or complete absence of ventilation; therefore, in principle, they can be imaged by sonography. Furthermore, the echotransparency of the lung allows the investigator to assess the parenchyma. Especially in the presence of obstructive atelectasis, atelectatic lung tissue serves as "an acoustic window" for the investigation of central structures that possibly underlie the atelectasis.

5.4.4 Compression Atelectasis

The most common form is accompanied by the formation of pleural effusion. Depending on the extent of intrapleural fluid, the patient may develop homogeneous hypoechoic transformations shaped like a wedge or a pointed cap (Fig. 5.52). The margin towards the adjacent aerated lung tissue is blurred. Usually the atelectatic lung is surrounded by fluid, but also may be partly adherent to the pleura. The following features help to confirm the diagnosis by sonography:

- Partial reventilation during inspiration (Fig. 5.53),
- Partial reventilation after aspiration of effusion (Fig. 5.54)

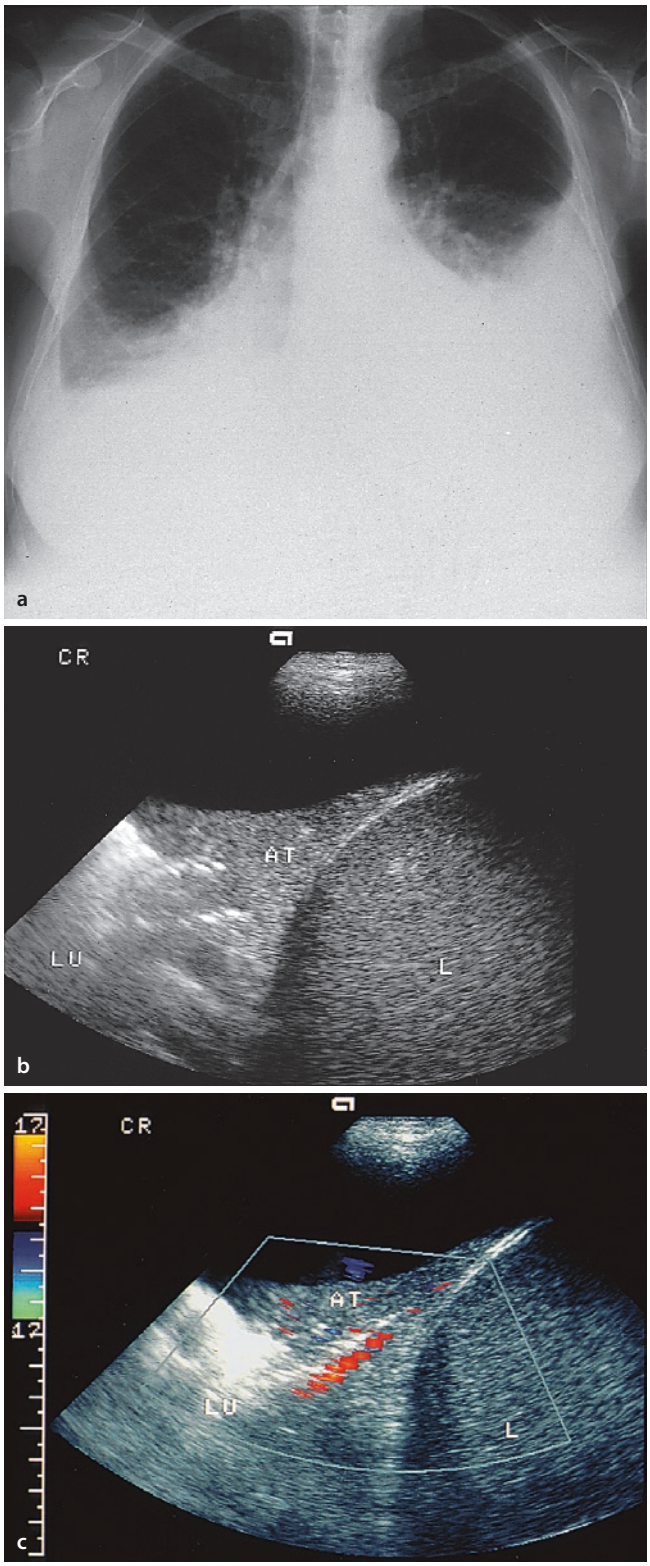

Fig. 5.52 **a** Chest X-ray: a 60-year-old man with global decompensated heart failure and bilateral pleural effusions. **b** Sonography: In right-lateral intercostal echo transmission one sees a pleural effusion with a wedge-shaped hypoechoic transformation of parts of the lower lobe of the lung as in the presence of atelectasis (*AT*). The demarcation to the ventilated lung (*LU*) is blurred. An extensive "air bronchogram" is seen. *L* liver. **c** Color-Doppler sonography reveals a flow signal along the bronchial branch filled with air

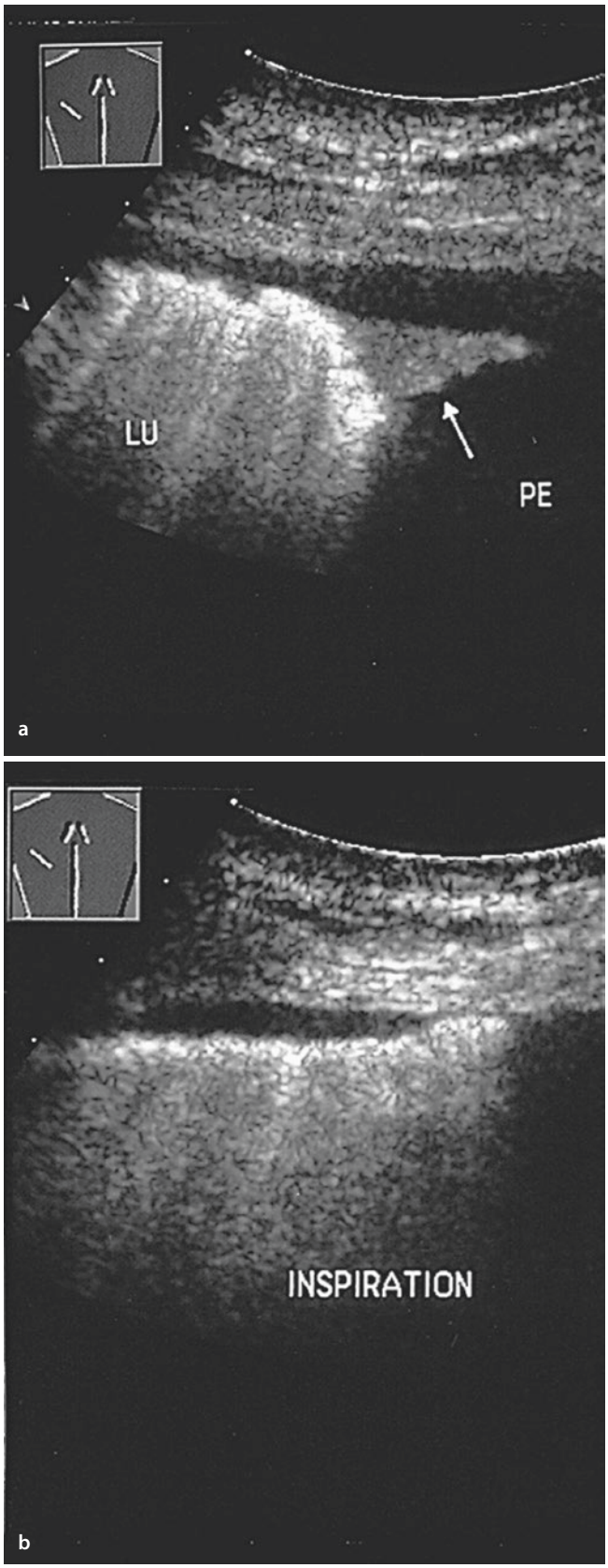

Fig. 5.53 **a** In left-lateral intercostal echo transmission one sees a pointed cap-like, smoothly margined hypoechoic transformation in the tip of the lower lobe of the left lung (*arrow*) in the presence of a pleural effusion. *Lu* lung, *PE* pleural effusion. **b** Reventilation of lung tissue is achieved after deep inspiration, as in the presence of compression atelectasis

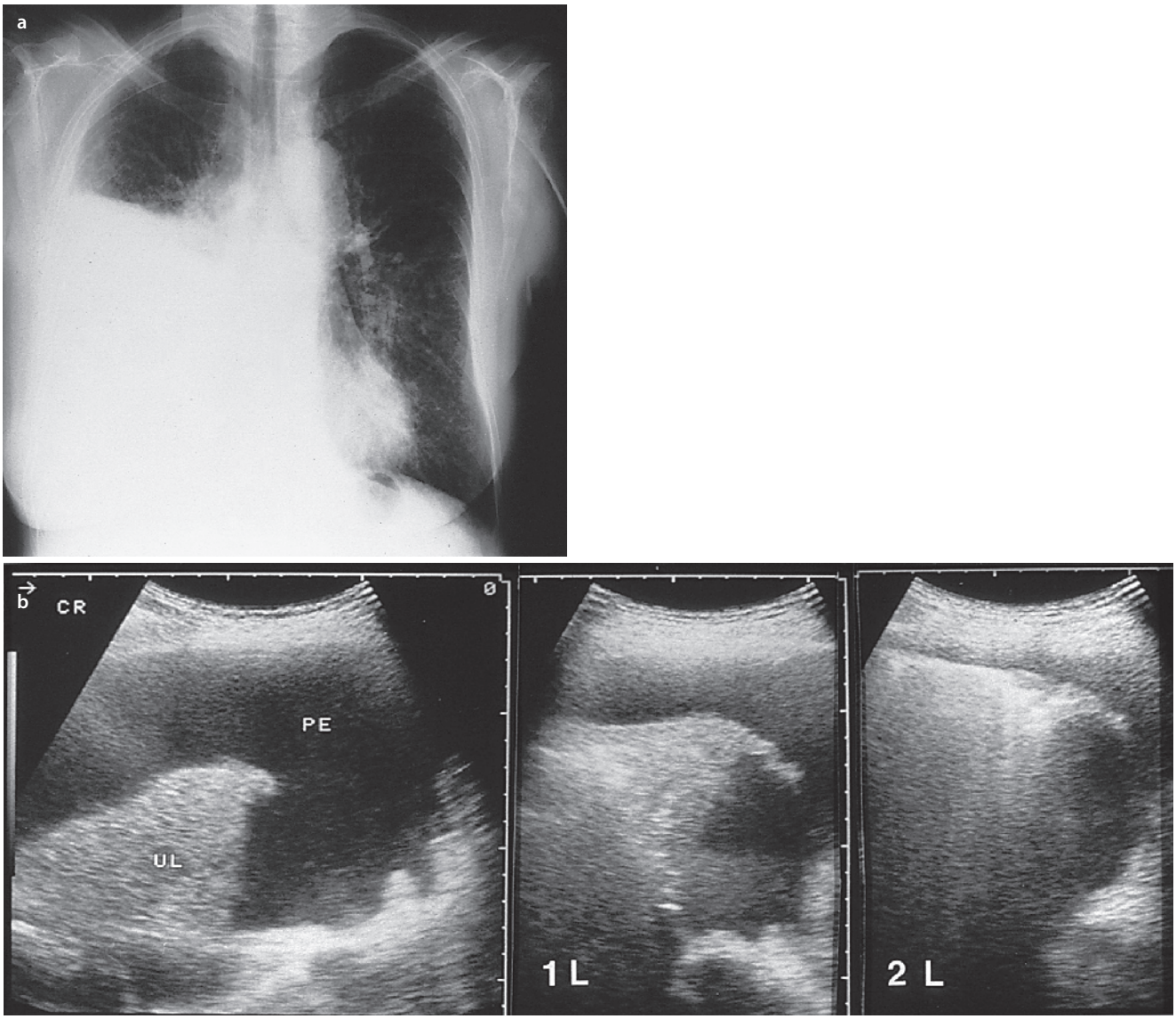

Fig. 5.54 A 66-year-old man with an alveolar carcinoma. **a** Chest X-ray: homogenous shadow of the caudal right-sided hemothorax. **b** Sonography: right-lateral intercostal echo transmission shows a marked pleural effusion (*PE*) with atelectasis in the lower lobe (*UL*). After aspiration of the effusion (1 l, *middle*), and (2 l, *right*) there is increasing reventilation

During inspiration sonography reveals an increasing quantity of air in atelectatic regions and the formation of a so-called air bronchogram. However, in the presence of exudative effusion, fibrin strands, septa and echogenic pleural effusion, one frequently observes poor reventilation during inspiration as a result of reduced elasticity of the lung. This condition has been described as a "trapped" lung (Lan et al. 1997).

Concomitant inflammatory invasion of parenchyma in atelectatic tissue is a further limitation. It leads to congestive pneumonia and restricts inspiratory ventilation. On the basis of sonomorphology alone this condition cannot be distinguished from pneumonia (Fig. 5.55).

Possible sonography findings in compression atelectasis:

1. B-mode sonography
   (a) Moderate to marked pleural effusion
   (b) Triangular pointed cap-like hypoechoic transformation of lung parenchyma
   (c) Blurred margins toward the ventilated lung parenchyma
   (d) Partial reventilation during inspiration ("air bronchogram")
   (e) Partial reventilation after aspiration of the effusion

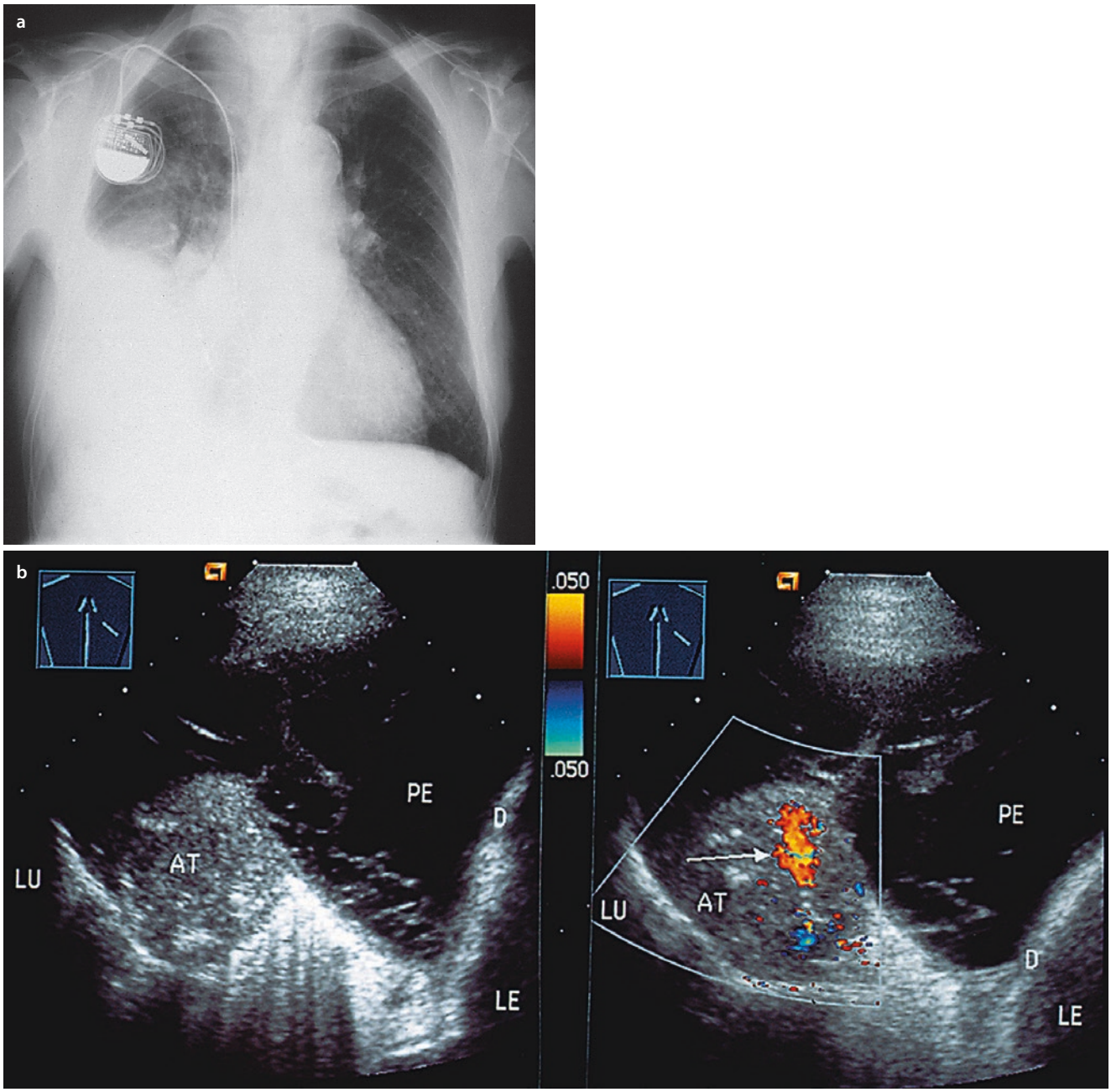

Fig. 5.55 A 75-year-old man with heart failure. **a** Chest X-ray: shadow in the region of the right caudal lung. **b** Sonography: right dorsal echo transmission shows a marked and partly septated pleural effusion (*PE*), and a circular hypoechoic consolidation of parts of the lung (*AT*). On color-Doppler sonography one finds pronounced flow signals. The marked pleural effusion and the absence of reventilation during inspiration are indicative of a fixed compression atelectasis. In principle, the image does not permit exclusion of concomitant congestive pneumonia. *LE* liver, *Lu* lung

2. Color-Doppler sonography: on intraindividual comparison with the liver one finds enhanced flow phenomena

In cases of compression atelectasis, lung tissue is partially reventilated after drainage of the effusion. This is also dependent on the elasticity of the lung. Of course, ventilation of the parenchyma after puncture of the effusion does not rule out the possibility of an additional central space-occupying lesion.

5.4.5 Obstructive Atelectasis

The sonographic image of obstructive atelectasis is marked by a largely homogeneous, hypoechoic presentation of lung tissue as in hepatization (Figs. 5.56 and 5.57). Effusion is absent or is very mild. In cases of lobar atelectasis the margin towards ventilated lung tissue is rather distinct (Fig. 5.58). Depending on the duration of atelectasis, intraparenchymatous structures also may be seen:

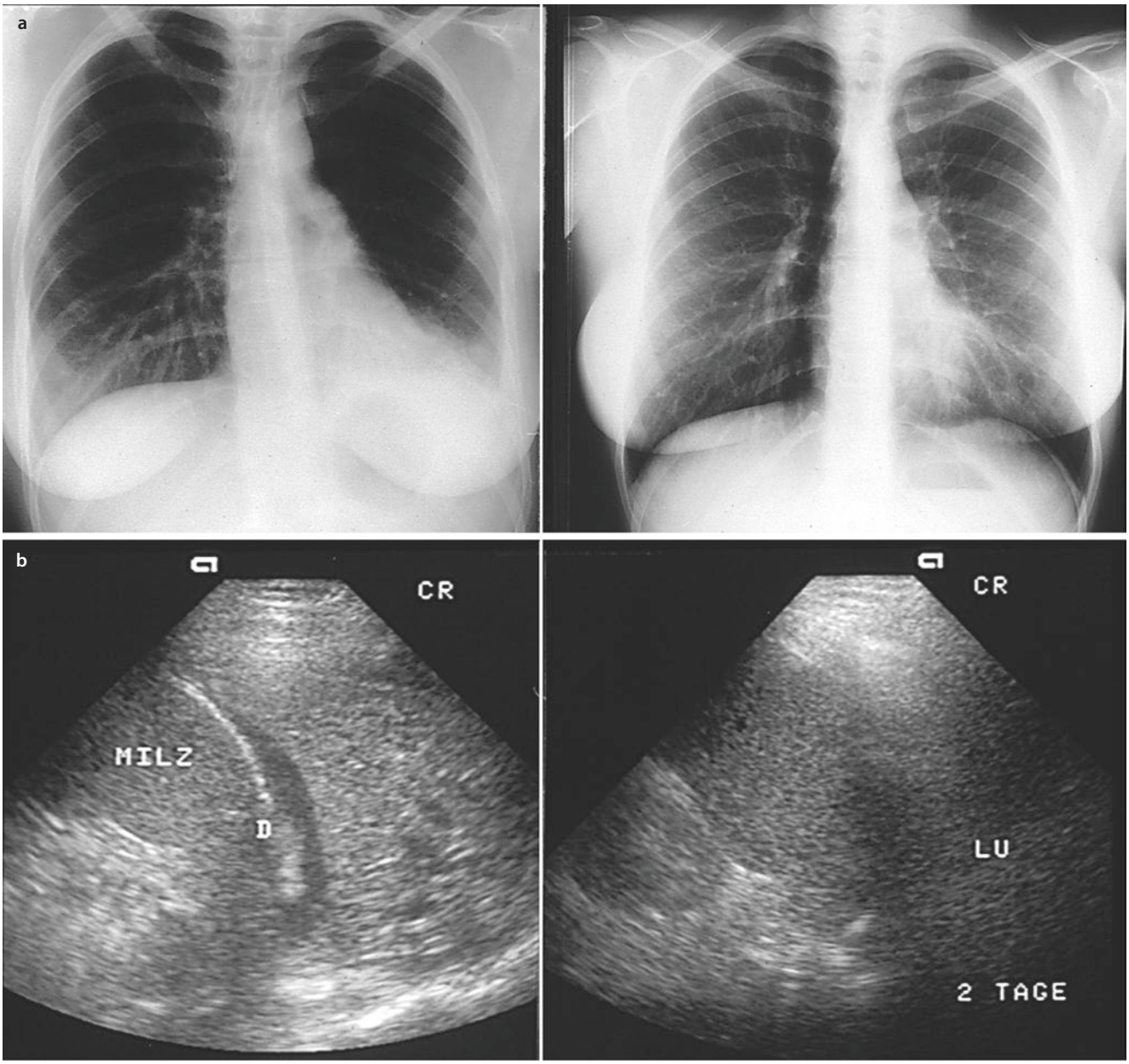

Fig. 5.56 A 20-year-old woman with fever and dyspnea. **a** Chest X-ray: signs of atelectasis in the lower lobe on the left side (*left*), which resolved spontaneously after 2 days (*right*). **b** Sonography: left-lateral intercostal echo transmission shows a homogenous lung consolidation with a mild pleural effusion as in the presence of obstructive atelectasis (*left*). This image taken after 48 h shows that the lung has been reventilated. The most likely condition in this case is displacement of the bronchus by inflammatory mucus. *Lu* lung, *D* diaphragm

- Hypoechoic vascular lines and echogenic reflexes (Figs. 5.59 and 5.60)
- Anechoic, hypoechoic, or echogenic focal lesions (Figs. 5.61 and 5.62)

Atelectasis of long duration is accompanied by sonographic reflexes in the lung parenchyma. The reflexes are caused by dilated bronchi, as a result of secretory congestion (so-called fluid bronchogram; Fig. 5.63). Vessels along the bronchi are seen as branches of the pulmonary artery and the pulmonary vein on color-Doppler sonography (Fig. 5.58; ▶ Chap. 8).

Possible findings on sonography in cases of obstructive atelectasis:

1. B-mode sonography
   (a) Mild to no pleural effusion
   (b) Homogenous hypoechoic transformation of lung parenchyma
   (c) Hyperechoic reflexes may be seen (fluid bronchogram)
   (d) Focal intraparenchymatous lesions may be seen
      (i) Liquefaction of parenchyma
      (ii) Microabscesses, gross abscesses
      (iii) Metastases

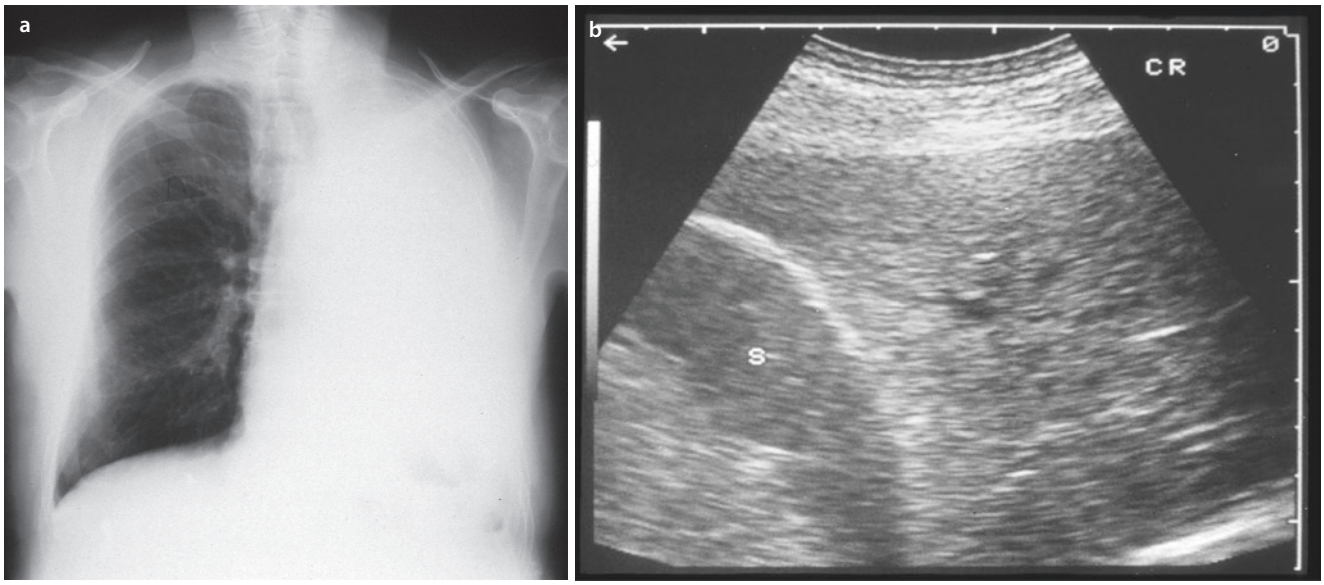

Fig. 5.57 A 68-year-old man with a bronchial carcinoma. **a** Chest X-ray: homogenous shadowing of the left hemothorax. **b** Sonography: left-lateral intercostal echo transmission shows a complete hypoechoic transformation of the left lung without effusion, similar to so-called hepatization in obstructive atelectasis. *S* spleen

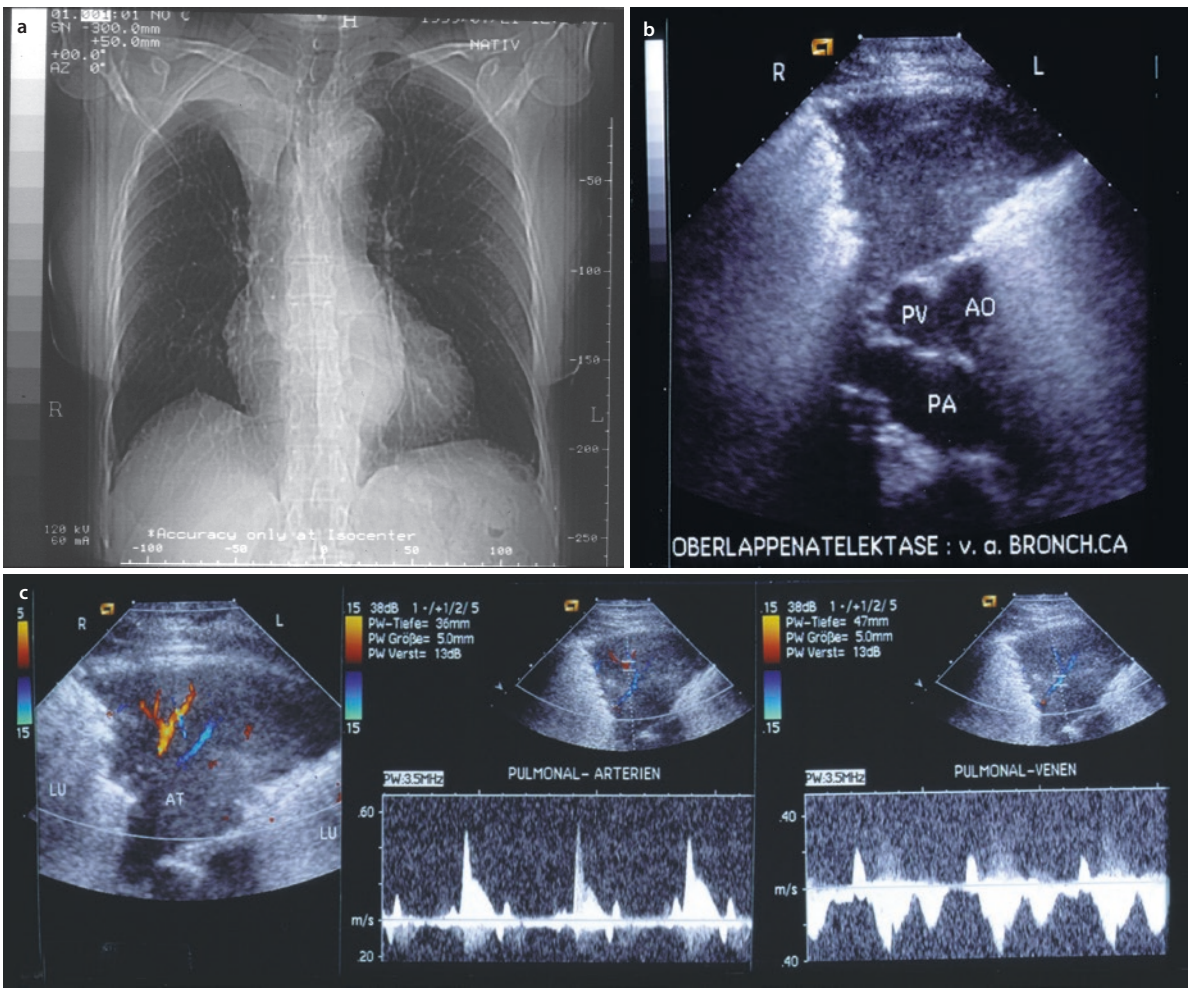

Fig. 5.58 A 74-year-old woman with dyspnea. **a** Chest X-ray: signs of right-sided upper-lobe atelectasis. **b** Sonography: right-ventral intercostal echo transmission shows a smoothly margined, wedge-shaped hypoechoic transformation of the lung as in atelectasis. The central vessels are seen; a shadow of the tumor core cannot be demarcated. *AO* aorta, *PV* pulmonary vein, *PA* pulmonary artery. **c** Color-Doppler sonography shows pronounced arterial and venous flow profiles. The characteristic flow profiles of the pulmonary artery and the pulmonary vein are seen

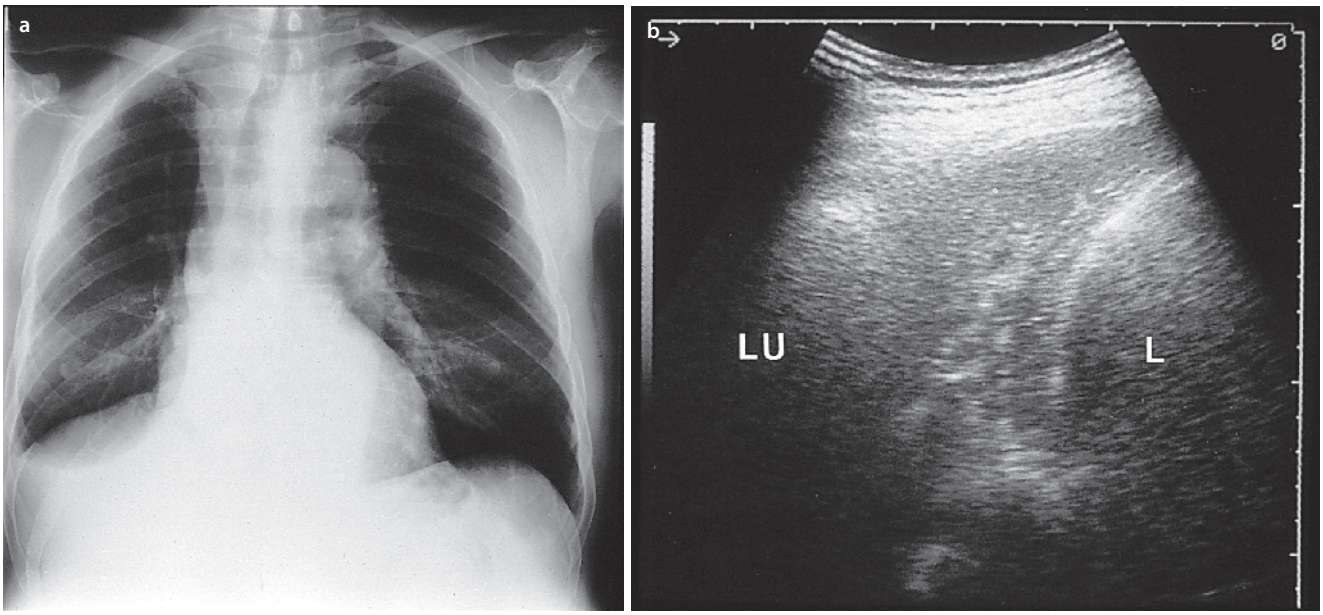

Fig. 5.59 An 84-year-old man with a bronchial carcinoma. **a** Chest X-ray: suspected lower-lobe atelectasis on the right side. **b** Sonography: right-lateral intercostal echo transmission shows a hypoechoic, poorly demarcated transformation with accentuated visualization of hyperechoic reflex bands in the atelectatic lung tissue

(e) A central space-occupying lesion may be seen
(f) No reventilation during inspiration

2. Color-Doppler sonography
   (a) On intraindividual comparison with the liver, enhanced flow phenomena are visualized
   (b) Triphasic spectrum of the arterial flow curve of pulmonary arteries (type, arteries of the extremities)

Quite often the investigator finds *focal lesions* in the lung parenchyma. As a result of dilated bronchi (due to congestion of secretion), one occasionally finds small anechoic, hypoechoic, or even echogenic lesions within the parenchyma. Given corresponding clinical features, the lesions are due to microabscesses. Occasionally the abscesses contain air echoes (Yang et al. 1992; Fig. 5.61). Atelectasis caused by tumor often leads to intraparenchymatous liquefaction, which is seen on sonography as large hypoechoic circular lesions with characteristic motion echoes on "real-time" investigation. This is primarily due to necrosis or tumor-related retention of secretion. Abscesses cannot be entirely excluded on the basis of sonomorphology alone. Here the clinical findings will be one of the main determinants of the diagnosis. However, sonography-guided aspiration will allow the investigator to confirm the diagnosis and obtain material for bacteriological investigation (Goerg 2003; Liaw et al. 1994; ▶ Chap. 8).

Occasionally echogenic circular lesions or metastases may be found in atelectatic lung tissue. They show intralesional flow signals on color-Doppler sonography (▶ Chap. 8).

Essentially, in the presence of lobar or pulmonary atelectasis, central portions can be imaged through atelectatic lung tissue by sonography. The main purpose here is to demonstrate the central tumor if there is one. On the basis of sonographic structural features, a definite distinction between atelectatic lung tissue and tumor tissue can be made in less than 50 % of cases (Goerg et al. 1996; Figs. 5.64 and 5.65).

5.4.6 Color-Doppler Sonography

Particularly in cases of compression atelectasis, the atelectatic lung tissue is characterized by accentuated flow phenomena compared with the liver (Goerg et al. 1996; Fig. 5.60). Investigation by color-Doppler sonography is limited by motion artifacts due to respiration and a possibly paracardiac position. Analysis of the venous Doppler flow curve will reveal the characteristic triphasic course of pulmonary veins.

Visualization of the arterial flow curve will show a triphasic spectrum as in the presence of high peripheral resistance (type, arteries of the extremities) with a steep increase in the systolic rate, a rapid fall in late systole, short diastolic backflow and late diastolic forward flow. Measurement of resistance will show high resistance (more than 0.80) and pulsatility (more than 2.50; Yuan et al. 1994; Fig. 5.58) indices.

Additional color-Doppler sonography may be helpful to distinguish between central tumors and atelectatic lung tissue (Yuan et al. 1994), as tumor tissue is characterized by poor visualization of flow signals (Fig. 5.66) compared with atelectatic lung tissue. Measurement of resistance in arterial vessels located within the tumor reveals flow signals with a high diastolic flow and correspondingly low resistance (less than 0.80) and pulsatility (less than 2.50; Yuan et al. 1994) indices. In obstructive atelectasis on the floor of a central bronchial carcinoma, during the progression of the tumor (independent of its structure), one finds increasing

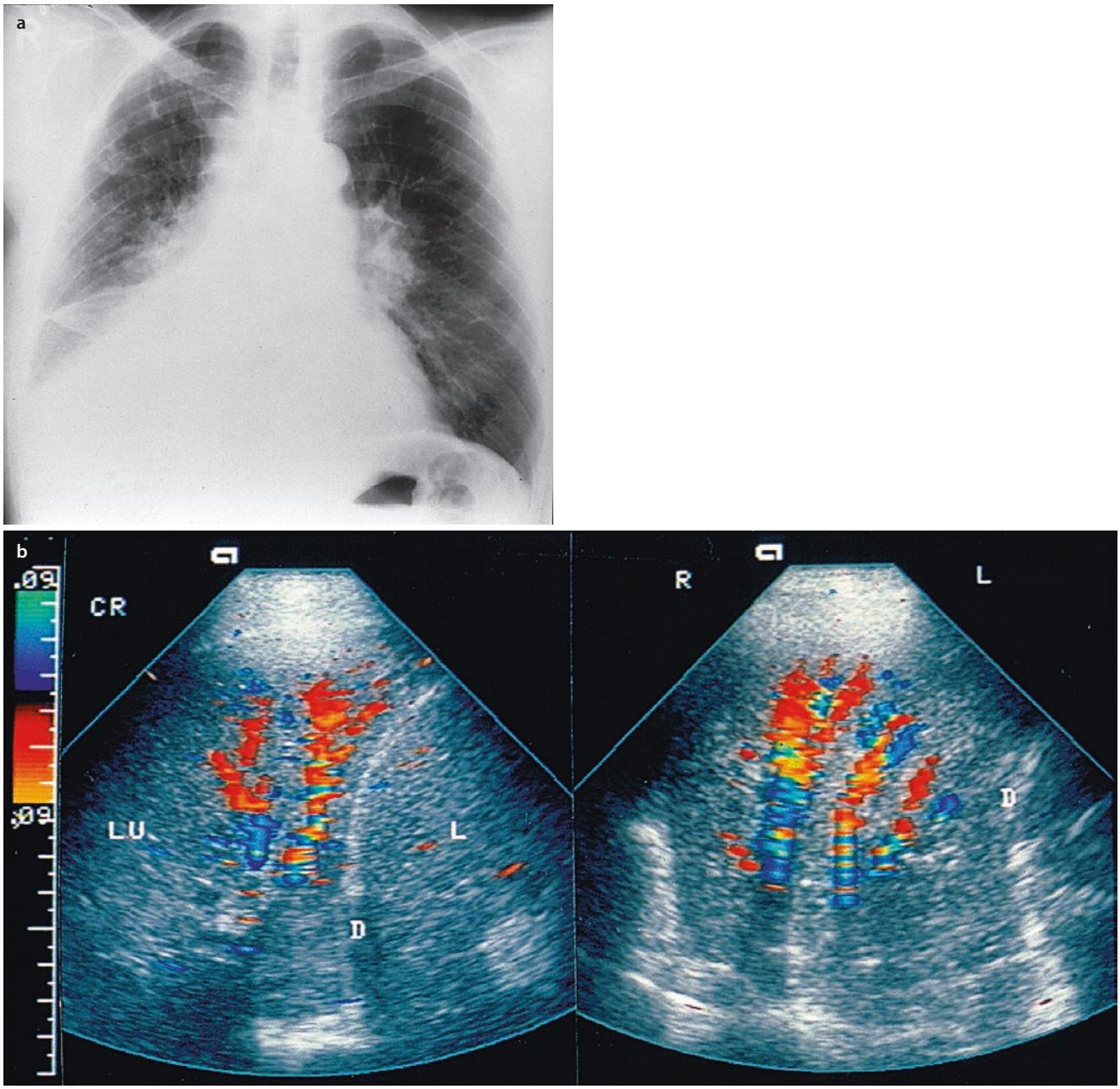

Fig. 5.60 A 58-year-old man with a bronchial carcinoma. **a** Chest X-ray: Signs of right-sided lower-lobe atelectasis. **b** Sonography: right-sided intercostal echo transmission shows a hypoechoic transformation of the lower lobe of the lung. In contrast to the liver, color-Doppler sonography shows enhanced flow signals which are characteristic evidence of atelectasis. *D* diaphragm, *L* liver, *Lu* lung

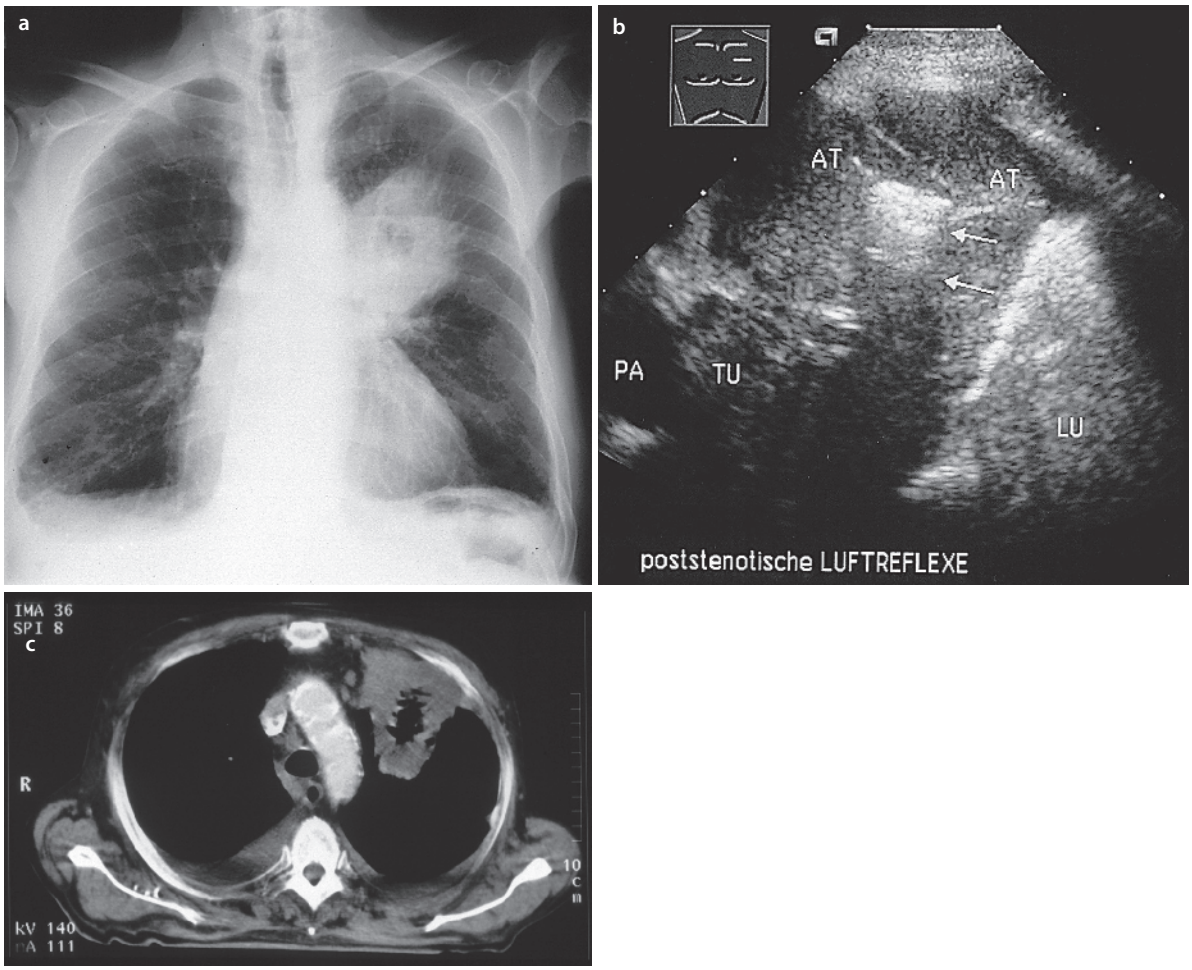

Fig. 5.61 A 68-year-old man with a bronchial carcinoma. **a** Chest X-ray: space-occupying lesion in the left hilum and a suspected central cavity. **b** Sonography: left-ventral intercostal echo transmission shows atelectasis in the upper lobe (*AT*) and, demarcated from the atelectasis, a hilar tumor formation (*Tu*). Centrally in the atelectatic lung tissue there is an air-filled cavity (*arrows*), most likely an inflammatory retention. *Lu* lung, *PA* pulmonary artery. **c** Computed tomography: atelectasis in the upper lobe with air-filled retention

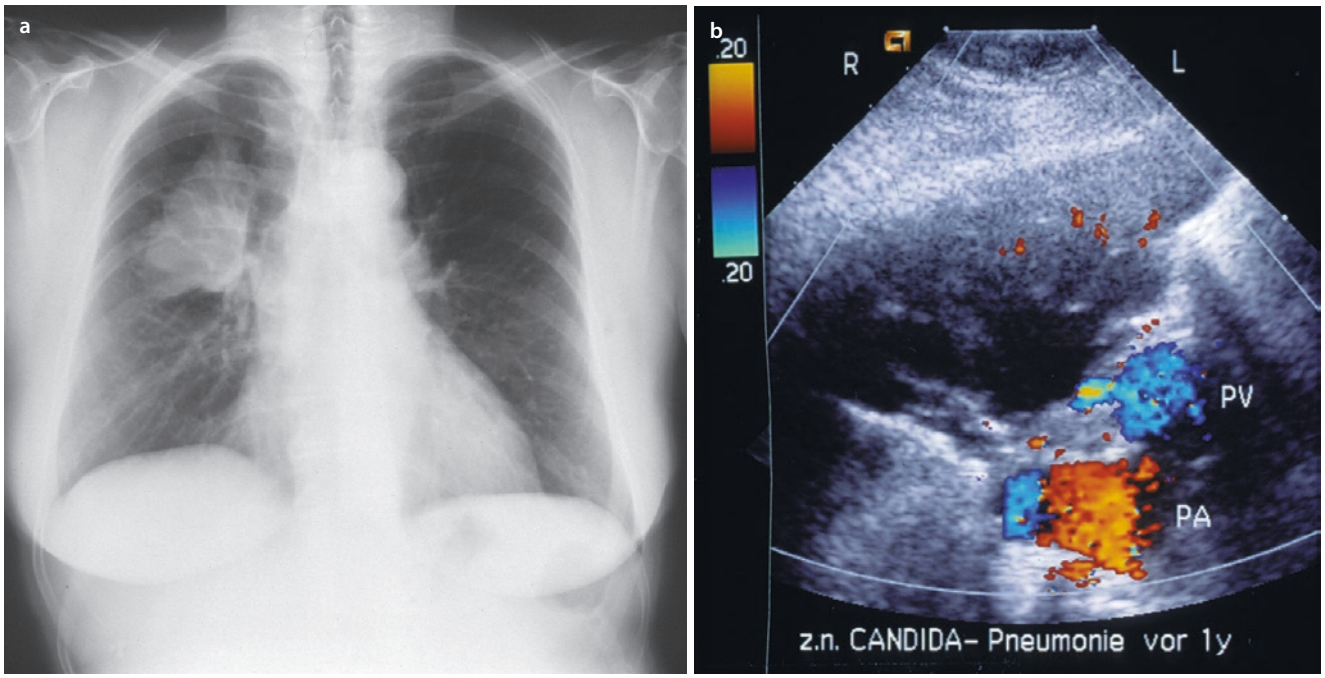

Fig. 5.62 A 63-year-old woman with a malignant lymphoma in the hilum after polychemotherapy and after *Candida* pneumonia. **a** Chest X-ray: central space-occupying lesion in the right hilum. **b** Sonography: right-ventral intercostal echo transmission shows partial atelectasis in the region of the upper lobe. A hilar tumor formation is not seen. Centrally in the atelectatic lung tissue there is an anechoic pseudocyst formation which has been constant for more than 12 months at sonography controls. *PA* pulmonary artery, *PV* pulmonary vein

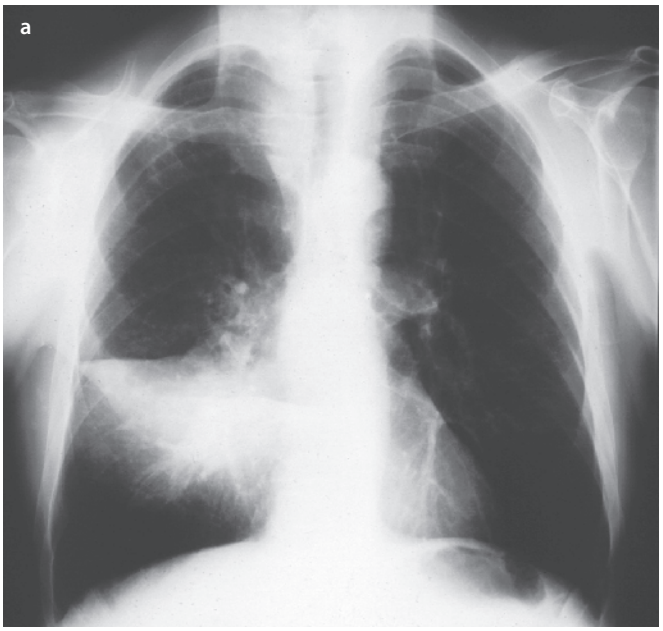

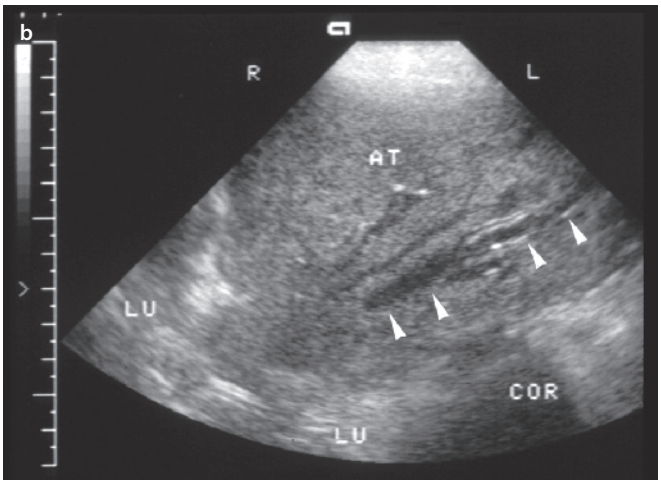

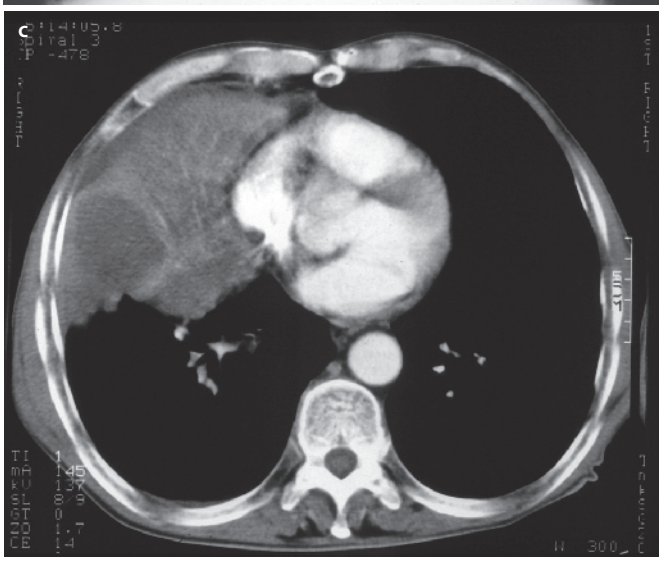

Fig. 5.63 A 68-year-old man with a bronchial carcinoma. **a** Chest X-ray: signs of middle-lobe atelectasis. **b** Sonography: right-ventral intercostal echo transmission shows atelectasis in the middle lobe (*AT*) with accentuated dilated bronchi, indicative of a fluid bronchogram ("sticks"). The central tumor formation cannot be clearly demarcated. **c** Computed tomography: visualization of atelectasis in the middle lobe

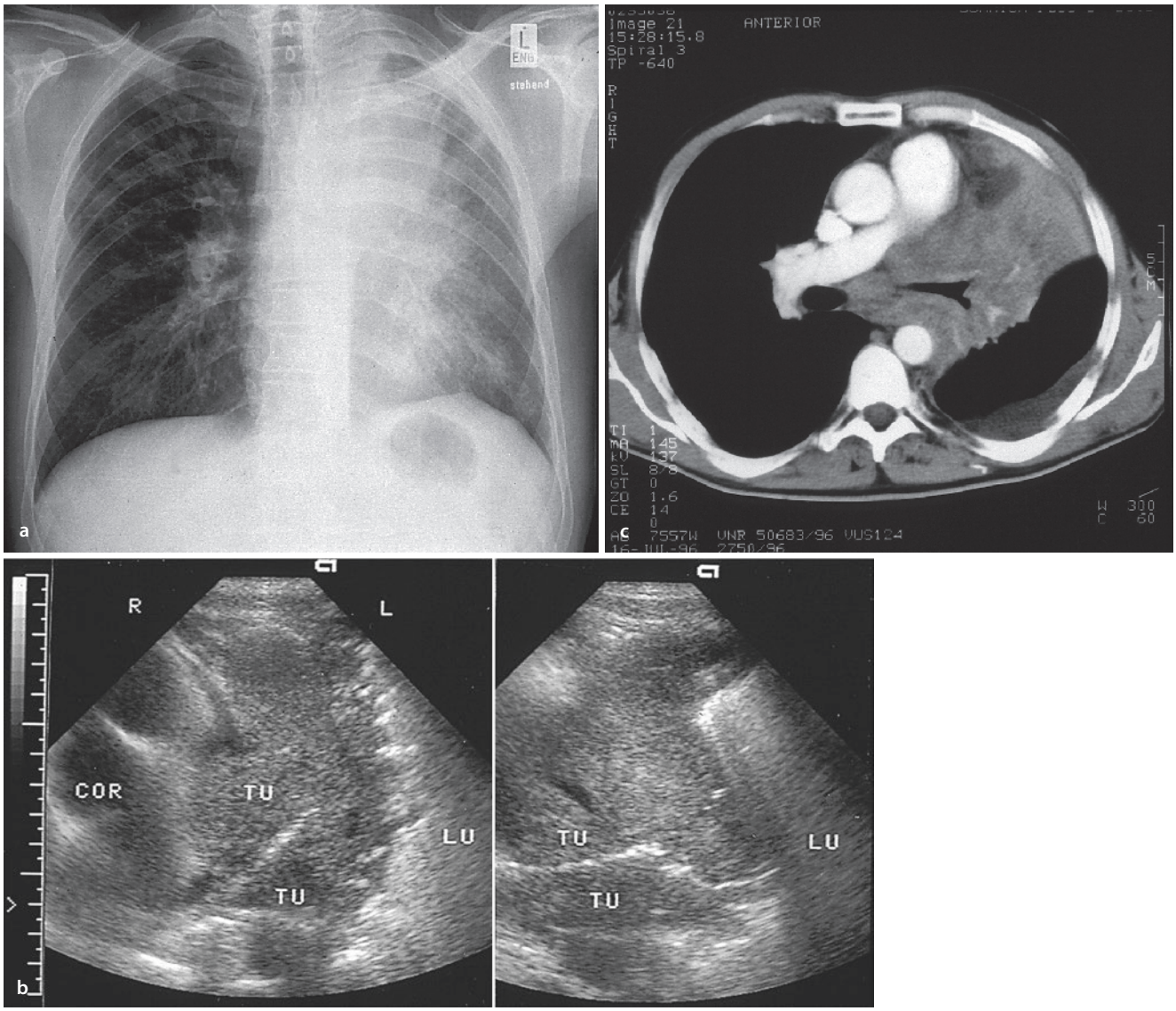

Fig. 5.64 A 44-year-old man with a bronchial carcinoma. **a** Chest X-ray: signs of left-sided upper-lobe atelectasis and dysatelectasis in the lower lobe. **b** Sonography: left-ventral intercostal echo transmission shows atelectasis in the upper lobe. The central tumor formation (*TU*) is rather poorly demarcated from the atelectasis. The highly constricted bronchus is seen as an air-filled band of several reflexes. *Lu* lung. **c** Computed tomography: visualization of the atelectasis in the upper lobe and the central tumor

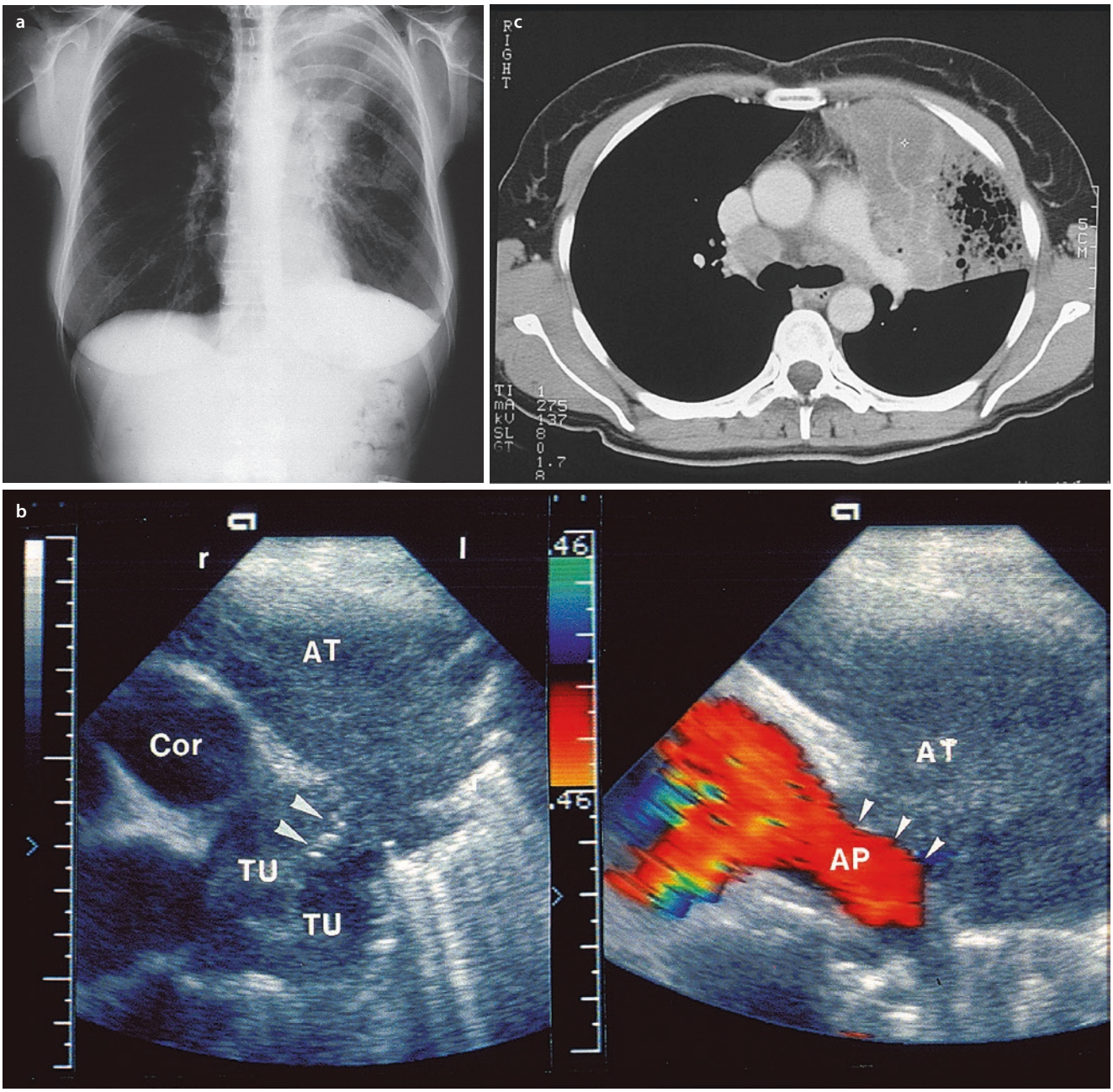

Fig. 5.65 A 48-year-old man with a bronchial carcinoma. **a** Chest X-ray: signs of upper-lobe atelectasis on the left side. **b** Sonography: left-ventral intercostal echo transmission shows the atelectasis in the upper lobe (*AT*) and the central tumor (*TU*) demarcated from the atelectasis. On color-Doppler sonography the tumor is seen immediately next to the pulmonary artery (*AP*; "sticks"). **c** Computed tomography: visualization of the atelectasis in the upper lobe and the tumor surrounding the pulmonary artery

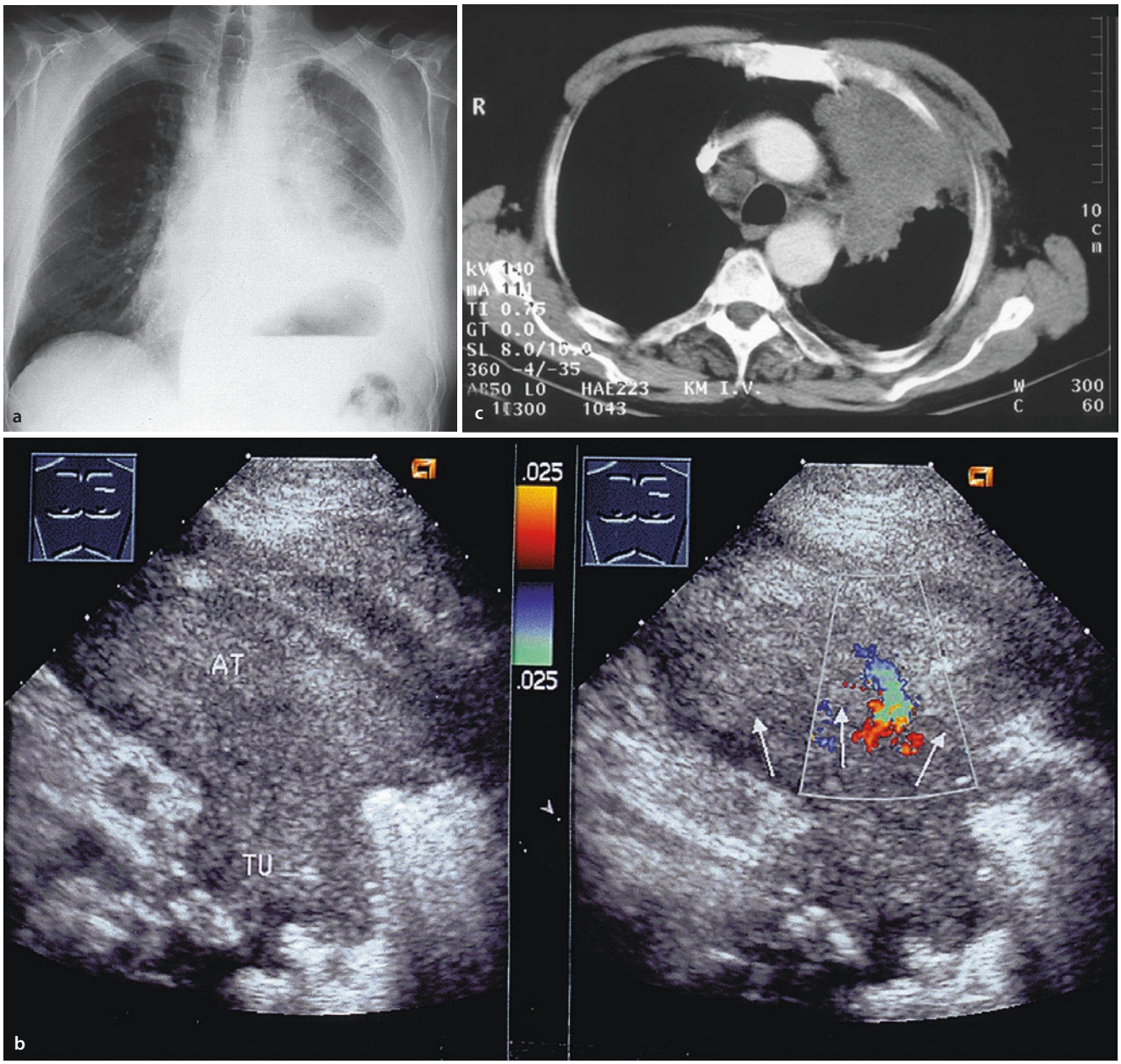

Fig. 5.66 A 70-year-old man with a bronchial carcinoma. **a** Chest X-ray: large tumor in the left upper field. **b** Sonography: hypoechoic tumor formation in the right upper lobe not clearly distinguishable from atelectatic lung tissue. On color-Doppler sonography one finds strong flow signals in the peripheral portions, possibly corresponding to atelectatic lung tissue. No flow signals are derived from the central part of the tumor. **c** Computed tomography: visualization of the tumor in the left hilum; suspicion of additional invasion of the chest wall

occlusion of the pulmonary arteries and, consequently, poor visualization of vessels in the atelectatic lung tissue on color-Doppler sonography (▶ Chap. 8).

In a few cases one finds central tumor spread into large vessels such as the aorta, the pulmonary artery, and the pulmonary vein (Fig. 5.67).

The significance of being able to visualize the central tumor lies in the fact that the tumor can be punctured through atelectatic lung tissue under sonographic guidance, with practically no risk of complications (Yang et al. 1990; Figs. 5.68 and 5.69).

5.4.7 Lung Contusion

In cases of chest trauma, particularly serial rib fractures, pulmonary contusions are visualized better on sonography than on radiographs. Alveolar edema and alveolar hemorrhage

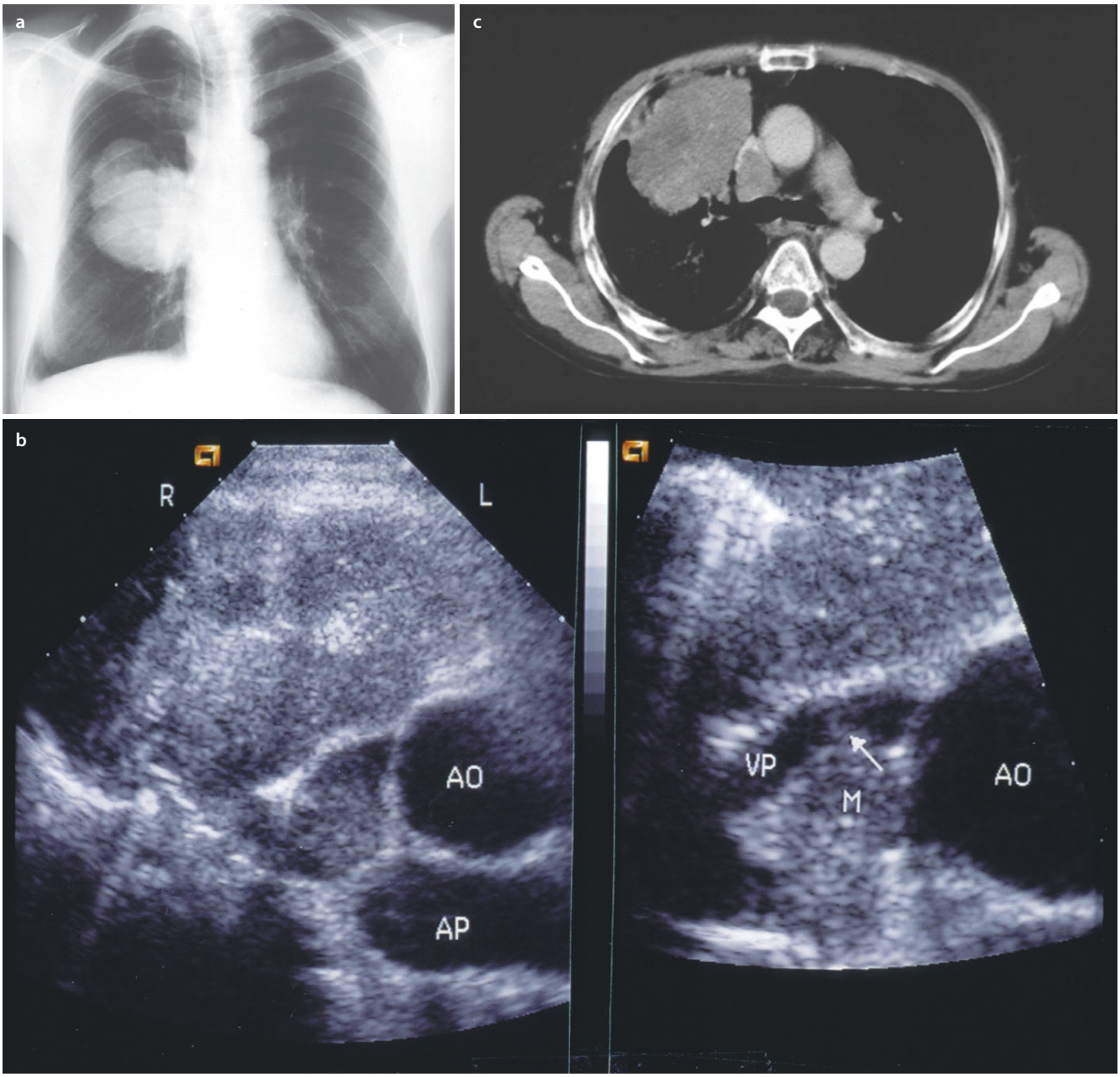

Fig. 5.67 A 49-year-old man with a bronchial carcinoma. **a** Chest X-ray: central space-occupying mass in the right hilum. **b** Sonography: right-ventral intercostal echo transmission shows a hypoechoic transformation. The atelectatic lung tissue cannot be demarcated from the central tumor in terms of its echomorphology. In the aortopulmonary window there are enlarged lymph nodes. Invasion of the aorta cannot be excluded. **c** Computed tomography: visualization of the tumor formation in contact with the aorta

caused by trauma are seen as moderately hypoechoic, blurred, pale lesions with indistinct margins (Figs. 2.17 and 5.70). These are more pronounced in the presence of concomitant minimal pleural effusions, but are also imaged on sonography in the absence of pleural effusion. In the event of any clinically relevant chest trauma, radiographs as well as sonograms should be obtained (Wuestner et al. 2005; ▶ Chap. 2). Including the presence of B-lines, chest ultrasonography can accurately predict lung contusion in blunt trauma victims, in comparison to CT scan (Soldati et al. 2006).

5.4.8 Summary

Depending on the extent of intrapleural fluid in case of compression atelectasis, one finds a pointed cap-like, wedge-shaped, homogenous, hypoechoic transformation with blurred margins towards the aerated adjacent lung tissue. The sonographic image of obstructive atelectasis is marked by largely homogenous hypoechoic lung tissue, similar to hepatization. An effusion is absent or is very mild. In cases of lobar atelectasis the margin towards the ventilated lung tissue

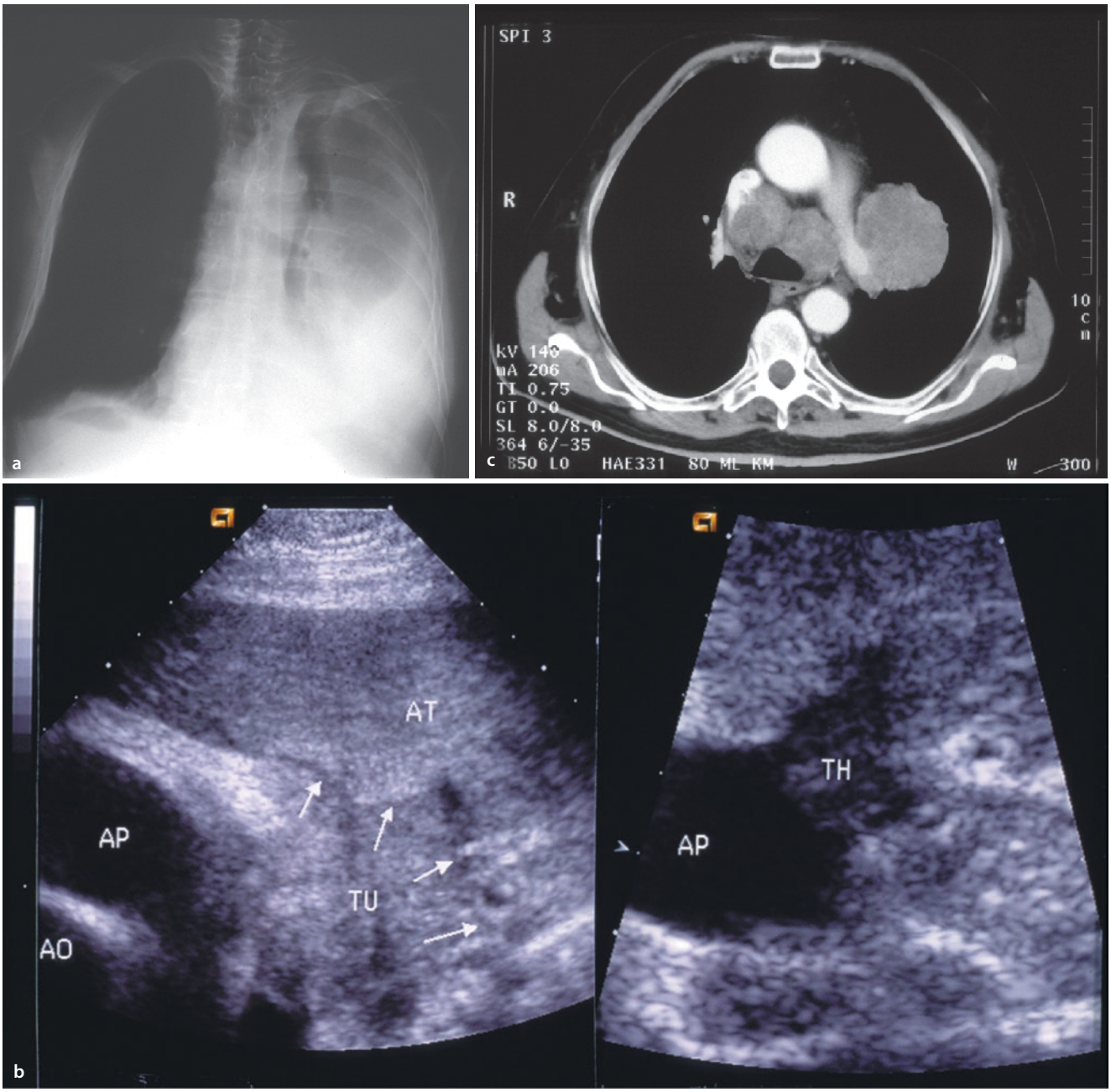

Fig. 5.68 A 77-year-old man with a bronchial carcinoma. **a** Chest X-ray: largely homogeneous shadowing of the left hemithorax. **b** Sonography: left-ventral intercostal echo transmission shows a central tumor (*TU*) and atelectasis (*AT*). The *arrows* point to the margin of the tumor where the atelectasis starts. Thrombotic material is seen in the pulmonary artery (suspected tumor thrombosis). **c** Computed tomography: visualization of the tumor formation in contact with the pulmonary artery

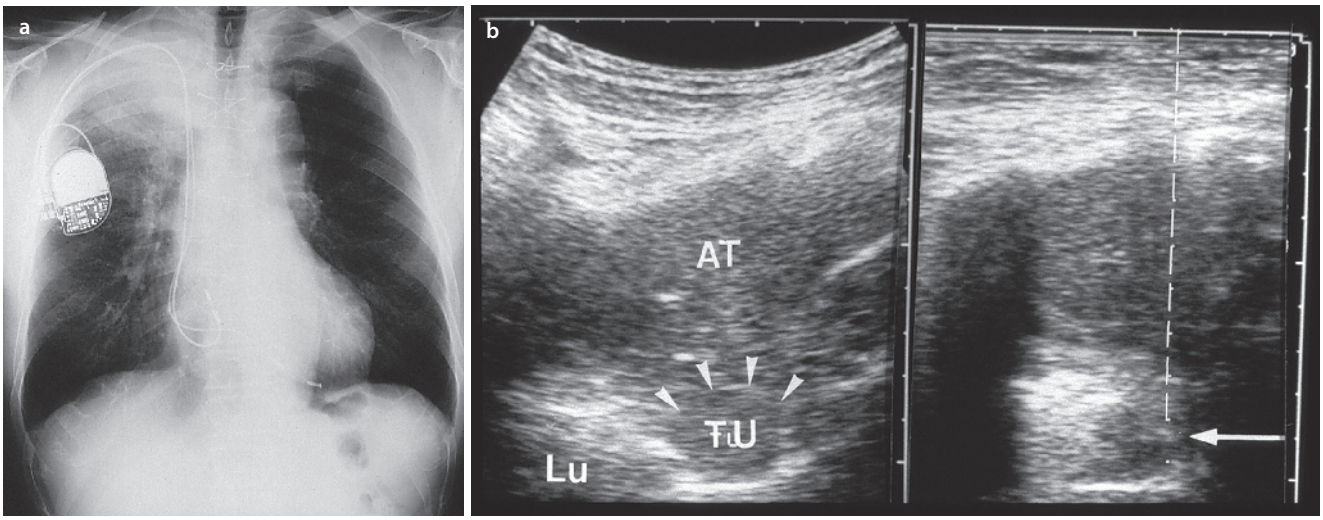

Fig. 5.69 A 67-year-old man with a bronchial carcinoma. **a** Chest X-ray: shadow in the region of the upper field on the right side. **b** Sonography: right-ventral echo transmission shows a small central tumor (*TU*) on the *left* with subsequent atelectasis (*AT*). The tumor could not be diagnosed by bronchoscopy. Under sonographic guidance, the tumor was aspirated through the atelectatic lung tissue by means of a 16-gauge punch biopsy. The *arrow* on the right marks the needle tip reflex. An adenocarcinoma was diagnosed

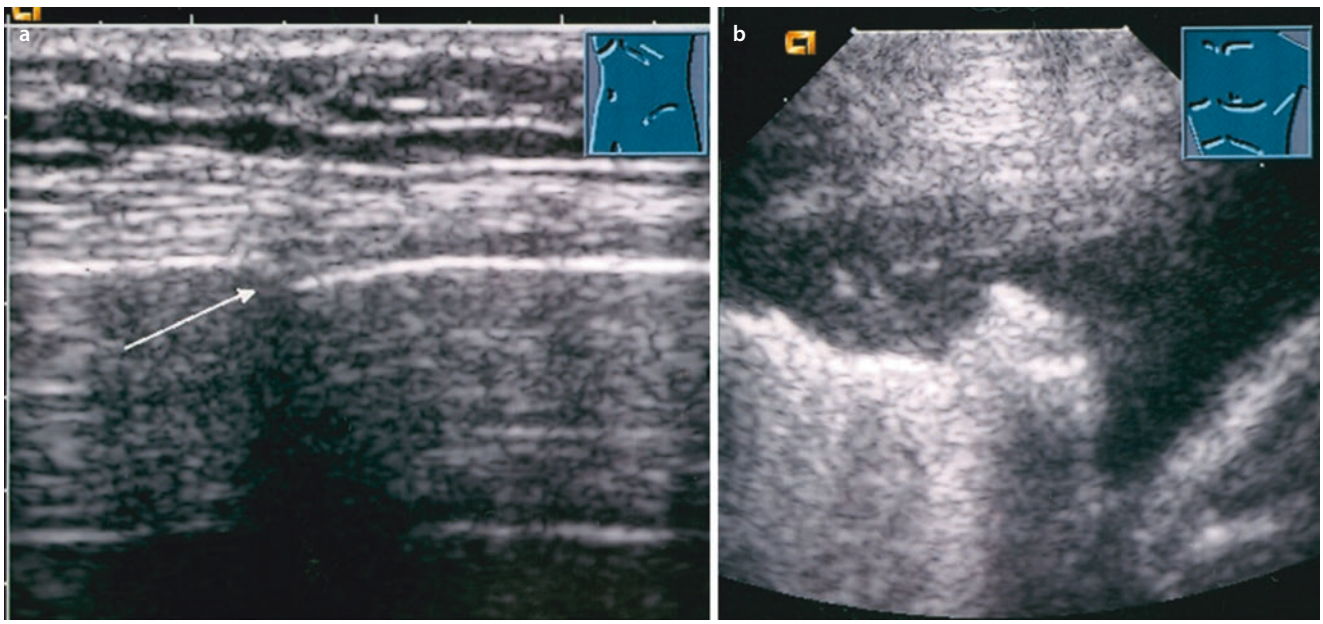

Fig. 5.70 Lung contusion and rib fracture. **a** On sonography one finds a step in the region of the rib – a sign of fracture. Additionally, free fluid is seen in the chest. Aspiration revealed a hemothorax. **b** The initial echo to the lung is irregular – a sign of contusion of the parenchyma

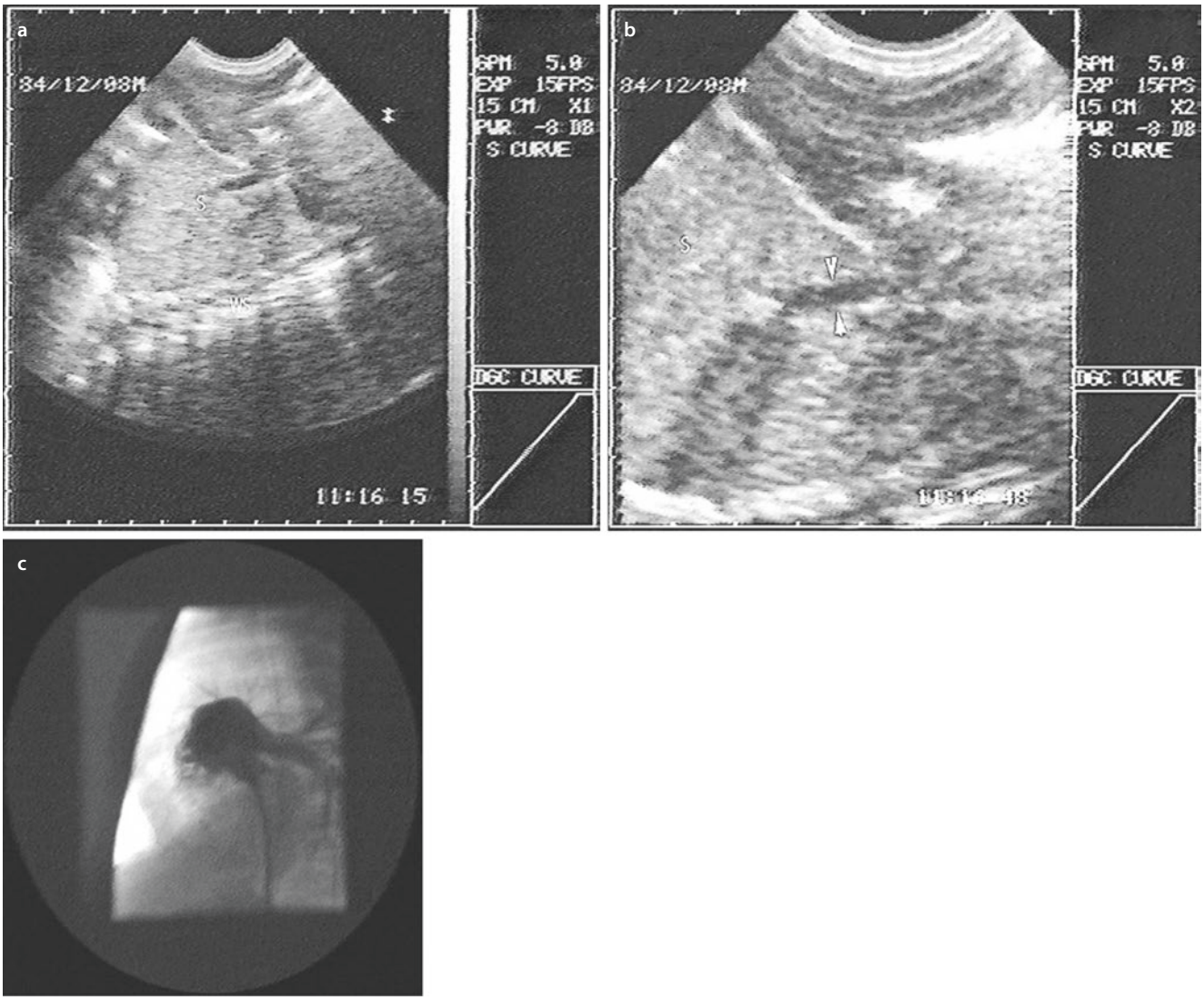

Fig. 5.71 Three-month-old boy with breathing difficulty and left thoracic swelling. Chest X-ray showed a left inferior tumor shadow with displacement of the mediastinum to the right. **a**, **b** Sonography shows a consolidation with a liver-like echo pattern over the left diaphragm; the vessels supplying this mass are depicted (*arrowheads*) *S* sequestration, *WS* spinal column. **c** Angiographic confirmation of the sonographic findings (Case report and images courtesy of A. Anderegg, Lausanne)

is rather blurred. Intraparenchymatous structures are seen as hypoechoic vascular lines, echogenic bronchial reflexes or focal lesions.

5.5 Congenital Pulmonary Sequestration

Gebhard Mathis

The very rare pulmonary sequestration underlines the value and importance of thorax sonography in neonatology and pediatrics. The neonate with this condition suffers from dyspnea and has a nonspecific systolic murmur. On chest radiograph, one may find a tumor-like shadow. On sonography, the echo texture of the pulmonary sequestration is similar to that of the liver, with wide arteries and veins (Gudinchet and Anderegg 1989). The supplying artery with the characteristic flow pattern can be identified on color-coded duplex sonography and the diagnosis is thus confirmed (Yuan et al. 1992). CT does not provide more information. If the lesion is imaged well on sonography, the infant can be spared the stress of angiography (Riccabona 2008; Fig. 5.71).

Acknowledgement: Neoplastic Consolidations in the Lung: Primary Lung Tumors and Metastases We thank R. Loose, Head of the Institute of Diagnostic and Interventional Radiology at the Klinikum Nürnberg Nord, for providing radiology reports.

References

Inflammatory Consolidations in the Lung

Bertolini FA, Goerg C, Mathis G (2008) Echo contrast ultrasound in subpleural consolidations. Abstract ECR 2008. Eur Radiol Suppl 18:S395

Busti C, Agnelli G, Duranti M, Orlandi C, Marcucci M, Paciaroni M (2014) Lung ultrasound in the diagnosis of stroke-associated pneumonia. Intern Emerg Med 9:173–178

Chavez MA, Shams N, Ellington LE et al (2014) Lung ultrasound for the diagnosis of pneumonia in adults: a systematic review and meta-analysis. Respir Res 15:50. doi:10.1186/1465-9921-15-50

Chavez MA, Naithani N, Gilmani RH (2015) Agreement between the World Health Organization Algorithm and lung consolidation identified using point-of-care ultrasound for the diagnosis of childhood pneumonia by general practitioners. Lung 193:531–538

Chen CH, Kuo ML, Shih JF, Chang TP, Perng RP (1993) Etiologic diagnosis of pulmonary infection by ultrasonically guided percutaneous lung aspiration. Zhonghua Yi Xue Za Zhi (Taipei) 51:5

Copetti R, Cattarossi L (2008) Ultrasound diagnosis of pneumonia in children. Radiol Med 113:190–198

Gehmacher O, Mathis G, Kopf A, Scheier M (1995) Ultrasound imaging of pneumonia. Ultrasound Med Biol 21:1119–1122

Goerg C (2007) Transcutaneous contrast-enhanced sonography of pleural-based pulmonary lesions. Eur J Radiol 64:213–221

Hu QJ, Shen YC, Jia LQ, Guo SJ, Long HY, Pang CS et al (2014) Diagnostic performance of lung ultrasound in the diagnosis of pneumonia: a bivariate meta-analysis. Int J Clin Exp Med 7:115–121

Kopf A, Metzler J, Mathis G (1994) Sonographie bei Lungentuberkulose Bildgebung 61(S2):12

Liaw YS, Yang PC et al (1994a) The bacteriology of obstructive pneumonitis. Am J Respir Crit Care Med 149:1648–1653

Lichtenstein D, Meziere G, Seitz J (2009) The dynamic airbronchogram. A lung ultrasound sign of alveolar consolidation ruling out atelectasis. Chest 135:1421–1425

Mathis G (1997) Thoraxsonography – part II: peripheral pulmonary consolidation. Ultrasound Med Biol 23:1141–1153

Mathis G, Metzler J, Fußenegger D, Feurstein M, Sutterluetti G (1992) Ultraschallbefunde bei Pneumonie. Ultraschall Klin Prax 7:45–49

Mathis G (2006) Ultrasound in pulmonary embolism: Killing three birds with one stone. Pneumologie 2006:600–606

Reissig A, Kroegel C (2003a) Transthoracic sonography of diffuse parenchymal lung disease: the role of comet tail artefacts. J Ultrasound Med 22:173–180

Reissig A, Kroegel C (2007) Sonographic diagnosis and follow-up of pneumonia: a prospective study. Respiration 74:537–547

Reissig A, Copetti R, Mathis G et al (2012) Lung ultrasound in the diagnosis and follow-up of community-acquired pneumonia. A prospective multicentre diagnostic accuracy study. Chest 142:965–972

Riccabona M. (2008) Ultrasound of the chest in children (mediastinum excluded). Eur Radiol 18: 390–399

Talayanagi N, Kagiyama N, Ishiguro T, Tokunaga D, Sugita Y (2010) Etiology and outcome of community-acquired lung abscesses. Respiration 80:98–105

Ticinesi A, Lauretani F, Nouvenne A, Meschi (2016) A Lung ultrasound and chest x-ray for detecting pneumonia in an acute geriatric ward. Medicine 95(27):e4153

van Sonnenberg E, Agostino H, Casola G, Wittich GR, Varney RR, Harker C (1991) Lung abscess: CT-guided drainage. Radiology 178:347–351

Weinberg B, Diaboumakis EE, Kass EG, Seife B, Zvi ZB (1986) The air bronchogram: sonographic demonstration. AJR Am J Roentgenol 147:593–595

Wohlgenannt S, Gehmacher O, Mathis G (2001) Thoraxsonographische Veraenderungen bei interstitiellen Lungenerkrankungen. Ultraschall Med 22:27–31

Yang PC, Luh KT, Lee YC (1991) Lung abscesses: ultrasonography and ultrasound-guided transthoracic aspiration. Radiology 180: 171–175

Yang PC, Luh KT, Chang DB, Yu CJ, Kuo SH, Wu HD (1992) Ultrasonographic evaluation of pulmonary consolidation. Am Rev Respir Dis 146: 757–762

Yuan A, Yang PC, Chang DB et al (1993a) Ultrasound guided aspiration biopsy for pulmonary tuberculosis with unusual radiographic appearances. Thorax 48:167–170

Neoplastic Consolidations in the Lung: Primary Lung Tumors and Metastases

Bandi V, Lunn W, Ernst A, Eberhardt R, Hoffmann H, Herth FJF (2008) Ultrasound vs CT in detecting chest wall invasion by tumor. A prospective study. Chest 133:881–886

Beckh S, Boelcskei PL (2003) Die Bedeutung der dynamischen Untersuchung in der Diagnostik thorakaler Herdbildungen. Praxis 92:1223–1226

Beckh S, Boelcskei PL, Lessnau KD (2002) Real-time chest ultrasonography. A comprehensive review for the pulmonologist. Chest 122:1759–1773

Corrin B (1999) Actinomycosis. In: Corrin B (ed) Pathology of the lungs. Churchill Livingstone, London, pp 194–195

Detterbeck FC, Malcolm M, DeCamp J et al (2003) Invasive staging – the guidelines. Chest 123:167S–175S

Detterbeck FC, Postmus PE, Tanoue LT (2013a) The stage classification of lung cancer. Diagnosis and management of lung cancer, 3rd ed: American College of Chest Physicians evidence-based clinical practice guidelines. Chest 143:e191S–e210S

Detterbeck FC, Zelman Lewis S, Diekemper R et al (2013b) Executive summary. Diagnosis and management of lung cancer, 3rd ed: American College of Chest Physicians evidence-based clinical practice guidelines. Chest 143:7S–37S

Fultz PJ, Feins RH, Strang JG et al (2002) Detection and diagnosis of nonpalpable supraclavicular lymph nodes in lung cancer at CT and US. Radiology 222:245–251

Goeckenjan G, Sitter H, Thomas M et al (2011) Prevention, diagnosis, therapy, and follow-up of lung cancer: interdisciplinary guideline of the German Respiratory Society and the German Cancer Society. Pneumologie 65:39–59

Goerg C, Bert T (2004) Transcutaneous colour Doppler sonography of lung consolidations. Ultraschall Med 25(221–226):285–291

Goerg C, Seifart U, Holzinger I et al (2002) Bronchioloalveolar carcinoma: sonographic pattern of "pneumonie". Eur J Ultrasound 15:109–117

Gompelmann D, Eberhardt R, Kreuter M et al (2012) Transthorakale und endobronchiale Thoraxsonographie beim Bronchialkarzinom. Pneumologe 9:416–424

Hoosein M, Barnes D, Khan AN et al (2011) The importance of ultrasound in staging and gaining a pathological diagnosis in patients with lung cancer – a two year single centre experience. Thorax 66:414–417

Hsu WH, Ikezoe J, Chen CY et al (1996) Color Doppler ultrasound signals of thoracic lesions. Am J Respir Crit Care Med 153:1938–1951

Hsu WH, Chiang CD, Chen CY et al (1998) Color Doppler ultrasound pulsatile flow signals of thoracic lesions: comparison of lung cancers and benign lesions. Ultrasound Med Biol 24:1087–1095

Knopp MV, Hawighorst H, Flömer F (1998) Magnetresonanztomographie. In: Drings P, Vogt-Moykopf I (eds) Thoraxtumoren. Springer, Berlin/Heidelberg/New York/Tokyo, pp 180–190

Ko JC, Yang PC, Yuan A et al (1994) Superior vena cava syndrome. Am J Respir Crit Care Med 149:783–787

Landreneau RJ, Mack MJ, Dowling RD et al (1998) The role of thoracoscopy in lung cancer management. Chest 113:6S–12S

Mathis G, Bitschnau R, Gehmacher O et al (1999b) Ultraschallgeführte transthorakale Punktion. Ultraschall Med 20:226–235

Pan JF, Yang PC, Chang DB et al (1993) Needle aspiration biopsy of malignant lung masses with necrotic centers. Chest 103:1452–1456
Piscaglia F, NolsØe C, Dietrich CF et al (2012) The EFSUMB guidelines and recommendations on the clinical practice of contrast enhanced ultrasound (CEUS): update 2011 on non-hepatic applications. Ultraschall Med 32:33–59
Prosch H, Strasser G, Sonka C, Oschatz E, Mahaal S, Mohn-Staudner A, Mostbeck GH (2007) Cervical ultrasound (US) and US-guided lymph node biopsy as a routine procedure for staging of lung cancer. Ultraschall Med 28:598–603
Rettenbacher T (2014) Sonografie der peripheren Lymphknoten Teil 2: Doppler-Kriterien und typische Befunde bestimmter Entitäten. Ultraschall Med 35:10–32
Rivera MP, Mehta AC, Wahidi MM (2013) Establishing the diagnosis of lung cancer, 3rd ed: American College of Chest physicians evidence-based clinical practical guidelines. Chest 143:e142S–e165S
Schoenberg SO (2003) Magnetresonanztomographie. In: Drings P, Dienemann H, Wannenmacher M (eds) Management des Lungenkarzinoms. Springer, Berlin, pp 117–124
Silvestri GA, Gonzalez AV, Jantz MA et al (2013) Methods for staging non-small cell lung cancer. Diagnosis and management of lung cancer, 3rd ed: American College of Chest Physicians evidence-based clinical practice guidelines. Chest 143:e211S–e250S
Suzuki N, Saitoh T, Kitamura S et al (1993) Tumor invasion of the chest wall in lung cancer: diagnosis with US. Radiology 187:394
van Kaick G, Bahner ML (1998) Computertomographie. In: Drings P, Vogt-Moykopf I (eds) Thoraxtumoren. Springer, Berlin/Heidelberg/New York/Tokyo, pp 165–179
Volpicelli G, Elbarbary M, Blaivas M et al (2012a) International evidence-based recommendations for point-of-care lung ultrasound. Intensive Care Med 38:577–591
Yang PC (1996) Review paper: color Doppler ultrasound of pulmonary consolidation. Eur J Ultrasound 3:169–178
Yuan A, Chang DB, Yu CJ et al (1994a) Color Doppler sonography of benign and malignant pulmonary masses. Am J Roentgenol 163:545–549

Vascular Lung Consolidations: Pulmonary Embolism and Pulmonary Infarction

AMWF-guidelines (2016) Thrombosis and pulmonary embolism. Vasa 45(Suppl 90):1–48
Burge AJ, Freeman KD, Klapper PJ, Haramati LB (2008) Increased diagnosis of pulmonary embolism without a corresponding decline in mortality during CT era. Clin Radiol 63:381–386
Gehmacher O, Mathis G (1994) Farkodierte Duplexsonographie peripherer Lungenherde – ein diagnostischer Fortschritt? Bildgebung 61(S2):11
Goldhaber SZ, Visani L, De Rosa M (1999) Acute pulmonary embolism: clinical outcomes in the International Cooperative Pulmonary Embolism Registry. Lancet 353(9162):1386–1389
Horner D, Hogg K, Body R, Jones S, Nash MJ, Mackway-Jones K (2014) Single whole-leg compression ultrasound for exclusion of deep vein thrombosis inn symptomatic patients: a prospective observational study. Br J Haematol 164:422–430
Jackson RE, Rudoni RR, Hauser AM, Pascual RE, Hussey M (2000) Prospective evaluation of two-dimensional transhoracic echocardiography in emergency department patients with suspected pulmonary embolism. Acad Emerg Med 7:994–998
Jaeger K, Eichlisberger R, Frauchinger B (1993) Stellenwert der bildgebenden Sonographie für die Diagnostik der Venenthrombose. Haemostaseologie 13:116–123
Janata K, Holzer M, Domanovits H, Müllner M, Bankier A, Kurtaran A, Bankl HC, Laggner AN (2002) Mortality of patients with pulmonary embolism. Wien Klin Wochenschr 113:766–772
Konstantinides SV, Torbicki A, Agnelli G, Danchin N, Fitzmaurice D, Gale N et al (2014) 2014 ESC guidelines in the diagnosis and management of acute pulmonary embolism. Eur Heart J 35: 3033–3073
Mathis G (2014) Thromboembolism in ultrasound: killing three birds with one stone. Chest 145:931–932
Mathis G, Dirschmid K (1993) Pulmonary infarction: sonographic appearance with pathologic correlation. Eur J Radiol 17:170–174
Mathis G, Bitschnau R, Gehmacher O et al (1999c) Chest ultrasound in diagnosis of pulmonary embolism in comparison to helical CT. Ultraschall Med 20:54–59
Mathis G, Blank W, Reissig A, Lechleitner P, Reuss J, Schuler A, Beckh S (2005) Thoracic ultrasound for diagnosing pulmonary embolism. A prospective multicenter study of 352 patients. Chest 128: 1531–1538
McConell MV, Solomon SD, Rayan ME, Come PC, Goldhaber SZ, Lee RT (1996) Regional right ventricular dysfunction detected by echocardiography in acute pulmonary embolism. Am J Cardiol 78:469–473
Miniati M, Monti S, Pratali L et al (2001) Value of transthoracic echocardiography in the diagnosis of pulmonary embolism. Results of a prospective study of unselected patients. Am J Med 110: 528–535
Nazerian P, Vanni S, Volpicell G, Gigli C, Zanobetti M, Bartolucci M et al (2014) Accuracy of point-of-care multiorgan ultrasonography for the diagnosis of pulmonary embolism. Chest 145:950–957
Newman DH, Schriger DL (2011) Rethinking testing for pulmonary embolism: less is more. Ann Emerg Med 57:622–627
Niemann T, Egelhof T, Bongratz G (2009) Transthoracic sonography for the detection of pulmonary embolism – a meta analysis. Ultraschall Med 30:150–156
Reissig A, Kroegel C (2003b) Transthoracic ultrasound of lung and pleura in the diagnosis of pulmonary embolism: a novel non-invasive bedside approach. Respiration 70:441–452
Reissig A, Heyne JP, Kroegel C (2001) Sonography of lung and pleura in pulmonary embolism: sonomorphologic characterization and comparison with spiral CT scanning. Chest 120:1977–1983
Reissig A, Haase U, Schulze E, Lehmann T, Kroegel C (2010) Diagnosis and therapy of pulmonary embolism prior to death. Dtsch Med Wochenschr 135(30):1477–1483, Epub 20 Jul 2010
Squizzato A, Rancan E, Dentali F, Bonzini M, Guasti L, Steidl L et al (2013) Diagnostic accuracy of lung ultrasound for pulmonary embolism: a systematic review and meta-analysis. J Thrombo Haemost 11: 1269–1278
Volpicelli G, Blaivas M, Elbaray M, Lichtenstein D, Mathis G, Kirkpatrick A et al (2012b) International evidence-based recommendations for point of-care lung ultrasound. Intensive Care Med 38: 577–591
Wacker P, Wacker R, Golnik R, Kreft HU (2003) Akute Lungenembolie: Ein neuer Score zur Quantifizierung der akuten Rechtsherzinsuffizienz. Intensivmed 40:130–137
Yuan A, Yang PC, Chang CB (1993b) Pulmonary infarction: use of color doppler sonography for diagnosis and assessment of reperfusion of the lung. AJR Am J Roentgenol 160:419–420

Mechanical Lung Consolidations: Atelectasis

Burke M, Fraser R (1988) Obstructive pneumonitis: a pathologic and pathogenetic reappraisal. Radiology 166:699–704
Goerg C (2003) Focal lesions in the opacified lung: a sonographic pictorial essay. Ultraschall Med 24:123–128
Goerg C, Weide R, Walters E, Schwerk WB (1996) Sonographische Befunde bei ausgedehnten Lungenatelektasen. Ultraschall Klin Prax 11:14–19
Grundmann E (1986) Spezielle Pathologie, 7th edn. Urban & Schwarzenberg, Munich
Lan RS, Lo KS, Chuang ML, Yang CT, Tsao TC, Lee CM (1997) Elastance of the pleural space: a predictor for the outcome of pleurodesis in patients with malignant pleural effusion. Ann Intern Med 126:768–774
Liaw YS, Yang PC, Wu ZG et al (1994b) The bacteriology of obstructive pneumonitis. Am J Respir Crit Care Med 149:1648–1653

Soldati G, Testa A, Silva FR, Carbone L, Portale G, Silveri NG (2006) Chest ultrasonography in lung contusion. Chest 130:533–538
Wuestner A, Gehmacher O, Haemmerle S, Schenkenbach C, Haefele H, Mathis G (2005) Ultraschalldiagnostik beim stumpfen Thoraxtrauma. Ultraschall Med 26:285–290
Yang PC, Luh KT, Wu DH, Chang DB, Lee NL, Kuo SM, Yang SP (1990b) Lung tumors associated with obstructive pneumonitis: US studies. Radiology 174:717–720
Yuan A, Chang DB, Yu CJ, Kuo SH, Luh KT, Yang PC (1994b) Color Doppler sonography of benign and malignant pulmonary masses. AJR Am J Roentgenol 163:545–549

Congenital Pulmonary Sequestration

Cortellaro F, Colombo S, Coen D, Pier Giorgio P, Duca PG (2012) Lung ultrasound is an accurate diagnostic tool for the diagnosis of pneumonia in the emergency department Emerg Med J 29: 19e23
Gudinchet F, Anderegg A (1989) Echography of pulmonary sequestration. Eur J Radiol 9:93–95
Yuan A, Yang PC, Chang DB et al (1992) Lung sequestration diagnosis with ultrasound and triplex doppler technique in an adult. Chest 102:1880–1882

Mediastinum

Wolfgang Blank, Alexander Heinzmann, and Jouke T. Annema

G. Mathis (ed.), *Chest Sonography*, DOI 10.1007/978-3-319-44072-9_6

6.1 Transthoracic

Wolfgang Blank and Alexander Heinzmann

Mediastinal structures can be visualized comprehensively by computed tomography as well as magnetic resonance tomography. Sonography in contrast identifies only parts of the mediastinum.

As early as in 1971 Goldberg (1971) pointed out the suprasternal sonographic access to the mediastinum. This access was used by cardiologists for the representation of the thoracic aorta and aortic valve. (Herth 2009). In the mid-1980s sonography of the mediastinum was researched in pediatrics (Lengerke and Schmid 1988; Liu et al. 1988) as well as in adult medicine and its efficiency was proved (Braun 1983; Blank et al. 1986; Wernecke et al. 1986; Brüggemann et al. 1991). In the following years the diagnostic potential of sonography was systematically researched (Heizel 1985; Wernecke et al. 1986; Wernecke 1991; Blank et al. 1996b; Bosch-Marcet 2007; Supakul and Karmazyn 2013). Further possibilities were disclosed by the application of color-Doppler sonography and, recently, through contrast-enhanced sonography (Betsch et al. 1992, 1994; Dietrich et al. 1997, 1999; Caremani et al. 2009; Chen et al. 2014).

6.1.1 Sonographic Investigation Technique and Reporting

Profound knowledge of anatomy is absolutely essential (Figs. 6.1 and 6.2). Because of the small sonic window and the penetration depth only 3.5- and 5-MHz sector, convex and vector transducers with small apertures are suitable for sonographic diagnosis. In sonography the mediastinum is accessed from the suprasternal and the parasternal approach, occasionally also from the infrasternal approach (Blank et al. 1996a). The large vessels and their spatial relationship to the heart in the various planes serve as cardinal structures. The investigation from suprasternal is performed with the patient in the supine position. Viewing the upper mediastinum is facilitated by having the patient recline his/her head, ideally by cushioning the thoracic spine. Turning the head to the right and left is additionally helpful. In the right- and left-sided position described by Wernecke et al. in 1988 and by Brüggemann et al. in 1991 the mediastinum is shifted and the pulmonary cavity is displaced, which permits better viewing of the mediastinum. It is easier to assess the mediastinum in expiration (Beckh et al. 2002; Koh et al. 2002; Braun and Blank 2005; Herth 2009).

Transsternal sonographic access to the mediastinum is possible in children in the cartilage stage (Supakul and Karmazyn 2013).

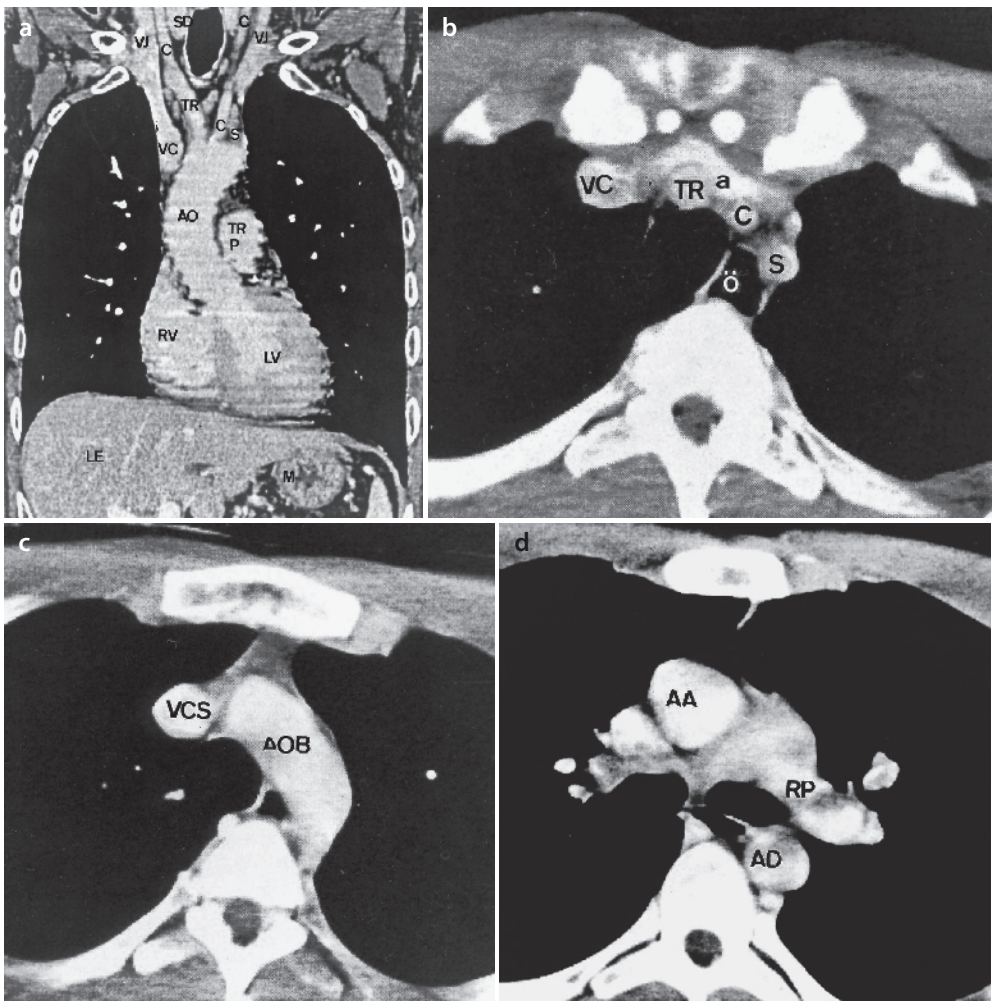

Fig. 6.1 Anatomy of the mediastinum on a computed tomogram. **a** Computed tomography reconstruction of the coronary section level. **b–d** Transverse sections of the mediastinum from caudal.*a*brachiocephalic veins, *AA* aorta ascendens, *AD* aorta descendens, *AO* aorta, *AOB* aortic arch, *C* carotid artery, *LP* left pulmonary artery, *LV* left ventricle, *Ö* esophagus, *RA* right atrium, *RP* right pulmonary artery, *RV* right ventricle, *S* subclavian artery, *SD* thyroid, *TP* pulmonary trunk, *TR* brachiocephalic trunk, *VC*, *VCI* inferior vena cava; *VJ* jugular vein. **e–g** Transverse sections of the mediastinum from caudal.*a*brachiocephalic veins, *AA* aorta ascendens, *AD* aorta descendens, *AO* aorta, *AOB* aortic arch, *C* carotid artery, *LP* left pulmonary artery, *LV* left ventricle, *Ö* esophagus, *RA* right atrium, *RP* right pulmonary artery, *RV* right ventricle, *S* subclavian artery, *SD*, thyroid, *TP* pulmonary trunk, *TR* brachiocephalic trunk, *VC*, *VCI* inferior vena cava, *VJ* jugular vein

Fig. 6.1 (continued)

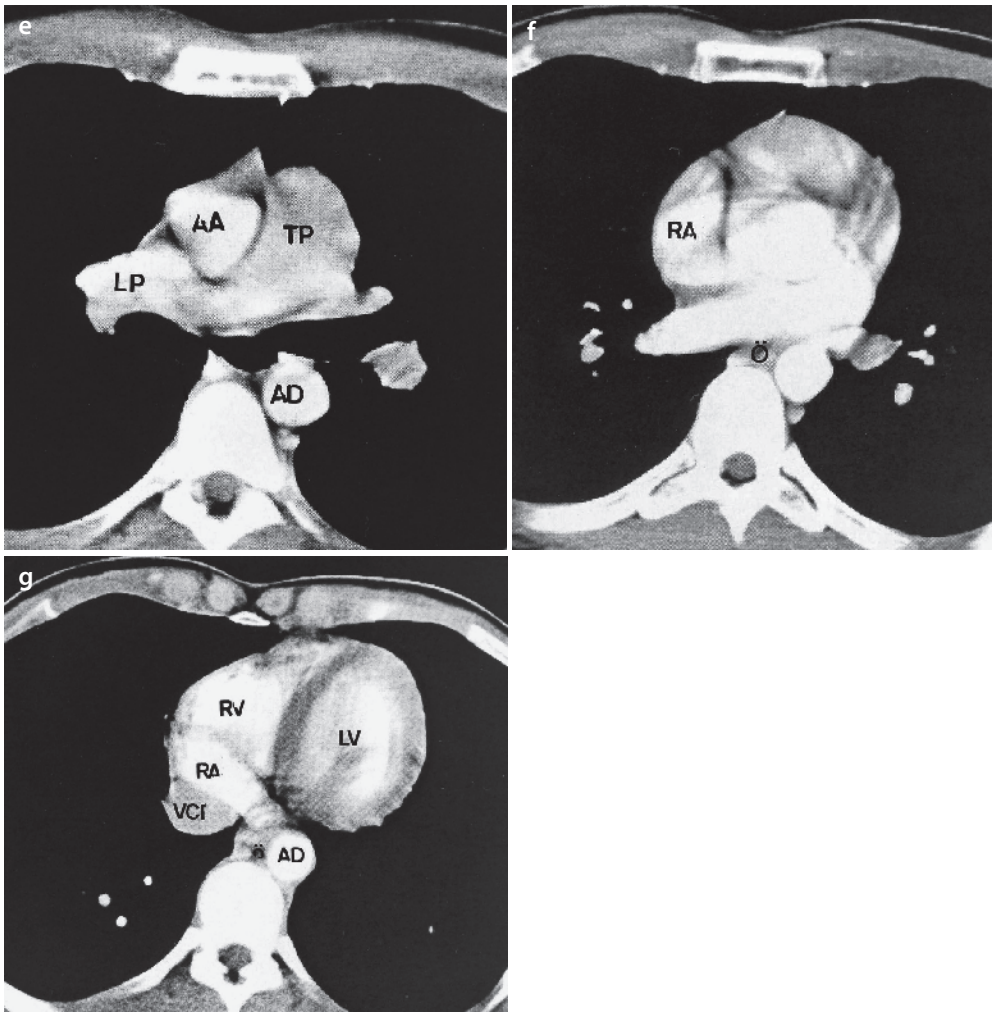

6.1.2 Sonoanatomy

In principle, from suprasternal the supraaortic and paratracheal region and the aorticopulmonary window can be imaged (Figs. 6.3, 6.4, 6.5, and 6.6):

Suprasternal access (supine position): superior/anterior mediastinum

- Right side—tracheal region
- Truncus brachiocephalicus, a. carotis, a. subclavia
- Arcus aortae
- V. cava superior, veins brachiocephalicus
- Truncus pulmonalis, arteries pulmonales
- Left atrium, veins pulmonales
- Thymus
- Retrosternal space

For this purpose half-sagittal (from the right and left sides), coronary and transverse images are needed. Cervical portions of the esophagus (posterior mediastinum) can also be visualized (5–8 cm) (Blank et al. 1998; Zhu et al. 2005; Palabiyik et al. 2012 Fig. 6.4d). From parasternal the combined use of right-sided and left-sided lateral decubitus position permits evaluation of the anterior and mid-mediastinum (Figs. 6.7 and 6.8). For this purpose the transducer is placed adjacent to the sternum, cranially, and then moved caudad. Anatomical structures visualized through transverse and sagittal sections in angulated planes are summarized as follows (Figs. 6.4, 6.5, and 6.6):

1. Parasternal access (lateral decubitus, right side): anterior/middle mediastinum
   - V. cava superior
   - Ascending aorta
   - A. pulmonalis dextra
   - Left atrium, vv. pulmonales
   - Left ventricle, right ventricle
2. Parasternal access (lateral decubitus, left side): anterior/middle mediastinum
   - Descending aorta
   - Truncus pulmonalis
   - Left atrium, vv. pulmonales
   - Left ventricle, right ventricle, right atrium

The infrasternal access only provides a limited view of caudal portions of the posterior mediastinum. The esophagus, aorta and vena cava are seen at the point where they pass through the diaphragm. Transverse and sagittal images in

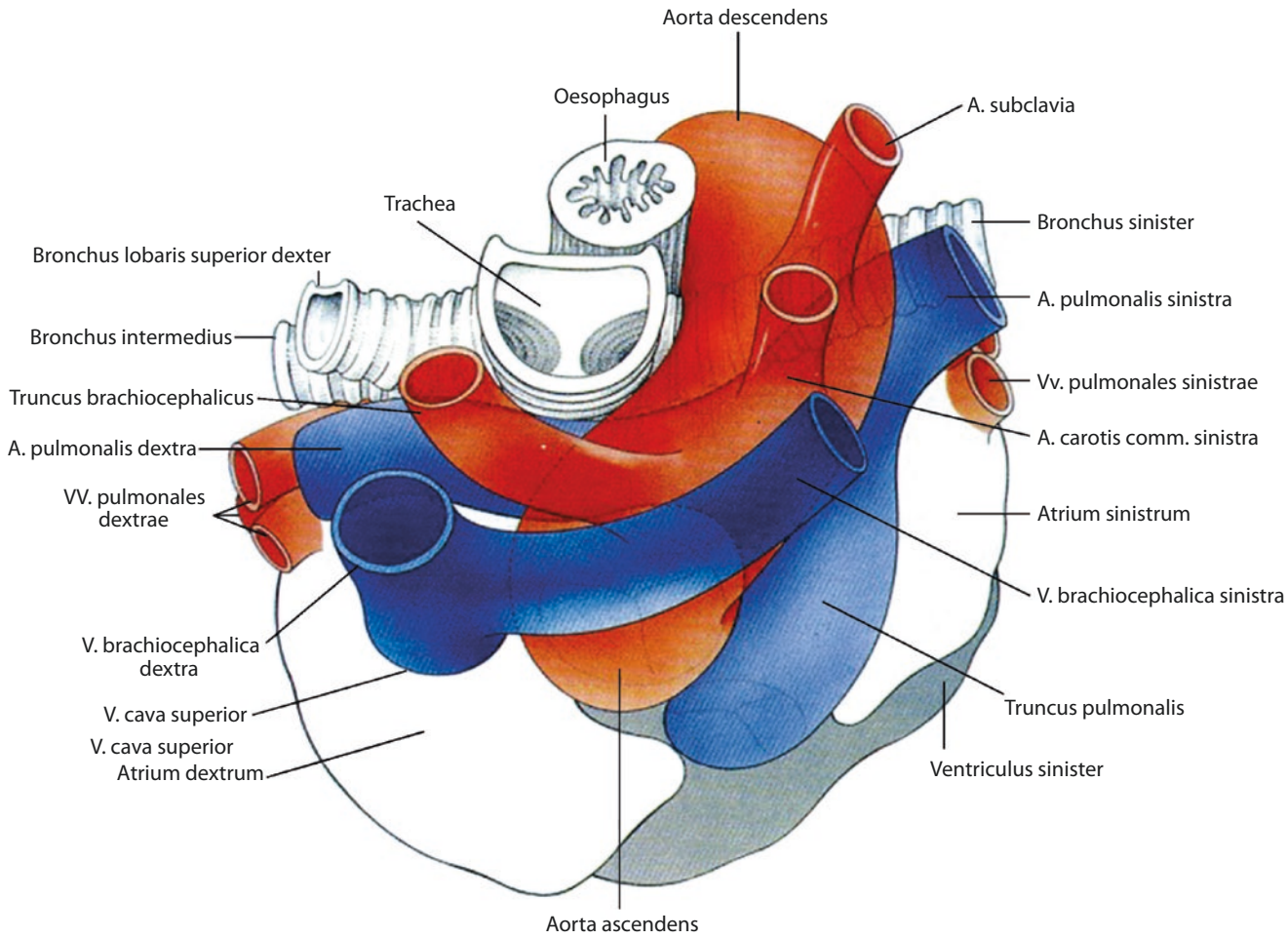

Fig. 6.2 Topographic anatomy of the mediastinal vessels—suprasternal view (From Wernecke 1991)

angulated planes are obtained through the left lobe of the liver (Blank et al. 1996a; Janssen et al. 1997; Fig. 6.9).

6.1.3 Imaging Compartments of the Mediastinum

The upper and mid-mediastinum can be imaged well on sonography. The suprasternal access permits adequate evaluation in 90–95 % of cases. The posterior mediastinum, paravertebral region, the hilum of the lung and the immediate retrosternal space, however, can only be partly assessed from a transthoracic approach. Transthoracic sonography may be severely hampered by obesity, pulmonary emphysema, mediastinal distortion as well as spinal deformities.

Factors that limit visualization of mediastinal structures:

- Low-lying structures
- Adiposity, large breasts
- Pulmonary emphysema
- Distortion of the mediastinum (surgery, inflammation, radiotherapy)
- Deformity of the vertebral column

6.1.4 Imaging Tumors in the Mediastinum

Approximately 75 % of clinically relevant space-occupying masses in the adult mediastinum are located in the anterior and mid-mediastinum and are therefore readily accessible for sonographic assessment (Rosenberg 1993). The topographic position of a mediastinal space-occupying mass, its size and mobility can be determined by sonography. High-resolution sonography permits good differentiation of tissue on the basis of echogenicity (cystic, solid to calcified). Surrounding vessels can usually also be imaged well in the B mode. More detailed information (differentiation of vessels, indicators of vessel infiltration, tumor vascularization) may be gathered by color-Doppler sonography (Betsch 1994; Blank and Braun 1995; Chen et al. 2014). Tumor vascularity can be demonstrated with much more sensitivity and without motion artifacts through contrast-enhanced sonography, if good-quality equipment is provided (Blank and Braun 1995; Görg et al. 2003). Various space-occupying masses in the mediastinum have a characteristic sonomorphology (Table 6.1). A definite diagnosis, however, is usually made after removal of tissue and its histological investigation (▶ Chap. 9).

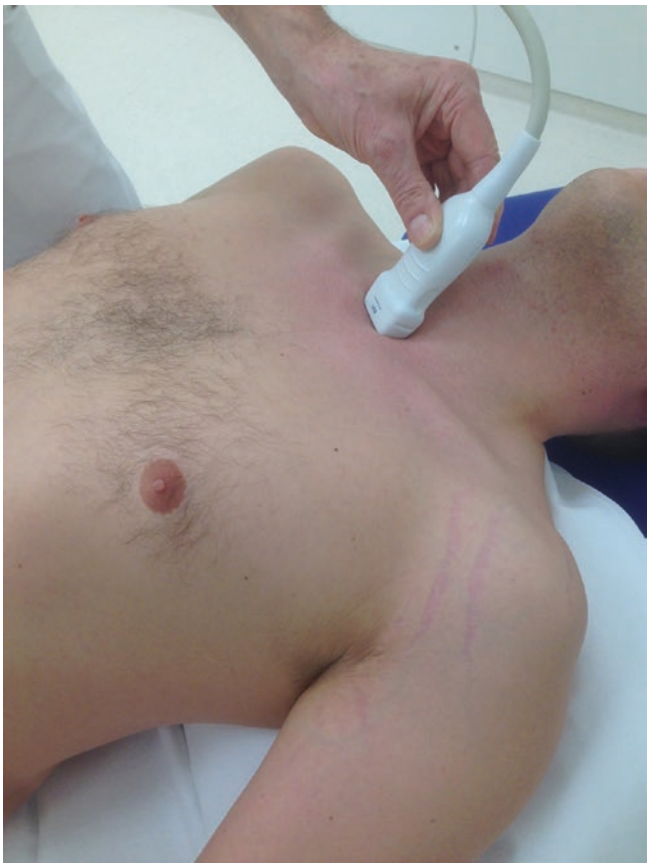

Fig. 6.3 Suprasternal examination. The ultrasound head is located in the jugular fossa; there is a cushion under the shoulders and the head is reclined at the maximum angle

6.1.5 Diagnostic Value of Sonography, Chest Radiographs and Computed Tomography

Sonography is superior to survey radiographs of the chest in the assessment of nearly all portions of the mediastinum (with the exception of the paravertebral region). In the evaluation of supraaortic, pericardial, prevascular and paratracheal regions, sonography has a sensitivity 90–100 % and is nearly as reliable as computed tomography. However, in the aorticopulmonary window and the subcarinal region, sonography achieves a sensitivity of only 82–70 % (Wernecke et al. 1988; Wernecke 1991; Brüggemann et al. 1991; Betsch 1994; Dietrich et al. 1995). Thus, sonography occupies an intermediary position between chest radiographs and computed tomography (Castellino et al. 1986; Bollen et al. 1994).

6.1.6 General Indications

Sonographic investigation of the mediastinum is performed after chest radiographs have been obtained, when the findings of the latter are not distinct or if a mediastinal space-occupying mass is suspected.

For an initial examination, medistinal sonography can be rapidly implemented in preclinical and emergency diagnosis as a point-of-care sonography for adults with acute thoracic symptoms (pain, upper inflow congestion; important diagnoses such as thoracic aortaic aneurism, a Vena cava superior thrombosis (Fig. 6.10) or a malignant lymphoma (Blank et al. 2014) can be made without delay. The procedure is also appropriate for primary imaging of children, and helps to reduce exposure to radiation. Reliable identification of medistinal tubercular lymph nodes in children is thus made possible (Bosch-Marcet et al. 2007; Supakul and Karmazyn 2013; Mosem and Andronikou 2014).

Sonography is the first investigation procedure in cases of acute chest symptoms (Fig. 6.10). The general indications for transthoracic sonography of the mediastinum are:

- Acute thoracic symptoms (Schmerz, obere Einflussstauung) (pain, upper inflow congestion)
- Suspected pulmonary tuberculosis, especially in children)
- Chest radiograph: space-occupying mass in the mediastinum
- Chest radiograph: undefined space-occupying mass
- Tumor staging (vascular complications)
- Monitoring the course of disease/therapy (tumor therapy)
- Puncture and drainage

6.1.7 Specific Sonographic Findings in Selected Space-Occupying Masses in the Mediastinum

Lymph Node Disease

Lymphomas account for approximately one quarter of all primary mediastinal tumors, whereas lymph node metastases of bronchial carcinomas, for instance, are more common.

On the basis of their hypoechoic transformation, inflamed and enlarged lymph nodes (e.g., Boeck's diseasetuberculosis,) or lymph nodes invaded by tumor (Hodgkin's or non-Hodgkin's lymphoma, lymph node metastases) can be well differentiated from the surrounding hyperechoic tissue (Wernecke 1991; Bosch-Marcet et al. 2007; Alvarez-Alvarez et al. 2013; Mosem and Andronikou 2014) (Figs. 6.11 and 6.12).

In contrast to the mostly "avascular" carcinoma metastases, lymphomas show strong blood flow in Color-Doppler Sonography (Chen et al. 2014); however, reliable differentiation of the above mentioned lymph node disease cannot be achieved through sonographic investigation without a tissue sample being taken (Gulati et al. 2000).

Differentiation of the above-mentioned diseases of lymph nodes by sonography alone is not possible without biopsy (Gulati et al. 2000).

Under treatment lymph nodes again become increasingly echogenic. Color-Doppler Sonography and, as an even more sensitive method that has been recently employed, contrast-enhanced sonography will reveal reduced blood circulation (Betsch 1994; Braun and Blank 2005). With the use of high-resolution devices, normal mediastinal lymph nodes (hypoechoic) are also visualized very often (paratracheal, aorticopulmonary window). A reliable differentiation of

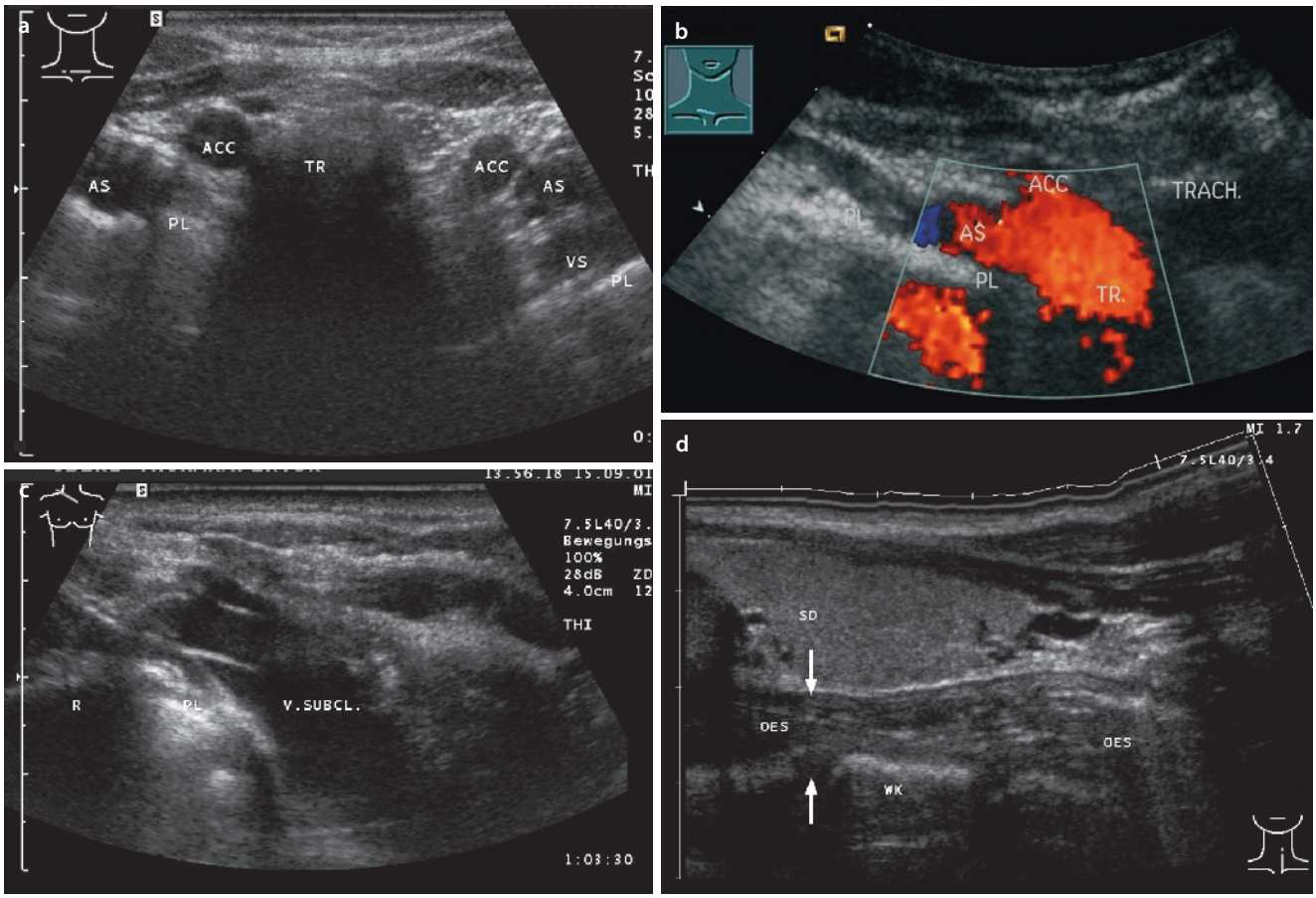

Fig. 6.4 Suprasternal examination. Supraaortal vessels. **a** The suprasternal transverse section demonstrates the cross section of the supraaortal vessels, right, distal to the branching of the brachiocephalic trunk. *ACC* common carotid artery, *AS* subclavian artery, *VS* subclavian vein, *TR* trachea, *PL* pleura/pulmonary reflex. **b** Half-sagittal right-hand section. The brachiocephalic trunk (*TR*) is shown by color-Doppler sonography, branching into the subclavian artery (*AS*) and the common carotid artery (*ACC*). The paratracheal region with its lymph nodes can be seen dorsal to the trunk in this section. Lateral to the reflex of the pleura/lung (*PL*), there is a mirror artifact of the artery. **c** A slight ventral tilting of the probe demonstrates the right subclavian vein. A venous valve can be distinguished. *PL* pleura/pulmonary reflex, *R* rib. **d** The cervical portions of the esophagus (*arrows*) show the left thyroid gland dorsomedial if the sonography probe is tilted slightly laterally. High-resolution sonography probes allow a five-layer separation to be made of the esophagus wall (*arrows*). When the patient swallows, the course of the peristaltic wave and the passage of a high reflexogenic air–liquid portion can be observed. Average wall thickness is 2.5 mm. *OES* esophagus, *SD* thyroid, *WK* cervical vertebra

pathological processes (► Chap 10), however, is not possible without obtaining bioptic material (Dietrich et al. 1995, 1999; Bosch-Marcet et al. 2007).

Tumors of the Thymus

The thymus is located in the anterior mediastinum, behind the sternum. In adults it cannot be distinguished from its hyperechoic surroundings. Approximately one quarter to one third of all primary mediastinal tumors originate from the thymus. There are various malignant tumors; thymomas and lymphomas are the most common ones (more rarely, germ cell carcinoma, carcinoids and carcinomas). These entities have characteristic sonographic features (Fig. 6.13, Table 6.2). The diagnosis is verified by performing a sonography-guided or computed tomography-guided biopsy (Schuler et al. 1995; ► Chap 10).

Germinal Cell Tumors

Teratomas and seminomas are mostly situated in the ventral and middle part of the mediastinum, accounting for approximately 10 % of primary mediastinal tumors. Teratomas usually occur in the second and third decades, grow slowly and only produce symptoms if they have grown to a large size (encroaching upon surrounding structures). These tumors are clearly delineated, and contain cystic as well as epithelial structures (skin and appendages) and also tissue of mesenchymal origin (cartilage, bone, smooth muscle). Twenty-five to thirty percent of tumors show malignant transformation (Fig. 6.14).

Neurogenic Tumors

Neurogenic tumors originate from the sympathetic trunk, intercostal nerves or the vagus nerve, and therefore commonly grow in the posterior mediastinum. They can therefore only be demonstrated by transthoracic sonography if they have displaced pul-

monary structures paravertebrally or extend cranially (retrosternal approach) or caudally (infrasternal approach). Transesophageal imaging and puncture, if necessary, are usually easy to perform.

Retrosternal Portions of the Thyroid and Parathyroid

These can be reliably assigned to the thyroid or the parathyroid on the basis of their topography and typical sonographic pattern. In problematic cases color-Doppler sonography may be used to prove the source organ of the lesion.

Parathyroid adenomas extending retrosternally usually appear as markedly hypoechoic well-vascularized space-occupying masses (typical laboratory constellation is increased parathyroid hormone and calcium). Puncture may be helpful to differentiate lymph node enlargement (Braun 1992).

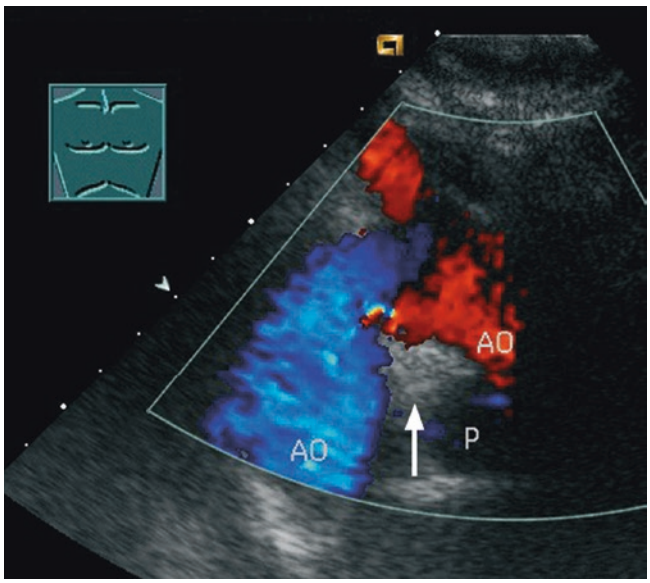

Fig. 6.5 Suprasternal examination. Suprasternal, sagittal section. The aorticopulmonary window (*arrow*) between the aortic arch and the pulmonary artery (*P*) shown in the cross section. If conditions for examination are difficult, the vessels can often be better differentiated from the surrounding soft-tissue structures by color-Doppler sonography and may be identified with more certainty (pulsed-Doppler sonography with characteristic frequency spectrum)

Mediastinal Cysts

Pericardial and bronchial cysts usually can be clearly identified. If they contain highly viscous fluid, however, differentiation may not always be possible even by dynamic B-mode imaging (change of patient positioning, etc.). Absence of vascularization (in color-Doppler or contrast-enhanced sonography) verifies the diagnosis (Fig. 6.15).

Pericardial Alterations

Pericardial alterations like pericardial effusion, hemopericardium and tumor infiltration are easily demonstrable.

Esophageal Disease

Proximal and distal portions of the esophagus can be clearly visualized by the suprasternal and infrasternal access. Esophageal tumors crossing the wall are seen as hypoechoic tumor formations with blurred margins (Figs. 6.16 and 6.17). In cases of surgical replacement of the esophagus, the upper anastomosis can be viewed. Recurrent tumors can also be detected (Blank et al. 1998; Palabiyik et al. 2012).

Sonography is a valuable aid in the detection of "dysphagia close to the cardia" (Blank et al. 1996a; Janssen et al. 1997).

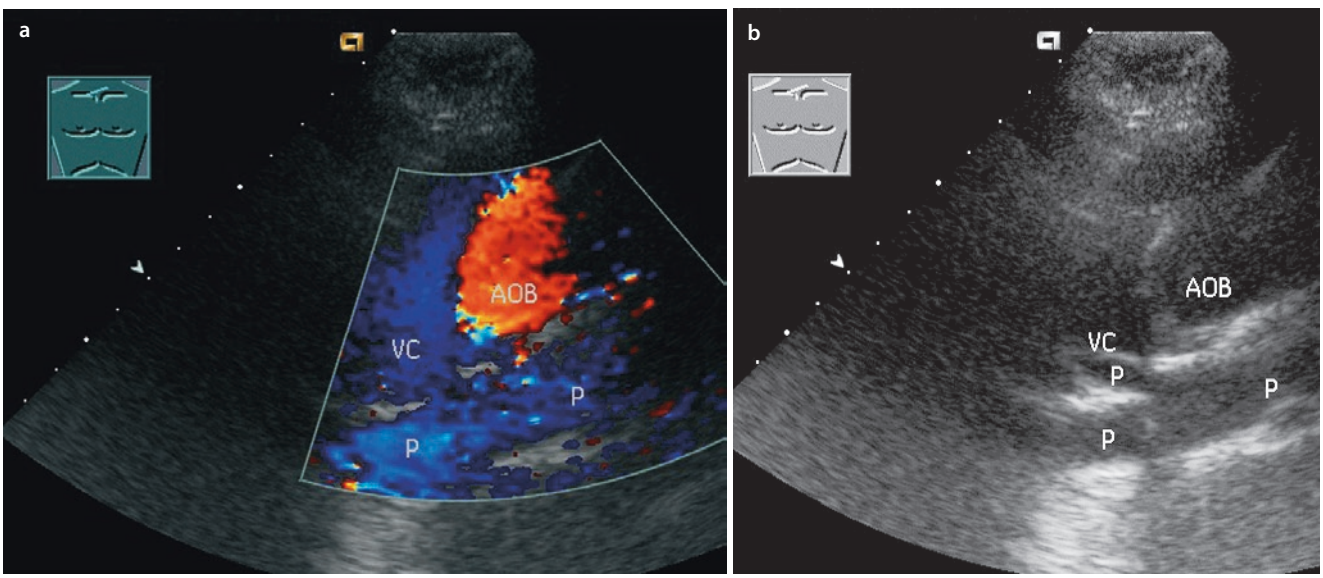

Fig. 6.6 Suprasternal examination. Suprasternal coronary section. **a** Lateral to the aortic arch (AOB), which is shown in an oblique section, the vena cava (VC) can be distinguished with certainty by color-Doppler sonography because of its reverse direction of flow (coded blue). **b** The branching of the pulmonary artery (P) and the aorticopulmonary window can be demonstrated better on B-mode after switching off the color Doppler

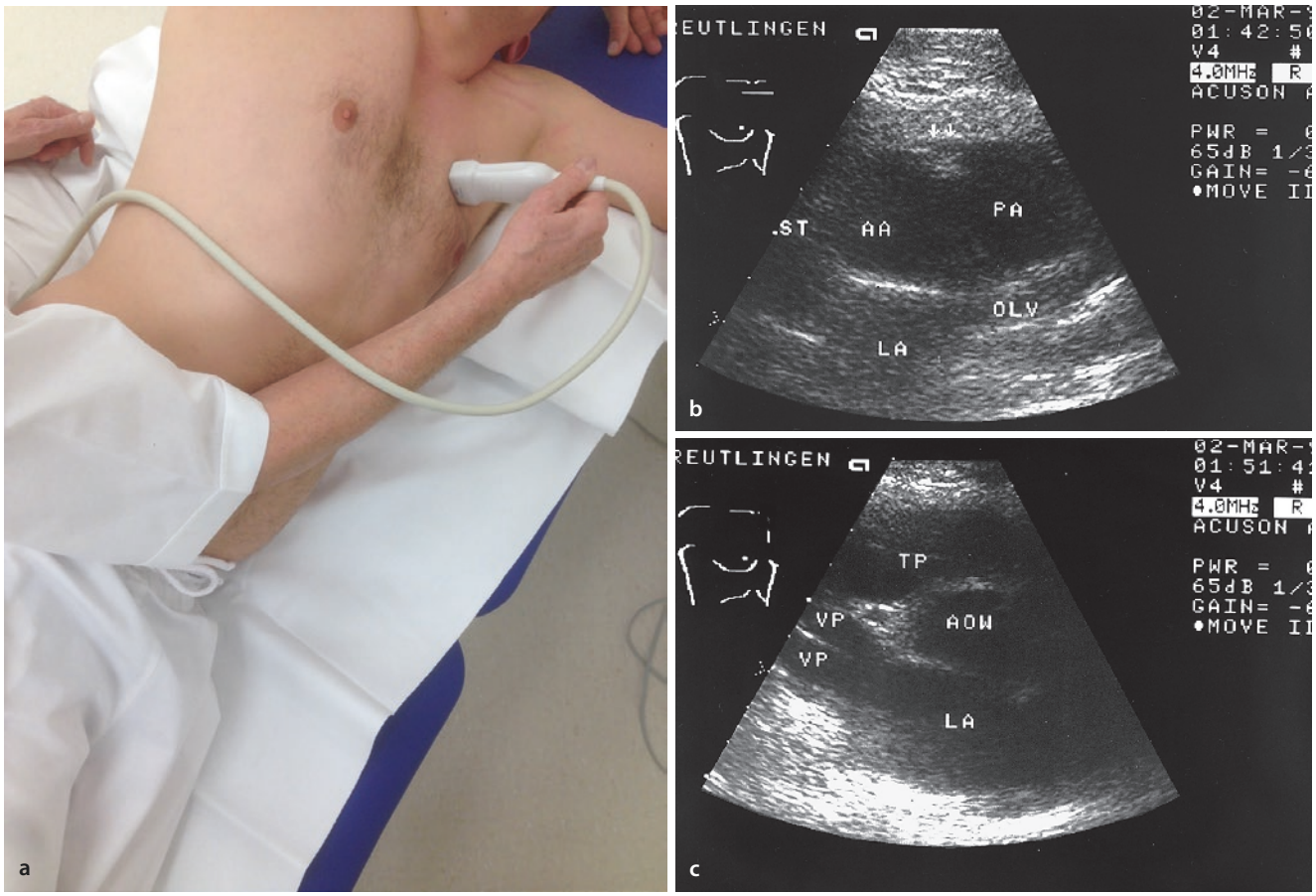

Fig. 6.7 **a** Parasternal examination in the left lateral position. **b** Left parasternal, transversal section. The pulmonary artery (*PA*) winds around the cross-sectional ascending aorta (*AA*). In-between is the upper pericardial recess (*double arrow*), sternum (*ST*), left atrium (*LA*) and upper lung veins (*OLV*). **c** Left parasternal, sagittal section. At the level of the aortic root (*AOW*) ventral crossing through the truncus pulmonalis (*TP*), dorsal left atrium (*LA*) joining pulmonary veins (*VP*)

6.1.8 Summary

Mediastinal space-occupying masses are most frequently found in the anterior upper mediastinum. They can be evaluated with transthoracic sonography nearly as reliably as with computed tomography, and histological material can usually be easily obtained by sonography-guided puncture (Chen et al. 2014) (▶ Chap. 10).

In case of acute thoracic symptoms, this procedure can be implemented as a point-of-care sonography in emergency diagnosis (Blank et al. 2014).

The disadvantages of sonography, however, are significant. The procedure is strongly investigator dependent and only reveals portions of the mediastinum compared with computed tomography. Moreover, the image quality is highly variable. Some of these disadvantages (Table 6.3) can be balanced by the application of endoluminal transesophageal and endobronchial sonography (▶ Sect. 6.2).

Acknowledgments I would like to express my thanks to Martin Lenz (chief consultant surgeon in the Radiology Department of the Steinenberg Clinic, Reutlingen) for preparing and providing the radiological findings, and my son Valentin for the technical photographic work.

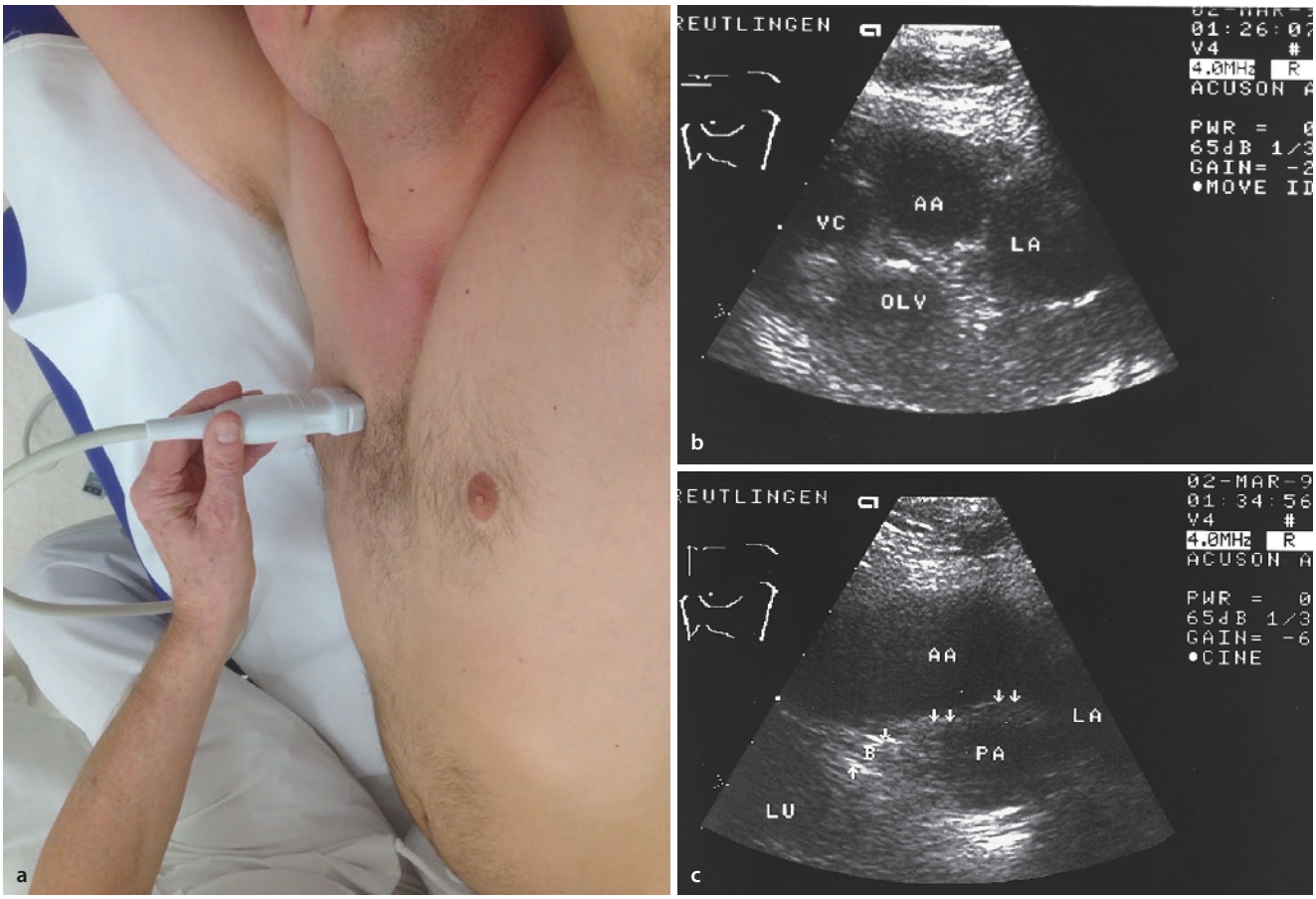

Fig. 6.8 **a** Parasternal examination in right lateral position. **b** Right parasternal transversal section. *AA* ascending artery, *VC* superior vena cava, *LA* left atrium *OLV*, upper lung vein. **c** Right parasternal sagittal section. A successful depiction of the ascending aorta (*AA*), the pulmonary artery (*PA*) in cross section with the aorticopulmonary window (*double arrow*) in-between, and of the subcarinal region. A bronchus (*B*) can be depicted as an echogenic reflection (*single arrow*). *LU* lung, *LA* left atrium

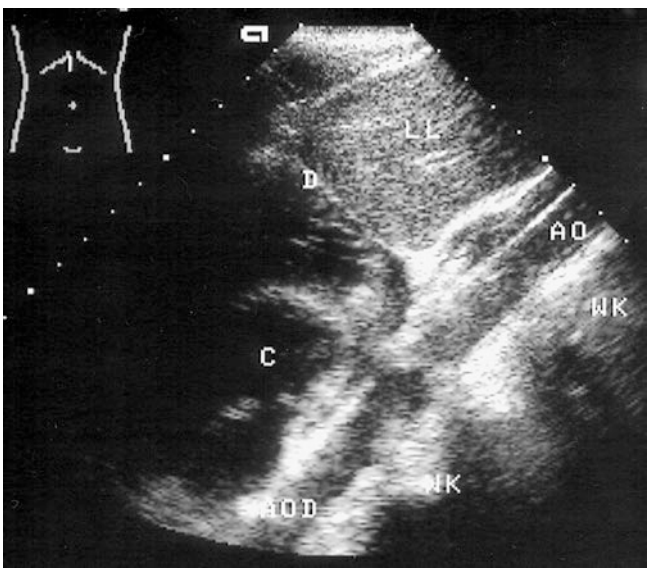

Fig. 6.9 Infrasternal sonography. Sagittal section. The esophagus can be observed at the passage through the diaphragm (*D*) ventrolaterally to the aorta (*AO*). The descending aorta (*AOD*) is partly covered by artifacts. *WK* vertebral body, *C* cor

Table 6.1 Sonomorphology of space-occupying masses in the mediastinum. Modified according to Wernecke (1991)

Appearance	Type of space occupation
Anechoic	Cystic formations, vessels
Hypoechoic	Lymphomas, "active" lymph nodes, more rarely "silent" lymph nodes
Hypoechoic–inhomogeneous echoes	Carcinoma, filiae, inflammation, aneurysm
Echodense	Physiological structures, thymus, scar (exception, rare liposarcoma and teratocarcinoma)

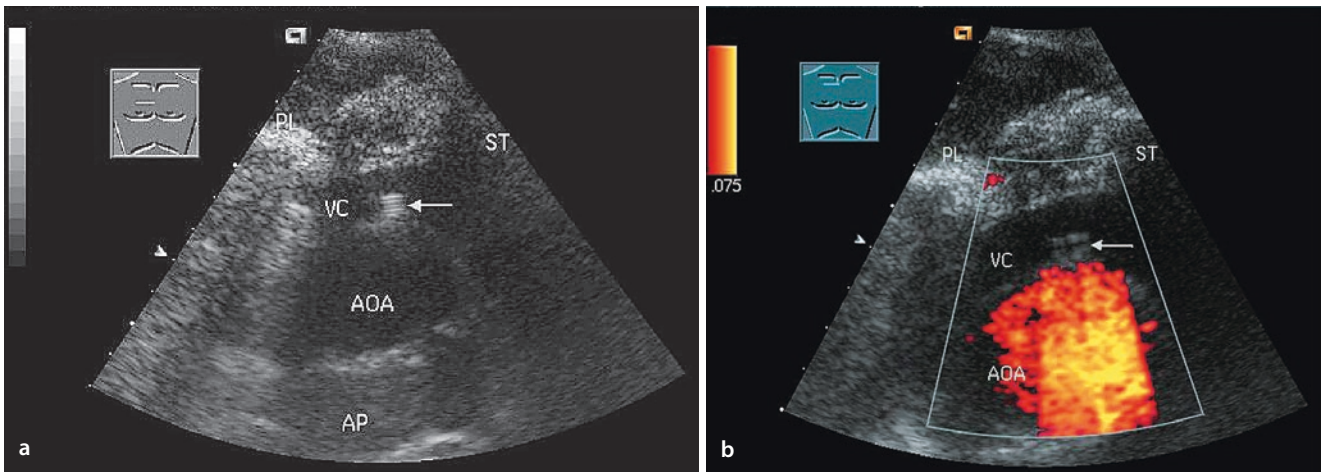

Fig. 6.10 Known non-Hodgkin's lymphoma. **a** Acute upper inflow congestion. Condition after port implantation. B-image sonography of still parasternal tumor masses. The port catheter can be differentiated as an echogenic double structure (*arrow*) in the hypoechoic vena cava. *AOA* ascending aorta, *AP* right pulmonary artery, *ST* sternum, *PL* pleura. **b** Thrombosis of the vena cava superior (*VC*) can be substantiated

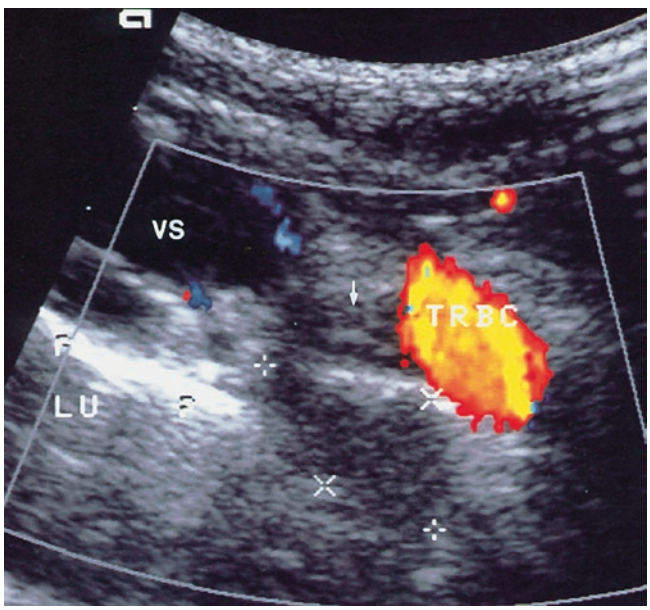

Fig. 6.11 Lymph node tuberculosis. Suprasternal semisagittal section, *right*. Dorsally to the color-Doppler sonography image of the brachiocephalic trunk (*TRBC*), one can see a hypoechoic, indistinctly delineated lymph node (*crosses*) in the paratracheal region, which normally has a homogeneous, hyperechoic structure. The diagnosis of lymph node tuberculosis was made possible by color-Doppler sonography of the fine-needle puncture. *LU* lung

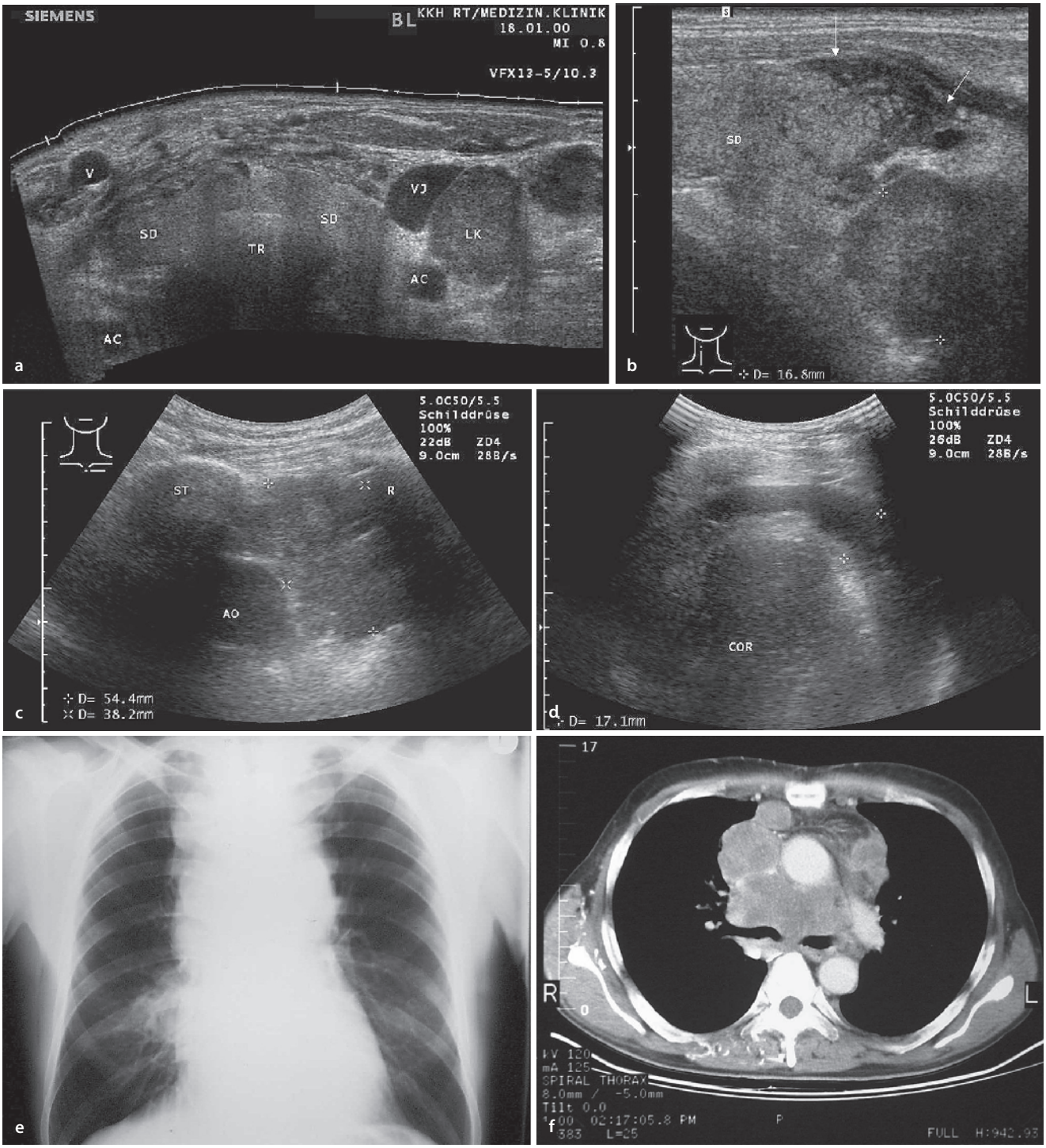

Fig. 6.12 Primary sonographic examination of an upper inflow congestion. **a** Multiple lymph nodes (*LK*) suspected of malignity in the neck region. The panorama presentation (SieScape, from Siemens) enables an impressive documentation of a relatively large region of the body. **b** Low-echo tumor infiltration into the thyroid gland. Tumor masses (*crosses*) reaching into the retrosternal region. **c** Left parasternal section, in the vicinity of the infiltrating low-echo mass (*crosses*). The wall of the aorta (*AO*) can no longer be sharply delineated. *ST* sternum, *R* rib. **d** Pericardial deposits and pericardial effusion (*crosses*). Suspected diagnosis of bronchial carcinoma (man, smoker) with substantiation of a mass suspected of being a metastasis in the region of the right adrenal gland (*crosses*). The diagnosis was confirmed by a sonographically controlled parasternal punch biopsy (Sonocan neddle, 1.2-mm diameter). Histology indicated smallcell bronchial carcinoma. **e** Chest X-ray overview. Mediastinal dissemination. **f** Computed tomogram. Tumor on the *right* lower lobar bronchus with extensive mediastinal metastases

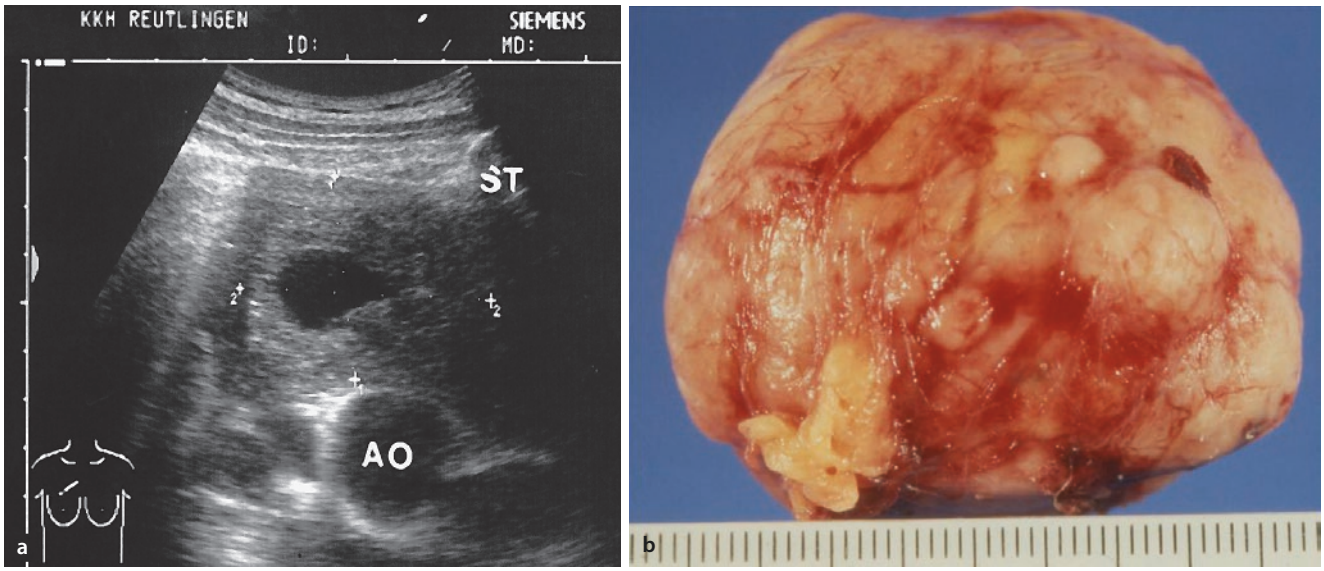

Fig. 6.13 Thymoma. **a** Parasternal, transversal section. Even with the patient in the supine position, it was possible to see a low-echo mass in a ventral position to the aorta and well delineated. Central liquid area. Sonographically controlled incision biopsy (diameter 1.2 mm). *AO* aorta, *ST* sternum. **b** Slide of pathology specimen. The tumor is clearly delineated

Table 6.2 Sonomorphology of thymomas

Benign	Malignant
Hypoechoic	Hypoechoic, inhomogeneous
Sharp margins	Blurred margins
Rounded, partly lobed	Tumor cones
No infiltration	Infiltration (pericardium, vessels)

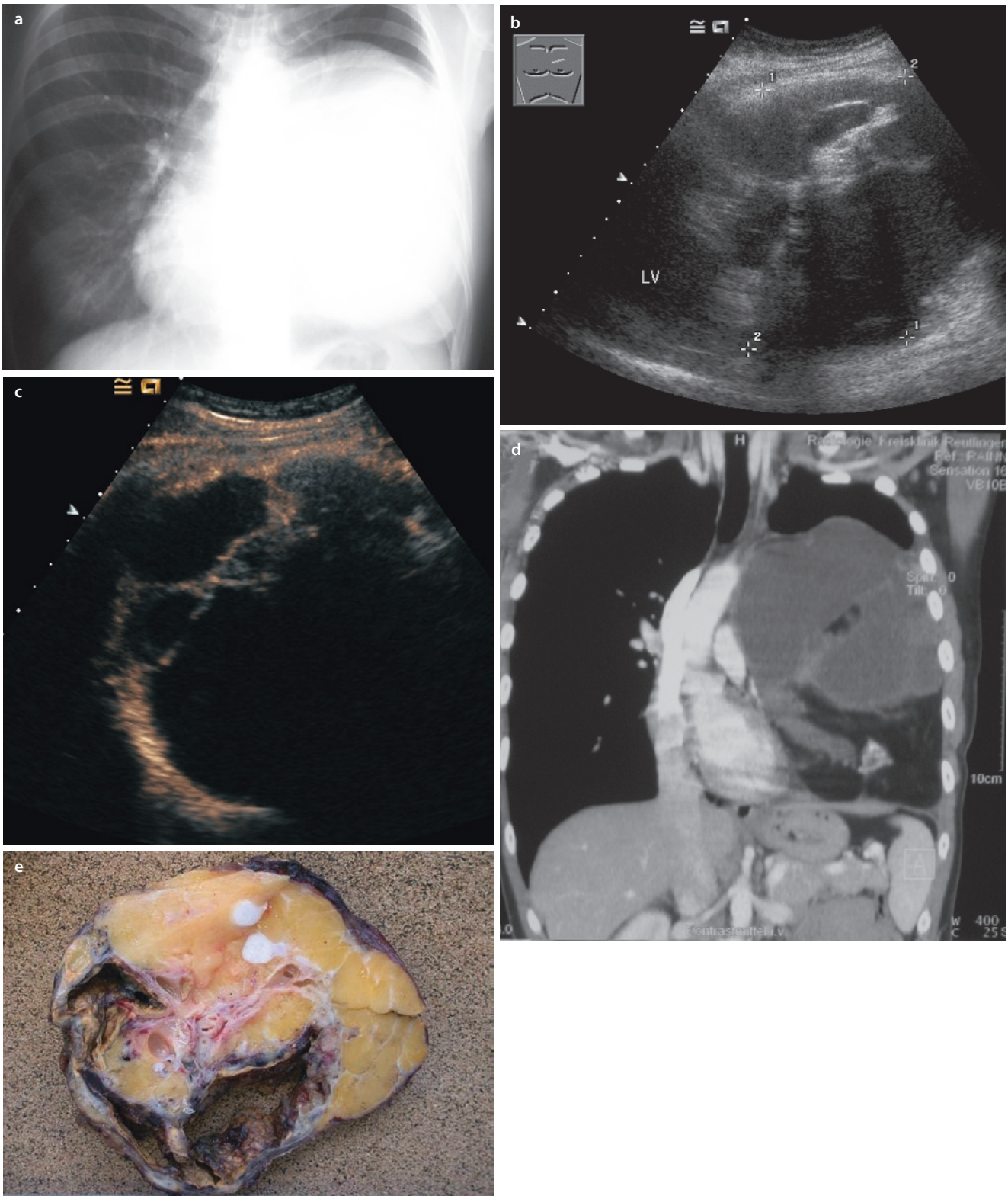

Fig. 6.14 Cystic teratoma. A 32-year-old patient, slight dyspnea when jogging. **a** Plain chest radiograph with tumor and mediastinal distortion to the right. **b** Left parasternal section in supine position. Clearly delineated mass with echogenic septum- like structures. In the *center*, high amplitude reflexes with dorsal shadowing. The space-occupying lesion displaces the pleura to the side toward the thoracic wall, which moves with breathing. The feeding vessels suggest a mediastinal origin of the lesion. **c** Contrast-enhanced sonography clearly demonstrates cystic parts of the tumor which otherwise only shows moderate vascularization and has a smooth border. A teratoma is suspected (central calcifications), and further preoperative diagnostics include computed tomography and transesophageal echocardiography. **d** Computed tomography reconstruction of the coronary section. **e** The gross pathological specimen demonstrates the smoothly demarcated tumor with septae, cystic areas, fatty tissue and cartilage/bone. Histology reveals a benign teratoma

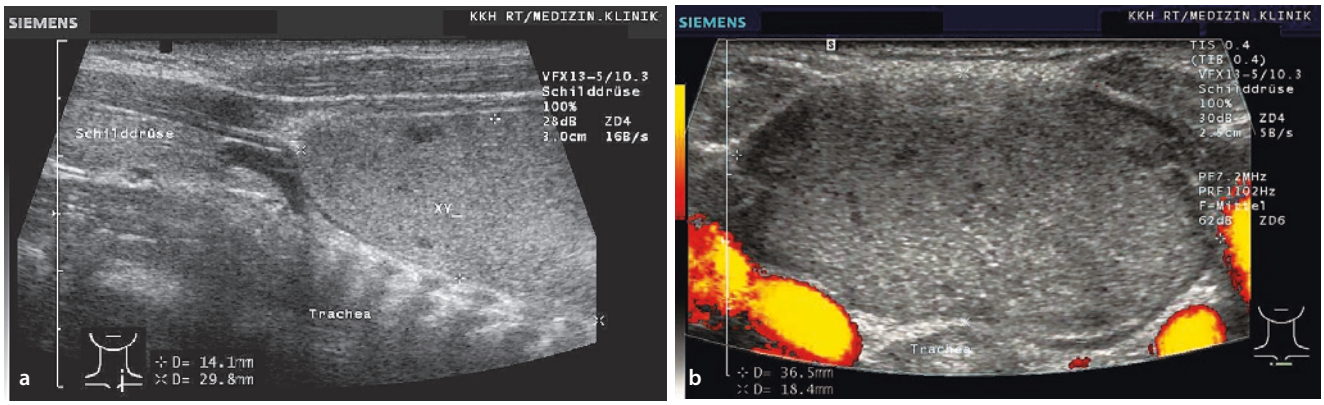

Fig. 6.15 Mediastianal cyst. **a** Suprasternal sagittal section. Smooth edged, homogeneously structured mass (*crosses*), ventral to the trachea. The proximal esophagus is recognizable dorsal to the thyroid gland on the *left*. **b** No blood circulation is detectable in the cross section even with highly sensitive technology. Movement of liquid is made recognizable in the B-image and in the color-Doppler sonography by a shaking movement. Diagnostic fine-needle puncture. Therapeutically operative resection due to compression syndrome

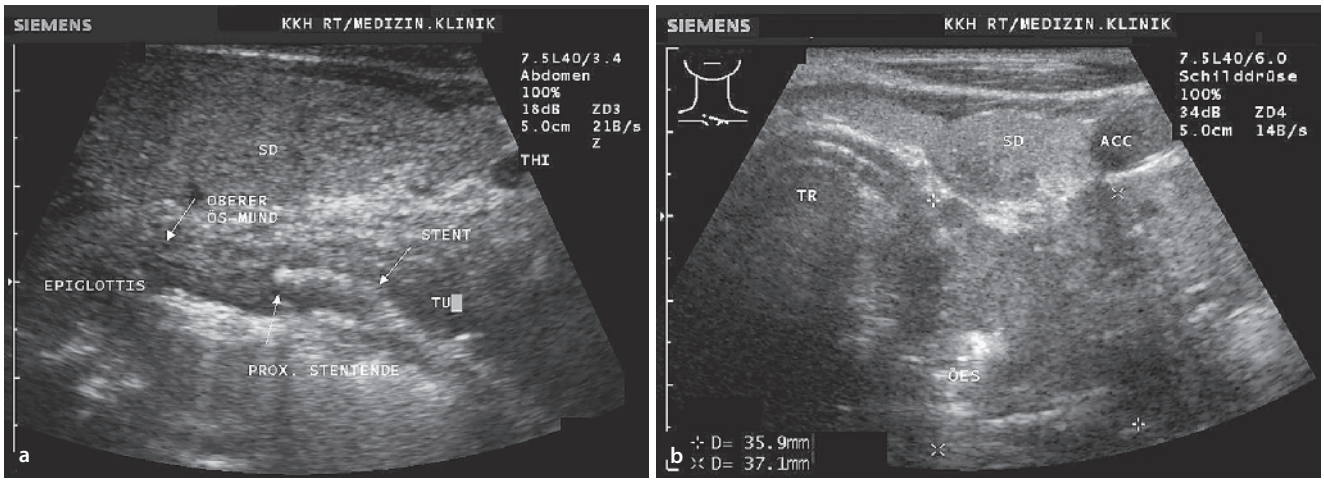

Fig. 6.16 **a** Proximal esophageal carcinoma spreading over the wall (*TU*) with infiltration into the epiglottis, upper esophageal sphincter (*OBERER ÖS-MUND*, *arrow*). The overgrown metal stent (*arrow*) is well delineated. An image with plenty of contrast and low in artifacts as a result of tissue-harmonic imaging. *THI* thyroid. **b** Tumor masses (*crosses*) with infiltration and stenosis of the esophagus (*OES*)

Table 6.3 Transthoracic sonography of the mediastinum

Advantages	Disadvantages
Dynamic imaging	Investigator dependent
Free selection of sectional planes	Only parts of the mediastinum are accessible
Good imaging of the aorticopulmonary window	–
Punctures: low rate of complications	Only punctures in the anterior mediastinum are possible

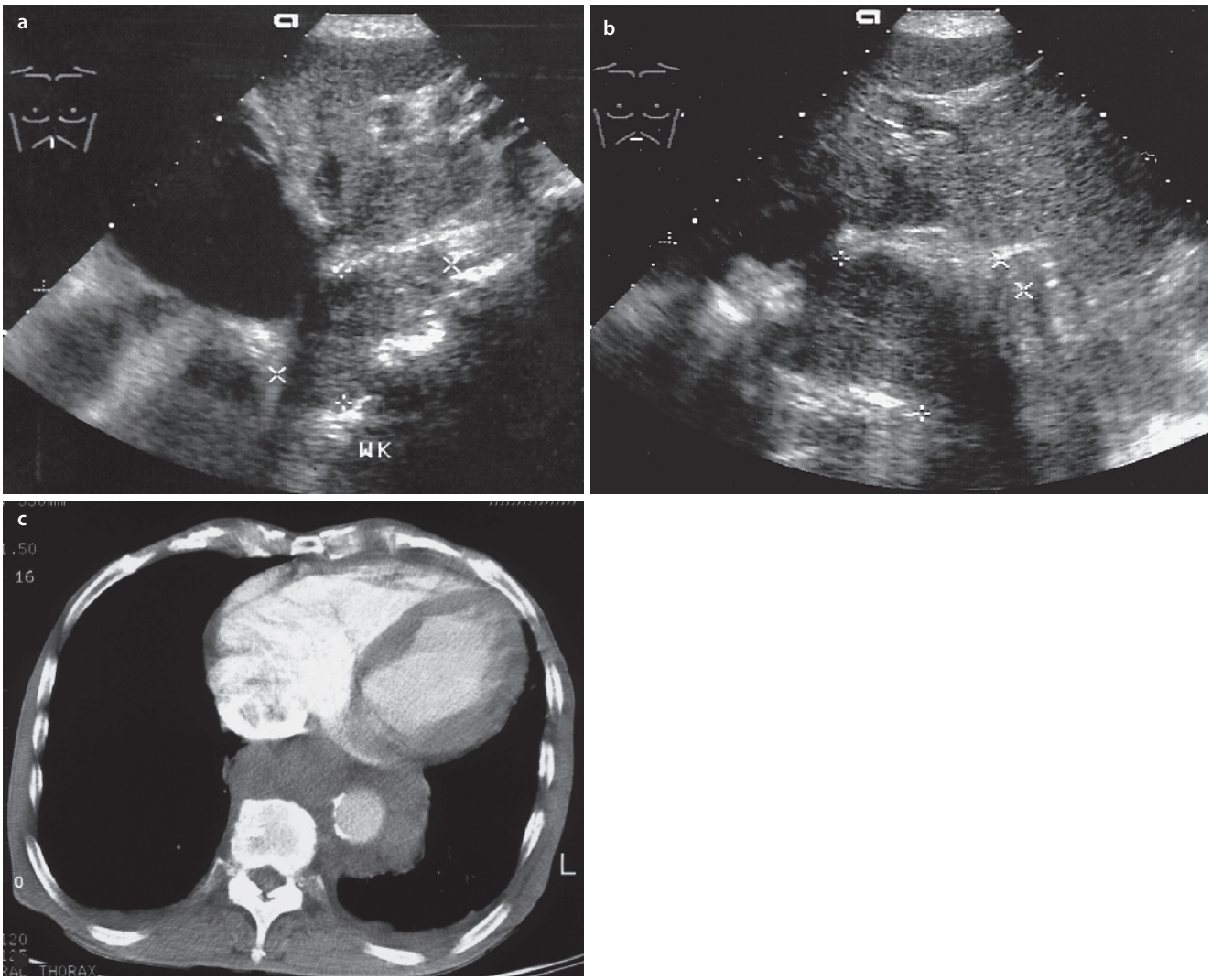

Fig. 6.17 Extensive esophageal carcinoma. **a** Clinical dysphagia. Endoscopic distal esophageal stenosis. No tumor could be established with certainty by biopsy. Sonography with infrasternal, sagittal section of the tumor formation lying ventrally to the spinal column (posterior mediastinum). *WK* vertebral body. **b** Tumor (*crosses*) located infrasternally in transverse section at the distal esophagus (*large crosses*) cannot be delineated. Percutaneously controlled transhepatic fine-needle cut biopsy (Sonocan, 0.9 mm). Histology indicated esophageal carcinoma. (**c**) Computed tomography. Mass in the posterior mediastinum surrounding the descending aorta

6.2 Transesophageal Sonography for Lung Cancer and Mediastinal Lesions

J.T. Annema

Assessing a tissue diagnosis of mediastinal lesions, for example in patients with lung cancer and enlarged mediastinal lymph nodes, is often of major clinical importance. To date, surgical staging—such as mediastinoscopy and mediastinotomy—is still regarded as the standard of care for mediastinal assessment. However, these procedures are not only invasive and require clinical admission with associated high costs, they also have limitations in their diagnostic reach.

The development of transesophageal sonography-guided fine-needle aspiration (FNA) provides a minimally invasive alternative for mediastinal analysis. Transesophageal sonography-guided FNA is currently used for the staging for various gastrointestinal malignancies. Since the first report in 1996 on transesophageal sonography-guided FNA for mediastinal staging (Pedersen et al. 1996), this method has evolved to an important diagnostic tool in chest medicine. In this part of the chapter, technical aspects as well as the use of transesophageal sonography-guided FNA in pulmonology will be discussed with an emphasis on the diagnosis and staging of lung cancer). To date, lung cancer staging guidelines advise endosonography when tissue verification of mediastinal nodes is indicated. Recently, it was demonstrated that endonosography (EBUS-TBNA) should be considered the initial diagnostic/staging test of choice in patients supected of have lung cancer as it reduces time to treatment decision in comparison with conventional (bronchoscopic) diagnostic and staging techniques.

6.2.1 Technical Aspects

Transesophageal sonography is performed with technology which is also used by gasteroenterologists.

Both radial and linear sonography probes are available, which both enable visualization of paraesophageal lesions. Real-time sonography-controlled FNAs (Fig. 6.18), however, are only possible with linear or longitudinal probes. The fine needle aspirates obtained can be used for cytological as well as molecular analysis—for instance, PCR analysis in patients with suspected tuberculosis.

In chest medicine, only linear sonography probes are used as tissue sampling is indicated in the vast majority of cases. Patients are investigated in a left lateral position in an ambulatory setting under conscious sedation using a low dose of midazolam. After the pharynx has been anesthetized with a lidocaine spray, the echo-endoscope is introduced into the distal esophagus until the left liver lobe is visualized. From this point the echo-endoscope is slowly retracted—meanwhile making circular movements, which enables complete visualization of all paraesophageal lesions that are located in the mediastinum. Once lymph nodes have been identified, size, shape, echo texture and borders of lesions can be described. Mediastinal nodes with a short axis exceeding 1 cm, a hypoechoic texture, a round shape and sharp borders are suspected to be malignant. When indicated, images and short movies of mediastinal abnormalities can be recorded. In order to prove malignant nodal involvement it is necessary to obtain tissue (Toloza et al. 2003b). Suspected paraesophageal lesions can be aspirated under real-time sonographic guidance (Fig. 6.19). Nodes from which tissue is obtained should be classified according to the IASLC-classification (Tournoy et al. 2008; Fig. 6.20). In the case of suspected adrenal metastases, left-sided adrenal masses can by aspirated from the stomach (Eloubeidi et al. 2004). On-site cytological evaluation of aspirates has been proven be useful in order to ensure that representative samples are obtained. In experienced hands, a complete trans-

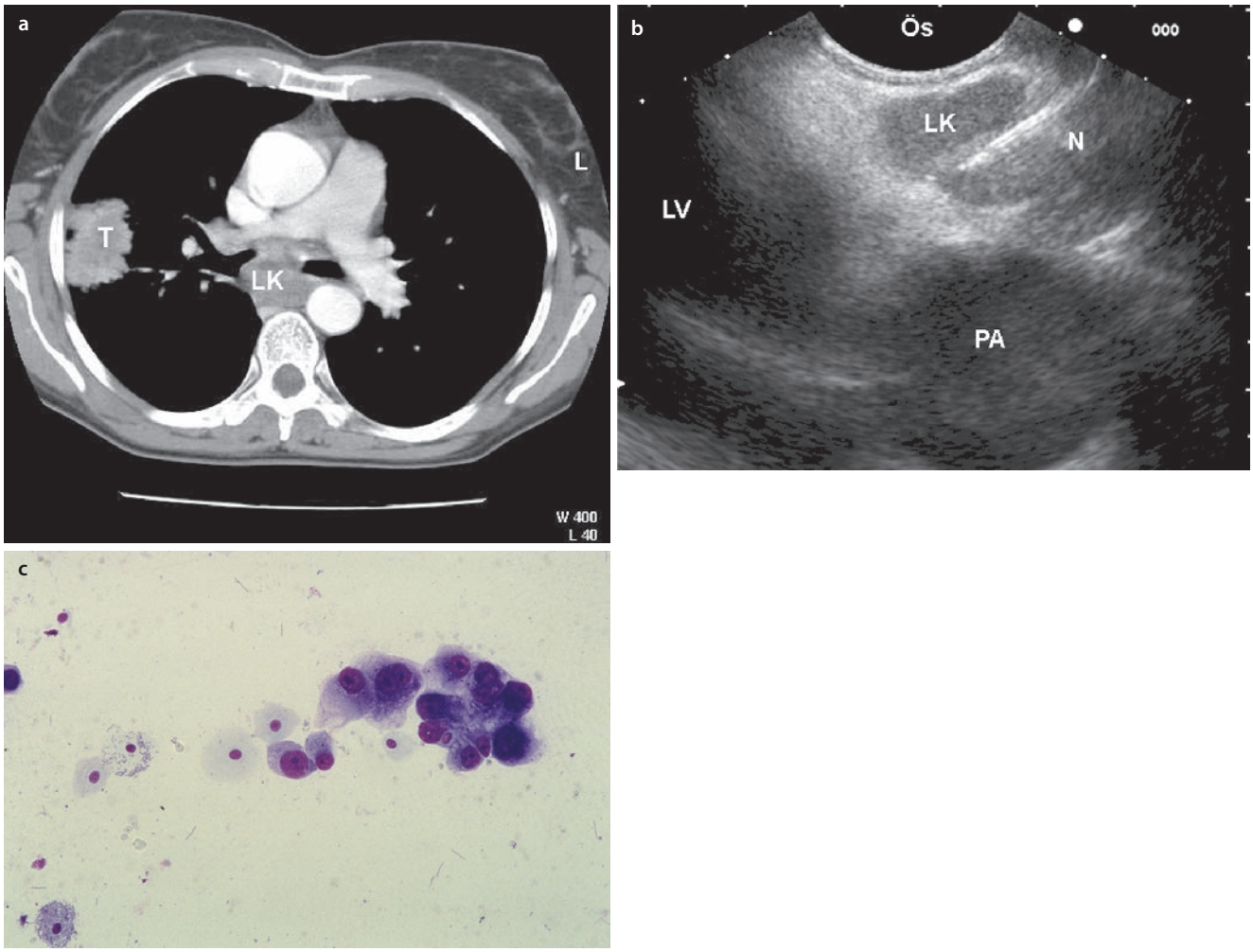

Fig. 6.18 **a** Computed tomography of the thorax. Right upper-lobe tumor (*T*) and enlarged subcarinal lymph node (*LK*). **b** Endosonography. Sonography-guided fine needle aspiration (*N* needle) of a hypoechoic lymph node with sharp borders located between the esophagus (*Ös*), pulmonary artery (*PA*) and *left* atrium (*LV*) (lymph node station 7). **c** Cytology. Fine-needle aspirate demonstrating adenocarcinoma with vacuoles and enlarged central nuclei. Squamous cells from the esophagus can be recognized on the *left*

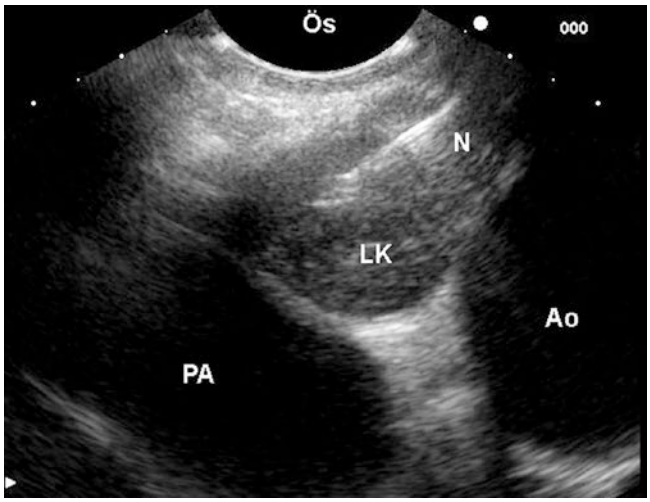

Fig. 6.19 Endosonography. Sonography-guided fine-needle aspiration (*N* needle) of a round hypoechoic lymph node with sharp borders, situated between the esophagus (*Ös*), aorta (*Ao*) and pulmonary artery (*PA*) (lymph node station 4 L)

esophageal sonographic examination for the diagnosis and staging of lung cancer takes about 25 min. Regarding the learning of mediastinal EUS, more important than absolute numbers, is competency assesment which is best assesed using a structured validated tool such as EUSAT (Konge et al. 2013). In recent years, there are several publications that EUS-FNA can be performed with the EBUS (Endobronchial ultrasound) scope, by inserting the EBUS scope in the esophagus (Herth et al. 2005). The advantage of the use of a single echo endoscope is related to time, investment and operational costs.

Although few absolute contraindications exist for transesophageal sonography procedures of the upper gastrointestinal tract, esophageal strictures and diverticula exhibit an increased perforation risk. Complications related to mediastinal lymph sampling are rare (Annema et al. 2005c, d; Eloubeidi et al. 2005b; Fritscher-Ravens et al. 2000a; Kramer et al. 2004; Larsen et al. 2002; Wallace et al. 2001; Williams et al. 1999). A cyst, however, poses an increased risk of infection and therefore should not be aspirated owing to an increased risk of mediastinitis (Annema et al. 2003a; Wildi et al. 2003).

The advantages of this novel diagnostic tool—as compared with radiological and surgical alternatives–are numerous (Table 6.3). Regarding mediastinal nodal staging, transesophageal sonography has a superior sensitivity compared with computed tomography (Hawes et al. 1994; Toloza et al. 2003a, b) and additionally provides the opportunity for tissue sampling. Compared with surgical alternatives, transesophageal sonography is less invasive, is performed in an outpatient setting and is therefore more cost-effective (Kramer et al. 2004).

The lower mediastinum is the area which can be visualized completely by transesophageal sonography, especially regarding the subcarinal (station 7) and the lower paraesophageal (station 8) nodes as well as those nodes located in the pulmonary ligament (station 9) (Fig. 6.21). Although nodes located in the aortopulmonary window (station 5) and adjacent to the aorta (station 6) can be detected by transesophageal sonography, tissue sampling is not always possible owing to intervening vascular structures. Limitations of EUS are its inability to reach the upper (station 2) and lower (station 4) paratracheal nodes as air in the trachea and main bronchi regularly inhibits visualization of these areas of the mediastinum. Mediastinoscopie and EBUS have a largely similair diagnostic reach whereas EUS has an added value by providing acces tot he lower mediastinum (Annema et al. 2005d; Eloubeidi et al. 2005a).

6.2.2 Transesophageal Sonography-Guided Fine-Needle Aspiration and Lung Cancer

Diagnosing Lung Cancer

Patients with suspected lung cancer and enlarged or PET-positive mediastinal nodes—for whom no diagnosis is obtained after bronchoscopy–are often good candidates for a transesophageal sonography-guided FNA investigation. If mediastinal metastases are assessed by transesophageal sonography-guided FNA, both a tissue diagnosis and locoregional staging are obtained with a single diagnostic test. In a prospective study of 142 patients with suspected lung cancer and enlarged mediastinal nodes, transesophageal sonography—after a nondiagnostic bronchoscopy—assessed a tissue diagnosis in 73 % of patients (Annema et al. 2005d). Recently, it was demonstrated that endonosography (EBUS-TBNA) should be considered the initial diagnostic/staging test of choice in patients supected of have lung cancer as it reduces time to treatment decision in comparison with conventional (bronchoscopic) diagnostic and staging techniques.

Transesophageal sonography-guided FNA is also indicated for diagnosing intrapulmonary tumors directly, provided they are located adjacent to the esophagus (Annema et al. 2005b; Varadarajulu et al. 2004a; Fig. 6.22). In a study of 32 patients with a centrally located lung tumor—in which bronchoscopy failed to achieve a tissue diagnosis—lung cancer was proven by transesophageal sonography-guided FNA in 97 % of cases (Annema et al. 2005b).

Staging of Lung Cancer

Mediastinal staging of lung cancer is the most common indication for a transesophageal sonography-guided FNA investigation, and the accuracy is between 76 and 98 % (Annema et al. 2005c, d; Eloubeidi et al. 2005b; Fritscher-Ravens et al. 2000a; Kramer et al. 2004; Larsen et al. 2002, 2005; Leblanc et al. 2004; Savides and Perricone 2004; Wallace et al. 2001, 2004; Williams et al. 1999; ▶ Table 5.6). So far, most studies have included selected patient with enlarged (short axis greater than 1 cm) or PET-positive (Annema et al. 2004; Eloubeidi et al. 2005b; Kramer et al. 2004) mediastinal nodes. For mediastinal restaging—an emerging indication for transesophageal sonography-guided FNA—an accuracy of 83 % has been reported (Annema et al. 2003b; Stigt et al. 2009).

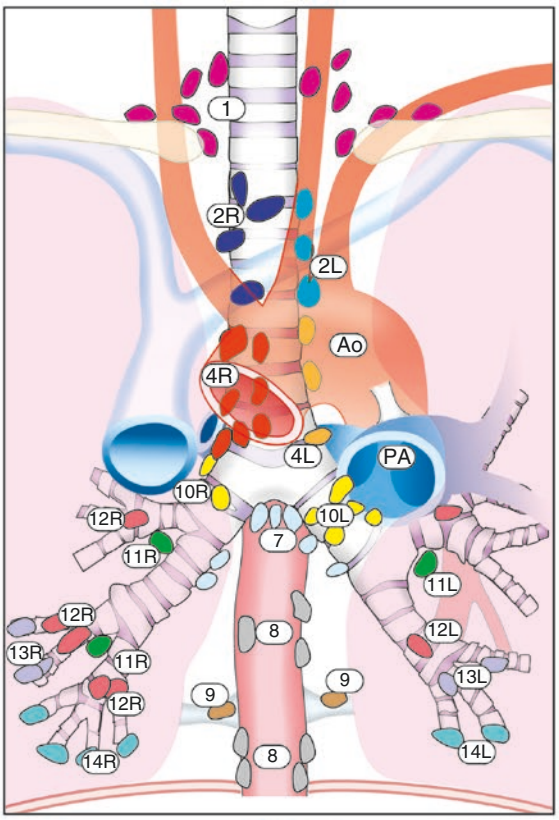

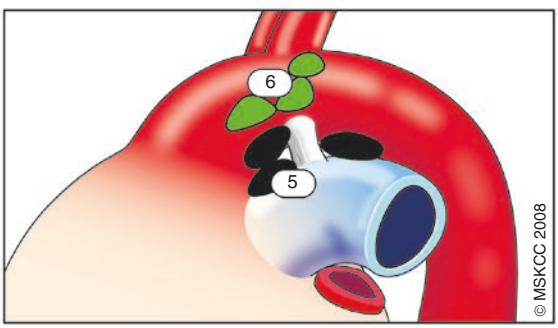

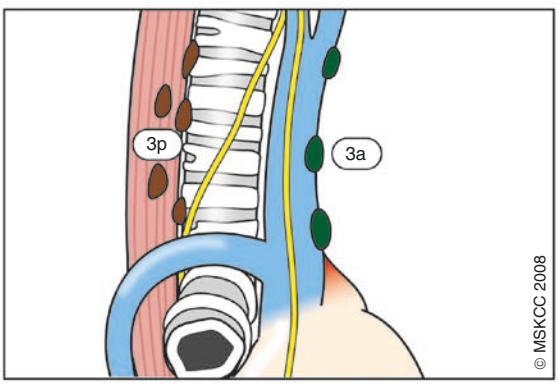

Supraclavicular zone

- 1 low cervical, supraclavicular, and sternal notch nodes

Superior Mediastinal Nodes

Upper zone

- 2R Upper Paratracheal (right)
- 2L Upper Paratracheal (left)
- 3a Pre-vascular
- 3p Retrotracheal
- 4R Lower Paratracheal (right)
- 4L Lower Paratracheal (left)

Aortic Nodes

AP zone

- 5 Subaortic
- 6 Para-aortic (ascending aorta or phrenic)

Inferior Mediastinal Nodes

Subcarinal zone

- 7 Subcarinal

Lower zone

- 8 Paraesophageal (below carina)
- 9 Pulmonary ligament

N_1 Nodes

Hilar/Interlobar zone

- 10 Hilar
- 11 Interlobar

Peripheral zone

- 12 Lobar
- 13 Segmental
- 14 Subsegmental

Fig. 6.20 IASLC: Nodal chart

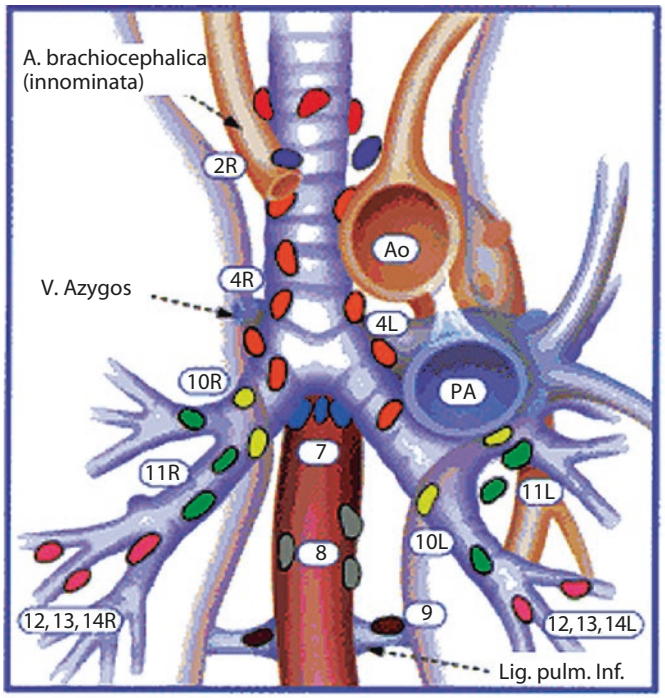

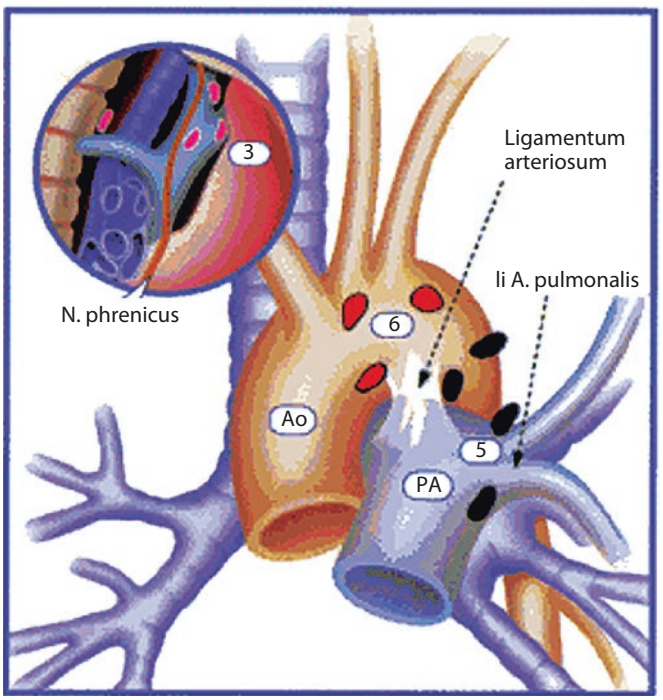

Superior mediastinal nodes

- 1 Highest medinastal
- 2 Upper paratracheal
- 3 Pre-vascular and retrotracheal
- 4 Lower paratracheal (including Azygos nodes)

N_2 = single digit, ipsilateral
N_3 = single digit, contralateral or supraclavicular

Aortic nodes

- 5 Subaortic (A-P window)
- 6 Para-aortic (ascending aorta ar phrenic)

Inferior mediastinal nodes

- 7 Subcarinal
- 8 Paraesophageal (below carina)
- 9 Pulmonary ligament

N_1 nodes

- 10 Hilar
- 11 Interlobar
- 12 Lobar
- 13 Segmental
- 14 Subsegmental

Fig. 6.21 Regional lymph node classification for lung cancer staging (Adapted from Mountain and Dresler 1997)

Centrally located lung tumors can often be detected by transesophageal sonography, and in these cases it is often possible to assess whether mediastinal tumor invasion (T4) is present (Schroder et al. 2005; Varadarajulu et al. 2004b; Fig. 6.23). In a study with 97 patients with a lung tumor located immediately adjacent to the esophagus, transesophageal sonography had an accuracy of 92 % regarding invasion in the aorta (Schroder et al. 2005).

The left adrenal gland, a common site for distant metastases in patients with lung cancer, can be visualized from the stomach by transesophageal sonography (Fig. 6.24). In a study of 31 patients with enlarged left adrenal glands on computed tomography, transesophageal sonography provided tissue proof of metastatic involvement in 42 % of cases (Eloubeidi et al. 2004). A multicentre study in patients with NSCLC and suspected left adrenal metastasis demonstrated metastases in

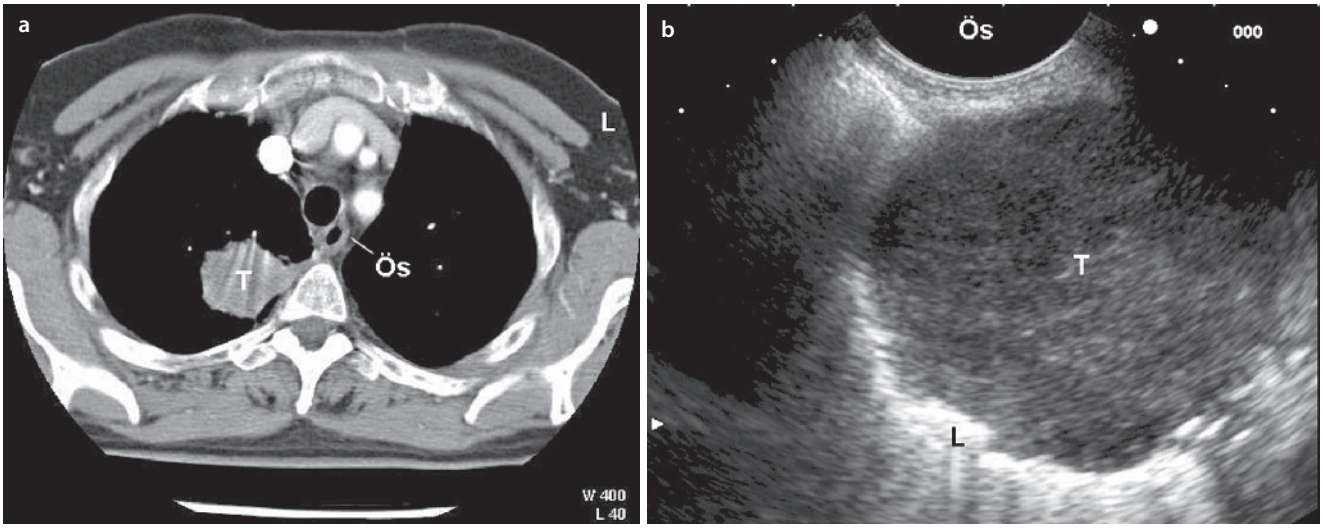

Fig. 6.22 **a** Computed tomography of the thorax. Relatively smooth shaped intrapulmonary lesion (*T*) located in the right upper lobe (3 cm ×3 cm ×6 cm) located adjacent to the esophagus (*Ös*). The esophagus is located behind the trachea. **b** Endosonography. Lesion with an inhomogeneous echo texture with irregular borders and bronchial carcinoma (*T*) which comprised lung tissue (*L*)

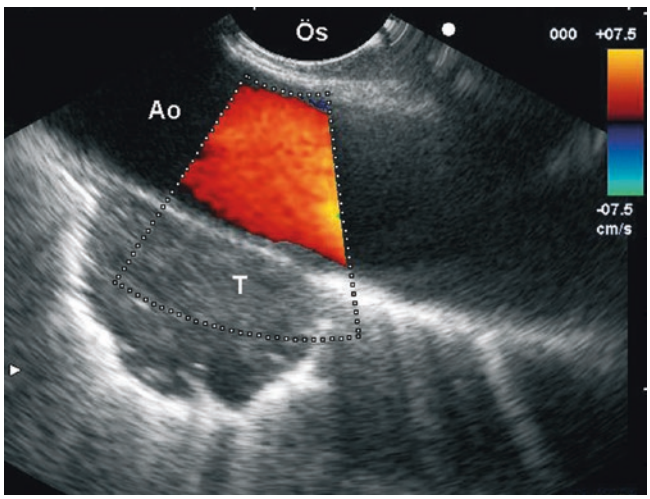

Fig. 6.23 Endosonography. Lung tumor (*T*) located in the left upper lobe with a close relation to the aorta (*Ao*). There are no signs of tumor invasion (T4) in the aorta. *Ös* esophagus

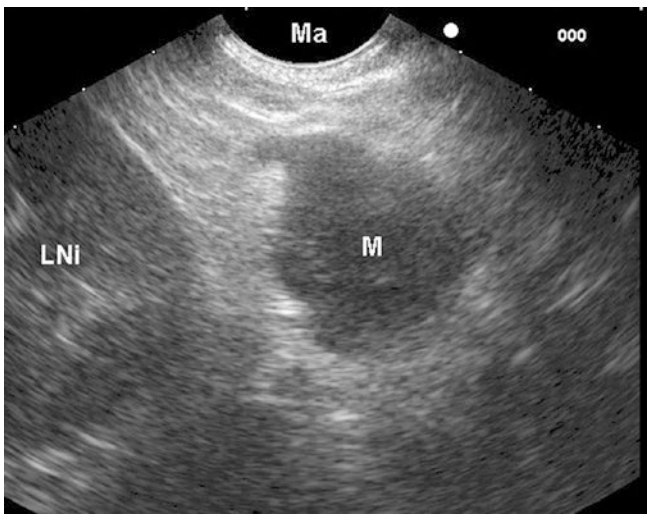

Fig. 6.24 Endosonography. Enlarged left adrenal gland with metastatic involvement (*M*) as assessed by transesophageal sonograph

53 patients (62 %) with a sensitivity of at least 85 %. Whether the left adrenal gland should be investigated routinely during a transesophageal sonographic investigation for lung cancer staging is the subject of debate (Ringbaek et al. 2005).

Clinical Implications

It is evident that the esophageal approach has important value in both the diagnosis and staging of lung cancer. Transesophageal sonographic investigations in patients with (suspected) lung cancer can prevent up to 70 % of scheduled mediastinoscopies by providing tissue proof of mediastinal metastases (Annema et al. 2005c; Larsen et al. 2002). Patients prefer an ambulatory transesophageal sonographic investigation to surgical staging, which involves clinical admission and general anesthesia (Annema et al. 2005d).

Transesophageal Sonography in Lung Cancer Staging Algorithms

What are the indications for transesophageal sonography-guided FNA in the diagnosis and staging of lung cancer? In patients with suspected NSCLC, initially an integrated CT-PET scan is made for staging purposes. In the ASTER randomized trial, endosonography (EBUS and EUS) followed by surgical staging (in case of the absence of mediastinal metastases) was superior to immediate surgical staging (sensitivity (94 vs 79 %) (Annema et al. 2010). Therefore, guidelines clearly indicate that endosonography (EBUS and or EUS) should be performed first in case of suspected mediastinal or hilar nodal involvement (enlarged or FDG avid nodes) (De Leyn et al. 2007). If complete nodal staging is to be achieved – as opposed to a diagnostic mediastinal nodal biopsy-, the combination of

EBUS and EUS is advised due to their complementary reach of various nodal stations. Surgical staging by mediastinoscopy is advised in those nodes that are suspected on CT-PET imaging but staged tumor negative by endosonography.

For diagnostic purposes of left sided and subcarinal mediastinale nodes, EUS is often prefered over EBUS as it results in less cough and desaturations and fewer doses of anesthetics. EUS can be performed with a conventional EUS scope or be putting the EBUS scope in the esophagus.

A very recent study indicated that the endoscopic approch for patients with suspected lung cancer should start with endosnography (EBUS) and not with conventional bronchoscopy as it reduces time to treatment desicion.

Transesophageal sonography-guided FNA indications in chest medicine:

- Suspected lung cancer, enlarged mediastinal nodes
- Suspected lung cancer, tumor located adjacent to the esophagus
- Mediastinal (re-) staging
- Analyzing PET-positive mediastinal lesions
- Staging of centrally located lung tumors suspected for tumor invasion (T4)
- Suspected left adrenal metastases (left-sided)
- Suspected sarcoidosis
- Suspected tuberculosis
- Suspected mediastinal cysts (no FNA)

6.2.3 Transesophageal Sonography-Guided Fine-Needle Aspiration and Sarcoidosis

Sarcoidosis is the most common interstitial lung disease in which mediastinal nodes are often involved. Frequently, a tissue diagnosis supporting the presumed diagnosis of sarcoidosis is needed, either before treatment with steroids or to rule out other diseases such as tuberculosis, lymphomas or malignant epithelial diseases. For the diagnosis of sarcoidosis, a state-of-the-art bronchoscopic evaluation—including several peripheral lung biopsies—has a diagnostic yield of 66 % (Costabel and Hunninghake 1999). However, peripheral biopsies include the risk of a pneumothorax or hemoptysis.

Transesophageal sonography has both a high yield (82 %; Annema et al. 2005a) and a high sensitivity 89–94 % (Fritscher-Ravens et al. 2000b; Wildi et al. 2004) in assessing noncaseating granulomas and so far no adverse events have been reported. Sonographic images of mediastinal nodes in patients with sarcoidosis often demonstrate a specific ultrasound pattern consisting of multiple, well-defined mediastinal nodes with an isoecpoic or hypoechoic texture and the absence of a centrally located hypoechoic area (Fig. 6.25a, Annema et al. 2005a). Often vessels within these nodes can be detected by color-Doppler sonography (Fritscher-Ravens et al. 2000a). On cytological evaluation, mediastinal nodes in patients with sarcoidosis present as noncaseating granulomas without necrosis (Fig. 6.25b). In a large randomized trial in patients with suspected sarcoidosis stage I/II, it has been shown that endosonography resulted in greater diagnostic yield in comparison with onventional bronchsocopic techniques (Bartheld von et al. 2013).

6.2.4 Transesophageal Sonography and Cysts

Paraesophageal and parabronchial cysts account for a considerable portion of mediastinal lesions. Cysts located adjacent to the esophagus (Fig. 6.26a) can be visualized by transesophageal sonography and often present with a round shape, well-defined borders and a echo-free or echo-poor content (Fig. 6.26b). Aspiration of cysts is not indicated owing to the risk of mediastinitis (Annema et al. 2003a; Wildi et al. 2003).

6.2.5 Summary

Almost twenty years after the first mediastinal EUS-FNA, it is evident that EUS-FNA has an important role in the diag-

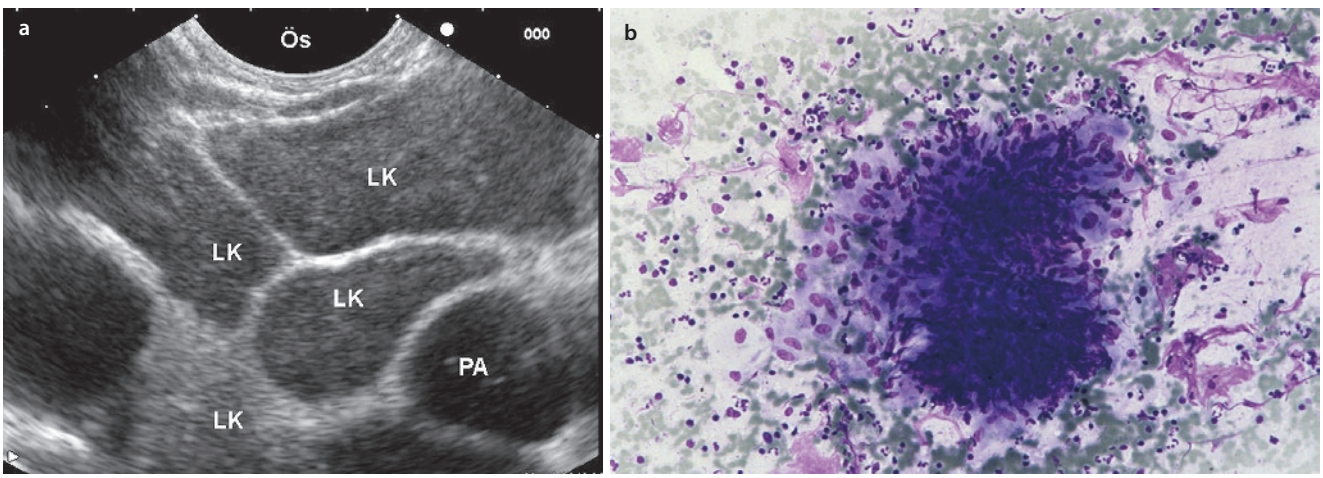

Fig. 6.25 (**a**) Endosonography. Multiple nodes (*LK*) with sharp borders and an isoechoic ultrasound pattern suggestive of sarcoidosis. *PA* pulmonary artery. (**b**) Cytology of this lymph node indicates a typical granuloma without central necrosis

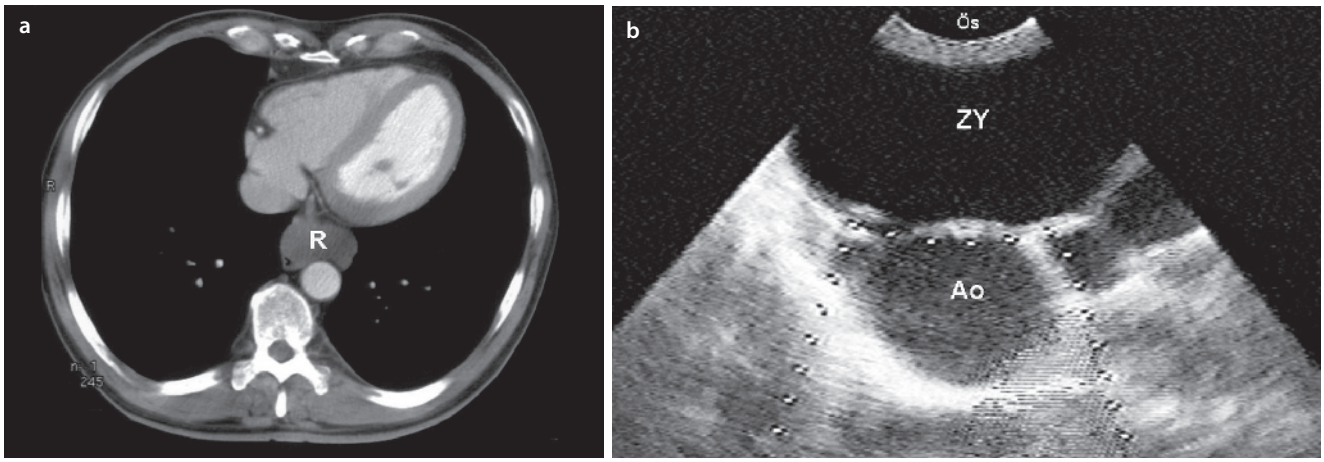

Fig. 6.26 (**a**) Computed tomography of the thorax. Sharp well-defined lesion (*R*) (2 cm × 1 cm × 1 cm) located in the lower mediastinum. The heart and descending aorta are easily identified. (**b**) Endosonography. Remarkably echo-poor, well-demarked, easily compressible lesion (cyst located immediately adjacent to the esophagus (*Ös*)) without a signal on color-Doppler sonography—sonographically compatible with a cyst. *Ao* aorta

nosis in staging of lungcancer. Additionally this test is helpful for the analysis of various other mediastinal lesions and the diagnosis of sarcoidosis. When used in clinical practice, transesophageal sonography-guided FNA not only prevents surgical diagnostic procedures to a large extent, it also reduces the number of futile thoracotomies and is cost-effective. The implementation of EUS in the pulmonary community will be facilitated by the use oft he EBUS scope.

References

Transthoracic

Alvarez-Alvarez C, Otero Fernandez M, Cabero-Perez MJ, Guerra Dietz L, Galan Cuesta M, Agüeo Balbin J (2013) Description of tuberculosis outbreak and usefulness of mediastinal ultrasound. An Pediatr (Barc) 79(5):293–299

Beckh S, Bolcskei PL, Lessnau KD (2002) Real-time chest ultrasonography. A comprehensive review for the pulmonologist. Chest 122:1759–1773

Betsch B (1994) Farbdopplersonographie des Mediastinums. Radiologe 34:599–604

Betsch B, Knopp MV, van Kaick G (1992) Malignant tumors and lymphomas of the mediastinum: diagnosis and follow-up with color assisted doppler sonography. Eur J Cancer Res Clin Oncol 118:107

Betsch B, Berndt R, Knopp MV, Schmähl A, Trost U, Delorme S (1994) Vergleich von Computertomographie und B-Bild-Sonographie in der bildgebenden Diagnostik des Mediastinums. Bildgebung 61:295–298

Blank W, Braun B (1995) Gewebsdiagnostik durch Dopplersonographie. Bildgebung 62:31–35

Blank W, Braun B, Gekeler E (1986) Ultraschalldiagnostik und Feinnadelpunktion pleuraler, pulmonaler und mediastinaler Prozesse. In: Hansmann M (ed) Ultraschalldiagnostik. Springer, Berlin/Heidelberg/New York/Tokyo, pp 562–565

Blank W, Braun B, Schuler A, Wild K (1996a) Die percutane Sonographie zur Differenzierung der Dysphagie. Ultraschall Med 17(S1):32

Blank W, Schuler A, Wild K, Braun B (1996b) Transthoracic sonography of the mediastinum. Eur J Ultrasound 3:179–190

Blank W, Schwaiger U, Wild K, Braun B (1998) Die percutane Sonographie zur Darstellung des cervicalen Ösophagus. Ultraschall Med 19(S1):4

Blank W, Mathis G, Osterwalder J (2014) Kursbuch Notfallsonographie. Stuttgart, Georg Thieme verlag 2014

Bollen EC, Goci R, van't Hof-Grootenboer BE, Versteege CWM, Engelshove HA, Lamers RJ (1994) Interobserver variability and accuracy of computed tomographic assessment of nodal status in lung cancer. Ann Thorac Surg 58:158–162

Bosch-Marcet J, Serres-Creixams X, Borras-Perez V et al (2007) Value of sonography for follow-up of mediastinal lymphadenopathy in children with tuberculosis. J Clin Ultrasound 35(3):118–224

Braun B (1983) Abdominelle und thorakale Ultraschalldiagnostik. In: Bock HE (ed) Klinik der Gegenwart. Urban & Schwarzenberg, Munich, pp 1141–1145

Braun B (1992) Schilddrüse. In: Braun B, Günther R, Schwerk WB (eds) Ultraschalldiagnostik. Lehrbuch und Atlas, vol III-3.1. Ecomed, Landsberg/Lech

Braun B, Blank W (2005) Sonographie von Hals und oberem Mediastinum. Internist 46(10):1133–1145

Brüggemann A, Greie A, Lepsien G (1991) Real-time-sonography of the mediastinum in adults: a study in 100 healthy volunteers. Surg Endosc 5:150–153

Caremani M, Benci A, Tacconi D et al (2009) Sonographic management of mediastinal syndrome. J Ultrasound 12(2):61–68

Castellino RA, Blank N, Hoppe RT et al (1986) Hodgkin disease: contributions of chest CT in the initial staging evaluation. Radiology 160:603–605

Chen HJ, Liao WC, Liang SJ, Tu Cy LICH, Hsu WH (2014) Diagnostic impact of color ultrasound-guided core biopsy on fine-needle aspiration of anterior mediastinal masses. Ultrasound Med Biol 40(12):2768–2776

Dietrich CF, Liesen M, Wehrmann T, Caspary WF (1995) Mediastinalsonographie: Eine neue Bewertung der Befunde. Ultraschall Med 16:61

Dietrich CF, Liesen M, Buhl R, Herrmann G, Kirchner I, Caspary WF, Wehrmann T (1997) Detection of normal mediastinal lymphnodes by ultrasonography. Acta Radiol 38:965–969

Dietrich CF, Chickakli M, Burgon I, Wehrmann T, Wiewrodt R, Buhl R, Caspary WF (1999) Mediastinal lymphnodes demonstrated by mediastinal sonography: activity marker in patients with cystic fibrosis. J Clin Ultrasound 27:9–14

Goldberg GG (1971) Suprasternal ultrasonography. JAMA 15:245–250

Görg C, Seifart U, Görg K, Zugmaier G (2003) Color Doppler Sonographic Mapping of Pulmonary Lesions. J Ultrasound Med 22:1033–1039

Gulati M, Venkataramu NK, Gupta S (2000) Ultrasound guided fine needle aspiration biopsy in mediasinal tunerculosis. Int J Tuberc Lung Dis 4(12):1164–1168

Heitzmann EK (1988) The mediastinum. Springer, Berlin/Heidelberg/New York/Tokyo
Heizel M (1985) Sonographische Topographie des oberen vorderen Mediastinums. Ultraschall 6:101–109
Herth FJF (2009) The Mediastinum. In: Bolliger CT, Herth FJF, Mayo PH, Miyazawa T, Beamis JF (eds) Clinical chest ultrasound. From the ICU to the Bronchoscopy Suite. Karger, Basel
Herth FJF, Becker HD (2003) Chest ultrasound; thoracic imaging; pleura mass; pleural effusion: ultrasound guidance. Respiration 70:84–94
Janssen J, Johanns W, Lehnhardt M, Jakobeit C, Greiner L (1997) Die transkutane Sonographie des gastroösophagealen Übergangs im prospektiven Vergleich mit der Endoskopie. Dtsch Med Wochenschr 122:1167–1171
Koh DM, Burke S, Davies N et al (2002) Transthoracic US of the chest: clinical uses and applications. Radiographics 22:E1. http://radiographics.rsnajnls.org/cgi/content/full/22/1/e1
Liu P, Daneman A, Stringer DA (1988) Real-time-sonography of mediastinal and juxtamediastinal masses in infants and children. J Can Assoc Radiol 39:198–203
Mosem T, Andronikou S (2014) Through the eye of the suprasternal notch: point-of-care sonography for tuberculous mediastinal lymphadenopathy in children. Pediatr Radiol 44:681–684
Palabiyik FB, Bayramoglu S, Gunert NT, Daglar S, Cimilli T (2012) Use of sonography for evaluation of the cervical and thoracic esophagus in children. J Ultrasound Med 31(9):1375–1379
Rosenberg JC (1993) Neoplasms of the mediastinum. In: De Vita VT, Hellman S, Rosenberg SA (eds) Cancer: principles and practice of oncology. Lippincott, Philadelphia, pp 759–775
Schuler A, Blank W, Braun B (1995) Sonographisch-interventionelle Diagnostik bei Thymomen. Ultraschall Med 16:62
Supakul N, Karmazyn B (2013) Ultrasound of the pediatric chest- the ins and outs. Semin Ultrasound CT MR 34(3):274–285
von Lengerke HV, Schmid HC (1988) Mediastinalsonographie im Kindesalter. Radiologe 28:460–465
Wernecke K (1991) Mediastinale Sonographie, Untersuchungstechnik, diagnostische Effizienz und Stellenwert in der bildgebenden Diagnostik des Mediastinums. Springer, Berlin/Heidelberg/New York/Tokyo
Wernecke K, Peters PE, Galanski M (1986) Mediastinal tumors: evaluation of suprasternal sonography. Radiology 159:405–409
Wernecke K, Pötter R, Peters PE (1988) Parasternal medisatinal sonography: sensitivity in the detection of anterior mediastinal and subcarinal tumors. AJR Am J Roentgenol 150:1021–1026
Zhu SY et al (2005) Sonographic demonstration of the normal thoraxic esophagus. J Clin Ultrasound 33(1):29–33

Transesophageal Sonography for Lung Cancer and Mediastinal Lesions

Annema JT, Veselic M, Versteegh MI, Rabe KF (2003a) Mediastinitis caused by EUS-FNA of a bronchogenic cyst. Endoscopy 35(9):791–793
Annema JT, Veselic M, Versteegh MI, Willems LN, Rabe KF (2003b) Mediastinal restaging: EUS-FNA offers a new perspective. Lung Cancer 42(3):311–318
Annema JT, Hoekstra OS, Smit EF, Veselic M, Versteegh MI, Rabe KF (2004) Towards a minimally invasive staging strategy in NSCLC: analysis of PET positive mediastinal lesions by EUS-FNA. Lung Cancer 44(1):53–60
Annema JT, Veselic M, Rabe KF (2005a) Endoscopic ultrasound-guided fine-needle aspiration for the diagnosis of sarcoidosis. Eur Respir J 25(3):405–409
Annema JT, Veselic M, Rabe KF (2005b) EUS-guided FNA of centrally located lung tumours following a non-diagnostic bronchoscopy. Lung Cancer 48(3):357–361
Annema JT, Versteegh MI, Veselic M, Voigt P, Rabe KF (2005c) Endoscopic ultrasound-guided fine-needle aspiration in the diagnosis and staging of lung cancer and its impact on surgical staging. J Clin Oncol 23(33):8357–8361
Annema JT, Versteegh MI, Veselic M, Welker L, Mauad T, Sont JK et al (2005d) Endoscopic ultrasound added to mediastinoscopy for preoperative staging of patients with lung cancer. JAMA 294(8):931–936
Annema JT, Bohoslavsky R, Burgers S et al (2010) Implementation of endoscopic ultrasound for lung cancer staging. Gastrointest Endosc 71(1):64–70
Costabel U, Hunninghake GW (1999) ATS/ERS/WASOG statement on sarcoidosis. Sarcoidosis Statement Committee. American Thoracic Society European Respiratory Society World Association for Sarcoidosis and Other Granulomatous Disorders. Eur Respir J 14(4):735–737
De Leyn P, Lardinois D, Van Schil PE, Rami-Porta R, Passlick B, Zielinski M et al (2007) ESTS guidelines for preoperative lymph node staging for non-small cell lung cancer. Eur J Cardiothorac Surg 32(1):1–8
Eloubeidi MA, Seewald S, Tamhane A, Brand B, Chen VK, Yasuda I et al (2004) EUS-guided FNA of the left adrenal gland in patients with thoracic or GI malignancies. Gastrointest Endosc 59(6):627–633
Eloubeidi MA, Tamhane A, Chen VK, Cerfolio RJ (2005a) Endoscopic ultrasound-guided fine-needle aspiration in patients with non-small cell lung cancer and prior negative mediastinoscopy. Ann Thorac Surg 80(4):1231–1239
Eloubeidi MA, Cerfolio RJ, Chen VK, Desmond R, Syed S, Ojha B (2005b) Endoscopic ultrasound-guided fine needle aspiration of mediastinal lymph node in patients with suspected lung cancer after positron emission tomography and computed tomography scans. Ann Thorac Surg 79(1):263–268
Fritscher-Ravens A, Sriram PV, Bobrowski C, Pforte A, Topalidis T, Krause C et al (2000a) Mediastinal lymphadenopathy in patients with or without previous malignancy: EUS-FNA-based differential cytodiagnosis in 153 patients. Am J Gastroenterol 95(9):2278–2284
Fritscher-Ravens A, Sriram PV, Topalidis T, Hauber HP, Meyer A, Soehendra N et al (2000b) Diagnosing sarcoidosis using endosonography-guided fine-needle aspiration. Chest 118(4):928–935
Hawes RH, Gress F, Kesler KA, Cummings OW, Conces DJ Jr (1994) Endoscopic ultrasound versus computed tomography in the evaluation of the mediastinum in patients with non-small-cell lung cancer. Endoscopy 26(9):784–787
Herth FJ, Lunn W, Eberhardt R, Becker HD, Ernst A (2005) Transbronchial vs. transesophageal ultrasound-guided aspiration of enlarged mediastinal lymph nodes. Am J Respir Crit Care Med 171(10):1164–1167
Kramer H, van Putten JW, Post WJ, van Dullemen HM, Bongaerts AH, Pruim J et al (2004) Oesophageal endoscopic ultrasound with fine needle aspiration improves and simplifies the staging of lung cancer. Thorax 59(7):596–601
Larsen SS, Krasnik M, Vilmann P, Jacobsen GK, Pedersen JH, Faurschou P et al (2002) Endoscopic ultrasound guided biopsy of mediastinal lesions has a major impact on patient management. Thorax 57(2):98–103
Larsen SS, Vilmann P, Krasnik M, Dirksen A, Clementsen P, Maltbaek N et al (2005) Endoscopic ultrasound guided biopsy performed routinely in lung cancer staging spares futile thoracotomies: preliminary results from a randomised clinical trial. Lung Cancer 49(3):377–385
Leblanc JK, Devereaux BM, Imperiale TF, Kesler K, Dewitt JM, Cummings O (2004) Endoscopic ultrasound in non-small cell lung cancer and negative mediastinum on computed tomography. Am J Respir Crit Care Med 171:177–82
Mountain CF, Dresler CM (1997) Regional lymph node classification for lung cancer staging. Chest 111(6):1718–1723
Pedersen BH, Vilmann P, Folke K, Jacobsen GK, Krasnik M, Milman N et al (1996) Endoscopic ultrasonography and real-time guided fine-needle aspiration biopsy of solid lesions of the mediastinum suspected of malignancy. Chest 110(2):539–544
Ringbaek TJ, Krasnik M, Clementsen P, Skov BG, Rasmussen EN, Vilmann P (2005) Transesophageal endoscopic ultrasound/fine-needle aspiration diagnosis of a malignant adrenal gland in a patient with non-

small cell lung cancer and a negative CT scan. Lung Cancer 48(2):247–249
Savides TJ, Perricone A (2004) Impact of EUS-guided FNA of enlarged mediastinal lymph nodes on subsequent thoracic surgery rates. Gastrointest Endosc 60(3):340–346
Schroder C, Schonhofer B, Vogel B (2005) Transesophageal echographic determination of aortic invasion by lung cancer. Chest 127(2):438–442
Stigt JA, OostdijkAH TPR et al (2009) Comparison of EUS-guided fine needle aspiration and integrated PET-CT in restaging after treatment for locally advanced non-small cell lung cancer. Lung Cancer 66(2):198–204
Toloza EM, Harpole L, McCrory DC (2003a) Noninvasive staging of non-small cell lung cancer: a review of the current evidence. Chest 123(1 Suppl):137S–146S
Toloza EM, Harpole L, Detterbeck F, McCrory DC (2003b) Invasive staging of non-small cell lung cancer: a review of the current evidence. Chest 123(1 Suppl):157S–166S
Tournoy KG, De Ryck F, Vanwalleghem LR, Vermassen F, Praet M, Aerts JG et al (2008) Endoscopic ultrasound reduces surgical mediastinal staging in lung cancer: a randomized trial. Am J Respir Crit Care Med 177(5):531–535
Varadarajulu S, Hoffman BJ, Hawes RH, Eloubeidi MA (2004a) EUS-guided FNA of lung masses adjacent to or abutting the esophagus after unrevealing CT-guided biopsy or bronchoscopy. Gastrointest Endosc 60(2):293–297
Varadarajulu S, Schmulewitz N, Wildi SF, Roberts S, Ravenel J, Reed CE et al (2004b) Accuracy of EUS in staging of T4 lung cancer. Gastrointest Endosc 59(3):345–348
Wallace MB, Silvestri GA, Sahai AV, Hawes RH, Hoffman BJ, Durkalski V et al (2001) Endoscopic ultrasound-guided fine needle aspiration for staging patients with carcinoma of the lung. Ann Thorac Surg 72(6):1861–1867
Wallace MB, Ravenel J, Block MI, Fraig M, Silvestri G, Wildi S et al (2004) Endoscopic ultrasound in lung cancer patients with a normal mediastinum on computed tomography. Ann Thorac Surg 77(5):1763–1768
Wildi SM, Hoda RS, Fickling W, Schmulewitz N, Varadarajulu S, Roberts SS et al (2003) Diagnosis of benign cysts of the mediastinum: the role and risks of EUS and FNA. Gastrointest Endosc 58(3):362–368
Wildi SM, Judson MA, Fraig M, Fickling WE, Schmulewitz N, Varadarajulu S et al (2004) Is endosonography guided fine needle aspiration (EUS-FNA) for sarcoidosis as good as we think? Thorax 59(9):794–799
Williams DB, Sahai AV, Aabakken L, Penman ID, Van Velse A, Webb J et al (1999) Endoscopic ultrasound guided fine needle aspiration biopsy: a large single centre experience. Gut 44:720–726

Endobronchial Sonography

Felix J.F. Herth and Ralf Eberhardt

G. Mathis (ed.), *Chest Sonography*, DOI 10.1007/978-3-319-44072-9_7

The endobronchial application of ultrasound was first described in 1992 (Hürther and Hanrath 1990). In the following years technical difficulties had to be solved and a clear view of the indication and diagnostic properties of endobronchial sonography had to be developed. Many abnormalities of the airways involve the bronchial wall and the parabronchial structures The view of the endoscopist, however, is limited to the lumen and the internal surface of the airways. Processes within the airway wall and outside the airways can only be assessed by indirect signs. Especially in malignancies this can be of decisive importance for the fate of the patient. External mediastinal thoracic sonography is insufficient for imaging of the paratracheal and hilar structures. By endoesophageal sonography, the pretracheal region and the right hilar structures are inaccessible because of limited contact and interposition of the airways. Therefore, expanding the endoscopist's view beyond the airways is essential (Herth and Becker 2000).

Radiologic imaging is disappointing unreliable in diagnosis of mediastinal lymph nodes. Because of this it is important to have an additionally look over the bronchial wall because radiologic practises like CT and NMR are not adequate reliable at the staging of lung cancer. Only 50% of tumor invasion in the lymph nodes are captured correctly. Approximately 25% are false-positive, 25% are false-negative interpreted (Rivera et al. 2013). An improved method were needed. (Herth and Becker 2000).

7.1 Instruments and Technique

7.1.1 Endobronchial Sonography Miniprobes

The different impedance of soft tissues has made sonography an indispensable diagnostic tool in medicine. Instruments that are used for gastrointestinal application could not be applied inside the airways because of their diameter (Ono et al. 1994). For application inside the central airways, therefore, flexible catheters for the probes with a balloon at the tip were developed, which allows circular contact for the ultrasound, providing a complete 360° image of the parabronchial and paratracheal structures (Fig. 7.1). Thus, under favorable conditions structures at a distance of up to 4 cm can be visualized (Herth and Becker 2000). The probes have been on the market since 1999 and can be applied with regular flexible endoscopes that have a biopsy channel of at least 2.6 mm.

7.1.2 Endobronchial Sonography Transbronchial Needle Aspiration

The latest developments are special bronchoscopes with an integrated curvilinear electronic transducer at the tip (Olympus BF-UC160F; Fig. 7.2). So a real-time needle puncture under endoscopic control is possible. The outer diameter of the insertion tube is 6.2 mm. The angulation range of the distal end of the endoscope is 160° upward and 90° downward. The instrument has a small curved linear-array electronic transducer, of length 10 mm, located at the distal end of the endoscope in front of a 30° oblique forward viewing fiber- optic lens (angle of view 80). The endoscope has a biopsy channel of 2 mm. The ultrasonic frequency is 7.5 MHz with a penetration depth of 5 cm. The scanning direction is parallel to the longitudinal axis of the endoscope with a scanning angle of 50°, which enables full sonographic monitoring of a needle when it is inserted via the biopsy channel during scanning (Krasnik et al. 2003).

7.2 Sonographic Anatomy

The wall of the central airways show a seven-layer structure which can be demonstrated by high magnification only. The layers represent the mucosa and submucosa, the three layers of the cartilage and the adjacent external structures of loose and dense connective tissue, respectively (Kurimoto et al. 1999). Under low-power magnification and in the periphery only a three-layer structure is visible. Orientation by sonography

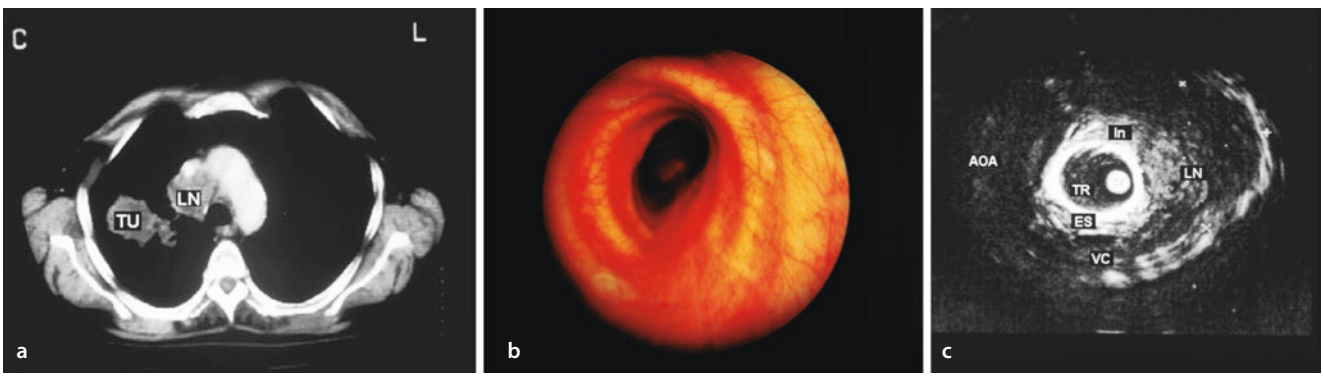

Fig. 7.1 Excision of the wall infiltration. (**a**) Possible infiltration of the tumor in the CT. (**b**) Possible infiltration in the endoscopic image. (**c**) Exclusion of tumor infiltration by EBUS. *TU* tumor, *LN* lymph node, *AOA* ascending aorta, *TR* trachea, *ES* endoscopic probe, *In* small lymph node, *VC* vena cava

Fig. 7.2 Head of the sonography bronchoscope

within the mediastinum is difficult. Besides the complex mediastinal anatomy this is due to motion artifacts by pulsation and respiration as well as the unusual planes of the sonography images as with the probes we have to follow the course of the airways. For orientation, therefore, the analysis of characteristic anatomical structures is more reliable than observation of the position of the sonography probe inside the airway. Vessels can be diagnosed by their pulsation. Lymph nodes and solid structures can be differentiated down to a size of a few millimeters from the blood vessels by their higher echodensity.

7.2.1 Indications and Results for the Endobronchial Sonography Miniprobe

Since 1999 the probe has been on the market and endobronchial sonography is applied in several centers worldwide. For some indications the superiority of sonography over conventional imaging has been proven in prospective studies and in some centers endobronchial sonography is already established as a routine procedure. According to the structures that can be analyzed, current indications comprise endoluminal, intramural and parabronchial structures; with respect to medical indications, early detection and tumor staging, inflammatory destruction of the airways, mediastinal lesions and malformations of mediastinal structures.

7.2.2 Tumorstaging

Lokal Tumorstaging

In small radiologically invisible tumors the decision for local endoscopic therapeutic intervention is dependent on their intraluminal and intramural extent within the different layers of the wall. In contrast to radiological imaging by endobronchial sonography even very small tumors of a few millimeters can be analyzed and differentiated from benign lesions. As different authors demonstrated, endobronchial sonography is a very reliable tool in analyzing the extent of these small lesions. We could demonstrate that by endobronchial sonography in small autofluorescence-positive lesions that were negative in white light bronchoscopy we could improve specificity (predicting malignancy) from 50 to 90. Combination of endobronchial sonography with autofluorescence has been proven to be efficient in prospective studies and today has become the basis for curative endobronchial treatment of malignancies in some institutions (Herth et al. 2002b; Fig. 7.3).

Advanced cancer In preoperative staging, endobronchial sonography allows detailed analysis of intraluminal, submucosal and intramural tumor spread, which can be essential for decisions regarding resection margins. Endobronchial sonography proved especially useful in diagnosis of mediastinal tumor involvement in the great vessels such as the aorta, the vena cava, the main pulmonary arteries and the esophageal wall which by conventional radiology frequently is impossible. In a trial it was shown that differentiation of external tumor invasion from impression of the tracheobronchial wall by endobronchial sonography is highly reliable (94%) in contrast to computed tomography imaging (51%). One hundred and four patients with a central tumor were examined (Herth et al. 2002b) with endobronchial sonography and computed tomography and the tumors were classified into invasion or impression types. All patients underwent surgery, and the findings were compared with the initial classification. The sensitivity (from 89% to 25%) and also the specificity (from 100% to 89%) shows the superiority of the sonography technique in the differentiation between airway infiltration and compression by tumor (Takemoto et al. 2000; Kurimoto et al. 1999). Thus, many patients considered to be nonresectable by the radiologist owing to supposed T4

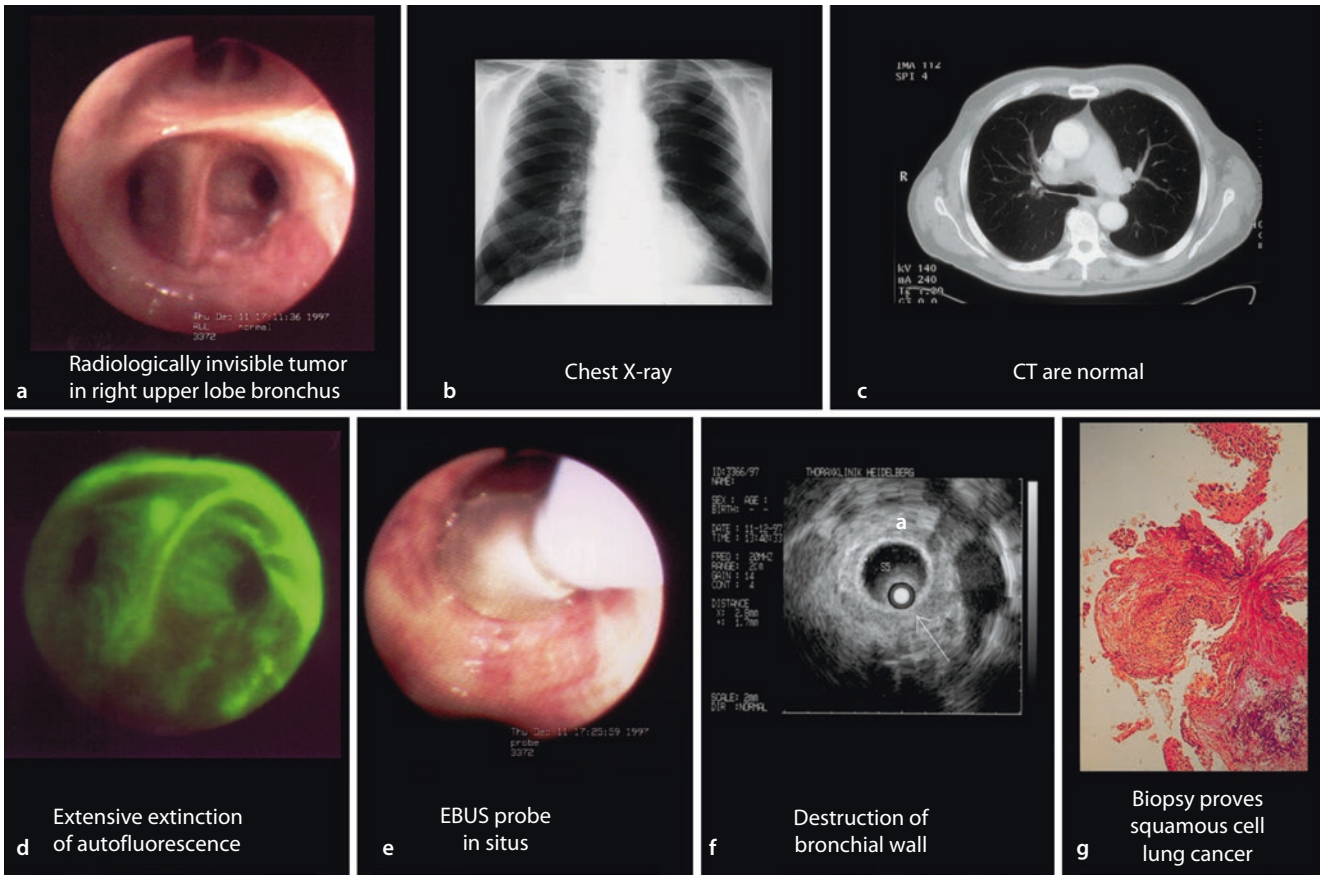

Fig. 7.3 Early cancer detection by different technologies and proof of extrabronchial tumor by EBUS

tumors could be operated on in a curative approach after use of endobronchial sonography (Herth et al. 2003) (Fig. 7.4).

For histological diagnosis of peripheral intrapulmonary lesions by bronchoscopy an instrumental approach under fluoroscopic or computed tomography guidance is the standard procedure (Fig. 7.5). This demands expensive X-ray equipment in the bronchoscopy suite or coordination with the radiology department and causes exposure to radiation for the patient and the staff. In a prospective study (Herth et al. 2002a) we were able to show that those lesions could be approached by endobronchial sonography guidance with the same success rate of approximately 75%. Recently these data were confirmed by different groups using the miniprobe as a guidance tool for the forceps (Omori et al. 2002; Herth et al. 2002a, b, 2006; Eberhardt et al. 2007; Kurimoto et al. 2002). Recently, the studies were summarised in a metananalysis (Steinfort et al. 2011) and the practise was integrated as state of the art (Rivera et al. 2013).

Lymph Node Staging

Under favorable conditions lymph nodes can be detected by endobronchial sonography down to a size of 2–3 mm and the internal structure (sinuses and folliculi) as well as small lymph vessels can be analyzed. By endosonographic localization of lymph nodes the results of TBNA can be significantly improved up to 85%. This is especially true for those positions in which reliable landmarks on the computed tomogram are missing, e.g., high and low paratracheal localization. (Herth et al. 2005) investigated the results of an endobronchial sonography guided TBNA compared with those of conventional TBNA. In this randomized study, they confirmed that the yield of an endobronchial sonography-guided TBNA is higher than that of the conventional TBNA (85 vs. 66%). In an additional analysis of the lymph node station they showed that especially in locations without endoscopic landmarks (lymph node stations 2, 3, 4, Mountain scheme) the detection technique is helpful to increase the yield. On the other hand, they showed that in the case of enlarged subcarinal nodes a conventional TBNA has the same yield as the TBNA after endobronchial sonography detection (Krasnik et al. 2003; Yasufuku et al. 2004; Herth et al. 2006; Herth et al. 2008). By now this practise count as the practise in the evaluation of the mediastinum. In every actual recommendation to the diagnostic procedure of lung cancer this practise is named as the first option (Rivera et al. 2013, Vansteenkiste et al. 2013, de Leyn et al. 2014).

Other developments in the ultrasound technic happen here too. Modern equipment provides options like harmonic imaging and elastography. If these type of depiction will provide additional information is tested in clinical studies.

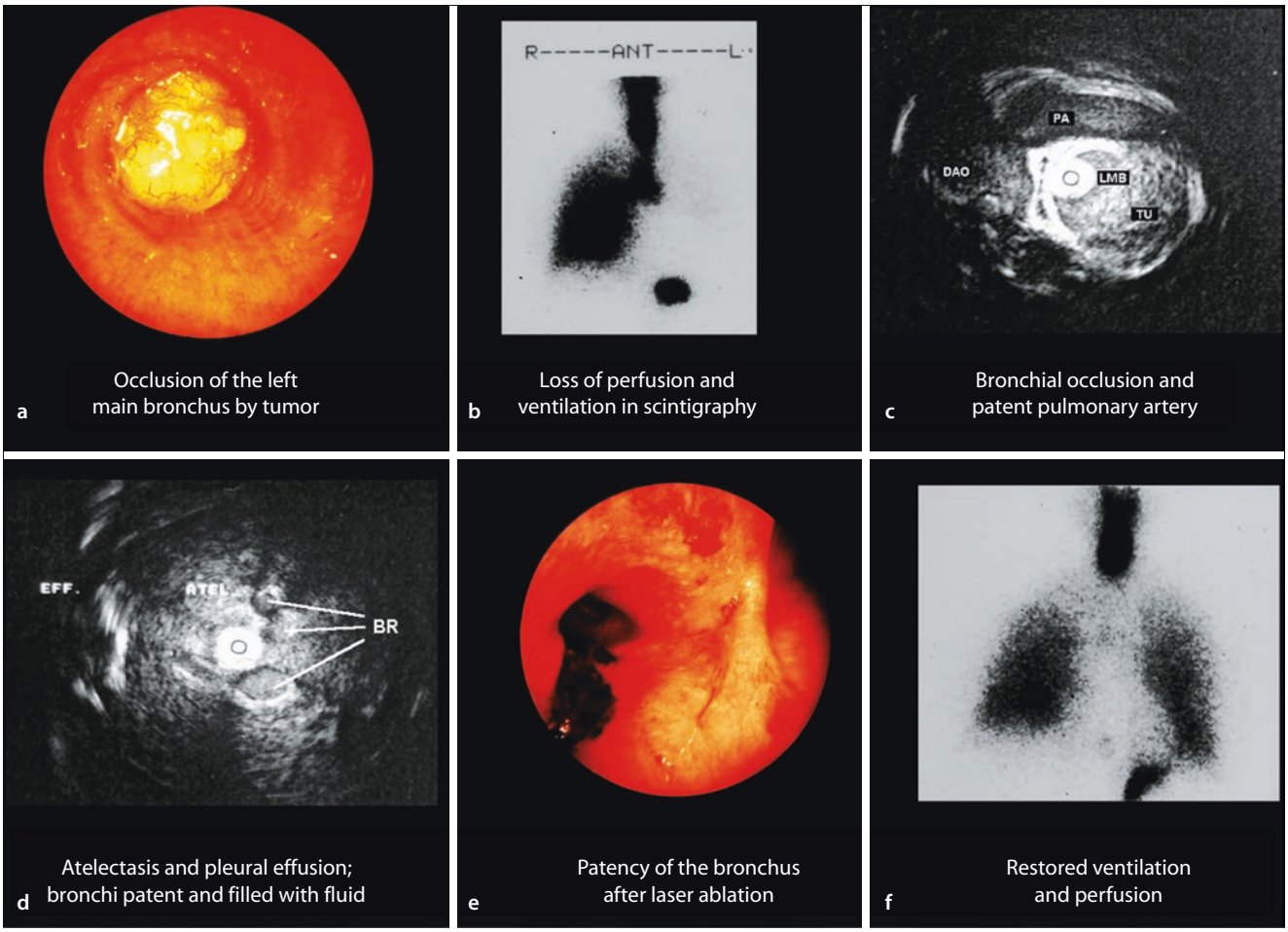

Fig. 7.4 EBUS guidance for tumor recanalisation

7.2.3 Endobronchial Sonography in Therapeutic Interventions

Especially for making decisions in potentially curative endobronchial therapy of malignancies such as photodynamic therapy or endoluminal high-dose radiation by brachytherapy, diagnosis of limitation of the lesion to the bronchial wall or to the close vicinity is essential. Here endobronchial sonography is superior to all other imaging procedures owing to the detailed analysis of the layers of the bronchial wall. In decision-making for endobronchial therapy of advanced lung cancer, endobronchial sonography provides important data (Herth et al. 2003). In complete bronchial obstruction, the base and the surface of the tumor assessed as can whether the different layers of the bronchial wall are involved, how far the tumor is penetrating into the mediastinal structures and whether the airways beyond the stenosis are patent. Also patency of the adjacent pulmonary artery can be diagnosed, which is important to predict postinterventional perfusion of the dependent lung and prevent increase of dead-space ventilation (Fig. 7.6). Endobronchial sonography is also useful for exploration of benign central airway stenosis to assess the extent and the cause of the disease, the relationship to vessels and other surrounding structures and to make the correct decision for therapy, such as mechanical dilatation, laser ablation or stent implantation and endoscopic control of the results (Fig. 7.7).

7.3 Summary

Endobronchial sonography has been widely available for more than 8 years. A growing body of good-quality literature supports its significant role in airway assessment and procedure guidance. Its usefulness is especially well documented in lymph node staging via guided TBNA and in lending support for therapeutic decision-making with regard to endoluminal or alternative treatment strategies for malignant airway abnormalities. Endobronchial sonography is a routine adjunct to endoscopy in many centers, and we expect its role to grow in the near future. Because of the evidence the endobrochial ultrasound is temporarily established in the diagnostic procedure of rounded lesions and also in the clarification of mediastinal procedures as the practise of choice.

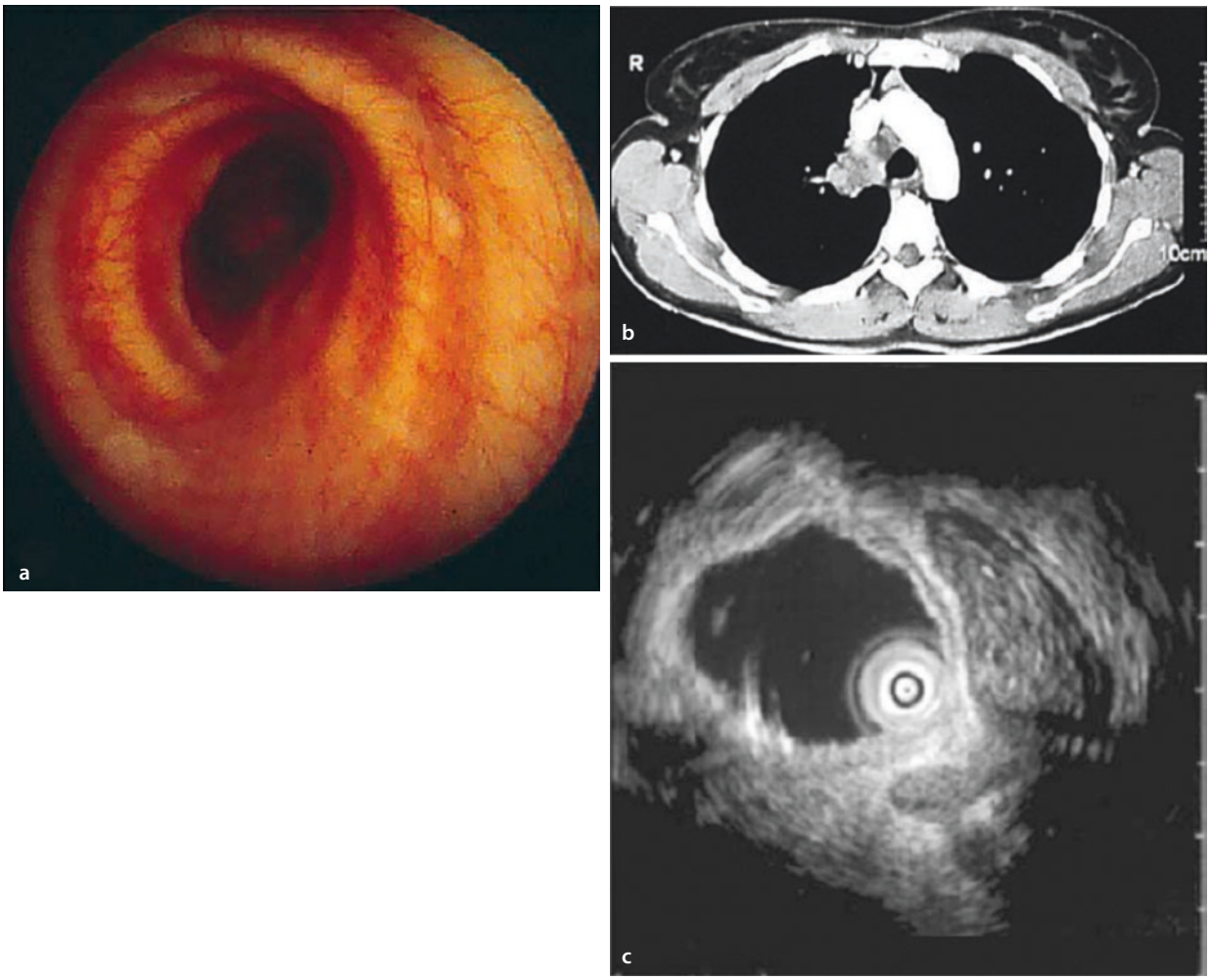

Fig. 7.5 Compression of the trachea by a tumor. (**a**) Bronchoscopy reveals an impression of the trachea. (**b**) The corresponding CT image shows a mass in the upper lobe. (**c**) Ultrasound reveals a well-defined tumor; an infiltration is unlikely

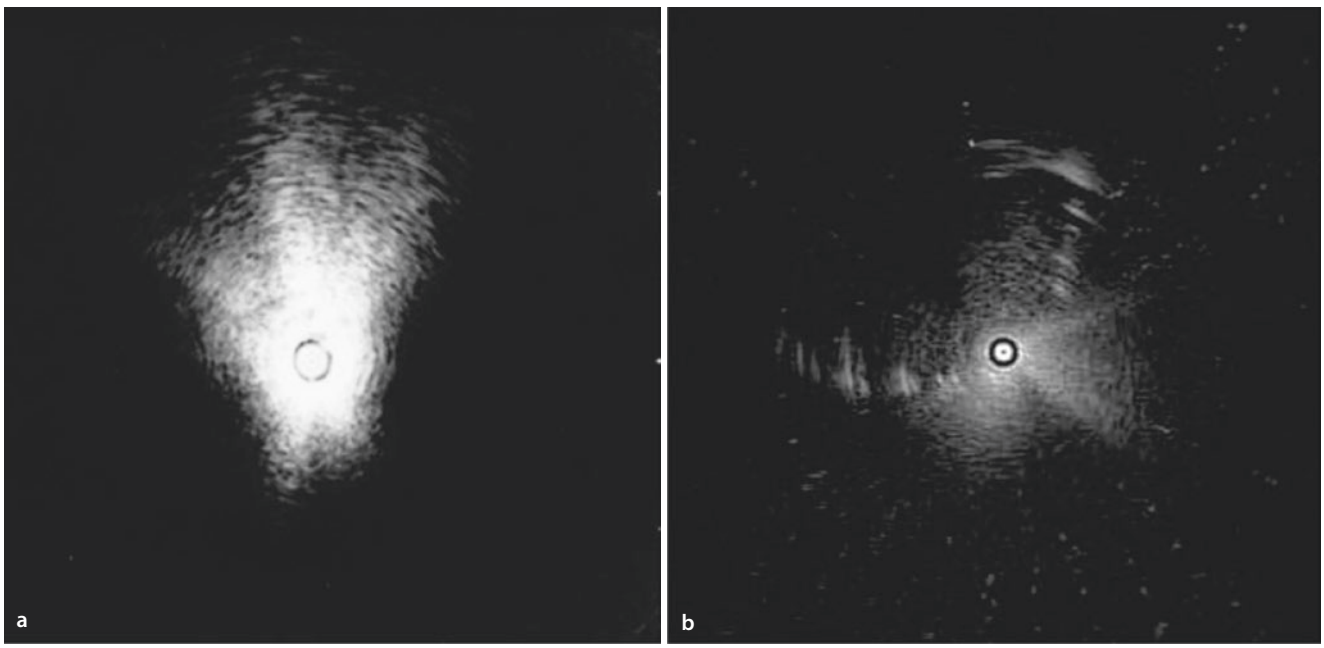

Fig. 7.6 (**a**) Complete reflection of sound waves in lung parenchyma. (**b**) A peripheral intrapulmonary lesion can be distinguished from the lung parenchyma with the probe head

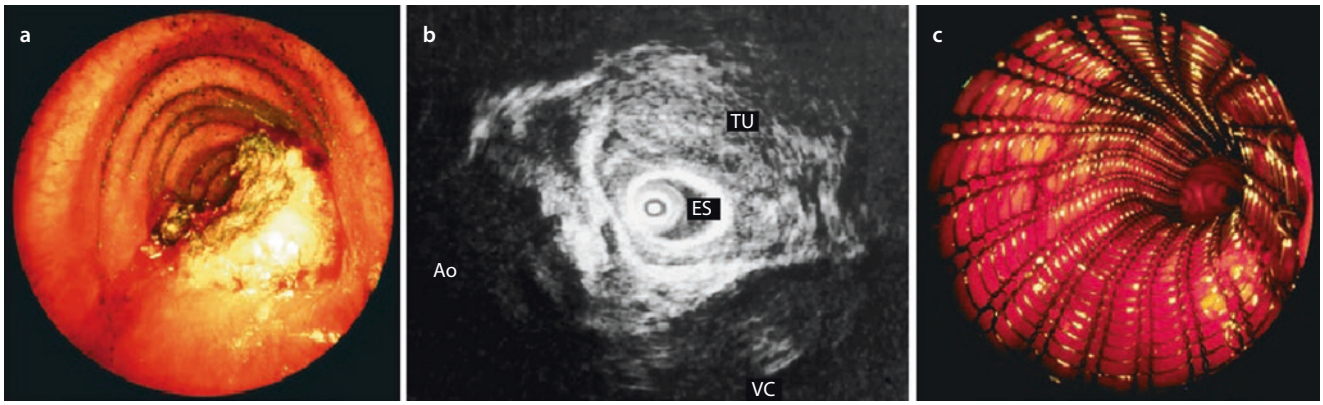

Tracheal tumor after partial laser ablation

Infiltration of anterior esophageal wall

Palliative stent insertion before external radiation due to risk of esophagotracheal fistula

Fig. 7.7 Ultrasound-guided lymph node puncture. The needle is well visible

References

Eberhardt R, Anantham D, Ernst A, Feller-Kopman D, Herth F (2007) Multimodality bronchoscopic diagnosis of peripheral lung lesions: a randomized trial. Am J Respir Crit Care Med 176:36–41

De Leyn P et al (2014) Revised ESTS guidelines for preoperative mediastinal lymph node staging for non-small-cell lung cancer. Eur J Cardiothorac Surg 45(5):787–798

Herth F, Becker HD (2000) Endobronchial ultrasound of the airways and the mediastinum. Monaldi Arch Chest Dis 55:36–45

Herth F, Ernst A, Becker HD (2002a) Endobronchial ultrasound (EBUS) guided transbronchial lung biopsy (TBBX) in solitary pulmo-nary nodules and peripheral lesions. Eur Respir J 20:972–975

Herth F, Ernst A, Becker HD (2002b) Endobronchial ultrasound in therapeutic bronchoscopy. Eur Respir J 20:118–121

Herth FJ, Ernst A, Schulz M, Becker HD (2003) Endobronchial ultrasound reliably differentiates between airway infiltration and compression by tumor. Chest 123:458–462

Herth FJ, Eberhardt R, Vilmann P, Krasnik M, Ernst A (2006) Real-time, endobronchial ultrasound-guided, transbronchial needle aspiration: a new method for sampling mediastinal lymph nodes. Thorax 61(9):795–798

Herth FJF, Krasnik M, Eberhardt R, Ernst A, Vilman P, Dienemann H (2005) EBUS guided biopsy for the staging of mediastinal lymph nodes in a radiologically normal mediastinum. Lung Cancer 49(2):26

Herth FJH, Annema JT, Eberhardt R, Yasufuku K, Ernst A, Krasnik M, Rintoul RC (2008) Endobronchila ultrasound with transbronchial needle aspiration for restaging the mediastinum in lung cancer. J Clin Oncol 26:3346–3350

Hürther Th, Hanrath P (1992) Endobronchial sonography: feasibility and preliminary results. Thorax 47:565–567

Krasnik M, Vilmann P, Larsen SS, Jacobsen GK (2003) Preliminary experience with a new method of endoscopic transbronchial real time ultrasound guided biopsy for diagnosis of mediastinal and hilar lesions. Thorax 58:1083–1086

Kurimoto N, Murayama M, Yoshioka S, Nishisaka T, Inai K, Dohi K (1999) Assessment of usefulness of endobronchial ultrasonography in determination of depth of tracheobronchial tumor invasion. Chest 115(6):1500–1506

Kurimoto N, Murayama M, Yoshioka S, Nishisaka T (2002) Analy-sis of the internal structure of peripheral pulmonary lesions using endobronchial ultrasonography. Chest 122(6):1887–1894

Ono R, Hirano H, Egawa S, Suemasu K (1994) Bronchoscopic ultrasonography and brachytherapy in roentgenologically occult bronchogenic carcinoma. J Bronchol 1:281–287

Omori S, Takiguchi Y, Hiroshima K et al (2002) Peripheral pulmonary diseases: evaluation with endobronchial US initial experience. Radiology 224(2):603–608

Rivera MP, Mehta AC, Wahidi MM (2013) Establishing the diagnosis of lung cancer: diagnosis and management of lung cancer, 3rd ed: American College of Chest Physicians evidence-based clinical practice guidelines. Chest 143(5 Suppl):e142S–e165S

Steinfort DP, Khor YH, Manser RL, Irving LB (2011 Apr) Radial probe endobronchial ultrasound for the diagnosis of peripheral lung cancer: systematic review and meta-analysis. Eur Respir J 37(4):902–910

Takemoto Y, Kawahara M, Ogawara M et al (2000) Ultrasound-guided flexible bronchoscopy for the diagnosis of tumor invasion to the bronchial wall and mediastinum. J Bronchol 7(2):127–132

Vansteenkiste J et al (2013) Early and locally advanced non-small-cell lung cancer (NSCLC): ESMO clinical practice guidelines for diagnosis, treatment and follow-up. Ann Oncol 24(Suppl 6):vi89–vi98

Yasufuku K, Chhajed PN, Sekine Y, Nakajima T, Chiyo M, Iyoda A, Yoshida S, Otsuji M, Shibuya K, Iizasa T, Saitoh Y, Fujisawa T (2004) Endobronchial ultrasound using a new convex probe: a preliminary study on surgically resected specimens. Oncol Rep 11(2):293– 296

Vascularization

Christian Görg

G. Mathis (ed.), *Chest Sonography*, DOI 10.1007/978-3-319-44072-9_8

8.1 Introduction

In addition to the sonographic characteristics of the B-mode image, the type of vascularization is of major importance for assessment of a lesion in terms of differential diagnosis. In sonographic examinations, the established procedures of color-Doppler sonography and, since recently, contrast-assisted sonography are used for this purpose.

However, the definitive value of color-Doppler sonography and contrast-assisted sonography for the diagnosis of solid peripheral consolidations in the lung, compared with other sectional imaging procedures for the chest, is yet to be fully established. In the last few years the color-Doppler sonography characteristics of bacterial pneumonia, obstructive atelectasis, lung infiltrates and bronchial carcinoma have been described (reviewed in Görg and Bert 2004a, b). Preliminary studies show that contrast-assisted sonography can be performed on the chest. Various diseases of the lung are characterized by specific contrast-assisted sonography findings (reviewed in Görg and Bert 2006).

Guidelines for the use of ultrasound contrast media (USCM) are discussed regularly at special consensus meetings and then published (2004, 2008, 2011). However, the authors' recommendation in favor of using contrast-enhanced ultrasound for the investigation of the chest is based on a meager body of evidence (Piscaglia et al. 2012).

The purpose of the present chapter is to describe color-Doppler sonography and contrast-assisted sonography findings in the presence of peripheral lung consolidations.

8.2 Pathophysiological Principles

The lung is characterized by dual vascularization. Perfusion is achieved on the one hand by lung circulation, which is responsible for pulmonary gas exchange. Lung circulation is accomplished by the pulmonary arteries and their ramifications as well as venules and lung veins. The lung itself is nourished by the bronchial arteries.

In contrast to systemic circulation, circulation by the pulmonary arteries is marked by specific characteristics. Pulmonary arteries and their initial branches are elastic. The subsequent arteries have muscular walls. From the level of the arterioles onward, these arteries turn into partly muscular and nonmuscular precapillaries. In contrast to systemic circulation in which arterioles are the main vessels of resistance, in lung circulation the resistance is more or less equally distributed between arteries, capillaries and veins. Thus, flow in the pulmonary arteries and capillaries is pulsatile and not continuous. In contrast to hypoxic vasodilatation in systemic circulation, hypoxic vasoconstriction occurs in lung circulation. The purpose of such vasoconstriction is to reduce the intrapulmonary shunt volume (Euler–Liljestrand mechanism). When lung tissue is affected by a malignant tumor, the carcinoma has been reported to invade the pulmonary arteries of the affected lung segment in 56–87 % of cases (Kolin and Koutllakis 1988; Fissler-Eickhoff and Müller 1994).

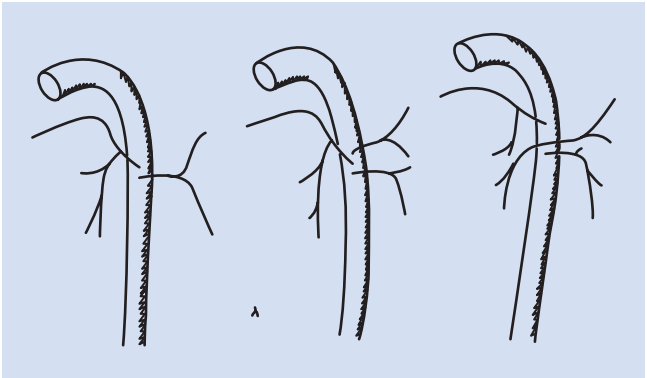

Fig. 8.1 The anatomy of the bronchial arteries

Particularly in the center of the tumor the regular vascular pattern is completely altered. Vascularization is reduced by stenosis and occlusion of the pulmonary arteries.

As a rule the bronchial arteries originate on the left side from the aortic arch and on the right side from the intercostal artery. They form a vascular ring at the hilum of the lung. From this vascular ring the branches run parallel to the bronchial branches and the pulmonary vessels (Fig. 8.1). The bronchial branches (rami bronchiales) supply the bronchi, pulmonary vessels, alveoli and supporting tissue. Interstitial branches run into the interlobar and interlobular septa and supply the visceral pleura. Anastomoses (blocked arteries) between the two systems are normally closed. In cases of occluded pulmonary vessels, the anastomoses become open owing to hypoxia and blood supply is provided by bronchial arteries. Angiographic studies have shown that particularly peripheral lung processes at the pleural wall, such as benign cavitary lesions, lung cysts, lung abscesses and liquefying pneumonia, are nourished by bronchial arteries (Görg and Bert 2004a). However, malignant primary lung tumors and lung metastases are vascularized by bronchial arteries to a differing extent (Müller and Meyer-Schwickerath 1978 (Fig. 8.2).

The intercostal arteries originate from the thoracic aorta and run a strictly intercostal course in the chest wall along the ribs. They are the only vessels that can be visualized on sonography, even in healthy volunteers. Particularly in cases of lesions in the chest wall, these vessels play an important role in tumor vascularization.

Tumor neoangiogenesis of primary bronchial carcinomas mainly originates in the bronchial arteries. The neoangiogenesis potential of pulmonary vessels appears to be low (Müller and Meyer-Schwickerath 1978; Hsu et al. 1996).

8.3 Principles of Color-Doppler Sonography

The hemodynamic parameters used in transcutaneous color-Doppler sonography at the chest to evaluate vessels can be divided into qualitative and semiquantitative parameters:

1. Qualitative findings of parenchymal vascularization
   (a) Absence of flow signals
   (b) Individual flow signals
   (c) Pronounced flow signals
   (d) Arterial turbulence phenomena
2. Spectral curve analysis: patterns of different arterial flow signals
   (a) Pulmonary artery
   (b) Bronchial artery
   (c) Intercostal artery
   (d) Tumor neoangiogenesis
3. Contrast-enhanced sonography
   (a) Time to enhancement
      – Pulmonary arterial phase
      – Bronchial arterial phase
   (b) Extent of enhancement

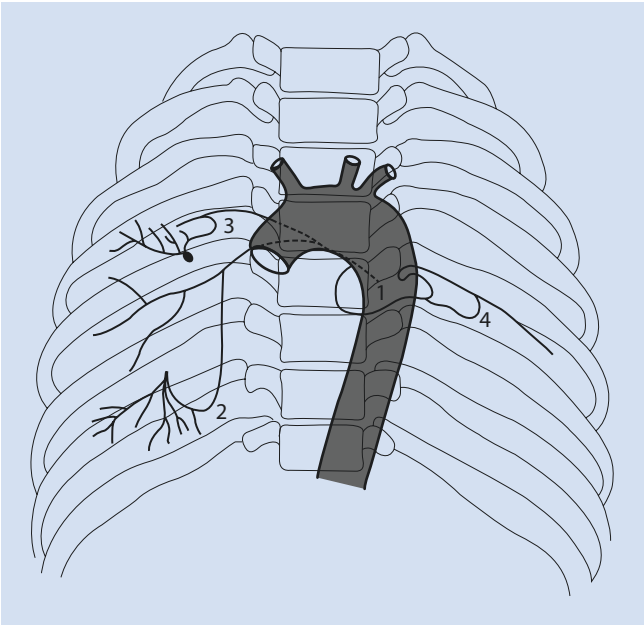

Fig. 8.2 The pathophysiology of the supply of the bronchial arteries. *1* Bronchobronchial anastomoses, *2* bronchopulmonary anastomoses, *3* intercostopulmonary anastomoses, *4* intercostobronchial anastomoses (After von Babo et al. 1979)

Qualitative findings include assessment of the presence, the direction and the characteristics of blood flow. In this regard a distinction is made between the absence of flow signals (Fig. 8.3), evidence of individual flow signals (Fig. 8.4), evidence of markedly disorganized vascularization (Fig. 8.5) or pronounced tree-shaped vascularization (Fig. 8.6), and evidence of arterial turbulence phenomena in consolidated areas (Fig. 8.7). Semiquantitative parameters such as the resistance index and the pulsatility index are used for spectral curve analysis of arterial blood flow. Spectral curves of pulmonary arteries, bronchial arteries, intercostal arteries and arteries of tumor angiogenesis can be differentiated within pathological processes, and can be used to differentiate ambiguous peripheral lung lesions. In principle, evidence and documentation of flow signals at the chest is device-dependent and is additionally influenced and limited by the location and the size of the lesion, its cause, and breath-dependent or pulsation-dependent movements. For instance, 20 % of peripheral lung lesions emit no flow signals (Yuan et al. 1994). Local fluid, lung cysts and lung infarctions show no flow signals on color-Doppler sonography. The color-Doppler sonography pattern of poorly visualized vessels is primarily seen in malignant pleural lesions. Markedly ramified vessels are characteristic for pneumonia and atelectasis (Yuan et al. 1994; Civardi et al. 1993). Turbulence phenomena within a lesion have been reported in pleural

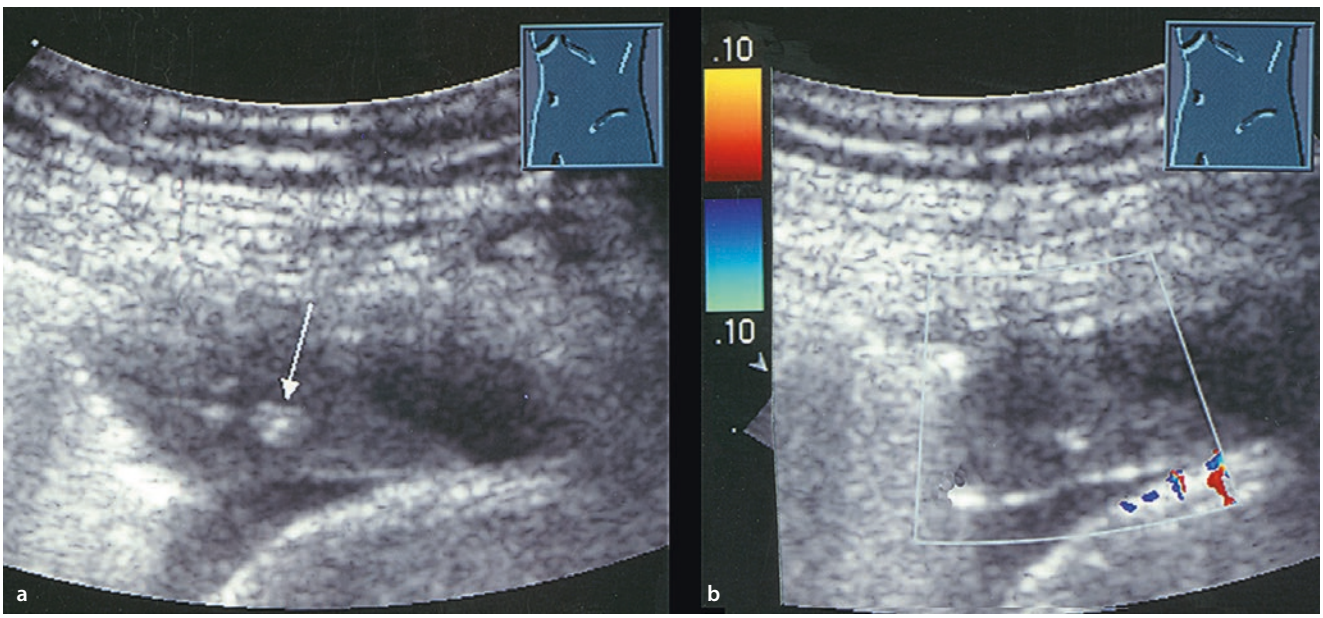

Fig. 8.3 A 43-year-old man with a lung infarction. **a** On the B-mode image one finds a hypoechoic wedge-shaped lesion with a central bronchial reflex (*arrow*). **b** Color-Doppler sonography shows the absence of vascularization

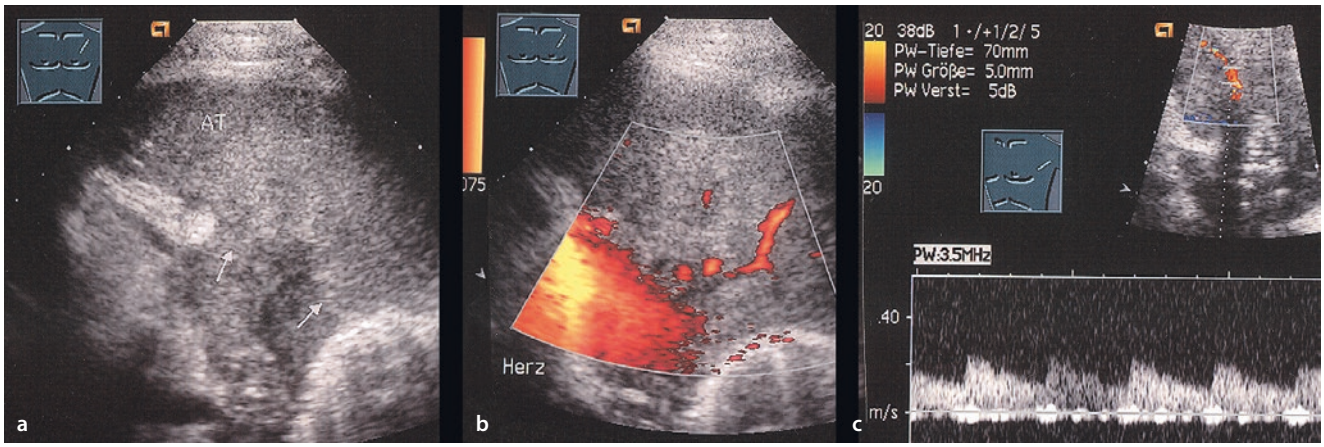

Fig. 8.4 A 36-year-old man with Hodgkin's disease in the mediastinum. **a** On the B-mode image one finds a hypoechoic central tumor formation with atelectasis (*AT*; *arrows*). **b** Color-Doppler sonography shows limited vascularization within the atelectasis, which is a sign of constriction of the pulmonary artery. **c** Spectral curve analysis shows a monophasic flow signal with reduced arterial flow resistance, indicative of a bronchial artery

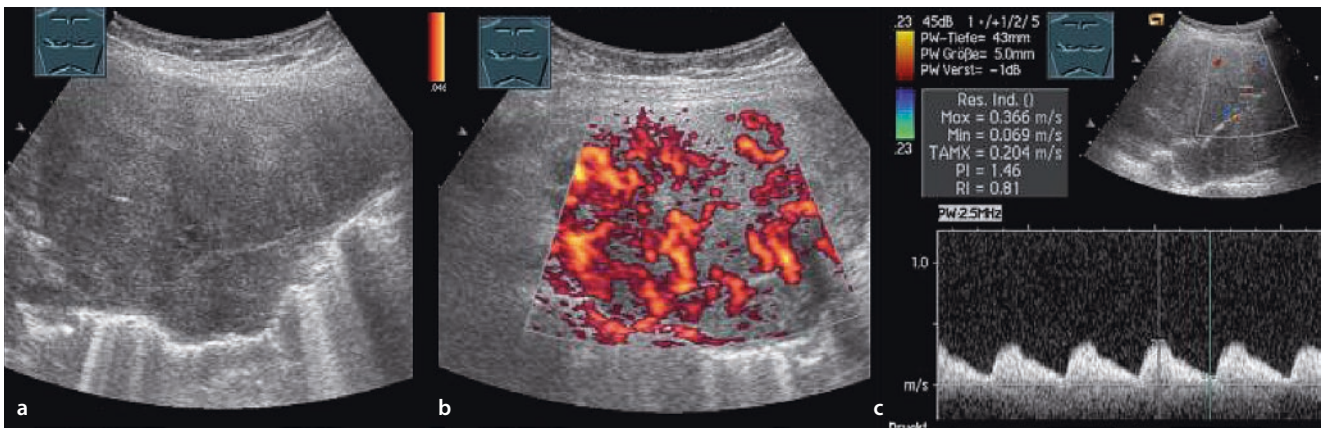

Fig. 8.5 A 62-year-old man with lung metastases in the presence of renal cell carcinoma. **a** The B-mode image reveals a large hypoechoic round lesion. **b** Color-Doppler sonography shows strong and disorganized vessels. **c** Spectral curve analysis shows a monophasic flow signal indicative of a bronchial artery

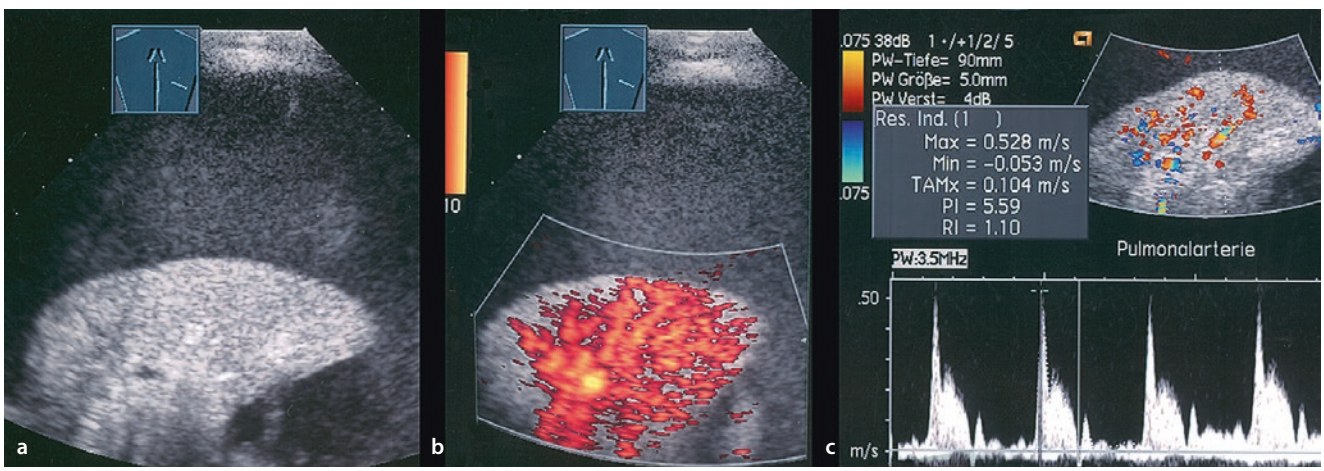

Fig. 8.6 A 37-year-old man with a pleural effusion and compressive atelectasis. **a** The B-mode image reveals a pleural effusion with atelectasis in the lung. **b** Color-Doppler sonography shows ramified vascularization. **c** Spectral curve analysis shows a high-impedance flow pattern, indicative of a pulmonary artery

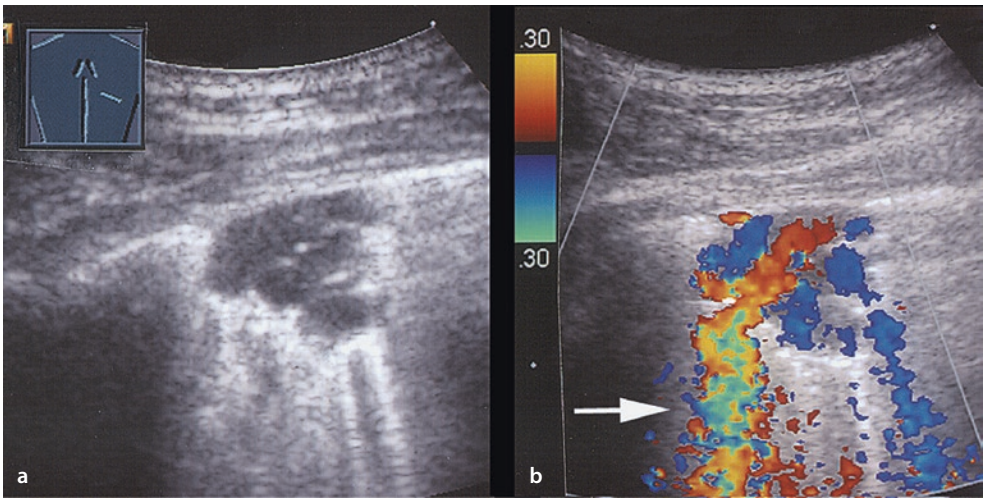

Fig. 8.7 A 14-year-old male patient with Osler–Weber–Rendu syndrome. **a** The B-mode image shows an anechoic space-occupying lesion close to the pleura. **b** Color-Doppler sonography reveals a large vessel that supplies the ectatic vessels close to the pleura. On spectral curve analysis this vessel was identified as a pulmonary artery

arteriovenous fistulae and vascular abnormalities in connection with Osler's disease.

Quantitative parameters such as the resistance index and the pulsatility index are used to analyze arterial spectral curves. Civardi et al. (1993) were the first to perform quantitative and qualitative spectral curve analyses for peripheral lung lesions. They found a triphasic flow signal more commonly in benign lesions and a monophasic flow signal in malignant lesions. Yuan et al. (1994) registered a sensitivity and specificity of more than 95 % for differentiation of benign lesions from malignant ones by the use of arterial spectral curve analysis. The authors interpreted the monophasic low-impedance flow primarily seen in tumors as flow signals of tumor neoangiogenesis, while they correlated the high-impedance flow of pneumonias and atelectases with vessels of the pulmonary arteries (Yuan et al. 1994). In a subsequent study the authors registered different resistance indices for atelectasis and pneumonia, indicative of differing vasoconstriction due to hypoxia (Yuan et al. 2000). In a controlled histological study, Hsu et al. (1996) were the first to show that the vessels from which low-impedance monophasic flow signals originated were not tumor vessels but were bronchial arteries. "True" tumor vessels are characterized by nearly constant flow without variations between the systolic and the diastolic phase (Hsu et al. 1996). Owing to the technical limitations of commercially available ultrasound devices for slow blood flow (less than 2 cm/s), tumor vessels are usually not seen on sonography (Harvey and Albrecht 2001). In a subsequent study, Hsu et al. (1998) registered a much lower sensitivity and specificity of 53 % and 72 % for differentiation of benign lesions from malignant ones by the use of arterial spectral curve analysis. A common feature of all of these studies is that the authors only used one arterial spectral curve pattern to analyze a lesion. By sonographic "mapping," the authors of a more recent study were able to demonstrate several different flow signals within a lesion in nearly half of the patients with pleural lesions examined (Görg et al. 2003) (Fig. 8.8). This may be interpreted as an indication of the fact that arterial blood supply to peripheral lung lesions is a complex phenomenon. In a subsequent study, chest wall lesions were examined with the aid of arterial spectral curve analysis and were found to be vascularized by intercostal arteries among other sources (Görg et al. 2005a). However, intercostal arteries have a monophasic high-impedance flow signal.

Thus, the following flow signals may be distinguished with the aid of arterial spectral curve analysis (Fig. 8.9):

1. *Pulmonary arteries* may be present in various locations, run a centrifugal course from the hilum to the surface of the lung and have a high-impedance, usually triphasic flow signal.
2. *Bronchial arteries* are present in various locations, vary in terms of their direction of flow and have a low-impedance monophasic flow signal.
3. *Intercostal arteries* are characterized by their strictly intercostal location, run a nearly horizontal course and have a high-impedance, usually monophasic flow signal.
4. Arterial vessels of *tumor neoangiogenesis* are present in various locations, vary in terms of their direction of flow and are marked by a nearly constant flow with no variation between the systolic and the diastolic phase (Fig. 8.10).

8.4 Basic Principles of Contrast-Assisted Sonography

In the last few years contrast-assisted sonography has become a widely used procedure to investigate the liver, particularly to describe focal liver lesions. The second generation of contrast media now available for clinical use causes microscopic blisters in the vessel lumen which lead to enhanced redispersion of the ultrasound wave, thus increasing the signal amplitude and eventually yielding better contrast of vessels than that achieved with color-Doppler sonography. The use of contrast-assisted sonography allows infinitesimally small vessels whose width is just a little larger than that of capillaries to be visualized. In the experimental setting, vessels with

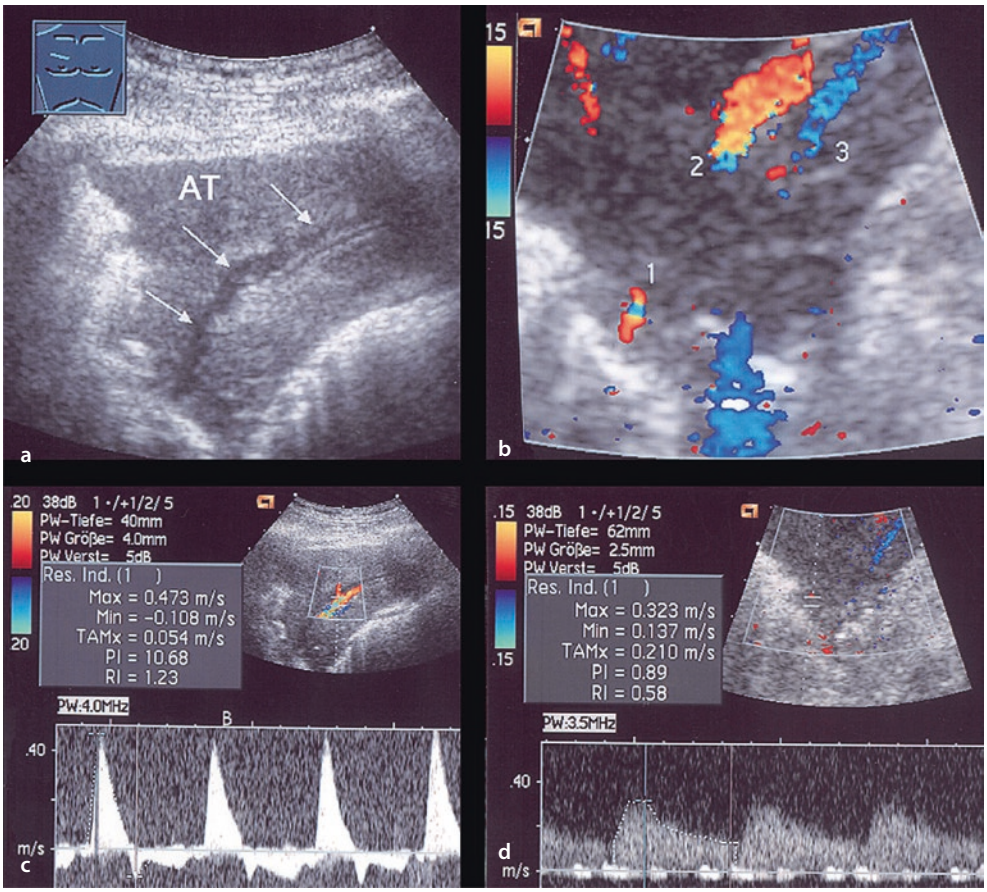

Fig. 8.8 A 65-year-old man with a centrally located bronchial carcinoid tumor and obstructive atelectasis. **a** The B-mode image shows a triangular hypoechoic consolidation with a fluid bronchogram (*arrows*). *AT* atelectasis. **b** Color-Doppler sonography reveals different vessels in the central region of the atelectasis (*1* bronchial artery, *2* pulmonary artery, *3* pulmonary vein). **c** Spectral curve analysis shows a high-impedance triphasic flow signal as a sign of a pulmonary artery (designated *2* in b). **d** Spectral curve analysis reveals a low-impedance arterial flow signal oriented toward the periphery, indicative of a bronchial artery (designated *2* in b)

a diameter of 74–134 µm were demonstrated by contrast-assisted sonography. Vessels smaller than 38 µm in diameter have not been visualized thus far even with the use of contrast medium. In principle, contrast-assisted sonography should be applied according to the guidelines of the EFSUMB (Albrecht et al. 2004).

With regard to the application of contrast-assisted sonography in the lung it should be noted that, as with all transcutaneous sonographic modalities, investigation of the healthy lung is not possible. However, like the liver, the lung is marked by dual arterial supply and is therefore predestined for the use of contrast-assisted sonography. Consolidated lung tissue can be examined with contrast-assisted sonography. Pathological lung lesions are first characterized by starting contrast enhancement. In cases of vascularization by the pulmonary arteries alone, this time point is marked by early arterial contrast enhancement about 1–6 s after application of contrast medium. The contrast medium can be demonstrated by sonography in the right side of the heart just a few seconds later. The time until the surge of contrast medium depends on hemodynamic parameters (heart failure, COPD) among other factors. The surge of contrast medium into a lesion before the chest wall or a parenchymatous organ is a sign of vascularization by the pulmonary artery. In cases of vascularization of a lesion by the bronchial arteries alone, contrast enhancement may be expected only after the contrast medium has passed through the lung. Thus, contrast enhancement of the left ventricle is seen at the earliest 7–10 s after application of contrast medium in the peripheral vein (Fig. 8.11). This always occurs in conjunction with enhancement of the chest wall or the parenchymatous organ, and is a sign of systemic arterial vascularization. The extent of contrast enhancement is basically dependent on the presence or absence of vascularization, the type of vascularization—whether through the pulmonary arteries or through the bronchial arteries—and also by the presence of collaterals or vessels of tumor neoangiogenesis. Depending on the phase, a distinction may be made between the arterial phase (1–30 s) and the parenchymatous phase (1–5 min). The extent of contrast enhancement has been quantified so far only in comparison with an intra-individual reference; a distinction is made between reduced and increased contrast enhancement. A parenchymatous organ such as the spleen is a suitable in vivo reference (Forsberg et al. 1999; Görg et al. 2006b). The healthy spleen is known to be characterized by organ-specific contrast tropism and homogenous contrast enhancement. Pathological changes in the spleen are rare compared with those in the liver.

A third assessment criterion is the differentiation between homogeneous and inhomogeneous contrast enhancement. Parenchymal lesions are assessed in terms of their numbers, shape (round, wedge-shaped), and location (central, peripheral). In summary, peripheral lesions of the lung may be evaluated according to the following criteria:

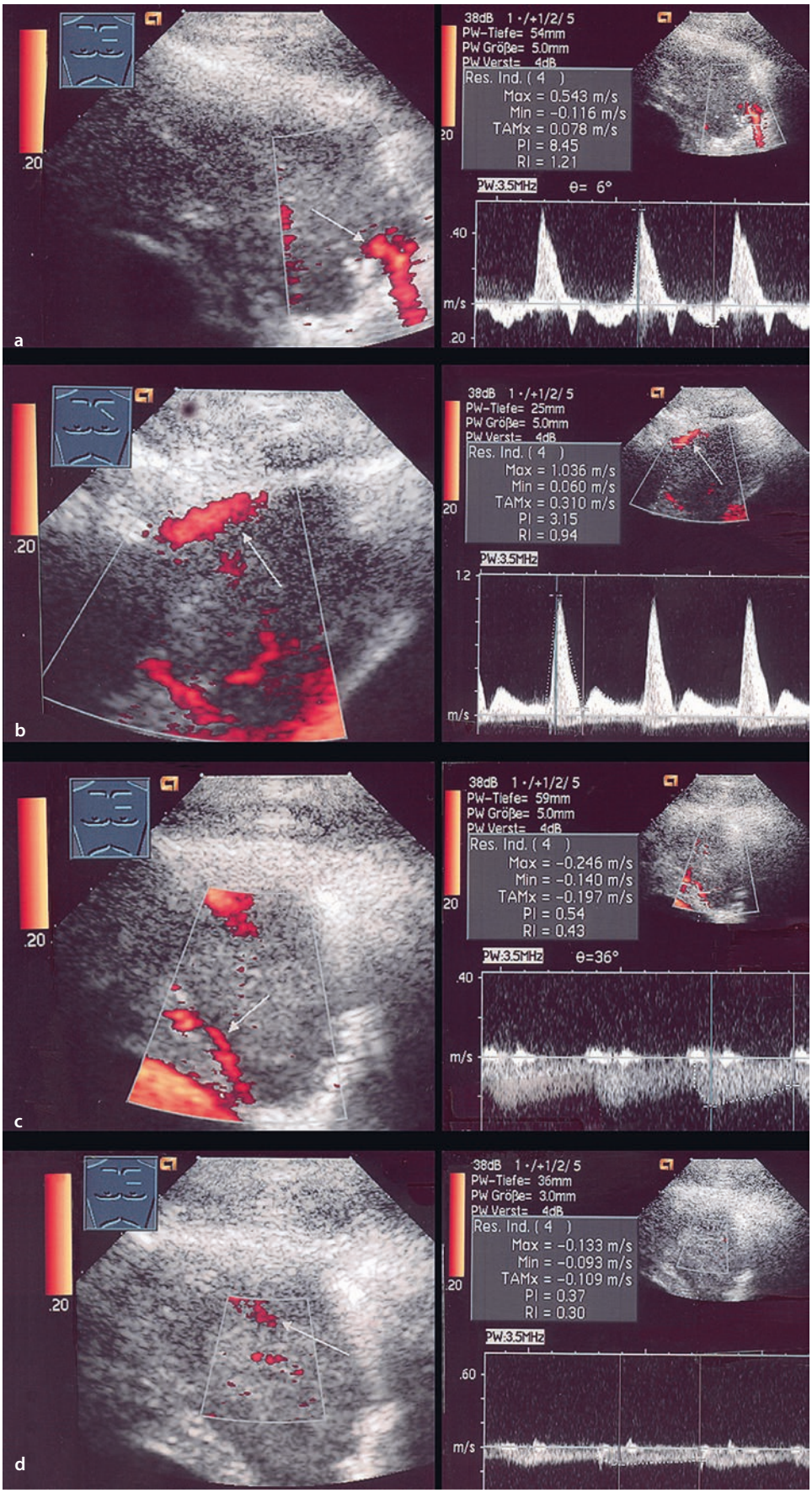

Fig. 8.9 A 31-year-old man with a malignant lymphoma affecting the lung. **a** Color-Doppler sonography shows a biphasic high-impedance flow pattern in the central portion of the consolidated lung—a sign of a pulmonary artery (*arrow*). **b** In the periphery of the tumor there is a monophasic high-impedance arterial flow pattern, typical of an intercostal artery (*arrow*). **c** In the central portion of the consolidated lung there is a monophasic low-impedance arterial flow signal—a sign of a bronchial artery (*arrow*). **d** Within the tumor one finds a nearly uniform flow signal without fluctuations in the diastolic and the systolic phase. Here one is inclined to suspect a vessel of tumor neoangiogenesis (*arrow*)

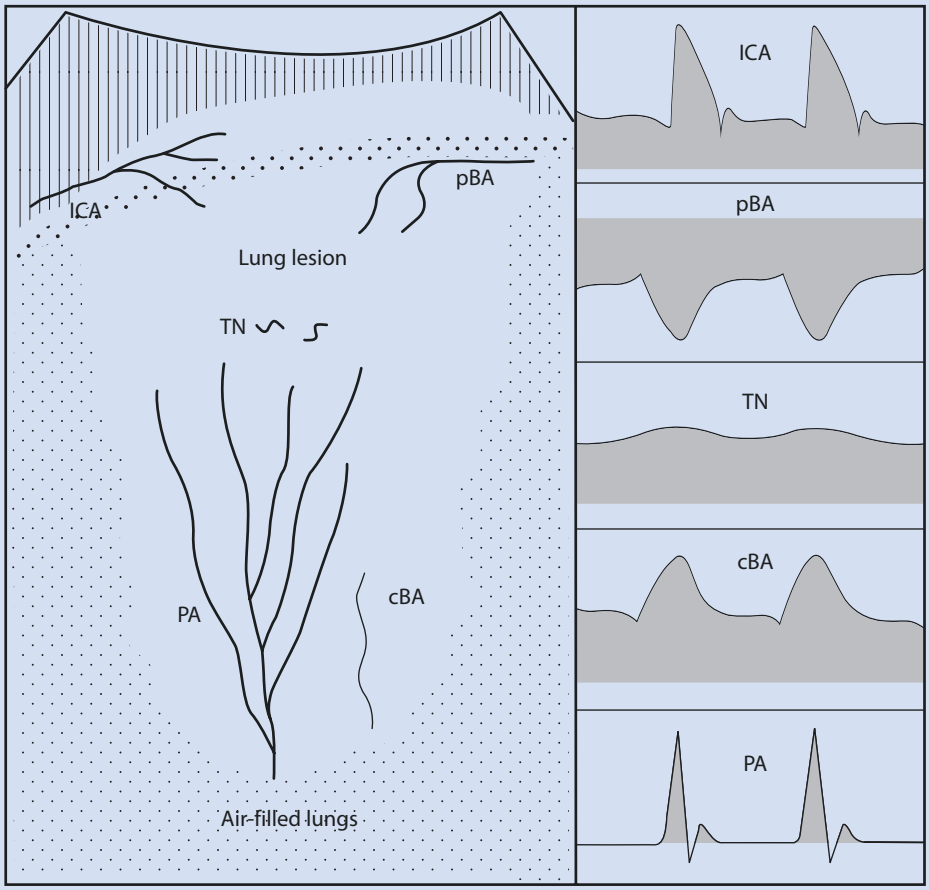

Fig. 8.10 Possible arterial supply of pulmonary lesions with corresponding spectral curves. *ICA* intercostal artery, *pBA* peripheral bronchial artery, *TN* tumor neoangiogenesis, *cBA* central bronchial artery, *PA* pulmonary artery

- The time until contrast enhancement permits a distinction between early vascularization by the pulmonary artery (Fig. 8.12) and delayed vascularization by a bronchial artery (Fig. 8.13).
- The extent of contrast enhancement compared to the enhancement of the spleen. (Fig. 8.14)
- Homogeneity of contrast enhancement with evidence of focal lesions in consolidated lung tissue (Fig. 8.15).

8.5 Predominantly Anechoic Peripheral Lung Consolidation

Color-Doppler Sonography

These lesions are rare and constitute an important differential diagnosis for localized effusion. Primary lung cysts at the pleural wall are seen on B-mode images as anechoic, usually polycystic tumors. Color-Doppler sonography shows qualitative flow signals in the septa and the region of the visceral pleura. On semiquantitative spectral analysis they show a monophasic pattern and thus correspond to bronchial and intercostal arteries (Fig. 8.16). Vascular tumors at the pleural wall, such as those associated with Osler's disease, have a characteristic appearance on color-Doppler sonography. The supplying pulmonary artery can be visualized (Fig. 8.7). The malignant cystic lung tumor shows centrally liquefied areas usually on a floor of liquefactions and is seen on the sonographic B-mode image as a semiliquid structure with septa in some cases. The tumor receives its blood supply from bronchial arteries, and more rarely from pulmonary arteries. Therefore, the spectral curve reveals a monophasic high-impedance arterial flow in keeping with bronchial arteries and occasionally a biphasic high-impedance arterial flow that corresponds to pulmonary arteries (Fig. 8.17). The aortic aneurysm at the dorsal wall of the pleura is a notable pitfall (Fig. 8.18); the same is true for the right lateral part of the heart at the chest wall in cases of cardiomegaly (Fig. 8.19).

Contrast-Assisted Sonography

Specific studies focusing on contrast-assisted sonography for the assessment of anechoic lung consolidations have not yet been published. Lung abscesses, pleural effusions, pleural empyema and liquefied lung tissue, however, are marked by the absence of contrast enhancement (Fig. 8.20).

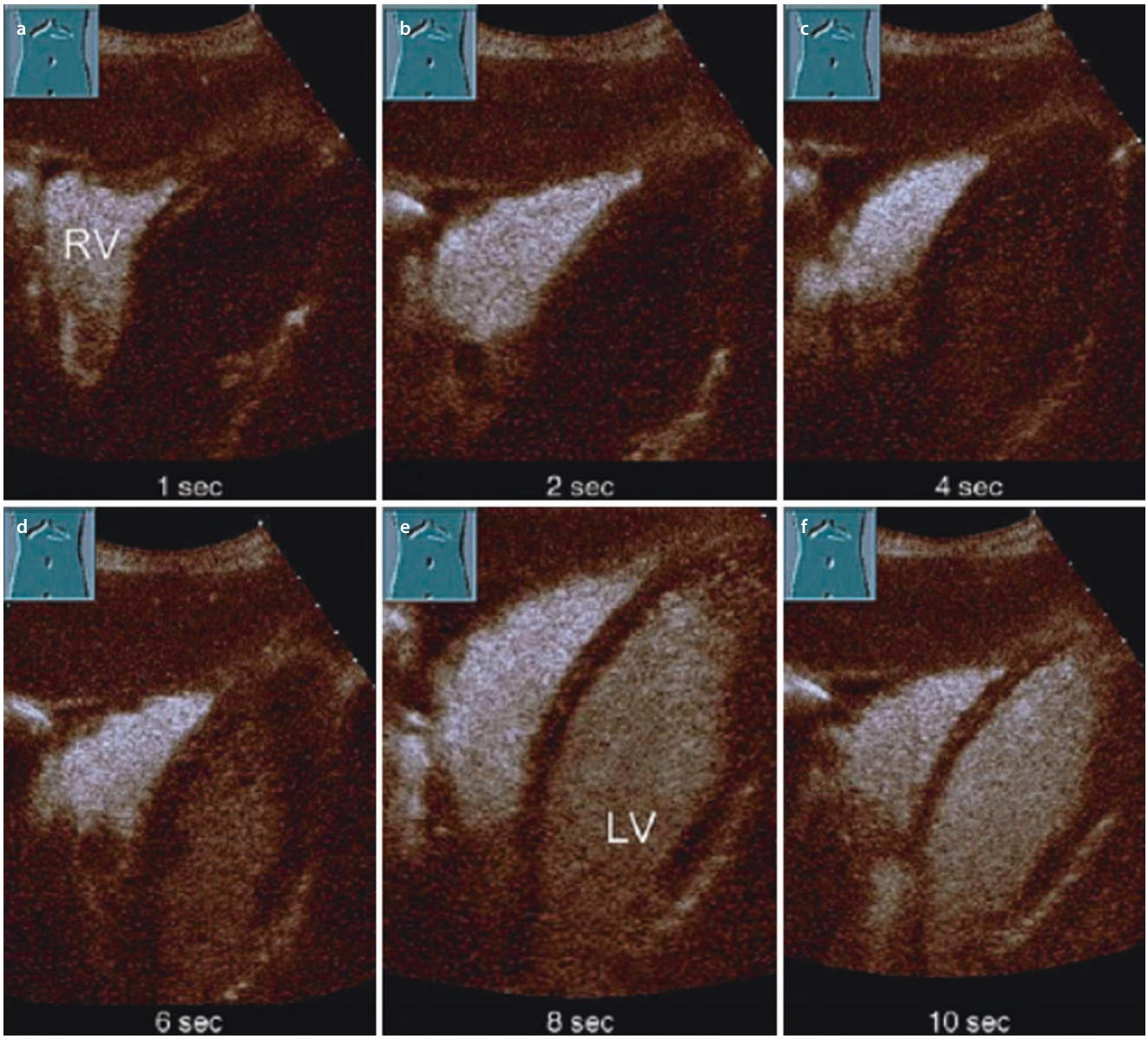

Fig. 8.11 Visualization of the time until contrast enhancement: four-chamber view in a healthy proband. After injection of contrast medium one sees contrast enhancement in the right ventricle as early as 1 s later (**a**–**d**). After 8 s there is contrast enhancement in the left ventricle (**e**, **f**)

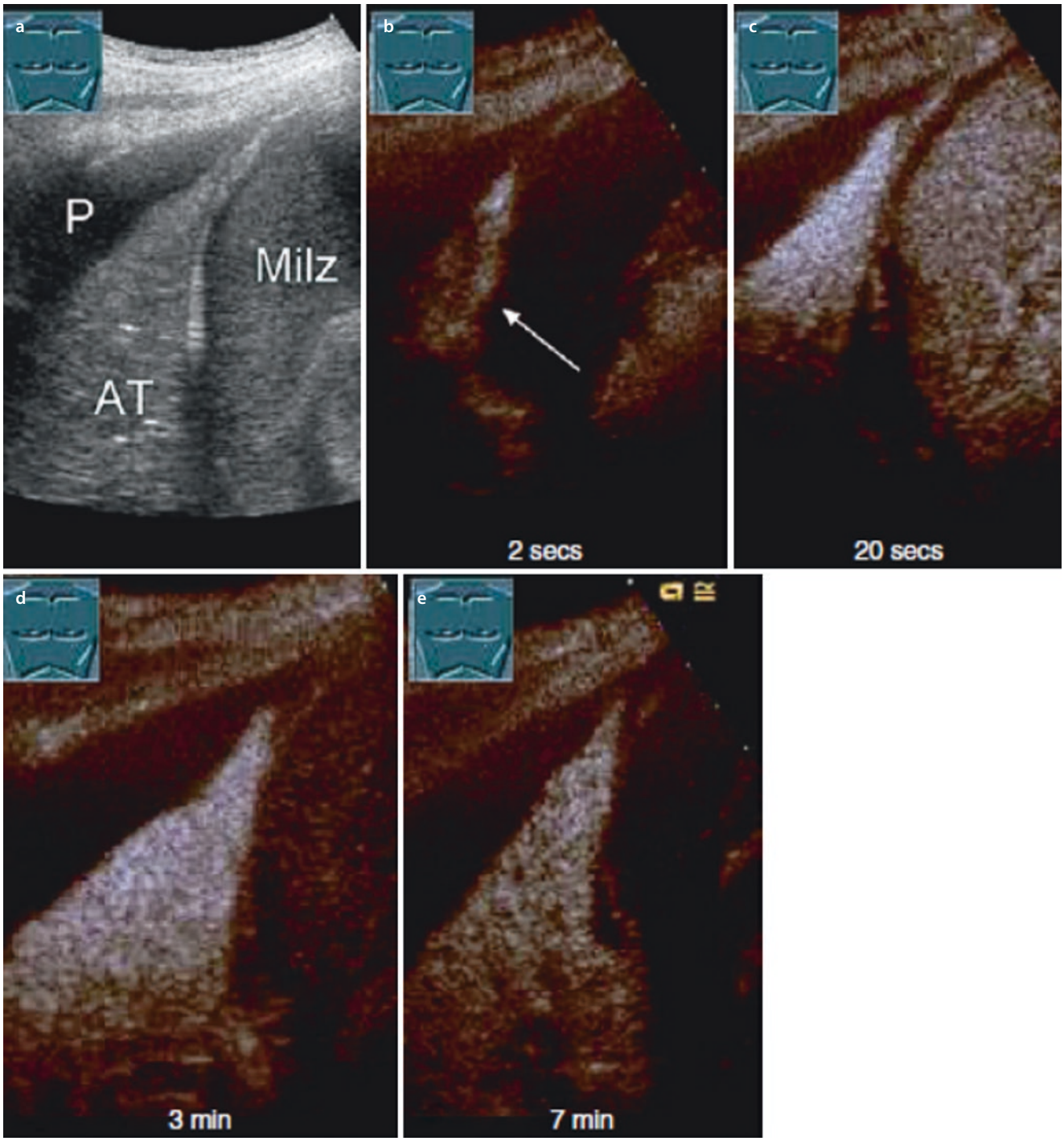

Fig. 8.12 A 24-year-old man with a pleural effusion and compressive atelectasis in the presence of amyloidosis. **a** On the B-mode image one finds a pleural effusion (*P*), an atelectasis (*AT*) and in subcostal location the spleen. Contrast-assisted sonography shows early arterial contrast enhancement after 2 s (**b**). The *arrow* marks the vessel with starting contrast enhancement. After 20 s there is marked contrast enhancement in the atelectatic tissue, which is hyperechoic compared with the parenchyma of the spleen (**c**). In the parenchymatous phase, after 3 min, one finds continued strong contrast enhancement in the atelectasis (**d**), which is also seen after 7 min (**e**). This contrast behavior is indicative of vascularization purely through the pulmonary arteries

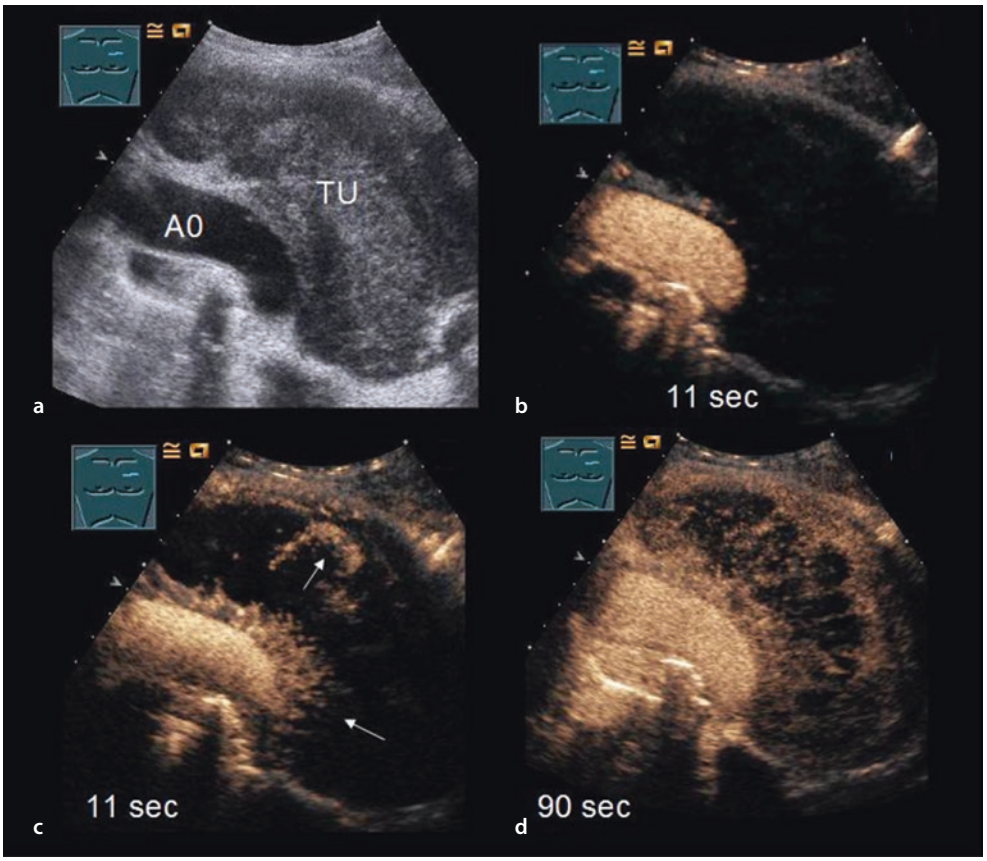

Fig. 8.13 Woman with a non-small-cell bronchial carcinoma in the left lung; a space-occupying lesion is seen. **a** B-mode ultrasonography shows an echogenic space-occupying lesion (*TU*) next to the aorta (*A0*) **b** Enhancement of the aorta occurs 11 seconds after the administration of contrast medium. **c** Mild contrast flow from the aorta (O) into the tumor tissue 11 seconds later, in keeping with central bronchial arteries (*arrow*), and corresponding mild contrast enrichment from peripheral bronchial arteries (*arrow*). **d** After 90 seconds the tumor shows inhomogeneous contrast enhancement

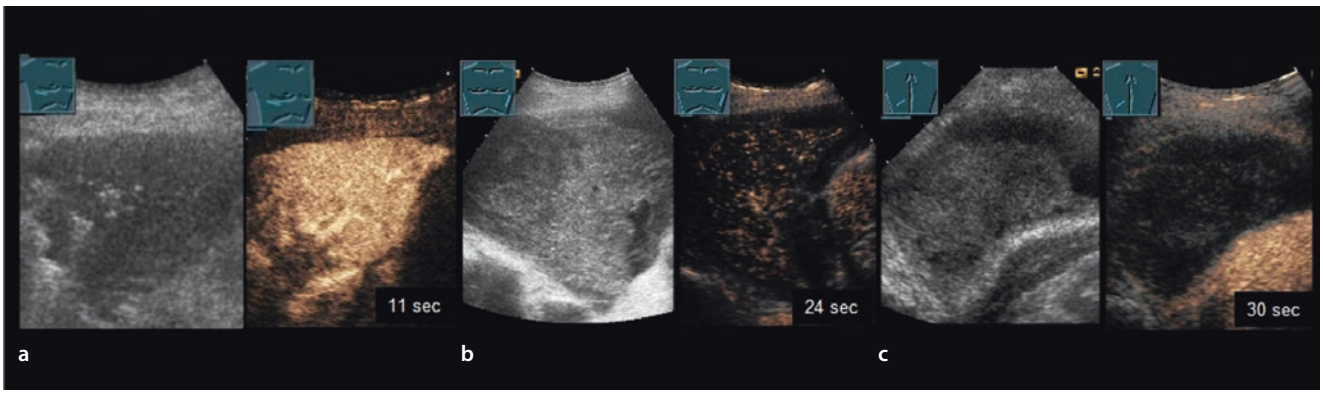

Fig. 8.14 Various degrees of contrast enhancement in three patients with an echogenic space-occupying lesion in the chest. **a** B-mode und contrast-enhanced ultrasonography in a man with pneumonia and strong contrast enhancement, **b** B-mode und contrast-enhanced ultrasound in a man with a lung tumor and poor contrast enhancement, **c** B-mode and contrast-enhanced ultrasound in a man with no contrast enhancement of an echogenic space-occupying lesion by way of a hematoma

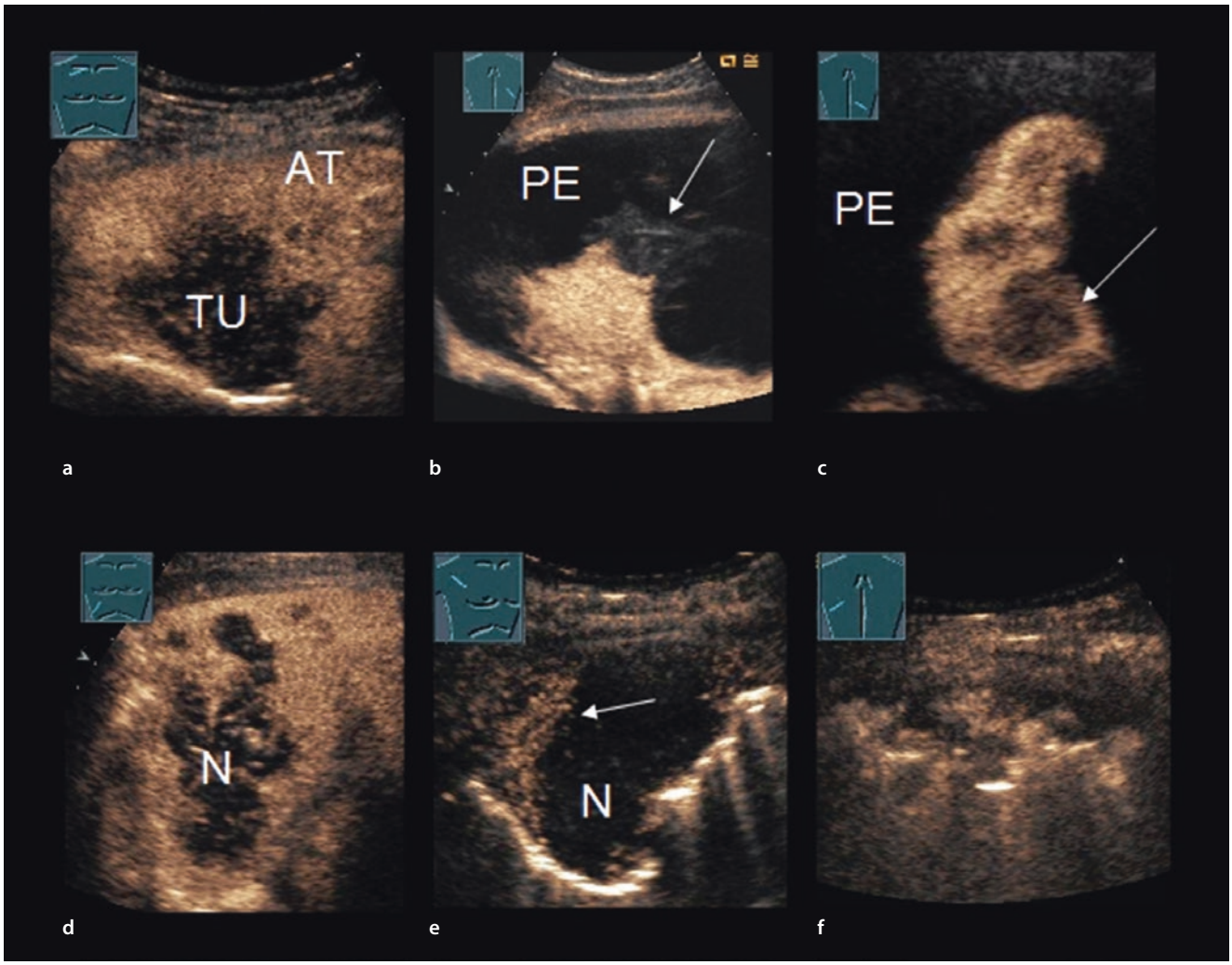

Fig. 8.15 Various patterns of inhomogeneous contrast enhancement in six patients: **a** central hypoechoic tumor (*TU*) und downstream atelectasis (*AT*), **b** Marked pleural effusion (*PE*) with echogenic atelectasis and a peripheral area with no contrast enhancement as in a pulmonary infarction (*arrow*), **c** Marked PE with echogenic atelectasis and central round lesions, with reduced contrast enhancement, most likely indicative of pulmonary metastases (*arrow*), **d** Echogenic space-occupying lesion after aspiration, with a central inhomogeneous area of no contrast enhancement as in necrosis (*arrow*), **e** Peripheral lung tumor with contrast enhancement only at the margins (*arrow*) and a large area of necrosis (*N*), **f** Inhomogeneous contrast enhancement in confirmed peripheral pulmonary embolism

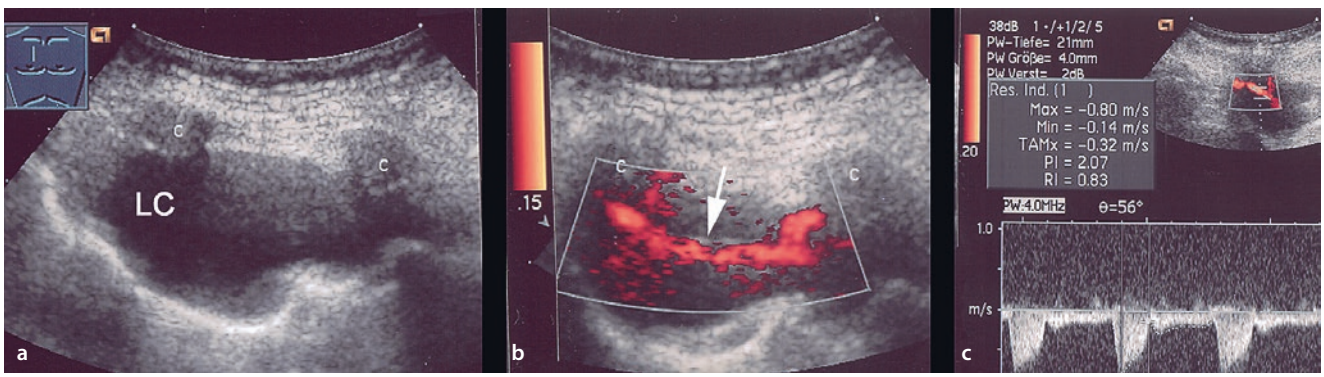

Fig. 8.16 A 70-year-old man with a primary lung cyst. **a** On the B-mode image one finds an anechoic lesion close to the pleura. *C* ribs, *LC* lung cyst. **b** Color-Doppler sonography in the power mode shows a strong vessel surrounding the lesion (*arrows*). **c** Spectral curve analysis demonstrates a monophasic high-impedance flow signal indicative of an intercostal artery

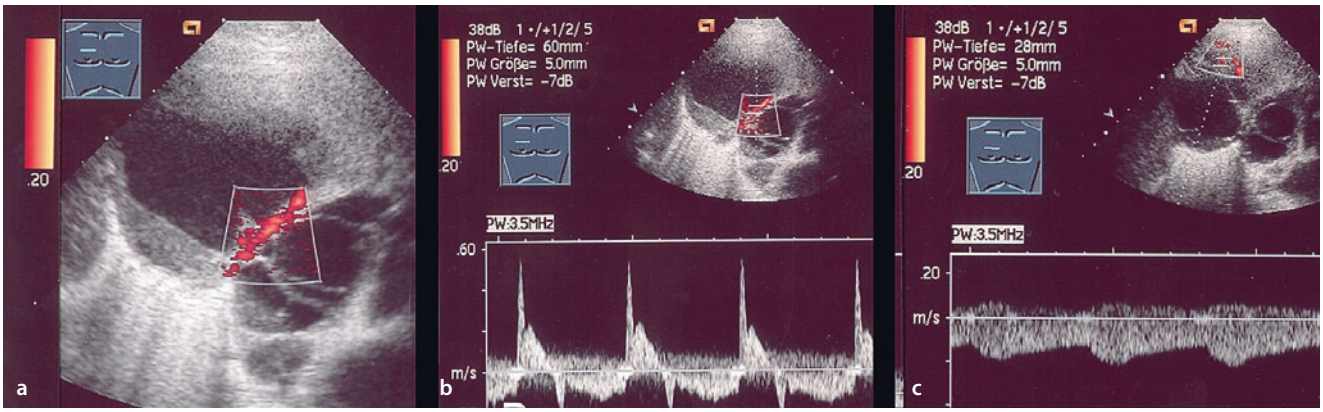

Fig. 8.17 A 44-year-old man with sarcoma of the lung. **a** Color-Doppler sonography shows a tumor with solid and cystic portions and vessels in the seventh course. **b** Spectral curve analysis reveals an arterial high-resistance flow signal. This is indicative of a pulmonary artery. **c** Visualization of a low-impedance flow signal in the margin of the lesion, indicative of a bronchial carcinoma

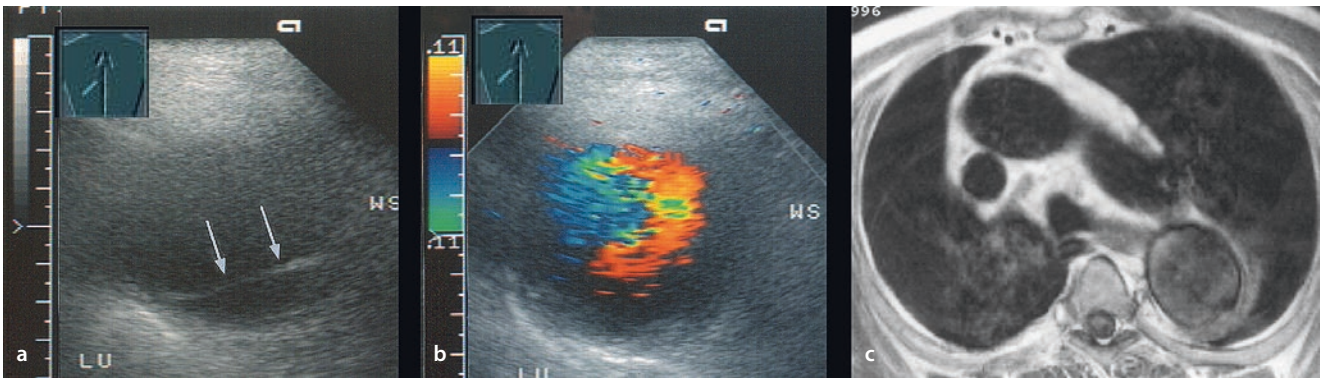

Fig. 8.18 A 49-year-old man with dissection of the aorta in the chest. **a** The B-mode image shows an anechoic septated round lesion close to the pleura (*arrow*). *LU* lung, *WS* spine. **b** Color-Doppler sonography reveals a turbulent flow pattern in the lesion, indicative of an aneurysm in the aorta. **c** The aneurysm in the aorta—on magnetic resonance tomography

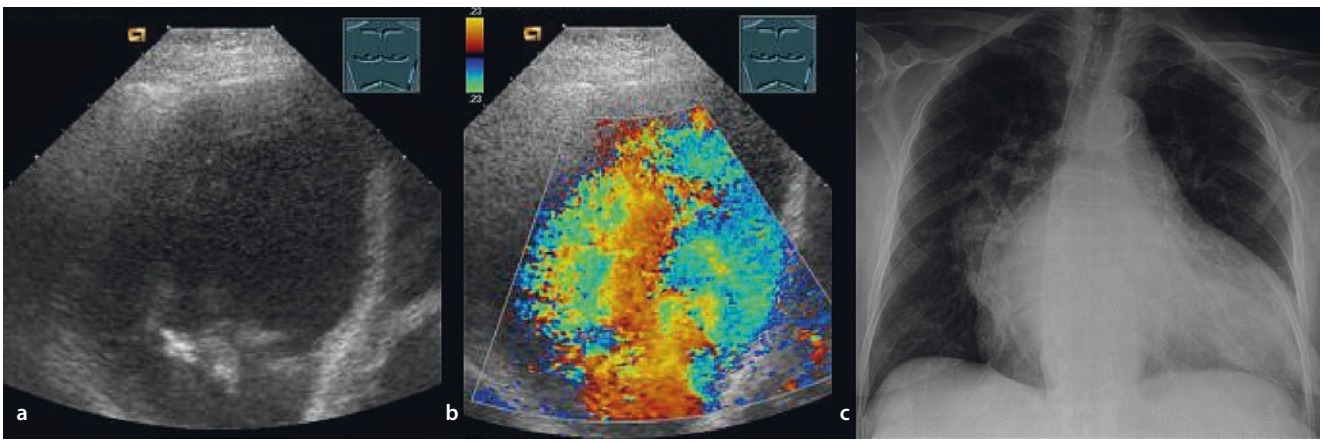

Fig. 8.19 A 78-year-old woman with dyspnea who came for puncture of a pleural effusion. **a** The B-mode image shows an anechoic space-occupying mass in the chest on the left side. **b** Color-Doppler sonography reveals a turbulent flow pattern within this lesion, indicative of the left ventricle being located at the chest wall. **c** The X-ray shows a large heart; the left ventricle is in contact with the lateral chest wall

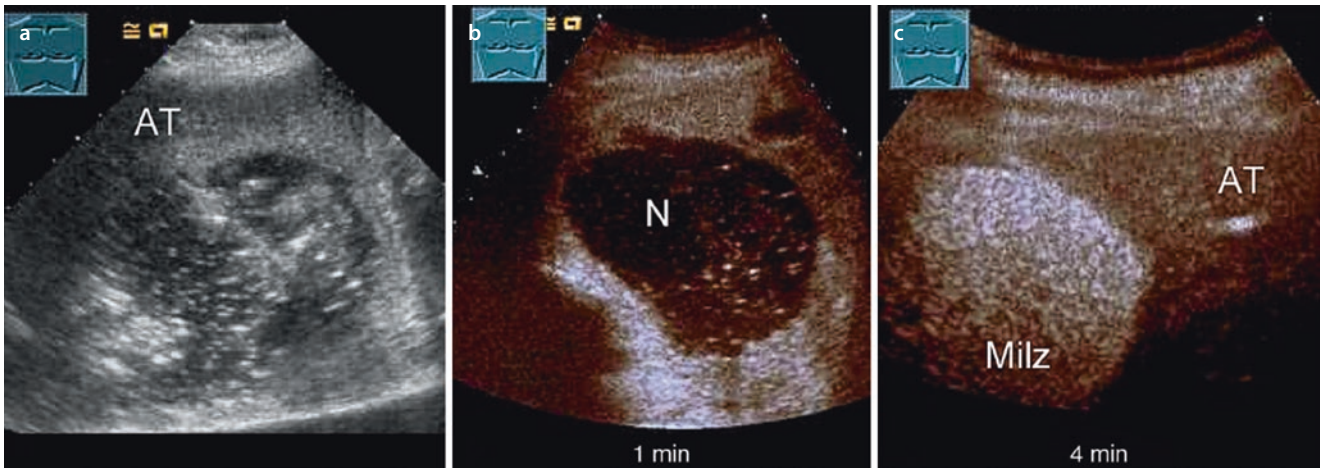

Fig. 8.20 A 54-year-old woman with a non-small-cell bronchial carcinoma. **a** A consolidated lung on the left side, with a central anechoic content with air reflexes. **b** After 1 min the contrast investigation shows no contrast enhancement in the central portion of the consolidated lung, indicative of liquefaction. **c** On the left-sided intercostal section one finds regular contrast enhancement of the spleen. The atelectatic lung tissue of the left lower lobe shows reduced contrast enhancement compared with the spleen

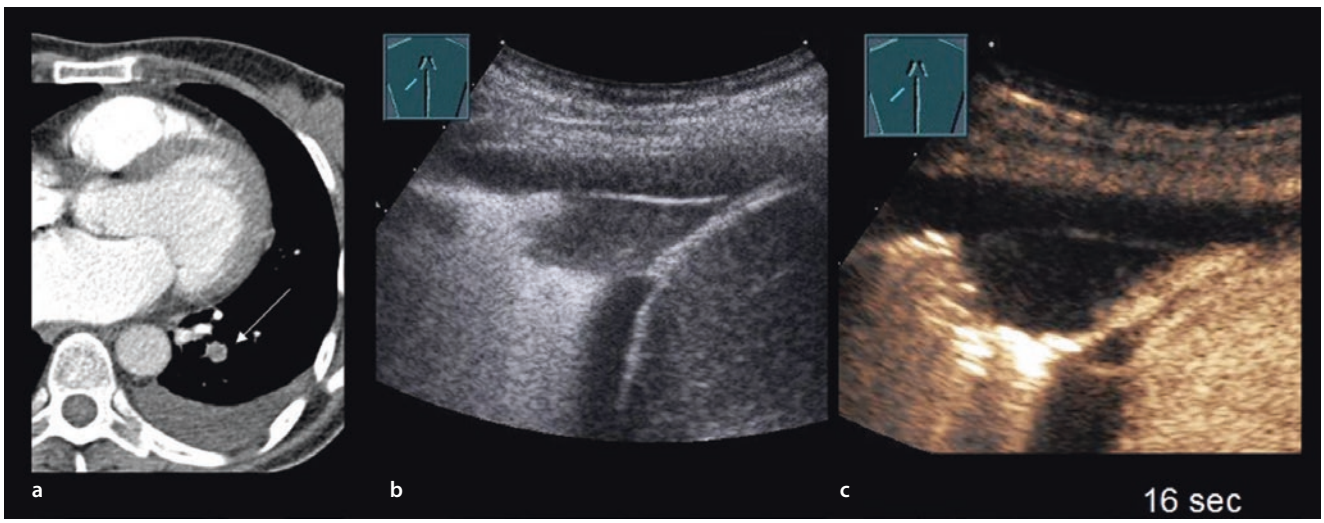

Fig. 8.21 **a** Woman with pulmonary embolism confirmed on computed tomography. **b** B-mode ultrasonography reveals a wedge-shaped, uniformly hypoechoic pulmonary consolidation with smooth margins. **c** The contrasted investigation shows no enhancement of the lesion

8.6 Predominantly Echogenic Lung Consolidation

8.6.1 Lung Infarction

Color-Doppler Sonography

The lung infarction could be a correlate of pulmonary embolism. In the case of peripheral obstruction of branches of the pulmonary arteries and insufficient nourishment from the bronchial arteries the patient may develop intra-alveolar hemorrhage which is visualized morphologically on the B-mode image as displaced air (Mathis and Dirschmid 1993). On qualitative color-Doppler sonography the lesion characteristically shows the absence of flow signals (Fig. 8.3). On semiquantitative spectral analysis one occasionally finds a monophasic pattern close to the pleura; this pattern can be attributed to bronchial arteries. In some cases the disconnected supplying branch of the pulmonary artery is visualized.

Contrast-Assisted Sonography

In keeping with findings on color-Doppler sonography, lung infarctions/lung hemorrhages are marked by the absence of contrast enhancement on contrast-assisted sonography (Fig. 8.21). One Occasionally the marginal portions show delayed and poor contrast enhancement by way of inhomogeneous contrast uptake, which is a sign of vascularization by the bronchial artery (Fig. 8.22). However, it should be noted that in a

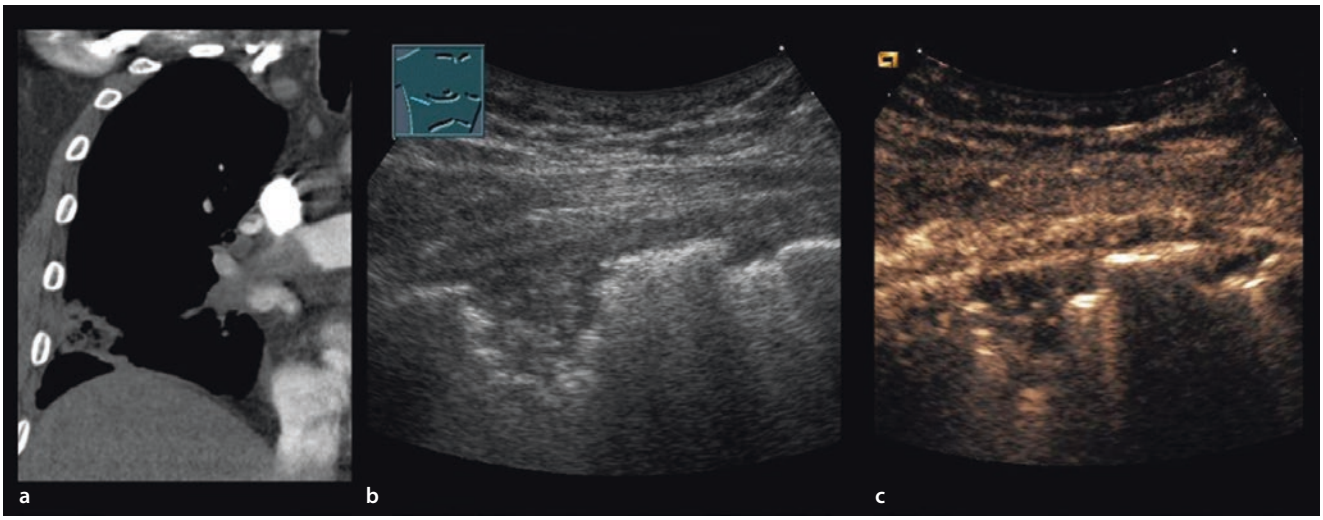

Fig. 8.22 **a** Man with a confirmed central pulmonary embolism and a peripheral consolidation on computed tomography. **b** The B-mode ultrasound image reveals a peripheral hypoechoic consolidation. **c** Contrast-enhanced ultrasound shows inhomogeneous enhancement after 25 seconds

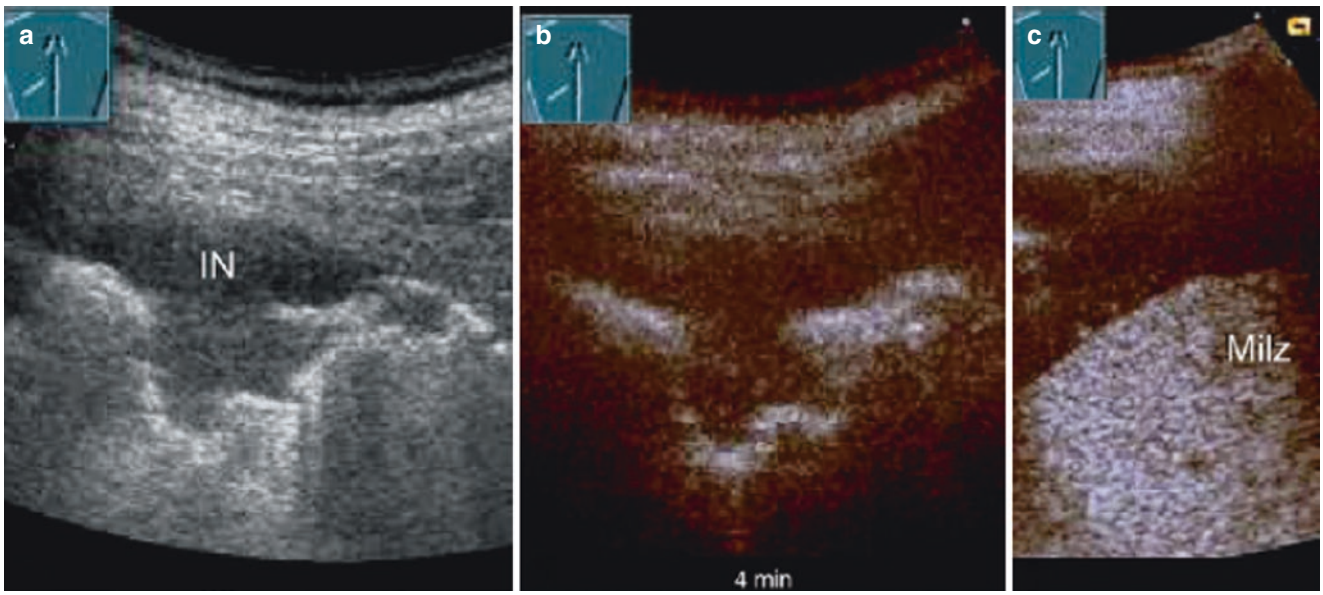

Fig. 8.23 A 55-year-old woman with breath-dependent pain and suspected pleurisy. **a** The B-mode ultrasound image shows a small wedge-shaped pleural defect. **b** Color Doppler reveals vessels within the defect. **c** On spectral curve analysis there is a high-impedance flow signal corresponding to that from a pulmonary artery

small number of patients with pulmonary embolisms on computed tomography, peripheral lesions may also show pure pulmonary artery enhancement on contrast-enhanced ultrasound, which may be sign of previously concluded repair processes.

It should be noted that contrast-assisted sonography allows the investigator to make a reliable distinction between vascularized and nonvascularized peripheral lung tissue and therefore possesses a potential for differential diagnosis in respect of delineating pleurisy or compressive atelectasis due to pleural effusion (Görg et al. 2006a) (Figs. 8.23, 8.24, and 8.25).

8.6.2 Pleurisy

Color-Doppler Sonography

The appearance of pleurisy on the B-mode image is similar to that of a lung infarction (Gehmacher et al. 1997). Depending on the size of the invasion, which is transformed into pleural pneumonia, the qualitative color-Doppler sonography characteristically shows pronounced vessels with predominant evidence of an arterial high-impedance flow profile on spectral analysis such as that seen in branches of the pulmonary artery (Fig. 8.26).

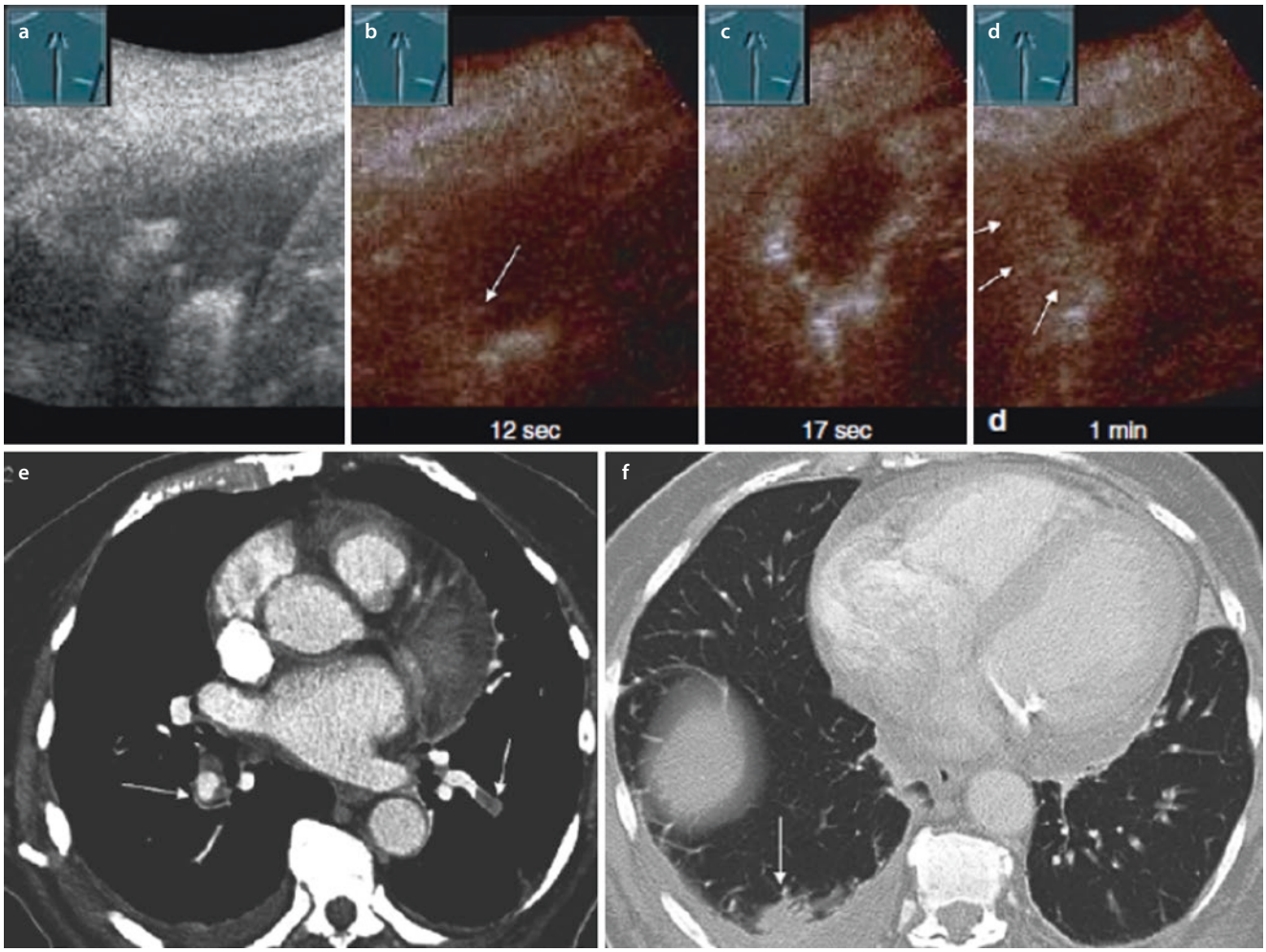

Fig. 8.24 Patient with breath-dependent pain and suspected pleurisy. **a** The B-mode ultrasound image reveals a long, irregular entry echo in the lower lobe of the right lung. **b** Contrast-assisted ultrasonography shows marked pulmonary artery enhancement of the lesion after 4 seconds **c** In the late parenchymal phase the lesion shows homogeneous contrast enhancement

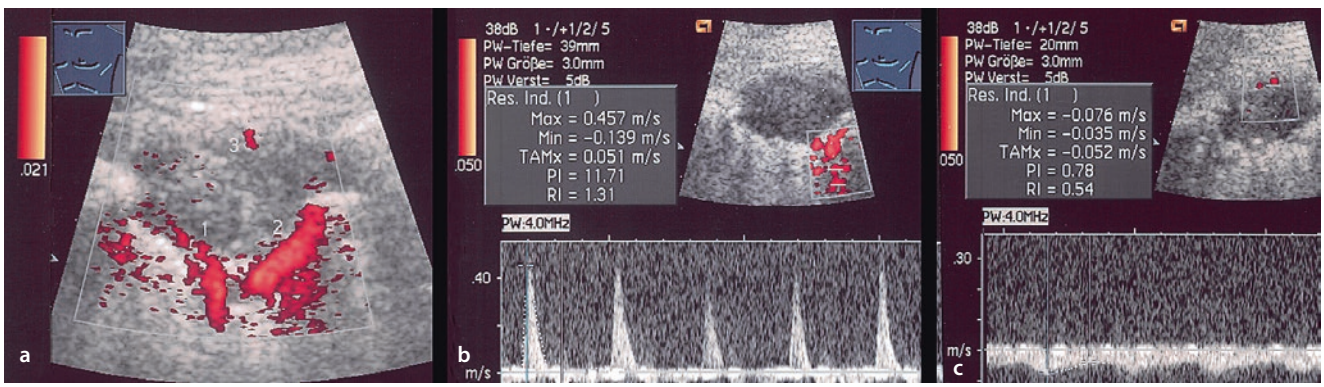

Fig. 8.25 A 56-year-old man with a plasmocytoma and histologically confirmed amyloidosis in the lung. **a** On color-Doppler sonography one finds several vessels. *1* pulmonary artery, *2* pulmonary vein, *3* bronchial artery. **b** Spectral curve analysis shows a high-impedance flow signal indicating a pulmonary artery (marked *1* in **a**). **c** Spectral curve analysis shows a low-impedance monophasic flow pattern oriented toward the hilum of the lung, as a sign of a bronchial artery close to the pleura (marked *3* in **a**)

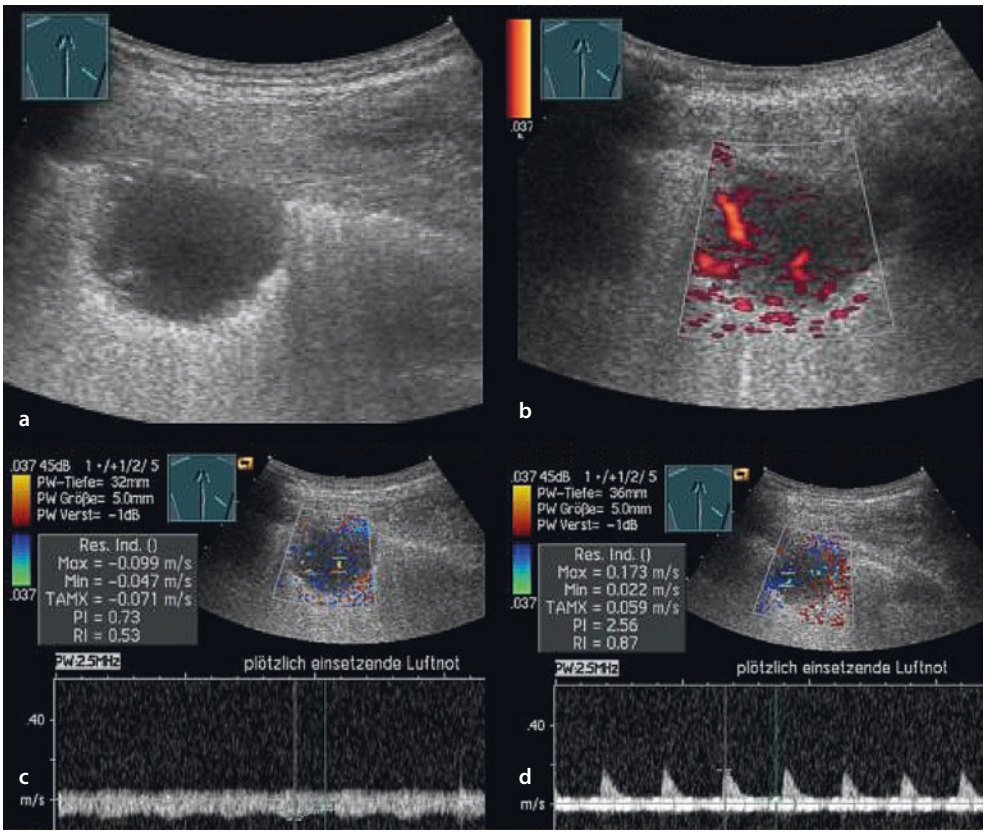

Fig. 8.26 A 30-year-old woman with sudden onset of dyspnea and fever. **a** B-mode sonography shows a peripheral hypoechoic round lesion of the lung. **b** On color-Doppler sonography one finds evident flow signals in the lesion. **c** Spectral curve analysis of a central vessel shows a low-impedance flow signal such as that seen in a bronchial artery. **d** Spectral curve analysis of a vessel from the margin shows a high-impedance flow signal such as that seen in pulmonary arteries. Under antibiotic therapy the lesion resolved completely

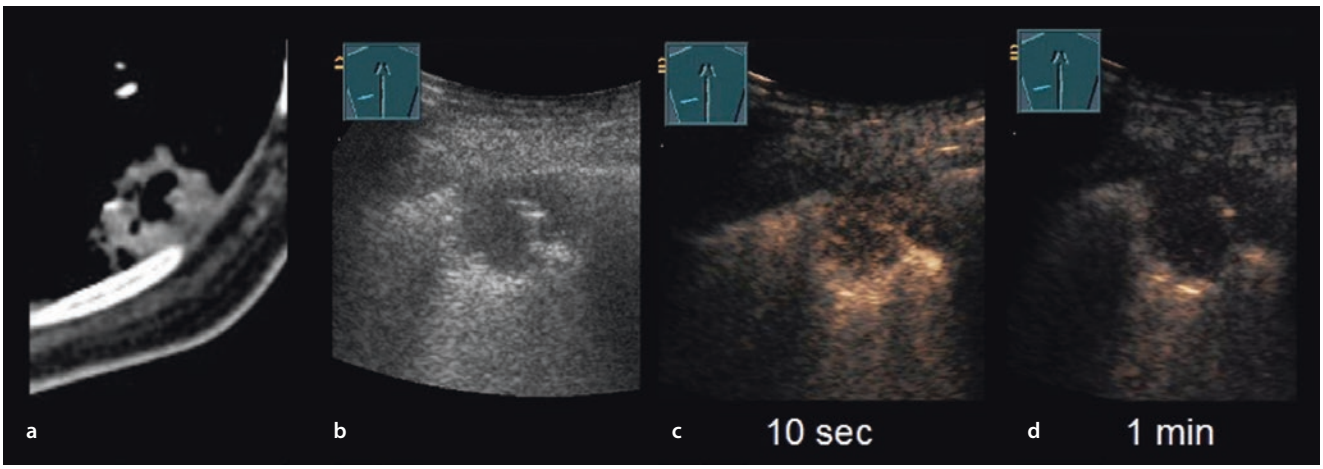

Fig. 8.27 Woman with a pancreatic carcinoma and histologically confirmed pulmonary metastases. **a** CT shows a round lesion with a suspected central consolidation. **b** The B-mode ultrasonography image shows an inhomogeneous hypoechoic lesion of the lung along the pleural margin, with a central air reflex. **c** Contrast-assisted ultrasound reveals reduced bronchial artery enhancement after 10 seconds. **d** In the parenchymal phase, after 1 minute, there is almost no further contrast enhancement in the lesion

Contrast-Assisted Sonography

In keeping with color-Doppler sonography findings, pleurisy takes very little time for contrast enhancement to start and is marked by strong contrast enhancement on contrast-assisted sonography. This is indicative of primary vascularization through pulmonary arteries (Fig. 8.27). The value of contrast-assisted sonography lies in its potential for differential diagnosis of non-vascularized peripheral lung lesions such as lung infarction, malignant lesions or scar tissue when the patient has respiration-related pain as the cardinal clinical symptom (Görg et al. 2005b).

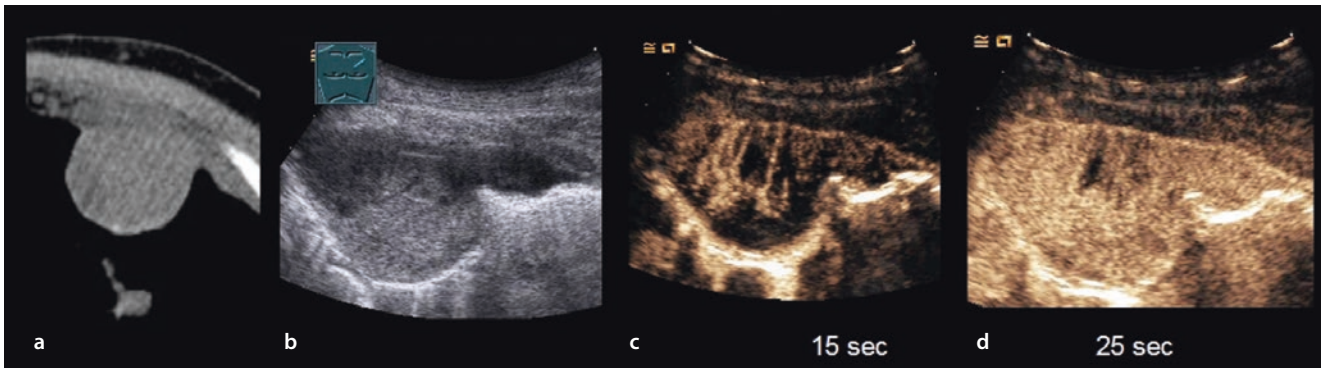

Fig. 8.28 Man with known sarcoma and histologically confirmed multiple lung metastases. **a** CT shows a round lesion along the pleura, **b** B-mode ultrasound reveals an oval, homogeneous, hypoechoic. lesion along the pleural margin. **c** Contrast-assisted ultrasonography shows, after 15 seconds, strong enhancement starting from the periphery, as a sign of peripheral vascularization from the bronchial artery. **d** After 25 seconds there is strong and homogeneous contrast enhancement of the lesion, as a sign of marked tumor angiogenesis

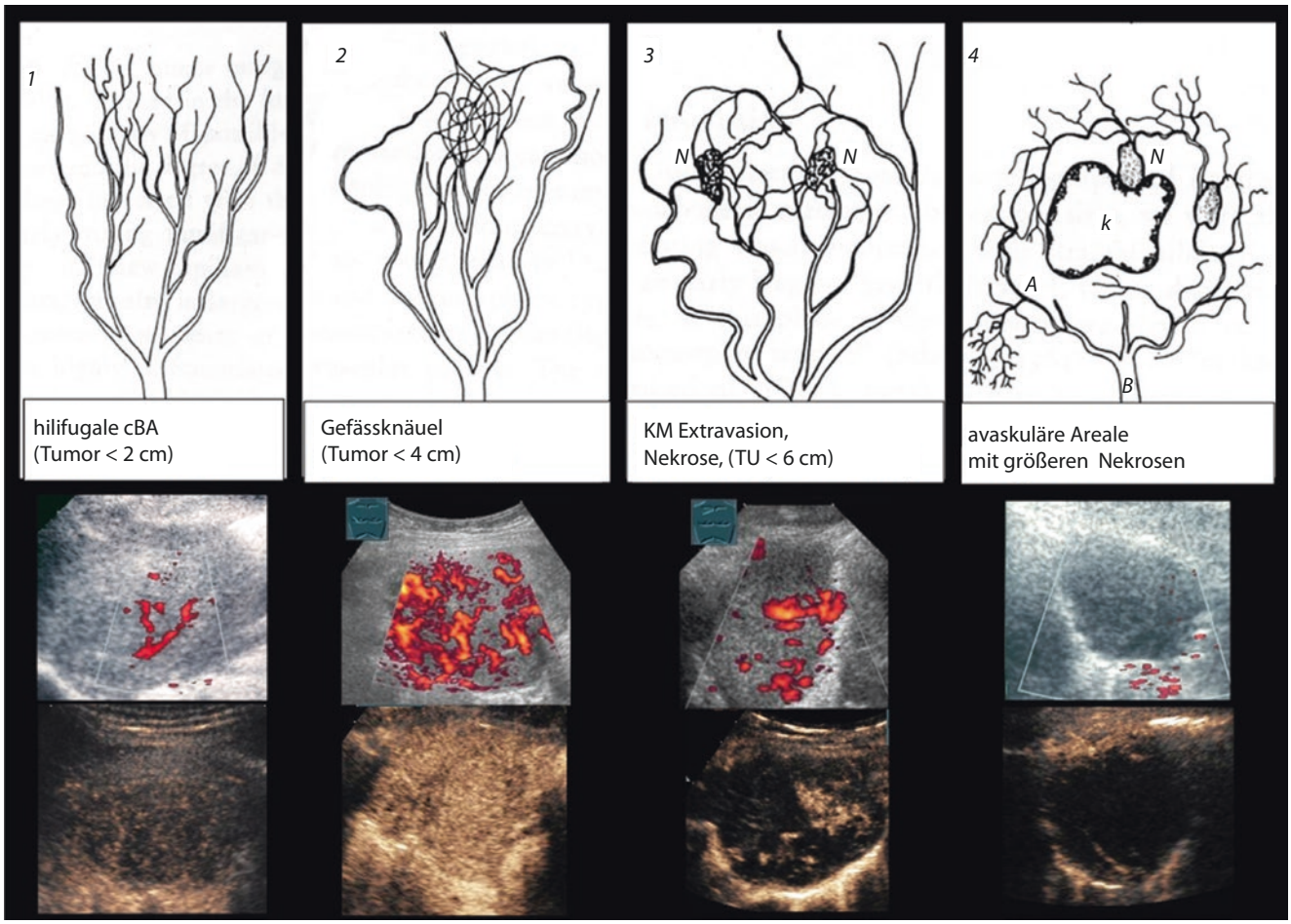

Fig. 8.29 Graphic diagram, color-coded Doppler ultrasound findings and contrast-enhanced ultrasound patterns of tumor vascularization by the bronchial artery to a varying degree, depending on tumor size (according to Müller, 1979)

8.6.3 The Peripheral Round Lesion

Color-Doppler Sonography

A peripheral round lesion of the lung at the wall of the pleura occurring as the cardinal symptom may be due to a benign or malignant lesion. Of decisive importance is the fact that, independent of the cause, the evidence of flow signals is dependent on the size of the lesion. On careful investigation one frequently finds arterial high-impedance flow signals from pulmonary arteries and low-impedance flow signals from bronchial arteries in benign as well as malignant peripheral lung lesions (Figs. 8.28 and 8.29).

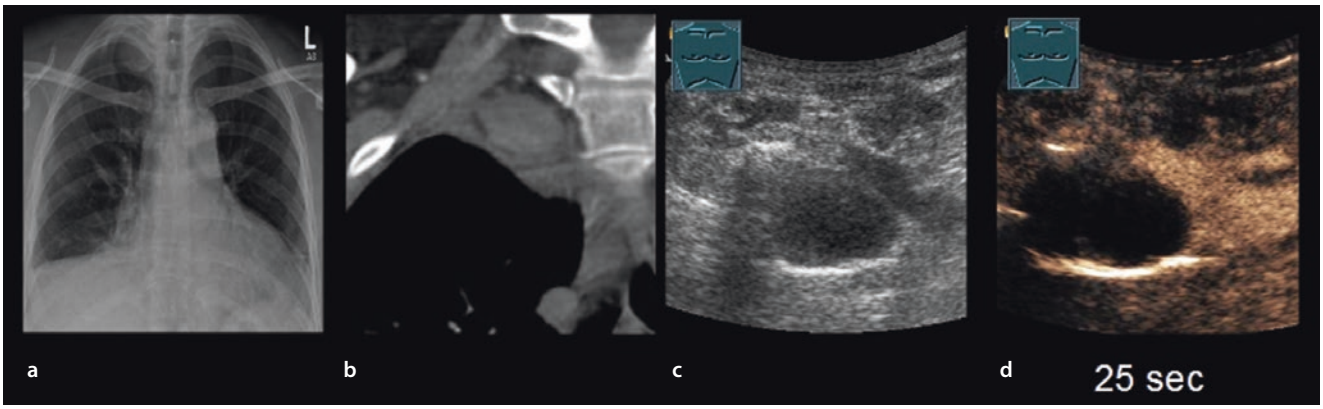

Fig. 8.30 Man with a space-occupying lesion in the right supraclavicular fossa, which is seen on conventional X-ray **a** as well as CT **b**. The patient's medical history mentions the insertion of a central venous access on the right side. **c** B-mode ultrasonography shows that the tumor is hypoechoic. **d** On contrast-enhanced ultrasound the tumor shows no contrast enhancement. Hence it appears to be a hematoma, which was confirmed by the fact that it resolved over time on ultrasound monitoring

Table 8.1 Time to enhancement (short vs. delayed) and extent of enhancement (reduced vs. marked) in 137 patients with pleural-based pulmonary lesions subdivided into patients with pneumonia, compression atelectasis, pulmonary embolism, benign pleural-based lesions, central lung cancer and peripheral malignant lesions

	Pneumonia (*n* = 32)		Compression atelectasis (*n* = 17)		Pulmonary embolism (*n* = 20)		Benign nodules (*n* = 8)		Central lung cancer (*n* = 31)		Peripheral malignant lesion (*n* = 29)	
	Reduced EE	Marked EE	Reduced EE	Marked EE	Reduced EE	Marked EE	Reduced EE	Marked EE	Reduced EE	Marked EE	Reduced EE	Marked EE
Delayed TE	2	4	0	0	20	0	4	2	8	5	18	4
Short TE	6	20	0	17	0	0	1	1	6	12	5	2

After Görg et al. (2006b)
TE time to enhancement, *EE* extent of enhancement

In the published literature, poor visualization of vessels on qualitative color-Doppler sonography and evidence of arterial monophasic flow signals with low resistance indices are reported to be characteristic features of malignant peripheral lung tumors or metastases (Yuan et al. 1994; Hsu et al. 1996, 1998; Civardi et al. 1993). In some cases the vessels seen on sonography may be identified as those resulting from tumor neoangiogenesis (originating from bronchial arteries) on pathological investigation (Hsu et al. 1998; Fig. 8.9d). However, studies that have used a single impedance measurement to assess the benign or malignant nature of a lesion must be viewed with caution. In principle color-Doppler sonography is not suitable for distinguishing between benign and malignant peripheral round lesions.

Contrast-Assisted Sonography

In keeping with the variable findings on color-Doppler sonography, contrast-assisted sonography also shows a heterogeneous pattern of vascularization. Malignant lesions—whether lung metastases or peripheral bronchial carcinomas—are marked by delayed start of contrast enhancement and reduced extent of contrast enhancement. This is indicative of predominant vascularization through bronchial arteries (Fig. 8.30, Table 8.1). Depending on the underlying structure, however, lung metastases of renal cell carcinomas and frequently also metastases of malignant lymphoma show pronounced contrast enhancement, as Sign of strong tumor angiogenesis (Fig. 8.31). The extent and homogeneity of tumor angiogenesis depend, among other factors, on tumor size (Fig. 8.32). In some cases contrast-enhanced ultrasound is useful to assess the malignant or benign nature of the lesion (Fig. 8.33). The traditional stumbling block is the bronchoalveolar carcinoma, which shows a typical pattern of "pneumonia" on the B-mode image, color Doppler ultrasound, as well as contrast-enhanced ultrasound.

Contrast-assisted sonography, like color-Doppler sonography, is not suitable for distinguishing between benign and malignant peripheral round lesions.

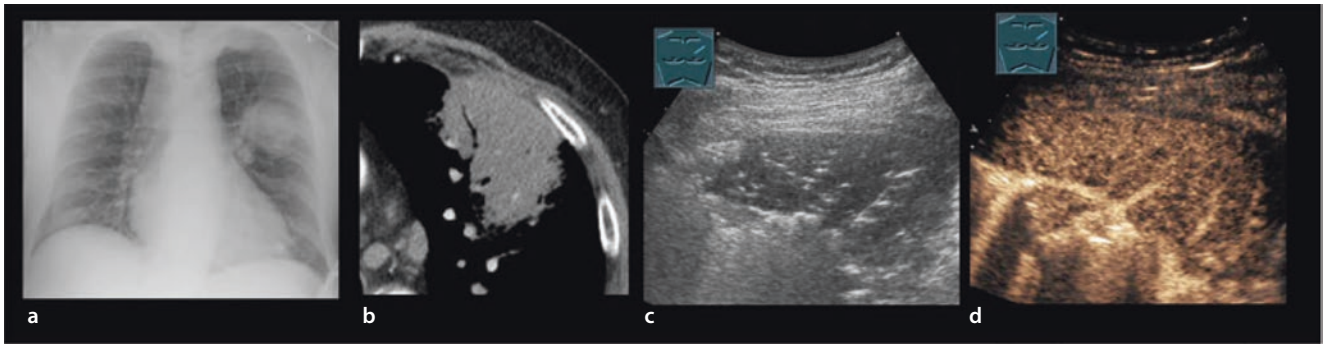

Fig. 8.31 Man with dyspnea, no fever, and a space-occupying lesion in the right middle lobe of the lung, which is seen on the conventional X-ray (**a**) and on CT (**b**) as typical pneumonia **c** B-mode ultrasound shows a hypoechoic consolidation with an air bronchogram, as in pneumonia. **d** On contrast-enhanced ultrasound the tumor shows marked and homogeneous contrast enhancement in the early arterial phase, as in pneumonia. The US-guided punch biopsy confirmed the presence of a bronchioloalveolar carcinoma

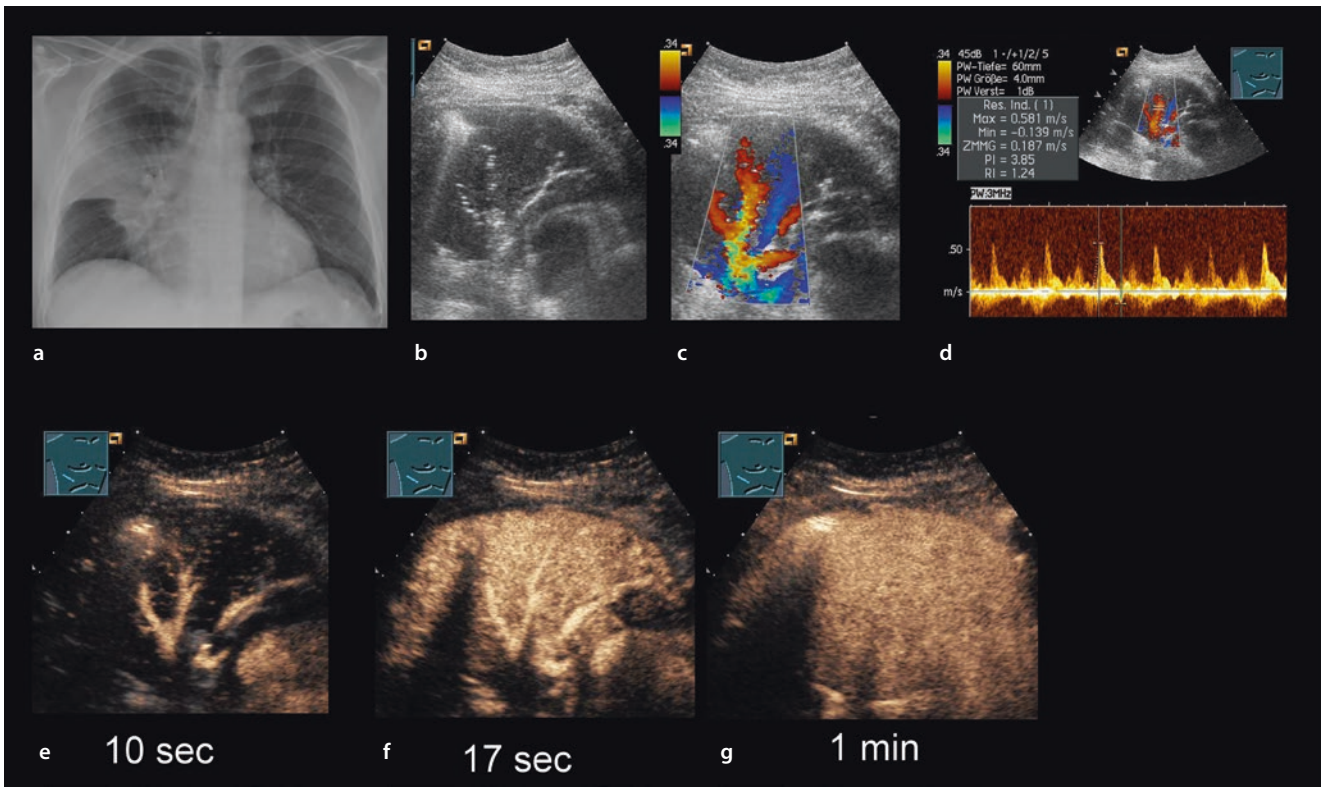

Fig. 8.32 **a** Man with pneumonia established by clinical and radiological investigation. **b** The B-mode ultrasound image reveals a typical widespread consolidation with a positive air bronchogram characteristic of pneumonia. **c** Color Doppler ultrasound clearly shows vessels arranged in orderly fashion. **d** On spectral curve analysis the arterial centrifugal vessels show a high-impedance flow signal similar to that of pulmonary arteries. **e–g** Contrast-enhanced ultrasound reveals, in the early arterial phase, the vascular tree of the pulmonary artery with strong and homogeneous contrast enhancement

8.6.4 Large Lung Consolidation: Pneumonia

Color-Doppler Sonography

Pneumonia is seen on X-rays and sonography in conjunction with the principal finding of a peripheral lung consolidation at the pleural wall. On B-mode image sonography, pneumonia is seen as a more or less pronounced air bronchogram (Gehmacher et al. 1995), while a complete consolidation is seen as so-called lung hepatization. On color-Doppler sonography, pneumonia is marked by significantly ramified vessels that correspond to segmental branches of the pulmonary artery (Fig. 8.34). Here also,

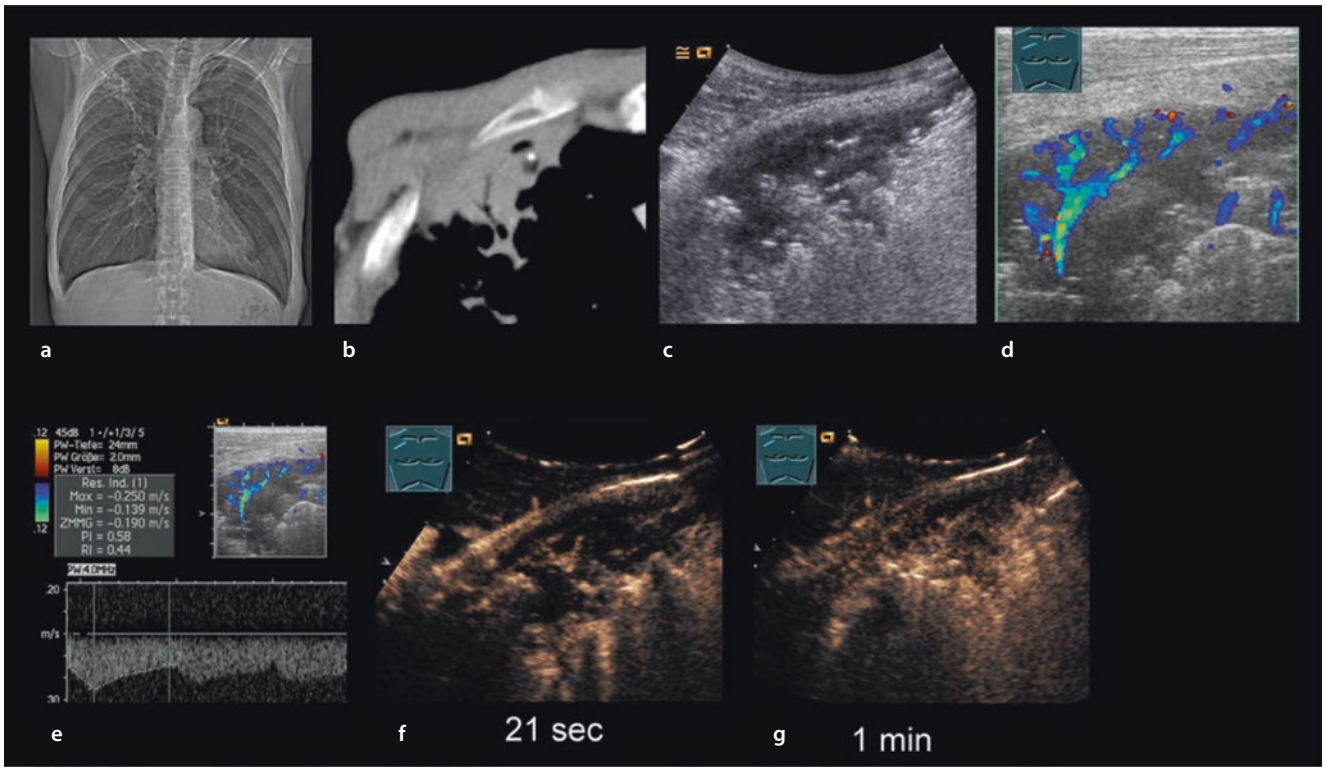

Fig. 8.33 **a** Man with chronic therapy-resistant pneumonia and an infiltrate in the apex, confirmed on radiographs; suspected tuberculosis. **b** The infiltrate and a mild consolidation are confirmed on CT. **c** B-mode ultrasonography shows a hypoechoic consolidation with standing air reflexes. **d** Color Doppler ultrasonography reveals vessels extending to the center from the surface of the lung. **e** With the aid of spectral curve analysis, the vessels can be identified as bronchial arteries by their low-impedance flow signal. **f–g** On contrast-enhanced ultrasound the lesion shows delayed bronchial artery enhancement with reduced and inhomogeneous contrast enhancement. The punch biopsy yielded the diagnosis of chronic carnifying pneumonia with marked fibrosis and no sign of tuberculosis

owing to hypoxia one frequently finds an arterial monophasic flow signal of central bronchial arteries in the invaded lung tissue (Fig. 8.35). In principle it should be noted that certain subtypes of adenocarcinoma may appear similar to pneumonia on the B-mode image and on color-Doppler sonography as well (Görg et al. 2002). Depending on the extent of hypoxic vasoconstriction in the pulmonary artery, the peripheral vascular tree of pulmonary arteries may not be visualized on qualitative color-Doppler sonography in the presence of advanced pneumonia. Bronchial arteries react to hypoxia by developing vasodilatation, as do all other arteries in the body. This explains the different resistance indices of pneumonia and atelectasis (Yuan et al. 2000). Thus, in the presence of lobar pneumonia parallel to the pulmonary arteries one occasionally finds an arterial monophasic flow pattern with low resistance indices, indicative of central bronchial arteries. The tuberculous infiltrate is a special phenomenon. It is characterized by marked vessels on color-Doppler sonography in terms of qualitative findings. On spectral analysis, however, it is seen as a monophasic curve, corresponding to bronchial arteries (Fig. 8.36). Cavitary lesions such as tuberculosis, liquefactions, necrosis, abscesses and pseudocysts are characterized by the presence of predominant vascularization through the bronchial artery in the marginal areas around the lesion.8.

Contrast-Assisted Sonography

In keeping with the findings on color-Doppler sonography, classic pneumonia is characterized by a short period until the start of contrast enhancement and strong contrast enhancement on contrast-assisted sonography. This is indicative of predominant vascularization though pulmonary arteries (Fig. 8.30). Reduced contrast enhancement is observed in cases of lobar pneumonia and can be explained by hypoxic vasoconstriction of the pulmonary artery (Fig. 8.31; Table 8.1). Delayed contrast enhancement indicates vascularization by the bronchial artery and is observed in cases of liquefaction and chronic pneumonia (Fig. 8.32). Such avascular areas in the region of pneumonia can be clearly demarcated on contrast-assisted sonography.

Inhomogeneous contrast enhancement is helpful in identifying typical courses of disease with evidence of consolidation, necrosis, infarct areas, inward bleeding, or abscesses. Especially in parapneumonic echogenic effusions with multiple septa and a suspected pleural empyema, the area can be clearly demarcated from the infiltrated lung (Fig. 8.37a).

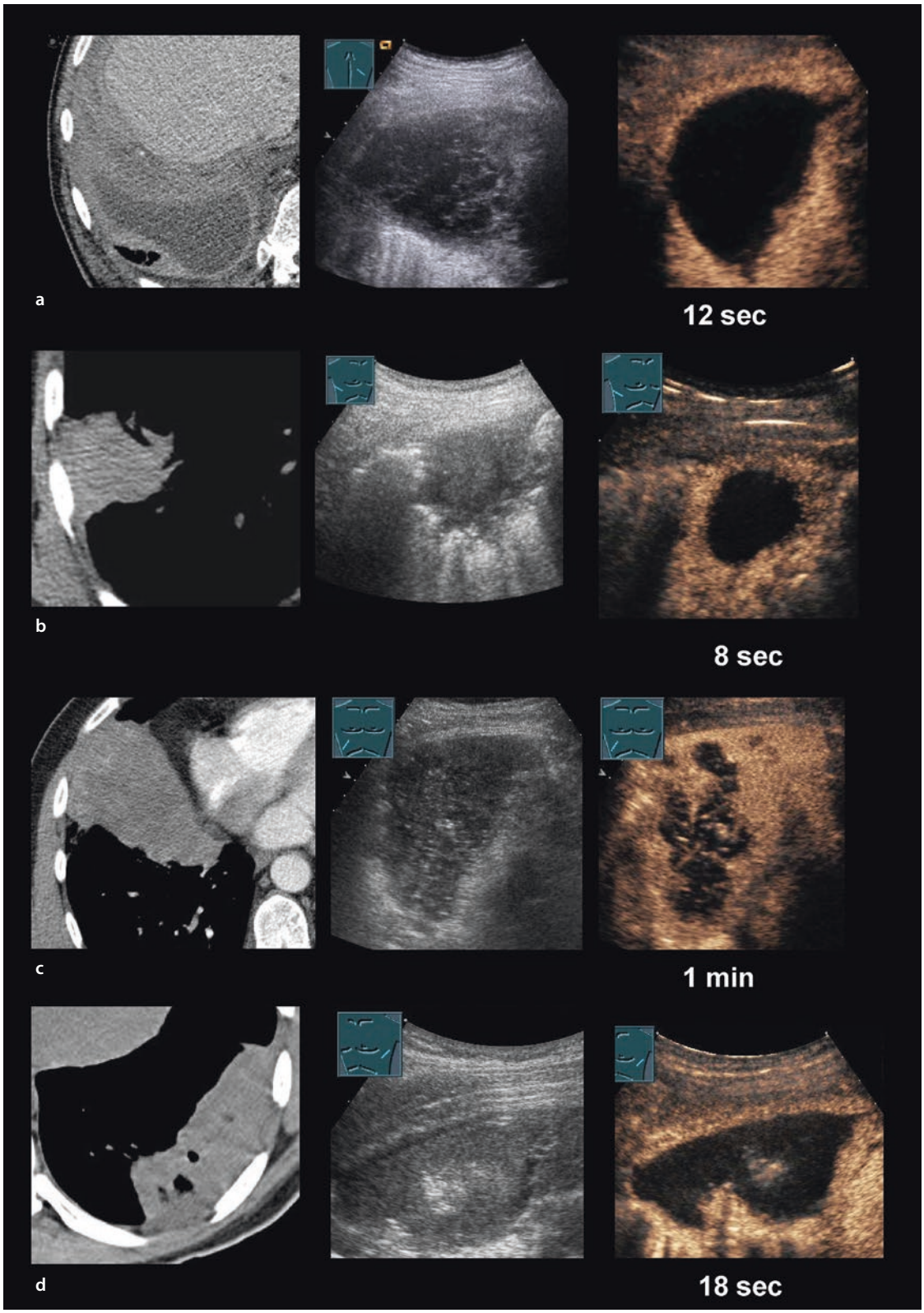

Fig. 8.34 Images (CT, B-mode image, and contrast-enhanced ultrasound) of patients with atypical courses of pneumonia. **a** Man with pneumonia and suspected parapneumonic empyema: contrast-enhanced ultrasound reveals the sharp demarcation of the empyema from the infiltration. **b** Man with AML, after pulmonary aspergillosis: contrast-enhanced ultrasound clearly shows a non-contrast-absorbing central region by way of necrosis. Resection of the infiltrate was performed prior to the planned bone marrow transplantation. **c** A fire-eater who had aspirated paraffinated hydrocarbon: contrast-enhanced ultrasound clearly shows the central necrosis in the infiltrated lung. **d** Man with ALL and a residual pneumonic infiltrate prior to bone marrow transplantation (BMT): contrast-enhanced ultrasound establishes the diagnosis of pulmonary infarction. BMT is performed subsequently

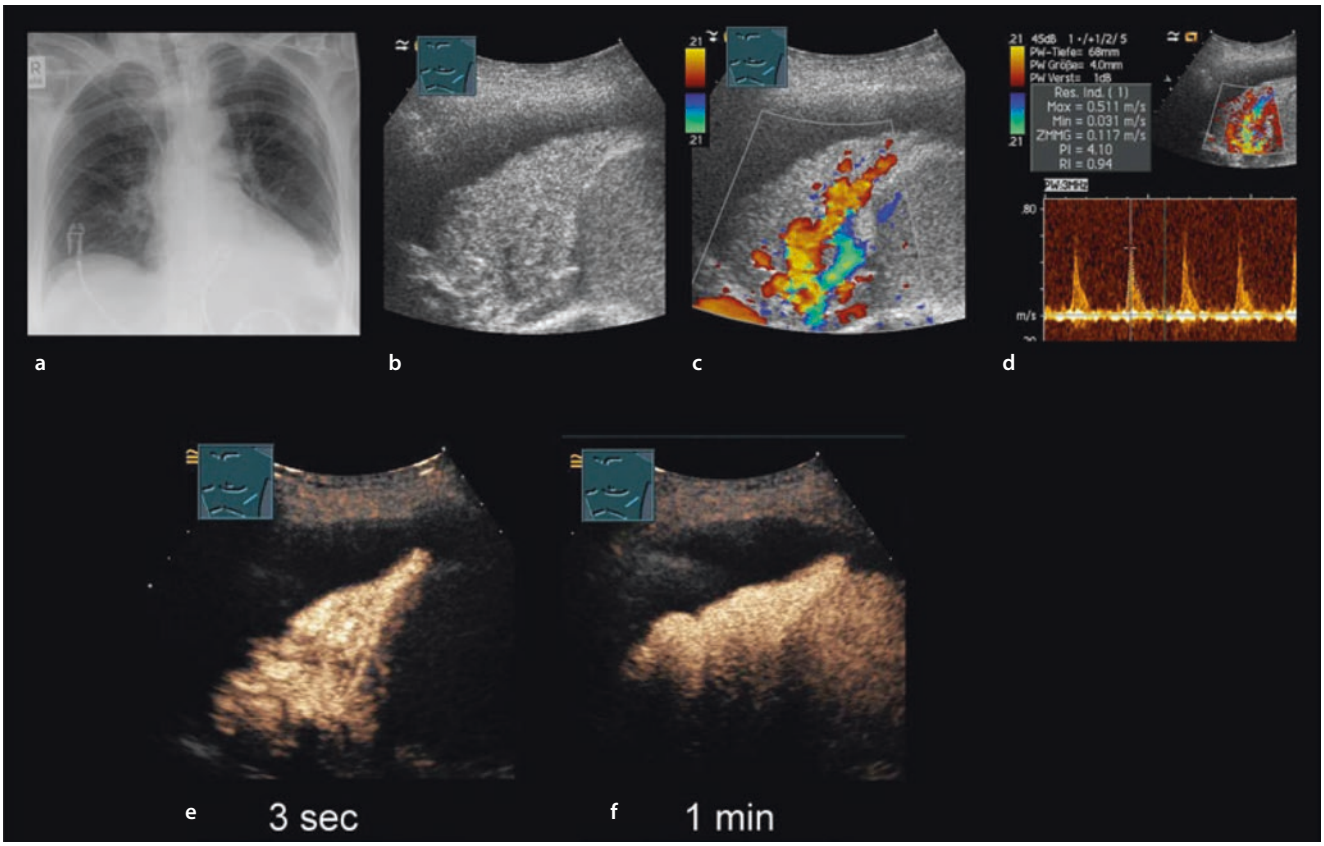

Fig. 8.35 **a** Man with a left-sided pleural effusion on the chest X-ray. **b** The B-mode image shows a homogeneous consolidation as in the presence of atelectasis. c Color Doppler ultrasound reveals specifically directed and pronounced vessels. **d** On spectral curve analysis the arterial centrifugal vessels show a high-impedance flow signal corresponding to that of pulmonary arteries. **e–g** Contrast-enhanced ultrasound, in the early arterial phase, shows the vascular tree of the pulmonary artery with marked and homogeneous contrast enhancement characteristic of atelectasis

Large Lung Consolidation: Compressive Atelectasis

Color-Doppler Sonography

Compressive atelectasis is seen on radiographs and sonography in conjunction with the cardinal finding of a peripheral basal lung consolidation at the pleural wall. The main finding is a pleural effusion, followed by the visualization of compressed lung tissue. On qualitative color-Doppler sonography atelectasis is seen as a strongly ramified vessel. On arterial spectral analysis one usually finds a high-impedance flow signal indicative of pulmonary arteries (Fig. 8.38).

Contrast-Assisted Sonography

In concurrence with color-Doppler sonography findings, compressive atelectasis is characterized by a brief period until the start of contrast enhancement and strong contrast enhancement on contrast-assisted sonography (Figs. 8.39 and 8.38). This is indicative of vascularization exclusively through the pulmonary arteries. The contrast-assisted sonography pattern of compressive atelectasis is very specific (Table 8.1). Round lesions in atelectatic lung tissue are marked by poor contrast enhancement (Fig. 8.40).

8.6.5 Large Lung Consolidation: Obstructive Atelectasis

Color-Doppler Sonography

The obstructive lung atelectasis is seen as a largely homogeneous hypoechoic transformation on the B-mode image. Depending on the duration of the obstruction, evidence of a "fluid bronchogram" is a characteristic feature in this setting. On qualitative color-Doppler sonography one finds pronounced vessels with evidence of an arterial high-impedance flow signal due to the branches of the pulmonary artery. Here also one finds an arterial monophasic flow profile of central bronchial arteries in atelectatic tissue as a result of hypoxia (Fig. 8.41). A frequent finding is the central tumor underlying the atelectasis, in which the con-

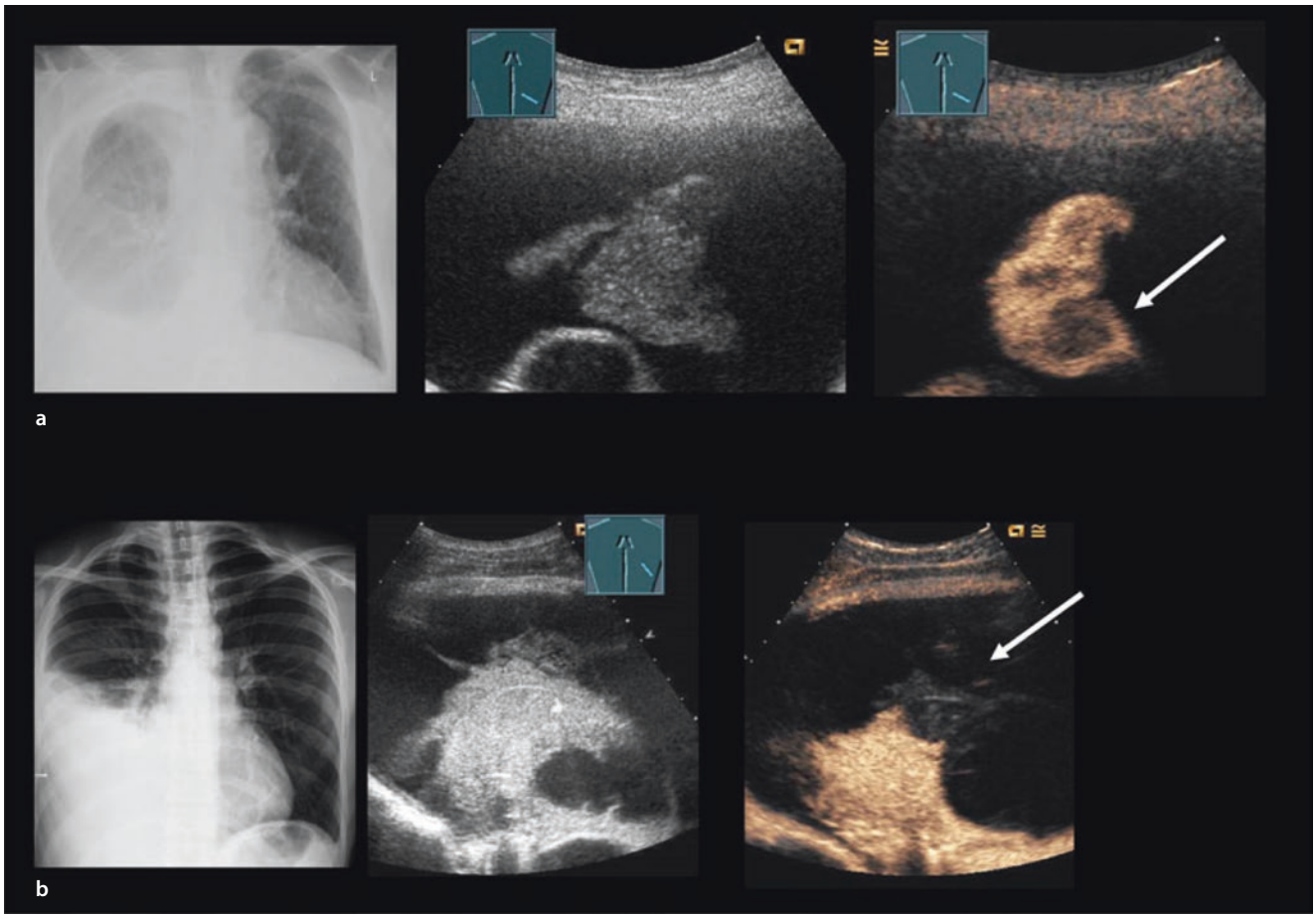

Fig. 8.36 Images (chest X-ray, B-mode ultrasound, und contrast-enhanced ultrasound) of patients with focal lesions in an atelectatic lung **a** Man with known breast carcinoma and a large pleural effusion; on contrast-enhanced ultrasound one finds several round lesions (arrow) in the atelectasis, as in metastases. **b** Man with deep vein thrombosis in his medical history and a large pleural effusion with multiple septa: contrast-enhanced ultrasound reveals a marginal zone without enhancement (*arrow*) in the atelectatic tissue, as in the presence of a pulmonary infarction

solidated atelectatic lung tissue serves more or less as an "acoustic window" to explore central lung structures (Fig. 8.42). According to Fissler-Eickhoff and Müller (1994), invasion and infiltration of the pulmonary arteries located in the region of the tumor occurs in 96 % of the cases of bronchial carcinoma investigated. This disturbed vascular architecture of the pulmonary artery is seen on sonography as reduced or no visualization of vessels in atelectatic lung tissue.

Contrast-Assisted Sonography

In keeping with the color-Doppler sonography findings, a recent obstructive atelectasis is marked by the same features as compressive atelectasis—a short period of time until contrast enhancement and strong contrast enhancement on contrast-assisted sonography. This is indicative of atelectatic lung tissue being entirely vascularized by the pulmonary arteries (Fig. 8.41). In this phase, in patients with a central tumor formation, the tumor may be demarcated from atelectatic lung tissue more clearly by contrast-assisted sonography than by B-mode sonography (Fig. 8.43). In cases of obstruction of longer duration, within the atelectasis one may find liquefactions and abscesses (Fig. 8.44). These potential lesions as well as metastases in atelectatic lung tissue can be reliably diagnosed by contrast-assisted sonography (Fig. 8.45). In the course of a tumor-related obstructive atelectasis, depending on the structure of the tumor there may be infiltration and occlusion of pulmonary arteries. In this situation contrast-assisted sonography shows delayed start of contrast enhancement and reduced contrast enhancement (Fig. 8.45). This is indicative of a switch to vascularization of atelectatic lung tissue by bronchial arteries (Görg et al. 2006a). In

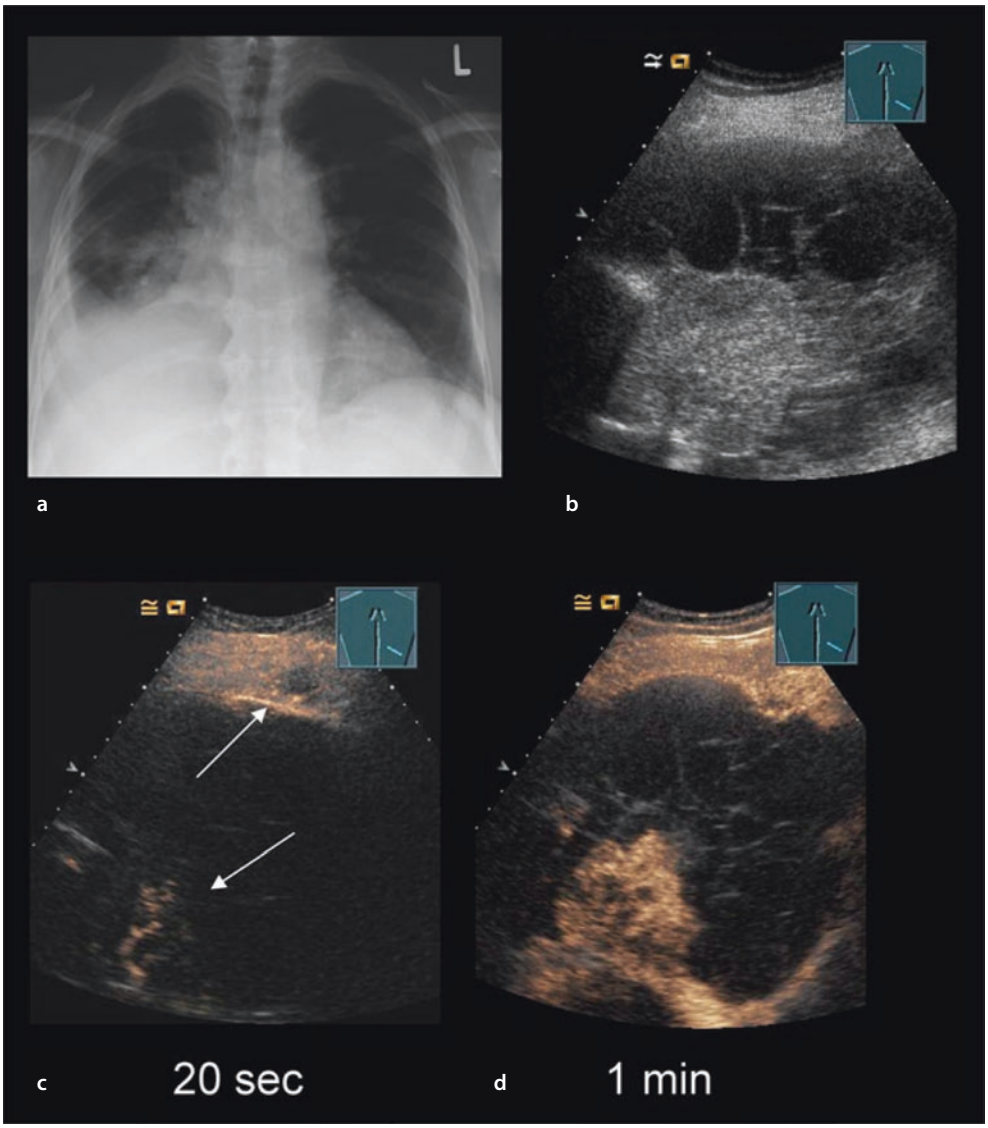

Fig. 8.37 **a** Man with NSCLC in his medical history, after undergoing chemoradiotherapy, now with a right-sided pleural effusion on the chest X-ray. **b** The B-mode image shows a homogeneous consolidation of the lung as in the presence of atelectasis. **c** After 20 seconds contrast-enhanced ultrasound shows systemic vessels in the atelectasis (arrow) and simultaneously in the chest wall (arrow), as a sign of central nutritive vascularization of the atelectasis through the bronchial artery. **d** After 1 minute the atelectasis shows homogeneous contrast enhancement, possibly as a sign of tumor angiogenesis

general the contrast-assisted sonography pattern in cases of obstructive atelectasis is heterogeneous (Table 8.1).

The pattern of compression atelectasis on contrast-enhanced ultrasonography is very specific. In atelectatic lung tissue, round lesions indicative of lung metastases (Fig. 8.43a), and wedge-shaped peripheral defects as a sign of infarctions (Fig. 8.43b), reveal poor or no contrast enhancement. In cases of chronic compression atelectasis, pulmonary artery vascularization may be transformed into purely nutritive bronchial artery vascularization (Fig. 8.44). Contrast-enhanced ultrasound can be very valuable in clarifying the etiology of a pleural effusion. An echogenic effusion with multiple septa can be clearly distinguished from tumor tissue (Fig. 8.45), and tumor tissue along the pleura (Fig. 8.46a) from a hematoma or fibrinous tissue (Fig. 8.46b).

8.6.6 Space-Occupying Lesion of the Chest Wall

- **Color-Doppler Sonography**

Sonography is the method of choice to explore the chest wall. The intercostal arteries supplying the chest wall are

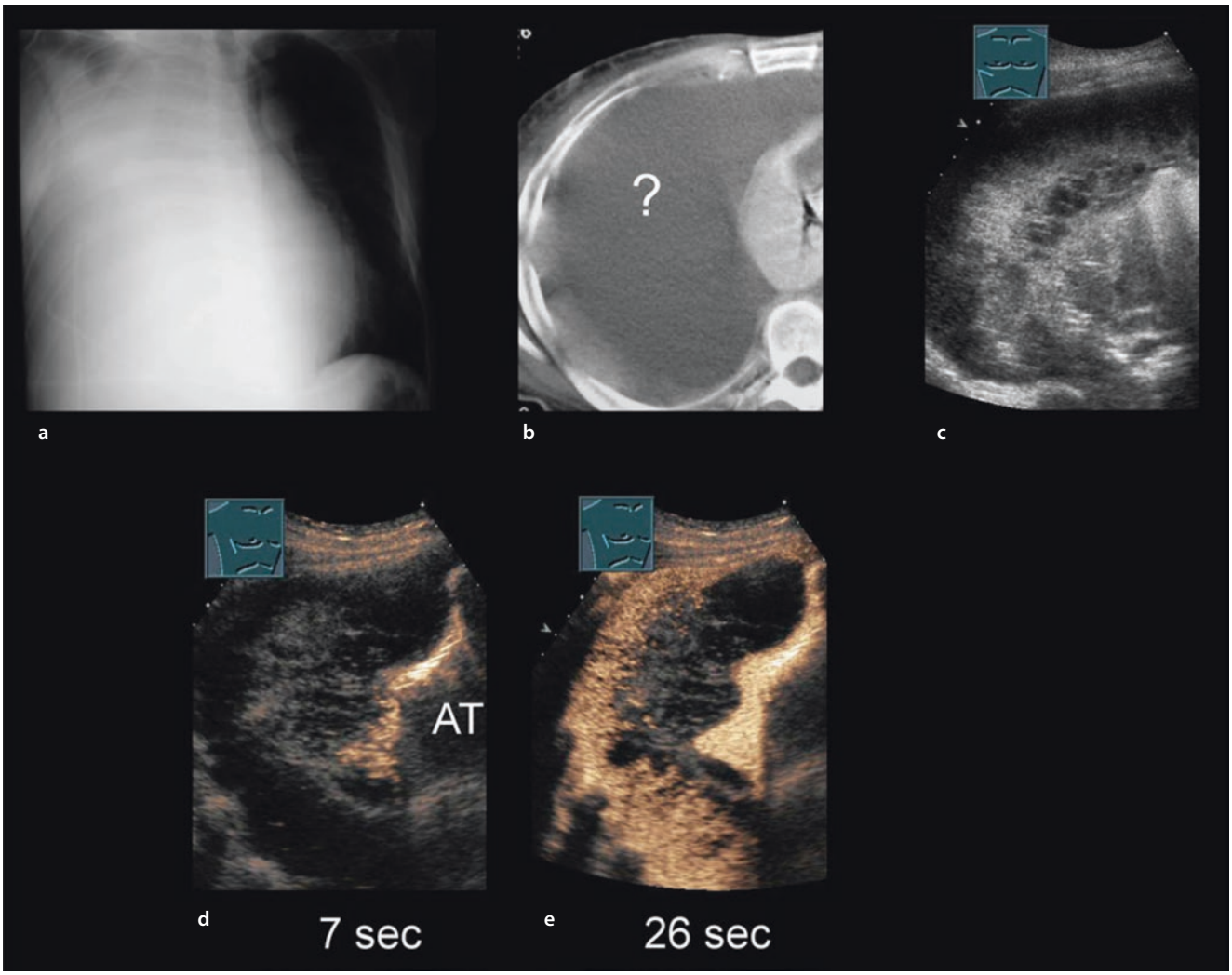

Fig. 8.38 Man with a known malignant melanoma. **a** The chest X-ray shows complete shadowing of the right half of the chest. **b** Solid portions cannot be clearly reliably identified in the effusion on CT. **c** The B-mode image shows a hemithorax with multiple septa. **d** Contrast-assisted ultrasonography reveals enhancement of the central atelectasis (AT) after 7 seconds. **e** Strong contrast enhancement after 26 seconds, starting from the periphery, as a sign of peripheral vascularization from the bronchial artery. Just a small part of the chest cavity shows an effusion with multiple septa.

usually seen even in healthy individuals by the use of color-Doppler sonography (Fig. 8.47). Tumors in the chest wall or pleural metastases are characterized by predominantly intercostal vascularization with a monophasic flow profile when the lesions are adherent to the chest wall (Fig. 8.48). When the tumor has invaded the lung, color-Doppler sonography may show different flow signals as a sign of complex arterial tumor vascularization (Görg et al. 2005a; Fig. 8.49).

Contrast-Assisted Sonography

Specific studies to assess the value of contrast-assisted sonography in cases of space-occupying lesions of the chest wall are not available. Intercostal arteries are strong vessels. On contrast-assisted sonography, intercostal arteries are marked by delayed start of contrast enhancement. The extent of contrast enhancement of the arterial phase may vary. Tumors with pronounced neovascularization reveal strong contrast enhancement (Fig. 8.50). Contrast-enhanced ultrasound is very important for the delineation of non-vascularized lesions such as hematomas or abscesses.

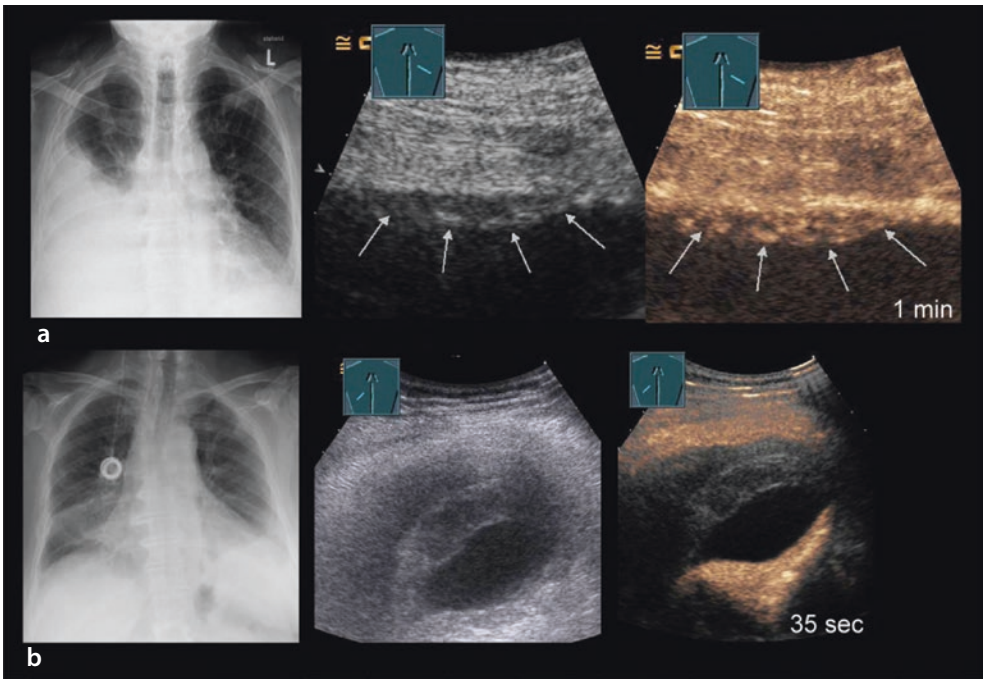

Fig. 8.39 Images (chest X-ray, B-mode image, and contrast-enhanced ultrasound) of patients with pleural effusions and tumor formations in the effusion. a Man with known bronchial carcinoma and a large pleural effusion: on the B-mode image the parietal pleura shows solid tissue over a large surface, with enhancement on the contrasted ultrasound investigation; a punch biopsy yielded the diagnosis of pleural carcinosis. b Woman with known breast carcinoma, after several pleural aspirations. The B-mode image shows echogenic space-occupying lesions in the pleural effusion. Contrast-enhanced ultrasound reveals no enhancement of the space-occupying lesions, as in the presence of a fibrin body or a blood clot

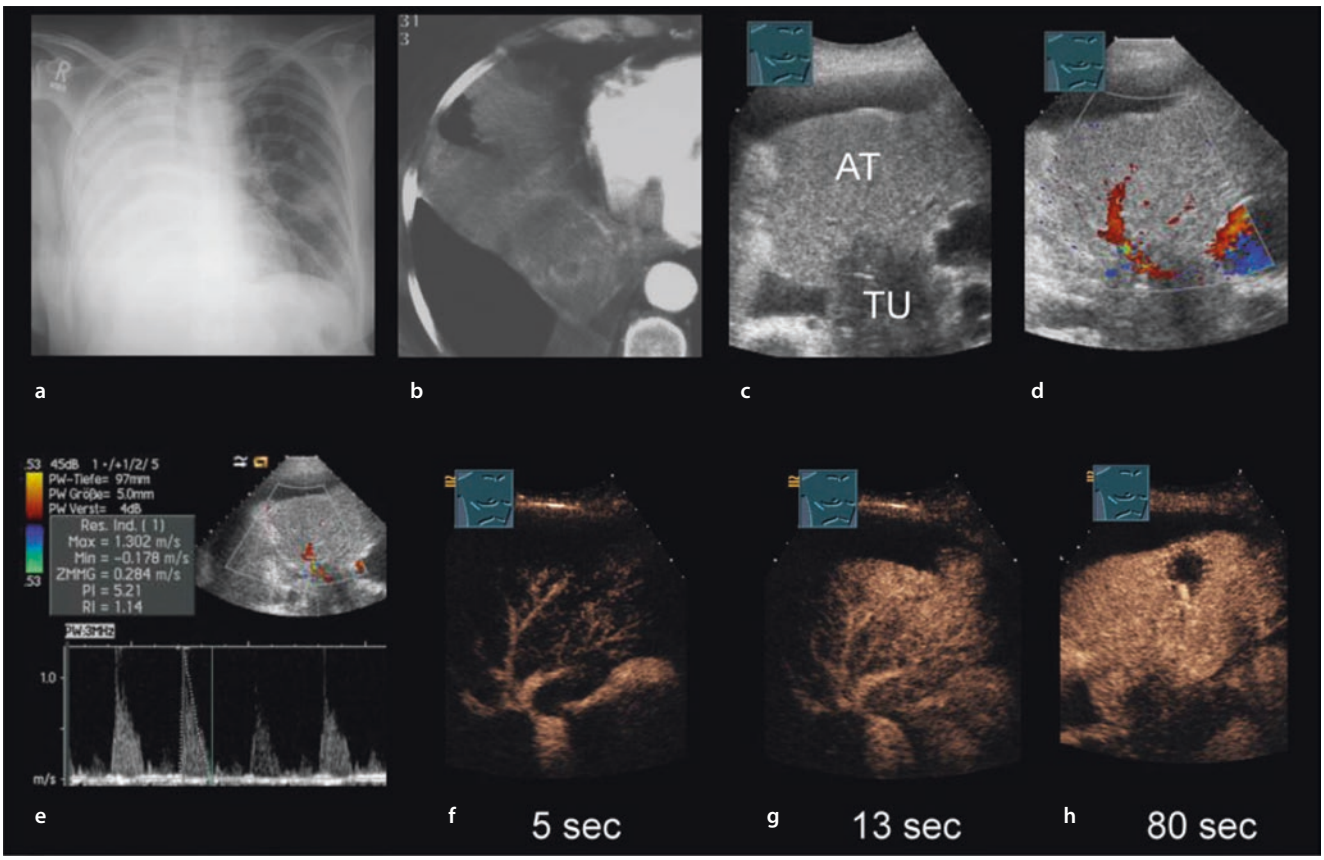

Fig. 8.40 Man with bronchial carcinoma. **a** The chest X-rays shows complete shadowing of the right half of the chest. **b** CT reveals a narrow effusion and a space-occupying lesion in the right-sided upper lobe. **c** B-mode ultrasonography shows atelectasis (AT) and an underlying central tumor formation (TU). **d** Color Doppler ultrasound reveals a large centrifugal vessel. **e** On spectral curve analysis the vessel shows a high-impedance arterial flow signal corresponding to that of the pulmonary artery. **f** On contrast-enhanced ultrasound, the vascular tree of the pulmonary artery is seen after 5 seconds. **g** Contrast enhancement of the AT after 13 seconds. **h** In the parenchymal phase there is a wash-out in the area of the central tumor formation; a focal parenchymal lesion is also seen (DD consolidation, abscess, metastasis)

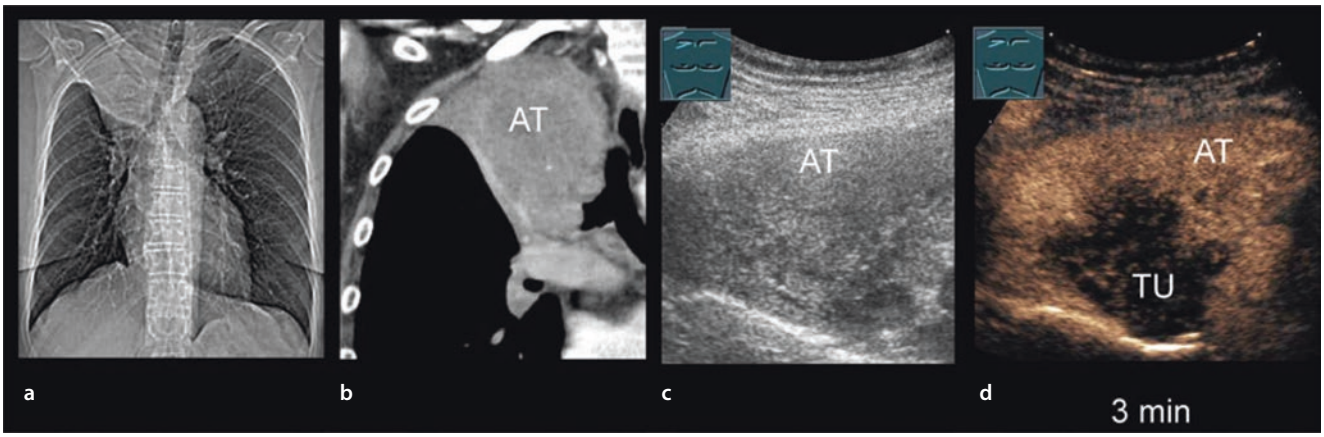

Fig. 8.41 Man with bronchial carcinoma. **a** The chest X-ray shows shadowing of the upper lobe on the right side. **b** CT reveals atelectasis (AT) with no central tumor formation. **c** B-mode ultrasound shows the atelectasis (AT) without a central tumor formation. **d** On contrast-enhanced ultrasound the atelectasis (AT) can be demarcated from a central tumor formation (TU)

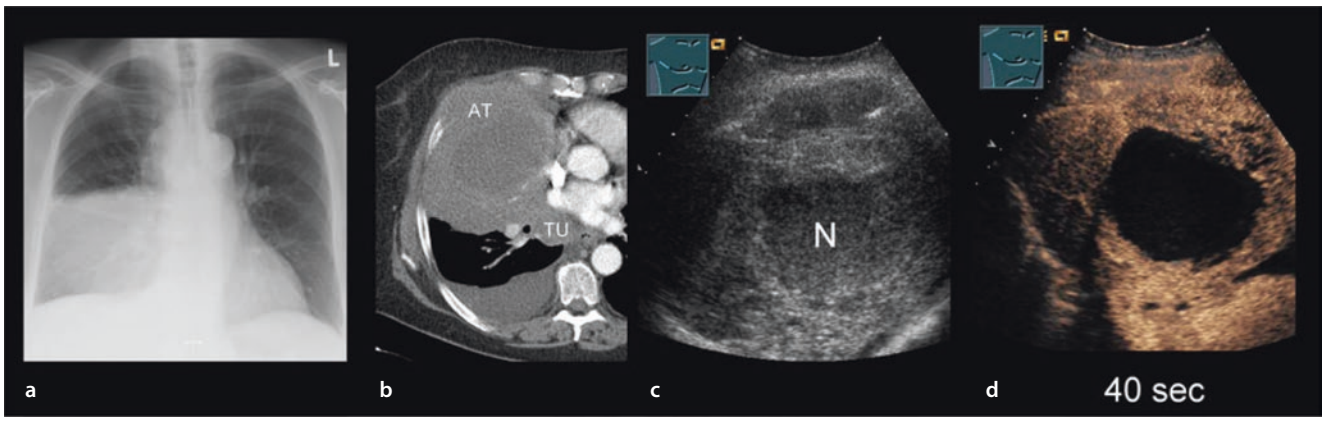

Fig. 8.42 Man with bronchial carcinoma. **a** The chest X-ray reveals shadowing in the lower field of the right lung. **b** CT shows a central tumor formation (*TU*) with downstream atelectasis (*AT*). **c** B-mode ultrasound reveals a clearly inhomogeneous space-occupying lesion without a central tumor formation. **d** On contrast-enhanced ultrasound a round space-occupying lesion is seen in the atelectasis, with no contrast enhancement, as in the presence of necrosis (*N*), an abscess or a consolidation

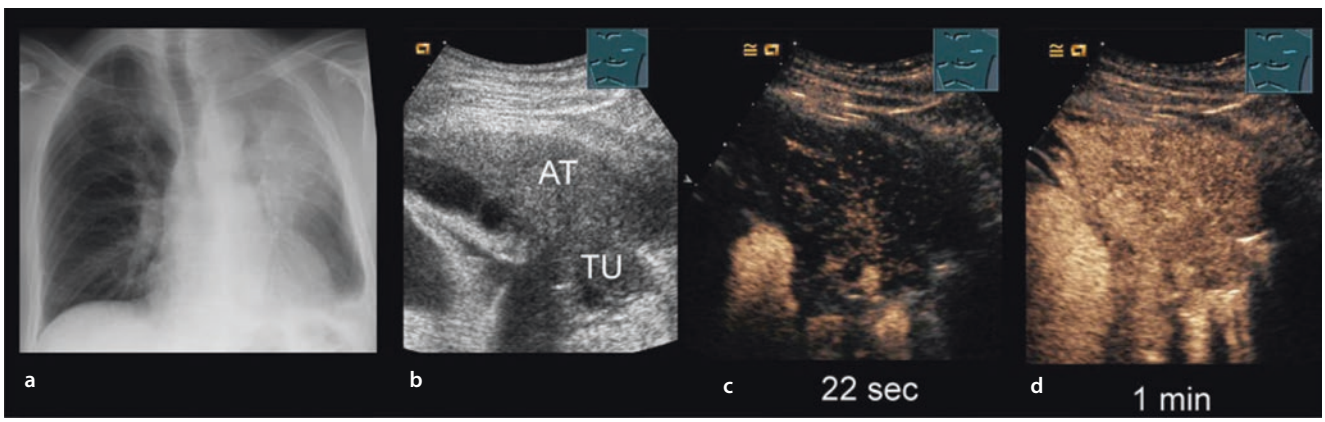

Fig. 8.43 Man with bronchial carcinoma, after chemoradiotherapy. **a** The chest X-ray reveals shadowing of the upper field in the left lung. **b** B-mode ultrasound shows a central space-occupying lesion (*TU*) with downstream atelectasis (*AT*). **c** On contrast-enhanced ultrasound, after 20 seconds there is undirected and slow contrast enhancement, as in the presence of vascularization by the bronchial artery. **d** After 1 minute the lesion is marked by strong and homogeneous contrast enhancement

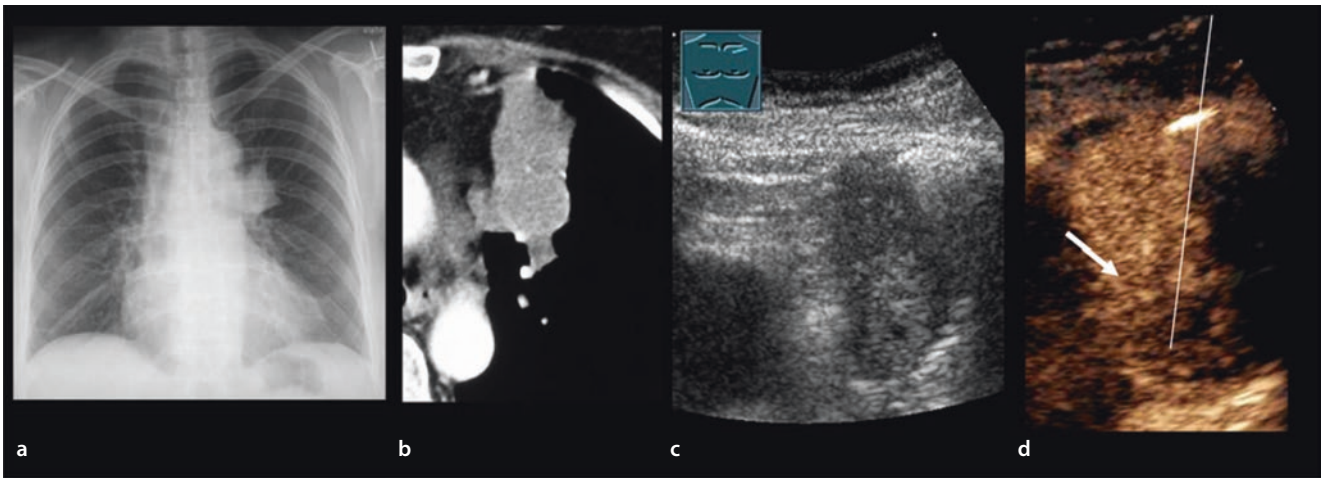

Fig. 8.44 Man with bronchial carcinoma. **a** The chest X-ray shows a space-occupying lesion in the left-sided hilum. **b** CT reveals a central tumor formation touching the chest wall. The tumor could not be seen on bronchoscopy. **c** Through a narrow "window", B-mode ultrasonography shows an inhomogeneous space-occupying lesion without a central tumor formation. **d** Contrast-enhanced ultrasound reveals, in the central aspect, a space-occupying lesion with reduced contrast enhancement, as in the presence of a central tumor (TU); the lesion was aspirated through the AT and yielded evidence of a bronchial carcinoma

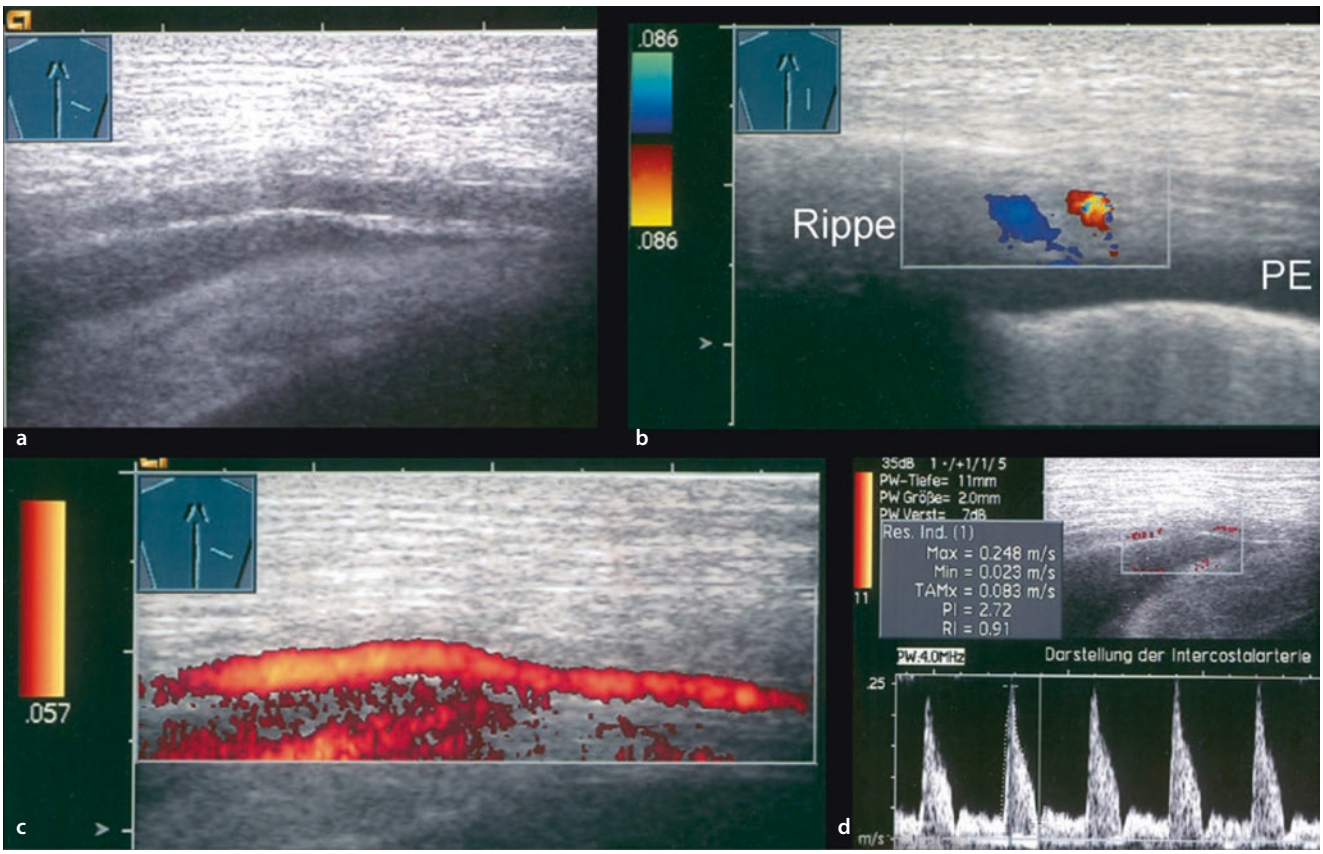

Fig. 8.45 US-Imaging of a normal intercostal artery. **a** Visible in B-Mode-Scan in intercostal section. **b** craniocaudal scan. **c** Color Doppler imaging of the intercostal arteria in longitudinal scan. **d** Spectral curve analysis shows a monophasic flow signal such as that seen in intercostal arteries

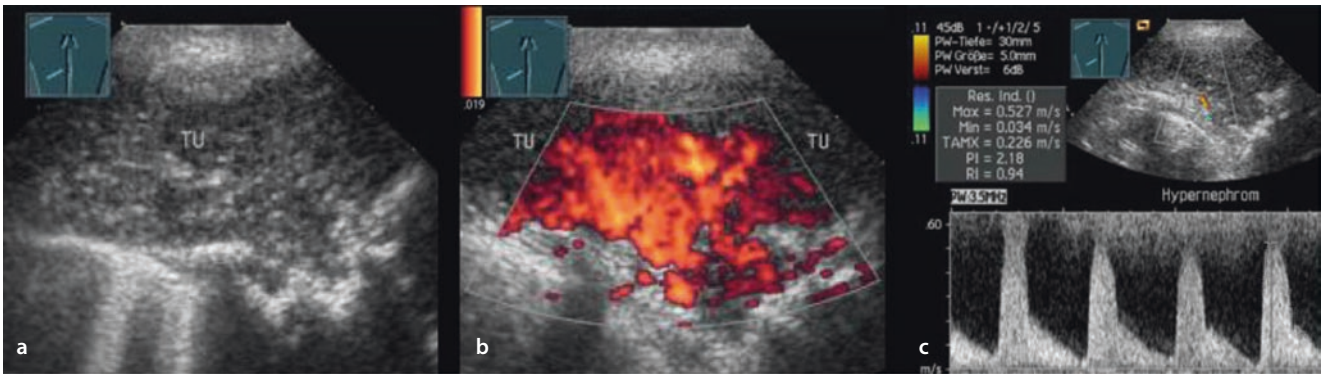

Fig. 8.46 50-year old patient with chest wall metastasis with known renal cancer. **a** Tumor infiltration in the chest wall. **b** Enhanced and irregular vascularization. **c** Spectral curve analysis shows a monophasic high impedance flow signal

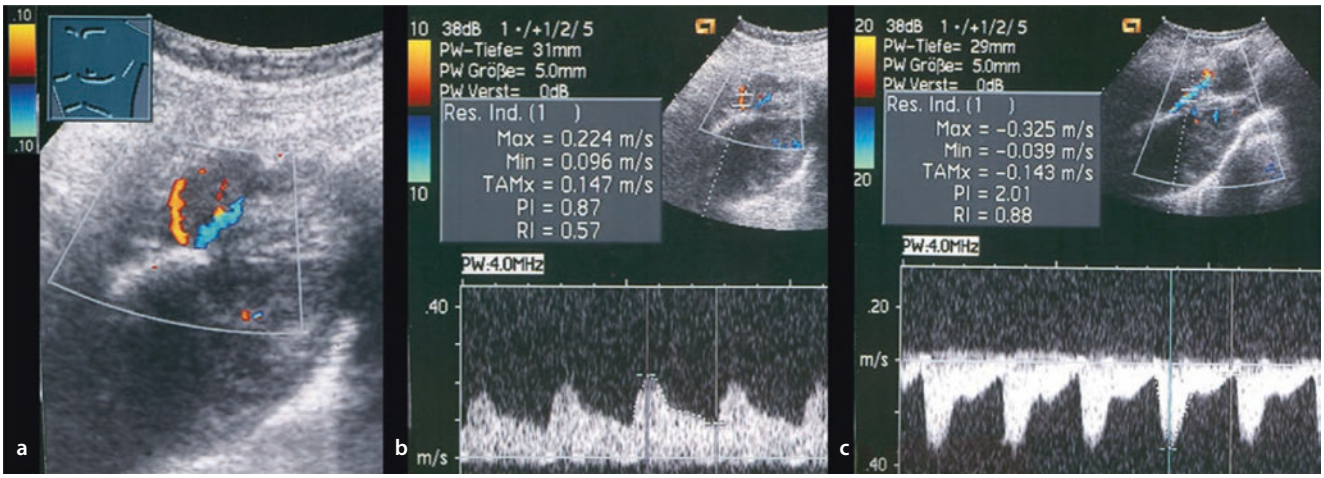

Fig. 8.47 34-years old man with testicular carcinoma and chest wall metastasis. **a** In B-Mode and color Doppler a tumor formation infiltrating in the lung. **b** Spectral curve analysis shows a monophasic low impendant flow signal as in bronchial arteria. **c** Monophasic high impendant flow signal as in intercostal arteria – complex tumorvascularization

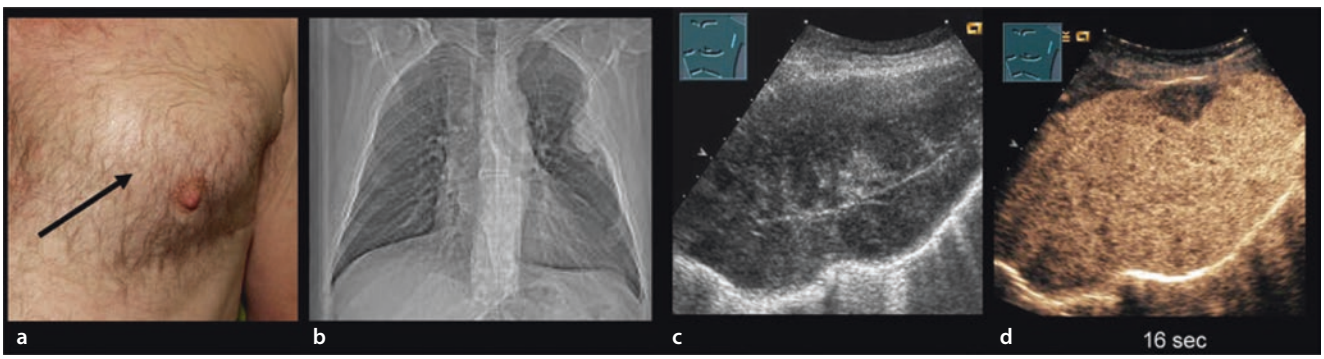

Fig. 8.48 **a** Man with a space-occupying lesion in the chest wall (*arrow*). **b** On the chest X-ray. a space-occupying lesion is seen in the apical lateral aspect on the left side. **c** The B-mode image shows a large hypoechoic lesion of the chest wall. **d** On contrast-enhanced ultrasound the lesion reveals homogeneous enhancement. The punch biopsy yielded the diagnosis of a plasmacytoma lesion

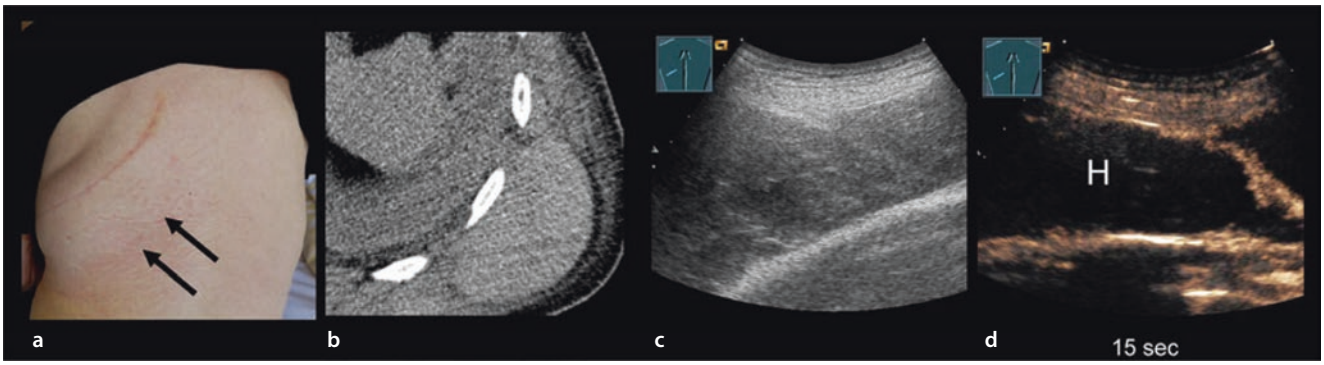

Fig. 8.49 **a** Patient with a primarily operated bronchial carcinoma and now a space-occupying lesion in the region of the scar (*arrow*). **b** CT reveals the space-occupying lesion in the chest wall. **c** The B-mode image reveals a large hypoechoic chest wall lesion. **d** On contrast-enhanced ultrasound the lesion shows no enhancement, as in hematoma, confirmed by a punch biopsy

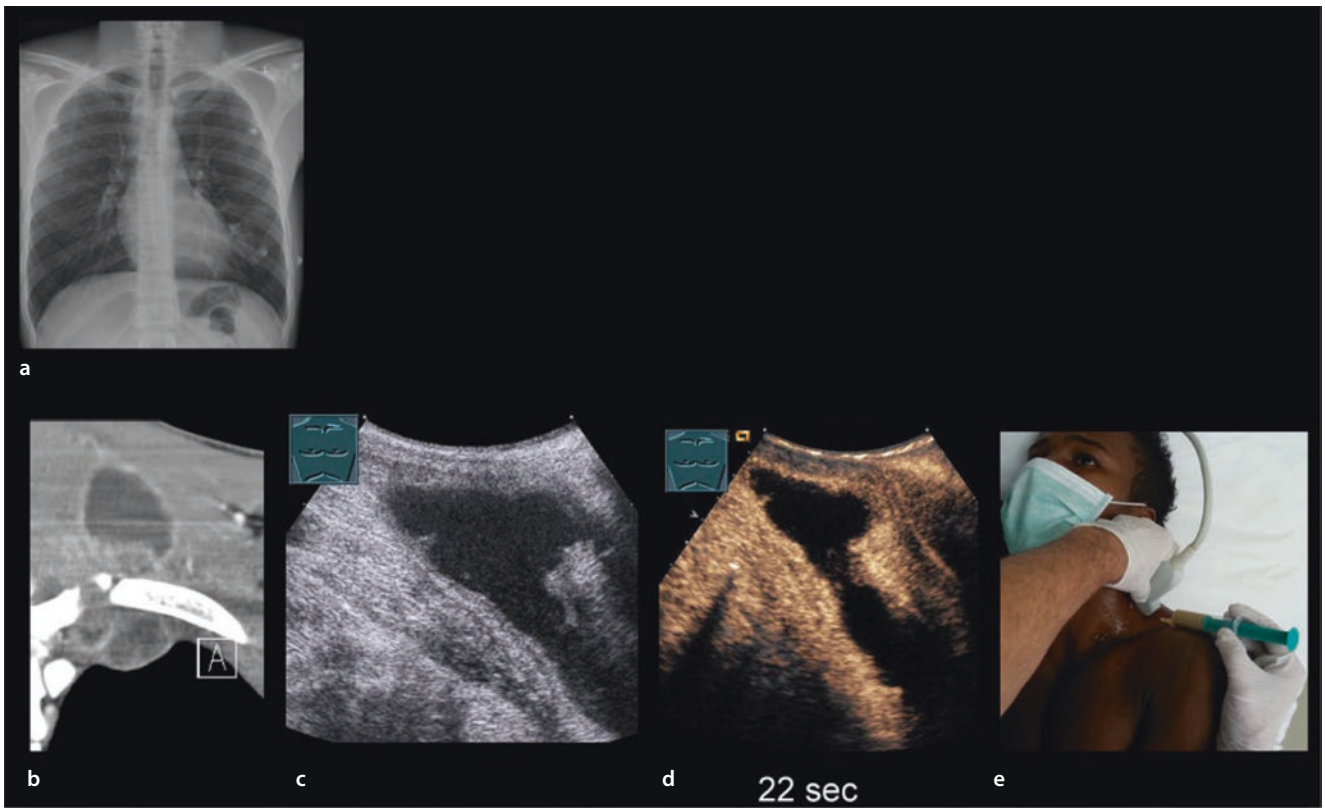

Fig. 8.50 Patient with pain in the thoracic spine for several months. **a** The chest X-ray is reported to be normal. **b** CT reveals a fluid-filled space-occupying lesion in the left-sided triangle of the neck, extending to the upper thoracic aperture. **c** The B-mode image shows a large fluid-filled structure at the neck, extending downward into the chest. **d** On contrast-enhanced ultrasound, the marginal wall of the retention shows marked absorption of contrast medium as in the presence of an abscess. **e** An US-guided diagnostic puncture yielded pus; tuberculosis was confirmed

8.7 Summary

Qualitative color-Doppler sonography shows varied and partly characteristic findings in the presence of various types of lung consolidations and is therefore a valuable adjunct to B-mode sonography with regard to the etiological classification of peripheral lung lesions. In keeping with the physiological dual vascularization of the lung by the pulmonary arteries and the bronchial arteries, on color-Doppler sonography one can distinguish between arterial high-impedance spectral curves and arterial low-impedance spectral curves in consolidated lung tissue. The former are assigned to pulmonary arteries and the latter to bronchial arteries. Within peripheral lung consolidations, different entities show characteristic distribution patterns of pulmonary-artery and bronchial-artery flow signals in respect of frequency and location. Arterial spectral curve analysis is time-consuming. Reliable demarcation of vessels of tumor neoangiogenesis is currently not possible with color-Doppler sonography.

Experience concerning contrast-assisted sonography in cases of peripheral lung lesions is limited. Contrast-assisted sonography at the chest can be performed easily and rapidly, and is therefore basically suitable for routine clinical use. Lung lesions can be distinguished by the time they require until the start of contrast enhancement and the extent of contrast enhancement. Initial studies show that contrast-assisted sonography at the chest can be helpful to differentiate ambiguous lung lesions (Görg et al. 2006b; ◘ Table 8.1).

8

References

Albrecht T, Blomley M, Bolondi L et al (2004) Guidelines for the use of contrast agents in ultrasound. Ultraschall Med 25:249–256

Babo HV, Müller KMG, Huzky A, Bosnjakovic-Buscher S (1979) Die Bronchialarteriographie bei Erkrankungen der Lunge. Radiologe 19:506–513

Civardi G, Fornari F, Cavanna L, Di Stasi M, Sbolli G et al (1993) Vascular signals from pleural-based lung lesions studied with pulsed doppler ultrasonography. JCU 21:617–622

Fissler-Eickhoff A, Müller KM (1994) Pathologie der Pulmonalarterien bei Lungentumoren. DMW 119:1415–1420

Forsberg F, Goldberg BB, Liu BB et al (1999) Tissue specific US contrast agent for evaluation of hepatic and splenic parenchyma. Radiology 210:125–132

Gehmacher O, Mathis G, Kopf A, Schreier M (1995) Ultrasound imaging of pneumonia. Ultrasound Med Biol 21:1119–1122

Gehmacher O, Kopf A, Scheier M et al (1997) Can pleurisy be detected with ultrasound? Ultraschall Med 18:214–219

Görg C, Seifart U, Holzinger I, Wolf M, Zugmaier G (2002) Bronchioloalveolar carcinoma: sonographic pattern of »pneumonia«. Eur J Ultrasound 15:109–117

Görg C, Seifart U, Görg K et al (2003) Color Doppler sonographic mapping of pulmonary lesions: evidence of dual arterial supply by spectral analysis. JUM 22:1033–1039

Görg C, Bert T (2004a) Trancutaneous colour Doppler sonography of lung consilidations: review and pictorial essay. Part 1: Pathophysiologic and CDS basics of pulmonary vascularity. Ultraschall Med 25:221–226

Görg C, Bert T (2004b) Trancutaneous colour Doppler sonography of lung consilidations: review and pictorial essay. Part 2: CDS patterns of pulmonary consolidations. Ultraschall Med 25:285–291

Görg C, Bert T, Görg K, Heinzel-Gutenbrunner M (2005a) Color Doppler sonographic mapping of chest wall lesions. BJR 78:303–307

Görg C, Bert T, Görg K (2005b) Contrast enhanced sonography for differential diagnosis of pleurisy and focal pleural lesions of unknown cause. Chest 128:3894–3899

Görg C, Bert T (2006) Transcutaneous contrast enhanced sonography of peripheral lung lesions: rewiew and pictorial essay. Am J Roentgenol 187:420–429

Görg C, Bert T, Kring R (2006a) Contrast enhanced sonography of the lung for differential diagnosis of atelectasis. JUM 25:35–39

Görg C, Bert T, Kring R, Dempfle A (2006b) Transcutaneous contrast enhanced sonography of the chest for evaluation of pleural based pulmonary lesions. Ultraschall Med 27:437–444

Harvey CJ, Albrecht T (2001) Ultrasound of focal liver lesions. Eur Radiol 11:1578–1593

Hsu WH, Ikezoe J, Chen CY, Kwan PC, Hsu CP et al (1996) Color doppler ultrasound signals of thoracic lesions: correlation with resected histologic specimens. Am J Respir Crit Care Med 153:1938–1951

Hsu WH, Chiang CD, Chen CY, Kwan PC, Hsu JY et al (1998) Color doppler ultrasound pulsatile flow signals of thoracic lesions: comparison of lung cancer and benign lesions. Ultrasound Med Biol 24:1087–1095

Kolin A, Koutllakis T (1988) Role of arterial occlusion in pulmonary scar cancers. Hum Pathol 19:1161–1170

Mathis G, Dirschmid K (1993) Pulmonary infarction: sonographic appearance with pathologic correlation. Eur J Radiol 17:170–174

Müller KM, Meyer-Schwickerath M (1978) Bronchial arteries in various stages of bronchogenic carcinoma. Path Res Pract 163:34–46

Piscaglia F, Nolsoe C, Dietrich CF et al (2012) The EFSUMB Guidelines and Recommendations on the Clinical Practice of Contrast Enhanced Ultrasound (CEUS): update 2011 on non-hepatic applications. Ultraschall Med 33(1):33–59

Yuan A, Chang DB, Yu CJ, Kuo SM, Luh KT, Yang PC (1994) Color doppler sonography of benign and malignant pulmonoray masses. Am J Roentgenol 163:545–549

Yuan A, Yang PC, Lee L, Wu DH, Kuo SH et al (2000) Reactive pulmonary artery vasoconstriction in pulmonary consolidation by color doppler ultrasonography. Ultrasound Med Biol 26:49–56

Image Artifacts and Pitfalls

Andreas Schuler

G. Mathis (ed.), *Chest Sonography*, DOI 10.1007/978-3-319-44072-9_9

9.1 Artifacts

Artifacts are a system-immanent aspect of ultrasonography. They arise due to physical phenomena when ultrasound waves pass through the human body (Table 9.1). Artifacts are disruptive artificial products that make it very difficult to image and evaluate the thorax, especially due to the anatomical features of this region. Artifacts can distort existing structures in terms of their size, position, form, and echogenicity; cause incorrect or incomplete imaging of their topography; or suggest the presence of structures that, in fact, do not exist. On the other hand, artifacts are indispensable and very important determinants of the diagnosis of specific diseases. The absence of certain typical artifacts (air: reverberation; bone: acoustic shadow) at the surface of the lung or in the bony thorax enables the investigator to diagnose certain diseases (lung lesion, rib lesion), as it is then possible to evaluate parenchyma, bone, and/or soft tissue. Artifacts also serve as a diagnostic criterion when they are seen at an unusual site, e.g., air with reverberation echoes in the pleural space in cases of pneumothorax.

9.2 Pitfalls

These are sources of error in ultrasonographic diagnosis, caused by anatomical, topographic, pathophysio-logical, or physical ultrasound-based misinterpretation on the part of the investigator, leading to incorrect diagnosis. Incomplete history taking, missing clinical information or examination, or insufficient knowledge of sonographic (and clinical) differential diagnosis may also be the reason for such "pitfalls." Last, but not least, every conscientious ultrasonographer must be aware of the limitations of the method so that additional diagnostic procedures can be applied efficiently, economically, and in a manner that is conducive to the patient's well-being. By so doing, several pitfalls can be avoided or resolved.

9.3 Ultrasound Physics in the Chest

Ultrasound images are created by the transmission and passage of ultrasound waves in the human body and the registration and processing of the backscattered/received echo of the emitted ultrasound beam. In an entirely homogeneous medium, a sound wave is carried forward in a uniform fashion. It is altered at the margin between two media. The phenomena/changes that are liable to occur in this process are summarized in Table 9.1. They include the geometry of the ultrasound wave, the angle at which it strikes the reflector, the physical properties of the reflector, and its surface consistency. The magnitude of the impedance difference between two different media is represented by various factors, one of them being the intensity of the backscattered echo. Thus, on the B-mode image, it is represented by the brightness of a pixel. Human tissue contains a number of marginal surfaces whose anatomical origin can be determined by characteristic ultrasound phenomena.

Table 9.1 Physical phenomena of ultrasound waves

Reflection	Refraction
Absorption	Dispersion
Diffraction	Attenuation

In contrast to the abdomen, ultrasonography of the chest is more frequently confronted with disturbing artifacts because of the surrounding "echo-opposing" structures (aerated lung, bony chest). Therefore, the specific ultrasound phenomena in air and bony structures will be briefly discussed in the following.

Air This is a strong ultrasound beam reflector. Depending on the structure of the surface, the impedance difference and the gas volume at the marginal surface, ultrasound waves differ in terms of their reflex behavior:

- Large extent of absorption
- Total reflection with acoustic shadow
- Partial reflections with change of transmission and a narrow acoustic shadow

The most common phenomenon is that up to 99 % of the ultrasound wave is reflected at the first marginal surface between tissue and air, i.e., the "initial lung echo." Therefore, it is not possible to visualize the deeper lung parenchyma by ultrasonography. Only when the structure of the surface is altered and in the presence of specific physical features (e.g., the absence of air in inflammatory or tumor-related processes, atelectasis, etc.) is it possible to image lung parenchyma. However, in such cases, the lung itself has several marginal surfaces (air in the bronchoalveolar space, bronchial wall, interstitial space, vascular wall, blood). The above-mentioned alterations in the ultrasound wave also occur at these marginal surfaces.

Bone In bone, there is nearly complete absorption of ultrasound energy. As a result, the "dorsal" ultrasound wave is obliterated (no further echoes in axial direction of the beam). When ultrasound waves hit bone at right angles, they may cause strong reflection and repetitive echoes of the bone surface in deeper portions (Fig. 9.1).

9.4 Imaging of Marginal Surfaces of the Pleura and the Diaphragm

The image varies, depending on the angle of incidence of ultrasound waves and the consistency (roughness) of the surfaces. Furthermore, the improved resolution of ultrasound probes and continuous advancement of technology permit differentiated imaging. At an angle of incidence of 0 to about

25°, total reflection may be expected to occur at the marginal surface between the pleura and the lung. Only when the surface of the pleura/lung is thickened due to inflammation or scars and the surface is irregular and "roughened," is it imaged even in the presence of a steeper angle of incidence.

Most of the diaphragm can be imaged by the transabdominal approach (as a rule through the liver from the right side and through the spleen from the right side). Due to the high impedance difference as well as scatter phenomena, the diaphragm is visualized as much thicker than it actually is (Fig. 9.2). Central portions of the diaphragm are not imaged well by the intercostal approach because of the unfavorable angle of incidence of the ultrasound wave. Apparent gaps might irritate the investigator. Moreover, lateral marginal shadow phenomena limit the assessment. Indistinct processes must be imaged in the complementary second plane.

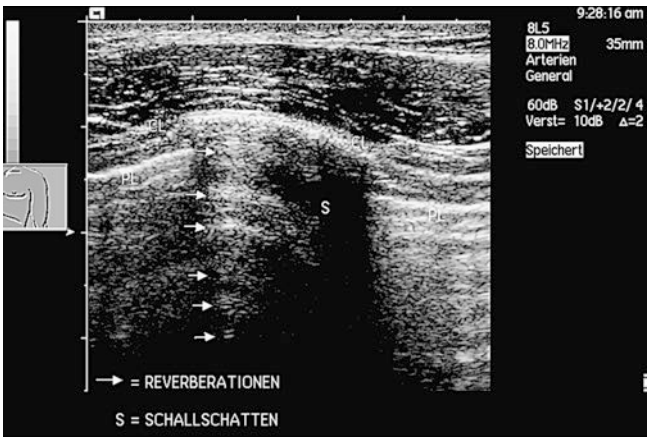

Fig. 9.1 Reflective shadowing at the clavicle (*CL*). Dorsal acoustic shadow (*S*) due to absorption of ultrasound waves at the surface of the clavicle. Additional reverberations (repetitive echoes, *arrows*) at the surface of the clavicle when the ultrasound waves hit perpendicularly. *PL* pleural reflex

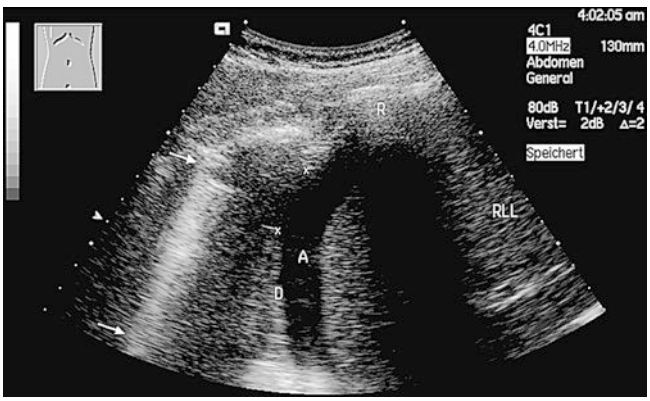

Fig. 9.2 "Diaphragmatic gap." A female patient with a primary peritoneal mesothelioma, ascites (*A*) and basal pleural pneumonia. The central portion of the diaphragm (*D*) is found to be markedly thickened. In areas dose to the transducer, there seems to be a gap (*x–x*). Furthermore, a lateral marginal shadow phenomenon is seen in the diaphragm and also a comet-tail artifact in air in the cranially located lung (*arrows*). *RLL* right lobe of liver, *R* rib with dorsal acoustic shadow

9.5 B-Mode Artifacts

Based on their mechanism of origin and physical ultrasound features, artifacts may be divided into four categories (Table 9.2; Kremkau and Taylor 1986; Schuler 1998).

9.5.1 Ultrasound Beam Artifacts in Chest Sonography

Reverberations (Repetitive Echoes): Margin Between Tissue and Air, Bone Fracture Fissures

They arise due to nearly complete reflection of the emitted ultrasound wave at the marginal surface between tissue and air (initial lung echo). This marginal surface acts as a strong reflector. It reflects the striking ultrasound wave back to the transducer membrane, where the wave is re-reflected and re-emitted, hits the marginal surface again, etc.

Depending on the duration, the marginal surface reflex is imaged dorsally, in axial direction of the ultrasound wave. Deeper reflectors are weaker and are imaged darker (Figs. 9.2 and 9.3). The artifact caused by insufficient probe-to-specimen contact (Fig. 9.10), e.g., when a linear ultrasound probe is used on the surface of the thorax, actually is a reverberation artifact (at the transducer membrane).

Table 9.2 Classification of artifacts

Ultrasound beam artifacts
Ultrasound enhancement artifacts
Ultrasound resolution artifacts
Other artifacts

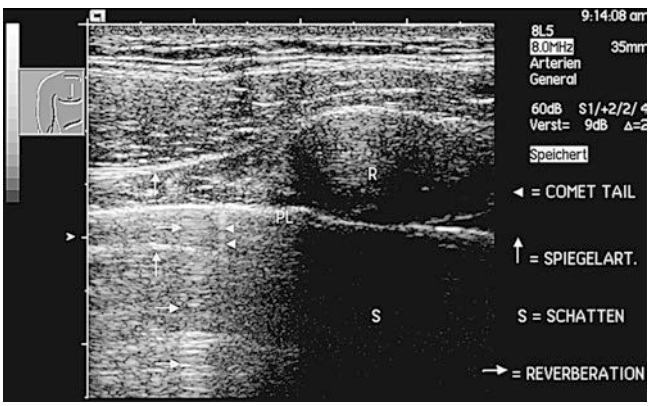

Fig. 9.3 Reverberations and comet-tail, parasternal longitudinal section from the right side. One finds reverberation artifacts (*horizontal arrows*) dorsally in the aerated lung, and a short comet-tail artifact (*arrowheads*). Furthermore, a muscle fascia of the thorax musculature is mirrored dorsally (*vertical arrows*) at the pleural reflex (*PL*). Rib (*R*) with an incomplete acoustic shadow (*S*); the pleural reflex acts as a strong reflector and is imaged here through partly cartilaginous rib with partial echo transmission

A narrow fissure in a rib fracture might become noticeable because of a reverberation artifact (so-called chimney phenomenon) (Dubs-Kunz 1992). The fracture end of the rib serves as a strong reflector in this setting (Fig. 2.17).

Mirror Artifacts: Liver Parenchyma in the Diaphragm, Vessels at the "Pleura"

These are caused by incidence-angle-dependent reflection of the ultrasound wave at a strong reflector (e.g., the diaphragm), oblique deflection in issue, repeated reflection on a reflector, back-scatter to the first reflector, and back-reflection to the ultrasound probe. This is imaged as a structure tot primarily in the axial direction of the ultrasound beam, within a region axialdistal to the actual reflector.

This causes the classical mirror artifact phenomena of the liver at the diaphragm (Fig. 9.4), but also of the subclavian artery at the initial lung reflex. This artifact phenomenon exists not only in B-mode sonography, but also in color Doppler and the Doppler frequency spectrum (Reading et al. 1990; Fig. 9.5). As a rule, the multiple backscattered echoes of mirror images are more hypoechoic and somewhat more blurred or distorted as a result of previous weakening of the ultrasound beam when it passes through tissue.

Arcuate Artifacts: Rib Reflex in Pleural Effusion

Arcuate artifacts may arise due to displacement of a reflex at a strong reflector in the lateral ultrasound beam or side lobe into the center of the main beam. Characteristically, in sector transducers and upwardly oriented curved arrays, one finds upwardly open circular arches. In linear probes, one finds a hyperbola. Thus, a reflection in a bony portion of the thorax could mimic a septation in a pleural effusion (Fig. 9.6). This problem can be resolved by altering the echo angle or the echo plane.

Scatter Lens Artifact/Shortening Phenomenon: Distortion of the Lung Surface Dorsal to Rib Cartilage

This artifact phenomenon is a result of the different transmission rates of ultrasound waves in rib cartilage (faster) than in the adjacent soft tissue of the chest wall. This may mimic a pseudolesion at the marginal surface of air/lung, because there is an apparent protrusion of contours in the direction of the ultrasound probe (Fig. 9.7). This artifact is simple to detect and plays a rather important role in abdominal diagnosis of the liver (apparent space-occupying mass on the surface of the liver) dorsal to rib cartilage (Bönhof and Linhart 1985).

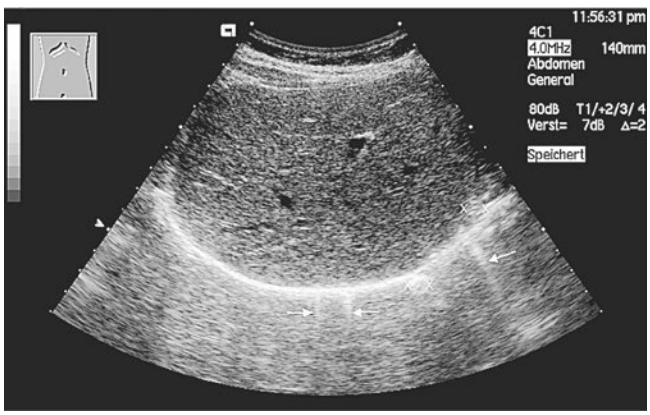

Fig. 9.4 Mirror artifact. Subcostal oblique section from the right side. "Classical" mirror artifact of the liver at the diaphragm. Portions lying at a distance from the transducer and the diaphragm, i.e., cranially by the subcostal approach, are not "lung parenchyma" but liver parenchyma reflected at the strong reflector, namely the diaphragm. A hemangioma (*x–x*) lying immediately subdiaphragmal in the original image is more clearly seen in the mirror image (*x–x*) and is displaced centrally to the mid portion of the image. In some cases, the mirror image might reveal structures outside the main beam that cannot be imaged (multiple beam artifacts) and cause considerable confusion. Additional comet-tail artifacts (*arrows*) in air

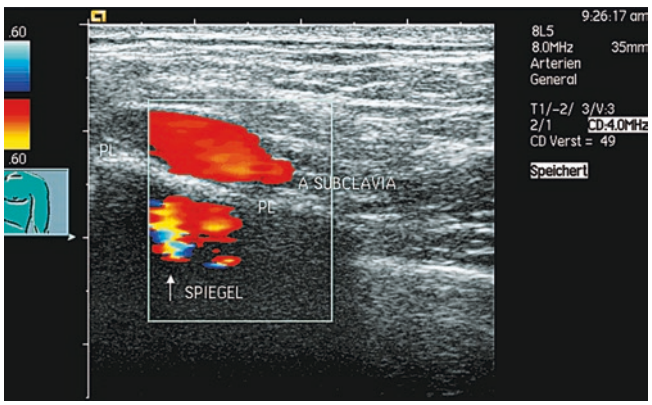

Fig. 9.5 Mirror artifact on color Doppler. The subclavian artery (*A. SUBCLAVIA*) is reflected at the pleura (*PL*). A vessel (*arrow*) lying dorsal to the pleura is seen on the mirror image; the vessel, however, does not really exist

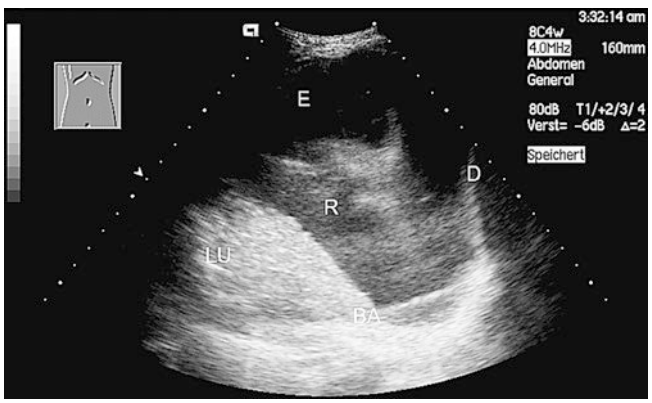

Fig. 9.6 Arcuate artifact in the pleural effusion. A female patient with pulmonary and pleural metastatic breast carcinoma. A strong reflector (bony thorax) lying outside the main beam is visualized as a circular arch (*AA* arcuate artifact), discretely opening upward. Distally, it may mimic septation of the pleural effusion (*E*). The internal echoes (*R*) are not corpuscular portions of the effusion but noise artifacts ("speckles"). *D* diaphragm, *LU* lung atelectasis in the presence of pleural effusion

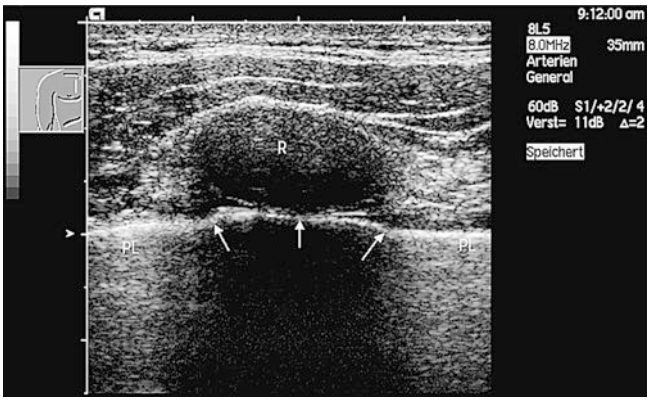

Fig. 9.7 Scatter lens artifact. The pleura (*PL*) dorsal to the rib cartilage (*R*) is shifted ventrally towards the transducer (*arrows*) as a result of various ultrasound beam rates in cartilage and soft tissue of the chest wall

Marginal Shadows: Diffraction/Refraction at Strong Reflectors ("Diaphragmatic Gap")

This artifact occurs when the ultrasound beam hits a surface obliquely. It is the result of diffraction and refraction phenomena at strong reflectors (e.g., the diaphragm; Fig. 9.2). The artifact is detected by the fact that it disappears when the echo plane or the echo angle is changed.

9.5.2 Artifacts Caused by Alterations in Echo Enhancement

Acoustic Shadow/Echo Obliteration: Formation of Plaque on All Bony Structures of the Chest

This certainly is one of the most common artifact phenomena in the thorax and greatly hinders the assessment of structures lying dorsal to such strong reflectors. Due to strong absorption, dorsal bone structures (ribs, scapula, clavicle, sternum, vertebral column) are nearly completely obliterated and practically all information is lost (Fig. 9.1). However, interruptions of the other-wise regular acoustic shadow in the bony thorax (bone contour, bone surface, joints) may be very helpful for diagnosis, as pathological changes will be present in such cases (fracture, bone tumor, joint effusion, joint empyema). Acoustic shadows in the pleura are also signs of pathological alterations, e.g., of plaque in the presence of asbestosis or calcification during the healing of pleural lung lesions or lung lesions dose to the pleura (pneumonia, tuberculosis) or in lymph nodes.

Echo Enhancement: Distal to Hypoechoic Structures (Pleural Effusion, Cyst, Vessel, Hypoechoic Space-Occupying Mass)

This phenomenon of "brighter," more hyperechoic areas distal to the above-mentioned structures is not due to echo enhancement but due to lesser weakening of ultrasound waves in the more hypoechoic portions closer to the probe. This causes distal parts to appear brighter (more hyperechoic and stronger

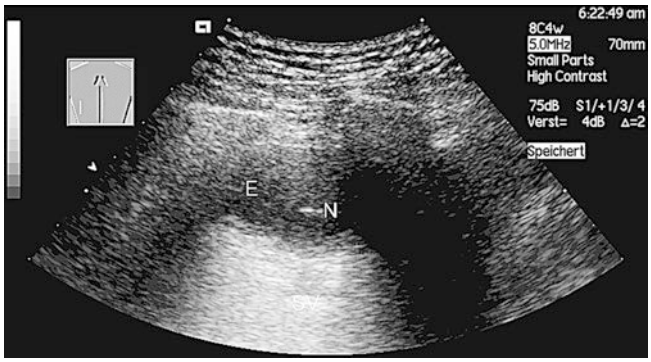

Fig. 9.8 Echo enhancement. Dorsal to a small, not entirely anechoic pleural effusion (*E*) there is marked "echo enhancement" (*EE*). This actually is reduced weakening of the echo, as the spread of the ultrasound beam in the pleural effusion is altered in comparison with adjacent tissue. Also note the nonanechoic effusion dose to the chest wall. The reflexes are noise artifacts. Furthermore, an echodense small bright linear reflex (*N*) is seen, the tip of the puncture needle introduced under sonographic guidance

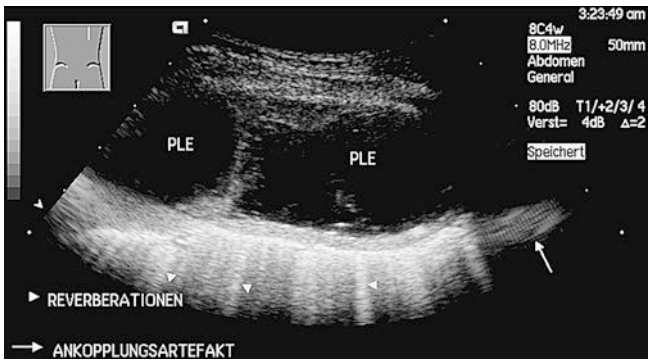

Fig. 9.9 Comet-tail and probe-to-specimen artifact. Dorsal to a septate pleural effusion in the presence of breast carcinoma one finds numerous comet-tail artifacts (*arrowheads*) arising in the air at the margin between the visceral pleura and the lung. Furthermore, given insufficient contact between the ultrasound probe and the chest wall, a shadow with an artifact reflex (*arrow*), although not like a classical ring-down artifact. Dorsal to the pleural effusion, there is marked echo enhancement. *PLE* pleural effusion

echoes) than the surrounding areas, which have uniformly weakened echoes. In the thorax, this is found in the presence of large quantities of fluid in the pleural space or hypoechoic peripheral pulmonary processes (Figs. 9.8 and 9.9).

Echo Resolution Artifacts

Noise: In Fluid-Filled Structures

At the surface of anechoic areas, one finds diffuse "noise" caused by interference from returning echoes at different marginal surfaces, such as those caused by "background noise," depending on general enhancement (this is also true for Doppler sonography). Here caution is advised, as apparently internal structures that in fact do not exist might be mimicked (e.g., in the pleural effusion; Figs. 9.6 and 9.8). Marginal surfaces are frequently blurred.

- **Slice Thickness Artifact: at Reflectors with a Strong Impedance Difference (Pleura, Diaphragm)**

This common and irritating artifact also belongs to the category of resolution artifacts. When the ultrasound beam hits strong reflectors obliquely and in the presence of a high impedance difference, the marginal layer is much thicker, (partly) blurred, and distorted. This phenomenon might mimic pleural and diaphragmatic lesions or thickening (Fig. 9.2), but also thrombosis or sediments in vessels.

9.5.3 Other Artifacts

Comet-Tail (Resonance Artifact), B-Lines: In Aerated Structures

At the margin, of the lung surface and air one frequently finds small comet-tail artifacts (Figs. 9.2, 9.3, 9.4 and 9.9). They are seen as bright, narrow strips of strong dorsal reflectors and their origin is controversially discussed. One explanation is reverberations (repetitive echoes) between two very closely located reflectors and resonance phenomena (vibrations) in a thin structure of soft tissue (e.g. thickened interstitial alveolar septa surrounded by air with a strong echo response). In addition to air or other gas bubbles, a common site of origin is metal foreign bodies.

Many authors refer to these artifacts as B-lines, the "sound of lung water" (Lichtenstein et al. 1997; Lichtenstein 2005; Gargani et al. 2008; Noble et al. 2009; Soldati et al. 2009). When occurring in large numbers in the region distal to the ultrasound reflection on the aerated lung, these artifacts indicate interstitial lung lesions such as interstitial edema or lesions in the presence of contusion, pneumonia, etc., (Soldati et al 2006; Volpicelli et al. 2008). In more rare cases, fibrotic lesions in the lung may also be present (Wohlgenannt et al. 2001; Reissig and Kroegel 2003). However, these artifacts are not sufficiently selective as regards their differentiation from the above-mentioned diseases. To put it simply, the evidence of these artifacts means that "the lung is not healthy" (Figs. 9.10, 9.11, and 9.12).

The 1st International consensus conference on pleura and lung ultrasound has defined B-lines as discrete laser-like vertical hyperechoic reverberation artifacts that arise from the pleural line (previously described as "comet tails"), extend to the bottom of the screen without fading, and move synchronously with lung sliding. Multiple B-lines are the sonographic sign of lung interstitial syndrome.

In the evaluation of *diffuse* interstitial syndrome, the sonographic technique ideally consists of scanning eight regions, but a more rapid anterior two region scan may be sufficient in some cases. A positive region is defined by the presence of three or more B-lines in a longitudinal plane between two ribs. However, focal multiple B-lines may be present in normal lung.

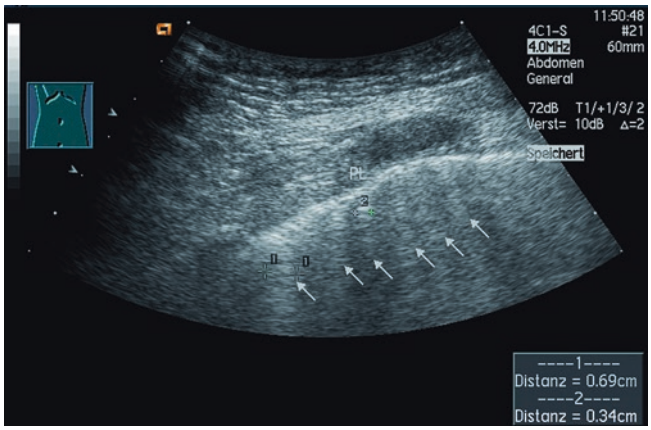

Fig. 9.10 B-lines (*arrows*, calipers: up to 7 mm wide) in pulmonary edema due to decompensated left ventricular heart failure (PL pleural reflex)

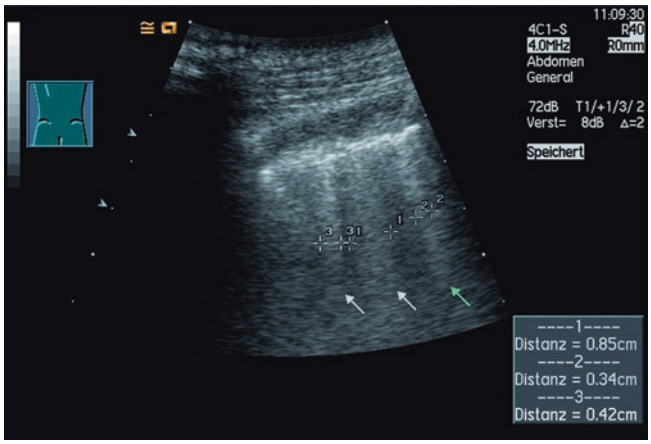

Fig. 9.11 Interstitial syndrome with comet-tail artifacts (*arrows*, calipers: 3–8 mm wide), bacterial pneumonia in the phase of healing, infiltrate not seen on the image

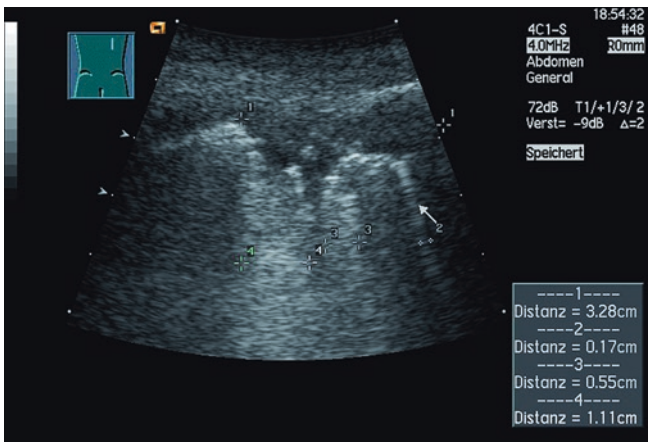

Fig. 9.12 Congestive pneumonia in chronic biventricular decompensated heart failure: infiltrate (calipers 1) and distal comet-tail artifacts (calipers 2–4: 2- to 11-mm-wide artifacts)

Focal sonographic pattern of interstitial syndrome may be seen in the presence of many lung diseases e.g.: Pneumonia and pneumonitis, atelectasis, pulmonary contusion, pulmonary infarction, pleural disease, neoplasia (Winfocus 2010).

Artifacts Caused by Foreign Bodies: Needle Tip, Drainage

Iatrogenic or accidental foreign bodies introduced into the body cause artifact phenomena. As a result, projectiles, fragments of glass or wood, other substances might be imaged in the chest wall and in soft tissue. This is significant when such artifacts are visualized during sonography-guided diagnostic or therapeutic measures. Small pulmonary consolidations dose to the pleura, pleural effusions a few millimeters in size, or pleural empyema can be punctured or drained under real-time sonographic guidance. Space-occupying masses in the soft tissue of the thorax or rib cage should also be punctured under sonographic guidance. Detection of the needle reflex in aerated structures might be difficult. Here, real-time control through subtle movement of the needle tip under simultaneous sonographic imaging is useful (Blank 1994; ◘ Fig. 9.8).

Ring-Down Artifact: Insufficient Probe-To-Specimen Contact

If the geometric configuration of the probe is unfavorable in relation to the investigated region (for instance a linear probe in a curved chest wall), this artifact can easily be detected by characteristic repetitive echoes (arising between the ultrasound crystal and the transducer membrane) (◘ Fig. 9.13).

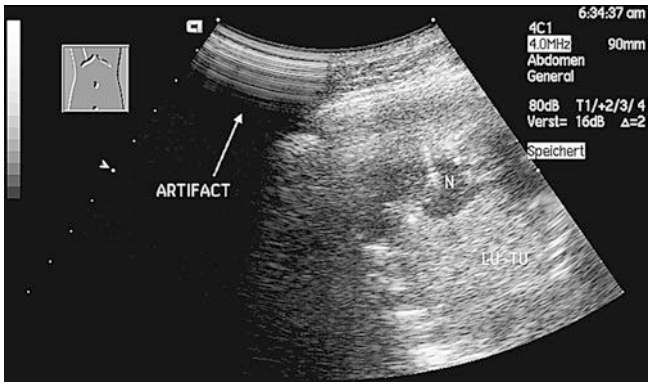

◘ **Fig. 9.13** Ring-down (probe-to-specimen artifact). Patient with a peripheral bronchial carcinoma in a ventral location on the right side. A probe-to-specimen artifact (*arrow*) is caused by insufficient contact between the transducer and the chest wall. A simultaneous fine-needle puncture performed for histological verification of the diagnosis shows the needle artifact (*N*) in the tumor (*LU-TU*)

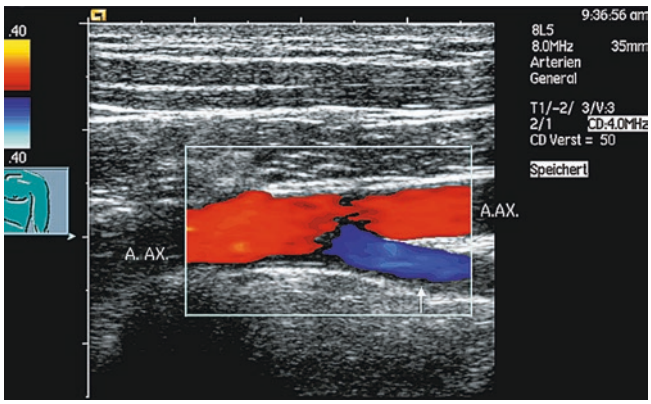

◘ **Fig. 9.14** Directional artifact (color Doppler). The axillary artery (infraclavicular) (*A.AX.*) with a branch for the musculature/chest wall. Blood flowing towards the ultrasound probe is coded *red*; blood flowing away from the probe is coded *blue* (see color scale). The branching artery (*arrow*) is *blue*, the change of color from *red* to *blue* occurs via *black*. Thus, here (at a 90° Doppler angle to the ultrasound probe), there is no blood flow relative to the ultrasound probe

9.6 Color Doppler Artifacts and Pitfalls in the Chest

The basic principles and settings of the various Doppler modalities will not be presented in this chapter. They have been discussed in detail elsewhere (Wild 1996).

9.6.1 Pulse Repetition Frequency, Overall Enhancement, Filter, Background Noise

Insufficient or incorrect setting of the overall enhancement of color Doppler either leads to incorrect imaging of actual blood flow (excessively low gain) or "over-radiation" due to numerous color pixels that do not represent blood flow but only background noise (poor signal-to-noise ratio).

A low pulse repetition frequency (PRF) should be selected for small vessels with low flow rates so that flow signals are not "overlooked." When large arteries are visualized (mediastinum, suprasternal, parasternal), it may be necessary to increase the PRF or reduce overall enhancement. The same is true for spectral Doppler. Selection of the wall filter should also be controlled, so that slow flow signals or signals of low intensity are not "filtered away."

9.6.2 Directional Artifact

The directional artifact is not actually an artifact phenomenon but evidence of directionally encoded visualization of blood flow on color Doppler (◘ Fig. 9.14). Thus, in a vessel with blood flow in the opposite direction of the ultrasound probe (for instance, when the vessel has a curved flow), the colors red and blue will be present in one and the same vessel. The actual change in the direction of blood flow is seen at the margin of the two colors; this area will be black (corresponding to null flow; see color scale).

9.6.3 Aliasing

In contrast to directional artifacts, aliasing is marked by a change of color through the bright color zones. This phenomenon is expressed as a colorful mosaic in the transition zone between two colors and will be seen at higher flow rates than the selected PRF (Fig. 9.15a). In spectral Doppler, portions of higher frequency appear as being "cut off" at the lower or upper margin of the Doppler frequency spectrum. Aliasing shows, for instance, higher-grade stenosis and disturbance of flow within vessels (Fig. 9.16). Increasing the PRF of color and spectral Doppler (up to the Nyquist limit) will help at least to reduce aliasing. It might also be possible to clearly determine the direction of flow (Fig. 9.15b, c).

9.6.4 Motion Artifacts

Mechanical movement of tissue against the ultrasound probe (breathing, musculature, cardiac and vascular pulsation, etc.) causes an apparent "frequency shift," which creates a signal in color Doppler as well. This disturbs, in particular, the assessment of structures dose to the heart and vessels due to persistent superimposition, and is a limitation of the method, e.g., in the detection of low blood flow in such areas. Various "artifact suppression" modalities proposed by manufacturers of ultrasound devices have achieved some improvement in this regard. Even in the presence of stenosis, movement of tissue due to concomitant motion (vibrations) on color Doppler might represent apparent flow signals outside the vessel (Fig. 9.16).

The gliding pleural reflex is very useful in terms of diagnosis. Due to motion, it also causes a strong power Doppler artifactual signal. The absence of this gliding sign, viewed in conjunction with the absence of comettail artifacts distal to the US reflection on the aerated lung, indicates a pneumothorax with a specificity of nearly 100 % (Kirkpatrick et al. 2004).

9.6.5 Unfavorable Angles

An angle of more than 60–90° may lead to incorrect Doppler measurements or incorrect imaging of blood flow (color Doppler and spectral Doppler). In such cases, the modality of power Doppler would at least help to image vessels in the thorax/lung (Yang 1996). In this setting, a largely angle-independent, directionally non-encoded, more sensitive documentation of blood flow is achieved by the visualization of amplitude (not frequency shift) of the backscattering echo.

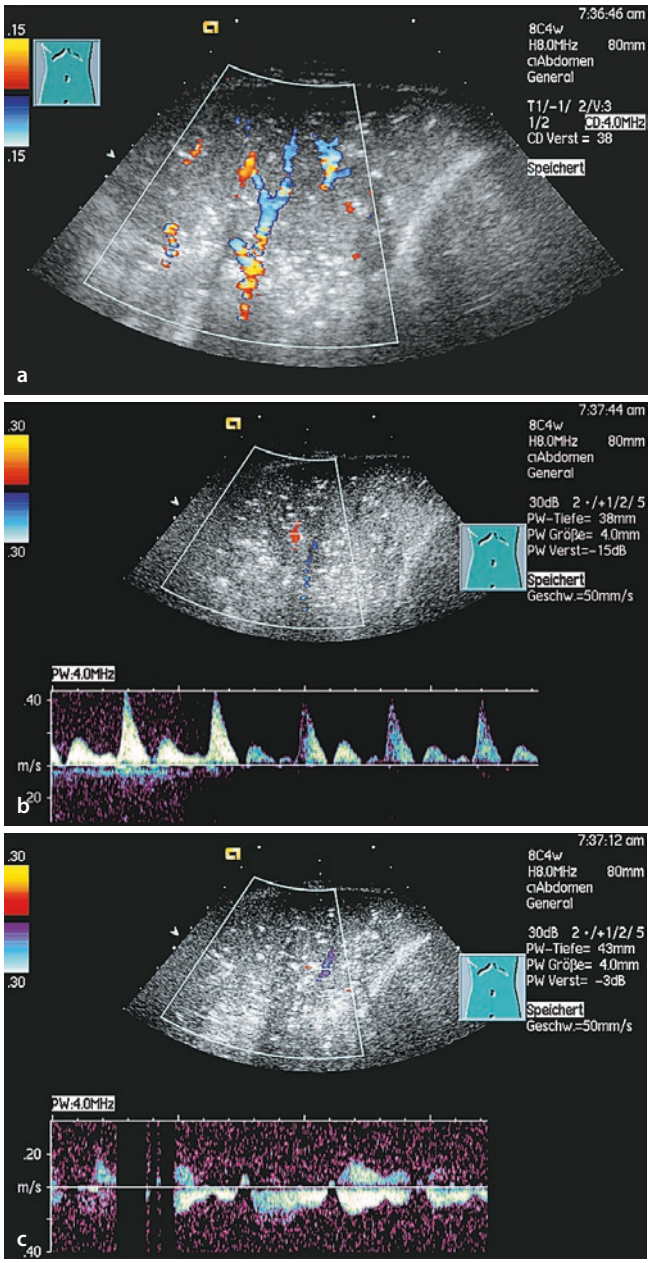

Fig. 9.15 **a** Aliasing on color Doppler in a pulmonary vessel in the presence of pneumonia. Given a low pulse repetition frequency in color Doppler (color scale, here 15 cm/s), color alone does not permit the investigator to conclusively establish the direction of flow. The change of color in the vessel is achieved via brighter colors. Thus, the mean flow rate in this vessel is more than 15 cm/s. **b** Pulmonary artery. Only when pulse repetition frequency is increased to 30 cm/s is it possible to clearly distinguish pulmonary vessels. On *red color* coding, color Doppler shows an afferent artery. On spectral Doppler, the corresponding Doppler frequency spectrum, suggesting four-phase flow. **c** Pulmonary vein. *Blue color* coding shows centrally aligned blood flow. Spectral Doppler shows the venous flow signal

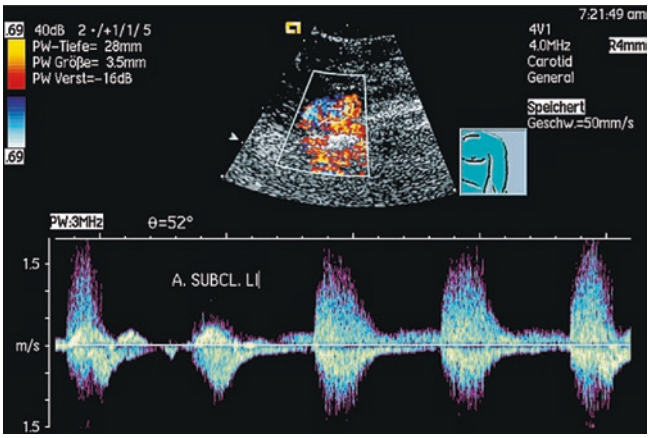

Fig. 9.16 Stenosis of the subclavian artery. In spite of high pulse repetition frequency (maximum 69 cm/s), there is markedly faster flow within the vessel, which is imaged by the bright color pixels in the vessel. Furthermore, the vessel itself is poorly delineated; color pixels are also seen outside of it. This is also known as a vibration artifact and is caused by tissue vibration secondary to stenosis and due to concomitant pulsations that cannot be reliably distinguished from the vessel in terms of space. Spectral Doppler shows flow maxima of about 1.5 m/s and retrograde flow (below the null line), as well as pathological, non-triphasic flow in this extremity artery

References

Blank W (1994) Ultrasound guided pucture and drainage. In: Braun B, Günther RW, Schwerk WB (eds) Ultraschalldiagnostik Lehrbuch und Atlas. ecomed, Landsberg. Bd III/11.1 pp 20 f

Bönhof JA, Linhart P (1985) A pseudolesion of the liver caused by rib cartilage in B-mode ultrasonography. J Ultrasound Med 4:135–137

Dubs-Kunz B (1992) Sonographische Diagnostik von Rippenfrakturen. In: Anderegg A, Despland P, Henner H (eds) Ultraschalldiagnostik 91. Springer, Berlin/Heidelberg/New York/Tokyo, pp 268–273

Gargani L, Frassi F, Soldati G, Tesorio P, Gheorghiade M, Picano E (2008) Ultrasound lung comets for the differential diagnosis of acute cardiogenic dyspnoea: a comparison with natriuretic peptides. Eur J Heart Fail 10:70–77

Kirkpatrick AW, Sirois M, Laupland B et al (2004) Hand-held thoracic sonography for detecting post-traumatic pneumothoraces: the Extended Focused Assessment with Sonography for Trauma (EFAST). J Trauma 57:288–295

Kremkau FW, Taylor KJW (1986) Artifacts in ultrasound imaging. J Ultrasound Med 5:227–237

Lichtenstein D, Meziere G, Biderman P (1997) The comet tail artifact: an ultrasound sign of alveolar-interstitial syndrome. Am J Respir Crit Care Med 156:1640–1646

Lichtenstein D (2005) General ultrasound in the critically ill, 2nd edn. Springer, Heidelberg

Noble VE, Murray AF, Capp R, Sylvia-Reardon MH, Steele DJR, Liteplo A (2009) Ultrasound assessment for extravascular lung water in patients undergoing hemodialysis. Time course for resolution. Chest 135:1433–1439

Reading CC, Charboneau JW, Allison JW, Cooperberg PL (1990) Color and spectral doppler mirror-image artifact of the subclavian artery. Radiology 174:41–42

Reissig A, Kroegel C (2003) Transthoracic sonography of diffuse parenchymal lung disease: the role of comet tail artefacts. J Ultrasound Med 22:173–180

Schuler A (1998) Untersuchungstechnik und Artefakte. In: Braun B, Günter RW, Schwerk WB (eds) Ultraschalldiagnostik Lehrbuch und Atlas. Bd I. ecomed, Landsberg, pp 1–42

Soldati G, Testa A, Silva FR, Carbone L, Portale G, Silveri NG (2006) Chest ultrasonography in lung contusion. Chest 130:533–538

Soldati G, Copetti R, Sher S (2009) Sonographic interstitial syndrome. The sound of lung water. J Ultrasound Med 28:163–174

Volpicelli G, Caramello V, Cardinale L, Cravino M (2008) Diagnosis of radio-occult pulmonary conditions by real-time chest ultrasonography in patients with pleuritic pain. Ultrasound Med Biol 34:1717–1723

Winfocus (2010) 1st International consensus conference on pleura and lung ultrasound

Wild K (1996) Periphere Gefäße. In: Braun B (ed) Ultraschalldiagnostik Lehrbuch und Atlas. ecomed, Landsberg, pp 10–13

Wohlgenannt S, Gehmacher O, Mathis G (2001) Thoracic sonography on interstitial lung disease. Ultraschall Med 22:27–31

Yang PC (1996) Color doppler ultrasound of pulmonary consolidation. Eur J Ultrasound 3:169–178

Interventional Chest Sonography

Wolfgang Blank and Thomas Müller

G. Mathis (ed.), *Chest Sonography*, DOI 10.1007/978-3-319-44072-9_10

10.1 General Indications

In addition to the frequent use of puncture for pleural effusion, space-occupying masses accessible to sonographic investigation, located in the chest wall, pleura, lung or anterior mediastinum, are important indications (Braun 1983; Börner 1986; Weiss and Weiss 1994; Pedersen et al. 1986; Yang et al. 2012).

Depending on their topographical position and the diagnostic availability and expertise, pathological changes not detectable by a transthoracic approach may be identified diagnostically by one of the interventional procedures displayed in the list in the previous section.

Interventions in the thorax: indications:

1. Space-occupying mass in the thoracic wall (tumors, abscesses, hematomas, changes in the skeletal parts)
2. Space-occupying masses in the pleura
3. Pleural effusion and pleural empyema (very small quantities, loculated effusions)
4. Peripheral lung consolidations (lung tumor, pneumonia, lung abscess)
5. Mediastinal processes (anterior mediastinum)

Because of the potential risk of complications, the indication for the procedure should be established with care.

Even if any sonographically demonstrable space-occupying lesion can be punctured in principle, one should only perform punctures if therapeutic consequences (e.g., radiation, chemotherapy) or important prognostic information is to be expected. In a patient who is operable, a suspected malignant tumor located in the periphery will normally not be punctured but will be resected as a first-line measure. It is not reasonable to merely seek confirmation of already established or plausible diagnoses. If the same information may be gathered in a less invasive way, puncture should not be performed (Beckh and Bölcskei 1997; Blank 2006; Müller and Blank 2011; Jeon et al. 2014).

10.2 Contraindications

The limits of acceptable coagulation parameters depend on the positioning of the mass and the invasiveness of the intervention. Urgent interventions require Individual assessment of risk (see ◘ Table 10.1). Special caution is necessary under Clopidogrel. Lung biopsies should not be undertaken; recommendations on superficial intervention are not univocal (see ◘ Table 10.1). Refererence is made to the literature (Ernst et al. 2006; Patel et al. 2013).

Bullous pulmonary emphysema and pulmonary hypertension are relative contraindications. When respiratory function is severely restricted or blood gas values are poor, a puncture should only be performed when the patient's condition is expected to be improved by the therapeutic intervention. High-risk puncture sites should be avoided (Yang et al. 1992; Mathis et al. 1999a; Dietrich and Nürnberg 2011).

10.3 Sonography-Guided or CT-Guided Puncture

In several diseases of the lung and mediastinum, CT provides the best overview. It should, however, only be used as an interventional measure when the target and pathway of puncture cannot be reliably assessed with sonography (Blank 2006; Mathis 1997a; Müller and Blank 2011).

The advantages of sonography-guided puncture are manifold: fast availability and bedside application (intensive care unit, emergency room), low rate of complications, absence of radiation exposure and low cost. In contrast to CT-guided puncture, the sonographic puncture can be carefully observed during the process. The investigator is free to use the pathway he/she desires in terms of direction; the ventilated lung is protected (low rate of pneumothorax). The nerve cords of the plexus in the region of the upper thoracic aperture may be

◘ **Table 10.1** Recommendations on coagulation diagnostics and coagulation management before thorax punctures

Procedure	Laboratory examination	Technique
Thoracocentesis Superficial biopsy	INR in case of pathologies involving anticoagulation and liver diseases PTT: Pat. with intravenous heparin Platelet count: not routinely recommended Hematocrit: not routinely recommended	INR > 2.0: threshold for treatment (ie, FFP, vitamin K) PTT: no consensus Thrombozyten <50.000/µl: Transfusion ASS/NSAR: do not withhold Thienopyridine (Clopidogrel) 0–5 Tage Pause LMWH (therapeutic dose): withhold one dose before procedure
Biopsy or drainage of abscesses Mediastinal and lung biopsy and thick catheters	INR recommended PTT: Pat. with intravenous heparin Platelet count: not routinely recommended Hematocrit: not routinely recommended	INR >1,5: threshold for treatment (ie, FFP, vitamin K) PTT: no consens Thrombozyten <50.000/µl: Transfusion ASS/NSAR: do not withold Thienopyridine (Clopidogrel) withhold for 5 d before procedure LMWH (therapeutic dose): withhold one dose before procedure

Adapted from Patel et al. (2012, 2013)
aPTT activated partial thromboplastin time, *INR* international normalized ratio, *LMWH* low molecular weight heparin

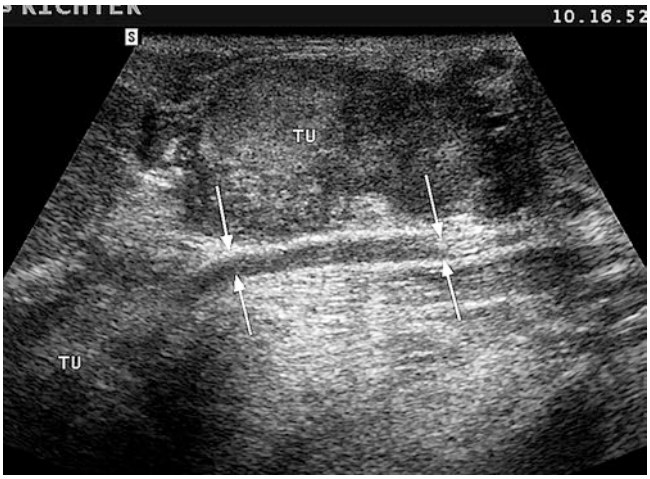

Fig. 10.1 Brachial plexus (*arrows*). Tumor masses (*TU*) in the region of the upper thoracic aperture

demonstrated with high-resolution ultrasound probes, thus avoiding injury through puncture (Fig. 10.1).

Vessels are detected with color-Doppler sonography (upper thoracic aperture, parasternal). Active (vascularized) sections of a tumor may be identified by color-Doppler sonography and, recently, by the even more sensitive method of contrast-enhanced sonography. Diagnostic puncture may be performed with a high success rate or the tumor may be ablated therapeutically, if advisable. Atelectatic or pneumonia-affected parts of peripheral lung consolidations may be differentiated from tumors by color-Doppler sonography or contrast-enhanced sonography (fewer motion artifacts) (Wang et al. 1995; Yang 1996; Zimmermann et al. 2003; Görg et al. 2006; Cao et al. 2011) (Fig. 10.2).

Sonography-guided percutaneous puncture also has its limitations, however. If the space-occupying mass is hardly or not at all visible percutaneously on sonography, or if the

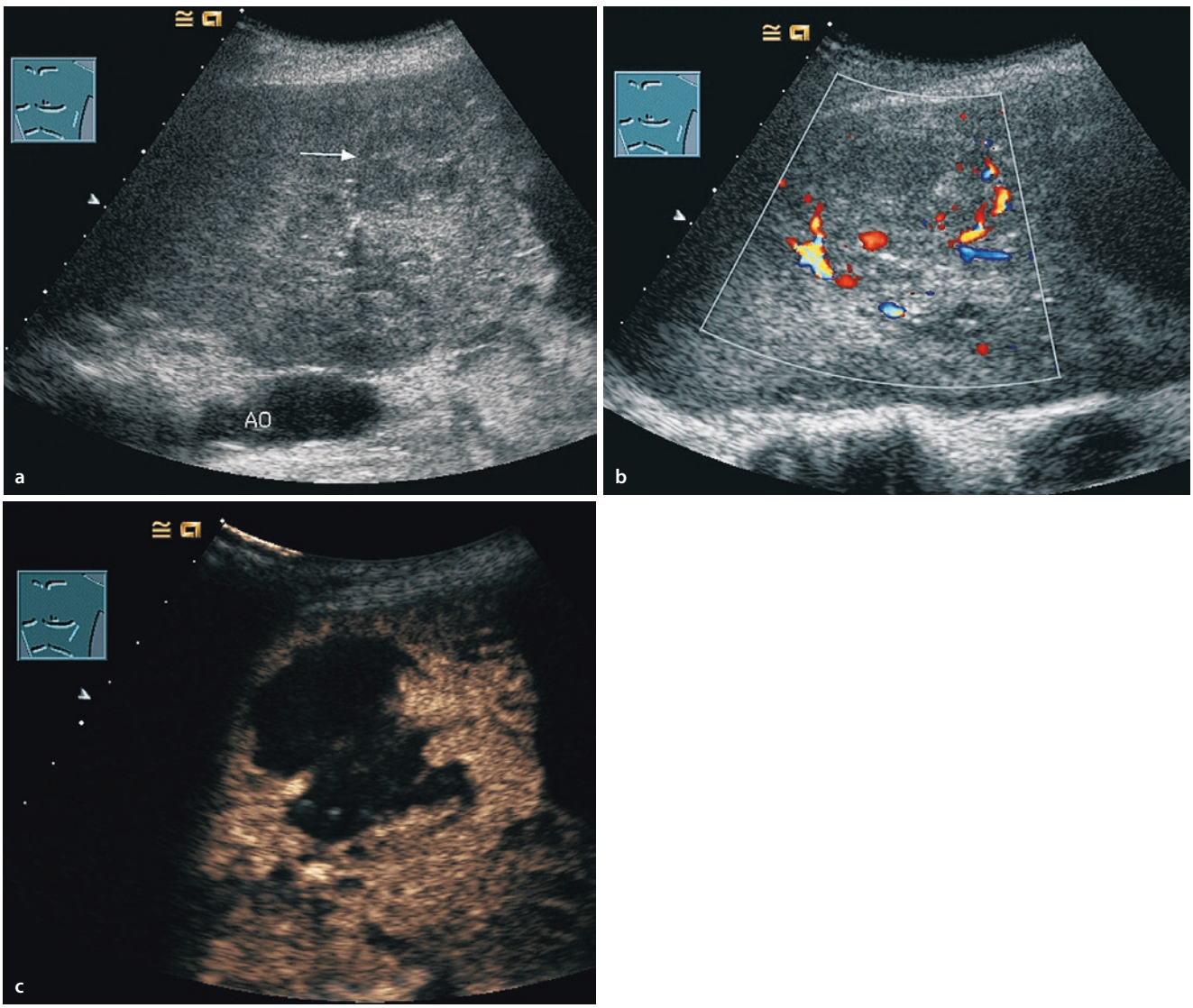

Fig. 10.2 Tumor inside an atelectasis. Computed tomography: obstruction atelectasis, cause not discernable. Bronchoscopy: no tumor found. **a** On B-mode sonography extensive atelectasis with a slightly conspicuous focal structural change (*arrow*). **b** In the area of structural irregularity there is no recognizable "normal" vessel architecture. **c** Space-occupying mass with little contrast on signal-enhanced sonography

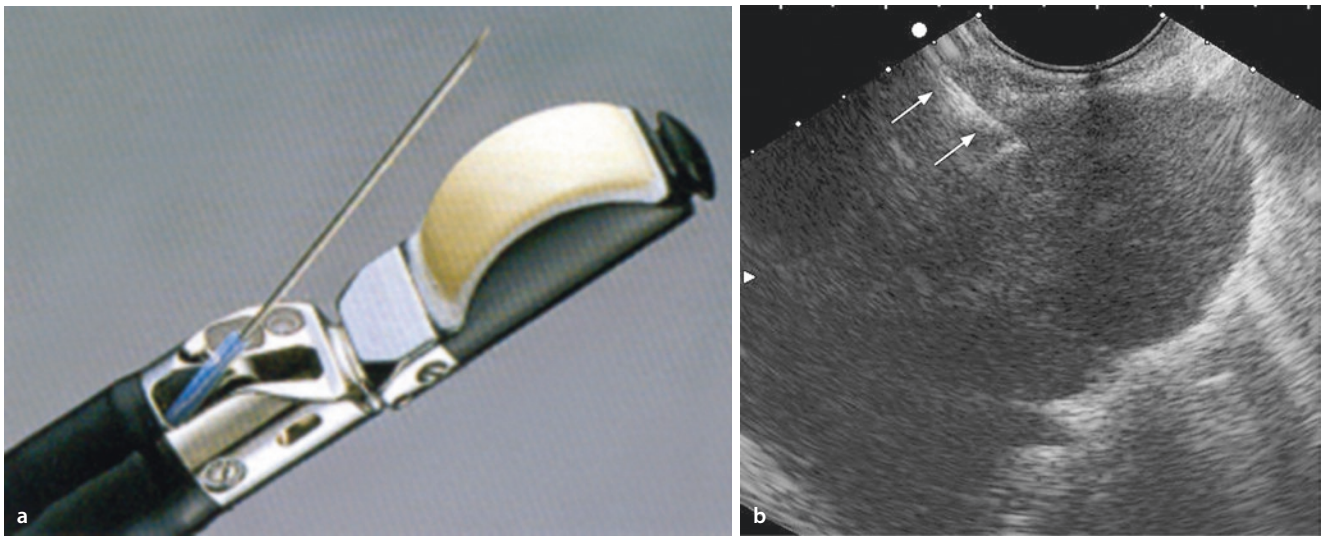

Fig. 10.3 Transesophageal puncture. **a** Longitudinal probe with puncture unit (Hitachi). **b** Paraesophageal hypoechoic tumor mass in the dorsal mediastinum. The puncture needle is easily recognizable (*arrows*). Cytology indicated small-cell bronchial carcinoma

puncture channel is not safe, other endoluminal procedures (bronchoscopy, endoluminal sonography) may be used or a computer-assisted puncture may be performed (Klose and Günther 1996; Mikloweit et al. 1991; Fig. 10.3).

In principle, the interventional procedure constituting the fastest means of arriving at the diagnosis and placing the least stress on the patient should be used.

The advantages of sonography-guided punctures are as follows:

1. The method can be carried out quickly and at the bedside.
2. There is no exposure of radiation to patients, assisting personnel or physicians.
3. The direction of puncture may be chosen freely, and the needle monitored continuously.
4. Nerves (plexus in the upper thoracic aperture), vessels (color-Doppler sonography), and the ventilated lung are spared (lower rate of pneumothorax).
5. Active tumor parts (color-Doppler sonography, contrast-enhanced sonography) may be punctured with a higher success rate.
6. Lung tumors may be differentiated from areas of pneumonia or atelectasis by color-Doppler sonography and contrast-enhanced sonography (fewer motion artifacts).
7. It is a low-cost procedure, and it may often be performed on an outpatient basis.

» "In US you see what you do, in CT you see what you have done" (Heilo 1996)

10.4 Apparatus, Instruments and Puncture Technique

For lesions of the chest wall, the investigator should use high-frequency linear probes. Lesions in the pleural space and lung should be investigated with sector-like probes equipped with a narrow covering. For endosonography-guided puncture, special intraluminal probes with biopsy canals are available (Kelbel et al. 1996; Jennsen et al. 2014).

The puncture needle can be guided in many ways (Fig. 10.4). A simple and economical method is so-called free puncture. Ninety percent of interventions are performed by the free-hand technique under sonographic visual control.

10.4.1 Puncture Needles

A distinction is made between fine (diameter less than 1 mm) and gross (diameter more than 1 mm) needles (Fig. 10.5). The rate of complications increases with the thickness of the needle and the duration of the procedure. The ideal puncture needle should fulfill the following criteria: it should be as thin as possible, sufficiently stiff to maintain the direction of puncture, cut sharply, be such that it can be advanced forward fast and be able to obtain sufficient material for investigation (Weiss and Düntsch 1996; Westcott 1980). Table 10.2 compares different classifications of needle diameters.

Fine Needles

For aspiration cytology, fine needles with a diameter of 0.7–0.9 mm are sufficient. They are available with and without a mandrin and have no cutting tip (economical injection needles, spinal puncture needles and Chiba needles).

Mandrins are usually not necessary, but their use is advisable if the pathway for puncture is long (through pulmonary tissue, for instance), because the needle bends less and there is no danger of abrading tissue outside the region to be punctured. A needle diameter of 0.7–0.9 mm is sufficient for cytological or bacteriological examination. If the liquid which needs to be aspirated is highly viscous (pus, blood), needles of a larger diameter must be chosen (1–2 mm maximum).

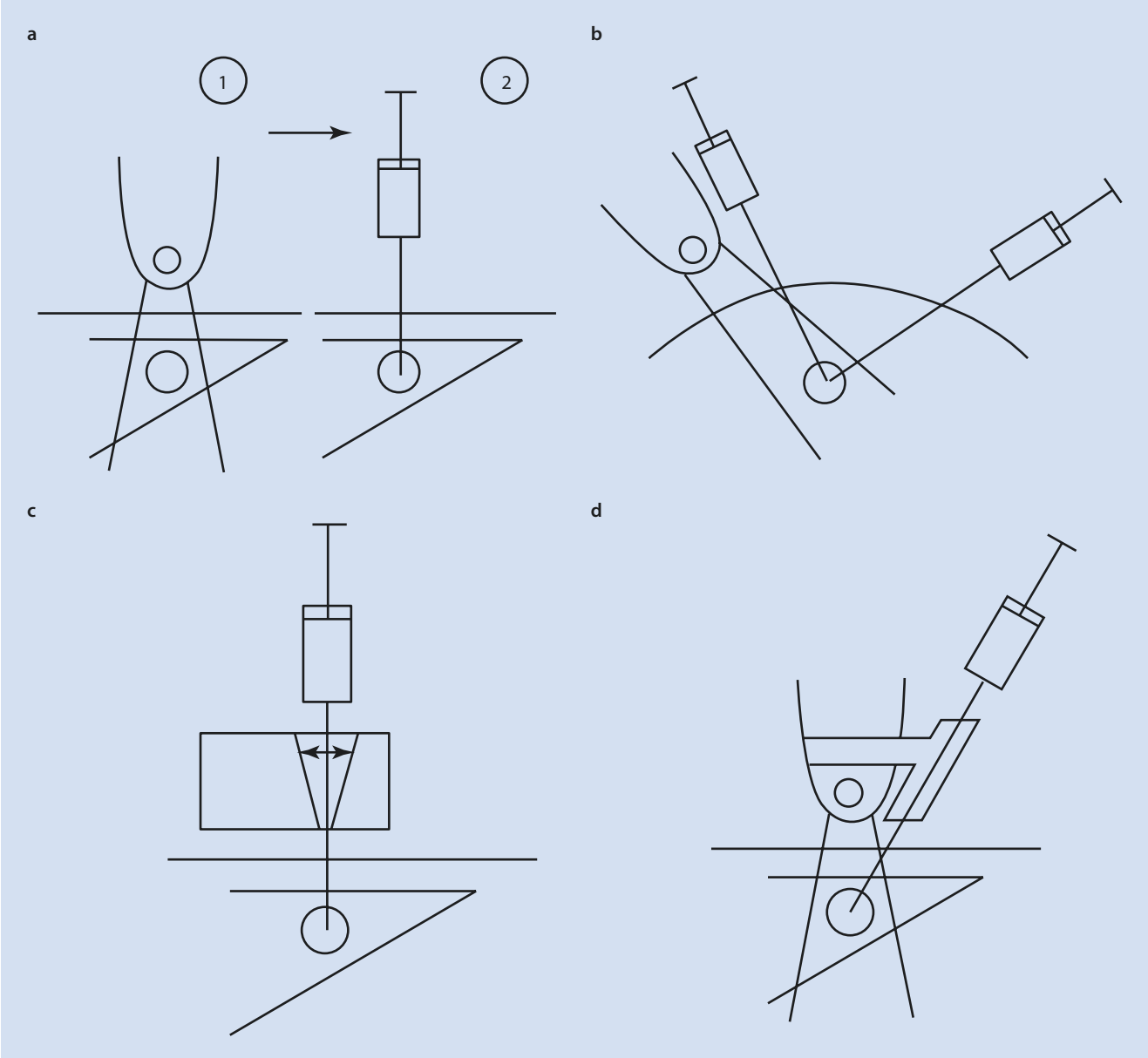

Fig. 10.4 Various puncture methods. **a**, **b** Free puncture. **a** Free-hand puncture after sonographic location. Inexpensive two-step method (no visual surveillance of the target area during the puncture). Very suitable for small processes located on the surface. **b** Puncture under sonographic observation. Low cost, puncture route variable, so punctures are possible from various areas, needle well visible, difficult with small processes located on the surface. Sterile gloves should be used for therapeutic procedures. **c**, **d** Guided puncture. **c** Ultrasound puncture probe. Expensive, puncture route not very variable, limited imaging through the perforation region, needle not easily visible, good view at close range. Seldom necessary for punctures of the thorax. **d** Sector/curved array scanner with attachment. Relatively cheap, needle is easily visible, but poor view at close range, puncture route prescribed but can be superimposed electronically, disinfection of the attachment necessary. Not sensible on the thorax

The puncture technique is as follows. Once the target of puncture has been reached, the puncture is performed, if possible, in a fan-like fashion under suction, in order to collect tissue from different areas (Fig. 10.6). With smaller tumors (less than 2 cm), it is often only possible to aim in one direction. In this case, turning the needle shaft may be helpful in collecting a tissue sample.

During forward and backward movement, cells are peeled off and aspirated into the tube. No suction should be applied during backward movement, so that material is not sucked into the syringe and dissemination of tumor tissue into the puncture canal is avoided.

A cytological slide is prepared by injecting the material collected onto the middle of the slide with high pressure. With use of a second slide, the material is spread with slight pressure and then, according to the agreement with the "house pathologist," fixated with alcohol (fixating spray, Merckofix, for instance) or air-dried. It is necessary to immediately scan the material under a microscope in order to make sure that there are enough cells for evaluation, so that a

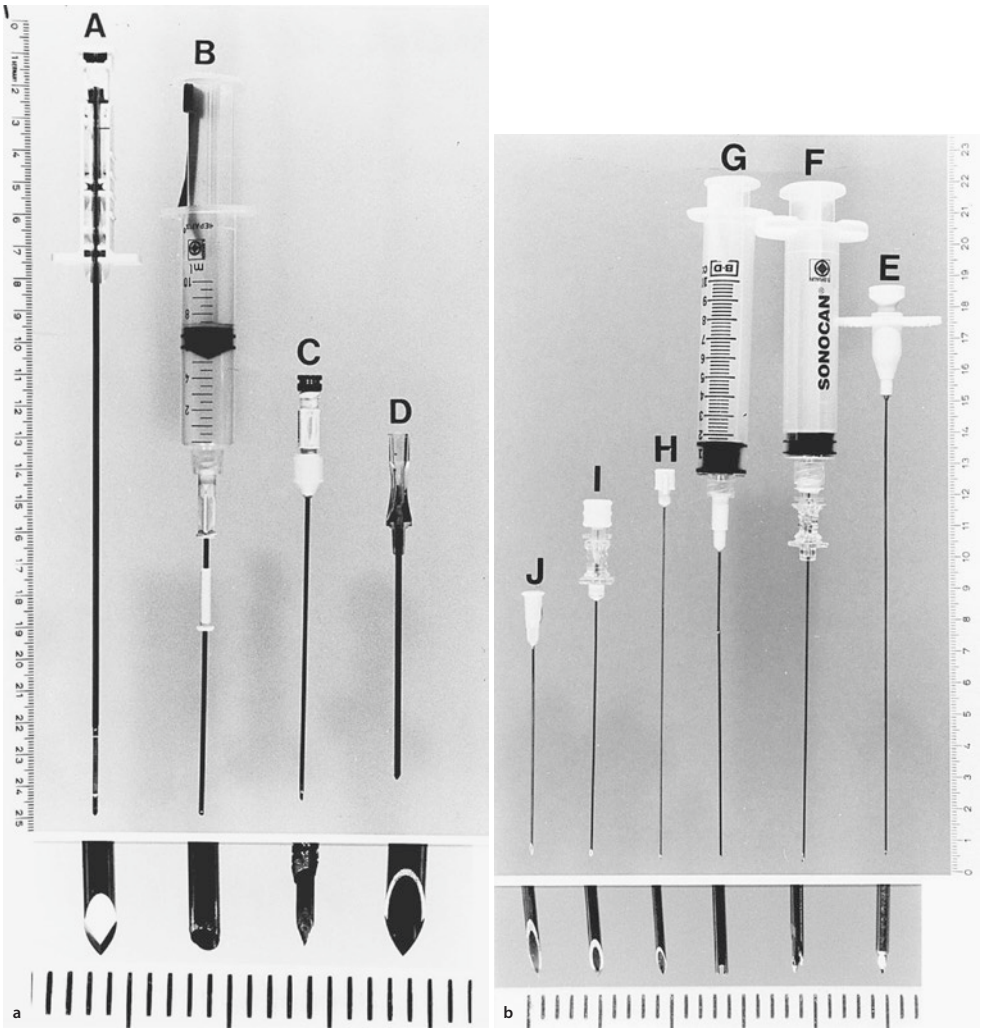

Fig. 10.5 Puncture needles. **a** Coarse needles. *A* Tru-Cut needle, diameter 1.4–2 mm. *B* Menghini needle, diameter 1.6 mm. *C* Bone punch needle (Angiomed).*D* Aspiration needle for viscous liquids, diameter 2.0 mm. **b** Fine needles. *E* Vaku-Cut needle based on Köhler (Angiomed). When the puncture destination has been reached, the stiletto is withdrawn three quarters of its length to create a partial vacuum. Diameter 0.8–1.2 mm. *F* Sonocan biopsy needle (Braun, Melsungen, Germany), diameter 0.8–1.4 mm, length 100–160 mm. Puncture technique as for the Otto needle, but without any rotating movement. *G* Cutting biopsy needle based on the Otto needle with a mandrin (Angiomed), diameter 0.8–1.2 mm, length 100–200 mm. *H* Chiba needle with a mandrin, diameter 0.6–0.9 mm. *I* Lumbal puncture cannula with a mandrin, diameter 0.9 mm. *J* Puncture cannula with no mandrin, diameter 0.7 mm

Table 10.2 Conversion table—needle diameter

Millimeters (mm)	Gauge (G)	French (Fr), Charriere (Charr)
0.7	22	
0.8	21	
0.9	20	
1.0	19	3
1.2	18	
1.35		4
1.4	17	
2.0	14	6
3.0	11	9
4.0	8	12
5.0	6	15

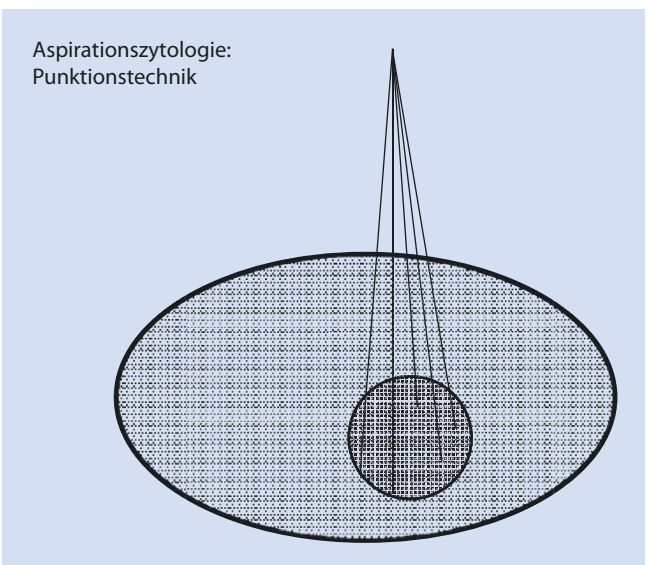

Fig. 10.6 Fine-needle aspiration puncture. Fan-shaped puncture technique

repeat puncture may be performed in the same session, which is necessary in one third of patients with suspected tumors. Bacteriological slides are made with Gram stain and bacteriological cultures started. If tuberculosis is suspected, special examinations are instigated (cultures, PCR, etc.)

The material obtained by this procedure usually only allows a cytological investigation which distinguishes between malignant and benign disease; it does not permit the investigator to determine the type of malignant lesion (e.g., lymphomas). If a quick diagnosis is needed and the proof of malignancy is sufficient, cytology is preferable at least as a first step (Diacon et al. 2007). Recent immunocytological techniques with specially coated slides have improved results, but determining the type of many malignant changes (lymphomas, for instance) is usually not possible, so examinations of histological material become necessary. Immunohistological techniques have also distinctly improved the results of cut biopsies (Müller and Blank 2011).

Possible mistakes in puncture cytology are:

1. Insufficient puncture technique
2. Little or useless material (possibly repuncture)
3. Aspiration of blood
4. False technique of slide preparation or fixation procedure
5. Little experience in cytology

Cutting Biopsy Needles

Tissue cylinders for histological assessment can be obtained with these needles. One-hand needles are useful, as *one* investigator performs the sonographic investigation and the puncture. Automatic one-hand needles (so-called puncture guns) are especially suitable in the thorax, as the procedure of puncture is fast, does not require the investigator to avoid the lung, and very representative puncture cylinders can be punched out from soft tissue (◘ Fig. 10.7). The results of puncture are better and the complication rate is lower—especially the rate of pneumothorax. In the case of hard tumors or tumors of the bony skeleton, the spring pressure of the automatic needle is often not sufficient to penetrate the tumor.

Disadvantages are the cumbersome procedure and the absence of the sensation of performing a puncture (Mathis 1997b).

In the meantime, there are a variety of equivalent needles available on the market. It is sensible to familiarize oneself with *one or two* needle types. Three needle techniques can be differentiated:

1. *Tru-Cut principle*: The True-Cut needle contains a biopsy chamber, securing the cylinder which has been cut. A disadvantage is that the volume of the tissue particle is thinner in comparison with the needle diameter and also is only half-cylindrical.
2. *Surecut principle*: The cutting process happens through a quick forward movement of the needle. On retraction, the tissue cylinder is held within the cylinder by suction. If the negative pressure fails, the tissue cylinder may be lost (◘ Fig. 10.8).
3. *BioPince principle*: Similar to the Surecut principle, complete cylinders are cut, thus yielding large tissue volumes (needle diameter 1.2 mm), producing better histological results. The needle combines the advantages of both principles mentioned above. A special "fixation wire" which gets propelled within the needle after the puncture procedure secures the tissue cylinder. Tumor seeding is very unlikely with this method (◘ Fig. 10.7).

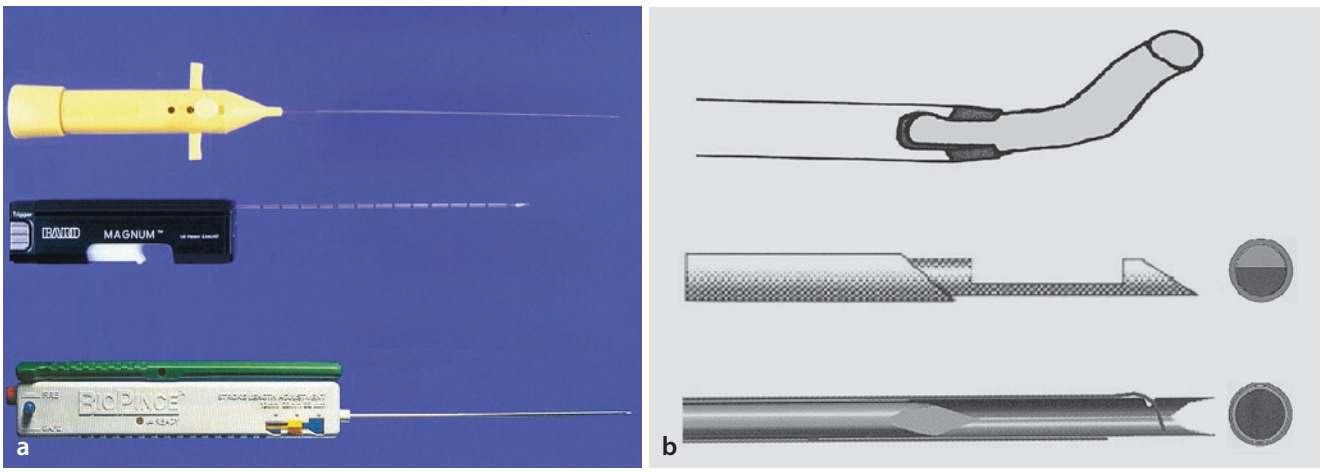

◘ **Fig. 10.7** **a** Automatic single-hand needle. The required depth of injection (measured sonographically) can be preset. *Top*: Auto-Vac puncture, disposable set (Bard). *Middle*: Reusable pistol from Barth with insertable Tru-Cut needles. The Tru-Cut needle contains a biopsy chamber. An advantage is that the cut cylinder of tissue cannot be lost when the needle is withdrawn. A disadvantage is the short tissue cylinder. *Bottom*: BioPince—biopsy pistol (Pflugbeil-Amedic). The full tissue cylinder is secured inside the needle by a special holding wire. **b** Surecut needle (*top*), Tru-Cut needle (*middle*) and BioPince needle (*bottom*)

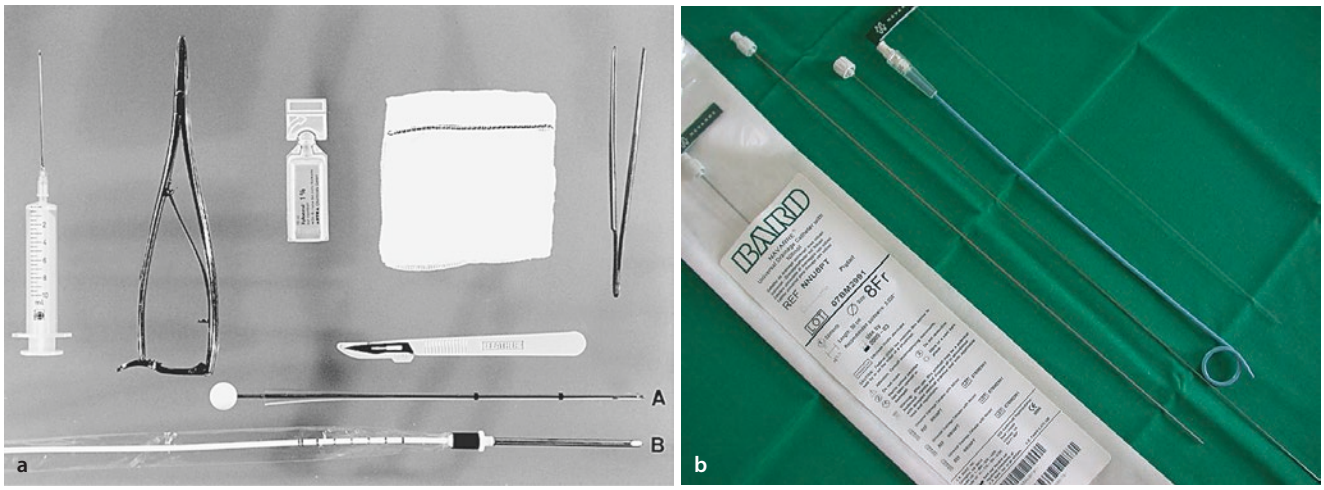

Fig. 10.8 **a** Pleural drainage set (trocar technique). *A* Thin (12-Fr) pneumo-catheter (Intra).*B* Trocar catheter (Argyle). **b** Navarre universal draining catheter (Bard—Angiomed 8–12 Fr). This catheter has many advantages: direct puncture only requires a small incision, introduction is possible without preceding dilatation, it does not kink, the lumen rarely occludes and the pig-tail prevents dislocation

Gross Needles

Gross needles (1.2–2 mm) are usually only needed for aspiration of highly viscous fluid. For histological differentiation of benign lesions of the thoracic wall, pleural afflictions or interstitial pulmonary disease, True-Cut needles of a large size might be necessary (Gleeson et al. 1990; Ikezoe et al. 1990; Fig. 10.7).

10.4.2 Drainage Catheter

The diameter of the selected catheter depends on the viscosity of the liquid formation. In principle, drainage may be performed using the trocar or Seldinger's technique. *The trocar technique* is commonly used in the thorax (Fig. 10.8). Both drainage techniques are preceded by diagnostic puncture (Fig. 10.9).

10.4.3 Checking the Position of the Needle and the Catheter

Correct placement of the needle is not demonstrated by sonography alone. Moreover, the "sensation of puncture" usually changes when the target of puncture is reached. Depending on the situation, resistance is noticeable. The feeling of hitting something hard suggests a malignant tumor. The absence of any palpable sensation when cutting a cylinder is one of the few disadvantages of using a "puncture pistol." Optical visualization of the needle depends on the angle of the needle and the ultrasound beam. Ideally, when a needle is introduced at the level of the transducer, the needle shaft is seen as an echogenic double reflex. However, in deeper lesions, only the tip of the needle is seen as a bright double reflex (Fig. 10.10b). A compromise must be found between demonstrability of the needle (better with a larger angle) and targeting precision (better with a smaller angle). The choice of the points of approach is often limited in the thorax by the anatomy.

In tissue with high echodensity it may be difficult to localize the needle. Here, it is useful to move the needle or the mandrin backward and forward and even to employ brief suction. Color-Doppler sonography will show the needle as a colored line (Fig. 10.11). When a gun is used, the incision canal (air) is visible even several seconds after the puncture.

A drainage catheter is typically visualized as a bright double contour, which might not show up the whole way, however. On color-Doppler sonography, the course of the catheter during instillation of fluid is clearly depicted by color-coding (Wang et al. 1995). If both techniques faile the correct positioning of the catheter can be checked by the injection of NaCl 0.9 %, mixed with a drop of SonoVue® (ultrasound contrast agent)

The coordination between the ultrasound probe and the needle tip works best if carried out as "one person—one hand puncture." Visualization of the spatial relations is better and necessary corrections in the position of the needle tip can be performed more quickly.

The inexperienced investigator should practice on models, e.g., on a steak interlarded with olives, or in a water bath or on puncture models commercially available (Mathis 1999a). Cheap puncture models for ultrasound-controlled drainage can be manufactured in homemade (Mohr et al. 2014).

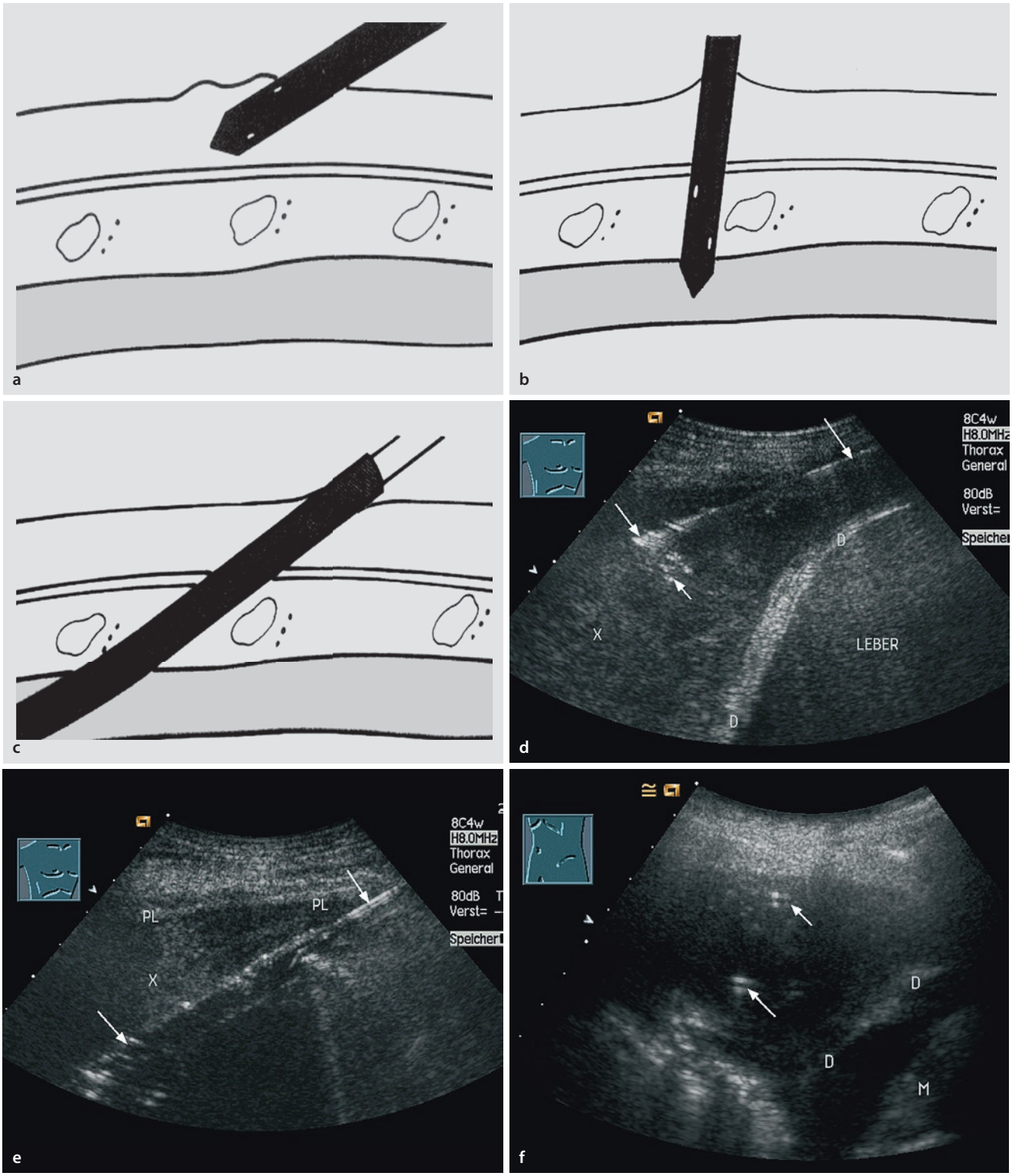

Fig. 10.9 Empyema of the pleura. **a**–**c** Pleural drainage. Outline of the technique. **d** On diagnostic puncture, the puncture needle (*large arrows*) is inserted in an upward direction at the upper edge of the rib. After instillation of liquid, an echogenic cloud shows up at the tip of the needle. *X* empyema. **e** On insertion, the trocar is visible as a straight echogenic reflex, partly producing acoustic shadowing (*arrows*). *X* empyema, *PL* parietal pleura. **f** After removal of the trocar, the soft draining tube (double reflex) is more difficult to recognize because of its winding course

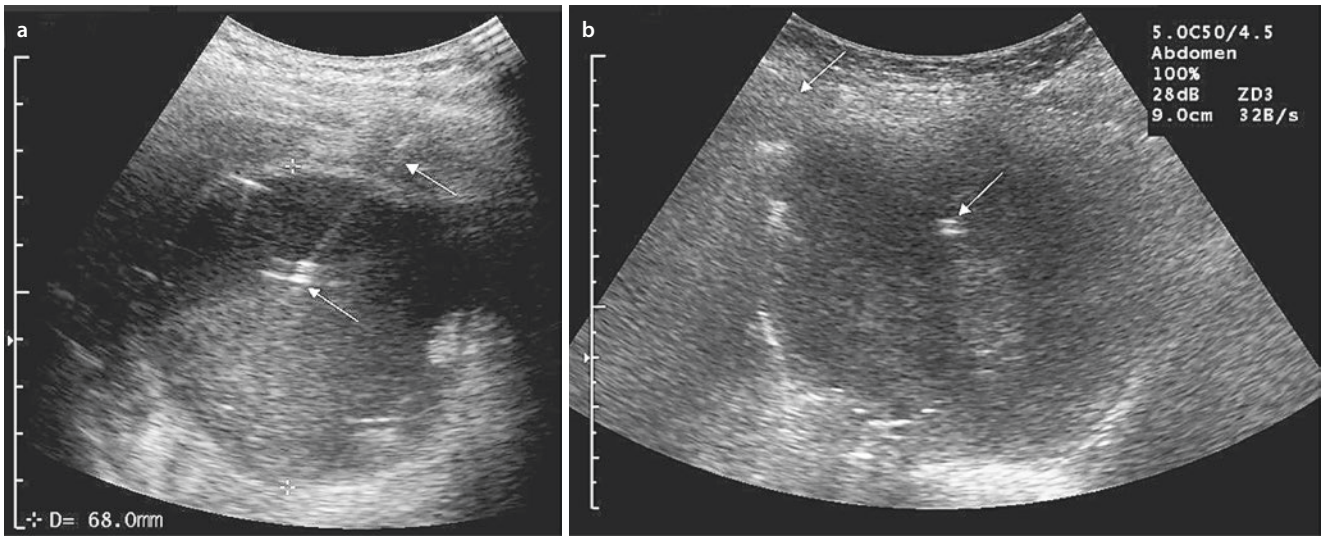

Fig. 10.10 **a** The needle shaft can be depicted at a great angle (45–90°) as an echogenous, straight-line reflex (*arrows*). The needle tip appears as an echogenic double reflex (*arrow* far from the sound head), but only if the needle is being guided correctly at the sound level. *Crosses* encapsulated pleural empyema. **b** Echogenic double reflex of the needle tip: double reflex is indicated by the *arrow* far from the sound head. As is so often the case, the puncture was not possible exactly at the insonation level. The needle shaft could only be indicated by wobbling movements (*arrow* close to the sound head). Hypoechoic tumor on the thoracic wall. Peripheral bronchial carcinoma (squamous cell)

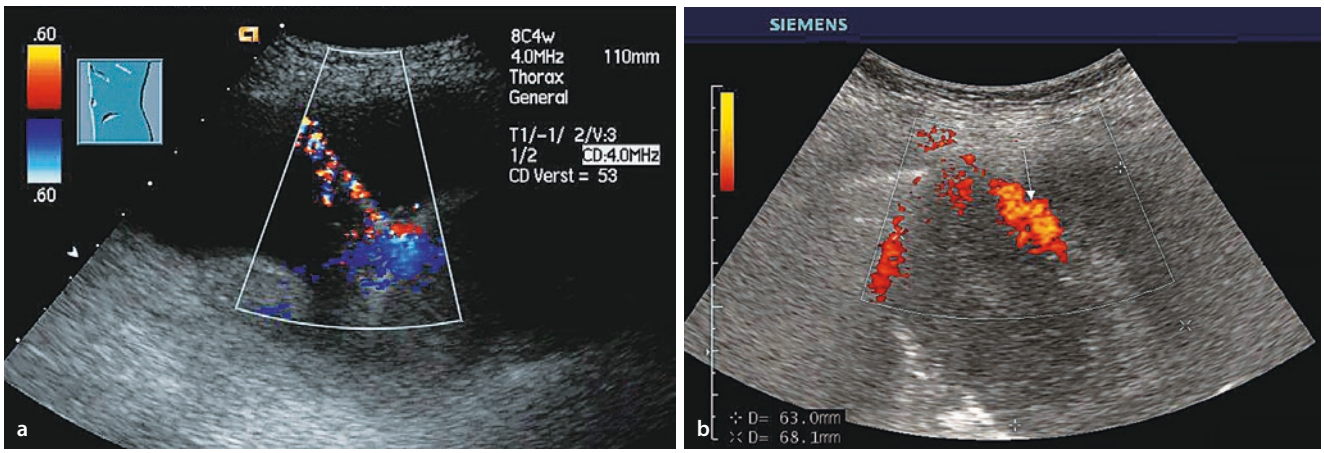

Fig. 10.11 **a** Color-Doppler sonography allows liquid movements in the needle to be detected. The exit of the liquid at the tip of the needle can be seen as a cloud of color. **b** Tissue shifts in the region of the needle tip (slight movement of the needle, or caused by suction) can also be detected by color-Doppler sonography (power Doppler). *Crosses* peripheral bronchial carcinoma

10.4.4 Preparation and Execution of Puncture

Most diagnostic puncture and draining procedures (of pleural effusions, for instance) may be performed on an outpatient basis. In principle, interventional procedures may be carried out in any room (emergency rooms, normal wards, intensive care wards), provided daily disinfection measures are guaranteed. Transportable ultrasound machines (Blank et al. 2014). may be advantageous.

Special puncturing equipment should be available: syringes, cannulas, puncture needles, drainage sets, gloves, disinfection spray, local anesthetics, sterile draping material and containers for further diagnostic processing (microbiological, chemical, cytological and histological examination) of the material obtained.

Coagulation status should be known (except in the case of lesions of the thoracic wall).

In an emergency case, the risk must be calculated individually.

As with any invasive procedure, the patient must be informed of the course and risk of the procedure. The sonographical status of the thorax is evaluated. Utilizing other imaging methods (plain chest radiograph, CT), the puncture goal, the site of puncture needle placement, puncture direction and puncture pathway are determined (the four P's).

The nonsterile ultrasound gel is removed. In cases of diagnostic puncture the investigator should use sterile gloves, local disinfectant spray and sterile catheter gel if necessary. The patient is positioned such that the focus is optimally accessible in a sitting, dorsal, lateral or ventral decubitus position. Local anesthesia is only required in cases of multiple puncture or needles with a thick lumen though many patients opt for it.

During the puncture the patient must be asked to briefly hold his/her breath.

Interventional procedures of the thorax—preparation and performance:

1. **Preparation**
   (a) Acknowledging preexisting findings (bronchoscopy, chest radiograph, CT).
   (b) Sonographic thorax status.
   (c) Verifying the indication for puncture.
   (d) Is a sonography-guided intervention technically feasible?
   (e) Are there contraindications for an intervention?
   (f) Has the patient received prophylactic antibiotic treatment (especially in the case of an abscess)?
   (g) Have information about the procedure and written consent by the patient obtained?
   (h) Cytology or histology?
   (i) Selection of puncture equipment (needle, drainage).
2. **Performance of intervention**
   (a) Positioning the patient (sitting, dorsal, lateral or ventral decubitus position).
   (b) Visualization of the goal of puncture, the pathway and direction.
   (c) Disinfection and local anesthesia, if wanted.
3. **Follow-up**
   (a) For outpatients
      – Three hours of surveillance after intervention.
      – Sonographical check before discharge of patient (pneumothorax? bleeding?).
      – Preliminary report for referring doctor.
      – Final evaluation of the procedure.
      – Immediate return to the hospital in case of symptoms.
      – Decision on who informs about the result and when.
   (b) For inpatients
      – Preliminary report for doctor in charge.
      – Instructions for nursing personnel (checkup examinations, suction for drainage, etc.).
      – Sonographic reevaluation after 3 h (pneumothorax?, bleeding?).
      – Checkup examinations after therapeutic punctures and drainage.
      – Possibly repuncture in cases of inconclusive result.

Sonographically guided interventions—conditions for achieving good results:

1. Careful formulation of indication (clinical experience).
2. Experience in sonography and puncturing.
3. Knowledge of possible complications and limitations of the method.
4. Quality of and preparation of material obtained.
5. Experience of the pathologist (immunohistology) and microbiologist.
6. Interdisciplinary cooperation.

10.5 Indications

10.5.1 Processes of the Chest Wall

Soft-tissue tumors should be punctured parallel to the surface of the lung as far as possible. The needle can then be (at a suitable angle) nearly completely imaged in its length and the risk of pneumothorax is minimized (◘ Fig. 10.12).

Needles with a large caliber may be used for this technique (1.4–2 mm). By doing so, even benign lesions are better differentiated (Gleeson et al. 1990; Bradley and Metreweli 1991; Sistrom 1997).

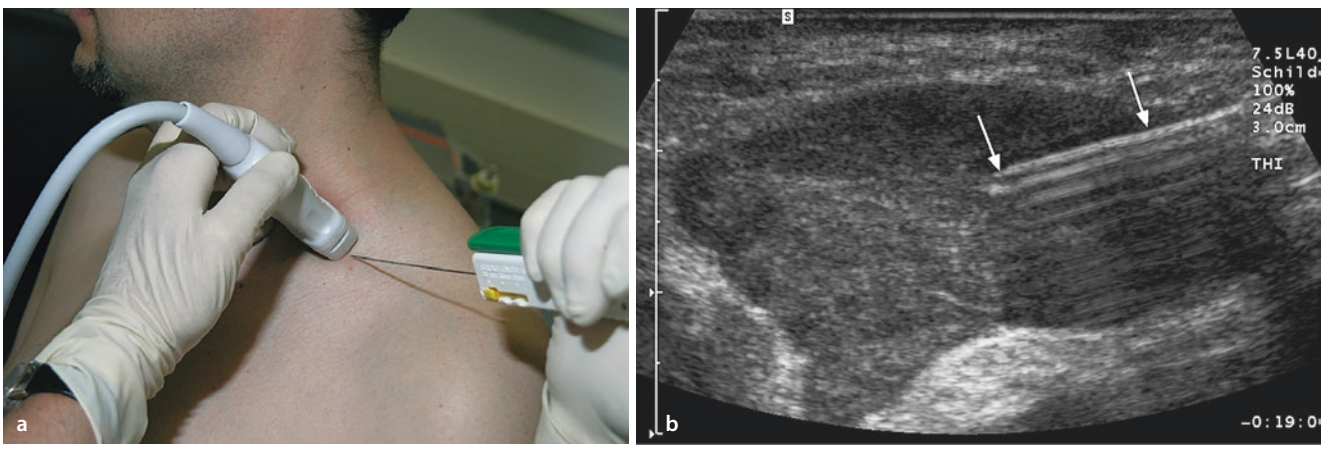

◘ **Fig. 10.12** **a** Classic puncture technique, upper thoracic aperture. **b** Classic puncture technique. Metastasis of the thoracic wall. The needle shaft (*arrows*) can be delineated very well at this favorable angle

Postoperative accumulation of fluid is treated by multiple puncture or, if necessary, with drainage.

Pathological processes of the bony skeleton are a domain of computer-assisted puncture, if the cortical bone is still intact. Frequently, diseases lead to defects in the cortical bone and may consequently be visualized well by sonography and also punctured (Fig. 10.13). Fine-needle aspiration puncture is usually sufficient for differentiation of inflammation/malignoma and carries a success rate of 88–100 %. If plasmocytoma is suspected, puncture is always preferable to cut biopsy, because diagnosis is easier from a slide preparation. For typification of a malignoma, a cut biopsy might be preferred in some cases.

Before puncturing tumors of the upper thoracic aperture, the nerve cords (brachial plexus) and vessels (color-Doppler sonography) should be identified in order to avoid injury to these structures (Vogel 1993; Civardi et al. 1994; Blank 1995, 2007).

10.5.2 Pleural Cavity

Thoracocentesis

In cases of large quantities of effusion, sonography helps to establish the extent of the effusion and mark the site of puncture in the optimal intercostal space. The puncture is then performed on the ward (Reuß 1996). In cases of complex effusions (small, loculated, encapsulated, inconvenient location), the puncture is safer when performed under continuous sonographic visual control (Figs. 10.14 and 10.15). By doing so, the rate of pneumothorax is markedly reduced (less than 1 %). The success rate is 97 % (O'Moore et al. 1987; Wang and Doelken 2009). Unsuccessful punctures can be avoided when "the fluid color sign" is demonstrated (Wu et al. 1995; Fig. 10.15). Synthetic indwelling catheters should be given preference over metal ones because of the risk of injury to the lung from metal.

After application of local anesthesia, the synthetic tube is pushed forward at the upper margin of the rib (in order to avoid injury of the nerve-vessel bundles running along the lower edge of the ribs) upward to the pleura with a mandrin (Abbocath; Abbott, Abbott Park III). Entry into the pleura is marked by a mild increase in resistance. The mandrin is then removed. In a closed system, special pleural drainage sets can be used to perform manual aspiration.

Uncomplicated pleural effusions in the presence of cardiac failure, pneumonia and even small pneumothorax after puncture can be treated with thoracocentesis.

Malignant pleural effusions, accumulation of pus or blood should be treated with a drain because of the risk of septation Müller and Blank 2011.

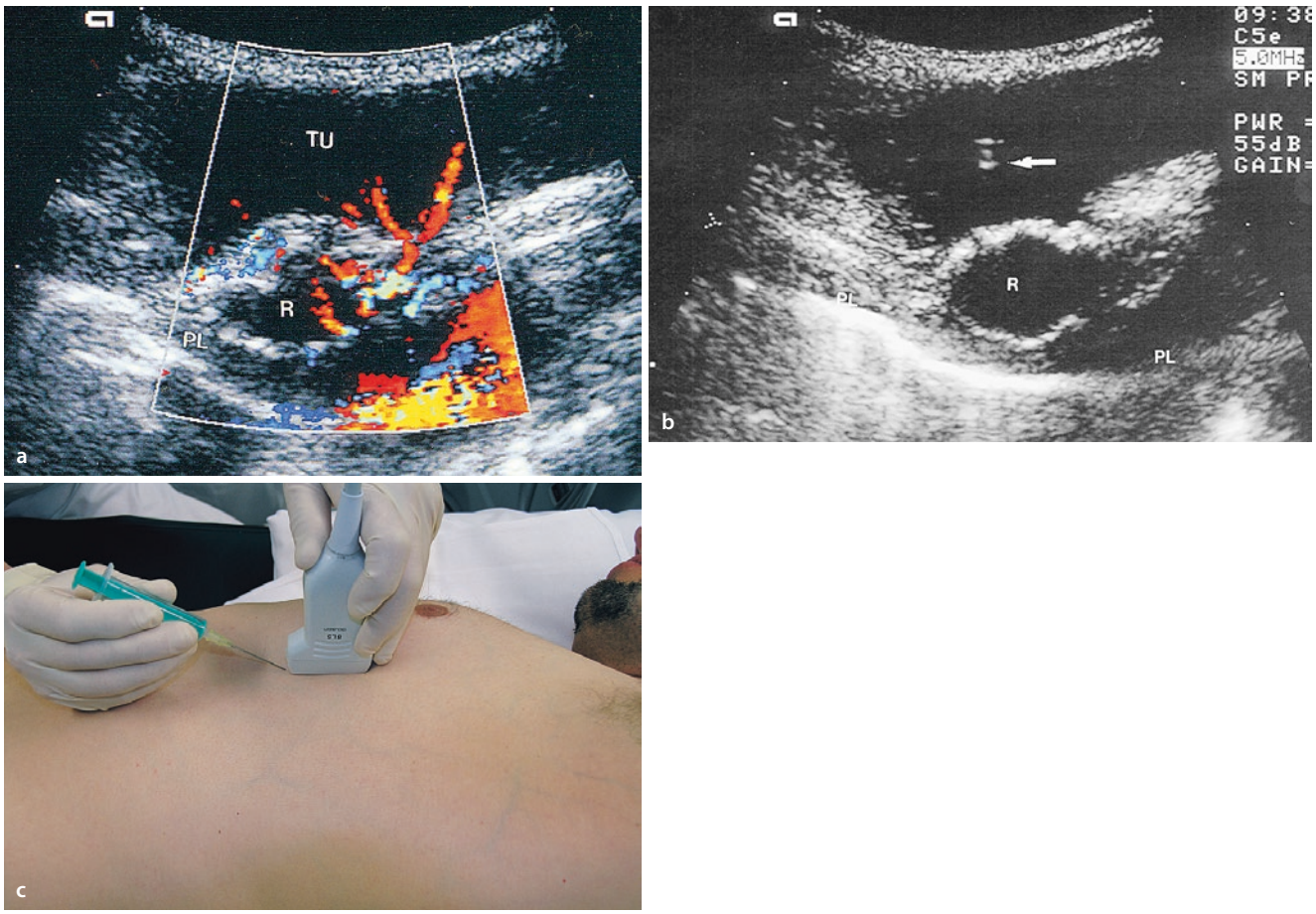

Fig. 10.13 **a** Destructed rib (*R*). Echo-free "soft tissue tumor" (*TU*). Color-Doppler sonography allows vessels to be depicted in the destructed rib and in the surrounding soft tissue tumor. *PL* pleura. **b** Fine-needle puncture of the soft-tissue tumor. The tip of the needle can be seen as an echogenous double reflex (*arrow*). Cytology indicated plasmocytoma. **c** Classic puncture technique

The success rate of cytology in malignant effusions is no more than 50–75 % (Gartmann 1988). In tuberculous effusions, pathogens are demonstrated in only 20–40 % of cases (Vladutiu 1986).

Pleura Biopsy

Since even the classic pleural blind biopsy according to Abrams or Ramell has an accuracy of no more than 50 % in malignant effusions, video-assisted thoracoscopy is being used more and more. Sonography-guided pleural biopsy is one alternative. The procedure has only been used in a very small number of cases so far, however (Mueller et al. 1988). As an alternative, automatic single-hand needles (BioPince needle, for instance) may be used successfully (sensitivity 70–80 %, specificity 100 %) (Adams et al. 2001; Chu et al. 1994; Heilo 1996; Koegelenberg and Diacon 2013). Fine-needle aspiration biopsy of tissue taken from a pleural thickening is of no value and is even hazardous (danger of bleeding). It may only be employed in the presence of focal lesions (Mathis et al. 1999).

Percutaneous Pleural Drainage

Given the appropriate indication, malignant, hemorrhagic and inflammatory pleural effusions may normally be treated with a sonography-guided pleural drain quickly, safely and successfully. Only rarely CT-guided puncture is necessary if the approach is difficult. Thin catheters (8–14 Fr, Pleurocat, for instance) are sufficient (Fysh et al. 2010; Davies et al. 2010). These thin catheters are tolerated better by most patients than thick catheters traditionally used in many hospitals. Their success rate is equivalent, and they carry a much lower complication rate. Puncture is usually performed with the trocar technique. The catheter should be placed in the lowest possible part of the pleural cavity.

Parapneumonic fluid collections should be drained soon in cases of septum formation and a pH level below 7.2. A drain should be left in place for 5–10 days, depending on the extent of inflammation (Kolditz and Höffken 2008).

In cases of malignant effusions, catheters with a narrow lumen (7–12 Fr, e.g., Pleurocat, Plastimed), will suffice. The puncture is usually performed using the trocar technique. The catheter is placed in the lowest part of the pleural cavity.

Early diagnostic verification of a pleural empyema is important, as percutaneous therapy is only successful (success rate, 72–88 %) in the acute phase (weeks 1–4) (Klose and Günther 1996; Müller und Blank 2011; ◘ Figs. 10.9, 10.16 and 10.19). The success of drainage in the presence of septation can be markedly improved by the instillation of urokinase (50–100,000 IU/treatment) (Sistrom 1997).

The correct positioning of the catheter can be checked by the injection of NaCl 0.9 %, mixed with a drop of SonoVue® (ultrasound contrast agent). This "off label" use has its advantages: it is possible to identify incorrect drainag and dislocations; septic developments and, as a result, insufficient drainage show up through the missing diffusion of the contrast medium in the pleural space (Heinzmann et al. 2012) (◘ Fig. 10.17). In the case of therapy resistant effusions the drainage with a tunneled catheter could be appropriate.

Pleurodesis

Malignant effusions are prone to build septa under recurrent thoracocentesis. It is therefore wise to proceed a early drainage treatment. Possibly. After the complete and possibly fractional emptying of the effusion (portions not to exceed 1.5 l) and the administering of a topical anesthetic follows the instillation of sclerosing substances, 4–5 g Talc mixed with 50 ml NaCl seems to be the most efficient; Bleomycin is

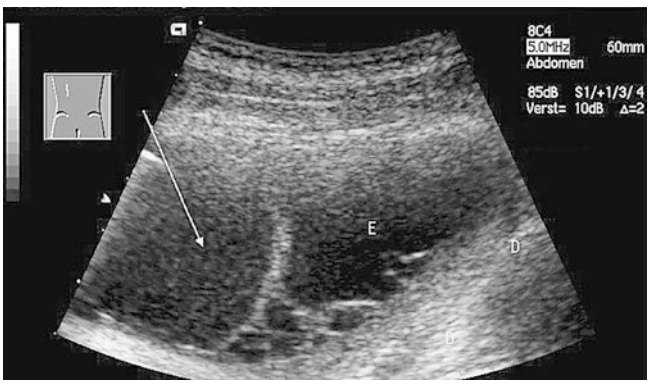

◘ **Fig. 10.14** Septated pleural effusion. Primary diagnostic puncture disclosing an encapsulated empyema (*arrow*). The secondary step involved pleura drainage. *D* diaphragm

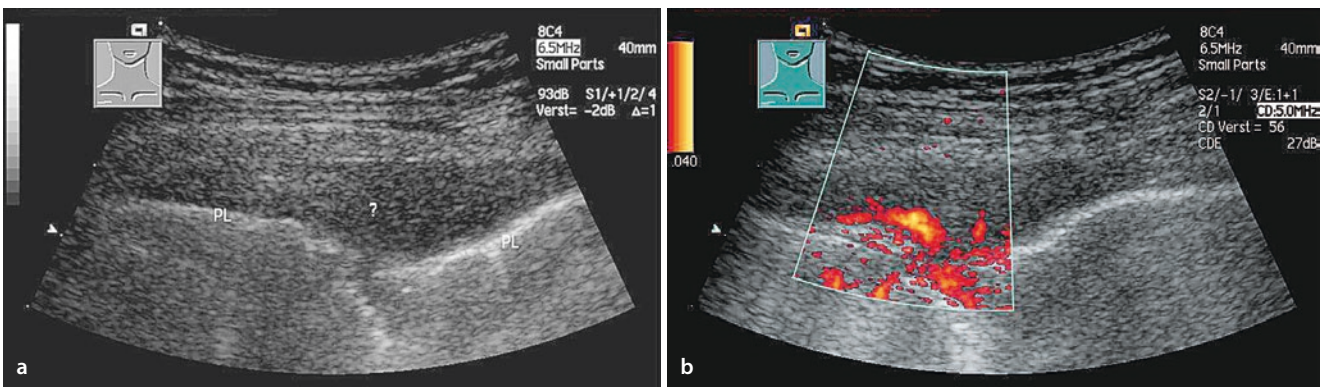

◘ **Fig. 10.15** **a** B-mode sonography for a differential diagnosis of an encapsulated effusion or fresh rind. *PL* visceral pleura. **b** Power Doppler demonstrates advanced vascularization with high-caliber vessels. Fresh pleural rind

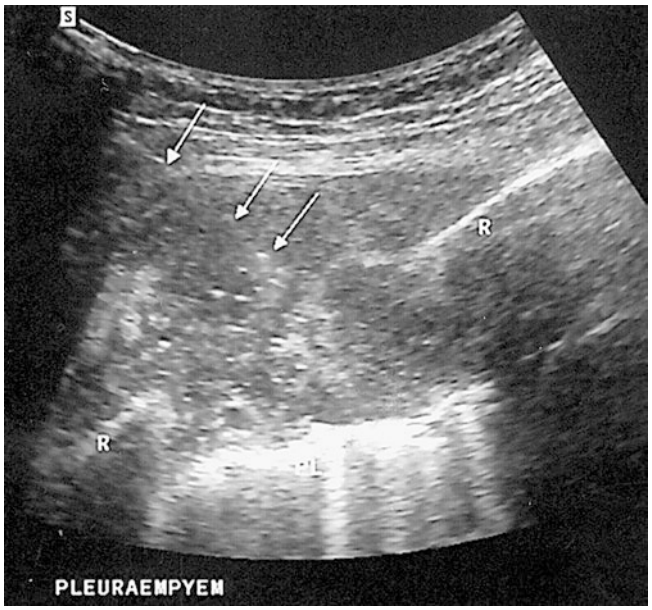

Fig. 10.16 An 80-year-old patient, whose temperature rose rapidly a few days after a fall which injured the left side of the thorax. X-ray image reveals a shadow located on the thoracic wall, suggestive of a fractured rib. Sonographic mass with infiltration into the thoracic wall. Minor liquid movements were perceptible during the dynamic examination. The diagnostic puncture was not successful until a coarse needle (with a diameter of 2 mm) was used. It proved possible to extract highly viscous pus. A pleural drainage was then inserted. *Arrows* needle shaft

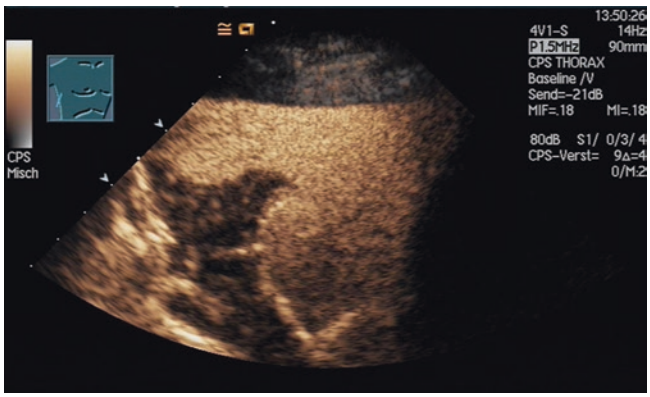

Fig. 10.17 The contrast medium spreads through the entire pleural space

an alternative (Roberts et al. 2011). Pleurodesis obtained by thoracoscopy is all the more effective (Tan et al. 2006).

10.5.3 Lung Consolidations

Peripheral pulmonary lesions may be visualized sonographically if they are situated in a favorable topographical position. They may be punctured if they reach the visceral pleura or if a poststenotic atelectasis or pneumonia provides an acoustic window.

At the time of diagnosis, two thirds of lung carcinomas are no longer curable by surgery. The histological type must be determined before palliative therapeutic measures are employed. In the diagnosis of the peripheral lung tumor, sonography-guided puncture is markedly superior to bronchoscopy, much easier and faster to perform than radiography or even computer-assisted percutaneous biopsy, and devoid of radiation (Chandresakar et al. 1976; Börner 1986; O'Moore et al. 1987; Hsu et al. 1996; Diacon et al. 2004a, b; Hoosein et al. 2011; Fig. 10.18).

Peripheral tumors larger than 3 cm in size should be diagnosed by fine-needle cut-biopsy (histology) (Mathis and Gehmacher 1999; Schubert et al. 2005). Peripheral tumors smaller than 3 cm in size can be better diagnosed by fine-needle aspiration cytology (Laio et al. 2000; Sistrom 1997). Biopsy is not always sufficient (accuracy 70 %) to distinguish benign tumors. Wedge resections obtained by thoracoscopy are given preference in many cases (Beckh and Bölcskei 1997).

Special Puncture Technique

A safe pathway for puncture circumventing the ventilated lung is an important prerequisite of avoiding pneumothorax. Larger tumors may be punctured in the classical way. The needle is inserted at the level of the ultrasound probe. The needle tip is pushed toward the parietal pleura under continuous sonographic observation. While the patient holds his/her breath, the lesion is punctured in such a way that the needle does not reach the ventilated lung. To achieve this, the puncture depth is measured beforehand and marked on the needle in the case of using an automatic one-hand needle.

Small (less than 1-cm) tumors located in the periphery may also be punctured if expertise is sufficient. Puncture technique must be adjusted to the individual type of lesion. Similar to puncture of the thyroid, atypical puncture is often necessary (Blank 2007). The tip of the needle must be inserted through the skin almost vertically, near the middle of and parallel to the probe, which has as little contact with the skin as possible. By tilting the probe in a plane vertical to the plane of the probe, one can identify the needle tip inside the thoracic wall, push it toward the pleura and insert it into the lesion under observation. Visualization of the needle tip is facilitated by moving it back and forth abruptly.

Alternatively, small lesions may be punctured "from memory" after marking the intended site of puncture with a ballpoint pen, for instance (small ring pressed into the skin). The results are no worse in the hands of experienced examiners.

If a small perforated ultrasound probe is available, this may also be used for a successful puncture.

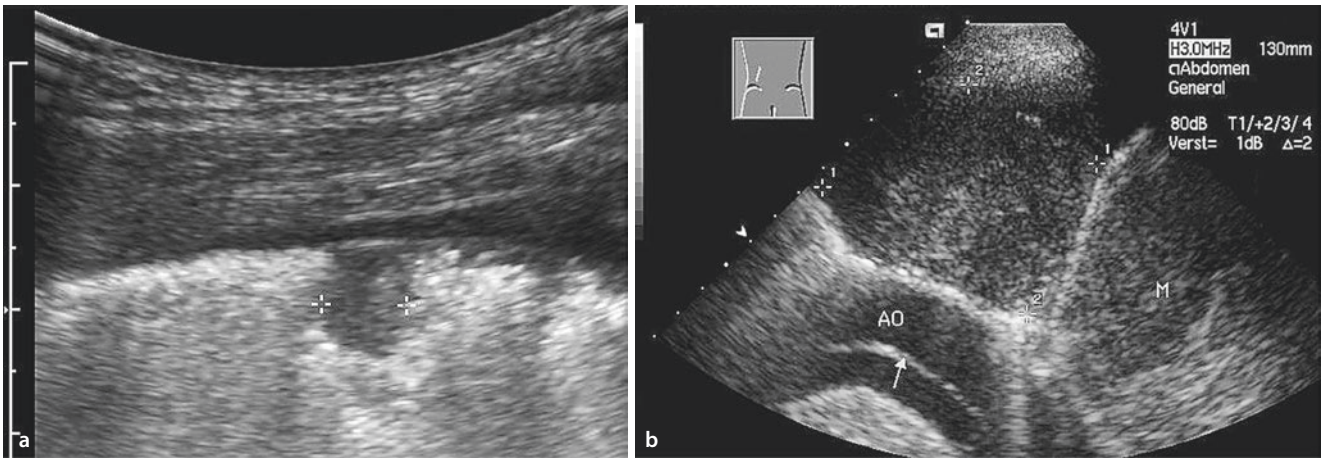

Fig. 10.18 **a** Several small peripheral lung tumors (maximum diameter 18 mm) located on the thoracic wall. Delicate pleural effusion. Fine-needle aspiration cytology indicated small-cell bronchial carcinoma. **b** Large mass, left dorsobasal location (*crosses*), alongside the diaphragm and also the descending aorta (*AO*). A dissecting aortic aneurysm had been identified in this patient 4 years earlier. *Arrow* dissection membrane. Fine-needle incision biopsy (Sonocan needle, 0.9 mm in diameter). Histology indicated squamous cell carcinoma

Pneumonia and Pulmonary Abscesses

The cause of consolidation of sections of the lung may be difficult to classify in immunosuppressed patients, especially. Aspiration puncture or cut biopsies of the areas with consecutive microbiological, cytological and histological examination of the material obtained allow a diagnosis in up to 93 % of cases (Yang et al. 1985).

Even small pulmonary abscess that escape detection on the radiograph can be imaged by sonography (6–7 mm) (Kolditz and Höffken 2008). If antibiotic therapy does not yield the desired result (75–90 % success rate), fluid may be aspirated from the region of the abscess under sonographic guidance. By this means, the pathogen can be isolated in about 65–93 % of cases (Gehmacher et al. 1986; Yang et al. 1992). If therapy continues to fail, a lung abscess drainage may be performed under sonographic guidance but this is rarely necessary (Sonnenberg et al. 1991; Klein et al. 1995; Fig. 10.19). The risk of bronchopleural fistula formation is minimized when the investigator uses the shortest access and traverses solid, homogeneous, infiltrated or atelectatic tissue (Mathis et al. 1999; Wali et al. 2002).

10.5.4 Mediastinum

Few space-occupying masses in the mediastinum (retrosternal goiter, cyst, aneurysm, thrombosis) can be reliably classified on the basis of characteristic sonographic features. An investigation of fine tissue is needed in order to determine the cause of the lesion. Gentle removal of tissue without causing a large defect is very important in the diagnosis of space-occupying masses that can be removed by surgery. Therefore, puncture under image guidance should be the first procedure. When this is done, space-occupying masses in the mediastinum can be easily punctured from a suprasternal or parasternal approach under sonographic guidance (Nordenstrom 1967; Rubens et al. 1997; Koegelenbug et al. 2009). The accuracy is 54–100 %, and the rate of complications is 0–4 %. Vessels should be avoided (Color-Doppler Sonography) (Blank et al. 1996; Figs. 10.20, 10.21 and 10.22). In cases of superficial lesions (thymomas, lymphomas), gross needles are given preference. With use of a needle with a thick lumen, correct histological classification is achieved in up to 93 % of cases and the rate of complications is only slightly higher, at less than 1 % (Fig. 10.23). In our experience, a needle diameter of 1.2 mm (BioPince needle) is normally sufficient.

In contrast to radiographic or CT-guided puncture (10–44 %), pneumothorax is rarely encountered (Yang et al. 1992; Heilo 1993, 1996; Schuler et al. 1995; Gupta et al. 1998; Koegelenberg et al. 2011; Marchevsky et al. 2011).

In recent years, endosonographic transesophageal-guided puncture has also been used successfully. It is a good complement to percutaneous puncture, as lesions in the anterior mediastinum are not easily accessed, in contrast to those in the posterior and lower mediastinum (Schlotterbeck et al. 1997; Pedersen et al. 1996; Hüner et al. 1998; Janssen et al. 1998; Jennsen et al. 2014).

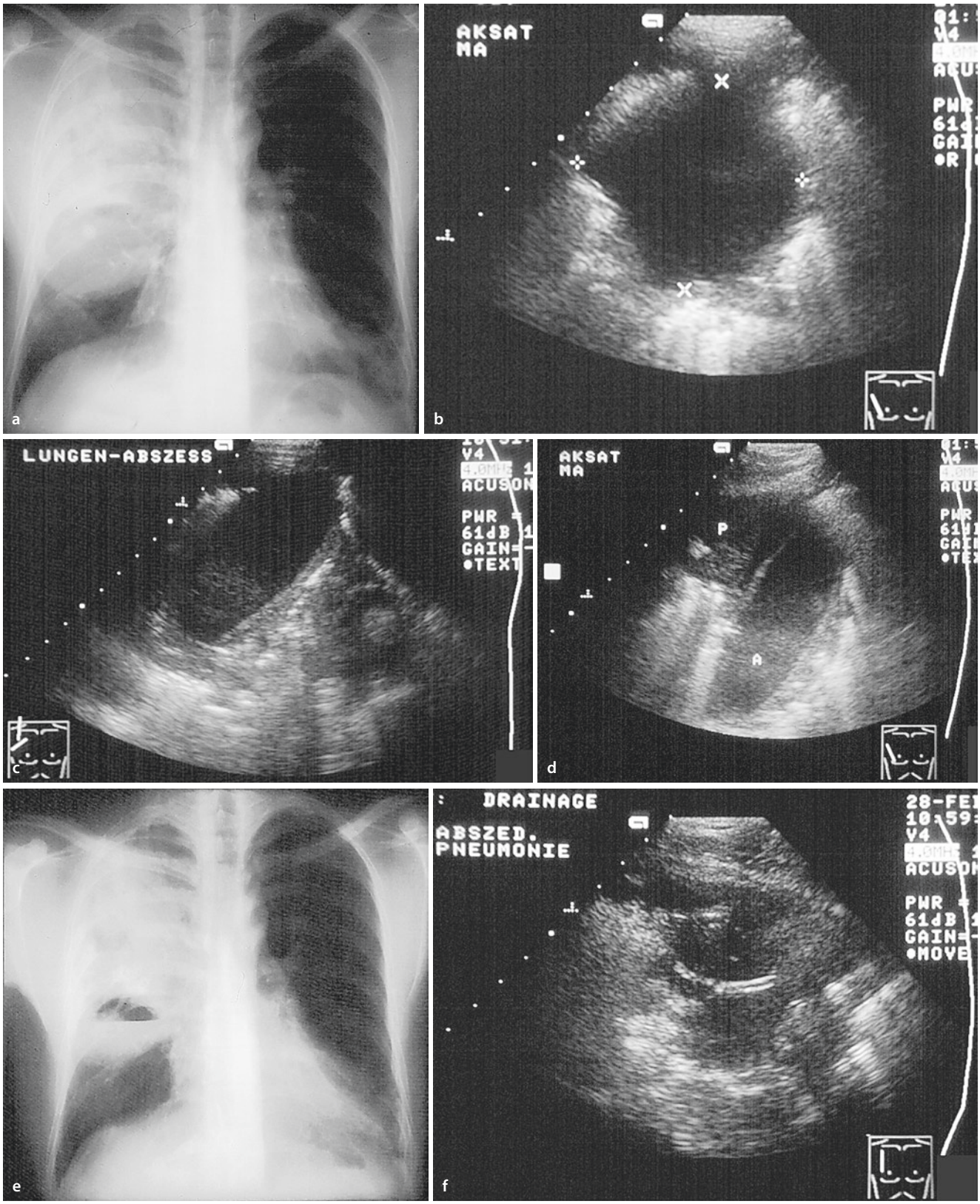

Fig. 10.19 Lung abscess with drainage. Young man with community-acquired pneumonia not responding to standard antibiotic therapy. Continuing high temperatures and respiratory deterioration. **a** On chest X-ray, extensive infiltration of the right upper lobe of the lung. **b** Sonography clearly demonstrates abscess formation. **c** Next to the abscess (*A*), pneumonic consolidation (*P*) is visible. If this does not contain air, puncture passing through this section would be feasible. The abscess is encapsulated by a membrane. **d** The shortest pathway for transthoracic puncture is chosen, and pus can be aspirated through the needle. **e** Abscess formation on chest X-ray. **f** The abscess is drained by a suction-rinse-drainage (echogenic double lumen) over 4 days. Quick recovery ensues

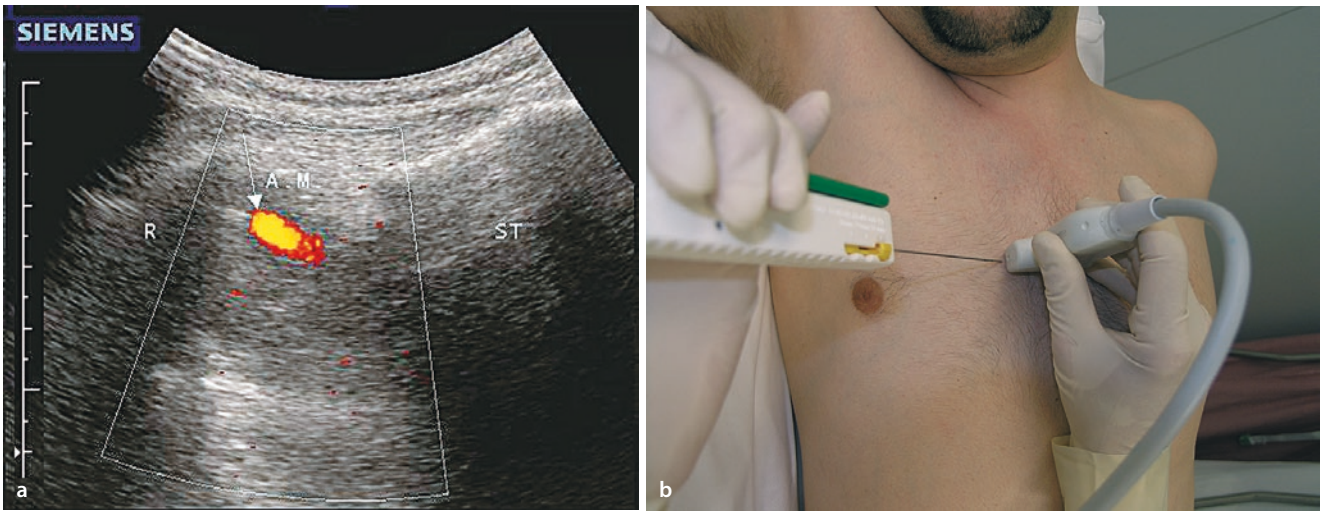

Fig. 10.20 **a** Mediastinal tumor. Parasternal plumb line in the right lateral position. Hypoechoic, indistinctly delineated mass (located in the color window). Color-Doppler sonography in "power" mode shows the mammary vessels located parasternally, **b** which have to be avoided during a punch biopsy

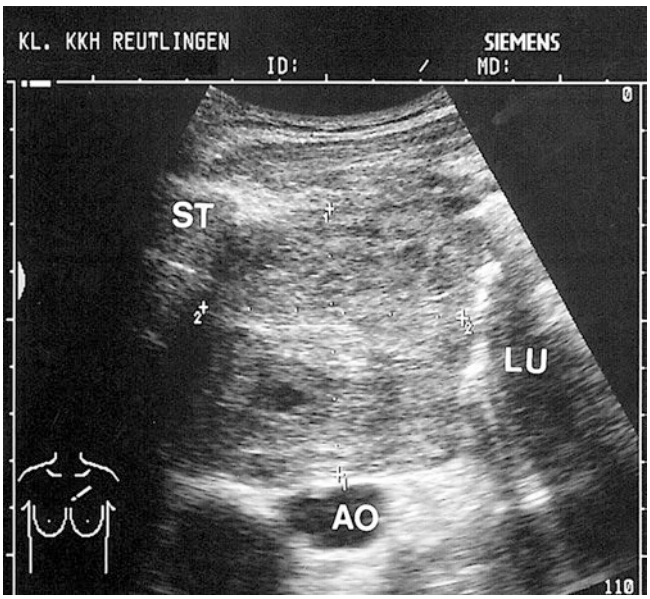

Fig. 10.21 A large mediastinal mass was discovered primarily by sonography, located parasternally on the left, in a 19-year-old patient during emergency treatment connected with a superior vena cava syndrome. A punch biopsy was performed immediately (Sonocan needle, 1.2-mm diameter). Histologically, a highly malignant non-Hodgkin lymphoma was diagnosed. *ST* sternum, *LU* lung, *AO* descending aorta

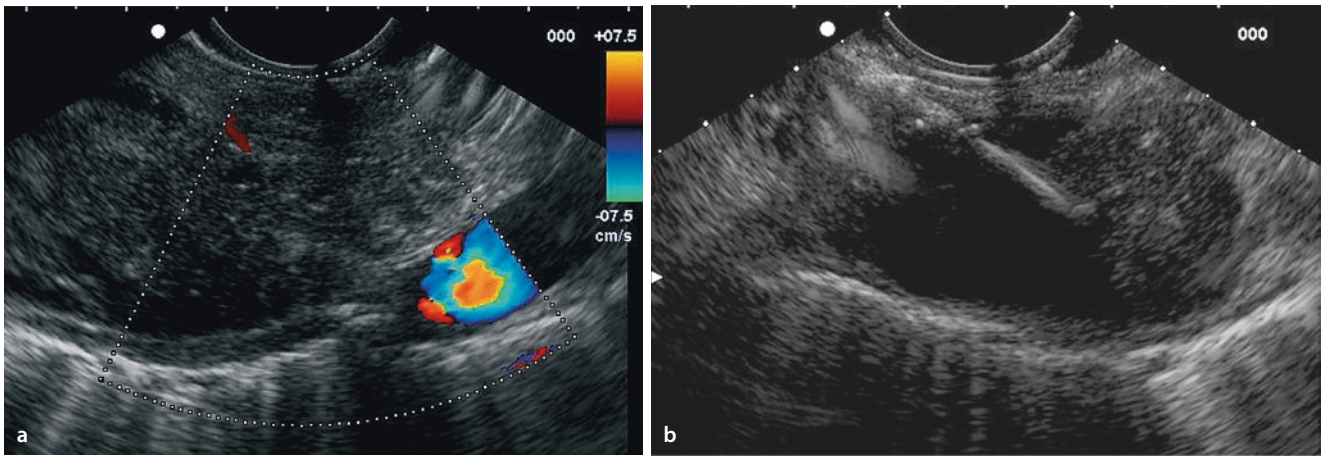

Fig. 10.22 Paravertebral abscess in a case of spondylodiscitis. At first, open surgical drainage of the spondylodiscitis was performed, followed by endosonographically guided nasal/transesophageal drainage used for rinsing with isotonic saline. **a** Space-occupying mass located next to the spine and the aorta. **b** Insertion of drain

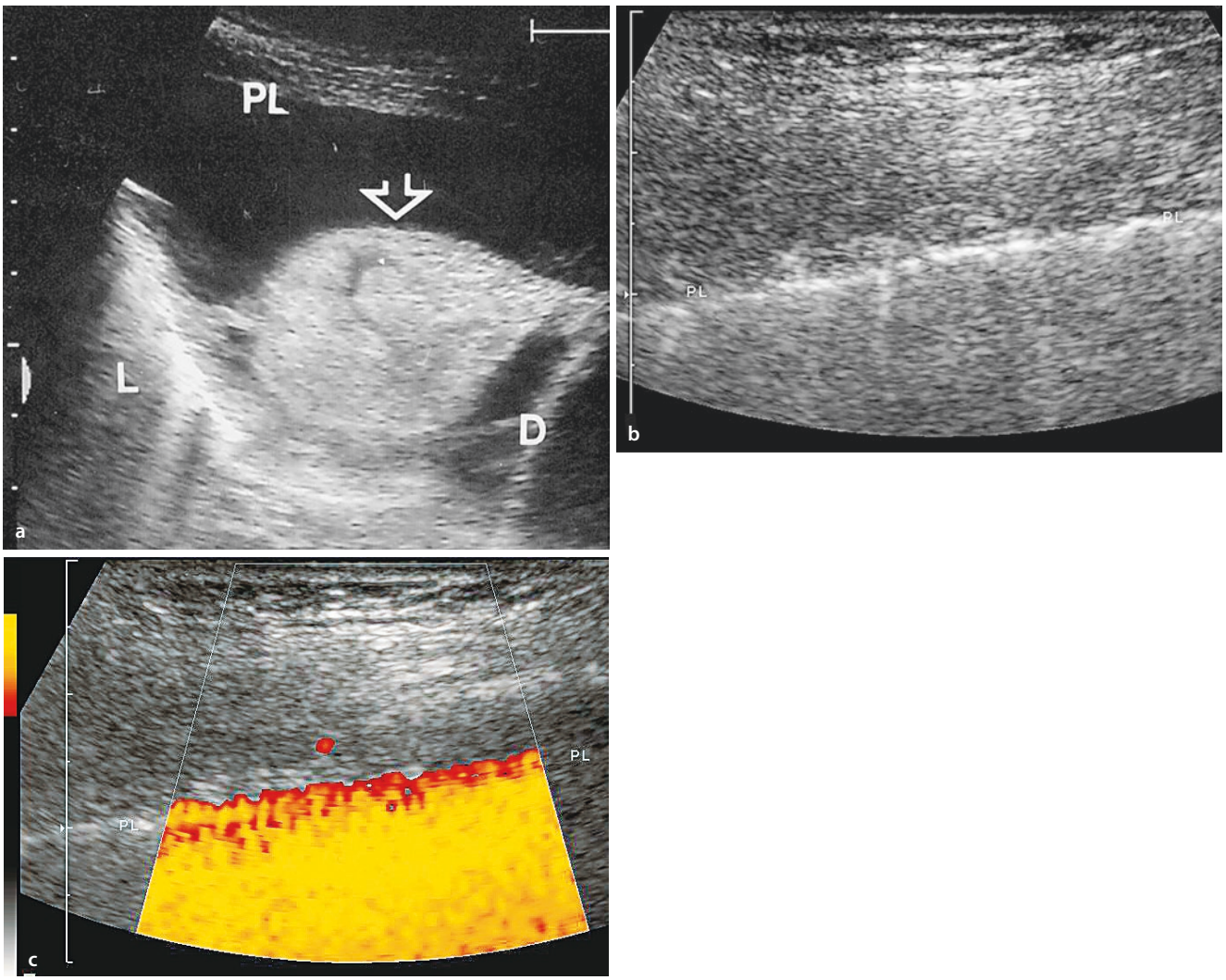

Fig. 10.23 **a** A blood clot (*arrow*) as a complication following a diagnostic puncture of a pleural effusion. *PL* parietal pleura, *L* compressed lung, *D* diaphragm. **b** Pneumothorax was excluded by showing the sliding sign of the pleura. **c** Color-Doppler sonography in "power" mode allowed the respiration-dependent sliding sign to be documented in an impressive way even in the static image. The repeat echoes that could be demonstrated with B-mode sonography (artifact) dorsal to the pulmonary surface show up accordingly as a color artifact. This cannot be demonstrated in cases of pneumothorax

10.6 Risks

Sonography-guided puncture has a low rate of complications. The rate of pneumothorax is 2.8 %; 1 % require drainage (Table 10.2). Hemorrhage or hemoptysis is observed in 0–2 %. Data concerning air embolism or even death are not available so far. Tumor dissemination through the procedure of puncture (vaccine metastases) is of little clinical significance and very rare, in less than 0.003 % of cases. In cases of malignant pleural mesothelioma, it is slightly more common. When surgery is performed, the site of puncture is also resected (Weiss and Düntsch 1996; Mathis et al. 1999; Bydder et al. 2004).

Pneumothorax After Puncture

If the focus is no longer visible after the puncture, the likelihood of a pneumothorax is high. This can be reliably detected by sonography, through the absence of respiration-dependent gliding movement of the pleura (Sensitivity 90–100 % Abb. 9.24b, c; Blank 1994; Ding et al. 2011; Herth et al. 2004; Reissig and Kroegel 2005; Volpicelli et al. 2012) Fig. 10.23.

The quantity of free air can only be measured by obtaining a chest radiograph. A pneumothorax usually reaches its maximum dimensions after 3 h, so the decision regarding a therapeutic procedure is made thereafter, when the pneumothorax is small. If the patient is symptomatic or if a larger volume is present, the patient is initially given protracted thoracocentesis. The success rate within the first 10 h is 90 % (Klose and Günther 1996; MacDuff et al. 2010). In the event of renewed collapse, the clinician should use a percutaneous drain and a catheter with a small lumen.

A routine chest radiograph is not required after sonography-guided puncture.

10.7 Summary

Provided the indication is established with care, interventional measures in the thorax are very successful. The rate of complications is low when the procedure is performed by trained therapists.

» The basic principle to be applied is: "try ultrasound first" (Sistrom 1997).

10.8 List of Materials

Sterican.Disposable injection cannula, size 1 (G 20/0.9 × 40/80 mm). B. Braun Melsungen AG, 34209 Melsungen, Germany

BioPince. Disposable full-cylinder biopsy pistol (G 18/1.2 × 100/150 mm).Inter.V, Gainesville, FL 32608 USA. Distributor Peter Pflugbeil GmbH, Georg-Wimmer-Ring 21, 85604 Zorneding, Germany, Fax: +44-8106-241333, email: info@pflugbeil.com, Internet: ▶ http://www.pflugbeil.com

Sonocan.Disposable set for sonography-guided full-cylinder biopsy by B. Braun Melsungen AG (G 20/0.9 × 100 mm/150 mm). Distributor Nicolai GmbH & Co. KG, Ostpassage 7, 30853 Langenhagen, Germany, Fax: +44-511-733235

Max Core Disposable biopsy pistol (G 20-16/0.9–1.2 × 100/160 mm). Bard

Magnum Core.Reusable biopsy pistol. Bard GmbH, Wachhausstrasse 6, 76227 Karlsruhe, Germany

Magnum disposable needles. (G 20-16/0.9–1.2 × 100/160 mm). Bard

Navarre universal drainage catheter with Nitinol (6–12 Fr × 30 cm). Bard

Universal adapter with Luer-Lock. Bard

Argyl trocar catheter (Charr 12–17/4–6 mm). Sherwood-Medical Company, Tullamore, Ireland

Argyl Sentinel Seal Thoracic drainage unit. Tyco Healthcare Company, Tullamore, Ireland

Acknowledgments I would like to express my thanks to Martin Lenz (chief consultant surgeon in the Radiology Department of the Steinenberg Clinic, Reutlingen) for preparing and providing the radiological findings, and my son Valentin for the technical photographic work.

References

Adams RF, Gray W, Davies RJ, Gleeson FV (2001) Percutaneous image-guided cutting needle biopsy of the pleura in the diagnosis of malignant mesothelioma. Chest 120:1798–1802

Beckh S, Bölcskei PL (1997) Biopsie thorakaler Raumforderungen—von der computertomographischen zur ultraschallgezielten Punktion. Ultraschall Med 18:220–225

Blank W (1994) Sonographisch gesteuerte Punktionen und Drainagen. In: Braun B, Günther R, Schwerk WB (eds) Ultraschalldiagnostik. Lehrbuch und Atlas, III-111th edn. Landsberg/Lech ecomed, pp 1–79

Blank W (1995) Weichteil- und Knochentumoren. In: Braun B, Günther R, Schwerk WB (eds) Ultraschalldiagnostik. Lehrbuch und Atlas, III-99th edn. Landsberg/Lech ecomed, pp 1–27

Blank W (2006) Sonographisch gezielte Punktionen und Drainagen. In: Seitz K, Schuler A, Rettenmaier G (eds) Sonographische Diagnose und Differenzialdiagnose. Thieme, Stuttgart

Blank W (2007) Sonographisch gezielte Punktionen und Drainagen. In: Seitz K, Schuler A, Rettenmaier G (eds) Sonographische Diagnose und Differenzialdiagnose. Thieme, Stuttgart

Blank W, Schuler A, Wild K, Braun B (1996) Transthoracic sonography of the mediastinum. Eur J Ultrasound 3:179–190

Blank W, Mathis G, Osterwalder J (Hrsg) (2014). Kursbuch Notfallsonographie. Georg Thieme Verlag, Stuttgart

Börner N (1986) Sonographische Diagnostik pleuropulmonaler Erkrankungen. Med Klin 81:496–500

Bradley MJ, Metreweli C (1991) Ultrasound in the diagnosis of the juxta-pleural lesion. Br J Radiol 64:330–333

Braun B (1983) Abdominelle und thorakale Ultraschalldiagnostik. In: Bock HE, Gerok W, Hartmann F et al (eds) Klinik der Gegenwart. Urban & Schwarzenberg, Munich, pp 1141–1145

Bydder S, Phillips M, Joseph DJ, Cameron F, Spry NA, Demelker Y, Musk AW (2004) A randomised trial of single-dose radiotherapy to pre-

vent procedure tract metastasis by malignant mesothelioma. Br J Cancer 91:9–10
Cao BS, Wu JH, Li XL, Deng J, Liao GQ (2011) Sonographically guided transthoracic biopsy of peripheral lung and mediastinal lesions: role of contrast-enhanced sonography. J Ultrasound Med 30:1479–1490
Chandresakar AJ, Reynes CJ, Churchill RJ (1976) Ultrasonically guided transthoracic percutaneous biopsy of peripheral pulmonary masses. Chest 70:627–630
Chu CY, Hsu WH, Hsu JY, Huang CM, Shih CM, Chiang DC (1994) Ultrasound-guided biopsy of thoracic masses. Chung Hua I Hsueh Tsa Chih 54:336–342
Civardi G, Livraghi T, Colombo MD (1994) Lytic bone lesions suspected for metastasis: ultrasonically guided fine-needle aspiration biopsy. J Clin Ultrasound 22:307–311
Davies HE, Davies RJO, Davies CWH (2010) Management of pleural infection in adults: British Thoracic Society pleural disease guideline. Thorax 65(Suppl 2):ii41–ii53
Diacon AH, Schurmanns MM, Theron J, Schubert PT, Wright CA, Bolliger CT (2004a) Safety and yield of ultrasound-assisted transthoracic biopsy performed by pulmonologists. Respiration 71(5):519–522
Diacon AH, Schurmanns MM, Theron J, Schubert PT, Wright CA, Bolliger CT (2004b) Safety and yield of ultrasound-assited transthoracic biopsy performed by pulmonologists. Respiration Internat Rev Thorac Dis 71(5):519–522
Diacon AH, Theron J, Schubert P, Bolliger CT (2007) Ultrasound-assisted transthoracic biopsy: fine-needle aspiration or cutting-needle biopsy? Eur Respir J 29:357–362
Dietrich CF, Nürnberg D (2011). Interventioneller Ultraschall. Lehrbuch und Atlas für die interventionlle Sonographie. Thieme Verlag, Stuttgart
Ding W, Shen Y, Yang J, He X, Zhang M (2011) Diagnosis of pneumothorax by radiography and ultrasonography: a meta-analysis. Chest 140:859–866
Ernst A, Eberhardt R, Wahidi M, Becker HD, Herth FJ (2006) Effect of routine clopidogrel use on bleeding complications after transbronchial biopsy in humans. Chest 129:734–737
Fysh ET, Smith NA, Lee YC (2010) Optimal chest drain size: the rise of the small-bore pleural catheter. Semin Respir Crit Care Med 31:760–768
Gartmann JC (1988) Der unklare Pleuraerguß: Praktisch-diagnostisches Vorgehen. Ther Umsch 45:308–313
Gehmacher O, Mathis G, Kopf A, Scheier M (1986) Ultrasound imaging of pneumonia. Ultrasound Med Biol 21:1119–1122
Gleeson F, Lomas DJ, Flower CDR, Stewart S (1990) Powered cutting needle biopsy of the pleura and chest wall. Clin Radiol 41:199–200
Görg C, Seifart U, Görg K, Zugmaier G (2003) Color Doppler sonographic mapping of pulmonary lesions. J Ultrasound Med 22:1033–1039
Görg C, Bert T, Kring R (2006) Contrast enhanced Sonography of the lung for differential diagnosis of atelektasis. JUM 25:35–39
Gupta S, Gulati M, Rajwanski A, Gupta P, Suri S (1998) Sonographically guided fine-needle aspiration biopsy of superior mediastinal lesions by the suprasternal route. Am J Roentgenol 171:1303–1306
Heilo A (1993) Tumors in the mediastinum: US-guided histologic core-needle biopsy. Radiology 189:143–146
Heilo A (1996) US-guided transthoracic biopsy. Eur J Ultrasound 3:141–153
Heinzmann A, Müller T, Leitlein J, Braun B, Kubicka S, Blank W (2012) Endocavitary contrast enhanced ultrasound (CEUS) – work in progress. Ultraschall Med 33:76–84
Herth FJ, Eberhardt R, Becker HD, Ernst A (2004) Diagnosis of pneumothorax (PTX) by means of transthoracic ultrasound—a prospective trial. Chest 126(49):892
Hoosein MM, Barnes D, Khan AN, Peake MD, Bennett J, Purnell D, Free C, Entwisle JJ (2011) The importance of ultrasound in staging and gaining a pathological diagnosis in patients with lung cancer – a two year single centre experience. Thorax 66:414–417
Hsu WH, Chiang DC, Hsu JY, Kwan PC, Chen CL, Chen DY (1996) Ultrasound guided fine-needle aspiration biopsy of lung cancers. J Clin Ultrasound 24:225–233
Hüner M, Ghadim BM, Haensch W, Schlag DM (1998) Transesophageal biopsy of mediastinal and pulmonary tumors by means of endoscopic ultrasound guidance. J Thorac Cardiovasc Surg 116:554–559
Ikezoe J, Morimoto S, Arisawa J, Takasgima S, Kozuka T, Nakahara K (1990) Percutaneous biopsy of thoracic lesions: value of sonography for needle guidance. Am J Roentgenol 154:1181–1185
Janssen J, Johann W, Luis W, Greiner L (1998) Zum klinischen Stellenwert der endosonographisch gesteuerten transoesophagealen Feinnadelpunktion von Mediastinalprozessen. Dtsch Med Wochenschr 123:1402–1409
Jennsen C, Gotschalk U, Schachschal G, Dietrich CF (2014). Kursbuch Endosonographie. Thieme Verlag, Stuttgart
Jeon KN, Bae K, Park MJ, Choi HC, Shin HS, Shin S, Kim HC, Ha CY (2014) US-guided transthoracic biopsy of peripheral lung lesions: pleural contact length influences diagnostic yield. Acta Radiol 55:295–301
Kelbel C, Stephany P, Lorenz J (1996) Endoluminal chest sonography. Eur J Ultrasound 3:191–195
Klein JS, Schultz S, Heffner JE (1995) Interventional radiology of the chest: image-guided percutaneous drainage of pleural effusions, lung abscess, and pneumothorax. Am J Roentgenol 164:581–588
Klose KC, Günther RW (1996) CT-gesteuerte Punktionen. In: Günther RW, Thelen M (eds) Interventionelle Radiologie. Thieme, Stuttgart, pp 750–775
Koegelenberg CF, Diacon AH (2013) Image-guided pleural biopsy. Curr Opin Pulm Med 19:368–373
Koegelenberg CF, Diacon AH, Irusen EM, von Groote-Bidlingmaier F, Mowlana A, Wright CA, Louw M, Schubert PT, Bolliger CT (2011) The diagnostic yield and safety of ultrasound-assisted transthoracic biopsy of mediastinal masses. Respiration 81:134–141
Koegelenbug CF, Bolliger CT, Diacon AH (2009) Diagnostic yield and safety of ultrasound-assisted biopsies in superior vena cavo syndrome. Eur Respir J 33:1389–1395
Kolditz M, Höffken G (2008) Management des parapneumonischen Ergusses und ds Pleuraempyems. Pneumologe 5:219.228
Liao WY, Chen MZ, Chang YL, Wu HD, Yu CJ, Kuo PH, Yang PC (2000) US guided transthoracic cutting biopsy for peripheral thoracic lesions less than 3 cm in diameter. Radiology 217:685–691
MacDuff A, Arnold A, Harvey J (2010) Management of spontaneous pneumothorax: British Thoracic Society Pleural Disease Guideline. Thorax 65(Suppl 2):ii18–ii31
Marchevsky AM, Marx A, Ströbel P, Suster S, Venuta F, Yousem S, Zakowski M (2011) Policies and reporting guidelines for small biopsy specimens of mediastinal masses. J Thorac Oncol 6:S1724–S1729
Mathis G (1997a) Thoraxsonography—part I: chest wall and pleura. Ultrasound Med Biol 23(8):1131–1139
Mathis G (1997b) Thoraxsonography—part II: peripheral pulmonary consolidation. Ultrasound Med Biol 23(8):1141–1153
Mathis G, Gehmacher O (1999a) Ultrasound-guided diagnostic and therapeutic interventions in peripheral pulmonary masses. Wien Klin Wochenschr 111:230–235
Mathis G, Bitschnau R, Gehmacher O, Dirschmid K (1999) Ultraschallgeführte transthorakale Punktion. Ultraschall Med 20:226–235
Mikloweit P, Zachgo W, Lörcher U, Meier-Sydow J (1991) Pleuranahe Lungenprozesse: Diagnostische Wertigkeit Sonographie versus Computertomographie (CT). Bildgebung 58:127–131
Mohr A, Jung EM et al (2014) Neuese und günstiges Trainingsmodellzur ultraschallgesteuerten Anlage von Drainagen. Z Gastroenterol 52(11):1257–1262
Mueller PR, Sanjay S, Simeone JF et al (1988) Image-guided pleural biopsies: indications, technique and results in 23 patients. Radiology 169:1–4
Müller T, Blank W (2011) Sonographisch gesteuerte Punktionen und Therapieverfahren. In: Braun B, Günther R, Schwerk WB (Hrsg.) Ultraschalldiagnostik. Lehrbuch und Atlas, III-11.1 edn. Landsberg/Lech ecomed, pp 1–79
Nordenstrom B (1967) Paraxiphoid approach to mediastinum for mediastinography and mediastinal needle biopsy: a preliminary report. Invest Radiol 2:141–146
O'Moore PV, Mueller PR, Simeone JF, Saini S, Butch RJ, Hahn PF (1987) Sonographic guidance in diagnostic and therapeutic interventions in the pleural space. Am J Roentgenol 149:1–5

Patel IJ, Davidson JC, Nikolic B, Salazar GM, Schwartzberg MS, Walker G, Saad WA (2012) Consensus guidelines for periprocedural management of coagulation status and hemostasis risk in percutaneous image-guided interventions. J Vasc Interv Radiol 23:727–736

Patel IJ, Davidson JC, Nikolic B, Salazar GM, Schwartzberg MS, Walker G, Saad WA (2013) Addendum of newer anticoagulants to the SIR consensus guideline. J Vasc Interv Radiol 24:641–645

Pedersen OM, Aasen TB, Gulsvik A (1986) Fine needle aspiration biopsy of mediastinal and peripheral pulmonary masses guided by real time sonography. Chest 89:504–508

Pedersen BH, Vilmann P, Folke K, Jacobsen GK, Krasnik M, Milman N, Hancke S (1996) Endoscopic ultrasonography and real-time guided fine-needle aspiration biopsy of solid lesions of the mediastinum suspected of malignancy. Chest 110:539–544

Reissig A, Kroegel C (2005) Accuracy of transthoracic sonography in excluding post-interventional pneumothorax and hydropneumothorax. Comparison to chest radiography. Eur J Radiol 53(3):463–470

Reuß J (1996) Sonographic imaging of the pleura: nearly 30 years experience. Eur J Ultrasound 3:125–139

Roberts ME, Neville E, Berrisford RG, Antunes G, Ali NJ (2011) Management of a malignant pleural effusion: British Thoracic Society pleural disease guideline 2010. Thorax 65(Suppl 2):ii32–ii40

Rubens DJ, Strang JG, Fultz PJ, Gottleib RH (1997) Sonographic guidance of mediastinal biopsy: an effective alternative to CT guidance. AJR 169:1605–1610

Schlotterbeck K, Schmid J, Klein F, Alber G (1997) Transesophageal sonography in the staging of lung cancer. Ultraschall Med 18:153–158

Schubert P, Wright CA, Louw M, Brundyn K, Theron J, Bolliger CT, Diacon AH (2005) Ultrasound assisted transthoracic biopsy: cells or sections? Diagn Cytopathol 33(49):233–237

Schuler A, Blank W, Braun B (1995) Sonographisch-interventionelle Diagnostik bei Thymomen. Ultraschall Med 16:62

Sistrom CI (1997) Thoracic sonography for diagnosis and intervention. Curr Probl Diagn Radiol 1:6–46

Sonnenberg E, Agostino H, Casola G, Wittich GR, Varney RR, Harker C (1991) Lung abscess: CT-guided drainage. Radiology 178:347–351

Tan C, Sedrakyan A, Browne J, Swift S, Treasure T (2006) The evidence on the effectiveness of management for malignant pleural effusion: a systematic review. Eur J Cardiothorac Surg 29:829–838

Vladutiu AO (1986) Pleural effusion. Futura Publishing, Mount Kisco

Vogel B (1993) Ultrasonographic detection and guided biopsy of thoracic osteolysis. Chest 104:1003–1005

Volpicelli G, Elbarbary M, Blaivas M, Lichtenstein DA, Mathis G, Kirkpatrick AW, Melniker L, Gargani L, Noble VE, Via G, Dean A, Tsung JW, Soldati G, Copetti R, Bouhemad B, Reissig A, Agricola E, Rouby JJ, Arbelot C, Liteplo A, Sargsyan A, Silva F, Hoppmann R, Breitkreutz R, Seibel A, Neri L, Storti E, Petrovic T (2012) International evidence-based recommendations for point-of-care lung ultrasound. Intensive Care Med 38:577–591

Wali SO, Shugaeri A, Samman YS, Abdelaziz M (2002) Percutaneous drainage of pyogenic lung abscess. Scand J Infect Dis 34:673–679

Wang JS, Doelken P (2009) Ultrasound-guided drainage procedures and biopsies. In: Bolliger CT, Herth FJF, Mayo PH, Miyazawa T, Beamis JF (eds) Clinical chest ultrasound. from the ICU to the bronchoscopy suite (progress in respiratory research), 37th edn. Karger-Verlag, New York

Wang HC, Yu DJ, Yang PC (1995) Transthoracic needle biopsy of thoracic tumor by Color Doppler ultrasound puncture guided device. Thorax 50:1258–1263

Weiss H, Düntsch U (1996) Komplikationen der Feinnadelbiopsie—DEGUM-Umfrage II. Ultraschall Med 17:118–130

Weiss H, Weiss A (1994) Therapeutische interventionelle Sonographie. Ultraschall Med 15:152–158

Westcott JL (1980) Direct percutaneous needle aspiration of localized pulmonary lesions: result in 422 patients. Radiology 137:31–35

Wu RG, Yang PC, Kuo SH, Luh KT (1995) "Fluid color" sign: a useful indicator for discrimination between pleural thickening and pleural effusion. J Ultrasound Med 14:767–769

Yang PC (1996) Color Doppler ultrasound of pulmonary consolidation. Eur J Ultrasound 3:169–178

Yang PC, Luh KT, Sheu JC, Kuo SH, Sang SP (1985) Peripheral pulmonary lesions: ultrasonography and ultrasonically guided aspiration biopsy. Radiology 155:451–456

Yang PC, Chang DB, Yu CJ, Lee YC, Kuo SH, Luh KT (1992) Ultrasound-guided core biopsy of thoracic tumors. Am Rev Respir Dis 146:763–767

Yang MA, Park MH, Shin BS, Ohm JY (2012) Ultrasonography-guided transthoracic cutting biopsy of pulmonary lesion: diagnostic benefits and safety. J Korean Soc Ultrasound Med 31:119–124

Zimmermann C, Werle A, Schuler A, Reuss J, Gemacher O, Blank W (2003) Echosignalverstärker in der sonographischen Diagnostik des Thorax. Ultraschall Med 24:31

From the Symptom to the Diagnosis

Sonja Beckh

G. Mathis (ed.), *Chest Sonography*, DOI 10.1007/978-3-319-44072-9_11

Technical advancements in sonography devices, which have led to the production of mobile and even portable units, have allowed rapid use of sonography at the bedside for a large number of indications (Sartori et al. 2007; Volpicelli 2008; Copetti and Cattarossi 2008; Lichtenstein and Mezière 2008; Reißig 2009; Moore 2011; Arntfield 2012; Gardelli 2012; Hyacinthe 2012; Kreuter 2012; Reißig 2012; Volpicelli 2013; Al Deeb 2014). The transducer virtually serves as a technical extension of the palpating hand or the stethoscope. In the presence of chest diseases the cardinal symptoms are chest pain, fever and dyspnea. These symptoms may occur either separately or in combination, and thus allow the diagnostician to orient himself/herself to the situation (◘ Fig. 11.1). The extent and the intensity of the individual symptoms are mainly determined by the severity of the respective disease.

The great diversity of symptoms in pulmonary embolism (Goldhaber 1998) may render the diagnosis of this condition extremely difficult (▶ Sect. 5.3).

11.1 Chest Pain

Chest pain is a common symptom in the emergency setting as well as the outpatient setting (Amsterdam et al. 2010). It is always necessary to identify the cause, and particularly the five life-threatening diseases, namely, myocardial infarction, acute dissection of the aorta, pulmonary embolism, tension pneumothorax and rupture of the esophagus (Kurz et al. 2005; Kontos et al. 2010; Arntfield and Millington 2012).

The character of pain and the findings of clinical and sonographic investigation provide information about differential diagnosis in the presence of various diseases (◘ Table 11.1).

The fibers responsible for the perception of pain are located in the parietal pleura, the soft tissues, and the bony structures of the chest wall in the aorta with its branches (◘ Fig. 11.2). The lung and the visceral pleura, on the other hand, are insensitive to stimuli that trigger pain. Pain that accompanies an inflammation in the medial portion of the diaphragm is projected into the ipsilateral shoulder and neck region (Murray and Gebhart 2005).

The ultrasound transducer is specifically targeted to the site of maximum pain, the site indicated by palpation or the physical investigation (Volpicelli 2008; Moore 2011; Gardelli 2012; Hyacinthe 2012; Kreuter 2012; Volpicelli 2013). In a physician's office, in the emergency setting or at the bedside, sonography contributes to the establishment of the diagnosis, may even provide an unequivocal diagnosis or may lead to further meaningful imaging procedures. Sonography is particularly useful to diagnose diseases of the chest in children (Kim et al. 2000).

11.1.1 Chest Pain as a Symptom of Life-Threatening Diseases

Tension Pneumothorax

Sudden onset of pain is the main characteristic of a tension pneumothorax. Depending on the magnitude of the pneumothorax, it may be accompanied by mild or excessive

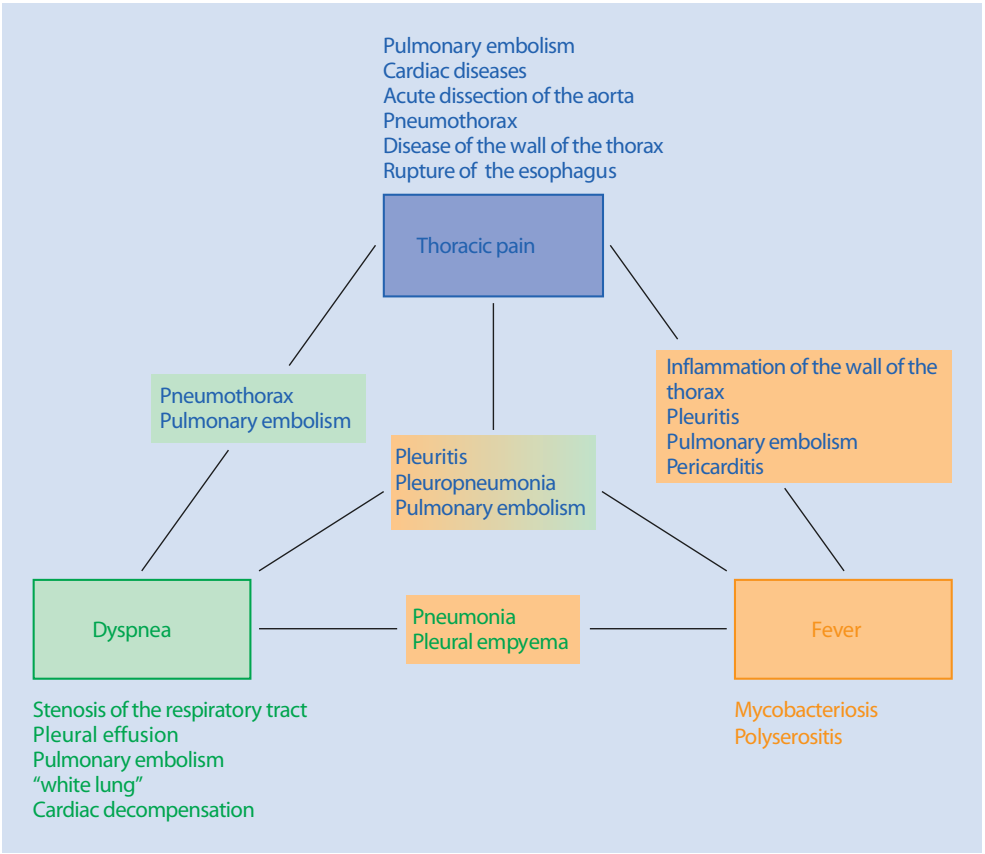

◘ **Fig. 11.1** Symptoms in diseases of the chest

Table 11.1 Findings in the presence of diseases accompanied by chest pain

Diagnosis	Characteristic of pain	Findings obtained from investigation	Sonographic findings
Tension pneumothorax	Sudden onset, sharp	Vesiculotympanitic resonance, no respiratory sounds, dyspnea, possibly symptoms of shock	The pleural reflex does not glide, repetitive echoes
Pulmonary embolism	Increased during inspiration	Pleural rales, dyspnea or fever may be present	Usually hypoechoic lesions in subpleural location; a small pleural effusion may be present
Acute dissection of the aorta	Strong pain, either in substernal location or between the shoulder blades, may radiate into the neck	Breath sounds are normal, diastolic murmur above the aortic valve may be present, symptoms of shock	Dissection of the aortic wall, dilated aorta
Myocardial infarction	Retrosternal, persistent, independent of breathing	Symptoms of shock may be present	Chest sonography is normal, diagnosis by ECG, laboratory findings, possibly echocardiography
Rupture of the esophagus	Retrosternal	Mediastinal emphysema	Not informative, diagnosis by X-ray
Chest wall processes	Local	Pain is increased on palpation or movement, fever in case of inflammation	Fracture: step formation and hematoma
			Abscess: hypoechoic, internal echoes
			Malignancy: destruction and infiltration
Pleuritis	Increased during inspiration	Pleural rales, fever; dyspnea may be present	Fragmentation of the pleural line, subpleural infiltrates, possibly pleural effusion
Pleuropneumonia	Increased during inspiration	Pleural rales, bronchial respiration, rales, fever, cough, dyspnea	"Hepatization" of lung tissue, aerobronchogram, hypervascularization, pleural effusion may be present
Pericarditis	Increased during inspiration and in relation to position	Pericardial rales, fever	A small pericardial effusion may be present; diagnosed by ECG

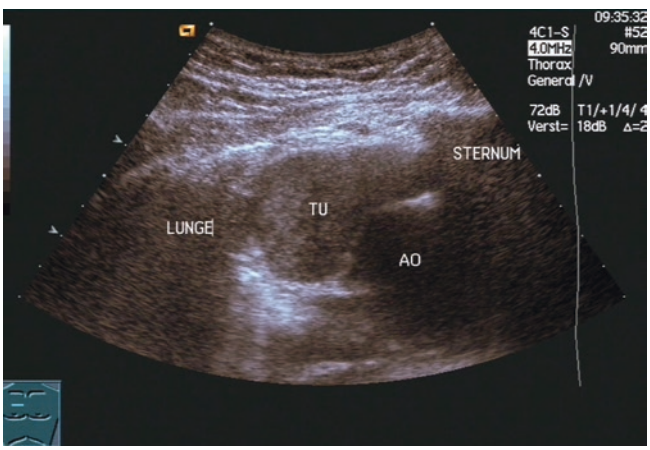

Fig. 11.2 A 56-year- old woman with retrosternal pain caused by a thymoma (*TU*) broad adjacent to the aortic wall. Diagnosis was established with sonographic biopsy and confirmed by operation

dyspnea. Within a very short period of time, the patient develops symptoms of shock owing to the pressure of mediastinal organs and vessels.

Sonography reveals repetitive echoes on the affected side and the absence of a gliding echogenic pleural reflex (▶ Chap. 3). An overview radiograph (Fig. 11.20) is needed to determine the depth of the pneumothorax space. High-resolution computed tomography reveals the extent and size of the emphysematous bulla (Fig. 11.3).

Pulmonary Embolism

A pulmonary embolism (▶ Sect. 5.3) is accompanied by pain on breathing when the parietal pleura is also inflamed. When the Doppler sonography investigation is extended to the leg veins in order to look for the site of thrombosis (Fig. 11.3) and when echocardiography is additionally performed in the case of circulatory symptoms to evaluate the right heart load,

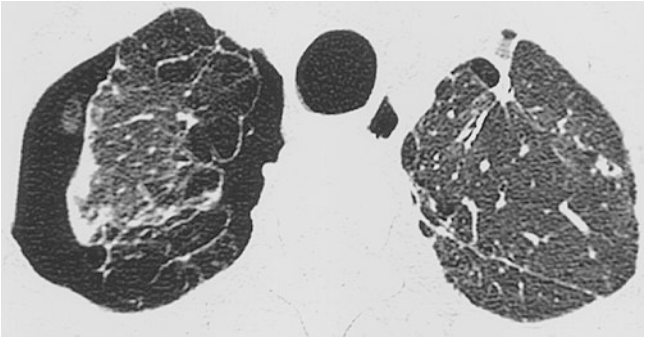

Fig. 11.3 Patient with a spontaneous pneumothorax. On high-resolution computed tomography one finds an extensive emphysematous bulla in the right upper lobe

the diagnosis can be made efficiently within a short period of time (Squizzato 2013; Mathis 2014).

Acute Dissection of the Aorta

This condition is typically accompanied by severe pain, frequently in dorsal location; maximum pain occurs between the shoulder blades. The pain may resolve for a short period of time but may also extend in the direction of dissection of vessels, for instance, in the neck when the carotid arteries are involved. Insonation from suprasternal or parasternal (▶ Chap. 5) permits immediate viewing of the ascending aorta, the aortic arch with the vessels connected to it, and the upper part of the descending aorta, even in the emergency setting (Arntfield and Millington 2012).

11.1.2 Pain Due to Diseases of the Chest Wall

The cardinal symptom is local pain, which is usually stronger during palpation or movement. In the case of irritated intercostal nerves or nerve roots the pain radiates into the area supplied by these nerves. The various structures of the chest wall are very well accessible to sonographic investigation (▶ Chap. 2).

Rib Fracture

Rib fractures are usually triggered by trauma of appropriate magnitude. In patients with osteoporosis, however, fractures may even be caused by severe coughing. Sonography reveals the formation of a step at the site of maximum pain (Wüstner et al. 2005), frequently a smaller hematoma and occasionally the so-called chimney phenomenon (▶ Figs. 2.13 and 2.143). Even in the presence of older fractures, the patient experiences pain, which is seen on sonography as a starting callus formation (◘ Fig. 11.4).

Tumor Invasion of the Chest Wall

A peripheral lung tumor that reaches the visceral pleura causes no pain. Only when it has invaded the parietal pleura and the muscular and bony structures of the chest does irritation of nerve fibers (which lead to pain receptors) occur.

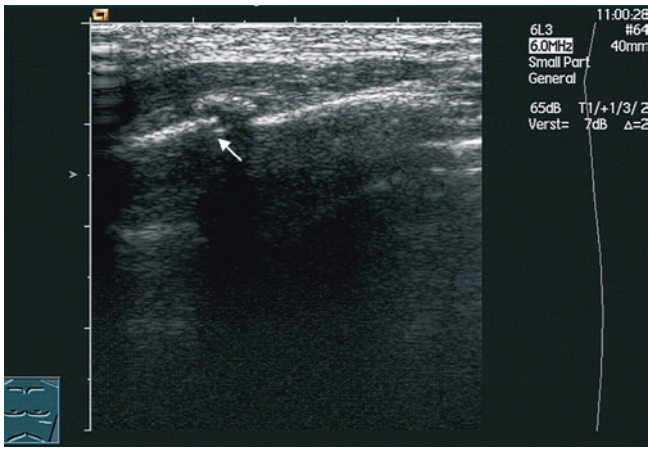

Fig. 11.4 Callus formation (the *arrow* is pointing to the fracture site) 2 weeks after a traumatic rib fracture

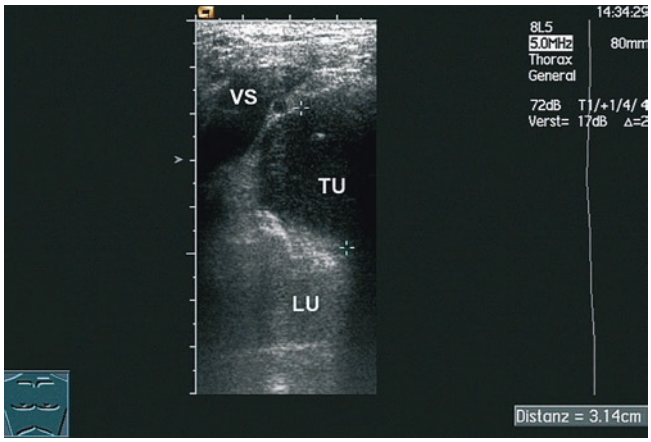

Fig. 11.5 A 46-year-old woman (40 pack years) with an adenocarcinoma (*TU*) in the left upper lobe which has perforated the superior sulcus and nearly reached the subclavian vessels. *VS* vena subclavia, *LU* lung

The term "Pancoast's tumor" (▶ Chap. 2, ▶ Sect. 4.2) refers to a tumor that passes through the apex of the lung. The high resolution of sonography visualizes branches of the brachial plexus (▶ Chap. 1), their erosion and their position in relation to the subclavian vessels in the event of penetration of the superior sulcus (◘ Fig. 11.5).

Tumor formations of the chest wall that extend across various structures can be identified well on B-mode sonography because of their different echogenicity and destruction of local tissue (◘ Fig. 11.6a, b). Pathological formation of new vessels is a further sonomorphological criterion of malignancy. Osteolytic metastases (◘ Fig. 11.7) and tumor manifestations in the joints are extremely painful (◘ Fig. 11.8).

11.2 Fever

The occurrence of fever is always an expression of inflammatory disease activity. The reasons may be numerous. Depending on the structures of the chest affected by inflammation, the

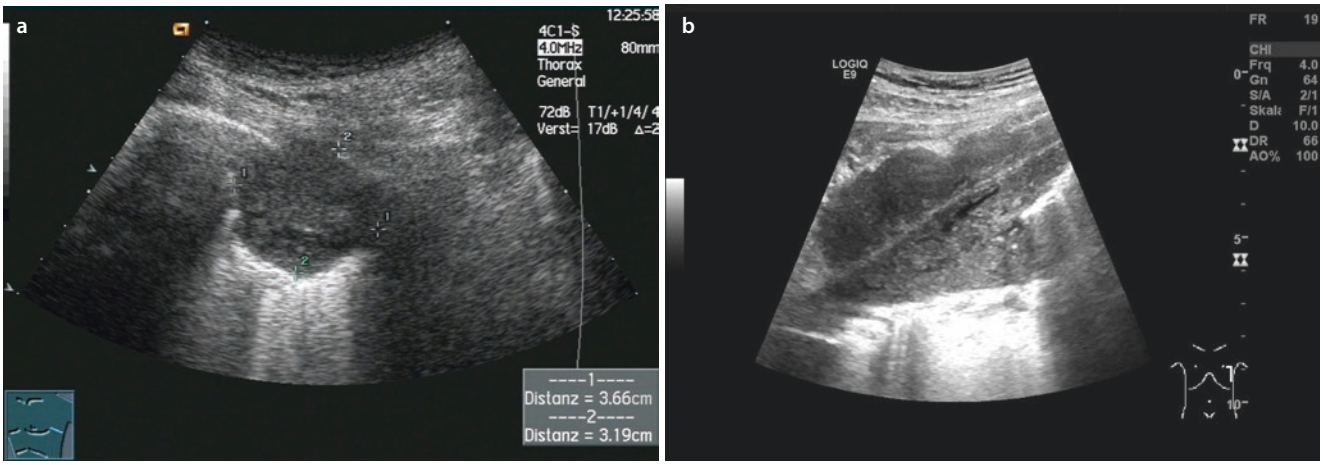

Fig. 11.6 **a** Peripheral lung carcinoma breaking through the pleural line and invading the muscles of the chest wall (sonographic biopsy: squamous cell carcinoma). **b** Pleural mesothelioma (histologic diagnosis gained with sonographic biopsy) showing a polycyclic formation in the chest wall and necrotizing infiltration of the adjacent lung

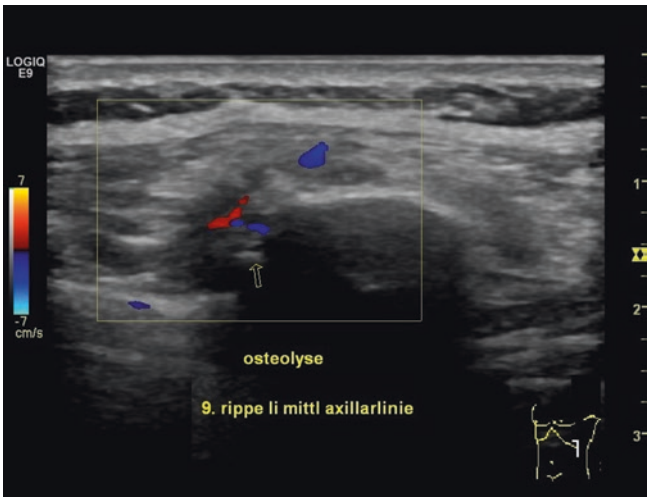

Fig. 11.7 Osteolytic destruction (*arrow*) of the ninth rib (left middle axillary line) in a patient with metastasizing lung carcinoma. Color Doppler depicts small vessels in the tumor

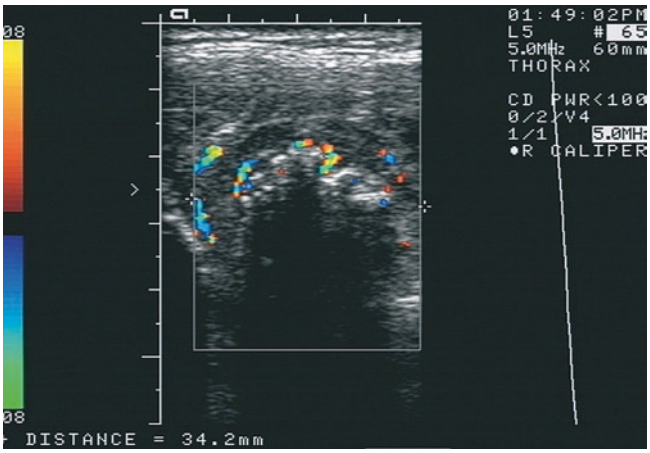

Fig. 11.8 A 51-year-old man with a painful swelling in the left sternoclavicular joint. Sonography reveals fragmentation of the cortical bone, which is surrounded by hypoechoic and strongly vascularized tissue. The surgical biopsy specimen yielded the diagnosis of a plasmocytoma. Clinically the patient had a solitary manifestation of a plasmocytoma which, however, was not secretory on laboratory investigation

condition may be accompanied by pain. Respiratory pain is indicative of pleural involvement. The intensity of fever—for instance, it may be low in the presence of pulmonary embolism or very high in the presence of pneumonia—as well as laboratory findings and bacteriological investigations serve as additional aids to establish the diagnosis.

11.2.1 Fever with Chest Pain

Abscesses in the Chest Wall

Inflammation in the soft tissues of the chest wall, for instance, in the presence of an abscess (▶ Fig. 2.3), causes local pain occasionally accompanied by swelling.

Abscesses in the chest wall may be quite extensive (Fig. 11.9).

Pleuritis

Inflammatory diseases of the pleura (▶ Chap. 3) cause pain which is enhanced during inspiration. Auscultation frequently discloses marked pleural rales. Most of all, sonography is a useful imaging procedure when one has to avoid irradiation.

Pulmonary Embolism

In some cases of recurrent pulmonary embolism (▶ Sect. 5.3) the only symptoms may be intermittent chest pain and fever for a long period of time; however, fever rarely exceeds 38.3 °C (Fedullo and Morrus 2005). In one investigation of geriatric patients, fever was frequently observed in connection with pulmonary embolism (Ceccarelli et al. 2003).

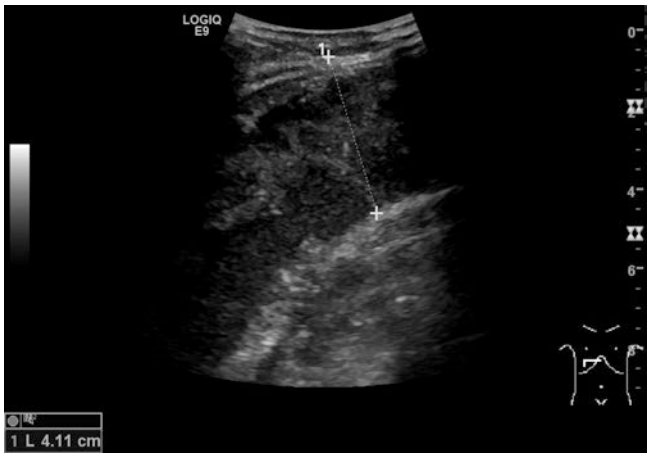

Fig. 11.9 A 35-year-old man with diabetes, renal insufficiency and a history of drug addiction. Extended abscess in the soft tissue of the right ventral chest wall (*markers*) caused by an infected central venous line in the jugular vein. Microbiological analysis of sonography-guided aspiration revealed *Staphylococcus*

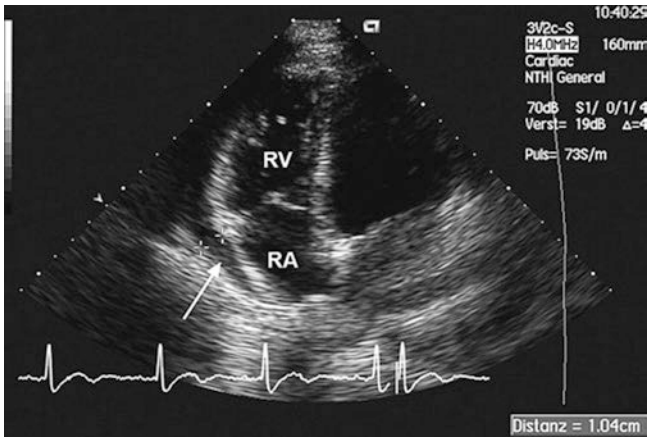

Fig. 11.10 A 25-year-old woman with a narrow pericardial effusion (*arrow*) in the presence of Churg–Strauss disease. *RA* right atrium, *RV* right ventricle

Pericarditis

Pericarditis is associated with moderately high fever, breath-related and position-related precordial pain. The main diagnostic tool is ECG, assisted by laboratory investigations. On sonography, at the onset of the disease one usually finds a fluid margin of lesser or greater magnitude in the pericardial space (Fig. 11.10). In every case sonography is the method of choice for further assessment of the progress of the disease.

11.2.2 Fever with Dyspnea

When a patient with fever develops dyspnea it is always a clinical sign of impairment of respiratory or ventilatory function.

Pneumonia

Pneumonia is usually associated with very high fever. In cases of pneumococcal pneumonia, the patient typically experiences sudden fever without prolonged onset of the disease. Inflammatory exudation of fluid in the alveoles eliminates air from the parenchyma and permits sonographic imaging even if the invasion extends up to the visceral pleura (▶ Sect. 5.1; Blaivas 2012; Reißig and Görg 2012; Chavez et al. 2014). Secretory retention due to obstruction secondary to a tumor leads to atelectasis and frequently also poststenotic pneumonia. The sonographic image shows the distribution of vessels as well as necrosis in the parenchyma. A bronchoscopy must be performed to assess the central bronchial system (Fig. 11.11).

Pleural Empyema

Pleural empyema, or collection of pus in the pleural space, is associated with fever, dyspnea and a severely impaired general condition. The disease is usually a threatening toxic condition which, if not identified on time or if treated too late, exposes the patient to the risk of sepsis and high lethality (Kolditz et al. 2004; Davies et al. 2010). Pleural empyema

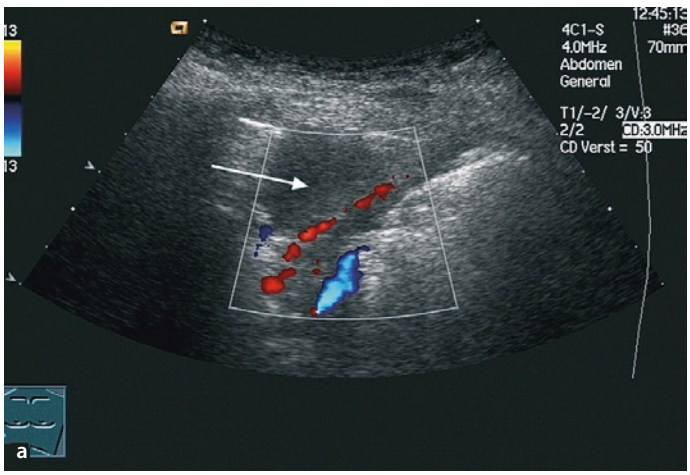

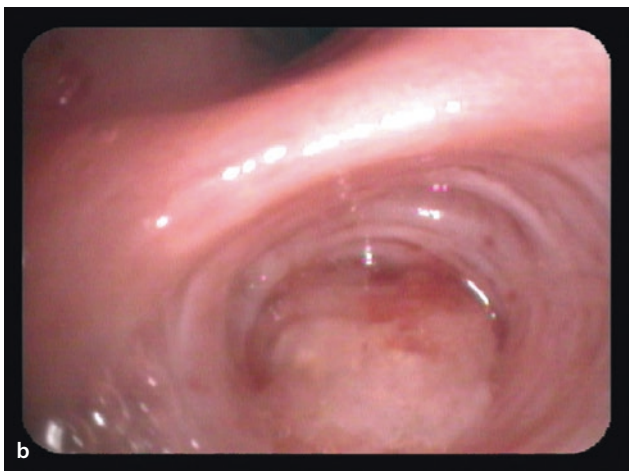

Fig. 11.11 A 91-year-old woman with middle-lobe pneumonia, a large peripheral colliquation (*arrow*) and regular central vessels (**a**). Bronchoscopy (**b**) reveals obstruction of the middle lobe secondary to the tumor, which proved to be an adenocarcinoma on histological investigation. Partial resolution of the middle-lobe invasion under antibiotic therapy

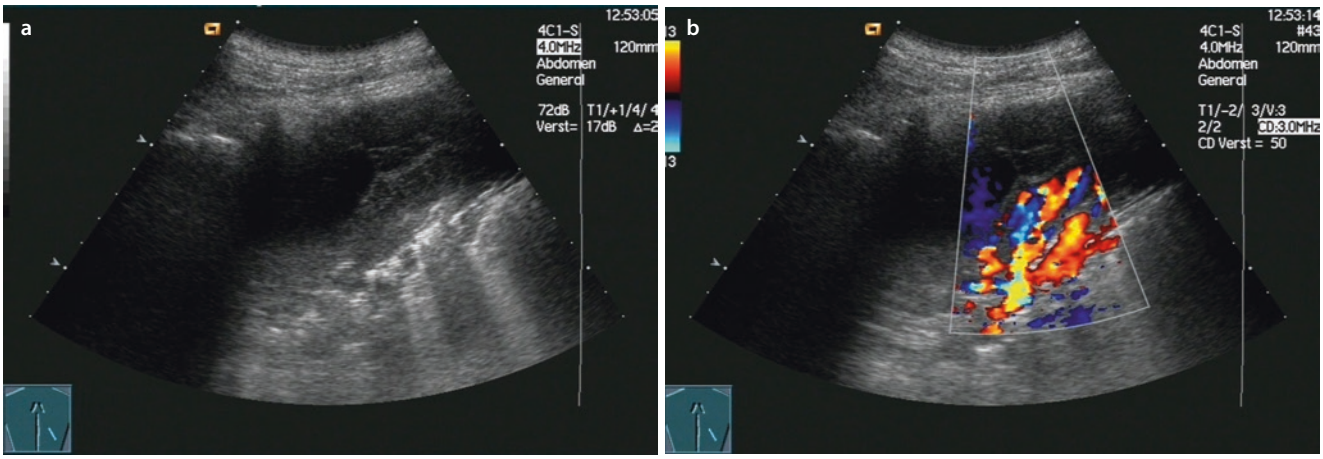

Fig. 11.12 **a** A 52-year-old man with fever and dyspnea. In the right lower lobe infiltration with air trappings, pleural thickening and several fibrinous bands. PH-value in the pleural fluid 6, 8. **b** Color Doppler shows hypervascularization in the infiltrated part of the lung. Successful treatment with drainage and antibiotics

may occur as an inflammation of the pleura, for instance, in the presence of a tuberculotic infection, or may be a complication of a parapneumonic effusion in case of bacterial pneumonia (Fig. 11.12a, b). The emergence of a pleural empyema always heralds a more severe course of disease, whether due to the impaired resistance of the individual or a particularly virulent pathogen. Pain usually occurs in the initial stage of the disease and disappears as the exudation in the pleural space increases. The longer an empyema exists, the more pronounced are the septations and chambers (Fig. 11.13a, b). Sonography also permits localization of the optimum site of aspiration, even at the bedside (Levin 1999, Davies et al. 2010; Heffner et al 2010), to obtain material for investigation and place a drain. On the basis of the sonography report, the extent of empyema can be assessed in children (Carey et al. 1998; Ramnath et al. 1998) and the investigator will be able to decide whether conservative or surgical treatment should be used. In adults—as far as possible— computed tomography should be performed to plan the treatment and determine the exact extent and size of the chambers (Fig. 11.13c).

When a suppurative effusion fills more than half a hemithorax, the patient has a pH below 7.2 and positive evidence of bacteria, a drain needs to be placed immediately (Colice et al. 2000; Davies et al. 2010; Heffner et al. 2010). In cases of chambered empyema, immediate intrapleural fibrinolysis therapy may be successful (Hamm 2005; Davies et al. 2010). The largest study conducted thus far on local fibrinolysis of empyema (Maskell et al. 2005) revealed no advantages in terms of the duration of disease or mortality in patients treated with streptokinase. However, the significant difference between chambered and nonchambered empyema was not taken into account. Video-assisted thoracoscopy and thoracotomy are surgical treatment procedures which, however, must be viewed under consideration of other factors present in the individual patient (Hamm 2005; Davies et al. 2010; Heffner et al. 2010).

11.2.3 Fever with Dyspnea and Chest Pain

The more extensively the pleura is affected in case of pleuritis, or the more extensively the lung parenchyma and pleura are affected in the case of pleuropneumonia, the more likely one will find a combination of all three symptoms. Fluid in the pleural space as well as invasion of peripheral portions of the lung can be viewed rapidly by sonography, independent of the patient's condition or mobility (Fig. 11.13d). Further investigations such as diagnostic aspiration of the pleura or additional radiological investigations serve to conclude the diagnostic procedures and make the diagnosis.

11.2.4 Fever as the Sole Symptom in Chest Diseases

In the case of ambiguous fever the investigator is confronted with a large number of possibilities in terms of differential diagnosis (Roth and Basello 2003). As a rule the first diagnostic step is laboratory investigations, which serve as the basis for further diagnostic procedures. The sonography investigation is not the first step for diseases of the chest because it does not provide a general overview of the chest organs. Sonography of the chest is usually requested in connection with a specific question in the case of an appropriate suspected diagnosis.

Polyserositis

Sonography, the most sensitive procedure to provide evidence of fluid, is used to investigate small pleural effusions (▶ Chap. 3) that frequently occur on both sides and usually cause no symptoms for the patient. Even small pericardial effusions (Fig. 11.10) in the course of autoimmune diseases or vasculitis can be very well demonstrated by sonography.

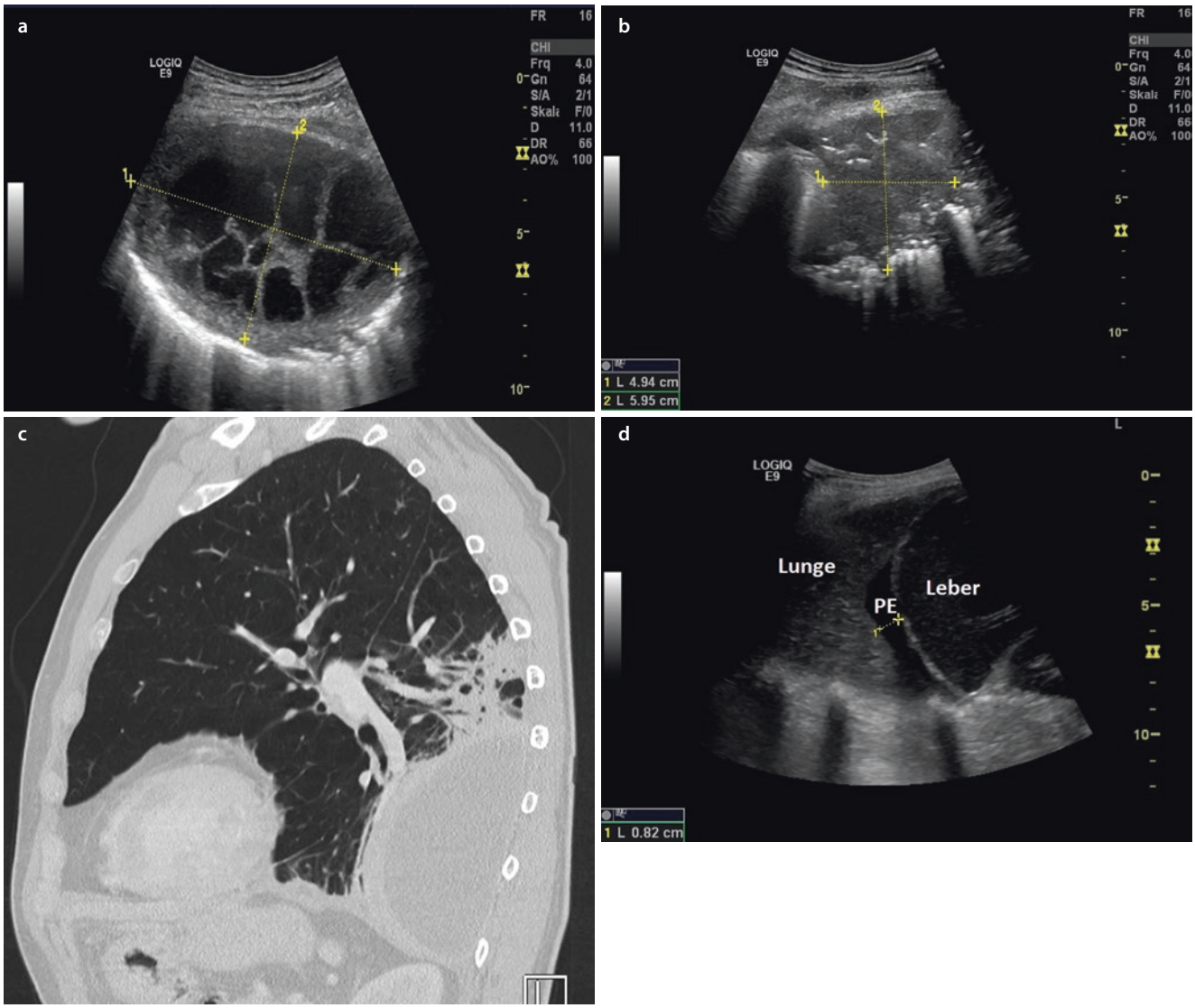

Fig. 11.13 **a** A 58-year-old man with high fever and critical sickness. On the left side dorsobasal pleural empyema with a thick wall and several loculations. **b** Above the empyema consolidated lung infiltration with air trappings. **c** Corresponding CT-image with section of the empyema and the infiltration. Therapy by means of VATS. **d** A 70-year-old woman with dyspnea and chest pain. The bedside sonographic examination from the right lateral aspect illustrates a compact consolidation in the right lower lobe and a small basal effusion (*PE, markers*)

Mycobacteriosis

The disease starts slowly and insidiously, and is associated with a gradual reduction of physical performance, nocturnal sweating and intermittent fever. Pulmonary symptoms might be entirely absent. Some patients have a persistent dry cough which initially misleads the clinician in terms of diagnostic procedures and treatment. Depending on the individual's immune defense and additional organs that may be affected, the symptoms of disease may be very diverse (Hopewell 2005).

In the case of active disease the conventional chest X-ray shows soft, pale infiltrates, occasionally in conjunction with colliquations. Peripheral inflammatory lesions are accessible to sonography (Figs. 11.14 and 11.15). Sonomorphological or radiological criteria that permit a reliable distinction between atypical mycobacteriosis and infection with *Mycobacterium tuberculosis* do not exist. The new interferon-gamma-release assays (IGRAs) measure the TB-antigen specific immunologic activation. These tests allow a differentiation between *Mycobacterium tuberculosis* and Mycobacteria other than tubercle bacilli (MOTT) (Diel et al. 2011, Schönfeld et al. 2013).

In cases of mycobacteriosis, sonography may be used in addition to radiological investigations, in order to evaluate the progress of peripheral lesions under treatment or when a sonography-guided biopsy is indicated for diagnostic purposes. However, conventional overview radiographs, possibly complemented by computed tomography, are always needed to assess the entire lung.

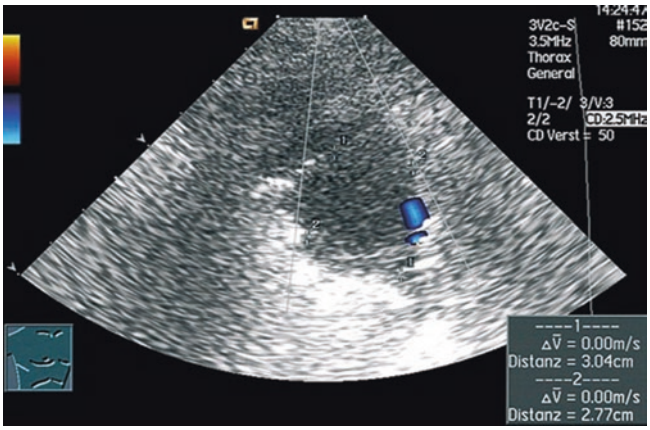

Fig. 11.14 A 68-year-old man with loss of strength and bouts of fever for several months. In the right upper lobe, in lateral location, there is a relatively homogeneous area with blurred margins and vessels at the margin. The sonographic biopsy (in NaCl!) showed bacteria on microscopic investigation; the bacteria were subsequently differentiated as atypical *Mycobacteria* using PCR

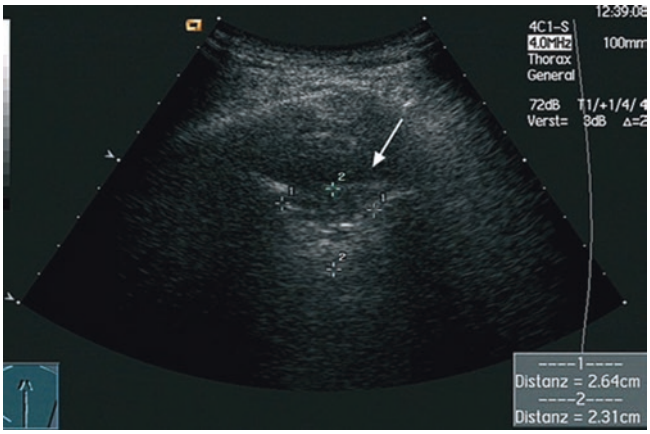

Fig. 11.15 A 73-year-old man with a chronic cough, who was known to suffer from chronic obstructive pulmonary disease. Sonography showed an area with blurred margins in dorsal and basal location, with residual air. A small pleural effusion (*arrow*). *Mycobacterium tuberculosis* was cultured in the bronchial and pleural secretion

Endocarditis

Fever, physical weakness and loss of physical performance may be the only signs of endocarditis. In the presence of good transthoracic insonation, vegetation in the heart valves is visualized. Blood cultures should be performed to obtain evidence of bacteria. In the case of Löffler's endocarditis, transient thrombi may be observed at the endocardium. A sonography investigation of the heart for the purpose of orientation can be performed even by the less experienced investigator. For a more detailed examination the investigator must possess the knowledge and skills required to perform echocardiography.

11.3 Dyspnea

The symptom of dyspnea is strongly dependent on the patient's subjective experience. Specific receptors that may be responsible for triggering dyspnea have not been identified thus far (Fitzgerald and Murray 2005). A multifactorial mechanism via medullary and peripheral chemoreceptors, pulmonary vagal afferences, and mechanoreceptors in the locomotor apparatus are presumed to exist (ATS 1999; Pfeifer 2005; Stulbarg and Adams 2005). In the meantime, clinically a distinction is made between acute, chronic, resting and stress dyspnea. Even the investigator finds it difficult to quantify dyspnea; therefore, particularly acute dyspnea should be rapidly investigated on the basis of clinical parameters (breath and pulse rate, auscultation, blood pressure), by laboratory investigation (blood gas analysis, determination of the acid–base balance of the body, blood count, typical enzymes associated with infarction) and imaging procedures. A strong respiratory drive is triggered by hypoxia and hypercapnia through afferent stimuli acting on the respiratory center.

Reduction of the gas-exchange surface, mechanical hindrance of dilatation of the lung, muscular and neurogenic deficits lead to greater respiratory effort. Cerebral disorders cause varying degrees of respiratory impairment. The possibilities of sonographic imaging in the presence of dyspnea, for the various compartments involved in respiration, are presented in the following.

11.3.1 Respiratory Tract

The upper and deeper respiratory tracts are the domain of endoscopy in terms of diagnosis. In the case of dyspnea with inspiratory stridor, sonography of the thyroid should always be considered as part of the routine investigation (Fig. 11.16).

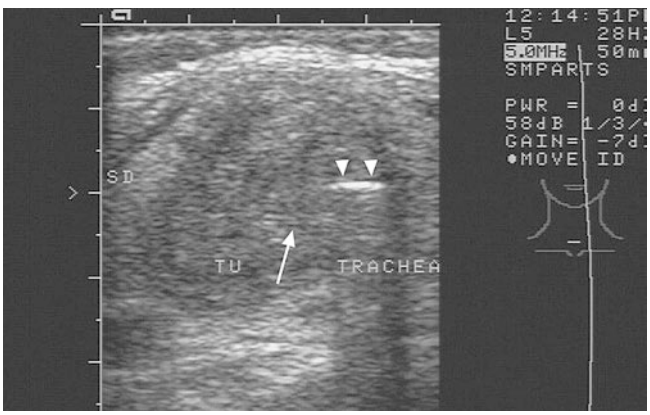

Fig. 11.16 A 55-year-old woman with advancing stress dyspnea for several weeks; inspiratory stridor. Sonography shows a space-occupying lesion arising from the right lobe of the thyroid, entering the trachea (*arrow*) and destroying the right lateral tracheal wall. A narrow air reflex (*arrowheads*) remains in the constricted trachea

11.3.2 Pleura

Fluid in the pleural space, depending on its quantity, leads to compression of lung tissue and reduces the respiratory surface. In patients with concomitant cardiopulmonary disease, even a few hundred milliliters of effusion can lead to dyspnea. Patients with a healthy contralateral lung may tolerate several liters of effusion and experience only mild dyspnea. Sonography allows rapid estimation of the quantity of effusion (Fig. 11.17) and the possibility of septation (Fig. 11.18).

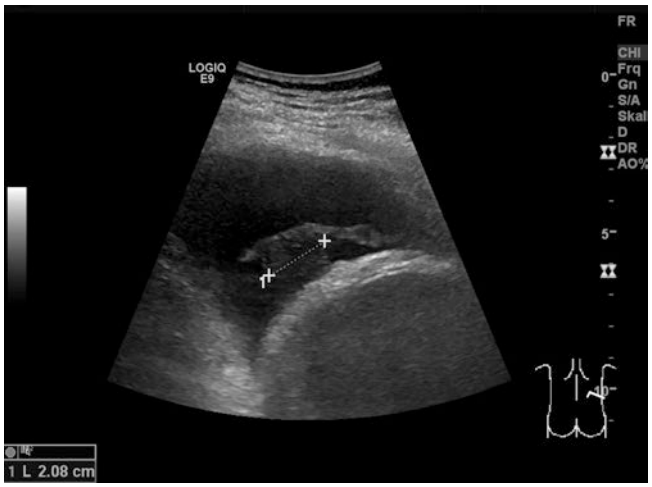

Fig. 11.17 A pleural effusion with a tumorous lesion based on the diaphragm (*cross markers*) turns out to be the cause of dyspnea in a 84-year-old woman. Malignant effusion is probable because of an operated breast cancer two years before (patient refused puncture and biopsy)

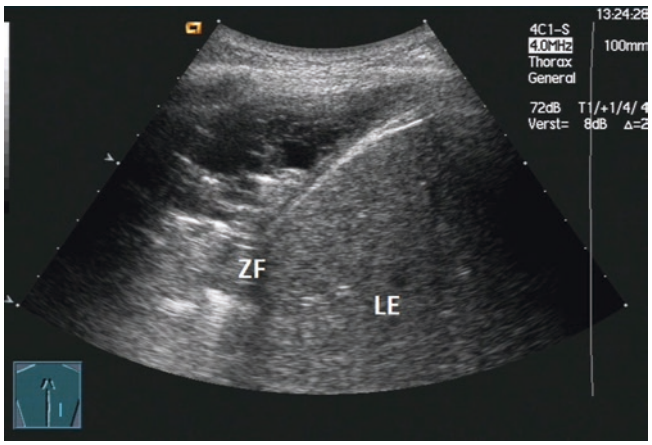

Fig. 11.18 After VATS due to complicated pleural empyema residuary small septate effusion and adherence of the lung to the diaphragm (*ZF, LE liver*)

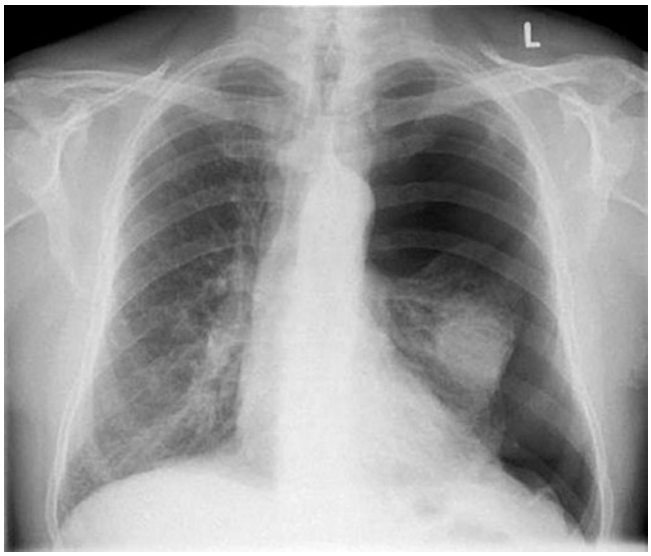

Fig. 11.19 A 63-year-old man with a tumor in the left upper lobe. Four hours after a biopsy had been obtained by transaxillary sonography, the patient developed dyspnea accompanied by elimination of gliding of the lung surface on sonography. The tumor previously seen on sonography was no longer visible. X-ray investigation showed a pneumothorax that needed drainage

As in a pleural effusion, the extent of a pneumothorax and the presence of concomitant diseases are of decisive importance for the emergence of dyspnea. A conventional X-ray is always needed to determine the size of the pneumothorax (Fig. 11.19).

11.3.3 Lung

Diseases of the lung parenchyma reduce the gas-exchange surfaces. Acute dyspnea may be caused by inflammatory, vascular or tumor diseases of the lung (▶ Chap. 5). Lung diseases accompanied by interstitial and chronic progressive loss of substance are more often accompanied by chronic and stress dyspnea. Pneumonia (▶ Sect. 5.1), tumors (▶ Sect. 5.2) and vascular consolidations (▶ Sect. 5.3) are accessible to sonographic diagnosis when ventilated tissue does not superimpose the path of insonation. Congested lung and pulmonary edema can be quickly identified by the findings of B-lines.

11.3.4 Heart

In cases of acute dyspnea the investigator must include cardiac diseases in the differential diagnosis. A physician trained in general internal medicine, as well as sonography, should be familiar with typical sonographic findings. In case of

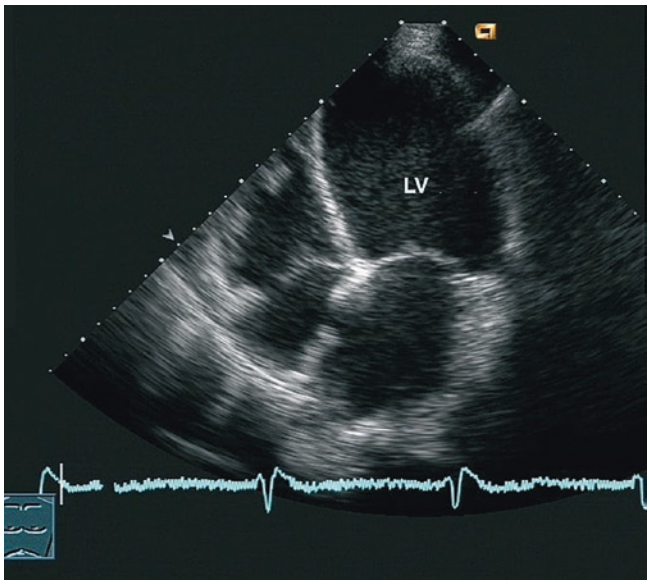

Fig. 11.20 A 55-year-old man with a pulmonary edema as a result of left-ventricular cardiomyopathy due to alcohol toxicity. The apical four-chamber view shows a dilated and ballooned left ventricle (*LV*)

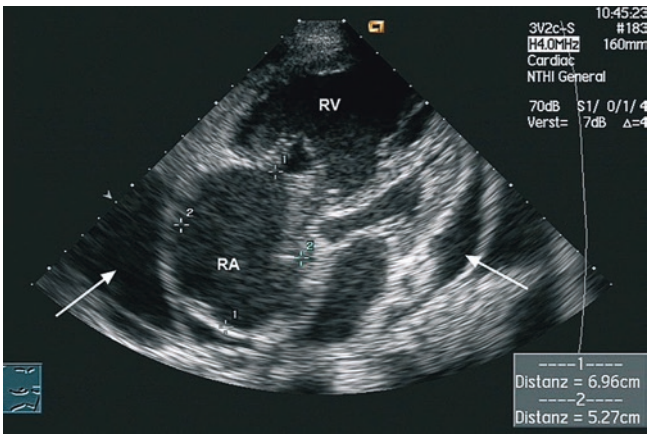

Fig. 11.21 A 64-year-old man with decompensated cor pulmonale as a result of pulmonary hypertension in the presence of the CREST syndrome. The apical four-chamber view reveals an enlarged right atrium (*RA*) and a massively dilated and hypertrophic right ventricle (*RV*). A pericardial effusion (*arrows*) lateral to the right atrium, the right ventricle and the left ventricle

failure of the left side of the heart (Ware and Matthay 2005; Arntfield and Millington 2012) owing to left-ventricular cardiomyopathy, one finds a massively dilated and ballooned left ventricle (Fig. 11.20).

In the case of cor pulmonale, diseases of the right side of the heart are manifested in terms of dilatation of the right side of the heart and hypertrophy of the right ventricle (Fig. 11.21).

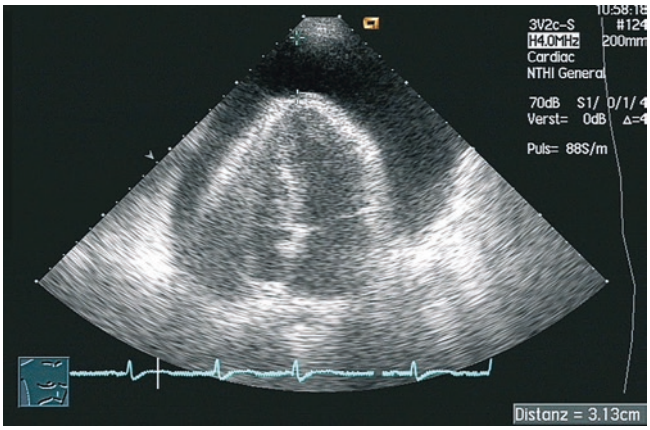

Fig. 11.22 A 91-year-old woman with global cardiac decompensation and a large circular pericardial effusion. Under diuretic therapy that reduced the cardiac load, the effusion resolved partially and dyspnea improved; therefore, in consideration of the patient's age a diagnostic aspiration was not performed

Determination of the size of the right side of the heart helps to assess the severity of disease in cases of a suspected pulmonary embolism (Goldhaber 1998; ▶ Sect. 5.3).

An indirect criterion of cardiac decompensation, easy to identify by sonography, is investigation of the vena cava in longitudinal section in the upper abdomen, through the left lobe of the liver. The diameter of the vena cava is more than 20 mm, and its diameter is inadequately reduced during inspiration.

A hemodynamically significant pericardial effusion leads to impairment of the systolic and diastolic function of the left ventricle, as well as congestion of venous blood flow. Large pericardial effusions can also be seen well in subcostal insonation from the epigastrium (Fig. 11.22).

11.3.5 Respiratory Muscles

The most important respiratory muscle is the diaphragm (▶ Chap. 3). In the rare event of bilateral paresis of the diaphragm the patient may be unable to lie supine because of dyspnea, which starts immediately (Fitzgerald and Murray 2005). Reduced mobility of the diaphragm due to fixation of the lung at the diaphragmatic pleura and unilateral partial or complete paresis of the diaphragm are seen well in the dynamic sonography investigation, particularly on comparison of the right and the left side (McCool and Tzelepis 2012). Local compression of the phrenic nerve may be visualized by supraclavicular placement of the probe (Fig. 11.23a, b).

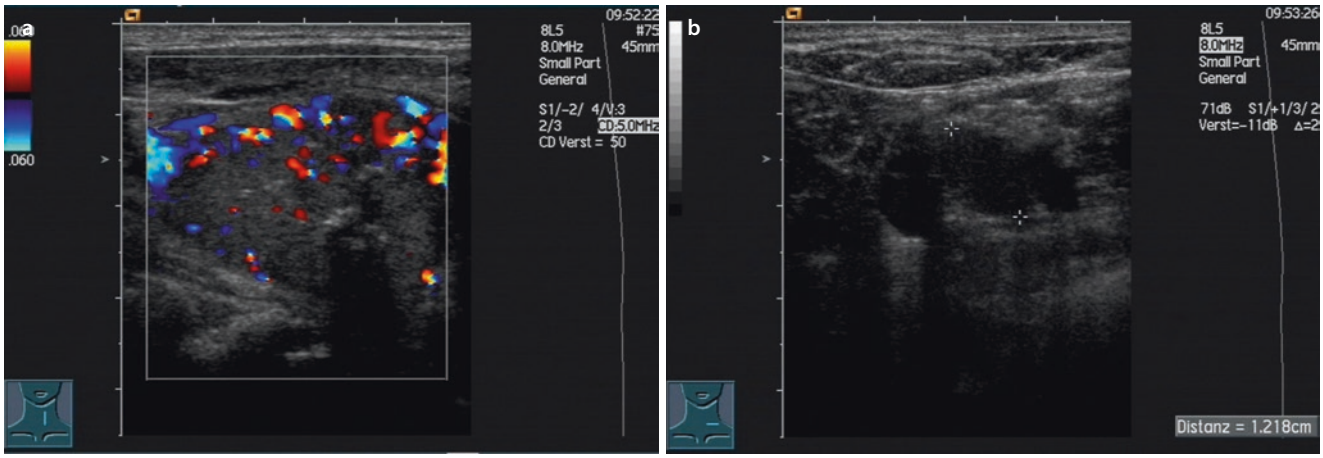

Fig. 11.23 **a** A 52-year-old man presenting with dyspnea, an elevated left diaphragm, local pain and increase of dyspnea on palpation left supraclavicular. Unremarkable radiologic findings except for the elevated diaphragm. In the left thyroid lobe (anamnestic "harmless node") inhomogeneous node with larger calcifications and irregular marginal vessels. **b** Next to the left thyroid lobe supraclavicular echo poor lymph node causing the elevated diaphragm by compression of the phrenic nerve. Diagnosis after curative surgery: papillary thyroid carcinoma with local lymph node metastasis

11.4 Summary

Chest pain, fever and dyspnea are frequent symptoms in cases of chest disease. The combination and varying intensity of symptoms allows conclusions to be drawn about the structures involved and the severity of the disease. Sonography, a readily available method that is very suitable for investigation at the bedside, makes a significant contribution to the diagnosis when investigating regions that can be viewed by the procedure. Sonography provides very significant information about the cause of sudden chest pain in the presence of a tension pneumothorax, in cases of pulmonary embolism, and in acute aortic dissection. Pathological changes in the chest wall can be visualized in an excellent manner because of the high quality of near-field resolution on the sonography image. Fever is a symptom in cases of inflammation of the chest wall, the pleura, and the lung. Sonography not only shows which structures are affected, but is also a reliable method for targeted diagnostic isolation of fluid and tissue. Sonography control investigations are particularly valuable in the course of pleural and pericardial effusions. In the case of dyspnea, sonography permits a distinction between a cardiac and a pulmonary cause of the condition. The dynamic investigation allows assessment of functional disorders of the diaphragm.

Acknowledgement We thank R. Loose, Head of the Institute of Diagnostic and Interventional Radiology at the Klinikum Nürnberg Nord, for providing radiology reports.

References

Al Deeb M, Barbic S, Featherstone R et al (2014) Point-of-care ultrasonography for the diagnosis of acute cardiogenic pulmonary edema in patients presenting with acute dyspnea: a systematic review and meta-analysis. Acad Emerg Med. 8:843–852

Amsterdam EA, Kirk JD, Bluemke DA (2010) Testing of low-risk patients presenting to emergency department with chest pain. Circulation 122:1756–1776

Arntfield RT, Millington SJ (2012) Point of care ultrasound applications in the emergency department and Intensive care unit – A review. Current cardiology reviews 8:98–108

ATS (1999) Dyspnea – mechanisms, assessment, and management: a consensus statement. Am J Respir Crit Care Med 159:321–340

Blaivas M (2012) Lung ultrasound in evaluation of pneumonia. J Ultrasound Med 31:823–826

Carey JA, Hamilton JR, Spencer DA, Gould K, Hasan A (1998) Empyema thoracis: a role for open thoracotomy and decortication. Arch Dis Child 79:510–513

Ceccarelli E, Masotti L, Barabesi L, Forconi S, Capelli R (2003) Pulmonary embolism in very old patients. Aging Clin Exp Res 15:117–122

Chavez MA, Shams N, Ellington LA et al (2014) Lung ultrasound for the diagnosis of pneumonia in adults: a systematic review and meta-analysis. Respiratory research 15:50

Colice GI, Curtis A, Deslauriers J et al (2000) ACCP consensus statement: medical and surgical treatment of parapneumonic effusions – an evidence-based guideline. Chest 118:1158–1171

Copetti R, Cattarossi L (2008) Ultrasound diagnosis of pneumonia in children. Radiol Med 113:190–198

Davies HE, Davies RJO, Davies CWH (2010) Management of pleural infection in adults: British Thoracic Society pleural disease guideline 2010. Thorax 65:ii41–ii53

Diel R, Loytved C, Nienhaus A et al (2011) Neue Empfehlungen für die Umgebungsuntersuchungen bei Tuberkulose

Deutsches Zentralkomitee zur Bekämpfung der Tuberkulose. Pneumologie 65:359–378

Fedullo PF, Morrus TA (2005) Pulmonary thromboembolism. In: Mason RJ, Murray JF, Broaddus VC, Nadel JA (eds) Textbook of respiratory medicine. Elsevier Saunders, Philadelphia, pp 1425–1458

Fitzgerald FT, Murray JF (2005) History and physical examinations. In: Mason RJ, Murray JF, Broaddus VC, Nadel JA (eds) Textbook of respiratory medicine. Elsevier Saunders, Philadelphia, pp 493–510

Gardelli G, Feletti F, Nanni A et al (2012) Chest Ultrasonography in the ICU. Respir Care 57:773–781

Goldhaber SZ (1998) Medical progress: pulmonary embolism. N Engl J Med 339:93–104

Hamm H (2005) Die Behandlung des parapneumonischen Ergusses and des Pleuraempyems. Pneumologie 59:696–703

Heffner JE et al (2010) Diagnostic utility and clinical applications of imaging for pleural space infections. Chest 137:467–479

Hopewell PC (2005) Tuberculosis and other mycobacterial diseases. In: Mason RJ, Murray JF, Broaddus VC, Nadel JA (eds) Textbook of respiratory medicine. Elsevier Saunders, Philadelphia, pp 979–1043

Hyacinthe AC, Broux C, Francony Gilles et al (2012) Diagnostic accuracy of ultrasonography in the acute assessment of common thoracic lesions after trauma. Chest 141:1177–1183

Kim OH, Kim WS, Kim MJ, Jung JY, Suh JH (2000) US in the diagnosis of pediatric chest diseases. Radiographics 20:653–671

Kolditz M, Halank M, Höffken G (2004) Parapneumonischer Erguss and Pleuraempyem—aktuelle Aspekte zu Einteilung, Diagnose and Therapie. Pneumologie 58:83–91

Kontos MC, Diercks DB, Kirk JD (2010) Emergency department and office-based evaluation of patients with chest pain. Mayo Clin Proc 85:285–295

Kreuter M, Herth FJF, Wenz H, Mathis G (2012) Sonographische Notfalldiagnostik des Thorax. Pneumologe 9:436–443

Kurz K, Giannitsis E, Meyer FJ (2 005) Thoraxschmerz. Pneumologie 2: 188–197

Levin DL, Klein JS (1999) Imaging techniques for pleural space infections. Semin Respir Infect 14:31–38

Lichtenstein DA, Mezière GA (2008) Relevance of lung ultrasound in the diagnosis of acute respiratory failure. The BLUE protocol. Chest 134:117–125

Maskell NA, Davies CWH, Nunn AJ et al (2005) U.K. trial of intrapleural streptokinase for pleural infection. N Engl J Med 352:865–874

Mathis G (2014) Thromboembolism in ultrasound. Killing three birds with one stone. Chest 145:931–932

McCool FD, Tzelepis GE (2012) Dysfunction of the diaphragm. N Engl J Med 366:932–942

Müller NL, Fraser RS, Lee KS, Johkoh T (2003) Diseases of the lung. Lippincott, Philadelphia, pp 45–46

Murray JF, Gebhart GF (2005) Chest pain. In: Mason RJ, Murray JF, Broaddus VC, Nadel JA (eds) Textbook of respiratory medicine. Elsevier Saunders, Philadelphia, pp 848–865

Moore CL, Copel JA (2011) Point-of-care ultrasonography. N Engl J Med 364:749–757

Pfeifer M (2005) Dyspnoe. Pneumologie 2:177–187

Ramnath RR, Heller RM, Ben-Ami T et al (1998) Implications of early sonographic evaluation of parapneumonic effusions in children with pneumonia. Pediatrics 101:68–71

Reißig A,Görg C, Mathis G (2009) Transthorakale Sonografie bei der Diagnostik pulmonaler Erkrankungen: ein systematischer Zugang. Ultraschall in Med 30:438–458

Reißig A, Görg C (2012) Pneumonie und diffus parenchymale Erkrankungen im Lungenultraschall. Pneumologe 9:444–451

Roth AR, Basello GM (2003) Approach to the adult patient with fever of unknown origin. Am Fam Physician 68:2223–2228

Sartori S, Tombesi P, Trevisani L, Nielsen I, Tassinari D, Abbasciano V (2007) Accuracy of transthoracic sonography in detection of pneumothorax after sonographically guided lung biopsy: prospective comparison with chest radiography. AJR 188:37–41

Schönfeld N, Haas W, Richter E et al (2013) Empfehlungen zur Diagnostik und Therapie nichttuberkulöser Mykobakteriosen des Deutschen Zentralkomitees zur Bekämpfung der Tuberkulose (DZK) und der Deutschen Gesellschaft für Pneumologie und Beatmungsmedizin (DGP). Pneumologie 67:605–633

Squizzato A, Rancan E, Dentali F et al (2013) Diagnostic accuracy of lung ultrasound for pulmonary embolism: a systematic review and meta-analysis. J Thromb Haemost 11:1269–1278

Stulbarg MS, Adams L (2005) Dyspnea. In: Mason RJ, Murray JF, Broaddus VC, Nadel JA (eds) Textbook of respiratory medicine. Elsevier Saunders, Philadelphia, pp 815–830

Volpicelli G, Frascisco M (2008) Lung ultrasound in the evaluation of patients with pleuritic pain in the emergency department. J Emerg Med 34:179–186

Volpicelli G (2013) Lung sonography. J Ultrasound Med 32:165–171

Ware LB, Matthay MA (2005) Acute pulmonary edema. N Engl J Med 353:2788–2796

Wüstner A, Gehmacher O, Hämmerle S et al (2005) Ultraschalldiagnostik beim stumpfen Thoraxtrauma. Ultraschall Med 26:285–290

Emergency Thoracic Ultrasound (Excluding Echocardiography)

Joseph Osterwalder and Gebhard Mathis

G. Mathis (ed.), *Chest Sonography*, DOI 10.1007/978-3-319-44072-9_12

12.1 Basic Principles

» Sonography is a continuation of the physical examination by other means Gerhard Rettenmaier (1975)

After a detailed description of the sonomorphology of various diseases in the main part of this book and the symptomatic approach detailed in ▶ Chap. 11, this chapter will be devoted to emergency situations. What is an emergency? Is it a life-threatening condition, severe trauma, or just excessive pain? Emergency sonography is defined as a well-performed problem-oriented bedside ultrasound examination of emergency patients; it is a continuation of the clinical assessment by the use of an auxillary. It is independent of the place where the patient is examined and of medical specialities. It may include several organs or regions of the body (Osterwalder 2011).

Preliminary reports of successful visualization of free fluid after abdominal trauma were first published more than 20 years ago (Hoffmann et al. 1989, 1992; Röthlin et al. 1993). The FAST concept (focused assessment with sonography for trauma) was later designed in the USA and further developed into E-FAST, P-FAST etc., all over the world (ACEP 2006, 2009). This revolutionary approach was followed by others such as focused ultrasound (Heller 1995), FEEL, and especially WINFOCUS (Word interactive Network focused on critical ultrasound). Each of them use different angles of view. Therefore, a trauma surgeon has different expectations of emergency sonography than a cardiologist. Despite increasing specialization, we should still maintain a general overview of our emergency patients based on medical history, clinical findings and addressing the right questions to the sonographer.

What is emergency ultrasound expected to do? Ultrasound makes the following contributions during the *primary survey*:

1. For initial assessment and decisions regarding resuscitation
2. In performing procedures

Its contributions during *the secondary survey* are as follows:

1. For the purpose of diagnosis
2. To narrow the differential diagnosis of signs and symptoms
3. For monitoring therapy and physiological variables
4. In performing procedures

In addition to resuscitation of life threatening conditions, emergency ultrasound is an important *strategic instrument*. In the preclinical setting, sonographic findings led to a change of treatment and selection of the appropriate hospital in 22 % of blunt abdominal traumas (Walcher et al. 2006). In the emergency department, sonography may significantly contribute to important decisions, such as whether a CT is needed, a specialist should be consulted, whether the patient needs to be hospitalized at all, or into which ward the patient should to be admitted. However, this task requires a high-quality ultrasound device with three transducers (convex, linear and phased array probe), basic software, as well as duplex-and-triplex Doppler. Quite often the investigation is performed alone by young residents on night duty. They should be trained early and thoroughly in performing ultrasound examinations. Several major abdominal and retroperitoneal, as well as thoracic, cardiovascular, and dermatological or musculoskeletal diseases and injuries can be identified immediately (Seitz et al. 2006; Breitkreutz et al. 2007; Walcher et al. 2009).

12.2 Chest Trauma

FAST initially focused on the abdomen. Not long after, fluids in the pleural cavity and the pericardium were added. Serious injuries in the chest can be identified by ultrasound in cases of penetrating as well as blunt trauma. In motor vehicular accidents leading to death, fatal injuries of the chest occur in 30 %, while a combination of injuries to the head and chest is found in a further 18 % (Ndiaye et al. 2009). In cases of pneumothorax or hemothorax, a drainage can be immediately performed. In addition to a pericardial effusion or even a tamponade, hypo-, dys- or akinesia and valve injuries are signs of heart failure. In cases of blunt trauma to the chest, contusions of the lung can be visualized by sonography in 18 % of cases. This type of injury should not be underestimated. We know that ARDS, although rare, may occur even 48 h after the accident (Wüstner et al. 2005). For the decision as to whether a CT is required in chest trauma, the full clinical picture has to be taken into consideration. However, sonography is the best predictor of chest injury—even better than conventional chest X-ray (Brink et al. 2009). One limitation is subcutaneous emphysema. It absorbs the ultrasound wave and therefore does not permit a view of the underlying regions (Mathis 2006).

Sonography in chest trauma

- Hematoma in the chest wall (Fig. 2.1)
- Fracture of the rib and sternum (Figs. 2.16, 2.17, and 2.18)
- Pneumothorax (Figs. 3.38, 3.39, and 3.40)
- Esophageale or main stem intubation
- Hemothorax (Fig. 12.1)
- Pericardial effusion—Cardiac contusion (Fig. 12.2)
- Injury to the aorta
- Contusion of the lung (Fig. 12.2)
- Rupture of the diaphragma (Fig. 12.3)
- Prandial status (Fig. 12.4)

Important before intubation

- Pericardial effusion (tamponade) (Fig. 12.5)
- Injuries to the heart (ventricular or septal rupture, valve rupture or lesion and regional wall motion abnormalities)
- Rupture of the aorta

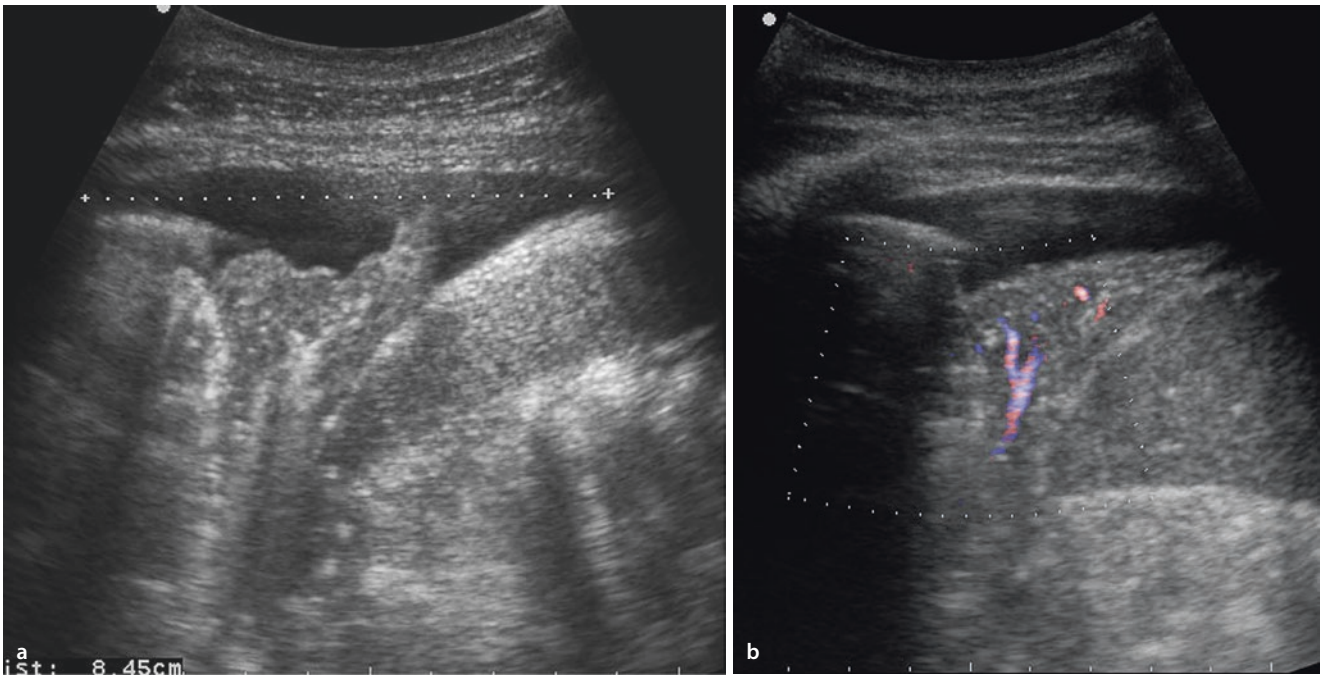

Fig. 12.1 Hemothorax due to a stab injury. **a** Four days after drainage, there is still a residual effusion, partly with internal echoes. **b** Compression atelectasis

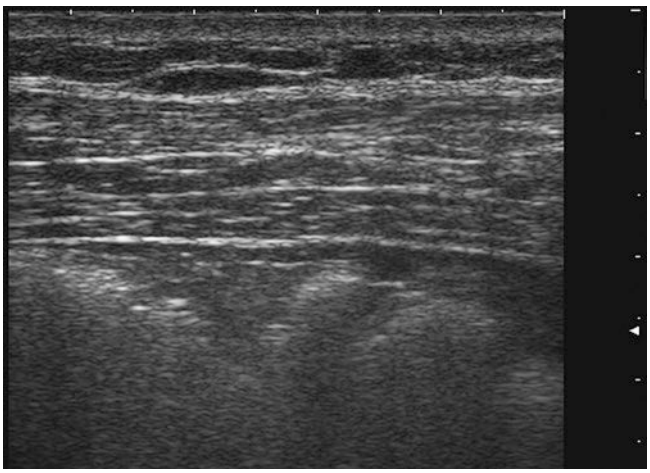

Fig. 12.2 Lung contusion due to a rib fracture after a fall from a ladder

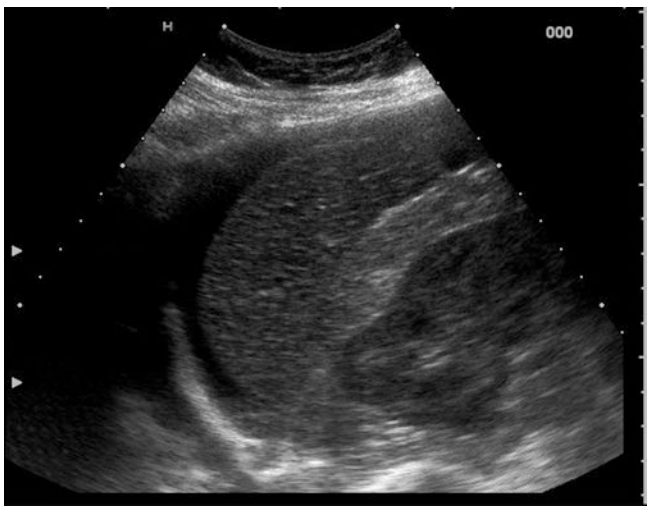

Fig. 12.3 Diaphragm rupture showing pleural effusion, perisplenic fluid collection and a gap in the ventral part of diaphragm

12.3 Nontraumatic Chest Emergencies

For a long time, emergency ultrasound of the chest (excluding echocardiography) in non-trauma patients was focused on obtaining evidence of pleural effusion and pneumothorax. Furthermore, the literature was mainly confined to the interpretation of comet-tail artifacts (B-lines) and more or less horizontal repetitive echoes (A-lines). This focus has been the consequence of various cultural customs/restrictions, which will not be further discussed here. However, there has been a change. In the meantime, recent data for certain diseases with typical pleural pain as well as without pain and with dyspnea and/or fever have clarified the remaining questions. The most common subpleural consolidations of the lung (pneumonia, pleurisy, pulmonary embolism) can easily be distinguished on the basis of their sonomorphology (Niemann et al. 2009). When CT is taken as the reference method, more pneumonias can be identified on ultrasonography than on the chest X-ray (Parlamento et al. 2009). We currently have two "silver standards" for the visualization of lung embolism. These methods complement each other: MSCT and ultrasonography (▶ see Sect. 4.3). CEUS—the signal-enhanced form of sonography—may help in cases of doubt (Goerg 2007).

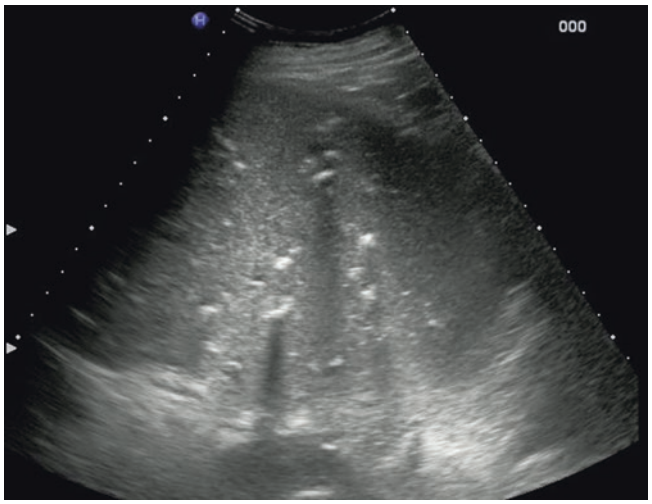

Fig. 12.4 Full stomach with fluid and leftovers from food

The following can be demonstrated accurately by chest ultrasound:
Pleural effusion (▶ Sect. 3.4)
Pneumothorax (▶ Sect. 3.6)
Pleurisy (Fig. 12.6, ▶ Sect. 3.5)
Lung atelectasis (▶ Sect. 5.4)
Pneumonia (Fig. 12.7, ▶ Sect. 5.1)
Pulmonary embolism (Fig. 12.8, ▶ Sect. 5.3)
DD: Carcinoma (▶ Sect. 5.2)

Chest ultrasound may be helpful in cases of:
Cardiac pulmonary edema
Pulmonary edema due to other causes (high-altitude pulmonary edema, inhalative-toxic)
ARDS
Interstitial lung diseases
Aspiration

One should also consider in which situation chest sonography is of no use for the differential diagnosis in pulmonary diseases with high-grade dyspnea.

Chest sonography is useless in cases of:
Bronchial asthma
COPD, except differentiation from pulmonary edema (none or less B-lines)
Pneumothorax/bullae
Hyperventilation

Dyspnea

Dyspnea is the most frequent respiratory symptom and occurs in over 50 % of patients due to cardiac or pulmonary pathologies. Additionally, acute dyspnea is an important sign of shock and is often a manifestation of a life-threaten-

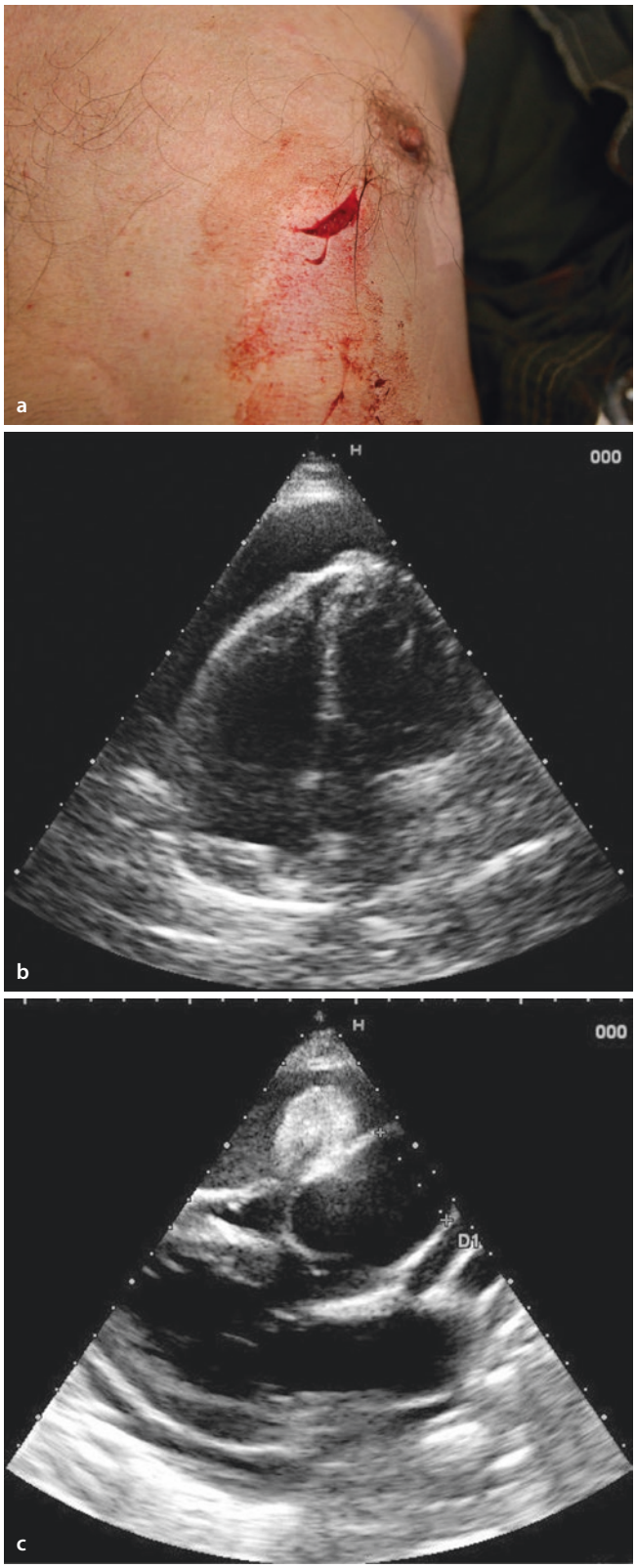

Fig. 12.5 Pericardial tamponade. **a** Stab injury. **b** Pericardial tamponade. **c** Blood clot in the hemopericard

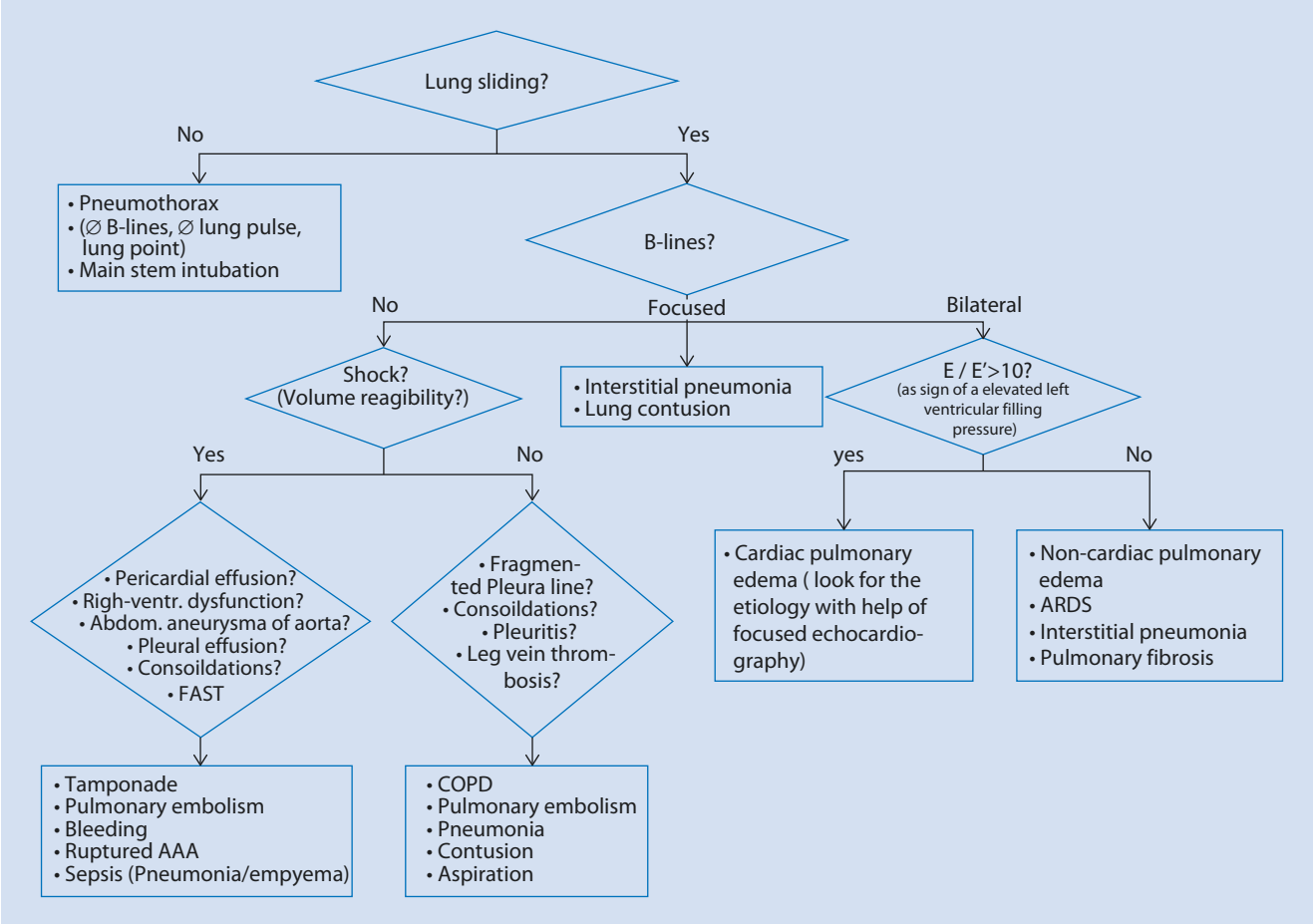

Fig. 12.6 Pleurisy: intense inspiratory chest pain. Fragmentation of the visceral pleura reflection, small subpleural consolidations

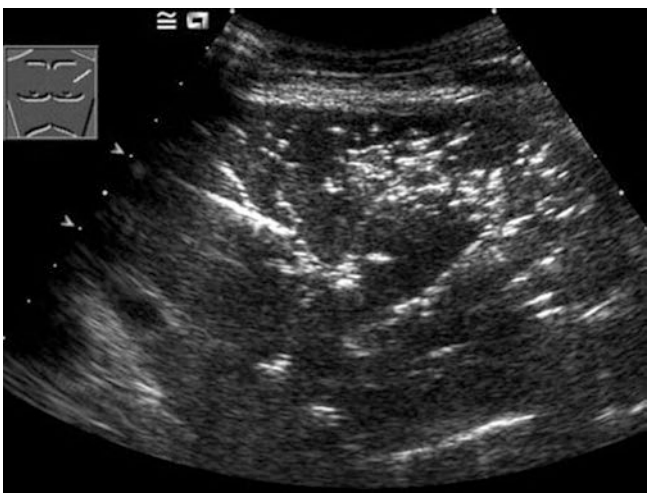

Fig. 12.7 Pneumonia: fever and dyspnea. Large liver- or tissue-like consolidation with bronchoaerogram

ing condition. Because of its subjective character the severity of dyspnea cannot be objectified and correlated to morbidity and mortality. This fact challenges the emergency physician. The first treatment is generally given without a definite diagnoses, f.ex. intubation. The physical examination and bedside auxillaries such as chest x-ray rarely lead to a definite diagnosis. Neither are specialists often present during the initial survey. In such situations focused bedside emergency sonography helps to quickly narrow the most important differential diagnoses. The examination includes heart, pleura, lung, abdomen and peripheral veins. The following algorithm summarizes the most important diagnostic steps and underlines the relevance of focused emergency echocardiography, FAST-exam, sonography of the abdominal aorta as well as veins of the lower extremity. These further possibilities are not the subject of this book. The interpretation of the findings are equally as important as a good performance of sonography. Relevant practical conclusions and safe decisions can only be made, when the clinical context and all available information are considered.

Algorithm Acute Dyspnea

The sonographic criteria of lung sonography for individual diseases are part of this book. Nevertheless, you should consult other literature for focused echocardiography, FAST-exam and sonography of lower extremity veins.

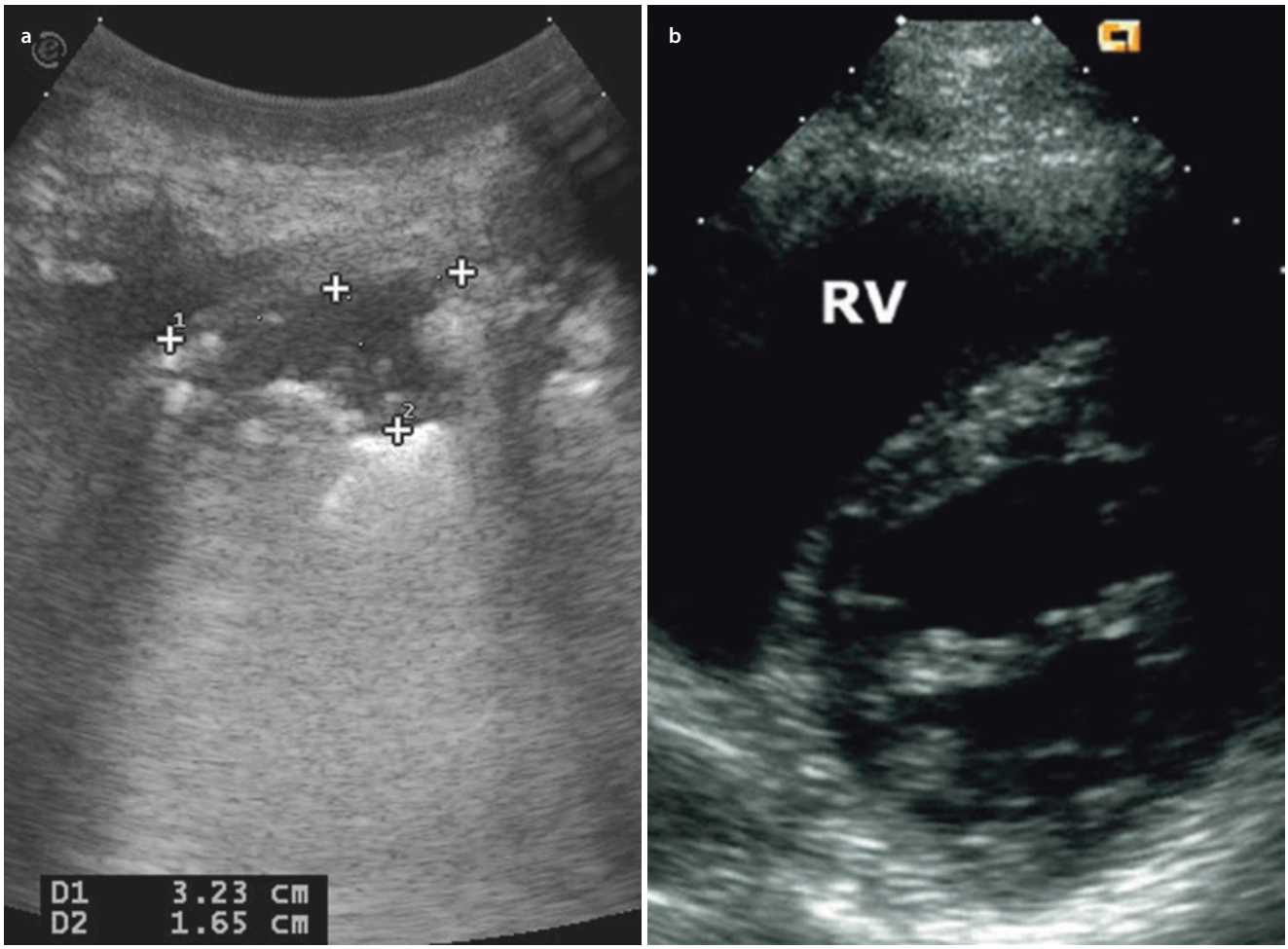

Fig. 12.8 Pulmonary embolism. **a** 1 cm triangular pleural-based lung consolidation. **b** Right heart failure seen as dilatation

References

ACEP (2009) Emergency ultrasound guidelines. Ann Emerg Med 53:550–570

Breitkreutz R, Walcher F, Seeger FH (2007) Focused echocardiographic evaluation in resuscitation management: concept of an advanced life support-confirmed algorithm. Crit Care Med 35(Suppl):150–161

Brink M, Kool DR, Dekker HM et al (2009) Predictors of abnormal chest CT after blunt trauma: a critical appraisal of the literature. Clin Radiol 64:272–283

Goerg C (2007) Transcutaneous contrast-enhanced sonography of pleural-based pulmonary lesions. Eur J Radiol 64:213–221

Heller WB (1995) Ultrasound in emergency medicine. WB Saunders, Philadelphia

Hoffmann R, Pohlemann T, Wippermann B et al (1989) Management of sonography in blunt abdominal trauma. Unfallchirurg 92:471–476

Hoffmann R, Nierlich M, Muggia-Sullam M et al (1992) Blunt abdominal trauma in cases of multiple evaluated by ultrasonography: a prospective analysis of 291 patients. J Trauma 32:452–458

Mathis G (2006) Notfallsonographie am thorax – a pictorial essay. Praxis 95:638–643

Ndiaye A, Chambost M, Chiron M (2009) The fatal injuries of car drivers. Forensic Sci Int 184:21–27

Niemann T, Egelhof T, Bongratz G (2009) Transthoracic sonography for the detection of pulmonary embolism – a meta analysis. Ultraschall Med 30:150–156

Osterwalder J (2011) 3-Länder-übergreifendes Ausbildungskonzept und Curriculum Notfallsonographie. Ultraschall Med 32

Parlamento S, Copetti R, Di Bartolomeo S (2009) Evaluation of lung ultrasound for the diagnosis of pneumonia in ED. Am J Emerg Med 27:379–384

Röthlin MA, Näf R, Amgwerde M et al (1993) Ultrasound in blunt abdominal and thoracic trauma. J Trauma 34:488–495

Seitz K, Mauch M, Vasillakis D (2006) Zentrale patientenaufnahme und ultraschall. Ultraschall Med 27:309–314

Tayal VS, Beatty MA, Marx JA (2004) FAST (focused assessment with sonography in trauma) accurate for cardiac and intraperitoneal injury in penetrating anterior chest trauma. J Ultrasound Med 23:467–472

Walcher F, Weinrich M, Conrad G et al (2006) Prehospital ultrasound imaging improves management of abdominal trauma. Br J Surg 93:238–242

Walcher F, Kirschning T, Brenner F et al (2009) Training in emergency sonography for trauma. Concept of a 1-day course program. Anaesthesist 58:375–378

World interactive network focused on critical ultrasound (2008) www.winfocus.org

Wüstner A, Gehmacher O, Hämmerle S, Schenkenbach C, Häfele H, Mathis G (2005) Ultraschalldiagnostik beim stumpfen thoraxtrauma. Ultraschall Med 26:285–290

Service Part

G. Mathis (ed.), *Chest Sonography*, DOI 10.1007/978-3-319-44072-9

Index

H

I

L

M

N

O

P

R

S

T

U

V

X